2017

SYNTHETIC METHODS FOR ESTER BOND FORMATION AND CONFORMATIONAL ANALYSIS OF ESTER-CONTAINING CARBOHYDRATES

Sven Hackbusch
University of the Pacific

Recommended Citation

SYNTHETIC METHODS FOR ESTER BOND FORMATION AND
CONFORMATIONAL ANALYSIS OF ESTER-CONTAINING CARBOHYDRATES.

by

Sven Hackbusch

A Dissertation Submitted to the

Office of Research and Graduate Studies

In Partial Fulfillment of the

Requirements for the Degree of

DOCTOR OF PHILOSOPHY

Department of Chemistry
Pharmaceutical and Chemical Sciences

University of the Pacific
Stockton, CA

2017

SYNTHETIC METHODS FOR ESTER BOND FORMATION AND
CONFORMATIONAL ANALYSIS OF ESTER-CONTAINING CARBOHYDRATES.

by

Sven Hackbusch

APPROVED BY:

Dissertation Advisor: Andreas H. Franz, Ph.D.

Committee Member: Vyacheslav V. Samoshin, Ph.D.

Committee Member: Liang Xue, Ph.D.

Committee Member: Jianhua Ren, Ph.D.

Committee Member: Wade A. Russu, Ph.D.

Department Chairs: Andreas H. Franz, Ph.D.; Michael McCallum, PhD.

Interim Dean of Graduate Studies: James A. Uchizono, Pharm.D., Ph.D.

SYNTHETIC METHODS FOR ESTER BOND FORMATION AND
CONFORMATIONAL ANALYSIS OF ESTER-CONTAINING CARBOHYDRATES.

Copyright 2017

by

Sven Hackbusch

ACKNOWLEDGMENTS

My deep and sincere gratitude goes out to Andreas Franz, who has gone above and beyond in his mentorship - not only in the laboratory, but in my private life, as well. Thank you for allowing me to grow and become an independent scientist and giving me the creative freedom to expand on our initial research proposals in my dissertation research.

Thank you to my committee for their continuous suggestions and helpful questions in shaping my dissertation research.

Without lab mates, this journey would have been quite lonely indeed, so thank you to all of those that have shared fume hoods and lab meetings with me over these five years, especially the always happy and upbeat Amelia Watson.

I want to thank the Pacific Mass Spec facility of David Sparkman, Matt Curtis and Patrick Batoon for many analyzed samples and the time taken to train me on running my own sample analysis.

Finally, thank you to my wife, parents and other family for their unwavering support and words of encouragement.

Synthetic methods for ester bond formation and conformational analysis of ester-containing carbohydrates.

Abstract

by Sven Hackbusch

University of the Pacific
2017

This dissertation encompasses work related to synthetic methods for the formation of ester linkages in organic compounds, as well as the investigation of the conformational influence of the ester functional group on the flexibility of inter-saccharide linkages, specifically, and the solution phase structure of ester-containing carbohydrate derivatives, in general.

Stereoselective reactions are an important part of the field of asymmetric synthesis and an understanding of their underlying mechanistic principles is essential for rational method development. Here, the exploration of a diastereoselective *O*-acylation reaction on a *trans*-2-substituted cyclohexanol scaffold is presented, along with possible reasons for the observed reversal of stereoselectivity dependent on the presence or absence of an achiral amine catalyst. In particular, this work establishes a structure-activity relationship with regard to the *trans*-2-substituent and its role as a chiral auxiliary in the reversal of diastereoselectivity.

In the second part, the synthesis of various ester-linked carbohydrate derivatives, and their conformational analysis is presented. Using multidimensional NMR experiments and computational methods, the compounds' solution-phase structures were established and the effect of the ester functional group on the molecules' flexibility and three-dimensional (3D) structure was investigated and compared to ether or glycosidic linkages. To aid in this, a novel Karplus equation for the $C(sp^2)OCH$ angle in ester-linked carbohydrates was developed on the basis of a model ester-linked carbohydrate. This equation describes the sinusoidal relationship between the $C(sp^2)OCH$ dihedral angle and the corresponding $^3J_{CH}$ coupling constant that can be determined from a *J*-HMBC NMR experiment. The insights from this research will be useful in describing the 3D structure of naturally occurring and lab-made ester-linked derivatives of carbohydrates, as well as guiding the *de novo*-design of carbohydrate based compounds with specific shape constraints for its use as enzyme inhibitors or similar targets.

In addition, the above project led to the development of a methodology for the synthesis of symmetrical ester molecules from primary alcohols using a mild oxidative esterification reaction, which proceeds in hydrous solvents using a nitrosyl radical catalyst. The reaction could be performed with a variety of alcohols and the resulting compounds are of interest in the fragrance and flavor industries.

TABLE OF CONTENTS

LIST OF TABLES

LIST OF FIGURES

LIST OF ABBREVIATIONS

Ac	acetyl
Bn	benzyl
bp	boiling point
borax	sodium borate, also known as sodium tetraborate
CH_2Cl_2	dichloromethane (see also DCM)
$CHCl_3$	chloroform
COSY	Homonuclear Correlation Spectroscopy
DART	Direct Analysis in Real Time
DBU	1,8-diazabicyclo(5.4.0)undec-7-ene
DCC	dicyclohexylcarbodiimide
DCM	dichloromethane
DEAD	diethylazodicarboxylate
DFT	density functional theory
DIC	N,N'-diisopropylcarbodiimide
DMAP	4-dimethylaminopyridine
dr	diastereomeric ratio
EDC	1-ethyl-3-(3-dimethylaminopropyl)carbodiimide
ESI	electrospray ionization
Et_2O	diethyl ether
EtOH	ethanol

EtOAc	ethyl acetate
J-HMBC	*J*-resolved Heteronuclear Multiple-Bond Correlation spectroscopy
HMBC	Heteronuclear Multiple-Bond Correlation spectroscopy
HMDS	hexamethyldisilazane
HMQC	Heteronuclear Multiple-Quantum Correlation spectroscopy
iPr$_2$O	diisopropyl ether
MD	molecular dynamics
MeOH	methanol
MS	mass spectrometry
mp	melting point
NMR	Nuclear Magnetic Resonance
NOE	nuclear overhauser effect
Oxone®	potassium peroxymonosulfate
ProtonSponge®	1,8-bis(dimethylamino)-naphthalene
PPh$_3$	triphenylphospine
QM	quantum mechanics
rt	room temperature, 25 °C (also RT)
TCCA	trichloroisocyanuric acid
THF	tetrahydrofuran
TMS	trimethylsilyl
TOCSY	Total Correlation Spectroscopy
TEMPO	2,2,6,6-tetramethyl-1-piperidinyloxy

Chapter 1: The ester functional group

In the enormous space of organic compounds, organic chemistry distinguishes between different classes of compounds based on similar carbon backbone skeletons and/or similar substructures, as illustrated in Figure 1.1.
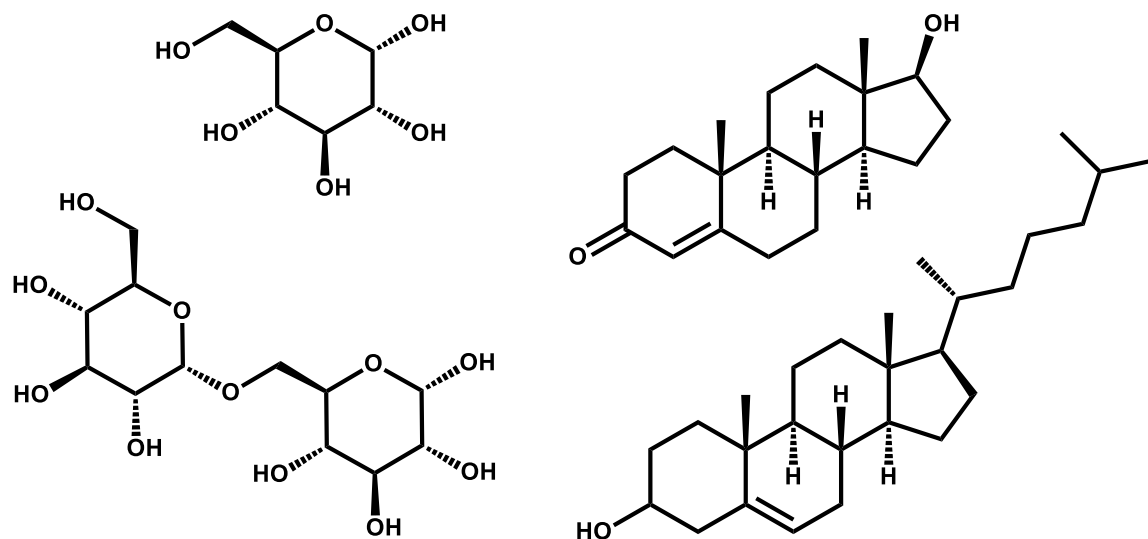
Figure 1.1. Examples of different organic compound classes: From left to right, the carbohydrates isomaltose and glucose and two steroids in testosterone and cholesterol, derived from the same characteristic four-ring core. All the above compounds share a common functional group, containing one or more alcohol or hydroxyl groups.

One key part of this classification is the distinction of specifically bonded atom combinations, known as functional groups. This distinction arises from the observed differences in chemical reactivity, as the same functional group will undergo the same or similar chemical reactions in several different molecules.[1] For example, all compounds in Figure 1.1 carry one or

more alcohol functional groups, which comprise a R_3C-O-H structural motif, where R denotes

one or up to three unclassified residues bound to the tetravalent carbon atom.

The functional group that is central to the work presented in this dissertation is the

carboxylate ester. A carboxylate ester is derived from the connection of a carboxylic acid to an

alcohol with the loss of one equivalent of H_2O, leading to a general structural motif of R-C(=O)-

O-R':
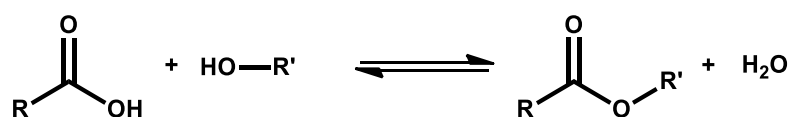
Figure 1.2. Schematic depiction of the ester formation from an alcohol and a carboxylic acid.

Additional types of esters are derived from different organic or inorganic acids to yield,

for example, phosphoesters, nitrate esters, thioesters or polyesters, examples of which are shown

in Figure 1.3. Because the body of work presented herein is primarily concerned only with esters

derived from carboxylic acids, in the following, the general term 'ester' will be employed to

specifically refer to carboxylate esters, unless otherwise notes.
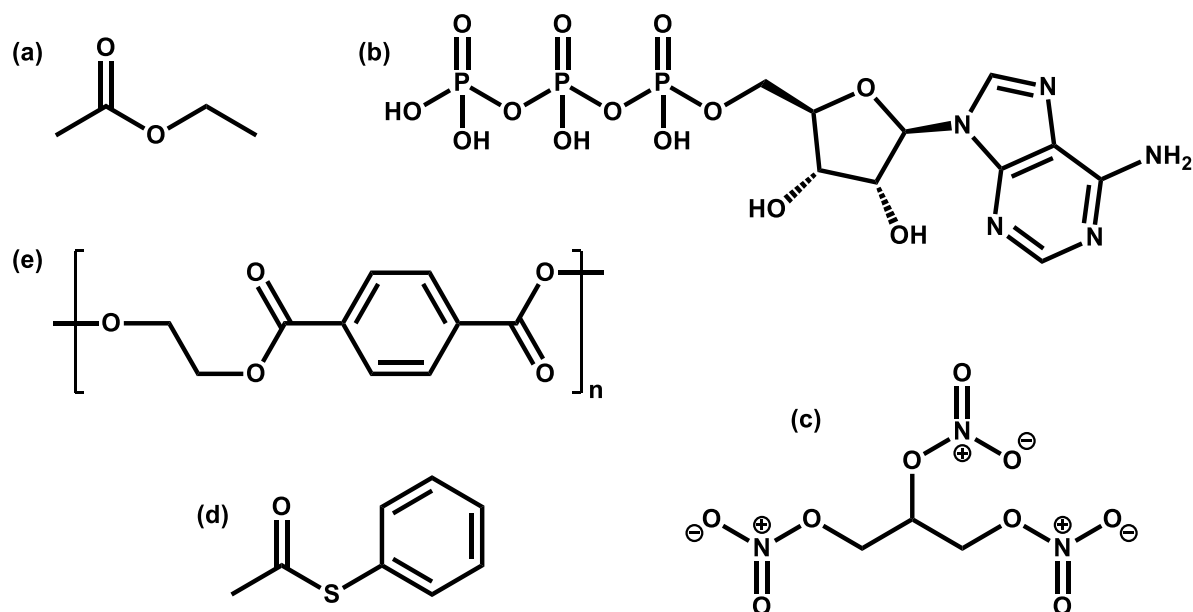
Figure 1.3. Examples of compounds in the different classes of carboxylate-, phosphor-, nitro- and polyesters; clockwise from top left: (a) ethyl acetate, (b) adenosine triphosphate (ATP), (c) trinitroglycerin, (d) phenyl thioacetate, and (e) polyethylene terephthalate (PET).

The names of chemical compounds have been standardized by the International Union of Pure and Applied Chemistry (IUPAC). By the IUPAC definition, the name of an ester is derived from the root of the acid's name and the root of the alcohol's name. The reaction of *n*-propionic acid and ethanol thus gives ethyl propionate, while the reaction of ethanoic acid and *n*-propanol gives *n*-propyl ethanoate. However, where applicable, the more common 'trivial names' will be used in this work. As such, the reaction of ethanoic acid and *n*-propanol will be referred to as the reaction of acetic acid and *n*-propanol to form *n*-propyl acetate. Additionally, an ester bond that leads to a cyclic structure classifies the compound as a lactone.

Esters in natural products and in the chemical industry

Esters are widely encountered in nature, as they permeate a wide range of compound classes that are of biological importance. Human nutrition relies on a substantial amount of fats, which are comprised of a significant amount of triglycerides – triesters of glycerol and three out of a large range of different saturated or unsaturated fatty acids.

Due to their high volatility and odor, low molecular weight esters are commonly used in the cosmetic and food and beverage industries as artificial or natural additives for flavoring or fragrances. Methyl salicylate ('oil of wintergreen') and isoamyl acetate, commonly referred to as 'banana oil' due to its characteristic odor, are examples of such esters. Additionally, parabens (esters of *p*-hydroxybenzoic acid) have found use as preservatives, due to bacteriocidal and fungicidal properties.[2,3] Lastly, polyesters, such as polyethyleneterephthalate (PET), comprise a large part of the polymers generated in the chemical industry for a wide variety of uses.

As mentioned, fats are of significant chemical importance. Besides their nutritional value, fats are a main component of lipid bilayers that form cell membranes and perform other functions. Specifically, 'fats' comprise a diverse range of triglycerides, from simple glycerides (carrying three identical acyl chains), mixed triglycerides (with two or three different acyl chains), glycerophospholipids to glyceroglycolipids and other saccharolipids. Two such examples are illustrated in Figure 1.4. In particular, glycolipids act as recognition sites for cell-to-cell interactions, with specific glycans binding to receptor lectins.[4] Secondly, glycolipids are important with regards to immune responses: Lipid A, which is a subunit of lipopolysaccharides of Gram-negative bacteria, is essential for the endotoxic activity it induces on the bacteria host's immune system, for example.[5-7]

In cases where specific glycolipids are overexpressed on the surface of cancer cells compared to healthy cells, strategies have been proposed to initiate B cell and T cell immune responses through recognition of the glycolipids on the cell surface, potentially leading to the development of cancer vaccines.[8]
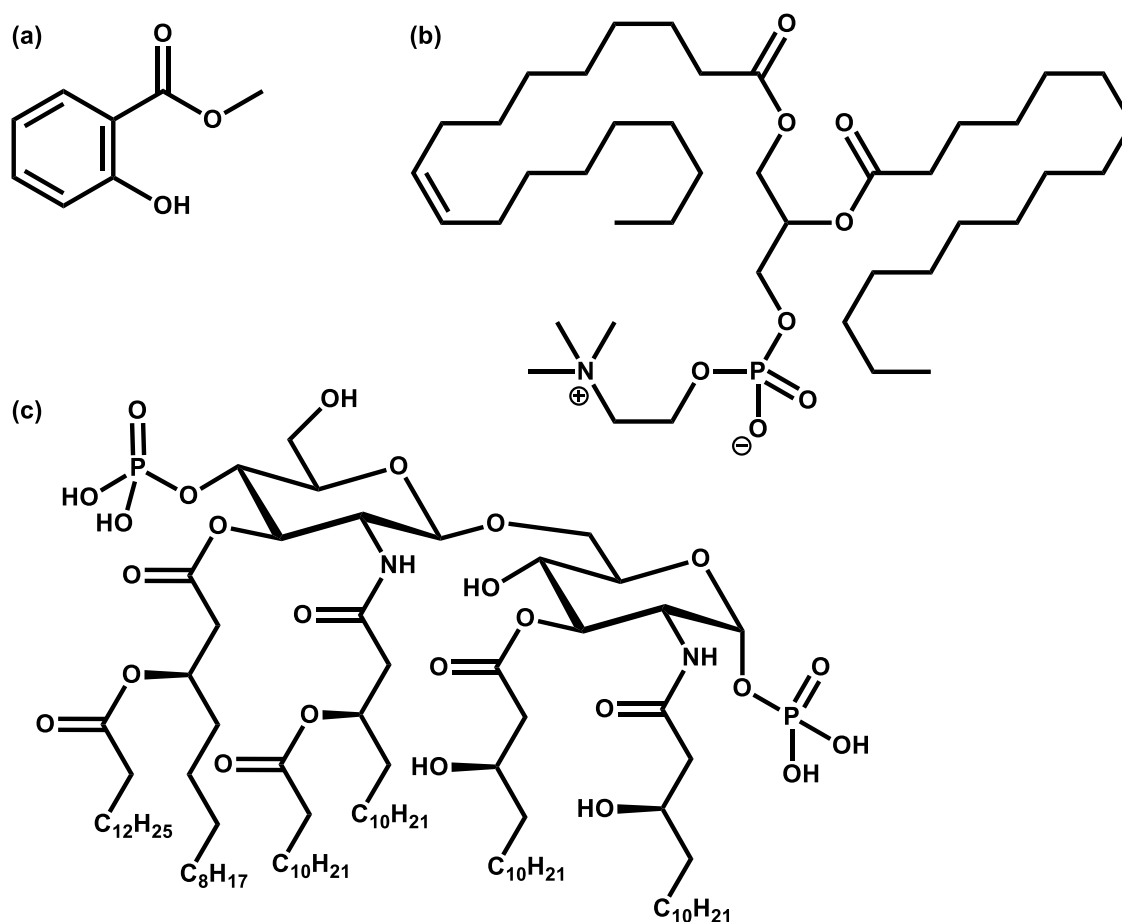
Figure 1.4. Examples of naturally occurring esters (clockwise from top left): (a) the fragrance compound methyl salicylate, (b) 1-oleoyl-2-palmitoyl-phosphatidylcholine, an example of a phospholipid, a group of compounds that are a major component of lipid membranes, and (c) lipid A, a glycolipid-specific to Gram-negative bacteria, as isolated from *E. coli*.[7]

Properties of the ester functional group

In terms of their physical properties, carboxylate esters are more polar than ethers, while being less polar than alcohols and carboxylic acids. The carbonyl oxygen can act as a hydrogen-bond acceptor, but unlike alcohols or acids, esters are not hydrogen-bond donors, making them more volatile than carboxylic acids and acids of similar molecular weight, but less volatile than comparable ethers.

The nature of the *sp*^{2} hybridization of the carbonyl carbon causes the R-C(=O)-O part of the ester functional group to be trigonal planar and the R-C=O, R-C-O and O=C-O angles to measure close to the ideal 120°. In addition, the C-O-R' angle is generally found to be close to the ideal 110° angle of the tetrahedral geometry of the sp^3 hybridized oxygen. Unlike in amides, the C-O bond has no partial double-bond character and as a result, the rotation about the C-O bond is more flexible. As such, esters can exhibit conformational isomerism between the two local minima of the *s-cis* (*Z*) or *s-trans* (*E*) conformations. As illustrated in Figure 1.5, there is a general preference for the *Z* conformer that can be explained by hyperconjugation and dipole effects, although steric hindrance of near substituents and solvent can influence the position of the equilibrium considerably. For example, 'smaller' cyclic lactones are usually restrained to the *E* conformer. In later chapters, this dihedral angle will be defined by the C-C-O-C angle, and as such the *Z* conformer in Figure 1.5 can also be considered *anti* with regards to the C-C-O-C dihedral angle.
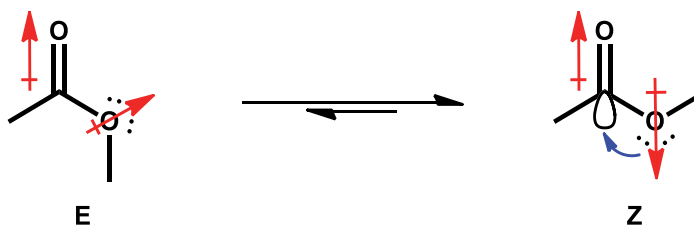
Figure 1.5. Equilibrium between the *E* and *Z* conformations of the ester and the influence of hyperconjugation and dipole moment compensation resulting in a shift in the equilibrium to the preferred *Z* conformation.

In addition, compared to the ether bond in R-CH$_2$-O-R', the ester bond is generally less stable due to the carbonyl oxygen withdrawing electron density from the carbonyl carbon, making it more susceptible to nucleophilic attack than the CH$_2$ group in ethers. However, unlike ketones or aldehydes, esters are less prone to reduction. This can be seen from the difference in reactivity

of NaBH$_4$ with esters, which are not reduced by NaBH$_4$ in ethanol, while ketones or aldehydes are converted into alcohols. Stronger reducing agents such as LiAlH$_4$ are needed to directly reduce esters to alcohols through an aldehyde intermediate.

Ester formation

As mentioned above, the ester functional group is derived from an alcohol and acid. As such, the simplest chemical reaction leading to the formation of an ester is shown above in Figure 1.2. The equilibrium can be shifted to the product side by a) increasing the concentration of one of the reactants or b) introducing a dehydrating agent, which removes any water formed in the reaction. Both of these are often employed in the Fischer esterification, which additionally uses an acid as a proton source to catalyze the otherwise sluggish reaction.[9]
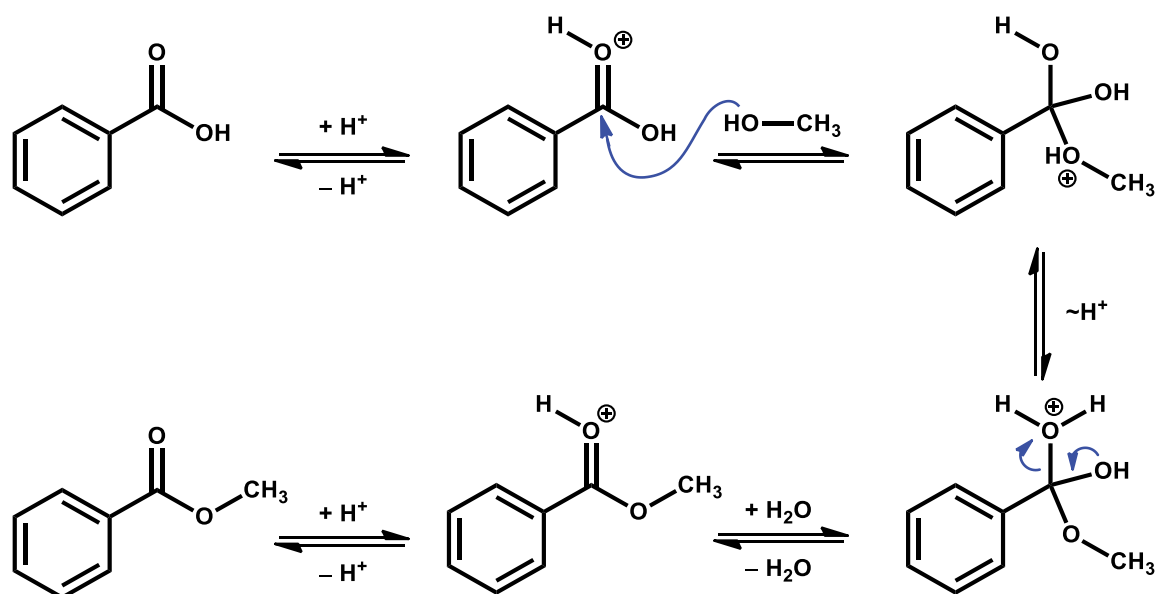
Figure 1.6. Mechanism of the acid catalyzed Fischer esterification between methanol and benzoic acid.

The Fischer esterification is typically carried out with the alcohol as both reactant and solvent. In instances where a large excess of one of the reactants is impractical, other synthetic

methods can be employed. Notably, the Steglich esterification uses dicyclohexylcarbodiimide (DCC) and 4-dimethylaminopyridine (DMAP) as a coupling reagent/catalyst combination to allow esterifications to be carried out in solvents such as dichloromethane at room temperature.[10] Other carbodiimides, such as 1-ethyl-3-(3-dimethylaminopropyl)carbodiimide (EDC) and N,N'-diisopropylcarbodiimide (DIC) have been frequently used for this transformation as well, due to their ease of handling and more easily removed byproducts, compared to DCC.

Another way to facilitate the ester formation with carboxylic acids is their conversion into a more reactive intermediate, which can be achieved through the formation of acyl chlorides or acid anhydrides, as illustrated in Figure 1.7. These compounds increase the electrophilicity of the central carbonyl carbon to allow more facile reaction with alcohols, often even in the absence of an acylation catalyst such as pyridine or DMAP.
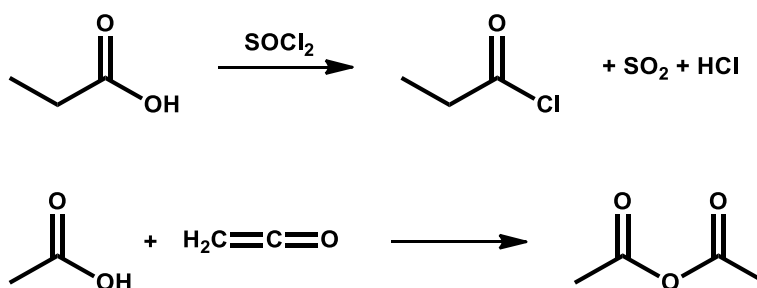
Figure 1.7. Formation of propionyl chloride or acetic anhydride from propionic acid using thionyl chloride or by reaction of acetic acid with ketene.

Primary or secondary alcohols can also be reacted with carboxylic acids in the Mitsunobu reaction, which employs triphenylphosphine (PPh$_3$) and diethylazodicarboxylate (DEAD), to form a phosphonium intermediate that can bind to and activate the alcohol oxygen as a leaving group, allowing for the carboxylic acid (with carboxylate as the reactive species) to attack with

inversion of the configuration. This reaction can be especially useful with secondary alcohols due to the controlled inversion of a chiral center.

Transesterifications can be useful to convert one type of ester into another, and is generally carried out in the presence of an acid or base catalyst. For example, PET (shown in Figure 1.3) is commercially produced through a transesterification of dimethyl terephthalate with ethylene glycol, with the methanol by-product removed by distillation to shift the equilibrium to the product side.[11]

Besides the formation of esters from their respective acid and alcohol pair, other methods starting from a variety of reagents have been explored, such as the alkylation of carboxylate salts, carbonylation reactions between alkyl or aryl halides, carbon monoxide and alcohols, the reaction of carboxylic acids with alkenes, among others.[12-15] The latter reaction falls under the umbrella of oxidative esterification reactions, which are of interest due to their potential as atom efficient and economical pathways toward useful ester compounds. In its basic form, an oxidative esterification can be achieved by reacting primary alcohols to form symmetrical ester – a topic that will be discussed in more detail in Chapter 3.[16]

Esters in organic synthesis

As previously mentioned, the nature of the carbonyl group in ester functional groups induces a partial positive charge in the carbonyl carbon, which makes it susceptible to nucleophilic attack. For this reason, the ester C-O bond can be cleaved by hydrolysis or alcoholysis under acidic or basic conditions. As described above, this can have synthetic applications in the transesterification, and when the ester functional group is only installed transiently, as is the case in protection group chemistry, as will be discussed hereafter. This is due to the reversible nature of the esterification reaction. However, if stronger nucleophiles, such as amines, are used, the attack of the nucleophile is often irreversible due to the less labile nature of the newly formed functional group (i.e. an amide group). This reactivity can be used to convert esters into other otherwise hard to access functional groups. Carbon-based nucleophiles

derived from Grignard reagents or organolithium compounds react with esters to form tertiary

alcohols by duplicate addition of the nucleophile, for example.

Esters can also be used in the Claisen condensation, as the α-hydrogens in esters are

similarly acidic as those in other carbonyl compounds. Using a strong base, an ester can thus be

inter- or intramolecularly reacted with another carbonyl-containing functional group to yield a ß-

keto ester or a ß-diketone, as depicted in Figure 1.8.[17,18]
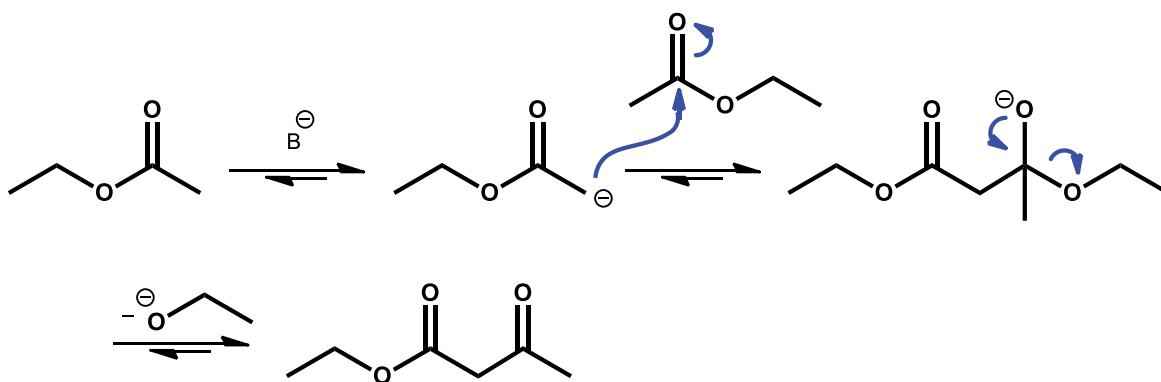
Figure 1.8. Mechanism of the intermolecular Claisen condensation between two molecules of
ethyl acetate to give ethyl acetoacetate, a ß-keto ester.

Ester function groups are widely used in protection group chemistry, where they can be

formed to temporarily shield alcohols or carboxylic acids to avoid reactivity during

transformations at other functional groups. For alcohols, acetyl and benzoyl protection groups

are frequently used for this purpose, partially because they are readily removed again by

relatively mild acid or base hydrolysis. In the field of carbohydrate chemistry, esters protection

groups can be particularly useful due to their ability to act as neighboring groups to direct

reactivity at, for example, the anomeric position.[19]
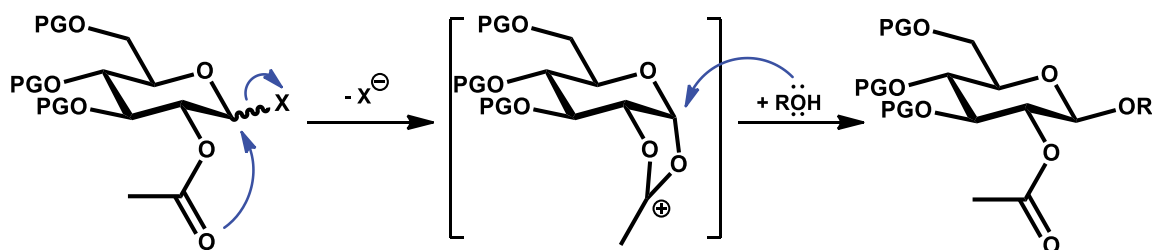
Figure 1.9. The 2-*O*-acetyl group participating in the stereochemical outcome of a glycosylation reaction through neighboring group participation to yield the *ß*-anomer as the major product.

In cases that call for a more stable ester protection group, a pivaloyl ester can be used, which is unusually resistant to hydrolysis and can thus act as an orthogonal protection to acetyl or benzoyl esters. Esters can likewise be used to protect carboxylic acids as methyl, benzyl or *tert*-butyl esters, the latter of which is particularly useful due to the ease of removal of side products during its deprotection.

In medicinal chemistry and chemical biology, esters are commonly used to increase bioavailability and facilitate cellular delivery by reducing the polarity of the molecule of interest. The polar nature of the hydroxyl functionalities of carbohydrates generally renders them cell-impermeable. To allow the crossing of a cell's lipid bilayers, sugars, for example, are routinely acylated with short chain fatty acids, such as butyrate. The thusly derivatized molecules, or 'prodrugs', are assumed to be converted into the active pharmaceutical moiety *via* endogenous esterase activity in the cell. Enalapril, the structure of which is shown in Figure 1.10, is one example of an ester-containing prodrug that is approved by the FDA for the treatment of hypertension, diabetic kidney disease and heart failure as an angiotensin-converting enzyme (ACE) inhibitor.[20,21] The bio-active form 'enalaprilat' suffers from insufficient GI absorption, which was improved by converting one of the two carboxylic acids into an ethyl ester. In the body, it is readily converted into its bio-active form by ester-hydrolysis mediated by a wide range of ubiquitous and non-specific esterase enzymes. Although this type of enzyme-catalyzed hydrolysis is often assumed to be faster than ensuing biological activity, examples exist which

suggest that ester bonds can persist intracellularly. For instance, acetylsalicylic acid, commonly known as aspirin, irreversibly inhibits cyclooxygenase (COX) by acetylation of a particular serine residue of the enzyme by transfer of the acetyl group – a reactivity that would not be possible, if aspirin was quickly hydrolyzed to salicylic acid.[22]

- cytotoxic
- not incorporated into glycans

- negligible cytotoxicity
- readily incorporated into glycans
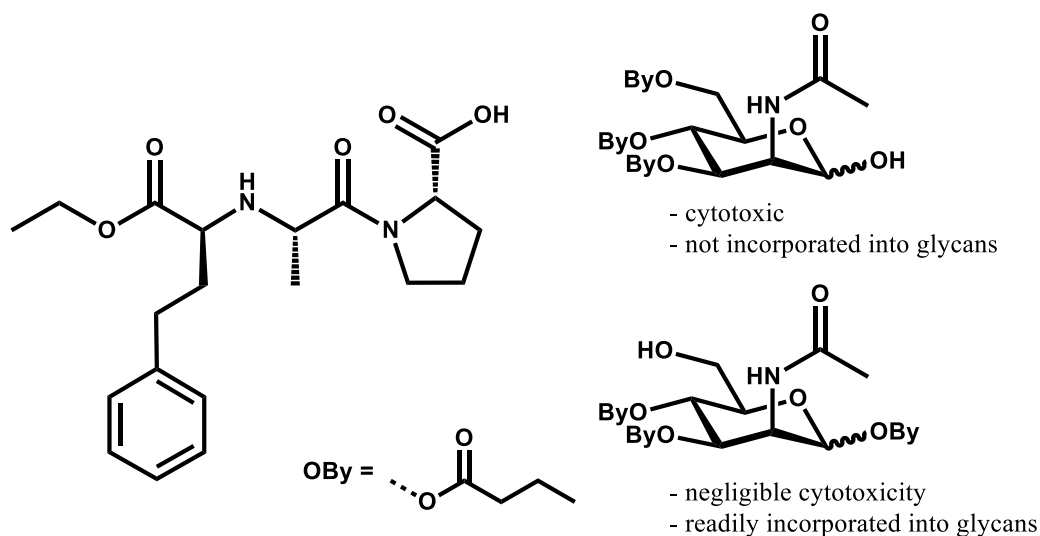
Figure 1.10. The structures of the ester-containing prodrug enalapril and two different *N*-acetyl-D-mannosamine prodrugs with different biological activity profiles, as reported by Aich *et al.*.[23]

Additionally, a study by Aich *et al.* on differently butyrated *N*-acetyl-D-mannosamine, which were synthesized to increase the bioavailability of the native *N*-acetyl-D-mannosamine, indicated different biological activity for the prodrugs depending on the site of esterification, as indicated in Figure 1.10.[23] These results suggested that esterase activity is not always faster than the desired target activity, contrary to what is commonly assumed, and that different activity profiles can result from different prodrugs, when ester bonds are in fact not immediately cleaved and thus possibly quite persistent upon traversing the cell membrane.

Relevance of esters in the present work

As can be understood from the title of this dissertation, the present work will elaborate on research findings concerned with a) the formation of ester linkages in organic compound classes and b) the synthesis of ester-containing carbohydrates and the investigation of the conformational influence of the ester functional group on the flexibility of inter-saccharide linkages, specifically, and the solution phase structure of the synthesized compounds, in general.

To that end, Chapter 2 will discuss the exploration of a diastereoselective esterification or *O*-acylation reaction on a substituted cyclohexanol scaffold and possible reasons for the reversal of the observed stereoselectivity through the addition of achiral pyridine catalysts. In Chapter 3, the development of a synthetic method toward symmetric esters from primary alcohols through an oxidative esterification is presented. Chapter 4 discusses the development and validation of an empirical Karplus equation for the C(=O)-O-C-H dihedral angle in ester-linked glucopyranoses. The methods presented in Chapters 3 and 4 are applied in the final Chapter 5, which is concerned with the synthesis of various ester-linked carbohydrate derivatives, particularly several acetyl-derivatives and a 6,6'-ester linked glucose disaccharide analog, and their conformational analysis to establish their solution structure based on the combination of spectroscopic and computational evidence and to elucidate the effect of the ester functional group on the molecules' flexibility.

Chapter 2: Diastereoselective Esterification

Introduction

One important area of study in organic chemistry, but also in inorganic chemistry, is that

of stereochemistry. Two molecules that are made up of the same atoms, but that are bonded

together in different ways, are constitutional isomers. Dimethyl ether (CH_3OCH_3) and ethanol

(CH_3CH_2OH) are simple examples of this relationship. Differing from constitutional isomers,

stereoisomers are molecules that are connected in the same fashion as one another, but with their

atoms arranged differently in space, so as to be noninterchangeable. For this reason, the three-

dimensional representation of chiral molecules is of importance in stereochemistry. The term

chirality originates from the Greek χειρ (phonetic "khire") for hand. It describes the concept in

which a molecule is nonsuperimposable on its mirror image.
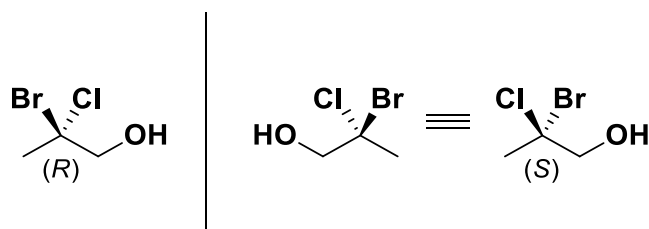
Figure 2.1. The mirror image of (*R*)-2-bromo-2-chloropropanol, (*S*)-2-bromo-2-chloropropanol,
is nonsuperimposable, illustrating the concept of chirality.

The spatial arrangement of the atoms in a chiral molecule, i.e. its absolute configuration,

is designated as either (*R*) or (*S*), referring to rectus or sinister, as exemplified in the case of 2-

bromo-2-chloropropanol in Figure 2.1. This and other nomenclature will be discussed hereafter.

The field of stereochemistry is considered by many to have originated with work by the French scientist Louis Pasteur (1822-1895). In his study of crystalline salts of tartaric acid obtained from lab-made sources, he observed the presence of nonsuperimposable mirror image crystals in the lab-made tartaric acid salt. As opposed to tartaric acid isolated from grapes, lab-made tartaric acid did not show to be optically active, that is it did not rotate plane-polarized light. With the use of tweezers and a magnifying glass, Pasteur was able to separate the two types of crystal shapes he observed and show that their solutions did indeed rotate plane-polarized light in opposite directions. In his landmark paper from 1848, Pasteur thus concluded that the molecules making up the crystals must be chiral, as well.[24,25] Until that time, the three-dimensional nature of chemical compounds at the molecular level was not readily apparent. In fact, it was not until 1874 that van't Hoff and Le Bel independently put forth that the four substituents around a carbon atom are arranged in tetrahedral fashion, as opposed to square planar.[26-28]

In nature, chirality is found on the macro scale in handedness and helical structures in animal and plant life. Beyond that it permeates to the micro scale, as the vast number of chemical compounds found in nature are chiral and often only one stereoisomer is present exclusively. For example, all 20 naturally occurring amino acids in proteins are L-amino acids. Carbohydrates largely exist only in their D-form in nature. The origin of this inherent preference in stereochemistry is not known at present, but is widely researched, and multiple hypotheses about the origin of chiral preference in the observed universe exist.[29,30]

Before the absolute configuration of stereoisomers was known, chiral molecules were initially classified by their interaction with plane-polarized light. For example, tartaric acid obtained from grapes rotated plane-polarized light in counterclockwise fashion and was thus termed to be levorotatory, *l*-tartaric acid or (–)-tartaric acid. The not naturally-occurring enantiomer of tartaric acid is dextrorotatory, as denoted by the *d*- or (+)- prefixes. There is however, no causal relationship between this property and a compound's absolute configuration.

Until 1951, chemists had no direct way to determine the absolute configuration of an optically active compound. In that year, J.M. Bijvoet *et al.* devised a technique based on X-ray diffraction to conclusively determine the absolute rotation of (+)-tartaric acid.[31] Before that time, only the relative configuration of stereoisomers could be known. To aid in this assignment, the convention based on the Fisher projection was to arbitrarily assign (+)-glyceraldehyde to D-glyceraldehyde, which is now known to in fact be (*R*)-glyceraldehyde, with its opposite being L-glyceraldehyde. This is also known as the Fischer–Rosanoff convention.[1] Through a series of chemical reactions that were known to either retain or reverse the stereochemistry of glyceraldehyde, other small biomolecules could be related to it and thus their stereochemistry established relative to it as D or L. Although based on a guess, the D/L-nomenclature is still commonly used today such as with the L-amino acids and D-sugars. This is because unlike in the *R*/*S* system, the substitution of residues on the stereocenter does not change the D/L designation, which is not necessarily the case for *R*/*S*.

In the above example of 2-bromo-2-chloropropanol in Figure 2.1, the molecule exists in two forms, classified as enantiomers, which differ in the absolute configuration at one stereocenter, namely the C-2 carbon. Enantiomers exhibit identical melting and boiling points and are otherwise indistinguishable in terms of their physical properties except for their behavior toward plane-polarized light. Because of this property, enantiomers in particular and chiral molecules in general are often said to be 'optically active'. All chiral molecules with only one stereocenter exist in either of two enantiomeric forms or their mixture, which is called a racemate. Molecules with *n* number of stereocenters can potentially form up to 2^n stereoisomers. Stereochemistry classifies these as either enantiomers or diastereomers. Diastereomers are defined by IUPAC as stereoisomers that are not mirror images of one another.[1] As such, they generally exhibit different chemical and physical properties. In addition, a third classification exists for chiral compounds that are superimposable on their mirror images due to an internal

plane of symmetry. These compounds, carrying an even number of at least two stereocenters are

termed *meso* – they are optically inactive and thus achiral.
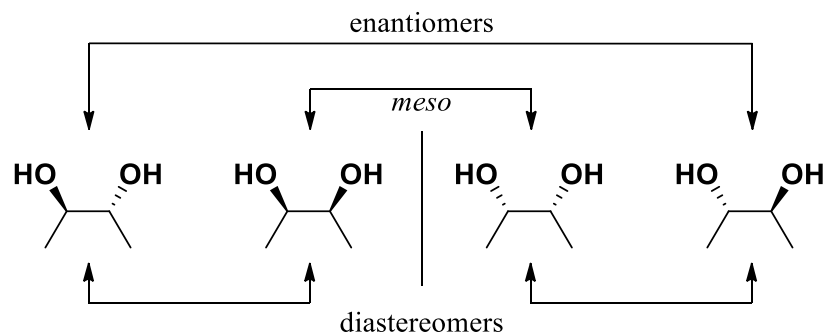
Figure 2.2. The relationships between the stereoisomers of 2,3-dihydroxybutane illustrating the concepts of enantiomers, diastereomers and *meso* compounds.

As pointed out above, the *R*/*S* designation is the most commonly used convention to

denote the absolute conformation at a given stereocenter. It is based on the Cahn-Ingold-Prelog

rules, which were first published in 1966.[32] The *R*/*S* nomenclature can even be used in the case of

axially chiral molecules. Under certain circumstances, molecules can be chiral despite a lack of a

stereocenter. 2,2'-bis(diphenylphosphino)-1,1'-binaphthyl (BINAP), for example, lacks a

stereogenic atom, but is chiral due to the restricted rotation of the two naphthyl moieties around

the central C-C single bond, as illustrated in Figure 2.3. Another notable example of this property

are substituted allenes. In all these cases, the molecules are said to exhibit an axial chirality or

helicity.[1]
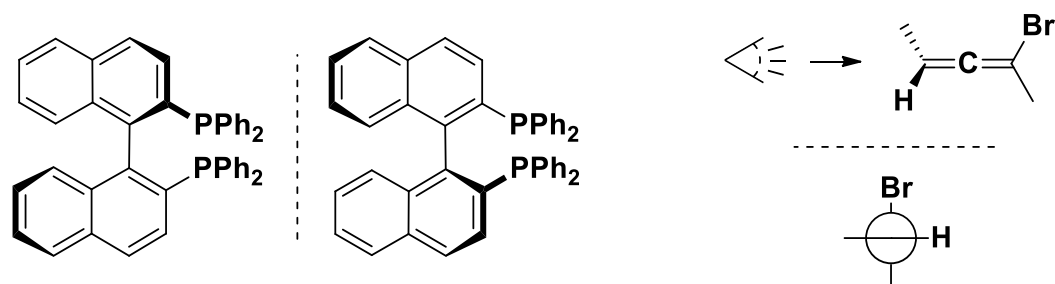
Figure 2.3. BINAP and some substituted allenes exhibit axial chirality.

In addition to this, in cyclic compounds the *cis*/*trans* designation can be used to describe the relationship of stereocenters, as the ring structure prevents free rotation around its single bonds. Two substituents are *trans* to one another if they are on opposite sides of the ring plane, when it is drawn flat, as illustrated in Figure 2.4.
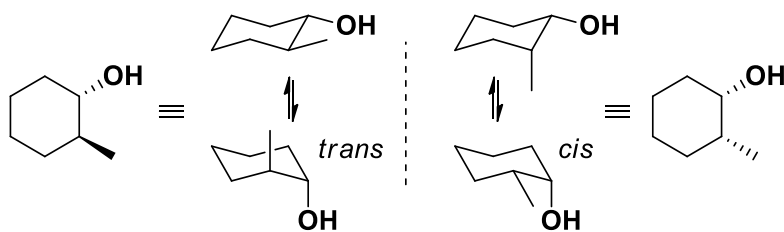
Figure 2.4. The relative configuration of substituents on cyclic compounds is described using *cis*/*trans*, as illustrated on the diastereomeric stereoisomers of 2-methylcyclohexanol.

Chiral resolution and stereoselectivity. As discovered by Louis Pasteur, in rare instances, the spontaneous resolution of two enantiomers by crystallization (as in the case of tartaric acid) is one way to achieve the separation of a racemic mixture. More often, chiral derivatizing agents, or chiral auxiliaries, are employed to achieve this so-called chiral resolution. With a chiral auxiliary, a stereogenic group is temporarily introduced into the molecule either to generate separable diastereomers or to steer the stereochemical outcome of a future synthetic step.

Chiral auxiliaries were first introduced by E.J. Corey in 1975 with the use of chiral (–)-8-phenylmenthol in his synthetic efforts toward prostaglandin.[33,34] A broad range of other auxiliaries has since been developed, such as trans-2-phenylcyclohexanol or the large group of oxazolidinone-derived compounds known as Evans auxiliaries.[35-37]
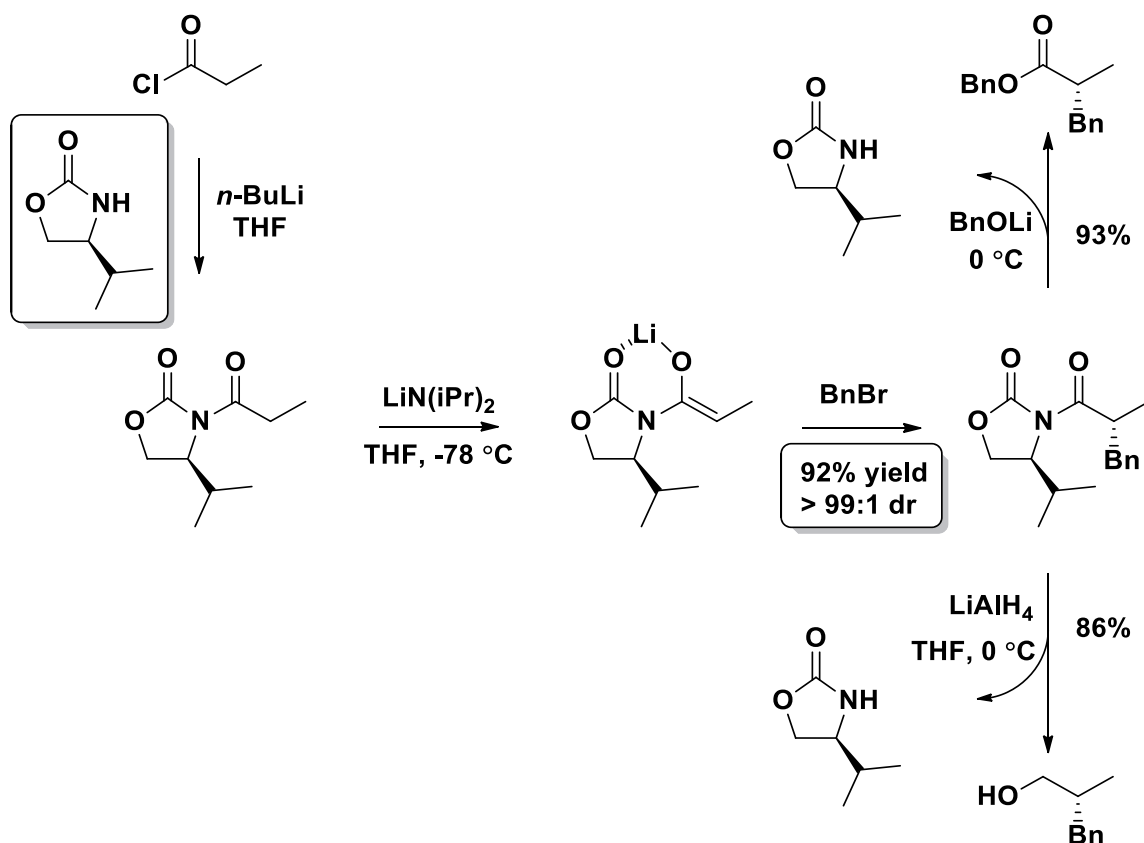
Figure 2.5. A variety of chiral auxiliaries have been developed, such as the chiral oxazolidinone employed in a stereoselective alkylation shown here.[37] Notably, the chiral auxiliary can be recovered at the end of the reaction sequence.

In general, chiral resolution through derivatization is based on the concept of stereoselectivity – that in the "handshake" of two respective chiral molecules, there is a matched-mismatched interaction leading to the formation of an unequal mixture of stereoisomers in the product.

Furthermore, kinetic resolution is another option to separate racemates. Kinetic resolution is based on the different chemical properties of the racemic starting materials, rather than different physical properties of diastereomeric products. The first reported kinetic resolution was in fact achieved by Louis Pasteur. He realized that in the presence of *Penicillium glaucum* mold, a racemic ammonium tartrate solution was partially consumed and the remaining tartrate was levorotatory.[38] Nowadays, enzymatic kinetic resolution is still one of the most efficient types of kinetic resolution due to the high selectivity many enzymes display toward chiral substrates. However, a multitude of examples of nonenzymatic alternatives has been reported.[39-41] Kinetic resolutions have been achieved using a variety of transformations, one example being acylation reactions involving amines or alcohols.[42-52] In the case of kinetic resolutions of alcohols, numerous chiral acylation catalysts have been developed, some of which are shown in Figure 2.6.
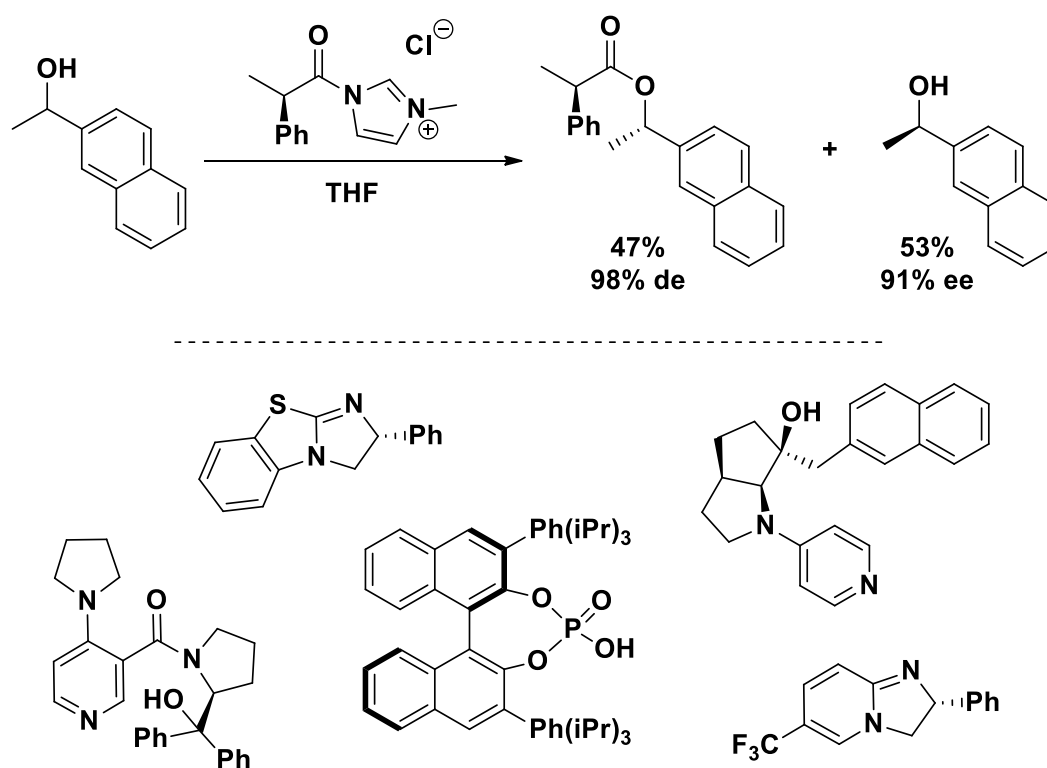
Figure 2.6. The kinetic resolution of secondary alcohols can be achieved with both acidic and basic chiral acyl transfer catalysts, a selection of which is shown here.[44,47-49,52]

Stereoselective reactions that yield stereo-enriched compounds are important tools in the field of asymmetric synthesis. At its heart, understanding the underlying mechanistic principles that govern stereoselective reactions is imperative if they are to find effective and broad scale use. In most cases, diastereoselectivity, much like enantioselectivity, is achieved through a 'matched-mismatched' interaction, leading to the preferential formation of one of the two possible diastereomers. This diastereoselectivity can arise either thermodynamically or kinetically from a difference in stability of the final products or by way of differentiation at the transition states. The inherent chirality in the substrate, reagent and the catalyst have a large influence on the stereochemical outcome of a reaction. This is also referred to as asymmetric induction.[1] Chiral catalysts or, in some cases, chiral ligands or additives are generally employed to induce or enhance diastereoselectivity.

Factors leading to Reversal of Diastereoselectivity. As pointed out above, stereoselective reactions are highly desirable and a field of intense research activity. Ideally, one and the same reaction can be used to selectively form all potential stereoisomers of a product with little change to the reaction conditions. In practice, this is often only achievable by changing the chirality of the catalyst or catalyst-ligand complex involved in the reaction. However, this is not always trivial, especially with catalysts or ligands derived from naturally occurring sources of chirality, such as L-amino acids.

Beyond the obvious influence of chiral catalyst, the observed preference for a given diastereomer or, in some cases, enantiomer is often dependent on the substrates involved in the reaction. Specific changes to the substrates in terms of steric and electronic properties have been observed to lead to reversals in stereoselectivity for a wide range of reactions, such as epoxidations,[53,54] conjugate additions,[55] cyclization reactions,[56,57] and rearrangement reactions,[58] among others.[59-61] Additionally, several other factors have been observed to lead to reversals in stereoselectivity in specific cases. Among these, temperature has been reported to be an important variable.[62-64] Likewise, changes to the solvent have been observed to change the

outcome of stereoselective reactions in a variety of cases, as well.[42,65-69] In one particular case,

Lazny *et al*. showed that with higher amounts of water added, the preferred diastereomeric

outcome of an aldol reaction changed from the *syn*- to the *anti*-aldol product.[70,71] Reactions that

are facilitated by organometallic compounds have been found to be particularly susceptible to

changes in terms of effects on their stereoselectivity. It is known for both Grignard and

organolithium reagents to exhibit different molecular aggregation states, both compared to one

another and at different concentrations of different solvents.[66,72-75] These changes can affect the

stereochemical outcome of reactions, by bringing about changes to the preferred conformation of

the substrates and intermediates. For example, the switch between magnesium and lithium

reagents was shown to cause a reversal in diastereoselectivity in multiple cases.[72,73,75] In another

example published by Ordóñez *et al*., the amount of base equivalent used in the deprotonation

step proved to be instrumental in controlling the diastereoselectivity in the benzylation of

phosphonopropanoamides by changing the aggregation state of the enolate to reject *Si face* attack,

as shown in Figure 2.7.[74]

 Lastly, a fair amount of research has shown that the addition of achiral additives, such as

Lewis bases or acids, often added to increase the performance of a given reaction, can impact the

stereochemical outcome of reactions and lead to a reversal of stereochemistry.[43,76-83] The fact that

an achiral moiety can affect the stereochemical outcome of some reaction in such an extensive

way is often unforeseen and the reason for the observed reversal in diastereoselectivity is not

always readily apparent. As such, some of the above examples will be discussed hereafter in

more detail to reveal the mechanisms by which achiral additives have been observed to effect

reversals in stereoselectivity.
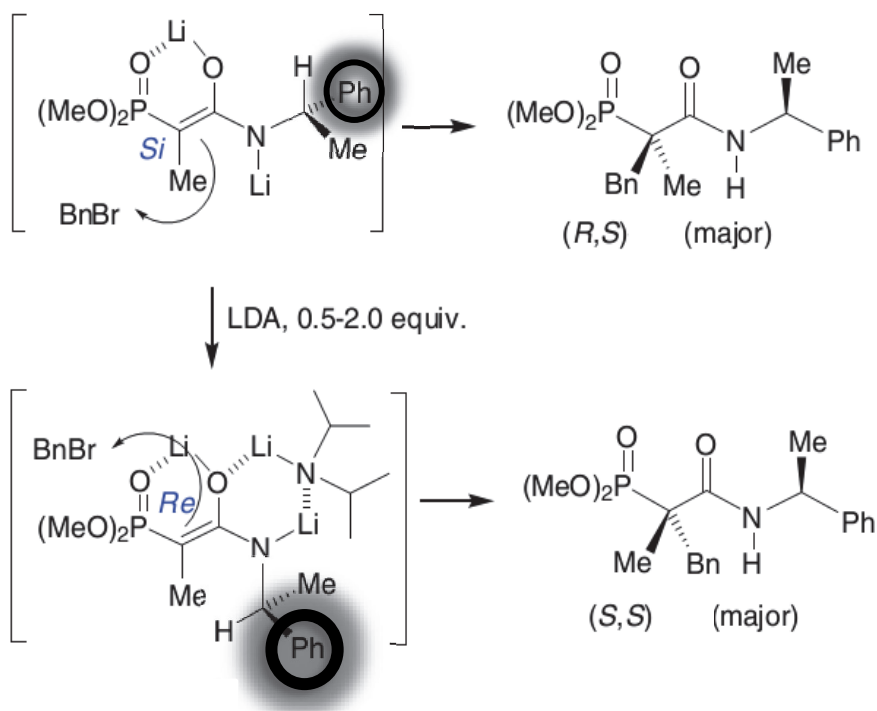
Figure 2.7. Suggested mechanism for the benzylation of the phosphonopropanoamides and reversal of diastereoselectivity induced by further addition of base forming an aggregate which sterically shields against *Si* attack of the benzyl electrophile, as published by Ordóñez *et al*..[74]

In the case of a proline-catalyzed aldol reaction involving cyclic ketones and various aromatic aldehydes, Martínez-Castañeda *et al.* were able to show that changing the counter ion of the employed achiral guanidinium salts, used as co-catalysts to improve the efficiency of the reaction, resulted in either *anti-* or *syn*-aldol adducts, as depicted in Figure 2.8.[80]
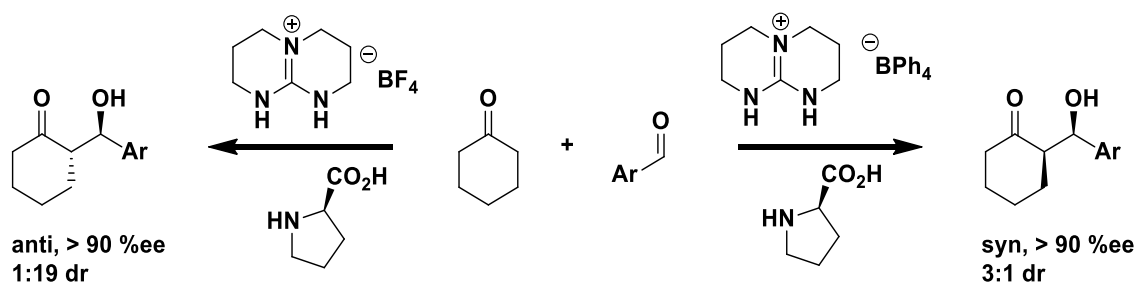
Figure 2.8. Switch of diastereoselectivity in proline-catalyzed aldol reactions based on the choice of anion of the co-catalyst leads to either *anti-* or *syn*-aldols.[80]

As shown in in Figure 2.9, the researchers monitored the reaction employing guanidinium tetraphenylborate leading to the *syn*-aldol product, which was the kinetically unfavorable product on the basis of quantum mechanical calculations. From this, it could be deduced that the *anti* diastereomer is initially created by the catalytic cycle and interconverted to the *syn* diastereomer in an equilibrium that exists "after the fact". The same equilibrium was not observed for tetrafluoroborate.
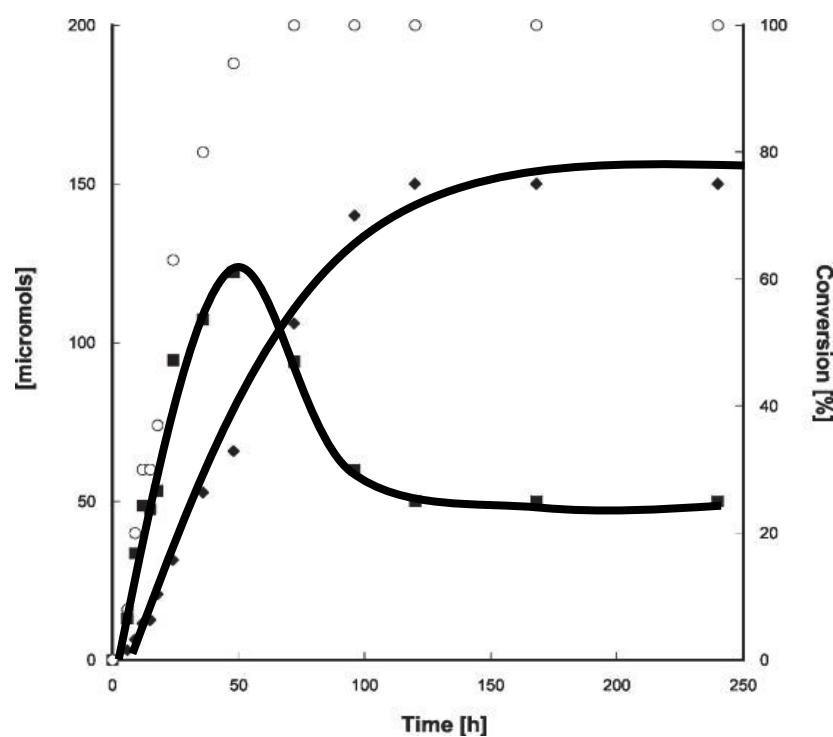
Figure 2.9. Concentration over time for the formation of aldol adducts (*syn* - diamonds; *anti* - squares) from cyclohexanone and 2-nitrobenzaldehyde and overall conversion (circles).[80]

In work presented by Sanji *et al.*, a reversal of diastereoselectivity was achieved in the addition reaction of *tert*-butyl alcohol to chiral silylenes through the addition of Lewis bases such as 2-methyltetrahydrofuran, triethylamine or quinuclidine, as depicted in Figure 2.10.[79]
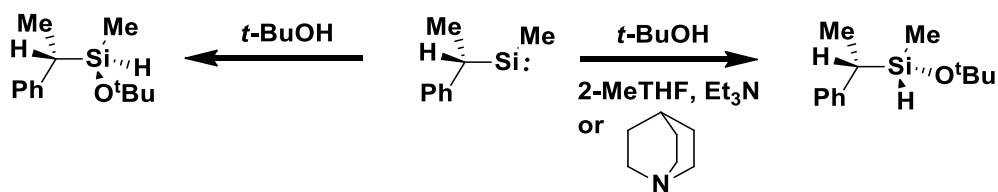
Figure 2.10. Introduction of a Lewis base changes the preferred diastereomeric product of the addition of *t*-butyl alcohol to (1-phenylethyl)-methylsilylene.[79]

Because silylenes, unlike carbenes, have a singlet groundstate, they possess a vacant *p* orbital and a lone pair in an *sp²* hybridized orbital. As illustrated in Figure 2.11, in the straightforward addition of the alcohol, the nucleophile will attack the vacant orbital lobe, thus leading to the addition from the least hindered side producing the *SR/RS* diastereomers preferentially. However, if a Lewis base is introduced to the system, it will coordinate with the empty *p* orbital in the aforementioned position and the alcohol can consequently only attack from the opposite side (in this case depicted as below the plane) resulting in the *SS/RR* diastereomers.

Similar observations to that of a Lewis base interfering with the preferred reaction pathway have been made by Yamamoto, Ivšić and Wang, independently, for Lewis acids that similarly coordinated with the substrates or substrate-catalyst complexes in ways that essentially block the otherwise preferred reaction pathway.[76,82,83]
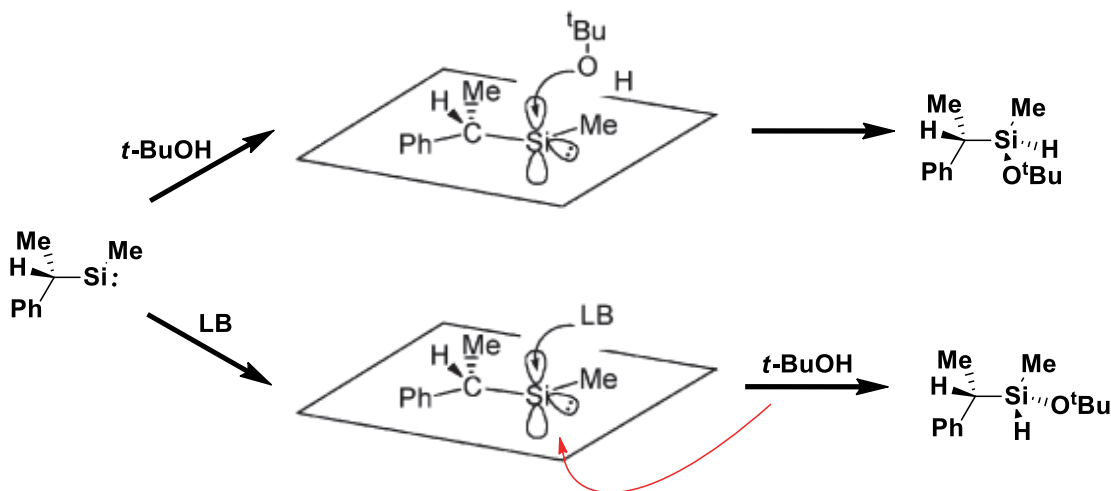
Figure 2.11. Schematic explanation for the reversal of diastereoselectivity upon introduction of Lewis base. The preferred angle of attack for the alcohol is blocked by coordination of the Lewis base to the vacant *p*-orbital and the reaction is rerouted to the otherwise unfavored diastereomer.[79]

In previous work from this research group, aimed at generating model precursors to potential chiral auxiliaries, it was discovered that the reaction between (±)-2-chloropropionyl chloride **3** and (±)-*trans*-2-(*p*-tolylsulfanyl)cyclohexanol **4** showed an appreciable double differentiation leading to the preferred formation of one of the two possible diastereomers. In order to increase the product yield, pyridine was added to the reaction as an acylation catalyst, which surprisingly resulted in an opposite distribution of diastereomeric products. Additional work revealed that pyridine was able to catalyze the acylation of a small set of racemic (±)-*trans*-2-substituted cyclohexanols with (±)-2-chloropropionyl chloride **3** in a way that also reversed the diastereoselectivity of the reaction for some of the substrates investigated.[84]

The purpose of this study was to further investigate this relationship and probe the substrate scope for the reversal of diastereoselectivity with pyridine and attempt to provide a rationale for the reversal of diastereoselectivity for the reaction. To that end, the reaction outcomes of a variety of *trans*-2-substituted cyclohexanols with (±)-2-chloropropionyl chloride **3** and (±)-2-chloro-2-phenylacetyl chloride **5** with or without pyridine as a catalyst were studied in depth, as depicted in Figure 2.12.
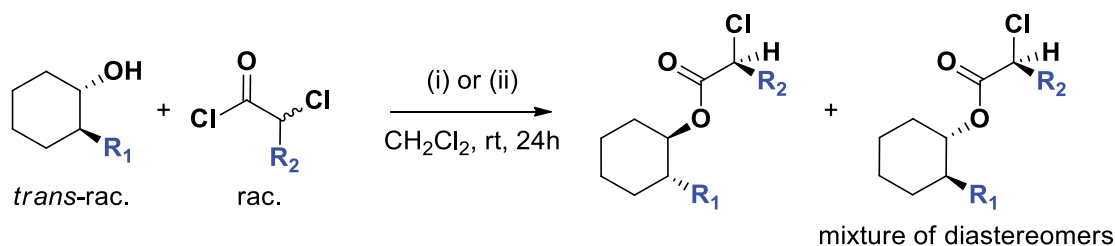
Figure 2.12. Reaction scheme for the acylation of racemic *trans*-2-substituted cyclohexanols with racemic acyl chlorides in the (i) absence or (ii) presence of pyridine (0.1 eq) and ProtonSponge® (1.0 eq) as auxiliary base. R_1 = variable (see Figure 2.16), R_2 = Me (**3**), Ph (**5**).

Results and Discussion

When (±)-*trans*-2-(*p*-tolylsulfanyl)cyclohexanol **4** was reacted with (±)-2-chloro-propionyl chloride **3** in dichloromethane without any other additives, as depicted in Figure 2.12, the desired reaction product could be isolated in 40% yield (Table 2.1, Entry 1). As shown in Figure 2.13, the product showed a characteristic quartet signal for the hydrogen on the 2-position of the propionyl for the two diastereomers formed. The quartets were separated sufficiently in terms of their chemical shift that they could be integrated without overlap and were thus used as the diagnostic peaks. Notably, this was not the case for the double-triplet signals of H-1 and H-2 on the cyclohexane moiety. The methyl group of the propionyl did give two separated doublets for the two diastereomers, however integration could not be readily performed due to signal overlap with CH_2 signals from the cyclohexane. The diastereomeric ratio (*dr*) was determined based on integration of the two quartet signals with the quartet at higher chemical shift designated as diastereomer A throughout this study. Thus, ratio of diastereomers could be determined to be 1:2.0. It bears mentioning that the assignment of the diastereomers is only relative and the absolute configurations of either diastereomer of the compounds discussed hereafter have not been established. The determination of the absolute configuration would require chromatographic separation of the diastereomers with subsequent analysis of crystalline products

by X-ray crystallography. However, the separation of the diastereomers proved unsuccessful due to their virtually identical R_f values in all tested mobile phases.

As previously observed, the addition of one equivalent of pyridine reversed the diastereoselectivity of the reaction (Table 2.1, Entry 6). However, upon closer examination, the diastereomeric ratio of the product of the acylation of **4** was found to be dependent on the catalyst/promoter load for pyridine (Table 2.1, Entries 2-9). Furthermore, the effect could be reproduced with two other achiral amine catalysts in DMAP (4-dimethylamino-pyridine) and collidine (2,4,6-trimethylpyridine). The obtained results were qualitatively similar (see Table 2.1, Entries 6, 13, 16, and Figure 2.14), suggesting that the observed diastereoselectivity for all three may be the result of matched/mismatched pairings of similar reaction pathways. The same concentration-dependent change in *dr* was observed, as well (Table 2.1, Entries 10-14 and 15-16).
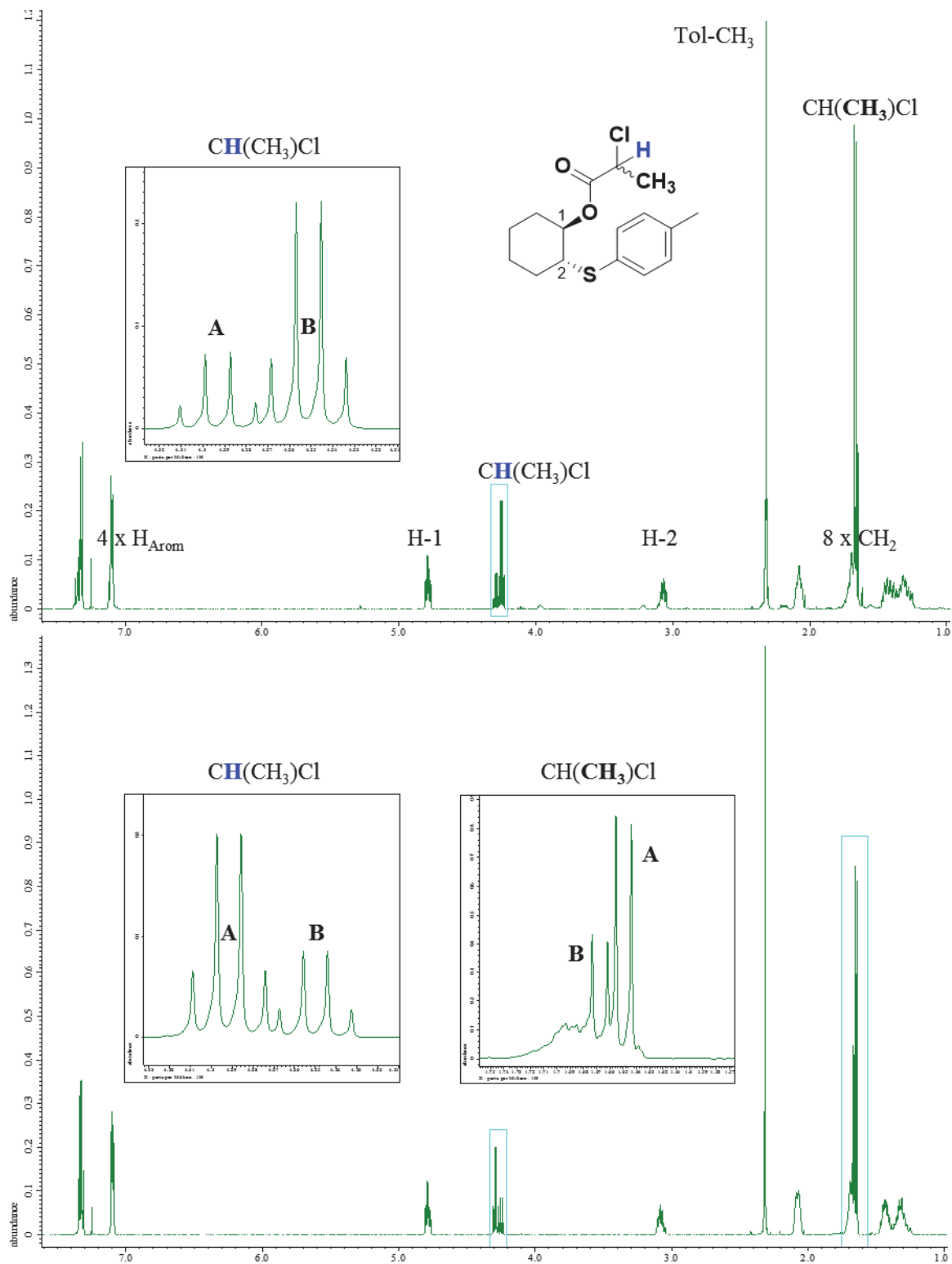
Figure 2.13. ^{1}H-NMR spectra of the isolated racemic product mixture from the reaction of **3** and **4** without pyridine (top) and with pyridine added (bottom, 100 mol%). Insets: quartet signals of **CH**(CH₃)Cl showing diastereomeric ratio based on integral size for A and B.

Table 2.1. Summary of catalyst-dependence study on the reversal of diastereoselectivity in acylation reactions between **3** and **4**. Reactions run in CH_2Cl_2 at 1.0 mmol scale for 24 h. ([a] Assignment of A and B arbitrary based on integration data of diagnostic quartet signal in ^{1}H-NMR spectrum. [b] 0.1 mmol scale.)

Entry	Catalyst - mol%		Isolated Yield	dr (A:B)[a]
1	-/-		40%	1:**2.0**
2	pyridine	10	61%	1:**1.2**
3	pyridine	20	41%	1:**1.1**
4	pyridine	51	45%	**1.5**:1
5	pyridine	80	52%	**2.2**:1
6	pyridine	104	51%	**2.3**:1
7	pyridine	151	66%	**2.2**:1
8	pyridine	201	61%	**2.5**:1
9	pyridine	308	43%	**2.2**:1
10	DMAP	10	35%	1:**1.7**
11	DMAP	20	37%	1:**1.3**
12	DMAP	51	46%	**1.7**:1
13	DMAP	100	47%	**2.6**:1
14	DMAP	197	50%	**2.2**:1
15	collidine	10	36%	1:**1.0**
16	collidine	97	43%	**2.7**:1
17	DBU	107	24%	**1.1**:1
18	DIPEA	48	30%	1:**1.0**
19	DIPEA	98	41%	**1.1**:1
20	TEA	103	46%	1:**1.1**
21[b]	DMAP + Et$_3$N	10+100	76%	**2.8**:1
22[b]	pyridine + Amberlite	10+ 100	35%	**3.0**:1

The catalyst/promoter load-dependent *dr* in the respective reactions for pyridine, DMAP and collidine was plotted in Figure 2.14 and appeared to show a near-linear dependence in the range of 0–100 mol%, with the maximum observed diastereoselectivity observed for 0 mol% and 100 mol% catalyst-loading respectively. This implies that the achiral acyl transfer catalysts are not simply speeding up the reaction and would indicate that they play a more essential role in the reaction pathway in interacting with the *trans*-2-substituted cyclohexanol substrate.

In contrast, non-nucleophilic bulky amines such as diisopropylethylamine (DIPEA), 1,8-diazabicyclo(5.4.0)undec-7-ene (DBU) and triethylamine (TEA) lead to a roughly 1:1 ratio of

diastereomers, with no apparent concentration dependence (Table 2.1, Entries 17-20) indicating

that here, the reaction pathway is likely different from the pyridine-promoted reaction. This

would be expected as the bulky bases should not be able to form an acyl-*nitrogen*-intermediate.
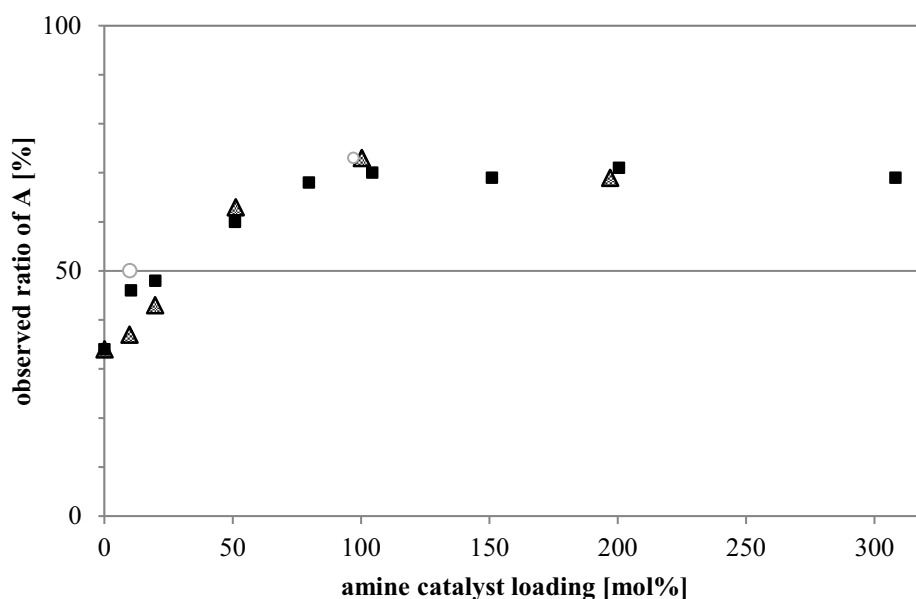
Figure 2.14. Observed amine-loading dependence of *dr* of the acylation product of **4** with **3** with pyridine (black squares), DMAP (dotted triangles) and collidine (gray circles) as catalysts.

Although the reason for the catalyst load-dependence was not immediately apparent,

further experimental evidence pointed to hydrochloric acid, which is produced as a byproduct in

the esterification reaction, as the reason for the above observations. Namely, when using DMAP

in catalytic quantities (0.1 equivalents) together with one equivalent of triethylamine, the overall

yield was improved and the observed *dr* was comparable to the case of equimolar amounts of

DMAP (Table 2.1, Entry 21). This effect of an auxiliary base was also seen when using a basic

ion exchange resin (Amberlite IRA-400 OH; Table 2.1, Entry 22).

The reason for this improvement in diastereoselectivity and yield through the addition of

an auxiliary base would appear to be the more effective neutralization of the hydrochloric acid

byproduct. When pyridine (or DMAP) is used in catalytic amounts, it is protonated by HCl over the course of the reaction and thus becomes unavailable for catalysis of the acylation. This reverts the reaction back to the non-catalyzed reaction pathway which yields opposite diastereoselectivity. The effect is an overall reduction of the *dr*. The addition of an auxiliary base causes its protonation in the place of pyridine, leaving the latter to remain available to catalyze the acylation reaction. The effect is an overall improvement of the *dr*.

  Influence of Solvent. Additionally, the solvent-dependence of the diastereoselectivity in the acylation was investigated. The results summarized in Table 2.2 showed that for acylation of the tolylsulfanyl-substituted cyclohexanol **4**, the uncatalyzed reaction was strongly influenced by the type of solvent used, as large variations in *dr* were observed. In the case of THF, the diastereoselectivity of the reaction was reversed when compared to dichloromethane, illustrating that the diastereoselectivity of the reaction could also be reversed on a solvent-dependent basis. However, as can be seen in Figure 2.15, these changes in diastereoselectivity are not clearly correlated with the change in solvent polarity (as portrayed by its dielectric constant ε).[85] Meanwhile, in the pyridine-promoted reactions (100 mol%), only little change in *dr* was observed compared to dichloromethane. This may be a result of the faster reaction in the presence of pyridine decreasing any solvent influence.

Table 2.2. Data from solvent variation in the acylation reaction between **3** and **4**. [a] ε: dielectric constant.[85] [b] Assignment of A and B arbitrary based on integration data of diagnostic quartet signal in ^{1}H-NMR spectrum.)

Entry	Solvent	ε[a]	Catalyst - mol%		Isolated Yield	dr (A:B)[b]
1	CH$_2$Cl$_2$	8.93	-/-		40%	1:**2.0**
2			pyridine	104	51%	**2.3**:1
3	THF	7.52	-/-		23%	**3.0**:1
4			pyridine	100	68%	**3.5**:1
5	EtOAc	6.08	-/-		51%	**1.2**:1
6			pyridine	102	31%	**3.5**:1
7	CHCl$_3$	4.81	-/-		53%	1:**3.3**
8			pyridine	110	59%	**2.7**:1
9	iPr$_2$O	3.81	-/-		17%	**1.4**:1
10			pyridine	97	42%	**5.7**:1
11	Et$_2$O	4.27	-/-		23%	1:**1.3**
12			pyridine	102	65%	**4.9**:1

As a general trend, in the presence of pyridine, larger dr were observed in less polar solvents than in more polar solvents. However, as pointed out above, no such trend was apparent for the uncatalyzed reaction. Overall, chloroform and dichloromethane showed the largest change in dr between the uncatalyzed and catalyzed reactions, considering only those where to diastereoselectivity was reversed, as opposed to enhanced, between the uncatalyzed and catalyzed reactions.
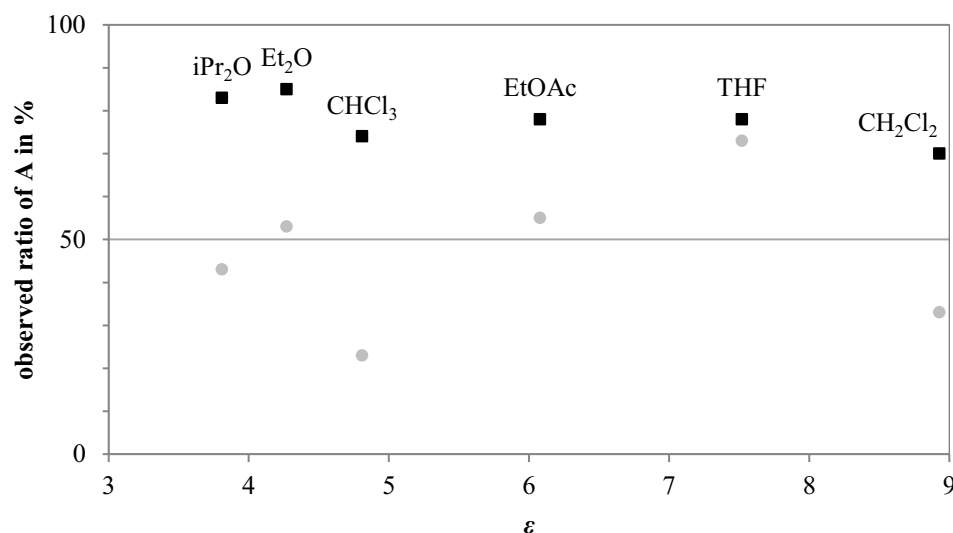
Figure 2.15. Observed solvent dependence of *dr* of the acylation product of **3** and **4**, as visualized by the observed *dr* plotted against the dielectric constant ε in different solvents with (black squares) and without (gray circles) pyridine present at approx. 100 mol% (see Table 2.2).

Optimization of reaction conditions. Next, the reaction conditions were optimized for product yield, as determined by ^{1}H NMR analysis, so as to increase its potential synthetic utility. It was noted from previous experiments that despite full conversion of **3** only relatively low yields of the desired ester were obtained. Thus, screening of the alcohol to acyl chloride ratio revealed the 2:1 ratio thereof to give optimal ester formation for use in further reactions (Table 2.3).

Table 2.3. Screening of alcohol **4** to acyl chloride **3** ratio for optimal yield at 0.1 mmol scale in 1 mL CH_2Cl_2 in the presence of 0.1 mmol pyridine for 24 h at rt. (Conversion of acyl chloride and yield determined by ^{1}H NMR.)

Entry	ROH (eq.)	AcylCl (eq.)	Conversion	Ester Yield
1	1.0	2.0	100%	41%
2	1.0	1.0	100%	63%
3	1.5	1.0	100%	67%
4	2.0	1.0	100%	91%
5	3.9	1.0	100%	91%

As discussed above, the use of an auxiliary base was found to allow the achiral amine catalyst to be employed at less than equimolar amounts. Since the choice of base appeared to influence the *dr* of the product mixture as well as the reaction yield, a small number of potential auxiliary bases, of both heterogeneous and homogeneous nature, were screened to find optimal conditions for the reaction of racemic *trans*-2-substituted cyclohexanols with racemic acyl chlorides. The results are summarized in Table 2.4. Based on the best combination of yield and *dr*, ProtonSponge® (1,8-bis(dimethylamino)-naphthalene) was chosen as a soluble auxiliary base to be employed in the reaction.

Table 2.4. Screening of auxiliary base using **4** (0.2 mmol) and **3** (0.1 mmol) in 1 mL CH_2Cl_2 for 24 h at rt. ([a] 1:1 ratio of reactants)

Entry	Catalyst (10 mol%)	Auxiliary base (1.0 eq)	Yield	*dr* (A:B)
1	-/-	-/-	24%	1:**2.7**
2	pyridine	Amberlite IRA-400 OH	60%	**3.7**:1
3	pyridine	ProtonSponge®	82%	**4.2**:1
4	pyridine	Amberlyst A21	40%	**5.4**:1
5[a]	DMAP	Et$_3$N	76%	**2.8**:1
6	pyridine	NaHCO$_3$	31%	**3.6**:1

Substrate scope. With these improved catalytic reaction conditions in hand, the source of the reversal of diastereoselectivity in the reaction was investigated. For this purpose, a small library of racemic (±)-*trans*-2-substituted cyclohexanols, carrying a variety of OR, SR and CH_2R motifs (where R=aryl, alkyl), was generated for substrate screening. The compound library is summarized in Figure 2.16.

Compounds **4**, **6**, **7**, **9**, **11**, **13**, **15** and **21** were synthesized via basic epoxide opening of cyclohexene oxide in ethanol, while the carba-analog of **7** (**25**) was obtained from benzyl magnesium bromide and cyclohexene oxide in THF. The epoxide opening with electron-deficient nitrophenol was unsuccessful even under basic conditions. Compound **17** with a

cyclohexyloxy substituent was obtained from the reaction of cyclohexene oxide and cyclohexanol

under basic conditions. The O*t*Bu-substitutent (**19**) was installed with catalytic amounts of

Cu(BF$_4$)$_2$ as activator for the epoxide opening of cyclohexane oxide with *tert*-butanol.

Compound **23** was synthesized from **4** through hydrogen peroxide oxidation in acetic acid.[86] A

second carba-analog (**27**) was commercially available.
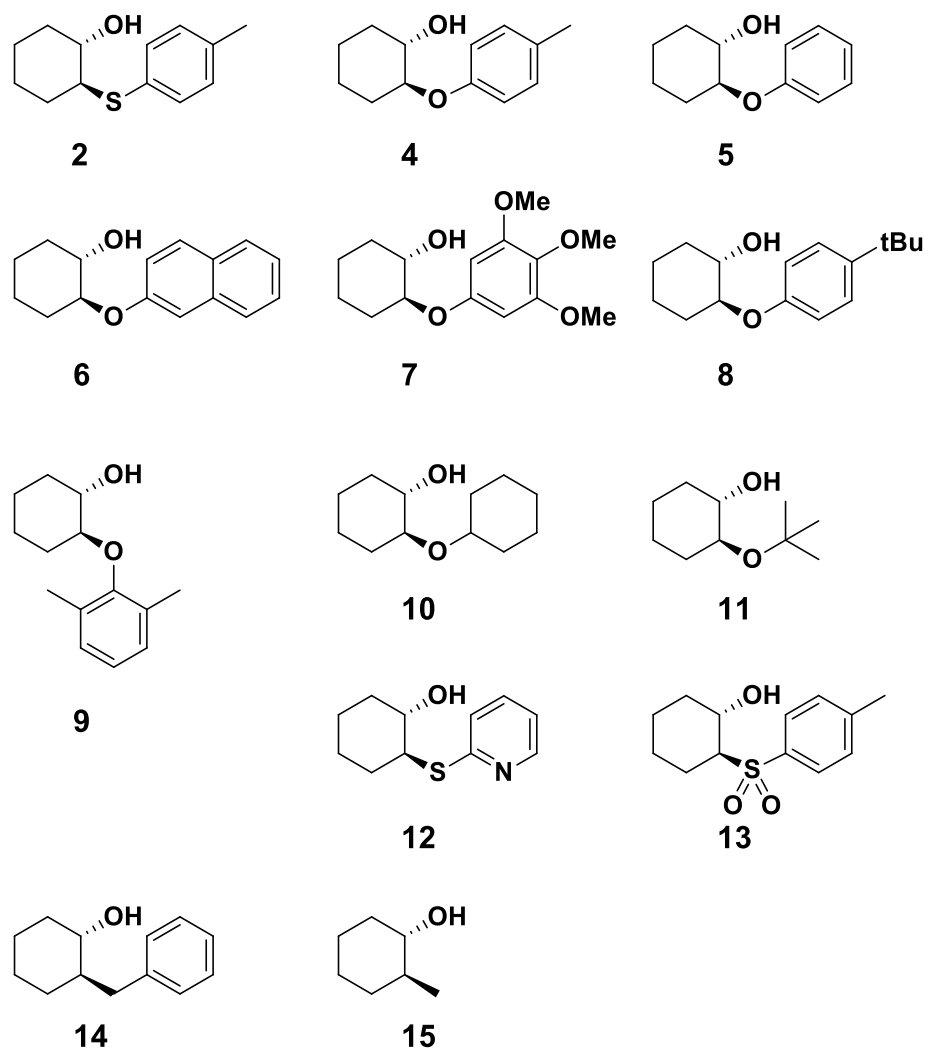
Figure 2.16. Generated library of racemic (±)-*trans*-2-substituted cyclohexanols used in screening of the substrate scope of the developed acylation methodology.

The collection of racemic (±)-*trans*-2-substituted cyclohexanols was then reacted with **3** in dichloromethane for 24 h at room temperature either (i) without or (ii) with the addition of pyridine (0.1 equiv) and ProtonSponge® (1.0 equiv.) based on the established optimal reaction conditions elaborated above. Yield and *dr* were determined from the crude reaction mixture by ^{1}H NMR (compare Methods section in Chapter 6 and Figure 2.13). All ester products were isolated by column chromatography and fully characterized using 1D & 2D NMR and MS analysis. The results of the substrate screening are summarized in Table 2.5.

Little change in the *dr* in either (i) the absence or (ii) presence of pyridine and ProtonSponge® was observed when the aromatic moiety on the *trans*-2-substituent carried *ortho*- or *para*-substituents (Table 2.5, Entries 11-14). The larger naphthyloxy-substituent in **9** also did not lead to higher *dr* in (ii), which indicated that extended π-π-stacking or other electronic effects on the aromatic moiety aside from the phenyl ring were not significant. However, **11** and **23** showed a strong increase in *dr* in the catalyzed reaction. This may be a result of an increased bulk in the substrate close to the reaction center or a significant change in conformation of the substituent relative to the cyclohexanol moiety.

Surprisingly, it was observed that alkyloxy-substituted compounds **17** and **19** gave higher absolute *dr* in the uncatalyzed reaction, contrary to the trend observed in aryloxy-substituted compounds. Although arguments related to electronic or steric effects of these substituents and potential interactions with **3** could be made, the exact reason for this observation remains unknown and further exploration is needed to elucidate the cause.

Table 2.5. Substrate screening of racemic (±)-*trans*-2-substituted cyclohexanols with **3** in the (i) absence or (ii) presence of pyridine (0.1 equiv) and ProtonSponge® (1.0 equiv.) under established reaction conditions.

mixture of diastereomers A:B
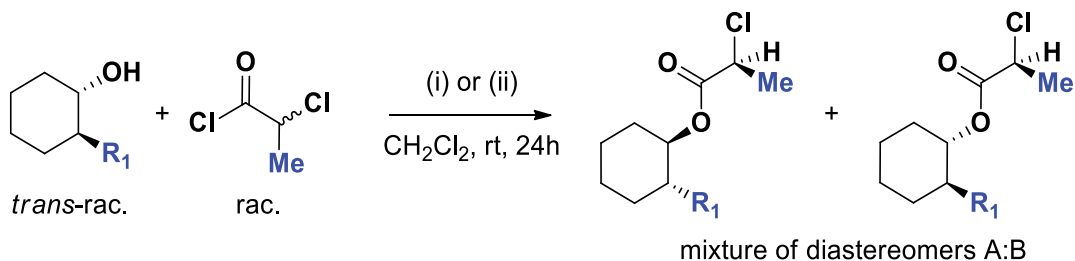
Entry	ROH	rxn cond.	NMR yield	*dr* (A:B)
1	4	i	40%	1:**3.2**
2	4	ii	80%	**3.2**:1
3	6	i	24%	1:**2.7**
4	6	ii	82%	**4.2**:1
5	7	i	22%	1:**2.7**
6	8	ii	73%	**3.7**:1
7	9	i	22%	1:**2.2**
8	10	ii	70%	**3.8**:1
9	11	i	16%	1:**1.7**
10	12	ii	57%	**3.8**:1
11	13	i	31%	1:**2.5**
12	14	ii	61%	**3.7**:1
13	15	i	27%	1:**3.3**
14	16	ii	63%	**7.5**:1
15	17	i	65%	1:**5.2**
16	18	ii	50%	**3.3**:1
17	19	i	94%	1:**5.5**
18	20	ii	77%	**1.8**:1
19	21	i	87%	**1.2**:1
20	22	ii	81%	**1.9**:1
21	23	i	0%	n.d.
22	24	ii	34%	**15**:1
23	25	i	53%	**2.0**:1
24	26	ii	77%	**1.2**:1
25	27	i	90%	1:**2.2**
26	28	ii	64%	1:**1.6**

Compound **21** showed no reversal of *dr* between (i) and (ii), however the *dr* was higher in the catalyzed reaction. Because **21** carries a pyridine moiety on the *trans*-2-substituent, it is

conceivable that it is acting as an intramolecular acyl-transfer catalyst in the absence of pyridine. The observed *dr* in favor of diastereomers A in both cases, which was found to be the predominant diastereomers for the other (±)-*trans*-2-substituted cyclohexanols, appears to lend further credence to this explanation. The carba-analogs **25** and **27** both did not show a reversal of diastereoselectivity upon the addition of pyridine and auxiliary base. This appears to be a direct consequence of the lack of a heteroatom on the *trans*-2-substituent. The heteroatom may significantly influence the transition state energies, as will be discussed hereafter, in the reaction with the acyl transfer catalyst relative to the reaction without it or even actively participate in the mechanism, as previously proposed.[13] A heteroatom (oxygen or sulfur, in the cases above) thus appears to be essential for the reversal of *dr* to be observed.

A small selection of racemic (±)-*trans*-2-substituted cyclohexanols was also subjected to 2-chloro-2-phenyl-acetyl chloride **5** in the same reaction scheme as above. The results are shown in Table 2.6. The initial expectation that a bulkier acyl chloride would yield higher *dr* was not borne out by the data. Although reversal of diastereoselectivity was seen generally, the *dr* was lower in the majority of cases with **5** than with **3**. The reason for this may be that the replacement of a methyl group with a phenyl group in the γ-position on the acyl chloride leads to steric crowding in the transition state, meaning that stereodifferentiation between the acyl chloride and the acyl pyridinium cases is actually more successful with a less sterically demanding acyl substrate. Curiously, no reversal of diastereoselectivity was observed for **17** with **5** (Table 2.6, Entries 7+8). This was opposite of the results for **17** with **3**.

Table 2.6. Substrate screening of selected racemic (±)-*trans*-2-substituted cyclohexanols with **5** in the (i) absence or (ii) presence of pyridine (0.1 equiv.) and ProtonSponge® (1.0 equiv.) under the established conditions.

mixture of diastereomers A:B
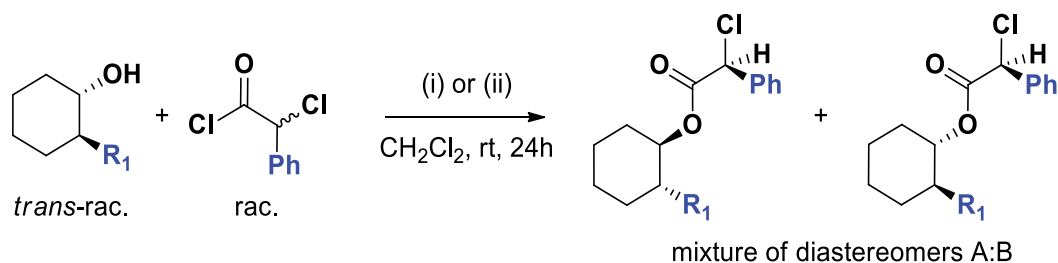
Entry	ROH	rxn cond.	NMR yield	*dr* (A:B)
1	4	i	32%	1:**1.1**
2	4	ii	85%	**2.5**:1
3	6	i	13%	1:**1.4**
4	6	ii	97%	**2.0**:1
5	15	i	18%	1:**2.0**
6	15	ii	>99%	**2.8**:1
7	17	i	69%	1:**6.8**
8	17	ii	> 99%	1:**10**
9	23	i	4%	1:**5.8**
10	23	ii	88%	**2.7**:1
11	27	i	99%	**1.7**:1
12	27	ii	> 99%	**1.1**:1

Mechanistic Considerations. The mechanism of the reaction is potentially very complicated and several distinct reaction pathways might contribute to the overall reaction, additionally influenced by the solvent in which the reaction takes place. It was previously shown that the presence of basic pyridine does not cause a change in diastereomeric ratio via post-reaction enolization and epimerization of the chiral center in the ester side chain.[84] As such, the observed reversal in *dr* is most likely the result of a change in relative activation energies required in the doubly-differentiated esterification.

The most straightforward mechanistic scenario for the ester formation in the case of reaction conditions (i) is the direct acylation of the hydroxyl group by racemic acyl chloride via a tetrahedral intermediate and the subsequent removal of HCl as a by-product of the reaction, as

depicted in Figure 2.17. By necessity, the approach of the racemic **3** to the racemic cyclohexanol

scaffold will lead to diastereomeric transition states and intermediates, which are different in their

respective free energies. This, in turn, will lead to differences in reaction rates. Such a simplified

scenario would also assume that the nearly non-polar solvent CH_2Cl_2 has no influence on the

reaction and all mechanistic steps are "intrinsic". In a mechanistic alternative, acylation could

transiently occur first at the heteroatom of the 2-substituent, particularly in the case of the

relatively polarizable sulfur (compare Figure 2.17, Intermediate **II**) to form a sulfonium ion.[87-89]

This intermediate can in turn react as an acylating reagent and react in intermolecular fashion

with another alcohol or through intramolecular acyl-transfer to the adjacent hydroxyl group of **II**.

However, based on little difference in the observed diastereoselectivities between sulfur and

oxygen containing compounds (compare **4** and **6** in the above Table 2.5 and Table 2.6), this may

not be the most likely pathway. In both hypothetical cases, diastereomeric transition states will

favor one or the other of the potential diastereomeric reaction products, **A** and **B**.
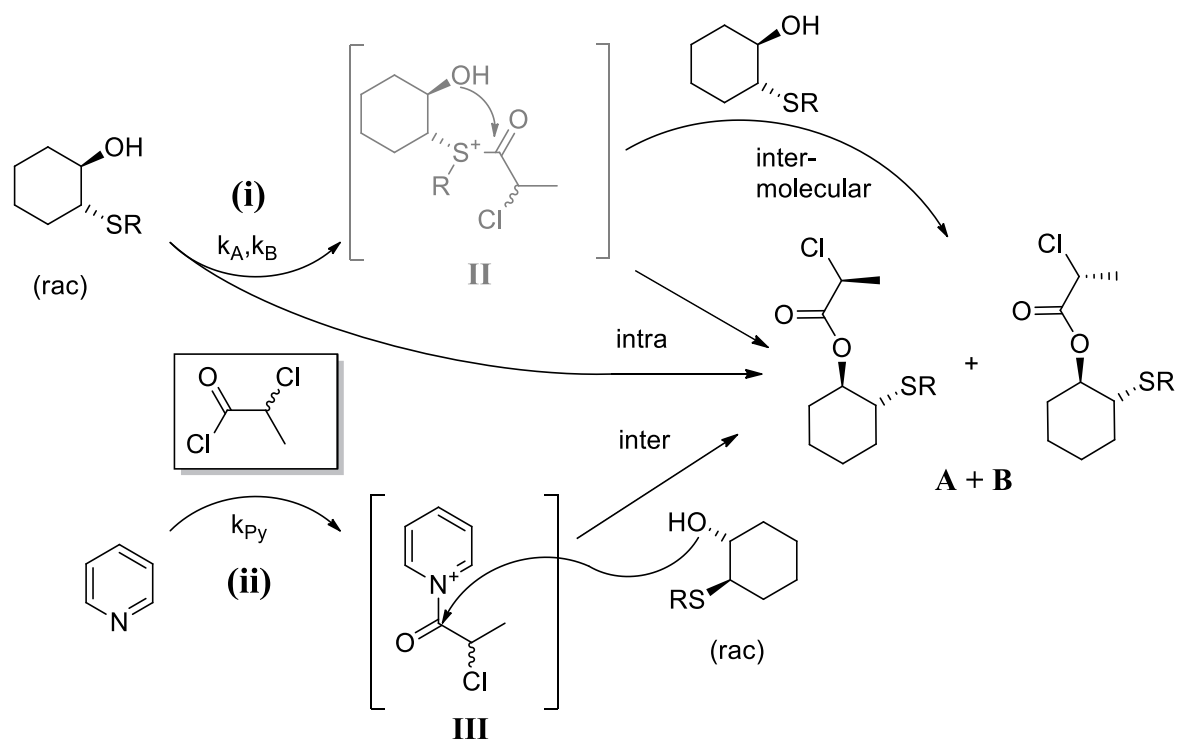
Figure 2.17. Possible reaction pathways for stereodifferentiation in the ester formation on (±)-*trans*-2-substituted cyclohexanols.

The alternative reaction conditions for (ii) including pyridine and the auxiliary base would cause the reaction medium to be slightly basic. While not basic enough to cause complete deprotonation of alcohols, pyridine will generate some alkoxide as opposed to neutral alkanol. Alkoxide is a more potent nucleophile than neutral alkanol, especially the case of an almost non-polar environment where the solvation shell around the nucleophile is minimal and nucleophilicity parallels basicity. Vastly higher reaction rates were observed in all pyridine-catalyzed/promoted cases where the reaction at room temperature showed significant conversion before an NMR sample could be prepared compared to pyridine-free experiments which required up to 24 hours for completion. It is also known that pyridine is an effective catalyst for the transfer of acyl groups onto hydroxyl groups to form ester bonds. The presence of pyridine during the acylation of alcohols with acetic anhydride for example causes the formation of acylpyridinium species, which are more powerful acylating reagents than acetic anhydride itself.

An even better catalyst is DMAP because of the dimethylamino-group's ability to stabilize the positive charge at the heterocyclic nitrogen after acylation. Therefore, it can be assumed that acylpyridinium species contribute to the esterification of the hydroxyl group in the cyclohexanol moiety and lead to an acceleration of the reaction rates. The additional influence on diastereoselectivity overall could potentially be a result of steric or stereoelectronic (dipole/π-stacking) effects with the *trans*-2-substituent and consequential rate differences in diastereoselective acyl transfer from the acylpyridinium species **III** to the chiral scaffold. It is known from other examples involving kinetic resolution of alcohols using acyl transfer catalysts, that π-stacking can play an important role in biasing a reaction toward certain pathways.[44,49] The experimentally observed product distribution of approximately 25:75 for the product of **3** and **4** under reaction condition (i) and its reversal to 75:25 under reaction condition (ii), along with the other experimental observations detailed above, imply that the pyridine-species, the solvent polarity, and the presence or absence of a heteroatom in the substituent at C-2 play a significant role on the relative rates of reaction for the formation of the diastereomers **A** and **B**.

In order to further investigate the reason for the reversal of *dr* with the addition of pyridine, the transition state structures of the ester formation were computed at the B3LYP/6-31G* level of theory with implicit Polarizable Continuum Model (PCM) solvent modeling for **4**, **6** and **27** with **3** and the acyl-pyridinium intermediate of **3**, respectively, under basic conditions (alcoholate). However, as depicted in Table 2.7, the reversal of diastereoselectivities due to the introduction of pyridine was not borne out quantitatively by the computed relative transition state energies for the different diastereomeric transition states. For example, in the case of the tolyloxy-substituted **6**, the lowest energy transition state leading to one diastereomer (*R,R,S*) in the uncatalyzed case was predicted to be 2.45 kcal/mol below the lowest energy transition state of the opposite diastereomer (*R,R,R*). Based on the experimental evidence this relationship should be reversed when considering the reaction with pyridine, however the first diastereomer (*R,R,S*) was also predicted to be formed preferentially through the lowest

energy transition state by 3.17 kcal/mol over the transition state leading to the opposite

diastereomer. The fact that the relative energies of the respective transition states do not follow

the experimentally observed pattern – that is, a change in the preference of diastereomers between

the uncatalyzed and catalyzed reaction for **4** and **6**, but not **27** – may partially be due to the fact

that the observed *dr* for the above compounds corresponds to relative difference in terms of the

activation barriers of less than 1 kcal/mol following the Boltzmann distribution:

$$\text{For } \mathbf{4}: \mathbf{A}: \mathbf{B} = 1.0 : 3.2 = 0.3126 = e^{-(\Delta E_A)RT} \Rightarrow \Delta E_A = 0.687 \text{ kcal mol}^{-1}$$

Although it is hard to give exact absolute error estimates for quantum mechanical computations,

commonly used DFT functionals and basis sets may not be as accurate as their ubiquitous use in

the organic chemistry literature would suggest.[90] The modeling of the reaction at a higher level of

theory and potentially with explicit consideration of the solvent may give a more accurate

representation of the experimentally observed situation, especially given the fact that the

observed *dr*'s would correspond to relatively small differences in the transition state energies.

However, the exponentially higher computational power required for such more accurate

calculations using the Møller–Plesset perturbation theory or Coupled-Cluster theory provided to

be a roadblock given the computational resources at hand. Instead, a qualitative interpretation of

the computational results revealed some interesting observations that could help explain the

experimentally observed reversal of *dr*.

Table 2.7. Relative energies of the computed transition states for the acylation of **4**, **6** and **27** with the lowest respective diastereomeric transition state bolded. See Figure 2.18 for explanation of the nomenclature of the stereochemistries involved. B3LYP/6-31G*(PCM).

$R =$ ΔE_{B3LYP}/kcal mol^{-1}	Methyl (**27**)		Tolyloxy (**6**)		Tolylsulfanyl (**4**)	
without pyridine	*R,R,R,R*	*R,R,R,S*	*R,R,R,R*	*R,R,R,S*	*R,R,R,R*	*R,R,R,S*
(e,e)	2.47	**0.47**	15.46	10.57	16.67	13.03
(a,a)	4.14	2.42	**2.45**	**0.00**	2.37	**0.00**
	R,R,S,R	*R,R,S,S*	*R,R,S,R*	*R,R,S,S*	*R,R,S,R*	*R,R,S,S*
(e,e)	**0.00**	1.32	10.41	11.40	7.70	8.15
(a,a)	1.39	3.16	4.56	6.47	**2.06**	3.68
with pyridine	*R,R,R,R*	*R,R,R,S*	*R,R,R,R*	*R,R,R,S*	*R,R,R,R*	*R,R,R,S*
(e,e)	1.44	5.25	16.23	18.67	19.82	23.28
(a,a)	**0.00**	3.80	9.27	11.75	**3.31**	7.14
	R,R,S,R	*R,R,S,S*	*R,R,S,R*	*R,R,S,S*	*R,R,S,R*	*R,R,S,S*
(e,e)	5.89	1.78	**3.17**	**0.00**	4.90	**0.00**
(a,a)	4.14	**0.91**	3.28	5.19	7.75	3.99
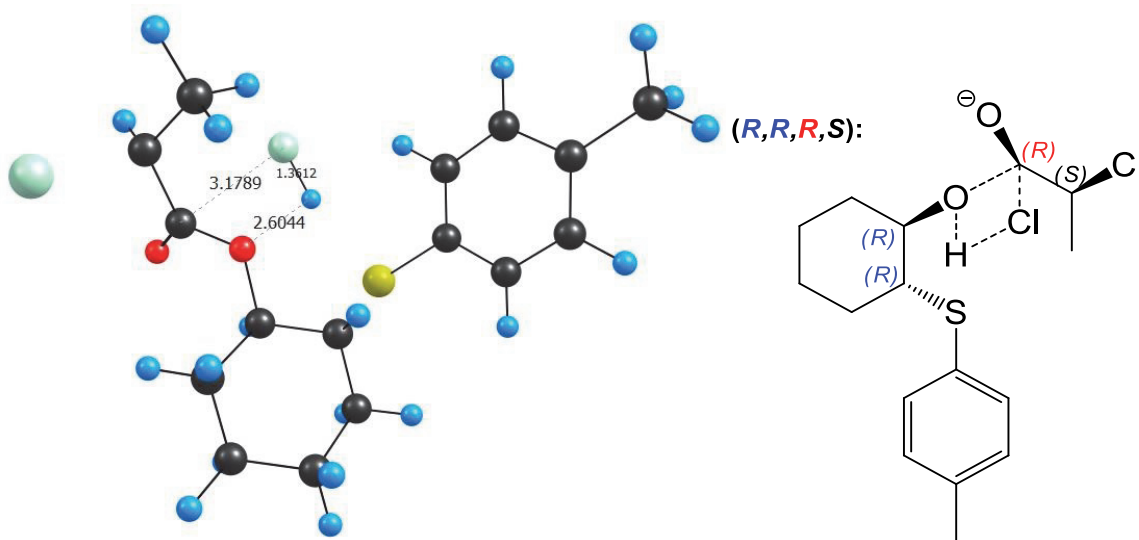
Figure 2.18. Nomenclature used in describing the stereochemistry of the diastereomeric transition state with the stereochemistry of the cyclohexanol denoted first, followed by the stereochemistry of the transient stereocenter and the stereochemistry of the 2-chloro propionyl, as exemplified for the (1*R*,2*S*)-1,2-dichloro-1-((1*R*,2*R*)-2-tolylsulfanyl-cyclohexyl)propan-1-olate transition state depicted here.
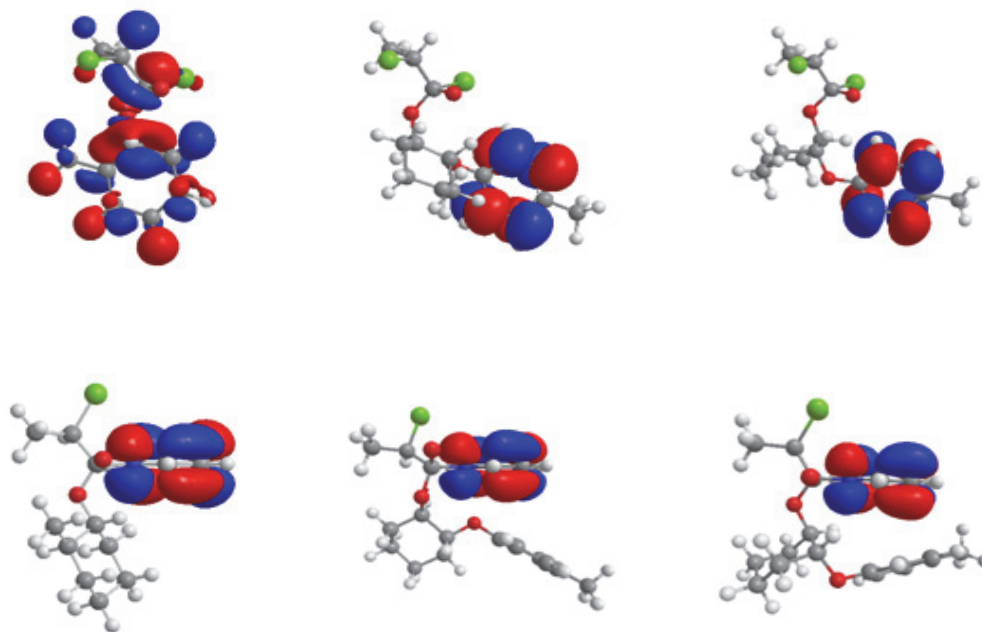
Figure 2.19. Representative transition state structures for the ester formation of **27** (top left structure) or **6** (top right two structures) with **3** or the acyl-pyridinium intermediate of **3** (bottom left for **27**, middle and right for **6**) under basic conditions (alcoholate) with the HOMO shown.

Figure 2.19 depicts representative structures of the lowest transition states found for the respective reactions of **6** and **27** with their HOMO shown. All structures for the obtained diastereomeric transition states for the two reaction pathways can be found in Appendix C. Notably, the lowest transition states obtained placed the *trans*-2-substituted cyclohexanol configured with both substituents in the axial position for **6**. The HOMO was found to be localized almost entirely in the pyridinium ring for the catalyzed reaction in all cases. In the catalyzed reaction, there appears to be an interaction of either the heteroatom or the aromatic moiety on the *trans*-2-substituent with the pyridinium ring, on which the HOMO is localized, for **4** and **6** causing the *trans*-2-substituent to be in close vicinity. This is not the case for **27**, where both heteroatom and aromatic moiety are absent. As a result, no clear preference in conformation of the transition state was observed. This interaction is also notably absent in the uncatalyzed reaction, where the HOMO was computed to be localized on the aromatic moiety for **4** and **6** and

no such interaction could be inferred between the heteroatom or the aromatic moiety and the chlorine leaving group for **6**. These computations suggest that the presence of a heteroatom and/or aromatic moiety on the *trans*-2-substituent of cyclohexanol causes it to interact favorably with the pyridinium species in the transition state, in support of the experimentally determined requirements for a reversal of diastereoselectivity to be observed between the reaction conditions (i) and (ii).

Conclusions

In summary, after optimization of the catalytic reaction conditions, using the auxiliary base to overcome the catalyst-load dependence on the *dr*, thirteen racemic (±)-*trans*-2-substituted alcohols were screened with two racemic acyl chlorides for reversal of *dr*. The highest *dr* was found with cyclohexyloxy-substituted **17** in the case of the uncatalyzed reaction with **5** (*dr* 1:10) and in the pyridine-catalyzed reaction with the tolylsulfonyl-containing compound **23** with **3** (*dr* 15:1). Stereoselectivity was generally higher with the less sterically demanding acyl chloride **3** as opposed to **5**. The heteroatom on the *trans*-2-substituent appears to be essential for the reversal of *dr* to be observed, acting as a chiral auxiliary of sorts. Computational modeling of the reaction points to the importance of the heteroatom and/or aromatic moiety on the *trans*-2-substituent, as well. With further improvements to the *dr*, especially through modification close to the alcohol functionality of the cyclohexanols substrate, this method may provide valuable in the stereodivergent resolution of racemic acyl chlorides.

Chapter 3: Oxidative Esterification using TEMPO/CaCl$_2$/Oxone

Introduction

As discussed in Chapter 1, various synthetic pathways exist to form esters and the "ideal" reaction for a given target molecule often depends on the available starting materials and functional groups already present. Specific to the present research, the synthesis of 6,6'-ester linked disaccharides was of interest to facilitate their conformational analysis and to gain insights into the influence of the ester functional group on the disaccharide's solution structure, the results of which will be discussed in the following chapters. Due to the nature of the desired products, among the possible reactions leading to ester-formation between two monosaccharides, oxidative esterification was considered first due to the symmetric nature of the target.

Oxidative esterification has been reported as a convenient pathway to both symmetric esters, as well as asymmetric esters.[16,91-94] The use of primary alcohols as starting material is potentially the most efficient way to form symmetrical esters, omitting the necessity for synthesis and isolation of aldehyde or carboxylic acid intermediates. Furthermore, symmetric esters have found broad application in the chemical industry, from flavor and fragrance industries to pharmaceutical and cosmetic preparations. Both metal-containing as well as metal-free reagents and catalysts have been developed for this type of reaction.[16,95-98]
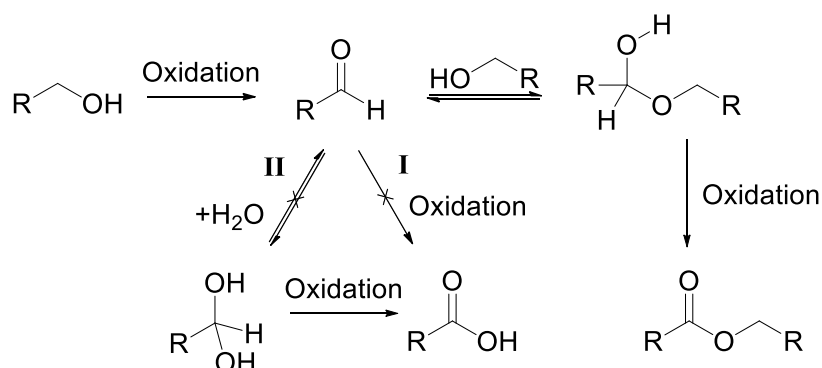
Figure 3.1. Accepted mechanism for the oxidative esterification of primary alcohols using TEMPO/CaCl$_2$/Oxone® and potential side reactions I and II.[94,97,99,100]

The mechanism of the reaction can be presented as a three step-two oxidation process (see Figure 3.1). The alcohol is first oxidized to the corresponding aldehyde, forms a hemiacetal with another alcohol and the hemiacetal is finally oxidized to the symmetric ester.[94,97,99,100] Nitroxyl radical derivatives, such as 2,2,6,6-tetramethyl-1-piperidinyloxy (TEMPO) and other stable derivatives have recently found larger use in oxidative transformations due to the generally mild conditions employed.[92,94,99,101] More specifically, Merbouh *et al.* showed that the TEMPO-derivative 4-acetylamino-TEMPO could be used to give symmetrical esters from primary alcohols containing a *β*-oxygen, including from carbohydrate derivates.[99] Meanwhile, work by Abramovich *et al.* demonstrated that TEMPO could be used catalytically in the oxidative esterification of primary alkyl alcohols given an appropriate terminal oxidant.[94] More recently, a catalytic TEMPO-mediated oxidation using Oxone® (potassium peroxymonosulfate) and calcium chloride giving aromatic aldehydes from a variety of benzylic alcohols was reported.[102] Interestingly, the same reaction conditions also produced *γ*-butyrolactone from 1,5-pentadiol with a 94% yield, however intermolecular ester formation was not reported. This finding suggested the likely possibility that the method may be adapted to form symmetrical esters from primary alcohols. The purpose of the present work was thus to explore the possibility of TEMPO/CaCl$_2$/Oxone® facilitated oxidative esterification from primary alcohols and investigate its substrate scope.

Results and Discussion

Initially, straight replication of the literature procedures of Tao *et al.* with benzyl alcohol in anhydrous solvents failed and showed no consumption of starting material after 1h by GC/MS.[102] However, the addition of a small amount of water lead to complete disappearance of the alcohol and formation of benzaldehyde, as observed by GC/MS after stirring at rt overnight.

This observation proved repeatable in the case of 1-hexanol **29**, with 0% conversion of the alcohol in the absence of water even after 24 h (Table 3.1, Entry 1). Conversely, in the presence of water the alcohol was converted into hexanal and the desired hexylhexanoate. Subsequently, the screening of a number of reaction conditions was undertaken to optimize the method for the oxidative esterification of **29** with the help of GC/MS for the analysis of the product mixture. The results are summarized in Table 3.1. In all reactions, aldehyde was found to be present as a side product. Over-oxidation was not observed to occur in significant amounts, with little to no amounts of hexanoic acid detected in the analysis of the product mixtures. These observations are in agreement with the stepwise mechanism of the oxidative esterification, as suggested by others (see Figure 3.1 above).[94,97,99,100]

Table 3.1. Optimization of reaction conditions for the oxidative esterification of 1-hexanol.

Entry	H_2O (mL)	$CaCl_2 \cdot 2H_2O$ (mmol)	Oxone (mmol)	t/h	Conv./%[a]	ester	aldehyde	side products	GC Yield
						Product ratio[a]			
1	0.0	0.5	1.0	24	0	-	-	-	0
2	1.0	0.5	1.0	2.5	44	90	10	0	39
3	0.5	0.5[b]	1.0	2.5	65	91	9	0	59
4	0.1	0.5	1.0	2.5	82	89	11	0	73
5	0.05	0.5	1.0	2.5	80	86	14	0	69
6	0.1	0.5	1.5	2.5	87	89	11	0	77
7	0.1	0.5	1.5	5	>99	83	14	3	82
8	0.1	0.5	2.0	2.5	90	88	12	0	79
9	0.1	0.5	2.0	5	>97	78	10	12	77
10	0.1	0.1	1.5	5	96	77	23	0	74
11	0.1	1.5	1.5	5	35	31	4	65	11
12	0.1	0.5	1.1	5[c]	91	88	12	0	80
13	0.1	0.5	1.3	4	97	88	12	0	**85**
14	0.1	0.5	1.5[d]	5	62	<10[e]	6	>84	<6
15	0.1	0.5[f]	1.3	4	82	9	52	39	7

[a]determined by GC/MS; [b]a control reaction with anhydrous $CaCl_2$ gave the same result; [c]no increase in conversion detected after 6h; [d]mCPBA instead of Oxone®; [e]overlap with 3-chlorobenzoic acid; [f]TBAB instead of $CaCl_2 \cdot 2H_2O$

Firstly, the amount of water needed for the reaction to proceed optimally was varied and it was found that a 1:20 ratio of water to dichloromethane gave the best combination of conversion and selectivity after 2.5 h (Table 3.1, Entries 2-5). The water appeared to associate with undissolved Oxone® and resulted in no apparent phase separation in the liquid phase. Next, the amount of the terminal oxidant Oxone® was varied and it was observed that, although higher amounts gave faster conversion of the starting material (Table 3.1, Entries 5-9), this was

accompanied by a decrease in selectivity when the reactions were allowed to proceed for longer times (Table 3.1, Entries 7 and 9). The decrease in selectivity could be attributed to the formation of chlorinated ester byproducts. Further investigation revealed that the formation of these side products could be suppressed partially by setting up the reactions in the dark or with reaction vessels covered in aluminum foil, which indicated that the side product formation might occur in a radical-type fashion (compare Figure 3.2 for GC/MS traces in the presence and absence of light).
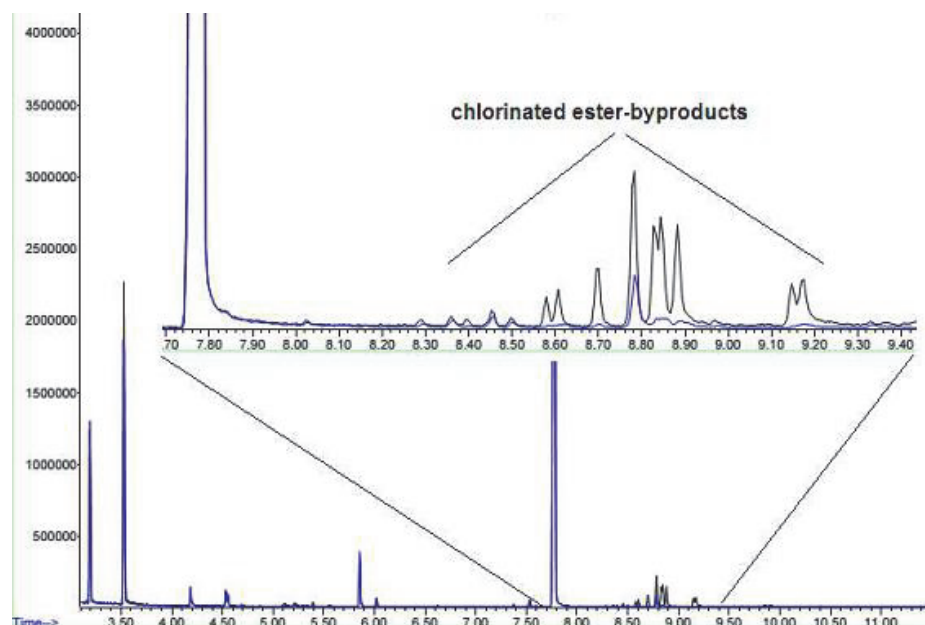
Figure 3.2. Indication of chlorinated ester-byproducts formed in clear glass vials (black trace), but not when vials were covered in aluminum foil (blue trace), as monitored by GC/MS of the product mixture. Chlorination was evident from characteristic isotopic peak pattern (X+2 peaks), not shown here.

When reducing the amount of chloride in the reaction, decreased selectivity for ester formation was observed (Table 3.1, Entry 10), while higher than 0.5 equivalents of $CaCl_2 \cdot 2 \ H_2O$ decreased conversion and lead to chlorinated side products (Table 3.1, Entry 11). This can likely be attributed to a higher concentration of hypochlorite in the mixture, which is an intermediate in

the catalytic cycle of the reaction when using Oxone® and $CaCl_2 \cdot 2\ H_2O$.[102] In fine-tuning the amount of Oxone® used in the reaction, 1.1 equivalents of Oxone® were found to give incomplete conversion of the alcohol, even after 6 h (Table 3.1, Entry 12). Meanwhile, 1.3 equivalents of Oxone® were found to give near complete conversion after 4 h with near optimal selectivity, leading to an overall GC/MS yield of 85 % for the reaction (Table 3.1, Entry 13).

Interestingly, when replacing Oxone® with *m*CPBA, a drastic increase in carboxylic acid yield was observed at the expense of hexanoate ester (Table 3.1, Entry 14). Likewise, the use of tetra-*n*-butyl ammonium bromide (TBAB) as the halide donor lowered the selectivity for ester-formation and over-oxidation to hexanoic acid was detected (Table 3.1, Entry 15). Taken together, these findings clearly illustrate the importance of the appropriate choice of oxidant and halide donor to avoid over-oxidation of the aldehyde intermediate prior to the formation of the hemiacetal intermediate (compare Figure 3.1, side reaction I).

Table 3.2. Solvent screening for the oxidative esterification of 1-hexanol using pre-optimized reagent conditions.
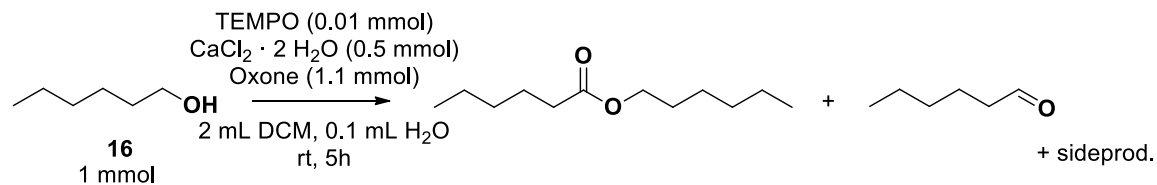
| Entry | Solvent | Conv./%[a] | Product ratio[a] | | | GC Yield[c] |
			ester	aldehyde	side products[b]	
1	CH$_2$Cl$_2$	84	69	28	3	**58**
2	EtOAc	47	79	2	19	37
3	Toluene	7	79	5	16	6
4	Et$_2$O	9	77	0	23	7
5	THF	10	20	4	77	2
6	Hexane	13	83	4	13	11
7	MeCN	88	61	8	31	**54**
8	Acetone	0	-	-	-	0
9	CHCl$_3$	74	68	26	6	**50**

[a] determined by GC/MS; [b] due to chlorination of **1a** or **2a** [c] calculated from product of conversion and **2a** product ratio.

A variety of differently polar and non-polar solvents was also screened, however only acetonitrile and chloroform gave similar but slightly inferior yield as compared to dichloromethane, as shown in Table 3.2.

As such, the procedure used going forward employed the following optimized reaction conditions: 0.01 equivalents of TEMPO, 0.5 equivalents of CaCl$_2$ · 2 H$_2$O and 1.1 equivalents of Oxone in 2 mL of dichloromethane with 0.1 mL H$_2$O added at a scale of 1 mmol of substrate.

As a next step, the substrate scope of the reaction was explored using the primary alcohols depicted in Figure 3.3. The results are encapsulated in Figure 3.3. Using the optimized reaction conditions described above, the isolated yield for hexyl hexanoate, produced from **29**, was improved over that previously estimated by GC/MS to 92% (Table 3.3, Entry 1). Other aliphatic alcohols, including those with branched alkyl chains and ring-structures, could be converted quickly and in moderate to good yields (Table 3.3, Entries 2-5, 10).
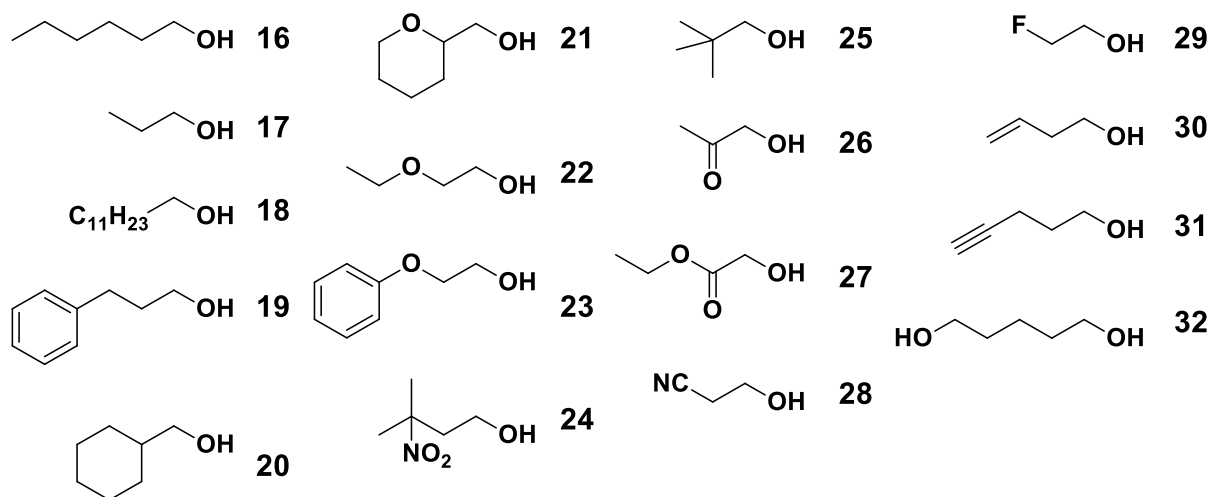
Figure 3.3. Substrate scope tested in the oxidative esterification using TEMPO/CaCl$_2$/Oxone®.

However, alcohols containing a *β*-oxygen substitution (**34 - 36)** failed to give good yields, as only traces of the desired ester products of **34** and **36** could be detected, while the ester derived from **35** was isolated in low yield. In all three cases, the reactions did not give full conversion after 24 h.

Table 3.3. Exploration of substrate scope.

$$2 \ R\text{—}OH \xrightarrow[\text{DCM/H}_2\text{O, rt}]{\text{TEMPO/CaCl}_2/\text{Oxone}} R\text{—}C(=O)\text{—}O\text{—}R$$

16-32

(1.0 mmol)

Entry	Reactant	t / h	Isolated Yield
1	29	4 h	92%
2	30	4 h	72%
3	31	24 h	29%
4	32	24 h	27%
5	33	2.5 h	89%
6	34	24 h	traces[a]
7	35	24 h	9% (25%[b])
8	36	24 h	traces[a]
9	37	24 h	NR[c]
10	38	4 h	93%
11	39	24 h	NR[c]
12	40	24 h	traces[a]
13	41	24 h	NRc
14	42	3 h	traces[a]
15	43	24 h	0%[d]
16	44	24 h	0%[d]
17	45	6 h	n.d.[e]

[a] detected by DART-HRMS; [b] with 2.0 eq Oxone® to achieve full consumption of ROH; [c] NR = no reaction; [d]chlorohydrin addition to double-bond; [e]lactone product and polymerization side products were inseparable via column chromatography

As exemplified in Table 3.3, Entry 7, using 2.0 equivalents of terminal oxidant, the ester derived from **35** could be isolated in 25% yield at near full conversion of starting material, with the aldehyde making up the majority of the product mixture. Similarly, the β-ketone and β-ester containing alcohols **39** and **40** did not give the desired esterification products. The low reactivity of these compounds, which is in contrast to that found by Abramovich *et al.* when using trichloroisocyanuronic acid as the terminal oxidant under anhydrous conditions and pyridine as a base additive, could potentially be a result of the presence of water, which might inhibit the

hemiacetal formation (compare Figure 3.1, side reaction II) or the relatively higher amount of hypochlorite formation.[94] However, it bears mentioning that in none of the above cases, overoxidation to the carboxylic acid (either directly or from the hydrate) was observed in appreciable amounts by GC/MS or NMR analysis of the crude product mixtures. Unlike in other methods, the addition of pyridine to the reaction mixture did not lead to improved yields in a test reaction with **35**, as isolated yield was virtually unchanged.[94,99]
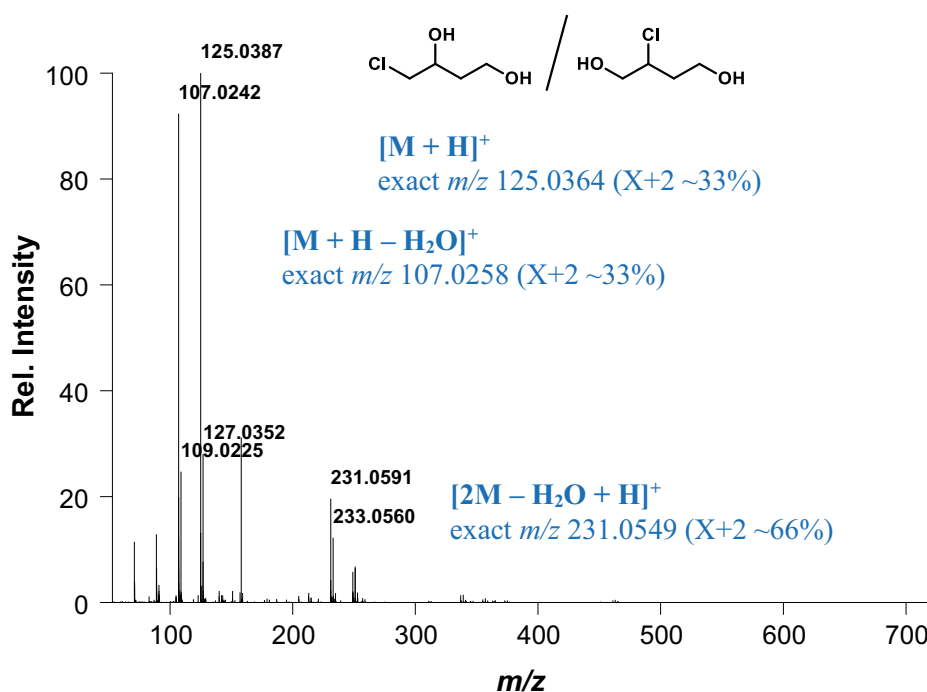
Figure 3.4. Evidence of chlorohydrin-addition products to **43** in the DART-HRMS spectrum.

The oxidative esterification of alcohols containing either an alkene (**43**) or alkyne (**44**) functional group was unsuccessful, due to the formation of chlorohydrin-addition products across the double bond and other unidentified side products, respectively. Figure 3.4 shows the identified side products for **43**.
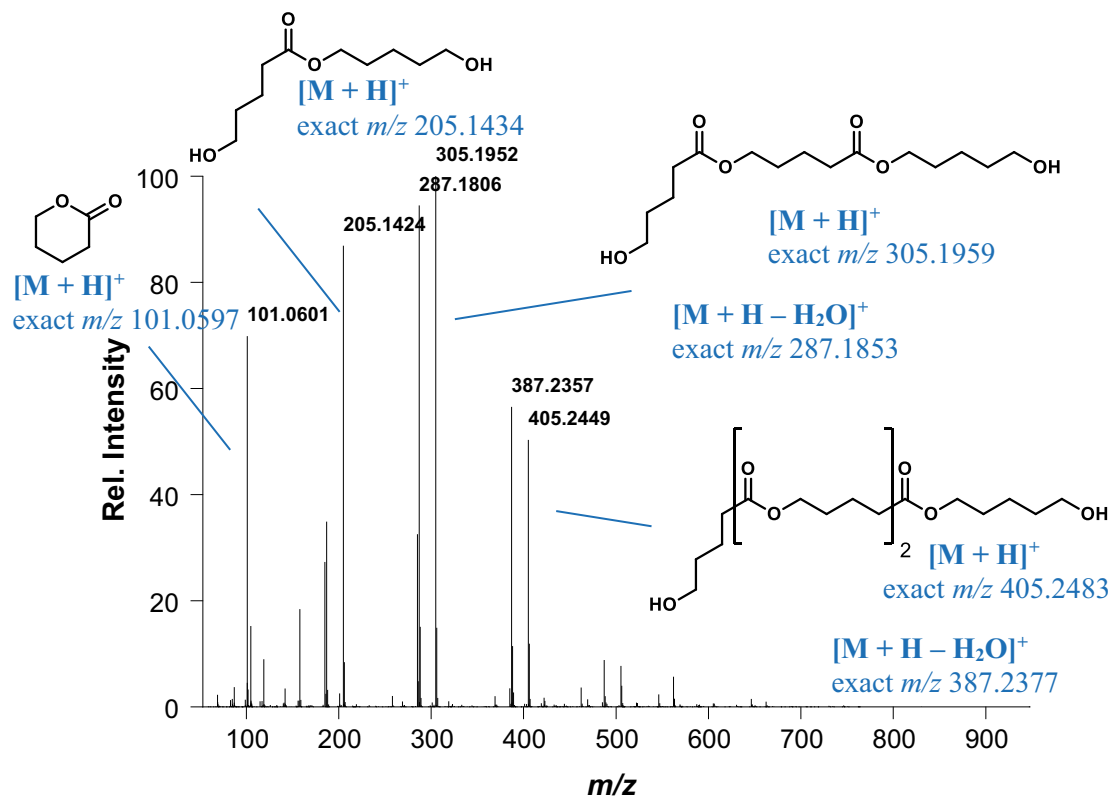
Figure 3.5. Evidence of polymerization products in the reaction of 1,5-pentanediol **45**, when monitored using DART-HRMS.

The β-cyano containing alcohol **41** was also unreactive under the given conditions, while only trace amounts of the product could be observed with 2-fluoroethanol **42**. Lastly, the reaction conditions were applied to 1,5-pentanediol **45** to form the corresponding lactone through intramolecular esterification; however, significant amounts of side products were evident from a cursory analysis of the crude product mixture. The identity of these could be determined using DART-HRMS analysis, as shown in Figure 3.5, revealing protonated molecular ions and dehydration fragments thereof for dimer, trimer and tetramer products of **45** with significant ion intensities. These side products were found to be inseparable via column chromatography due to near identical R_f values and their formation could not be significantly suppressed even when the reaction was performed at 5x higher (0.1 mmol/mL) dilutions.
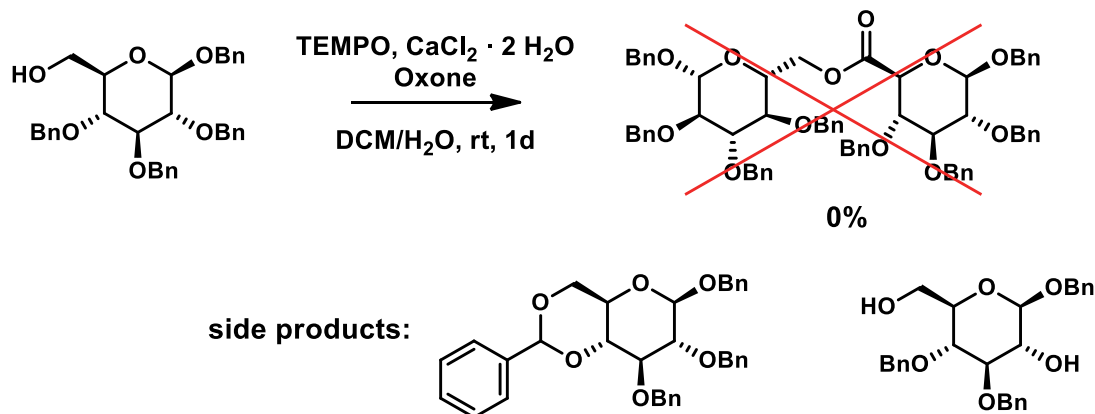
Figure 3.6. Reaction scheme for the expected transformation of benzyl 2,3,4-tri-*O*-benzyl-*β*-D-glucopyranose and the observed side products which were formed instead.

When the established method was used for the transformation of benzyl 2,3,4-tri-*O*-benzyl-*β*-D-glucopyranose, less than 50% conversion was observed after 24 h and the desired 6,6'-linked ester was not observed among the product mixture. Instead, the degradation of the starting material by oxidative cleavage of the benzyl group (at either the 2, 3 or 4-position) was identified as the major side reaction. In addition, traces of benzyl 2,3-O-benzyl-4,6-O-benzylidene-*β*-D-glucopyranoside, due to oxidative C-O bond formation, could be isolated as well. A more thorough literature search revealed that the reaction pathway leading to oxidative cleavage has been previously observed in a similar reaction involving various benzyl ethers and 4-acetamido-2,2,6,6-tetramethylpiperidine-1-oxoammonium tetrafluoroborate in wet acetonitrile, as reported by Pradhan *et al.*.[92] In the reported case, the oxidative cleavage was found to yield aromatic aldehydes. The authors reasoned that the oxidation could be due to a formal hydride abstraction from the benzylic carbon due to their evidence of slower reactions with substrates bearing electron-withdrawing substituents.

To gain additional knowledge about the selectivity of the established method, several competition experiments were performed. In a reaction of equimolar amounts of 1-octanol and 2-octanol under the established reaction conditions, as described above and using 1 mmol of each

alcohol with 1.1 mmol of Oxone®, little to no selectivity was observed for the consumption of

primary over secondary alcohol (58:42 ratio as determined by GC/MS). In addition, only trace

amounts of the mixed 2-octyl octanoate were observed in 1:6 ratio to the more prevalent 1-octyl

octanoate. This is likely a result of competing rates of hemiacetal formation, which are expected

to be higher for the primary alcohol. In reaction of either benzyl alcohol or benzaldehyde with

hexanol, no significant amount of cross-esterification was observed in neither case, with the main

products being benzaldehyde and hexyl hexanoate, respectively.
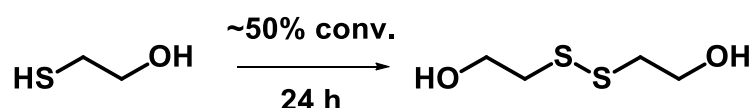
Figure 3.7. Oxidation of *β*-mercaptoethanol using established reaction conditions – product was not isolated.

Interestingly, the oxidation of 2-mercaptoethanol did not lead to the symmetrical ester,

but instead, the disulfide-linked dimer was detected by mass spectral techniques. As such, the

oxidation appears to be selective for thiols in the presence of alcohol functional groups, due to

their lower oxidation potential. This might be useful in the formation of disulfide-bridged

compounds, however the possibility was not explored further, as it would have been outside of

the scope of the work presented herein.

Conclusions

In summary, a convenient metal-free oxidative esterification methodology was

established with TEMPO/CaCl$_2$/Oxone as the oxidizer combination. The method gave

satisfactory ester yields for a range of primary alcohols. *β*-Substitution was not well tolerated

overall, as substrates were either unreactive or required additional terminal oxidant to lead to

appreciable amounts of product formation. However, the reaction does not require anhydrous

conditions and in fact water is required for the reaction to proceed. Although the adaption of the

newly established methodology to the transformation of 6-unprotected monosaccharide benzyl-derivatives was unsuccessful, this oxidative esterification to give 6,6'-ester linked disaccharides could be achieved with a similar method, as will be detailed in the Chapter 5.

Chapter 4: Development of a Karplus Equation for $^3J_{C(sp2)OCH}$.

Introduction

Carbohydrates are inherently flexible molecules and any attempt to shed light on the relation between structure and biochemical function of carbohydrates and their derivatives must be based on unambiguous structure assignment and the description of their solution geometries, otherwise known as Conformational Analysis. Although X-ray crystallography allows the unambiguous determination of molecular geometry for crystalline compounds, its disadvantage is that the dihedral angles that can be determined refer to the solid state, which often does not hold true in solution. On the other hand, NMR spectroscopy, taken in conjunction with computational techniques and statistical analysis, can provide a near-complete picture of a molecule's solution geometry.[103-108] A particularly useful tool to determine a molecule's geometry is the relationship between a coupling constant and dihedral angle of the coupled atoms. In 1959, Martin Karplus described this relationship for the first time for the $^3J_{HCCH}$ coupling constant and HCCH dihedral angle in ethane based on valence bond theory.[109-111] In his seminal paper, for which, together with his subsequent work, Karplus received a share of the Nobel Prize in Chemistry in 2013, he quantitatively described the correlation of experimental coupling constant to the dihedral angle between the coupled nuclei. The original equation published by Karplus expressed the relationship as follows:

$$^3J_{HCCH} \,/\, \mathrm{Hz} \,=\, 8.5 \cdot \cos^2 \varphi - 0.28 \ \text{ for } \ 0° \leq \varphi \leq 90° \ \text{ and} \qquad (1)$$

$$9.5 \cdot \cos^2 \varphi - 0.28 \ \text{ for } \ 90° \leq \varphi \leq 180°$$

In the above, φ is defined as the dihedral angle between the hydrogen atoms in question. This relationship can be rewritten as one quadratic equation:

$$^3J_{HCCH} / Hz = 9.0 \cdot \cos^2 \varphi - 0.5 \cdot \cos \varphi - 0.3 \qquad (2)$$

This theoretically allows one to obtain a value for φ from an experimental $^3J_{HH}$ value, however Karplus himself cautioned against this, due to the multiple solutions of the quadratic equation when solving for the dihedral angle and other caveats discussed hereafter. It was soon realized that electronegativity of other substituents in ethane, and other molecules, for that matter, had an effect on the $^3J_{HH}$ coupling pathway and the magnitude of the observed coupling constant. In 1979, Haasnoot, Altona and coworkers published several papers that studied the $^3J_{HCCH}$ values in differently substituted ethane and other molecules to arrive at the following equation that takes into account these substituents:[112-114]

$$^3J_{HCCH} — Hz = 13.88 \cdot \cos^2 \varphi - 0.81 \cdot \cos \varphi \qquad (3)$$

$$+ \sum \Delta\chi_i [0.56 - 2.32 \cdot \cos^2 (\zeta\varphi + 17.9 \cdot |\Delta\chi_i|)]$$

The sign parameter ζ takes the value of ± 1 based on the orientation of the electronegative substituent as illustrated in Figure 4.1, while $\Sigma\Delta\chi_i$ is the sum of the electronegativity differences between the substituents i and hydrogen.
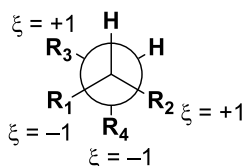
Figure 4.1. In the Haasnoot-Altona equation, substituents positioned clockwise relative to a hydrogen are assigned $\zeta = +1$, with substituents positioned counterclockwise $\zeta = -1$.

Nowadays, Karplus equations derived from a multitude of experimental data and extensive quantum mechanical calculations are available, that take bond lengths, electron densities, electron orbital terms, and dipolar electron spin terms into account implicitly or explicitly.[115-118]   Many Karplus equations have been derived based on both experimental and computational data for HCCH, CCCH and COCH torsions, both for generalized and carbohydrate-specific cases.[116,119-131]   Notably, the review by Coxon provides a good overview of the current state of the art.[116]

Specifically, one of the most commonly used Karplus equations for COCH linkages was derived by Tvaroška *et al.* from experimental coupling constants of conformationally restrained carbohydrate derivatives, including several anhydro-sugars, as shown in Figure 4.2.[122]   The coupling constants were fitted to dihedral angles obtained from X-ray crystallography data of the respective compounds to derive the following equation, which predicted coupling constants generally within ±1 Hz of the experimentally determined values:[122]

$$^3J_{\text{HCCH}} \; / \; \text{Hz} = 5.7 \cdot \cos^2 \varPhi - 0.6 \cdot \cos \varPhi - 0.5 \tag{4}$$

$\varPhi$ was defined as the dihedral angle between the vicinal hydrogen and the corresponding carbon three bonds removed, as illustrated in Figure 4.2.
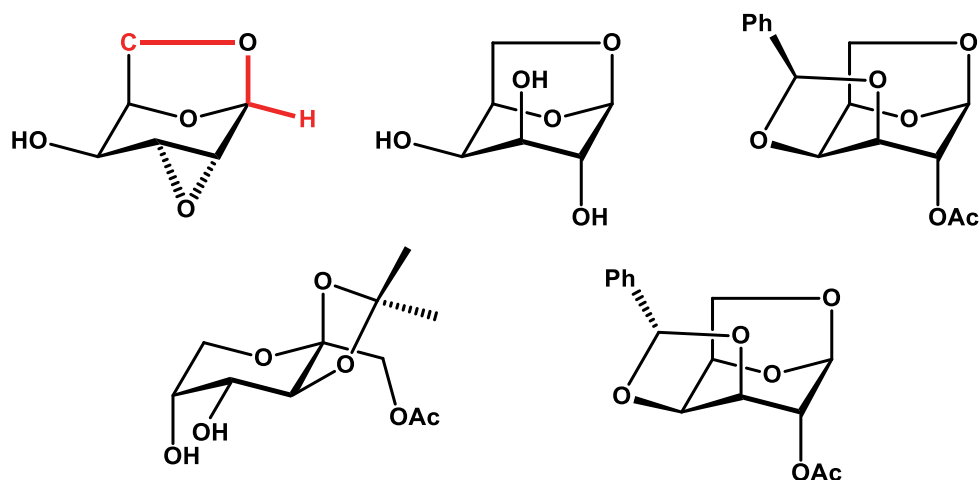
Figure 4.2. Conformationally restrained carbohydrate derivatives used by Tvaroška *et al.* to derive their Karplus equation for the COCH linkage.[122]

Similarly, Aydin *et al.* used a combination of experimental and DFT results from bicyclicly restrained compounds, i.e. adamantane and norborane derivatives, to arrive at their Karplus equations for $^3J_{CCCH}$.[124] Mulloy *et al.* likewise used experimental $^3J_{CH}$ values measured in carbohydrate-analogs together with molecular modeling data to derive their Karplus equation for COCH in the 1→2 linkage of sucrose.[128]

However, in most compounds the dihedral angle of interest is quite flexible and measured coupling constant is the result of averaging across the range of conformationally accessible dihedral angles and does not correspond to one angle unambiguously. As a result, the majority of published Karplus equations, including several carbohydrate-specific ones, have not been derived from experimental data, but were instead constructed from computed coupling constants and dihedral angles using, in the majority of more recent cases, density functional theory. Most commonly, such methods investigate one or multiple model compound(s) representative of the types of compounds of interest. After a relaxed rotational scan around the dihedral angle of interest at fixed increments (e.g. 30°) with geometry reoptimization of the rest of the molecule, a coupling constant is computed for each such rotamer employing a sufficiently expanded basis set.

Following this general approach, Karplus equations have been derived for specific classes of compounds: Grimmer *et al.* fitted Karplus equations for $^3J_{CCCH}$ and $^3J_{COCH}$ in substituted aromatic moieties, where carbon is sp^2 hybridized.[119] Munzarová *et al.* similarly used DFT calculations to arrive at a description of the CNCH coupling pathway in nucleosides for the investigation of the orientation of modified nucleobases relative to ribose.[120] Suardíaz *et al.* used valine as a model compound for the description of $^3J_{CNCH}$ in peptides to aid in the conformational analysis of the peptide backbone.[123] For carbohydrates, several published equations exist for the various two- and three-bond homo- and heteronuclear coupling constants related to the glycosidic linkage and the exocyclic CH_2OH group.[121,129-131] This work has been performed based on simple carbohydrate analogs for both pyranoses, as well as furanoses.

In the investigation of the conformational changes imparted by an ester linkage to several ester-containing carbohydrate derivatives, which will be detailed in the following chapter, an accurate description of the flexibility of the $C(sp^2)$-O-C-H torsional angle (highlighted in Figure 4.3 below) to accurately describe the solution phase structure of these molecules was required. However, the available Karplus equations for $C(sp^3)OCH$ torsions were not well suited for ester-linked compounds due to the different hybridization of the carbonyl carbon atom. Specifically, the Karplus equations by Tvaroška and others yield lower absolute values for the coupling in the sp^3-hybridized case compared to $C(sp^2)$-O-C-H in ester-functionalized compounds, as detailed hereafter. Based on their research on acetylated alcohols, González-Outeiriño *et al.* did publish one relevant Karplus equation in 2005 for the $C(sp^2)$-O-C-H coupling pathway. However, the researchers fitted experimentally obtained $^3J_{CH}$ values against MM3-computed static torsion angles based on the lowest energy conformer alone, resulting in an equation that does not represent the actual conformational behavior of said acetates.[132]

Thus, the present research aimed to establish the Karplus relationship between the $C1'(sp^2)$-$H6_{R/S}$ coupling constant and the corresponding torsion angle θ in carbohydrates (defined hereafter as C5-C6-O6-C1' based on IUPAC nomenclature, as shown in Figure 4.3) based on

experimental and computational data for a model carbohydrate derivative, namely 6-acetyl-α/β-D-glucopyranose **46**. This approach differs from the method of others outlined above by explicit consideration of the entire carbohydrate moiety, instead of modeling a simpler analog without all its OH functional groups.[121,129-131] In addition, four more compounds were synthesized in acetyl 6-*O*-acetyl-α/β-D-glucopyranoside **47**, 2,6-diacetyl-α/β-D-glucopyranose **48**, 3,6-diacetyl-α/β-D-glucopyranose **49** and methyl-α/β-D-glucopyranuronate **50** to serve as the test set for validation of the Karplus equation, which is shown in Figure 4.3.

It should be noted that while the current research was in progress, Turney *et al.* published their investigation on the conformation of O-acetyl side chains in monosaccharides, which also produced a Karplus relationship for the aforementioned C(sp^2)OCH torsion, albeit using a somewhat different methodology, along with equations for other coupling two- and three-bond coupling pathways affected by θ.[133] Their results corroborate our findings presented herein.
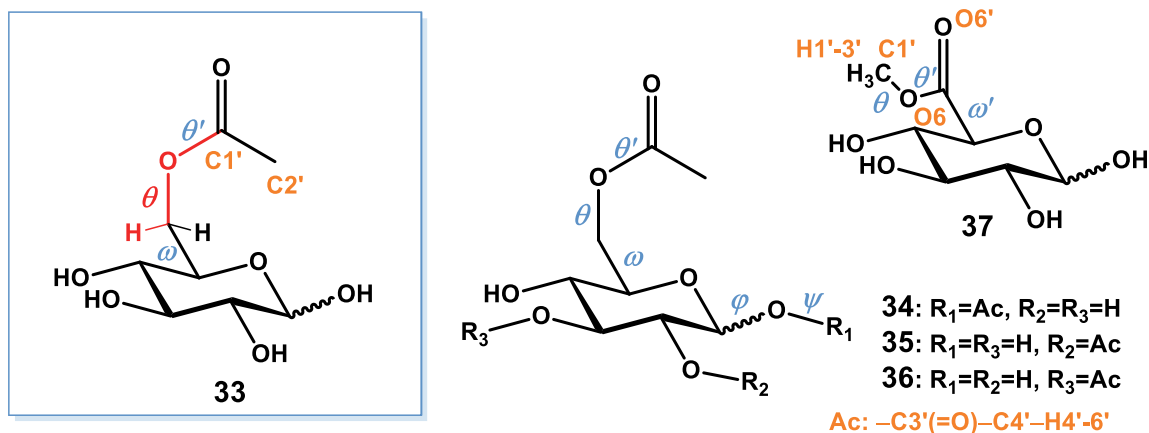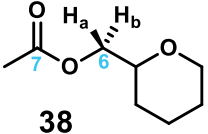
Figure 4.3. Model compound α/β-**46** and test set of compounds **51** − **52** used for the development of a Karplus equation for the relationship between ^3J(C$_{sp^2}$-O-C-H) and the θ (C5-C6-O6-C1') dihedral angle.

Results and Discussion

As mentioned above, when modeling a simple carbohydrate-like compound in (tetrahydropyran-2-yl)methyl acetate **53** with the AM1 force field, the back-calculated $^3J_{CH}$ coupling constants for the C7-O6-C6-H6$_{R/S}$ coupling pathways were underestimated by existing Karplus equations, such as that by Tvaroska, as illustrated in Table 4.1.[122]

Table 4.1. Comparison of experimental and theoretical coupling constants for $^3J_{C(sp2)OCH}$ in **53** using an existing COCH Karplus equation.[122]

	experimental J-HMBC	MD simulation (AM1, 500ps, backcalculated)
$^3J_{C7,H6R/S}$/ Hz	3.1 (H6$_R$), 2.9 (H6$_S$)	2.7 (H6$_R$) 2.2 (H6$_S$)

To ascertain, if a better fit could be obtained for the described linkage, a Karplus equation was generated using computational treatment of **53**. A conformational search using Spartan14 was performed to obtain an initial guess at the lowest energy conformers of **53**.[134] Based on their B3LYP/6-31G* optimized geometries, the Fermi contact term, which represents the experimental coupling constant, was computed using Gaussian09 at the B3LYP/6-31G*(PCM) level of theory with implicitly treated solvent (chloroform) for all rotamers ±10,20°.[135] The Fermi contact values were plotted against the C7-O-C6-C5 dihedral angle θ and fitted using a general four-parameter Karplus equation. The resulting Karplus equations for both $^3J_{C7-H6R}$ and $^3J_{C7-H6S}$, as shown in Figure 4.4, are given below:

$$^3J_{C7-O-C6-H6R} = 6.8 \cdot \cos{}^2(\theta + 118.7°) - 1.6 \cdot \cos(\theta + 118.7°) + 0.8 \qquad (5)$$

$$^3J_{C7-O-C6-H6S} = 7.1 \cdot \cos{}^2(\theta - 120.6°) - 1.7 \cdot \cos(\theta - 120.6°) + 0.8 \qquad (6)$$
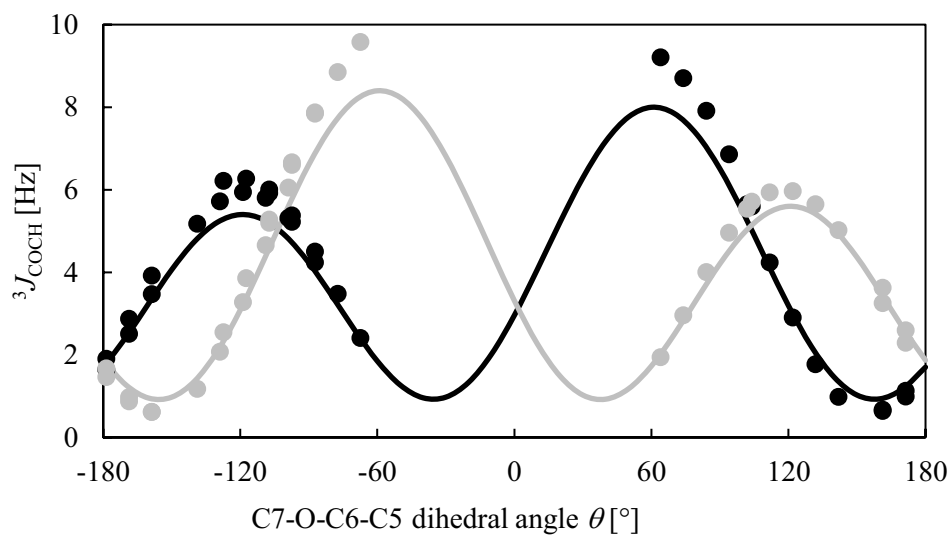
Figure 4.4. Computationally determined Karplus relationship between C7-O-C6-C5 dihedral angle θ (in accordance with IUPAC nomenclature) and $^3J_{COCH}$ for H6$_R$ (gray) and H6$_S$ (black) based on **53**.

Figure 4.5 shows a visual comparison between equations (5) and (6) to the Karplus

equation for C(sp^3)OCH coupling published by Tvaroška *et al*. (in black), which results in a

different Karplus relationship around the maximum at 60° and -60° for the two equations,

respectively.
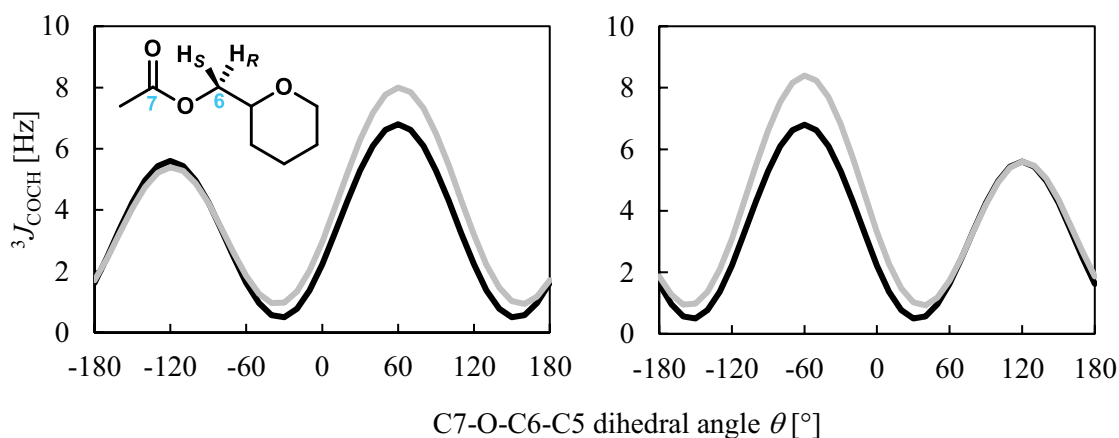
Figure 4.5. Comparison of preliminary Karplus equations (gray) obtained based on tetrahydropyran-2-methyl acetate **53** for C7-H6$_R$ and C7-H6$_S$ (left and right, respectively) and published equation based on Tvaroška et al. (black).[122]

With these equations, a recalculation of the back-calculated coupling constants from the MD simulation of **53** yielded values that fall closer to the experimentally determined ones (3.0 Hz for H6$_R$, 2.5 Hz for H6$_S$). This demonstrated the viability of the general method to obtain a better-fitting Karplus equation for $^3J_{Csp2OCH}$ in ester-linked compounds from computational treatment. Often, even for carbohydrate specific Karplus work, carbohydrate-like compounds (but missing hydroxyl groups in some positions) were chosen as model compounds to derive a Karplus equation from DFT calculations, similar to the example of **53**. Instead, a carbohydrate derivate was chosen for this study to more closely model the carbohydrate derivatives discussed in the following chapter.

Synthesis of model compounds. To study of the C(sp^2)OCH Karplus relationship on a carbohydrate ester model compound, a simple regioselective acetylation of glucose to give 6-*O*-acetyl-α/*ß*-D-glucopyranose **46** was envisioned initially. A number of enzymatic and non-enzymatic methods for regioselective acetylation of unprotected or partially protected carbohydrates have been discussed in the literature.[136-139] However, several attempts at regioselective acetylation using established non-enzymatic methods or adaptations thereof failed

using unprotected glucose, despite their demonstrated success with methyl-D-glucopyranoside.[138,140] The transformation was instead successful following a less direct synthetic route, as depicted in Figure 4.6. Using a regioselective acetylation of per-TMS protected D-glucose **54** followed by selective deprotection of the silyl protection groups, **46** was obtained as a 42:58 mixture of α/β-anomers.[141,142] In the regioselective acylation of per-TMS D-glucose **54**, in addition to giving the monoacetylated **55,** en route to **46**, the reaction also yielded the diacetylated **56** in 16% yield. As described by Witschi *et al*., the DOWEX 50WX8-mediated deprotection of **55** and **56** was observed to proceed with minimal acetyl migration to give a mixture of anomers of **46** and **47**, respectively.[142]
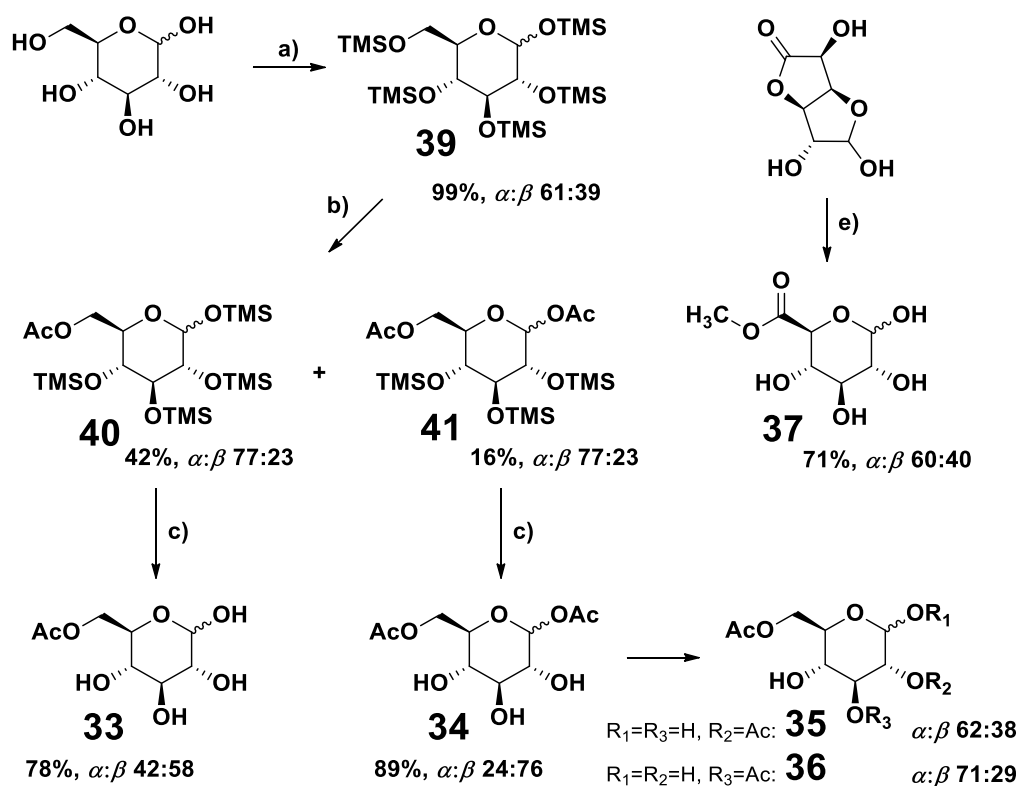
Figure 4.6. Synthetic scheme for the synthesis of model compounds α/β-**46**, α/β-**47**, α/β-**48**, α/β-**49** and α/β-**50** used in this study. Conditions: a) HMDS, TMSOTf, CH_2Cl_2, rt, overnight ; b) AcOH, Ac_2O, rt, 7 days; c) DOWEX 50WX8, MeOH, rt, 15 min; d) H_2O, MeOH, 40 °C, overnight; e) Na, MeOH, rt, 1h.

In addition, it was found that α/β-**47** could be converted through acetyl migration into a mixture containing the more thermodynamically stable 2,6- and 3,6-regioisomers (α/β-**48** and α/β-**49**) by heating of the diacetyl-glucose solution to 40 °C overnight. Their presence could be verified through 1D TOCSY experiments, which identified the hydrogens on the pyranose ring for α/β-**48** and α/β-**49**. See Methods section for the observed chemical shifts. In addition, a small amount of 6-acetyl-D-glucose **46** was found to be present in the mixture as a result of deacetylation. Meanwhile, no significant amounts of 4,6-diacetyl-D-glucose were observed by ^{1}H NMR. A fourth compound to be used in validating of the Karplus equation, the methyl ester of glucuronic acid **50**, was readily accessible from D-glucurono-6,3-lactone using methanol under basic conditions in 71% yield (α:β 60:40) after separation from unreacted lactone by column chromatography.[143] The above synthesized compounds (or mixtures of regioisomers in the case of **48** and **49**) were analyzed by 1D & 2D NMR and full spectral assignments could be made. Figure 4.7 illustrates the use of 1D-TOCSY experiments to separate the overlapping spectral regions of the respective anomeric mixtures. Compounds **46** and **50** were measured in D_2O, while **47**, **48** and **49** were measured in 2:1 D_2O:MeOD-d_4 due to their limited solubility in water alone. The addition of deuterated methanol is not expected to significantly affect the conformational behavior of the carbohydrates, due to the similar polarity of the solvents. The assignments were corroborated by those published in the literature, where applicable.[139,142]
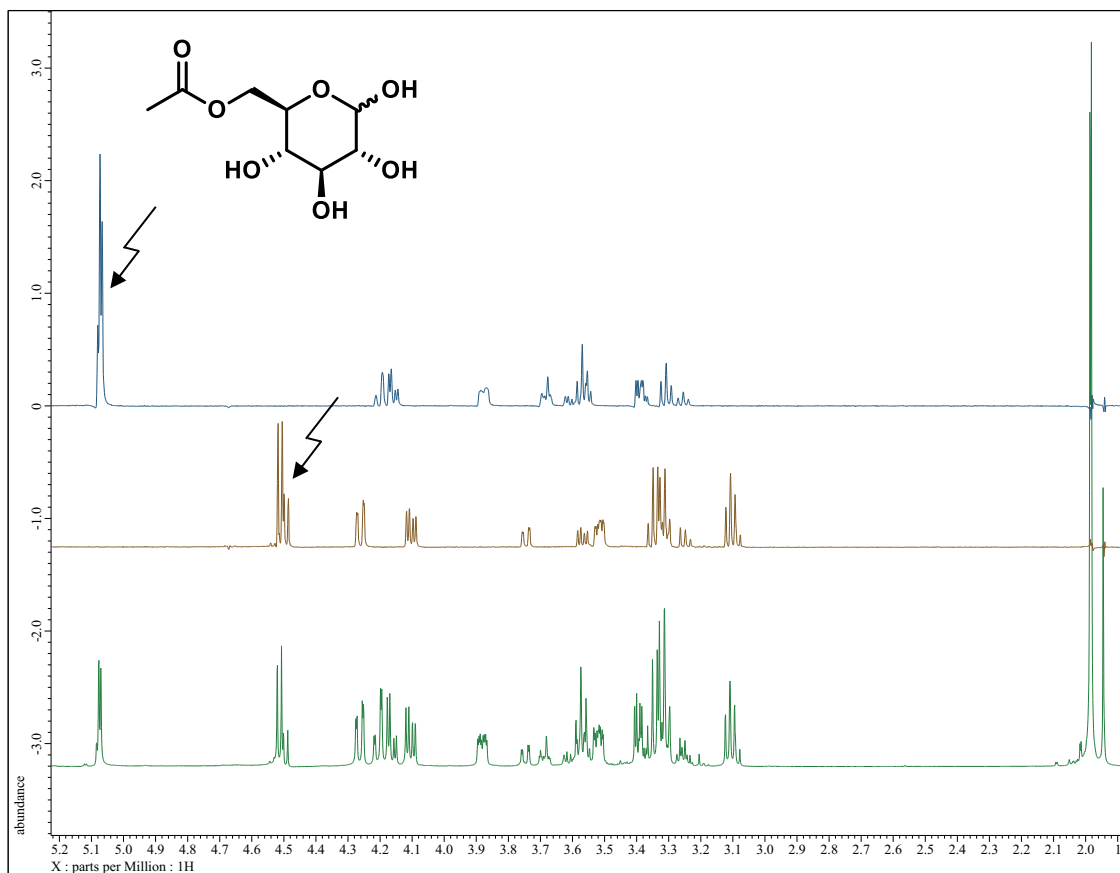
Figure 4.7. H$_2$O-Presaturation ^{1}H NMR of Compound **46** overlaid with 1D TOCSY data for α-**1** (top) and β-**1** (middle) to illustrate the distinction of the spectral peaks of the respective anomers.

Experimental determination of $^3J_{CH}$ coupling constants. Heteronuclear three-bond couplings could be measured using a gradient-selected *J*-HMBC experiment, which yielded pseudo-three dimensional HMBC spectra with the coupling evolution time τ on the z-axis.[144] Coupling constants could be extracted for a given crosspeak in the HMBC spectrum on the basis of the peak volume (*A*) of the cross-peak in the *J*-HMBC spectra: *A* fluctuates in sinusoidal fashion with increasing coupling evolution time τ. In the experiment, *A* is measured as |*A*| and thus every second lobe in the coupling evolution time slice was inverted to negative value, if applicable. The resulting data could be fitted using PSI-Plot to a sinusoidal function of $A = \sin(\pi \cdot {}^3J_{CH} \cdot \tau)$ to yield the coupling constants for the relevant three bond couplings along the dihedral angles of interest with an uncertainty of about ±0.6 Hz.[144,145] The relevant $^3J_{Csp2OCH}$

coupling constants that could be determined in this fashion are summarized in Table 4.5 and

Table 4.7 on pages 107 and 112, respectively.

$$A = 1.196 \cdot \sin(\mathbf{2.96\ Hz} \cdot \pi \cdot \tau)$$
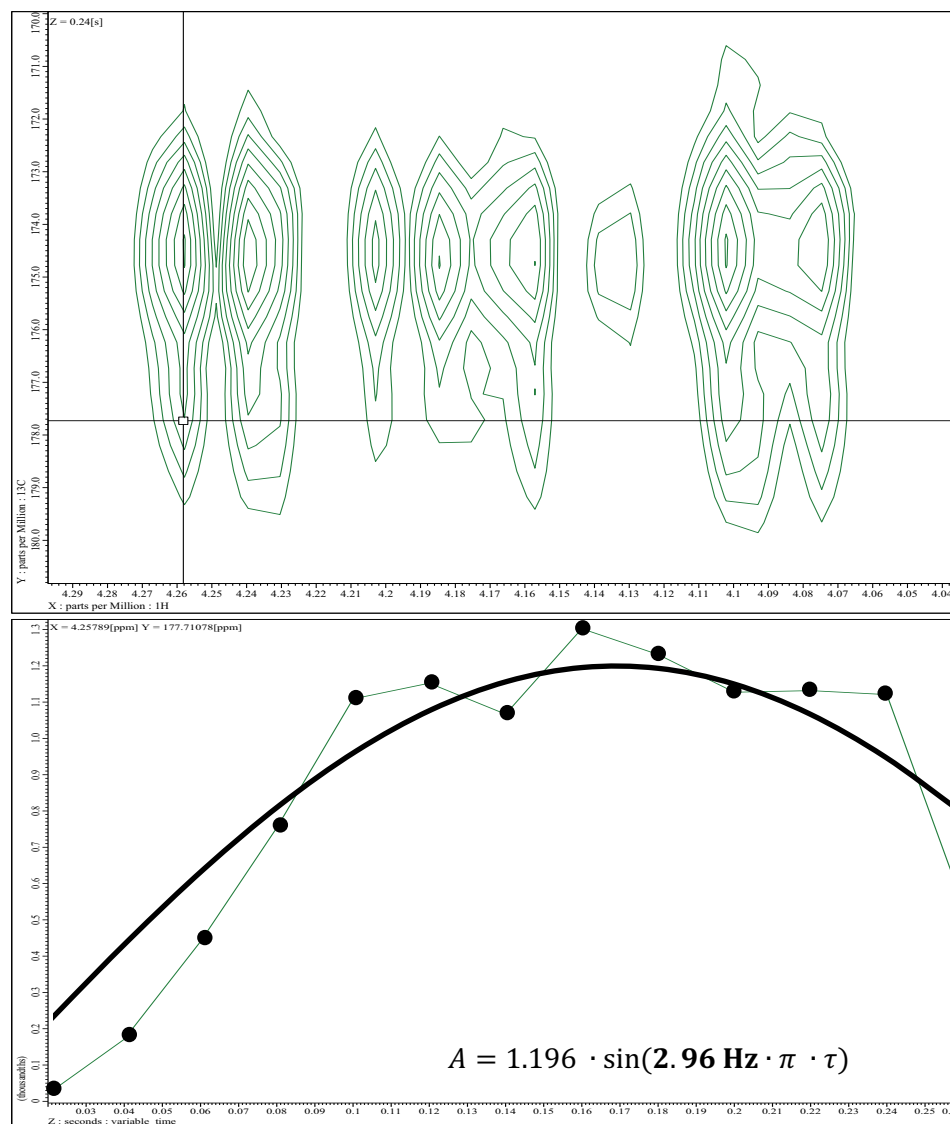
Figure 4.8. Expanded $^3J_{C5,H6a/b}$ cross-peak region of Compound 46 and example gradient enhanced *J*-HMBC data (thin lines) with data points in 20 ms intervals used in the determination of $^3J_{CH}$ (correlation at 4.26 ppm – 168 ppm) by fitting with a sinusoidal equation displayed using PSI-Plot.[145]

Development of a Karplus equation for C(*sp²*)OCH torsion angles. To establish a computational model for **46**, both molecular dynamics simulations and quantum mechanical calculations were performed. An exhaustive dihedral angle scan was performed on both α- and β-anomers of **46** using Spartan14 (for details see methods section) to arrive at an initial guess for the lowest energy conformers of **46**. After this, the Amber14 software package and the carbohydrate-specific GLYCAM06 force field employing the TIP3P water model was used to run a 500 ns molecular dynamics simulation to sufficiently sample the conformational space of both α-**46** and β-**46**.[146-148] The molecular dynamics treatment of the model compound was employed due to its known capability to characterize the internal molecular motion and flexible nature of carbohydrates.[103,149] The MD simulations were analyzed on the basis of the relevant dihedral angles ω, θ and θ' and categorized by their population maxima (taking into account the surrounding dihedral angle range of +/– 37°) and 9 major conformational regions could be distinguished for both α-**46** and β-**46** (see **Table 4.2** and **Table 4.3** and **Figure 4.9** and **Figure 4.10**). This captured 97% of the total 50000 conformers obtained for the two anomers, respectively.

Table 4.2. Summary of the conformational space of α-**46** established based on MD simulation covering 97% of the total conformers.

Conformer #	C4-C5-C6-O6 ω / °	C5-C6-O6-C1' θ / °	C6-O6-C1'-C2' θ' / °	Count	% abundance
1	58	180	180	17759	**37%**
2	58	103	180	5342	**11%**
3	58	-106	180	4194	9%
4	-73	180	180	4686	10%
5	-73	103	180	2381	5%
6	-73	-106	180	2189	4%
7	-168	180	180	6370	**13%**
8	-168	103	180	2774	6%
9	-168	-106	180	2661	5%
				48356	97% coverage

In the case of both *α*-**46** and *β*-**46**, conformer 1 ($\omega = 58°$, $\theta = 180°$, $\theta' = 180°$) was found to be the dominant conformational region at 37% and 38% respectively. For *α*-**46**, ω was found to largely favor g^+ (58°) with 57% abundance over the *st* (-168°) conformation at 24%, with the remainder of 19% present as g^- (-73°). The ω angle thus is predicted to behave similar to that of unsubstituted *α*-D-glucose.[131,150] For θ, a 60 % preference for the *st* (180°) conformation was predicted, with the g^+ (103°) and g^- (-106°) conformations contributing 22% and 18%, respectively. Meanwhile, the θ' angle was computed to entirely assume the *st* (180°) conformation due to the carbonyl on C1'. For *β*-**46**, the ω angle was found to assume a slightly larger proportion of the g^+ conformation at 64%, in favor of both the *st* and g^- conformations at 19% and 15%, thus differing slightly from unsubstituted *β*-D-glucose, which is assumed to have a higher amount of *st*.[131,150]

Table 4.3. Summary of the conformational space established for *β*-**46** based on MD simulation covering 97% of the total conformers.

Conformer #	C4-C5-C6-O6 $\omega/°$	C5-C6-O6-C1' $\theta/°$	C6-O6-C1'-C2' $\theta'/°$	Count	% abundance
1	58	180	180	18373	**38%**
2	58	103	180	8049	**17%**
3	58	-106	180	4280	9%
4	-73	180	180	4053	8%
5	-73	103	180	1755	4%
6	-73	-106	180	1686	3%
7	-168	180	180	5203	**11%**
8	-168	103	180	1971	4%
9	-168	-106	180	3035	6%
				48575	97% coverage

As a result, the second most abundant conformational region for *β*-**46** was conformer 2 ($\omega = 58°$ (g^+), $\theta = 103°$ (g^+), $\theta' = 180°$ (*st*)) at 17% in *β*-**46**, as opposed to conformer 7 ($\omega = -168°$ (*st*), $\theta = 180°$ (*st*), $\theta' = 180°$ (*st*)) at 13% in *α*-**46**, as shown in Table 4.3. For θ, the dihedral

angle population appeared largely unchanged between α-**46** and β-**46**, with β-**46** also displaying a large preference for the *st* conformation with 57%, and the g^+ and g^- conformations contributing 25% and 18% respectively. The broad distribution of θ in both α-**46** and β-**46** – as seen in Figure 4.9 and Figure 4.10 – can very likely be attributed to little steric hindrance from neighboring positions, as also observed by Turney *et al.*.[133] As was seen for α-**46**, the θ' angle in β-**46** was observed entirely in the *st* conformation due to the carbonyl.
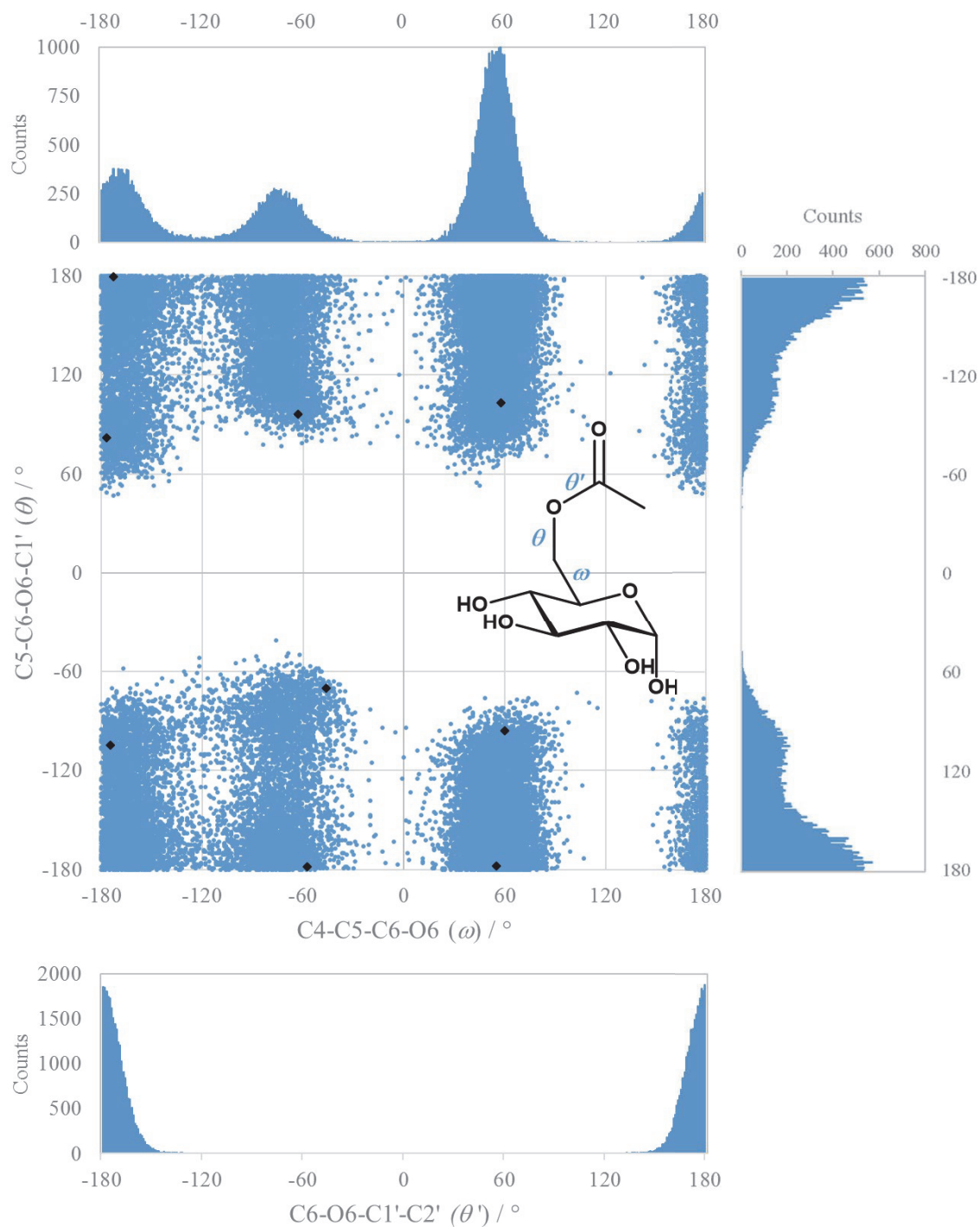
Figure 4.9. Summary of MD simulation for *α*-**46** showing population histograms and Ramachandran plot data for the relevant dihedral angles *θ* (C5-C6-O6-C1'), *ω* (C4-C5-C6-O6) and *θ*' (C6-O6-C1'-C2') – QM minimized conformers are overlaid as black diamonds to show their respective dihedral angle values.
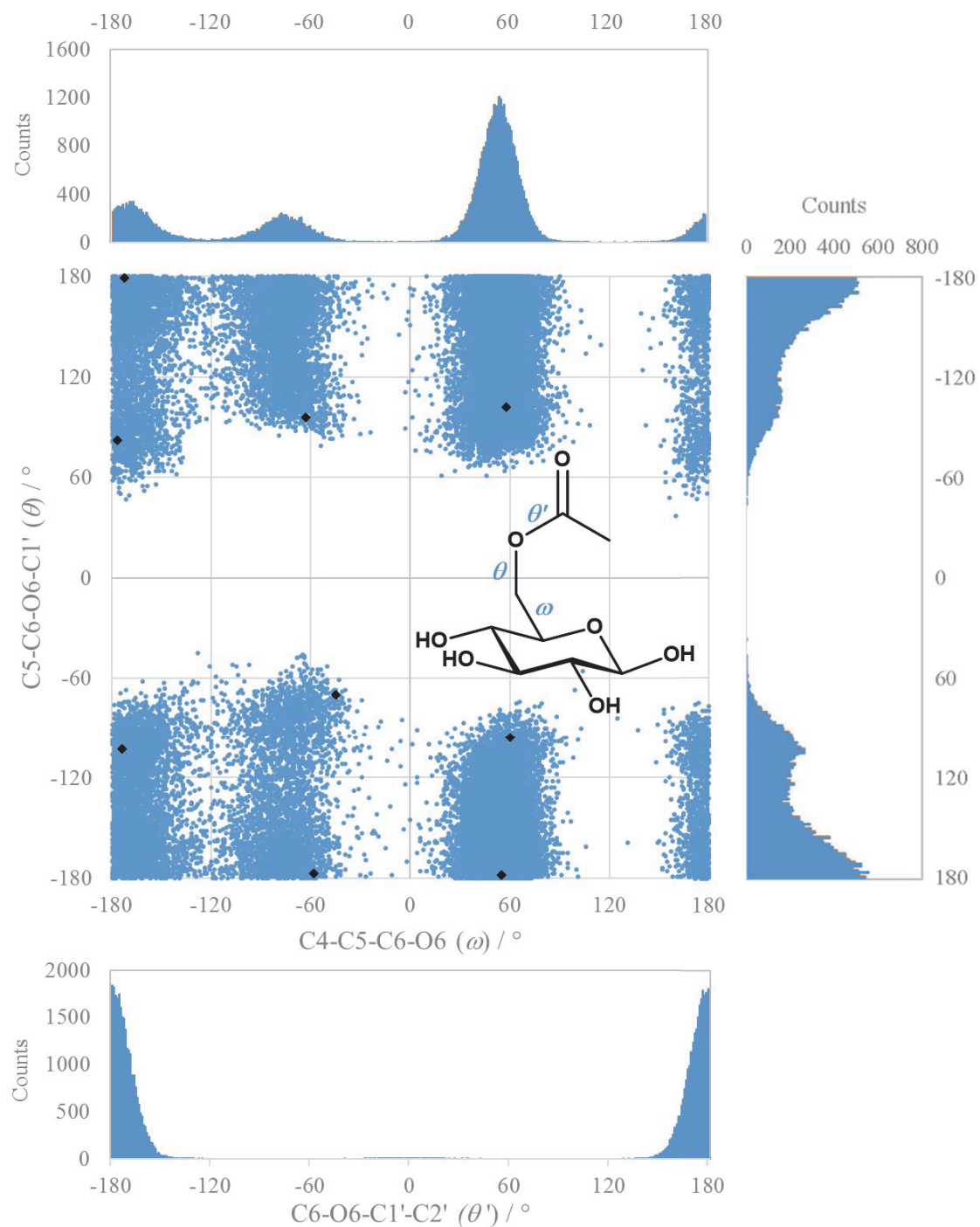
Figure 4.10. Summary of the MD simulation for β-**46** showing population histograms and Ramachandran plot data for the relevant dihedral angles θ (C5-C6-O6-C1'), ω (C4-C5-C6-O6) and θ' (C6-O6-C1'-C2') – QM minimized conformers are overlaid as black diamonds to show their respective dihedral angle values.

With the conformational space of α-**46** and β-**46** established, representative geometries for all 9 major conformation regions for both anomers (as described in Table 4.2 and Table 4.3 above) were extracted from the MD trajectories and the geometries minimized using Gaussian09 at the M05-2X/6-31G*(PCM) level of theory, as discussed in the Methods section. The θ and ω dihedral angle values for the minimized QM conformers are overlaid on the respective MD-derived Ramachandran plots in Figure 4.9 and Figure 4.10. Except for the cases of conformer region 6 ($\omega = -73°$, $\theta = -106°$, $\theta' = 180°$), where the QM geometry showed a slight deviation in the ω angle from the mode of the MD simulation, they were found to very closely match the maxima of the dihedral angle populations, which supported the adequateness of the MD simulations. Table 4.4 summarizes the relative Gibbs Free Energies of the conformers resulting from QM optimization. As can be seen, the order of the relative Gibbs Free Energies does not match the observed relative abundances derived from the MD simulation. However, the QM geometries were not optimized with regards to the additional flexibility of the hydroxyl groups that were not considered in the classification of the conformer populations above. Additionally, the main caveat with regard to the representativeness of the QM results is the poor consideration of solvent effects on the hydrogen bonding pattern in implicit solvent computations. Here, especially with the exclusion of explicit water molecules, the formation of intramolecular hydrogen bonding in the hybrid-*ab initio* model, which are absent in the 'real' structure, lead to changes in the relative Gibbs Free Energies that are not representative of the 'actual' molecular structure. Consideration of the solvation effect and potential water bridges that stabilize certain conformations were omitted due to the additional complexity they would have introduced to the investigation. As such, the relative energy of the QM conformers was not considered further.

Table 4.4. Summary of relative QM energies (M05-2X/6-311+G**(PCM)//M05-2X/6-31G*(PCM)) of the 9 conformers representative of the conformational space established for **46**.

ΔG^{298} / kcal mol^{-1}	α-**46**	β-**46**
1	1.17	1.12
2	0.16	0.37
3	0.07	0.27
4	2.09	2.25
5	2.58	2.72
6	2.89	2.99
7	0.00	0.00
8	0.56	0.23
9	2.27	0.43

For each of the computed conformers, all other rotational minima around θ were computed. Based on the optimized geometries, relaxed geometry optimizations were then performed to compute the +/– 10°/20° rotated conformations, giving 270 molecular geometries total for each α-**46** and β-**46**. This method, as opposed to a simple rotational scan of the dihedral angle at given angle increments, was chosen to avoid placing undue emphasis on data from energetically unfavorable conformers, thus potentially skewing the Karplus fit. Specifically, the region between $\theta = $ –60° and $\theta = $ +60°, which is expected to be unpopulated on the basis of the MD simulations for α-**46** and β-**46**, was omitted from impacting the fitting to a Karplus-type equation, in this way. Finally, Fermi contact value calculations were performed for all structures at the M05-2X/6-311G**[u+1s](PCM) level of theory to obtain values for the Fermi contact term for $^3J_{C1',H6R/S}$ in both α-**46** and β-**46**. Only the Fermi contact term was considered basis on findings from previous studies, as detailed in the Methods section.[151,152] The computed values were then plotted against the C5-C6-O6-C1' dihedral angle in accordance to the IUPAC convention for carbohydrate nomenclature.[153] The resulting data points for ($\theta \mid {}^3J_{C1',H6R}$) and ($\theta \mid {}^3J_{C1',H6S}$) showed the expected Karplus-type relationship and, notably, as apparent from the relatively small spread of the data, data from all 9 conformers gave congruent results.
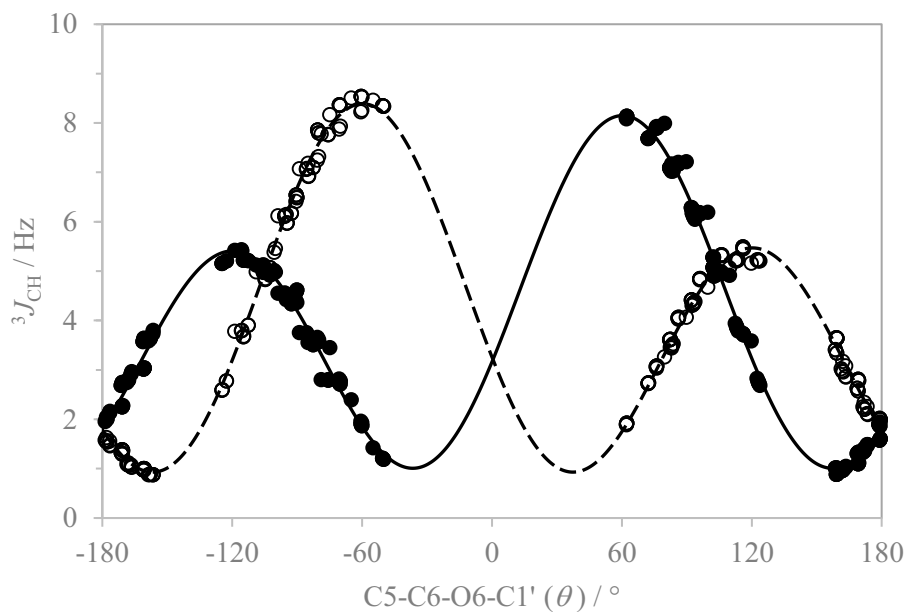
Figure 4.11. Computed coupling constants ^3J(C1',H6$_{R/S}$) for α/β-**46** plotted against θ (C5-C6-O6-C1', based on IUPAC definition) overlaid with the Karplus equation fit (H6$_R$ solid dots and line, H6$_S$ circles and dashed line).

This provides evidence for the small influence of the conformation away from θ and at the anomeric carbon on the coupling constants corresponding to the θ angle for α/β-**46**. As such, the 9 conformers of each anomer were not weighed based on their relative abundance from the MD simulation or the relative energies from their QM optimization. Instead, their computed coupling constants for $^3J_{C1',H6R}$ and $^3J_{C1',H6S}$ could be fit using a four parameter Karplus equation of the form $^3J = A \cdot \cos^2(\theta + B) + C \cdot \cos(\theta + B) + D$ (see Figure 4.11) for both anomers together to give the following two Karplus equations based on the C5-C6-O6-C1' dihedral angle:

$$^3J_{C1',H6_{proR}} = 5.69 \cdot \cos^2(\theta + 119.67°) - 1.37 \cdot \cos(\theta + 119.67°) + 1.09 \qquad (7)$$

$$r^2 = 0.996 \quad rms = 0.06$$

$$^3J_{C1',H6_{proS}} = 5.91 \cdot \cos^2(\theta - 120.29) - 1.46 \cdot \cos(\theta - 120.29) + 1.02 \qquad (8)$$

$$r^2 = 0.998 \quad rms = 0.11$$

As can be seen, the obtained coefficients were very similar for the two equations with the phase shift parameter B giving virtually the same absolute value. Because of this, the two sets of data could be combined by plotting the computed coupling constant values against the C1'-O6-C6-H6$_{R/S}$ dihedral angle θ^* to give a generalized Karplus equation for C(sp2)-O-C-H dihedral angles:

$$^3J_{C-O-C-H} = 5.81 \cdot \cos^2(\theta^* + 0.07°) - 1.42 \cdot \cos(\theta^* + 0.07°) + 1.05 \qquad (9)$$

$$r^2 = 0.997 \quad rms = 0.11$$

Because the parameter for the phase shift was determined to be virtually 0°, the data was refitted with a three-parameter version, which did not affect the fit to any significant amount while at the same time decreasing the number of parameters used:

$$^3J_{C1'-O6-C6-H6_{R/S}} = 5.81 \cdot \cos^2 \theta^* - 1.42 \cdot \cos \theta^* + 1.05 \qquad (10)$$

$$r^2 = 0.997 \quad rms = 0.12$$

It should be mentioned, that although the generalized equation is appropriate for the case where the diastereotopic environment of H6$_R$ and H6$_S$ does not largely influence the coupling constant for $^3J_{C,H}$, this is not necessarily the case for other molecules. Particularly, ongoing research in this laboratory indicates that the Karplus equation for the $^3J_{CH}$ coupling of the diastereotopic hydrogens of H-6$_{proS/R}$ to C-4 is best described by two distinct and separate Karplus equations.[a]

---

[a] Unpublished results – based on data related to D-glucose and D-galactose obtained with the same methodology as described here for **46**. "New Karplus equations for Conformational analysis of Monosaccharides", manuscript in preparation.
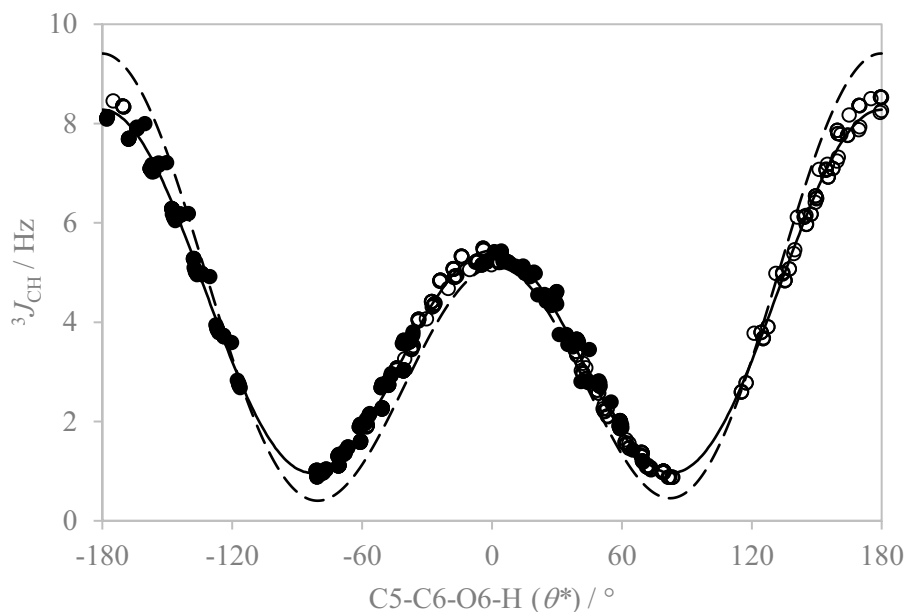
Figure 4.12. Overlay of fitted data for both $^3J(\text{C1'},\text{H6}_R)$ and $^3J(\text{C1'},\text{H6}_S)$ plotted against the θ^* (C5-C6-O6-H6$_{R/S}$) angle and fitted Karplus equation (solid line), along with Karplus equation published by Turney *et al.* (dashed line).

As seen in Figure 4.12, the resulting three parameter Karplus equation bears close resemblance to that obtained by Turney *et al.* which was fitted using a seven parameter equation.[133] Using the newly established Karplus equations (7) and (8), the MD simulations of α/β-**46** were used to backcalculate predicted values for $^3J_{\text{C1'},\text{H6}R/S}$ from the θ dihedral angle distribution. As seen in Table 4.5, the computed coupling constants based on MD data are in excellent agreement with those from the *J*-HMBC experiment. The identity of the two hydrogens on C-6 could be assigned unambiguously as H6$_R$ and H6$_S$ in both cases on the basis of homonuclear three-bond coupling constants. For this, the experimentally determined coupling constants were compared to theoretical values which were backcalculated using published Karplus equations for $^3J_{\text{H5},\text{H6}R/S}$ and $^2J_{\text{H6}R,\text{H6}S}$.[121] The resulting values do not compare as favorably to the experimentally determined coupling constants, as the $^3J_{\text{CH}}$ values, however the magnitude

of the coupling constants is sufficiently different to allow for the distinction between H6$_R$ and

H6$_S$. In the case of the $^3J_{HH}$ data, a more satisfactory fit could be obtained with a more specific

Karplus equation. This is seen in the additional data included in parentheses for $^3J_{HH}$ in Table 4.5

calculated with Karplus equations parameterized on QM data for α/β-D-glucose in our research

group, although the magnitude of the $^3J_{H5,H6R}$ coupling was not fully captured.[a]

Table 4.5. Experimental and theoretical data for ^3J coupling constants of α/β-**46**.

	α-**46**		β-**46**	
	exp.	MD[a]	exp.	MD[a]
$^3J_{C1',H6R}$	3.1	3.0 (2.8[133])	3.1	3.2 (2.8[133])
$^3J_{C1',H6S}$	2.8	3.1 (2.8[133])	2.9	3.2 (2.9[133])
$^3J_{H5,H6R}$	4.8	3.6[121] (3.5[b])	5.7	3.5[121] (3.4[b])
$^3J_{H5,H6S}$	2.4	3.1[121] (2.6[b])	2.1	2.8[121] (2.3[b])
$^2J_{H6R,H6S}$	12.0	-10.1[121]	12.3	-10.3[121]

a) Theoretical values are back-calculated from MD simulations using Karplus equations (7) and (8) or literature equations, as annotated.[121,133] b) calculated based on unpublished results for $^3J_{H5,H6R/S}$ based on data related to D-glucose and D-galactose obtained using the same methodology as described for 46. See Appendix C for a summary of the results.

Verification of equation using model test set. To test the newly established Karplus

equation, it was applied to the case of α/β-**47**, α/β-**48**, α/β-**49** and **50** shown in Figure 4.6 above.

For this, the compounds were treated using the established molecular dynamics procedure as

outline above for **46**. For the MD simulation of **47** and **50**, additional dihedral angle parameters

were needed to describe the ester-linkage on the anomeric carbon. This expansion of the

GLYCAM06 force field was performed following the same methodology used by Kirschner *et al.*

in the original GLYCAM06 publication on the basis of small model compounds and parameter

substitution.[146] Further details are discussed in the Methods section and the Supplemental

Information. Additionally, atomic charges of α/β-**47** and α/β-**50** were derived based on the RESP

two-step fitting procedure first published by Cornell et al., as described in the Methods section.[154]

Table 4.6. Summary of the relevant dihedral angle distributions for α/β-**47**, α/β-**48,** α/β-**49** and α/β-**57** based on their MD simulations.

Angle Preference		α-**47**	β-**47**	α-**48**	β-**48**	α-**49**	β-**49**	α-**57**	β-**57**
	g^+ / %	63	62	63	66	61	65	59	63
ω	g^- / %	15	15	16	15	18	16	34	30
	st / %	22	23	21	19	21	19	7	7
	g^+ / %	22	21	22	25	21	25	14	16
θ	g^- / %	18	19	17	18	19	18	24	25
	st / %	60	60	61	57	60	57	62	59
	g^+ / %	-	-	-	-	-	-	-	-
θ'	g^- / %	-	-	-	-	-	-	-	-
	st / %	100	100	100	100	100	100	100	100
		71	61	60	100	100	100	100	100
		(84°)	(-78°)	(83°)	(118°)	(-115°)	(-115°)	(120°)	(118°)
φ		29	39	40					
		(137°)	(-128°)	(132°)					
	g^+ / %	-	-	-	-	-	-	-	-
ψ	g^- / %	-	-	-	-	-	-	-	-
	st / %	100	100	100	100	100	100	100	100

Table 4.6 summarizes the results of the MD simulations for α/β-**47**, α/β-**48** and α/β-**49** with respect to the relevant dihedral angles. In α/β-**47**, φ was defined as O5-C1-O1-C3' in accordance with IUPAC recommendations.[153] By analogy, φ denotes the C1-C2-O2-C3' and C2-C3-C3-C3' dihedral angles in α/β-**48** and α/β-**49**, respectively. In Table 4.6, data for φ was summarized without assigning g^+/g^- or st, because of ambiguity in the definition of the respective dihedral angle. As can be seen, the θ, ω and θ' dihedral angles are unchanged from α/β-**46**. The φ angle is more restrained than θ in all cases, due to the neighboring hydroxyl groups. As illustrated in Table 4.6, φ is least flexible in α/β-**49** and β-**48**, where the acetyl group is flanked by two equatorial hydroxyl groups on both sides, leading to a unimodal distribution. In α/β-**47** and α-**48**, only one equatorial hydroxyl group results in a bimodal distribution around φ. In all compounds, ψ is constrained to the st conformation due to the carbonyl function, as already established for θ'.

In addition, the solution geometry of the undetected least stable regioisomer, namely 4,6-diacetyl-α/β-D-glucopyranose (57), was modeled by molecular dynamics, as well. Based on the MD simulation, φ was predicted to be even more restrained for 4-acetyl, as depicted in Figure 4.13. In addition, the close proximity of the 4-acetyl group altered the conformation of the 6-acetyl group, affecting both ω and θ populations. For ω, a shift in the minor population from *st* to g^- was predicted, along with a shift from g+ to g^- in the θ angle, as summarized in Table 4.6.
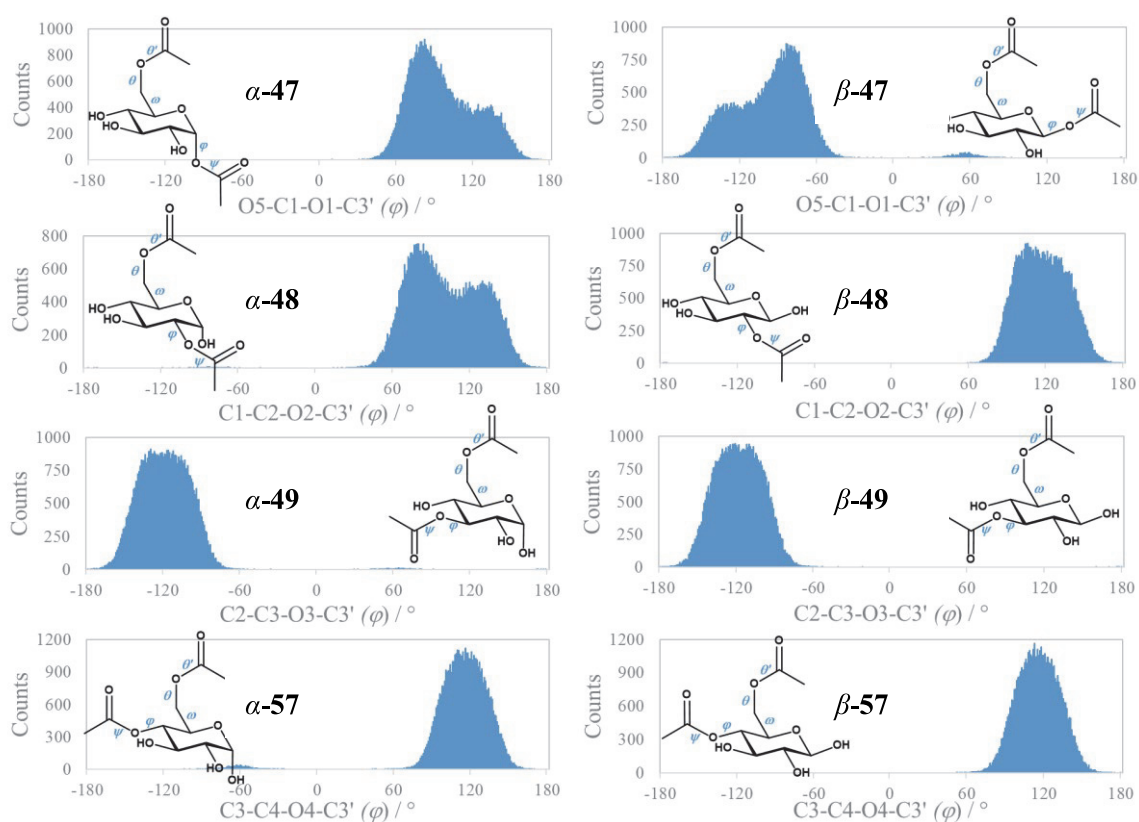
Figure 4.13. Summary of the φ dihedral angle for compounds α/β-**47**, α/β-**48,** α/β-**49** and α/β-**57** (top to bottom) showing the flexibility of the different acetyl linkages based on their MD simulations. A full graphical representation of the conformational analysis for each compound may be found in Appendix C.

The MD simulations of both α-**50** and β-**50** displayed the expected high flexibility in the θ (C6-O6-C1'-H1') angle, with the dihedral population equally distributed between the maxima

at g^+, g^- and *st*, since the methyl group attached to the carboxyl should be allowed to rotate freely. The θ' (C5-C6-O6-C1') angle was found to be constrained to ±180°, same as it was observed for α/β-**46**. However, unlike the ω angle in the aforementioned model compound, ω' (C4-C5-C6-O6) in α-**50** and β-**50** assumed only two maxima around –102° and +88°, roughly matching the g^- and g^+ conformers (α-**50**: 75% g^-, 25% g^+, β-**50**: 76% g^-, 24% g^+), as expected for the ester carboxylate.[146,155,156] There is no preference for the *st* conformation, due to the carbonyl moiety of the ester group. This is comparable to the effect of the carboxylate group, as described in the original GLYCAM06 publication, that also shows only two minima for this angle.[146] In the calculation of theoretical coupling constants for $^3J_{C6,Me-H}$ from α/β-**50**, the contribution from all three protons in the methyl group was averaged, as is the case in the experimental observable.[119]
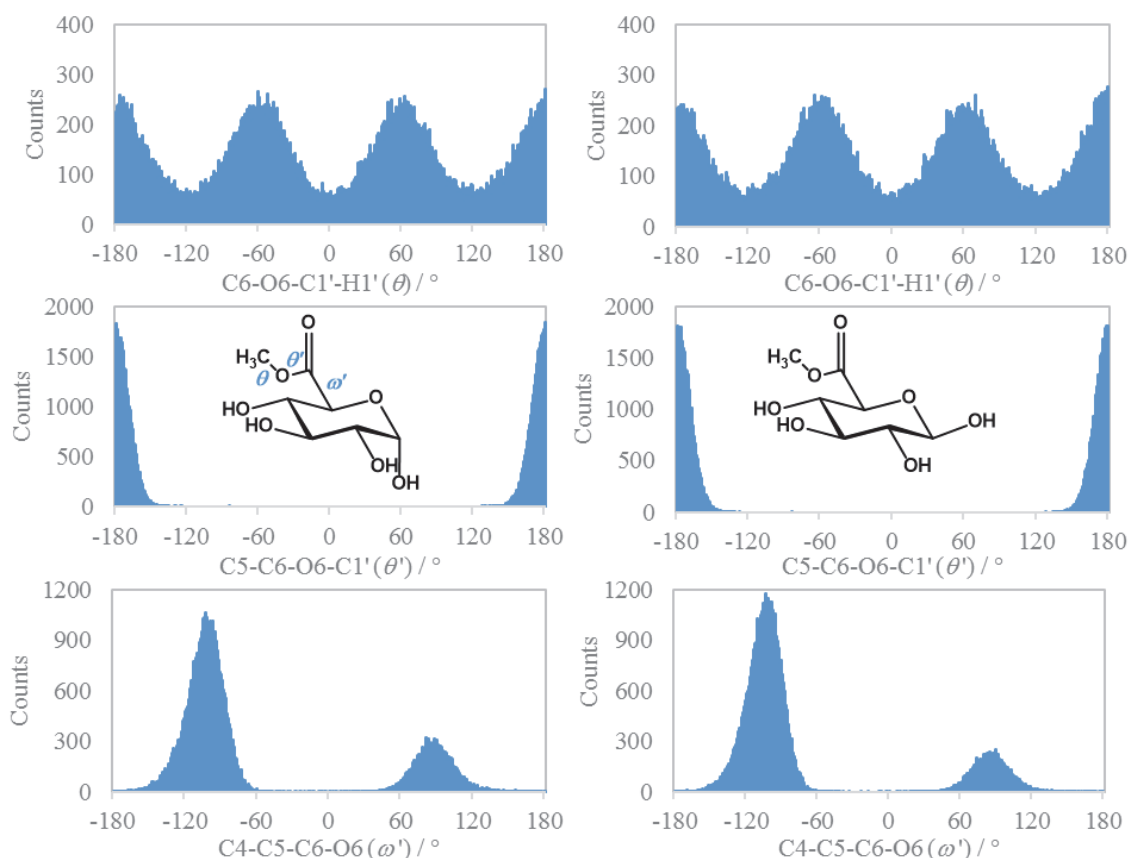
Figure 4.14. Histograms depicting the population distribution of the three relevant dihedral angles θ (C6-O6-C1'-H1'), θ' (C5-C6-O6-C1') and ω' (C4-C5-C6-O6) from the MD simulations of α-**50** and β-**50**.

As illustrated in Table 4.7, the experimental and back-calculated theoretical $^3J_{CH}$ coupling constant data for the test set was in generally good agreement within the range of the experimental error (about ± 0.6 Hz). The coupling constants determined for $^3J_{C1',H6R/S}$ in **47 - 49** were essentially unchanged from those in **46**, as was expected based on their MD simulations. The coupling constants determined from the MD simulations of α/β-**47** and α/β-**49** with equation (9) for the 1-and 3-acetyl linkage fall within the experimental error of the values determined from the *J*-HMBC experiment for α/β-**47** and α/β-**49**. In the case of the 2-acetyl linkage, a combined value was obtained for the $^3J_{C3',H2}$ correlation in α-**48** and β-**48**, as their crosspeaks overlap. The computationally derived coupling constant for α-**48** is comparable to the measured value, however the value determined for β-**48** falls outside the range of the experimental error. This

could be due to the overlap in the *J*-HMBC spectrum or the MD simulation being a less than perfect representation of the actual conformational behavior of *β*-**48**. For *α*-**50** and *β*-**50**, a satisfactory fit could be obtained between the computational and experimental coupling constant with the methyl group.

Table 4.7. Experimental and theoretical data (in parentheses) for the relevant $^3J_{CH}$ coupling constants in *α*/*β*-**47** , *α*/*β*-**48**, *α*/*β*-**49** and *α*/*β*-**50**.

exp. (MD)	*α*-**47**	*β*-**47**	*α*-**48**	*β*-**48**	*α*-**49**	*β*-**49**	*α*-**50**	*β*-**50**
$^3J_{C1',H6R}$	n.d.[a] (3.2,2.8)	3.0 (3.1,2.8)	3.1[b] (3.1,2.7)	3.2[b] (3.2,2.8)	3.1[b] (3.1,2.7)	3.2[b] (3.2,2.8)		
$^3J_{C1',H6S}$	2.6 (3.0,2.8)	2.6 (3.1,2.8)	2.8[b] (3.1,2.8)	3.0[b] (3.2,2.9)	2.8[b] (3.1,2.8)	3.0[b] (3.2,2.9)		
$^3J_{C3',H1}$	3.5 (4.0,3.5)	3.5 (4.2,3.8)						
$^3J_{C3',H2}$			3.6[c] (4.1,3.7)	3.6[c] (4.9,4.5)				
$^3J_{C3',H3}$					4.2 (3.5,3.6)	3.9 (3.6,3.7)		
$^3J_{C6,Me-H}$							3.9 (4.0, 3.9)	4.0 (4.0, 3.9)

Theoretical values are backcalculated from MD simulations using Karplus equation (10) for $^3J_{C1',H6R/S}$ (left) and using the equation from Turney *et al.* (right).[133] a) no data due to spectral overlap for $^3J_{C1',H6S}$ correlation in *α*-**47**; b) determined from crosspeak overlap of *α*-**48** and *α*-**49**, due to spectral overlap; c) determined from crosspeak overlap of *α*-**48** and *β*-**48**, due to spectral overlap.

Overall, the close fit between experimental and theoretical coupling constant data for the C(sp^2)-O-C-H coupling pathway in the test compounds lends support to the premise that both the newly established Karplus equation and the MD simulations presented herein are good approximations of the true relationships and conformational behavior of the studied compounds.

Application to (tetrahydropyran-2-yl)-methyl acetate. With the validation of the above Karplus equations and their application to acetylated glucopyranoses and methyl glucoronate in aqueous media completed, the potential extension to carbohydrates in other solvents was considered. As a first approximation, the application to the conformational analysis of the aforementioned (tetrahydropyran-2-yl)-methyl acetate **53** was reexamined with the newly developed Karplus equations (8), (9) and (10). Secondly, the MD simulations were carried out with three different force fields to compare their applicability to **53**.

In addition to the aforementioned GLYCAM06 force field, which has been thoroughly parameterized to represent carbohydrate compounds on the basis of QM calculations for small molecule analogs like **53**, two more generally applicable force fields, the General AMBER Force Field (*gaff*) and the MM2 force field were considered.[157,158] *gaff* and MM2 face the potential problem of being optimized for the lowest common denominator – they are design to be easily and broadly applicable to a wide variety of compounds, but will ultimately perform worse for a given compound than more specifically parameterized force fields designed to model that specific compound class.

The results of the three MD simulations with regard to ω and θ are summarized in Figure 4.15. As depicted by the dihedral angle histograms, the three force fields predicted drastically different conformational behavior for the two dihedral angles of **53**. While both GLYCAM06 and MM2 predicted a similar dihedral angle distribution for θ, as predicted for the compounds discussed above, *gaff* predicted a drastically shifted conformational equilibrium with the global maximum in the g^+ conformation (65°). More importantly, each force field predicted a completely different conformational region as the global maximum for the ω dihedral angle (GLYCAM06 g^+ 5%, g^- 87%, *st* 7%; *gaff* g^+ 11, g^- 7, *st* 82; MM2 g^+ 63%, g^- 0%, *st* 37%).
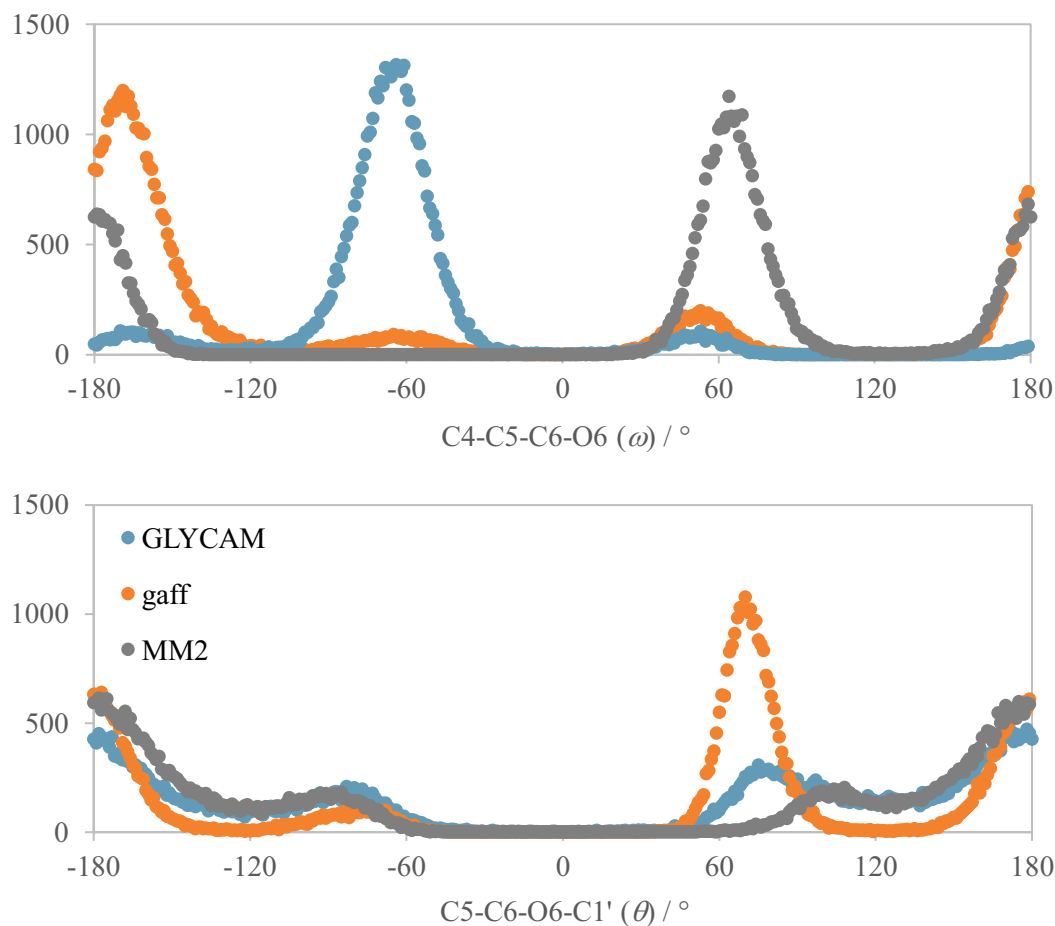
Figure 4.15. Graphical representation of the dihedral angle distributions of ω and θ for **53** - obtained from separate MD simulations using the three different force fields.

To determine, which of the three force fields lead to the most representative model of **53** in chloroform, the corresponding coupling constants for the ω and θ angles were back-calculated using the Karplus equations discussed above. The predicted coupling constants and the experimentally determined values are summarized in Table 4.8. From these data, GLYCAM06 was determined to most likely give the conformational model, that is closest to the true conformational equilibrium in solution, based on the following: MM2 and GLYCAM06 both predicted $^3J_{C5,H6R/S}$ values that are within the experimental error of those measured experimentally for θ, with GLYCAM06 giving the slightly better fit. For ω, both GLYCAM06 and MM2 gave

reasonable coupling constant predictions for $^3J_{H5,H6R/S}$, however resulting in opposite assignments of the H6R/S signals in the ^{1}H NMR. In the case of both dihedral angles, the MD simulation with *gaff* resulted in the worst agreement between predicted and experimental coupling constant data.

Table 4.8. Comparison of different force fields for modeling of **53** by comparison of their back-calculated coupling constants for ω and θ to the experimentally determined values.

(Hz)	exp.[a]	GLYCAM06	*gaff*	MM2
$^3J_{C1',H6R}$	3.1/2.9	3.0	5.0	3.7
$^3J_{C1',H6S}$		3.2	2.7	3.5
$^3J_{H5,H6R}$	6.9/3.6	2.0	6.6	5.9
$^3J_{H5,H6S}$		7.0	1.6	3.9

a) Assignment of H-6$_{R/S}$ was not possible from chemical shift data alone. b) calculated based on unpublished results for $^3J_{H5,H6R/S}$ based on data related to D-glucose and D-galactose obtained using the same methodology as described for 46. See Appendix C for a summary of the results.

To aid in the choice of the adequate force field for **53**, quantum mechanical geometry optimizations for all 9 combinations of ω and θ torsions were performed using M05-2X/6-31G*(PCM), followed with single point energy calculations at the M05-2X/6-311+G**(PCM) level of theory. The resulting relative Gibbs Free Energies are summarized in Table 4.9. Based on the results of the QM computations, the dihedral angle distributions were predicted to be 40% g^+, 23% g^- and 37% *st* for ω and 22% g^+, 15% g^- and 63% *st* for θ. Comparing these results to the dihedral angle distributions for the three force field methods in Figure 4.15 above, the MD simulations using GLYCAM06 and MM2 were found to closely reproduce the relative abundances for θ. However, none of the three force fields gave dihedral angle distributions congruent with the quantum mechanical data for ω, although again GLYCAM06 and MM2 performed significantly better than the generalized AMBER force field.

Table 4.9. Summary of the QM computations of the 9 relevant conformers of **53**.

Conformer	C4-C5-C6-O6 ω / °	C5-C6-O6-C1' θ / °	ΔG^{298} (M05-2X) kcal/mol	relative abundance
1	59 (g^+)	103 (g^+)	1.73	2%
2	56 (g^+)	-102 (g^-)	1.38	3%
3	57 (g^+)	-178 (st)	0.00	35%
4	-64 (g^-)	103 (g^+)	1.13	5%
5	-57 (g^-)	-82 (g^-)	1.08	6%
6	-63 (g^-)	179 (st)	0.63	12%
7	-176 (st)	82 (g^+)	0.49	15%
8	-176 (st)	-104 (g^-)	1.10	6%
9	-173 (st)	180 (st)	0.46	16%

The disparate computational predictions of the dihedral angle populations for **53** employing the different force fields detailed above underline the importance of choosing an appropriate computational method and validating its results, so as to avoid modeling something that does not mirror reality. This also illustrates that any molecular dynamics simulations should be validated against experimentally obtained data and higher level computations– and even then used with caution, due to the way that different population distributions can result in the same predicted coupling constants because of the periodic nature of the Karplus relationship.

Conclusions

In summary, a Karplus equation for the C(sp^2)-O-C-H coupling pathway in ester-linked carbohydrates was developed on the basis of quantum mechanical and molecular dynamics computations for 6-*O*-acetyl-D-glucopyranose **46**. The Karplus relationship was validated with a carbohydrate-based test set with the ester represented by an acetyl group on positions 1, 2, 3 and 6 of a carbohydrate moiety, as well as a pyranuronic acid methyl ester. The presented data support that a combination of computational (MD simulations using a carbohydrate specific force field) and experimental data (NMR data from *J*-HMBC experiments) can be used to establish the conformational space of ester-linked carbohydrates together with the Karplus equations

established herein. Additionally, the divergent results of different force fields for the

computational treatment of **53** illustrate the importance of carefully choosing an appropriate

computational method and validating it for the conformational analysis of the particular

molecules of interest. The application of the Karplus equations discussed above to the

conformational analysis of 6,6'-ester linked disaccharides and other ester-linkages in

carbohydrate derivatives is presented in the following chapter.

Chapter 5: Ester-linked Carbohydrates and their Conformational Analysis

Introduction

Carbohydrates are essential components of life and known to play numerous roles in biology, such as in energy storage (glycogen and starch) and macro-scale structural integrity of cells and organisms (cellulose and chitin). Furthermore, carbohydrate derivatives are found as structural motifs in important coenzymes (coenzyme A, NAD/NADH$^+$, ADP/ATP) and form part of the backbone of RNA and DNA. They are known to be involved in immune response, cell-to-cell signaling and many other vital functions.[159-161] However, many of the functions of carbohydrates are still not fully understood, partly because of the enormous structural diversity of the glycome.[162-164] The number of different isomeric forms of monosaccharides and the possible variations of linkages between monosaccharide units together are the main reason for the vast chemical space of carbohydrates.

Monosaccharides are the basic unit of carbohydrates, which can bond together to disaccharides, trisaccharides, and other oligo- and polysaccharides, also referred to as glycans. The most widely known type of monosaccharides are D-aldohexoses, of which there are 8 different ones, each of which can exist in either their *α*- or *ß*-hemiacetal form in solution, in equilibrium with their open chain form, as illustrated in Figure 5.1.
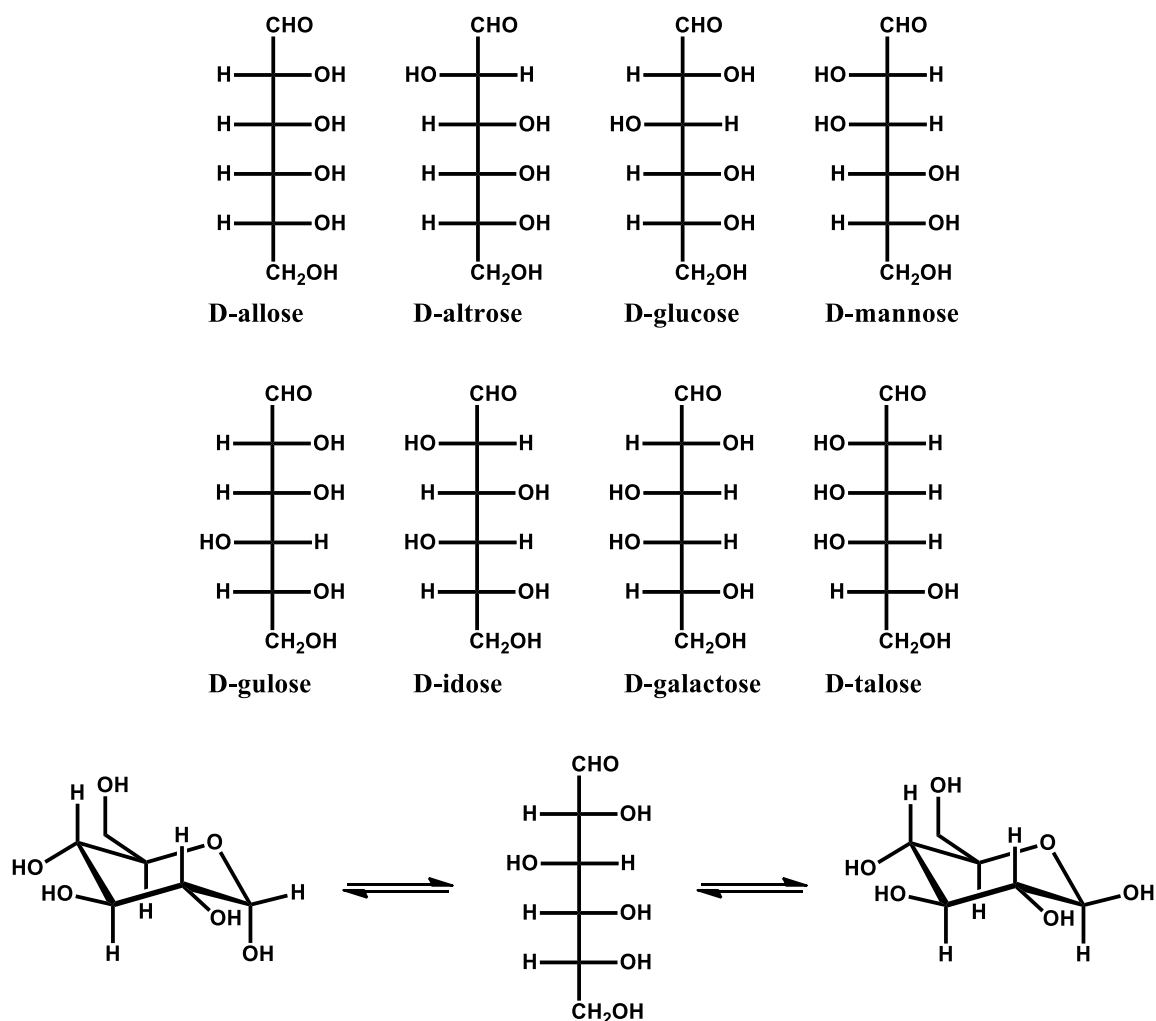
Figure 5.1. Graphical representation of the eight D-isomers of aldohexoses and the equilibrium between the α- and β-anomers of glucose and its open-chain form.

The linkage between monosaccharides is commonly referred to as the glycosidic linkage, which is comprised of an acetal-ether functional group between the anomeric hydroxyl group of one monosaccharide and any hydroxyl group on the other monosaccharide. Aside from the conformation of the 6-membered sugar ring, the glycosidic linkage is the primary cause for the large flexibility of carbohydrates, as alluded to in the previous chapter. When two monosaccharides are bound through their respective anomeric hydroxyl groups, such as in trehalose, this is termed a 1→1 or head-to-head linkage. More commonly, disaccharides are

formed from heat-to-tail glycosidic linkages (1→2, 1→3, 1→4 or 1→6). These linkages are defined by two (or three, in the case of 1→6) dihedral angles. Additionally, Cumpstey *et al*. proposed the term 'diglycose' for disaccharides which carry a non-glycosidic tail-to-tail linkage.[165,166] This type of linkage is very rare in nature.[166]
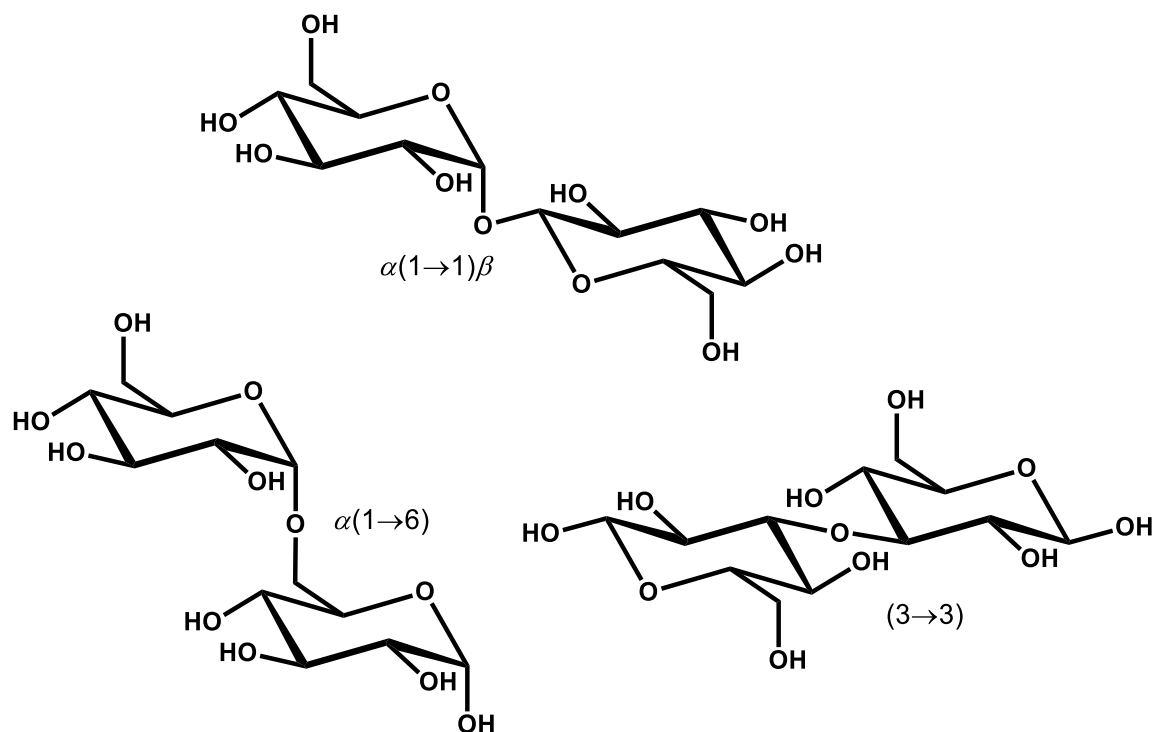
Figure 5.2. Examples of head-to-head (top), head-to-tail (left) and tail-to-tail (right) linkages between monosaccharides.[165,166]

As mentioned above, sugars are involved in a large number of biochemical processes. In these, they can interact with a number of enzymes and other proteins, which can either form or cleave glycosidic linkages (glycosyltransferases and glycosidases, respectively) or act as glycan recognition sites (lectins and glycosaminoglycan-binding proteins).[167-172] In all such interactions, the shape of the sugar molecule is of considerable importance. As mentioned, the variability in constitution and stereochemistry between different carbohydrates can result in large

conformational differences. For example, many glycosidases, such as mammalian muscle acid α-glucosidase, show high activity toward maltose and other $\alpha(1{\rightarrow}4)$-glucans, but will have low activity toward isomaltose or cellulose, which are $\alpha(1{\rightarrow}6)$- and $\beta(1{\rightarrow}4)$-linked, respectively.[173,174]

For this reason of substrate specificity and the importance of molecular shape on their biochemical activity, the conformational analysis of naturally occurring carbohydrates has received considerable attention.[103-108,149,175-181] Beyond that, molecules designed to act similar to naturally occurring carbohydrates, so called carbohydrate analogs or mimics, have been explored for a variety of reasons, such as therapeutic applications or the elucidation of enzyme mechanisms and biochemical pathways.[182] In a number of cases, glycosidases were found to be inhibited by carbohydrate analogs that were modified to replace the endocyclic oxygen. Examples for this are 1-deoxynojirimycin, a natural α-glucosidase inhibitor, which was first isolated from mulberry leaves, and the anti-diabetic medications acarbose and miglitol, which act on α-glucosidases and slow the digestion of carbohydrates into monosaccharides.[183-185] In all three cases an oxonium-ion mimicking substitution allowed for the compound's inhibitory activity.
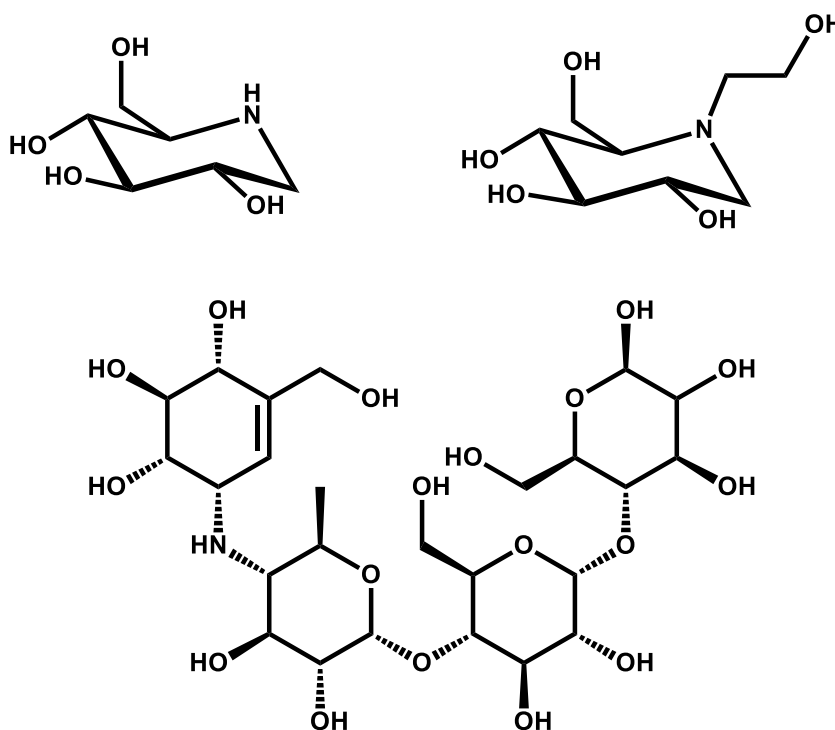
Figure 5.3. Examples of carbohydrate analogs that are α-glucosidases inhibitors: 1-Deoxynojirimycin, miglitol and acarbose (clockwise). [183-185]

With regards to possible carbohydrate mimics, understanding the changes to the solution phase structure induced by structural changes in the compounds, such as atom substitution, is of critical importance.

To that end, a variety of disaccharide analogs has been investigated in terms of their solution phase structure, to gain a better understanding of the induced changes to the conformations of the molecules. The ultimate goal of these endeavors is generally to improve the rational design of carbohydrate mimics to increase bioactivity. Many researchers have investigated the influence of changes to the glycosidic linkage between monosaccharides, for two main reasons: The glycosidic linkage represents a 'hinge' between the two monomer units and as such, any changes to the cross linkage would be expected to have a profound effect on the overall conformation. Additionally, substitution of the functional group, by replacing the glycosidic

oxygen with sulfur or carbon can increase the bioavailability of carbohydrate analogs by increasing their hydrolytic stability.

As mentioned previously, conformational analysis techniques are commonly used to characterize these changes in carbohydrate analogs. As stated in Chapter 4, X-ray crystallography has been a valuable analytical technique to determine solid phase structures – and these have at times proven to give vital insights into solution phase structures, as well. However, the limitations of comparing a rigid crystal structure to the free solution behavior of flexible molecules are readily apparent. In its place, NMR spectroscopy has been used widely for conformational analyses and to describe the molecular shape of molecules in solution. In particular, NOE experiments and coupling constant analysis generally allow chemists to propose reasonable solution phase structures.[104-106,108,186] However, there continues to be a need to supplement the experimental data with computational modeling, particularly in the case of molecules that have large conformational spaces and low rigidity, such as carbohydrates, where more than only a handful of conformers will be assessable to the molecule of interest.[103,105-107,187]

A large number of studies have been published on the conformational analysis of carbohydrate analogs using a combination of NMR and computational modeling. For example, Sabesan et al. investigated the effect of the introduction of a methyl group on the 6-position of a α(1→6)-linked sialoside analog to ascertain the structural requirements in neuraminidase hydrolysis through conformational locking, which was verified through coupling constant analysis using available Karplus equations.[188] Similarly, Vidal et $al.$ investigated the effect of a change from a $ß$(1→3)-linked disaccharide to its CH_2-linked C-glycoside analog. Using a combination of NMR and molecular mechanics, the researchers were able to show that this induced larger flexibility around the ψ dihedral angle, as illustrated in Figure 5.4.[189] Additionally, work by Asensio and others has been reported on the conformational analysis of aza-C-glycosides, designed as glycosidase inhibitors, and other C-glycosides, as well as carbasugars and $N(OCH_3)$-linked disaccharides, among others.[190-193]
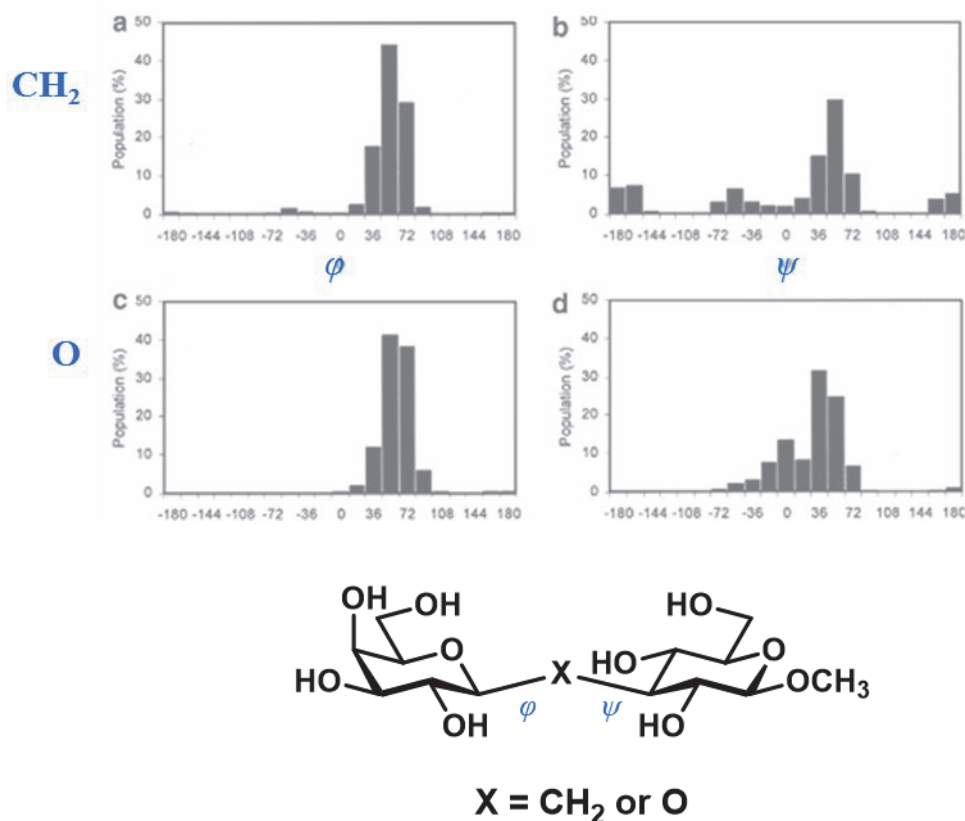
Figure 5.4. The C-glycoside analog of methyl *ß*-D-galactopyranosyl-(1→3)-*ß*-D-glucopyranoside was found to have higher flexibility in its ψ dihedral angle distribution by Vidal *et al.*.[189]

A common thread through all the carbohydrate analogs discussed hitherto is the substitution of the glycosidic linkage. As mentioned, the main rationale for this is the increased resistance to enzymatic and non-enzymatic hydrolysis of the sugar cross linkage. However, as discussed in Chapter 1, carbohydrates are also often found to be linked to proteins or fats and other structural motifs through ester linkage. However, the possibility of ester-linkage for the cross-linkage of monosaccharides has received little attention and only a small number of naturally occurring ester-linked di- or polysaccharides have been reported in the literature.[194-196]
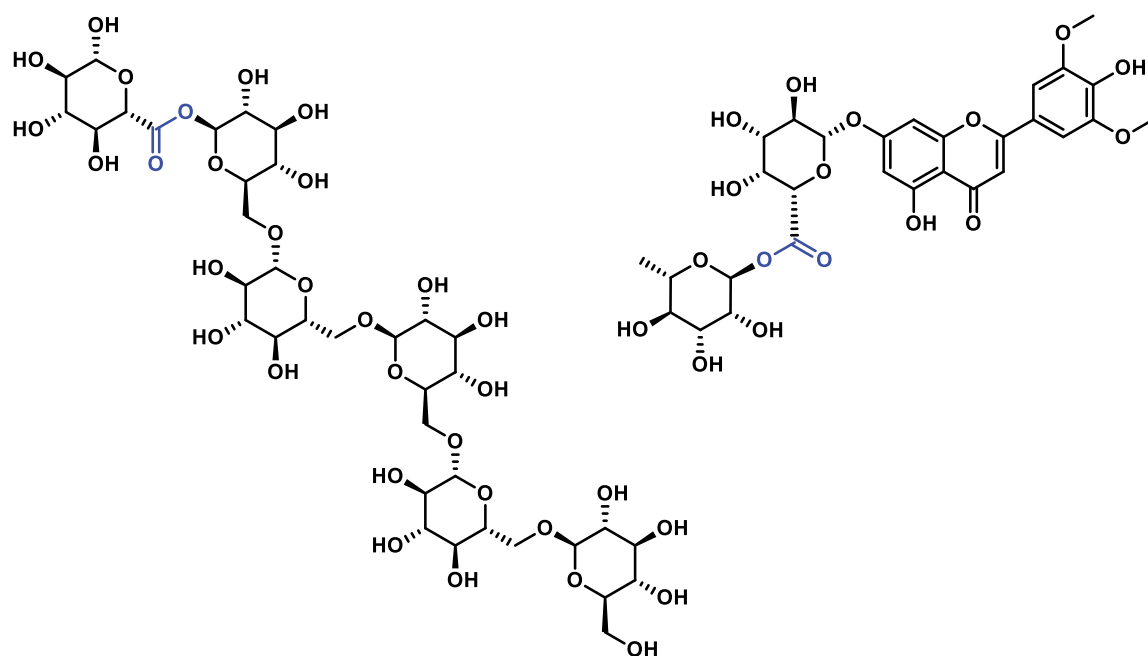
Figure 5.5. Examples of ester-linked carbohydrates: Tricin-7-*O*-rhamnosylgalacturonide (right), isolated from sugar cane and a glucuronopyranosyl polyglucopyranosyl constituent (left) found in Goji berries.[194-196]

Beyond that, ester-linked disaccharides or disaccharide analogs have previously been studied by Baddeley and others for their use in trehalose-based compounds for drug delivery matrices.[197,198] Kondratenko *et al.* synthesized ester-linked carbohydrates as modified triterpene saponins for antiulcer activity.[199] Additionally, ester disaccharides were studied for their potential to be used in a synthetic pathway to afford stereoselective glycosylation through a 'redox glycosylation' pathway.[200-203] Lastly, Brown *et al.* studied a small number of O-uronyl derivatives due to their potential implication as natural non-methyl O-galacturonyl esters in pectins or xylans.[204] However, the effect of the ester-linkage on the conformational behavior of the aforementioned ester-linked disaccharide analogs was not considered in the respective studies.

As such, the present work aimed to address two issues with regards to the conformational analysis of ester-linked carbohydrate analogs. Firstly, to investigate if the Karplus equation

developed in Chapter 4 and the computational methods on the basis of MD simulations using the 'extended' GLYCAM06 force field would be adequate in developing conformational models for ester disaccharides, as well as other acylated carbohydrate derivatives, both in water and organic solvents, such as chloroform. To that end, several acetylated carbohydrate derivatives were studied. Secondly, on the basis of such conformational models, the influence of the ester functional group on the flexibility of the linkage between two sugar monomers was to be elucidated. Based on the general conformational behavior of the ester functional group, it was hypothesized that it would decrease the flexibility of a carbohydrate analog when compared to a more conformationally labile ether or anomeric acetal linkage. This hypothesis was tested on a novel 6,6'-ester linked model disaccharide analog, which was synthesized using an oxidative esterification reaction similar to that discussed in Chapter 3.

Results & Discussion

Acetylated carbohydrate derivatives. To further investigate the utility of the newly developed Karplus equation detailed in Chapter 4, its use in the conformational analysis of per-*O*-acetylated monosaccharides was probed. At the same time, the secondary intent was to ascertain whether the GLYCAM06 force field, parameterized for the description of carbohydrate moieties in aqueous solution, would yield reasonable solution phase structures for acetylated carbohydrate derivatives in organic solvents, to gauge the potential for its use in the conformational analysis of per-acetylated di- and trisaccharides or polysaccharides in chloroform.
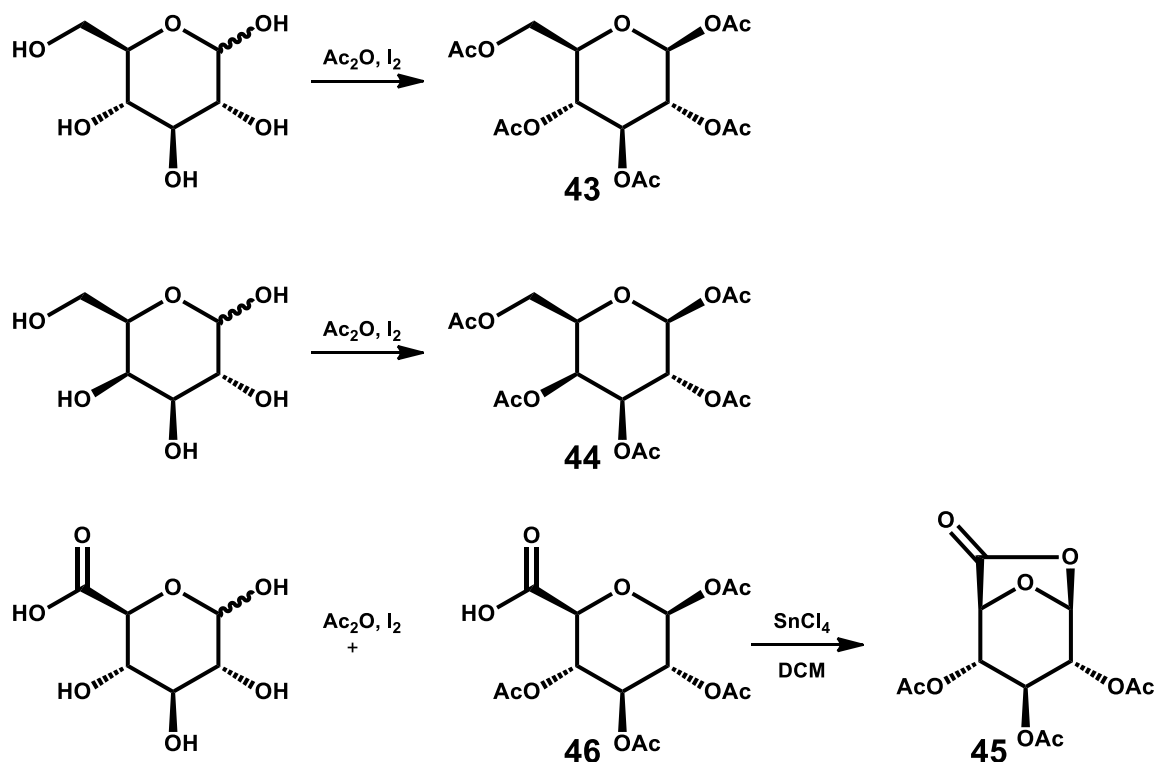
Figure 5.6. Synthetic routes to the three acetylated carbohydrate derivatives **58 – 60** that were studied by conformational analysis.

For this study, the per-acetylation of D-glucose and D-galactose was carried out in acetic anhydride with catalytic amounts of iodine, following established literature procedures, to afford acetyl 2,3,4,6-tetra-*O*-acetyl-*α/β*-D-glucopyranoside **58** and acetyl 2,3,4,6-tetra-*O*-acetyl-*α/β*-D-galactopyranoside **59** in 95% and 86% yield, respectively, with the *α*-anomer being the predominantly formed product in both cases (**58**: *α:β* 75:25; **59**: *α:β* 87:13).[205] In addition, tri-*O*-acetyl-D-glucurono-6,1-lactone **60** could be obtained in two steps from D-glucopyranuronic acid: Employing the acetylation conditions outlined above yielded 2,3,4,6-tetra-*O*-acetyl-*α*-D-glucopyranuronate **61** in 86% yield, which could in turn be transformed into the desired **60** through intramolecular transesterification mediated by SnCl4 in 21% yield.[206] All three compounds of interest were analyzed by NMR spectroscopy in deuterated chloroform. Both per-acetylated monosaccharides **58** and **59** were present in the expected $^4C_1$ chair conformation, as

indicated by the observed coupling in their ^{1}H NMR spectra. Closer examination of the ^{1}H NMR spectrum for **60** revealed notable second order signal splitting that could be attributed to W-coupling between the ring protons, as shown in Figure 5.7. This is due to the fact that **60** adopts the ^{1}C$_4$ conformation in solution because of the lactone formation, causing the acetyl groups to be in the axial position, with all hydrogens on the ring *gauche* to one another.
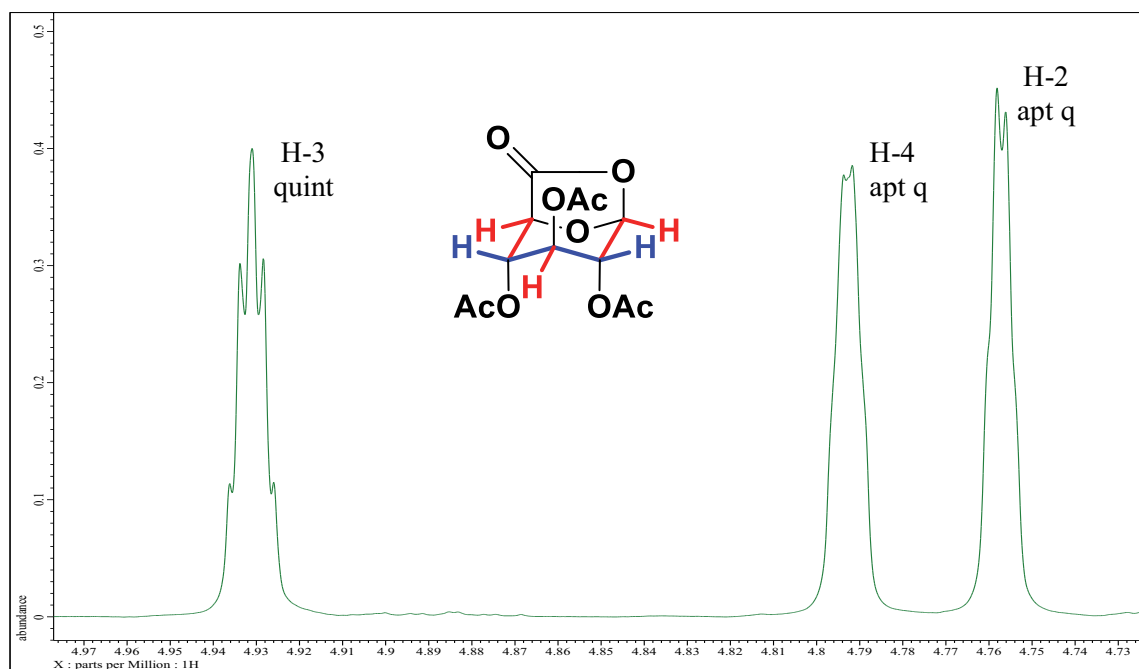
Figure 5.7. Close-up view of the second order splitting pattern of the ring protons in the ^{1}H NMR spectrum of **60**, with W-coupling highlighted between H-2 and H-4 and H-3 with H-1 and H-5.

To describe the solution structure of the per-acetylated **58** – **60**, they were treated computationally using the 'extended' GLYCAM06 forcefield. MD simulations were run over 500 ns trajectories using the same methodology as for the previously discussed compounds in Chapter 4. Because the NMR analysis of all three compounds was performed in deuterated chloroform solvent, the chloroform solvent model of AMBER14 was employed. In the case of **58** and **59**, only the α-anomer was investigated by MD, because it was the major anomer in solution.

The resulting 500 ns MD trajectories were analyzed to establish major conformational regions, as described previously on the basis of the important dihedral angle distributions describing the ester linkages.

Per-O-acetylated glucose and galactose (58 and 59). The analysis of the MD trajectories for the two per-*O*-acetylated monosaccharides investigated in this work resulted in the identification of a maximum of 72 and 24 conformers for α-**58** and α-**59**, respectively. The relevant dihedral angle histograms for the ω, θ and φ_n angles are shown in **Figure 5.8** and Figure 5.9. Of the identified conformational regions, those that were predicted to contribute more than 1% to the total sampled conformational space of α-**58** and α-**59** were summarized in **Table 5.1** and Table 5.2 on pages 132 and 134, respectively.
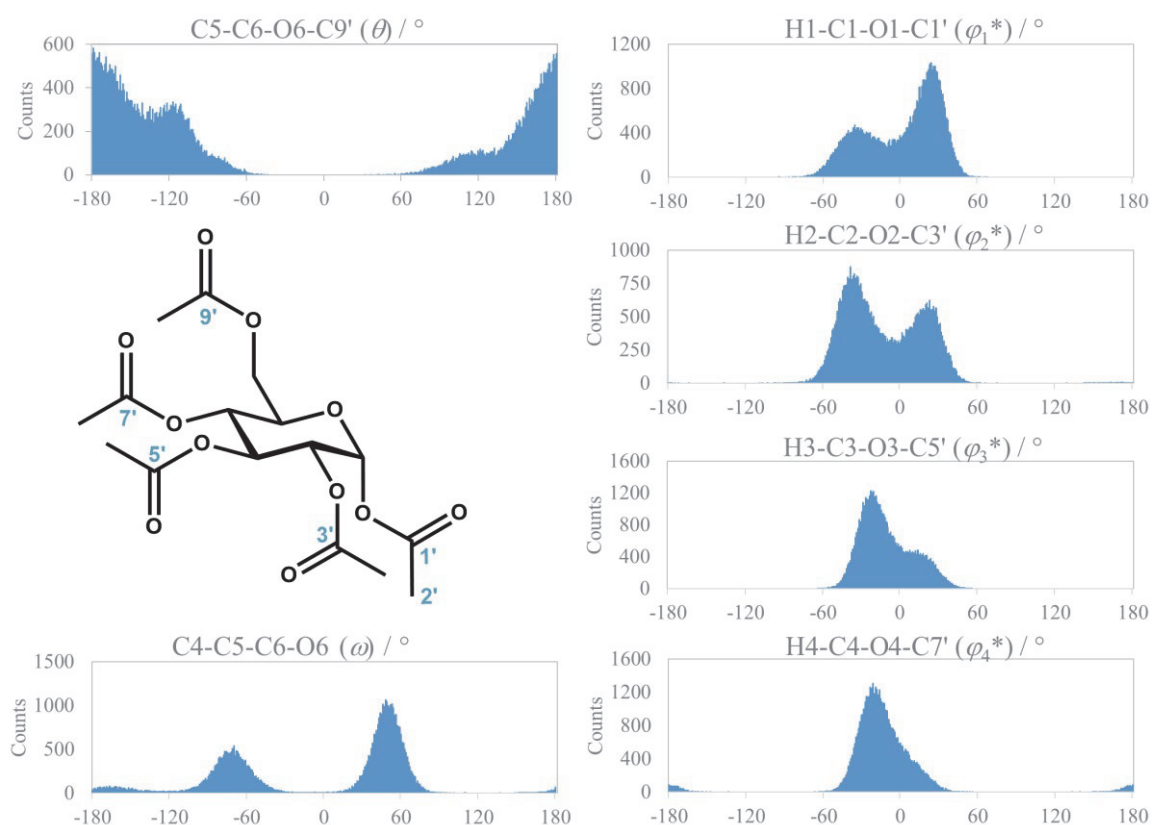
Figure 5.8. Relevant dihedral angle histograms of the ω, θ and $\varphi_n{}^*$ angles for **58** derived from the MD simulation of its α-anomer.

Compared to 6-*O*-acetyl-α/β-D-glucopyranose **46**, the MD simulation for acetyl 2,3,4,6-tetra-*O*-acetyl-α-D-glucopyranoside α-**58** predicted the g^- conformer (34%) to be more dominant at the expense of the *st* conformer (6%), while g^+ (60%) was predicted to be the dominant conformer for ω, as shown in Figure 5.8. This is possibly a result of unfavorable interactions between the 6-*O*-acetyl group and the endocyclic oxygen. Additionally, the presence of the 4-acetyl group biased the trimodal distribution of the θ angle away from the more sterically demanding g^+ population (13%) and to the g^- population (32%), as was expected based on the investigation of 4,6-di-*O*-acetyl-D-glucose **57** in Chapter 4. The MD simulation predicted *st* to be the major conformer of θ (55%), as shown in Figure 5.8. The φ_1 and φ_2 angles also closely matched the dihedral angle distributions for the diacetylated compounds **47**, **48**, **49** and **57** in Chapter 4, which carried acetyl groups on positions 1 and 2, respectively. For φ_3, the dihedral angle distribution was slightly bimodal and biased to rotate the 3-*O*-acetyl group toward C-2, due to the presence of the 2-*O*-acetyl and 4-*O*-acetyl groups. This was predicted similarly for the 4-*O*-acetyl group and φ_4, which was slightly biased toward C5. Interestingly, the 4-*O*-acetyl group was predicted to have a small contribution from the *E* conformer (< 4%), as well.

Table 5.1. Summary of the conformer regions (contributing > 1% to the total trajectory) of acetyl 2,3,4,6-tetra-*O*-acetyl-*α*-D-glucopyranoside *α*-**58** established based on its MD simulation. (For a tabular representation of the complete conformational space, see Table in Appendix C.)

Conformer #	C4-C5-C6-O6 ω / °	C5-C6-O6-C11' θ / °	O5-C1-O1-C1' φ_1 / °	C1-C2-O2-C3' φ_2 / °	C3-C4-O4-C7' φ_4 / °	Count	% abundance
1	53	180	142	83	100	5561	**12%**
2	53	180	142	139	100	2917	6%
3	53	180	89	83	100	2243	2%
4	53	180	89	139	100	2813	6%
5	53	-116	142	83	100	4368	**10%**
6	53	-116	142	139	100	2330	5%
7	53	-116	89	83	100	1826	4%
8	53	-116	89	139	100	2215	5%
9	53	118	142	83	100	1167	3%
10	53	118	142	139	100	611	1%
11	53	118	89	139	100	517	1%
12	-68	180	142	83	100	3735	**8%**
13	-68	180	142	139	100	1938	4%
14	-68	180	89	83	100	1571	3%
15	-68	180	89	139	100	2037	4%
16	-68	-116	142	83	100	1501	3%
17	-68	-116	142	139	100	726	2%
18	-68	-116	89	83	100	533	1%
19	-68	-116	89	139	100	642	1%
20	-68	118	142	83	100	934	2%
21	-68	118	89	83	100	474	1%
22	-68	118	89	139	100	455	1%
23	-163	180	142	83	100	696	2%
						41810	84% coverage

Compared to 58, acetyl 2,3,4,6-tetra-*O*-acetyl-*α*-D-galactopyranoside 59 has the opposite stereochemistry at the 4-position, with the acetyl substituent in the axial position. As a result, the conformational space of *α*-59 differed from *α*-58 primarily in the populations of the 4-*O*-acetyl group and the ω and θ angles. Notably, only the g^- conformer of the ω angle was predicted to be

populated in α-59, presumably due to the inversion of the neighboring stereocenter – the g^+ conformer, which dominates in α-58, would place the 6-*O*-acetyl group in close proximity to the axial 4-*O*-acetyl. Likewise, the population of θ was predicted to be shifted to avoid steric bulking at the g^- conformer (7%), favoring the g^+ and *st* conformer, predicted to contribute 53% and 40%, respectively. The 1-, 2- and 3-*O*-acetyl groups were predicted to be largely unchanged for α-59, as compared to α-58. Meanwhile, the φ_4 angle in the galactose analog was predicted to be biased opposite to that in α-58, as a result of the inversion of the stereocenter at the 4-position and the resulting change in the preferred conformer for ω.
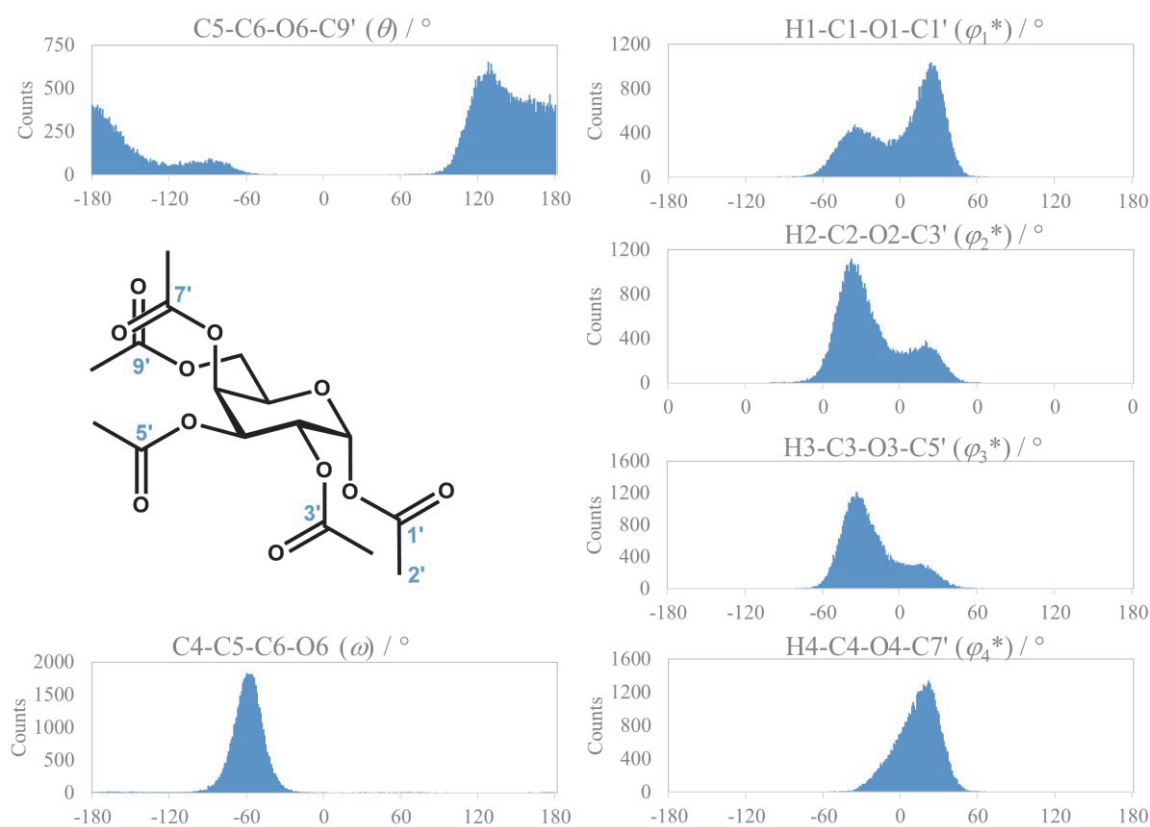
Figure 5.9. Relevant dihedral angle histograms of the ω, θ and $\varphi_n{}^*$ angles for 59 derived from the MD simulation of its α-anomer.

Table 5.2. Summary of the conformers (contributing > 1% to the total trajectory) of acetyl 2,3,4,6-tetra-*O*-acetyl-*α*-D-galactopyranoside *α*-59 established based on its MD simulation. (For a tabular representation of the complete conformational space, see Table in Appendix C.)

Conformer #	C4-C5-C6-O6 ω / °	C5-C6-O6-C11' θ / °	O5-C1-O1-C1' φ_1 / °	C1-C2-O2-C3' φ_2 / °	C2-C3-O3-C5' φ_3 / °	Count	% abundance
1	-56	130	145	85	-148	10102	**23%**
2	-56	130	145	85	-99	1850	4%
3	-56	130	145	143	-148	1795	4%
4	-56	130	145	143	-99	970	2%
5	-56	130	90	85	-148	4676	**11%**
6	-56	130	90	85	-99	1059	2%
7	-56	130	90	143	-148	1868	4%
8	-56	130	90	143	-99	1228	3%
9	-56	180	145	85	-148	7379	**17%**
10	-56	180	145	85	-99	1562	4%
11	-56	180	145	143	-148	1389	3%
12	-56	180	145	143	-99	898	2%
13	-56	180	90	85	-148	3174	7%
14	-56	180	90	85	-99	791	2%
15	-56	180	90	143	-148	1281	3%
16	-56	180	90	143	-99	955	2%
17	-56	-87	145	85	-148	1346	3%
18	-56	-87	90	85	-148	557	1%
						42880	86% coverage
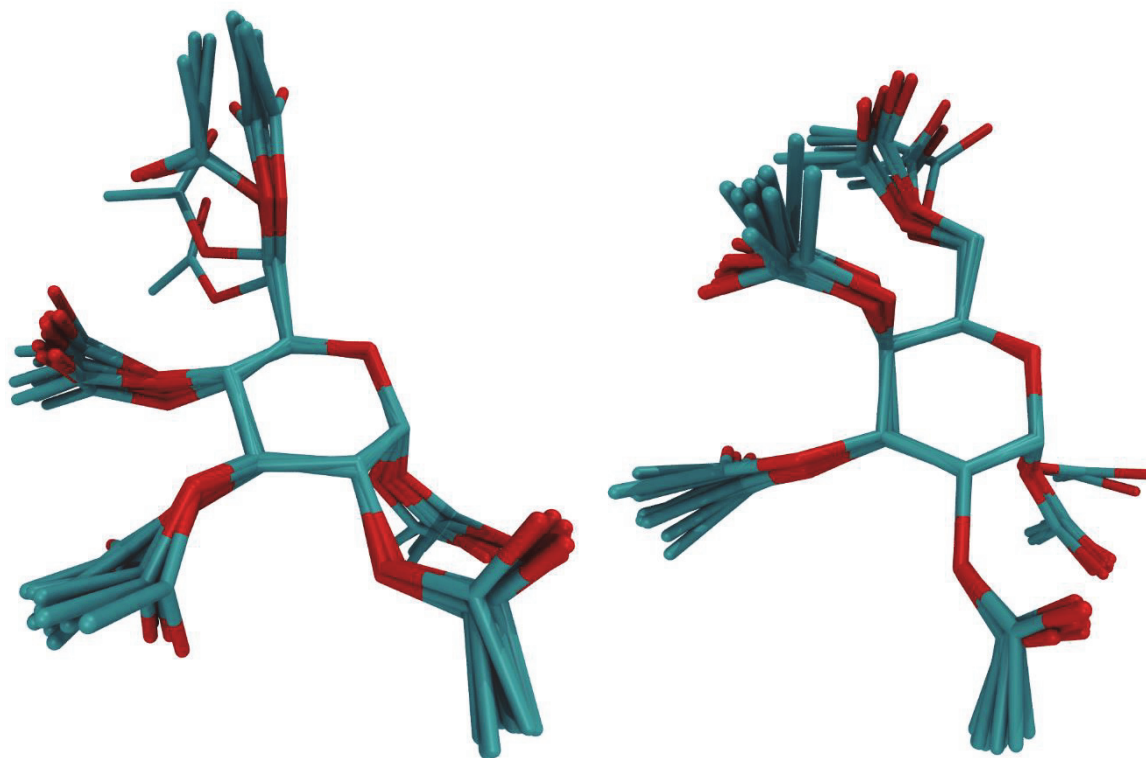
Figure 5.10. Graphical representation of the three most abundant conformational regions of α-**58** (left) and α-59 (right), illustrating the differences in ω predicted by the MD simulations. Hydrogen atoms removed for clarity.

To evaluate the above models for the conformational behavior of **58** and 59, the relevant coupling constants for the ω, θ and φ_{1-4} angles were back-calculated from the computationally predicted dihedral angle distributions using the respective Karplus equations (10) and (11) discussed in Chapter 4. The resulting theoretical ^3J values are summarized together with the experimentally measured values in Table 5.3 and Table 5.4 for **58** and 59, respectively.

Table 5.3. Summary of experimental and theoretical ^3J values (back-extracted from MD trajectory) for acetyl 2,3,4,6-tetra-*O*-acetyl-α/ß-D-glucopyranoside **58**.

(Hz)	Ac$_5$-α-D-Glc exp.[a]	MD	Ac$_5$-ß-D-Glc exp.[a]
$^3J_{C1',H1}$	3.4	4.3	3.5
$^3J_{C3',H2}$	3.6	4.2	n.d.[b]
$^3J_{C5',H3}$	3.8	4.7	3.8
$^3J_{C7',H4}$	4.1	4.9	n.d.[b]
$^3J_{C9',H6R}$	3.2	3.2	3.1
$^3J_{C9',H6S}$	2.3	2.9	n.d.[b]
$^3J_{H5,H6R}$	2.1	2.7[c]	n.d.[b]
$^3J_{H5,H6S}$	3.6	3.4[c]	3.6

a) measured in CDCl$_3$. b) not determined due to spectral overlap. c) calculated based on the Karplus equation for $^3J_{H5,H6R/S}$ as discussed in Chapter 4. See Appendix C for a summary of the results and equation (11) from Chapter 4.

Based on the data in Table 5.3, there was a reasonable match between the experimental and theoretical coupling constants for the C(sp^2)OCH coupling pathway of the five acetyl groups θ and φ_{1-4}). Although some of the computationally derived values were outside the experimental values, when accounting for experimental error, this could be a result of the nature of the Karplus equation. Specifically, the predicted φ_n angles fall on a steep region of the equation, which results in large deviations of the coupling constant for small changes in the dihedral angle. Notably, the predicted ω angle distribution of α-**58** resulted in theoretical coupling constants for $^3J_{H5,H6R}$ (using Karplus equation (11) from Chapter 4, detailed in the Appendix C) that closely matched those determined experimentally. Taken all together, the conformational behavior of acetyl 2,3,4,6-tetra-*O*-acetyl-α-D-galactopyranoside α-**58** appeared to be reasonably well modeled, within limitations, with the 'extended' GLYCAM06 force field – originally parameterized for water – in chloroform.

Table 5.4. Summary of experimental and theoretical ^3J values (back-extracted from MD trajectory) for acetyl 2,3,4,6-tetra-O-acetyl-α/β-D-galactopyranoside **59.**

| (Hz) | Ac$_5$-α-D-Gal | | Ac$_5$-β-D-Gal |
	exp.[a]	MD	exp.[a]
$^3J_{C1',H1}$	3.4	4.4	3.5
$^3J_{C3',H2}$	n.d.[b]	4.0	n.d.[c]
$^3J_{C5',H3}$	n.d.[c]	4.2	n.d.[c]
$^3J_{C7',H4}$	n.d.[b]	4.8	3.3
$^3J_{C9',H6R}$	3.4[b]	2.5	n.d.[b]
$^3J_{C9',H6S}$		3.8	n.d.[b]
$^3J_{H5,H6R}$	6.6[d]	2.2[e]	n.d.[b]
$^3J_{H5,H6S}$	6.6[d]	8.0[e]	n.d.[b]

a) measured in CDCl$_3$. b) due to spectral overlap. c) not determined due to insufficient signal. d) determined from dt splitting of H-5. e) calculated based on the Karplus equation for $^3J_{H5,H6R/S}$ as discussed in Chapter 4. See Appendix C for a summary of the results and equation.

In the case of acetyl 2,3,4,6-tetra-O-acetyl-α/β-D-galactopyranoside **59**, the coupling constants for the $\varphi_{2\text{-}4}$ angles of the 2,3,4-O-acetyl groups of α-**59** could not be determined experimentally, due to spectral overlap or insufficient signal, while the coupling constants for $^3J_{C9',H6R/S}$ could only be determined as an average value, due to AB-mixing of the closely spaced proton signals. The MD back-calculated coupling constants for the θ and $\varphi_{1\text{-}4}$ angles were predicted to be similar to those of α-**58**, as would be expected based on the similar dihedral angle distributions. The match to the experimental data was reasonable, with the aforementioned caveats with regards to the slope of the Karplus relationship, for φ_1 and θ. However, the predicted theoretical $^3J_{HH}$ values for the ω angle were significantly different from the experimentally determined values. Based on the experimental values of 6.6 Hz for both $^3J_{H5,H6R}$ and $^3J_{H5,H6S}$, the ω angle would be predicted to be roughly evenly distributed between the st and g^- conformers. g^- would give coupling constants of about 2.2 Hz and 8.0 Hz for $^3J_{H5,H6R}$ and $^3J_{H5,H6S}$, as was the case for the predicted values in Table 5.4, while st would result in $^3J_{HH}$ values of about 8.3 Hz and 1.4 Hz, respectively. Alternatively, the g^+ conformation would result in small

coupling constants around 1-3 Hz for both $^3J_{H5,H6R}$ and $^3J_{H5,H6S}$. Thus, an approximately 1:1 distribution between the *st* and *g$^-$* conformers would be predicted to closely match the experimentally determined coupling constants. However, as previously discussed, the MD simulation predicted the ω angle to exclusively adopt the *g$^-$* conformer. For comparison, in the original publication on the GLYCAM06 force field, it was used to simulate the conformational behavior of methyl α-D-galactopyranose, resulting in a predicted 8/18/75 distribution of *g$^+$/g$^-$/st* conformers of the ω angle, which was in close agreement to previous experimental results, that reported the *st* conformer to dominate (13/17/70).[146,207] In light of these results, the absence of the *st* conformer of ω in the MD simulation of α-59 and the deviation between experimental and theoretical coupling constants for $^3J_{H5,H6R/S}$ would indicate that the computational model of its conformational behavior is inaccurate.

It is possible that solvent effects on the relative Gibbs Free Energies of the conformer populations are insufficiently accounted for by the explicit chloroform solvent parameters in AMBER14, resulting in this deviation. Alternatively, the insufficient parameterization of the GLYCAM06 force field for the behavior of acetylated saccharides in chloroform could be the reason for the observed differences between experimentally determined and MD-back-calculated coupling constants. This is possibly because the GLYCAM06 force field was not developed with this application in mind. Nonetheless, as shown in Table 5.3 and Table 5.4, the coupling constants for the θ and φ_n angles that were determined from the *J*-HMBC experiment for α-**58** and α-59 were reasonably well reproduced by the MD simulation, indicating that the newly developed Karplus equation, as described in Chapter 4, is applicable to the conformational analysis of acetylated monosaccharides in chloroform.

Tri-O-acetyl-D-glucurono-6,1-lactone (60). In the case of the tri-*O*-acetyl-D-*glucurono*-6,1-lactone **60**, the analysis of its MD simulation yielded 8 conformers, which are summarized in Table 5.5, with the relevant dihedral angle histograms depicted in **Figure 5.11**.

Table 5.5. Summary of the conformational space of tri-*O*-acetyl-D-*glucurono*-6,1-lactone **60** established based on MD simulation covering 95% of the total conformers, shown in Figure 5.11.

Conformer #	C1-C2-O2-C1' φ_2 / °	C2-C3-O3-C3' φ_3 / °	C3-C4-O4-C5' φ_4 / °	Count	% abundance
1	75	-75	165	14862	**31%**
2	75	-165	165	13554	**28%**
3	75	-75	75	7290	15%
4	165	-165	165	3924	8%
5	75	-165	75	3081	6%
6	165	-75	165	2077	4%
7	165	-165	75	1341	3%
8	165	-75	75	1548	3%
				47677	95% coverage

Due to the bicyclic nature of the 6,1-lactone, the ω, θ and θ' dihedral angles were predicted to be restricted to narrow dihedral angle distributions around $\omega = 90°$, $\theta = 0°$ (*E* conformer) and $\theta^* = 145°$, respectively. The φ_n angles (C$_{n-1}$-C$_n$-O$_n$-C$_{n'}$) of the three acetyl groups were predicted to be bimodal, with φ_2 and φ_4 each favoring the presumably less sterically demanding conformation that point the acetyl groups away from the 'central' 3-acetyl group. For the 3-acetyl group, φ_3 was predicted to be evenly distributed between the two potential rotamers. Meanwhile, the ψ_n angles (C$_n$-O$_n$-C$_{n'}$-C$_{n+1'}$) were restricted to the *anti* conformer ($\psi_n = 180°$) in all cases (histograms not shown), as expected due to the nature of the ester bond, as indicated in the graphical representation of **60** in Figure 5.11**.**
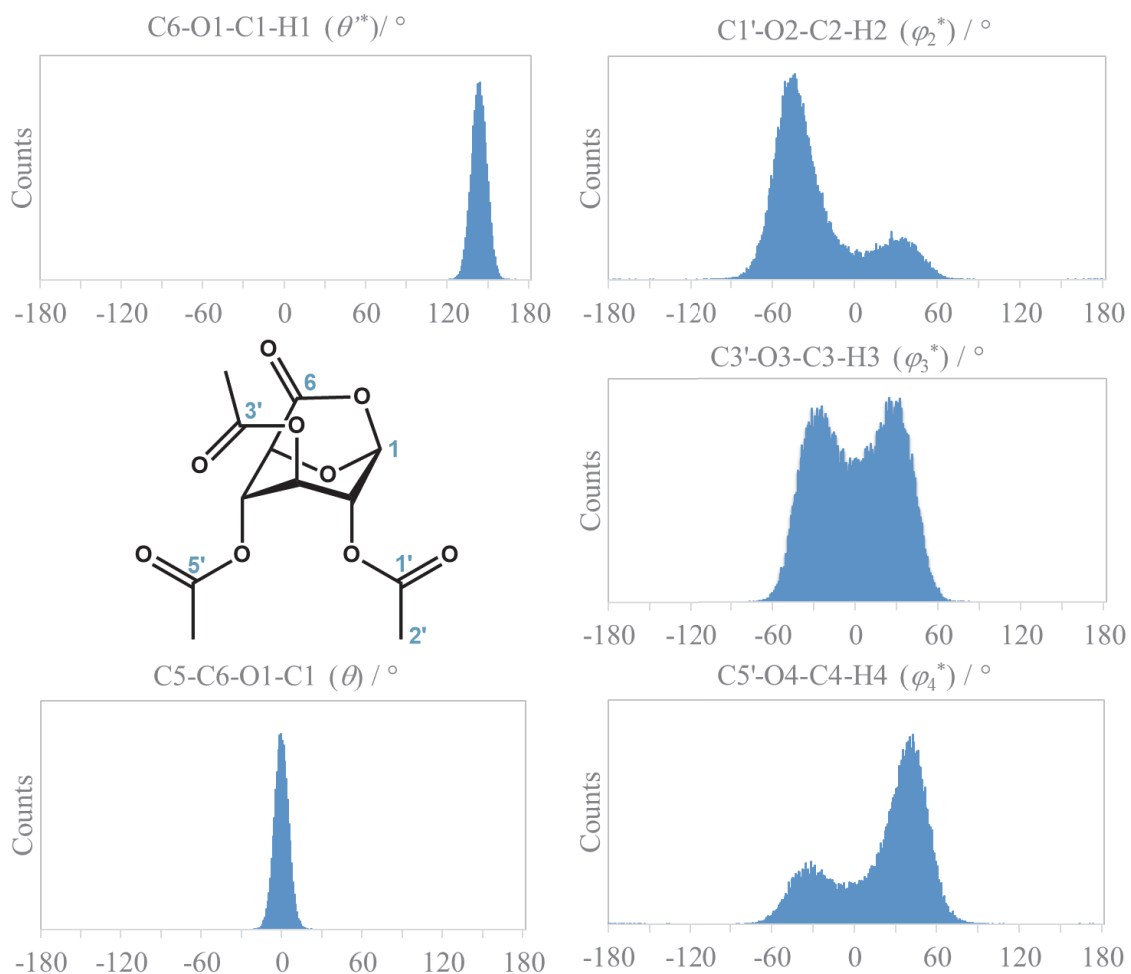
Figure 5.11. Summary of the relevant dihedral angle histograms from the MD simulation of tri-*O*-acetyl-D-*glucorono*-6,1-lactone **60**.

Because of the rigidity of the lactone and the relatively restrained torsions of the acetyl groups, representative geometries from the eight determined conformational regions of **60** were optimized at the M05-2X/6-31G* level of theory, which was chosen for the reasons discussed in the previous chapter. The relative Gibbs Free Energies of the 8 conformers, calculated based on single point energy calculations using DFT or *ab initio* methods (M05-2X/6-311+G**, as described in Chapter 4, and MP2/aug-cc-pVTZ), were summarized in Table 5.6 and the optimized structures are shown in Figure 5.12.

Table 5.6. Summary of the relative Gibbs Free Energies of the eight conformers of **60** derived from DFT and hybrid-*ab initio*/DFT computations and the resulting predicted relative abundances based on the Boltzmann distribution.

Conformer	M05-2X/6-311+G**//M05-2X/6-31G*		MP2/aug-cc-pVTZ//M05-2X/6-31G*		GLYCAM06
	ΔG^{298} kcal/mol	contribution	ΔG^{298} kcal/mol	contribution	contribution
1	0.84	14%	0.95	11%	31%
2	1.30	7%	1.32	6%	28%
3	0.00	58%	0.00	54%	15%
4	1.28	7%	1.12	8%	8%
5	2.55	1%	2.33	1%	6%
6	0.88	13%	0.64	19%	4%
7	3.04	0%	2.50	1%	3%
8	not a minimum	0%	not a minimum	0%	3%

As noted in the table, conformer 8 was not found to be a local minimum structure at the given level of theory, however local minima corresponding to the other 7 conformational regions of the MD simulation were optimized successfully. There was good agreement between the relative Free Gibbs energies of the conformers computed with DFT and *ab initio* methods; however, the results from the MD simulation using the 'extended' GLYCAM06 force field significantly deviated from those of the higher-level QM computations. As shown in Table 5.6, based on the DFT/*ab initio* computations, conformer 3 was predicted to be the global minimum and to contribute over 50% to the overall conformational space, while the MD simulation predicted it to only contribute 15%. This disagreement is likely due to the GLYCAM06 force field being insufficiently parameterized for the molecule of interest. As previously discussed, the GLYCAM06 force field was developed for the application to carbohydrates in aqueous solution, as opposed to acetylated lactone derivatives thereof in chloroform, as was the case for **60**.
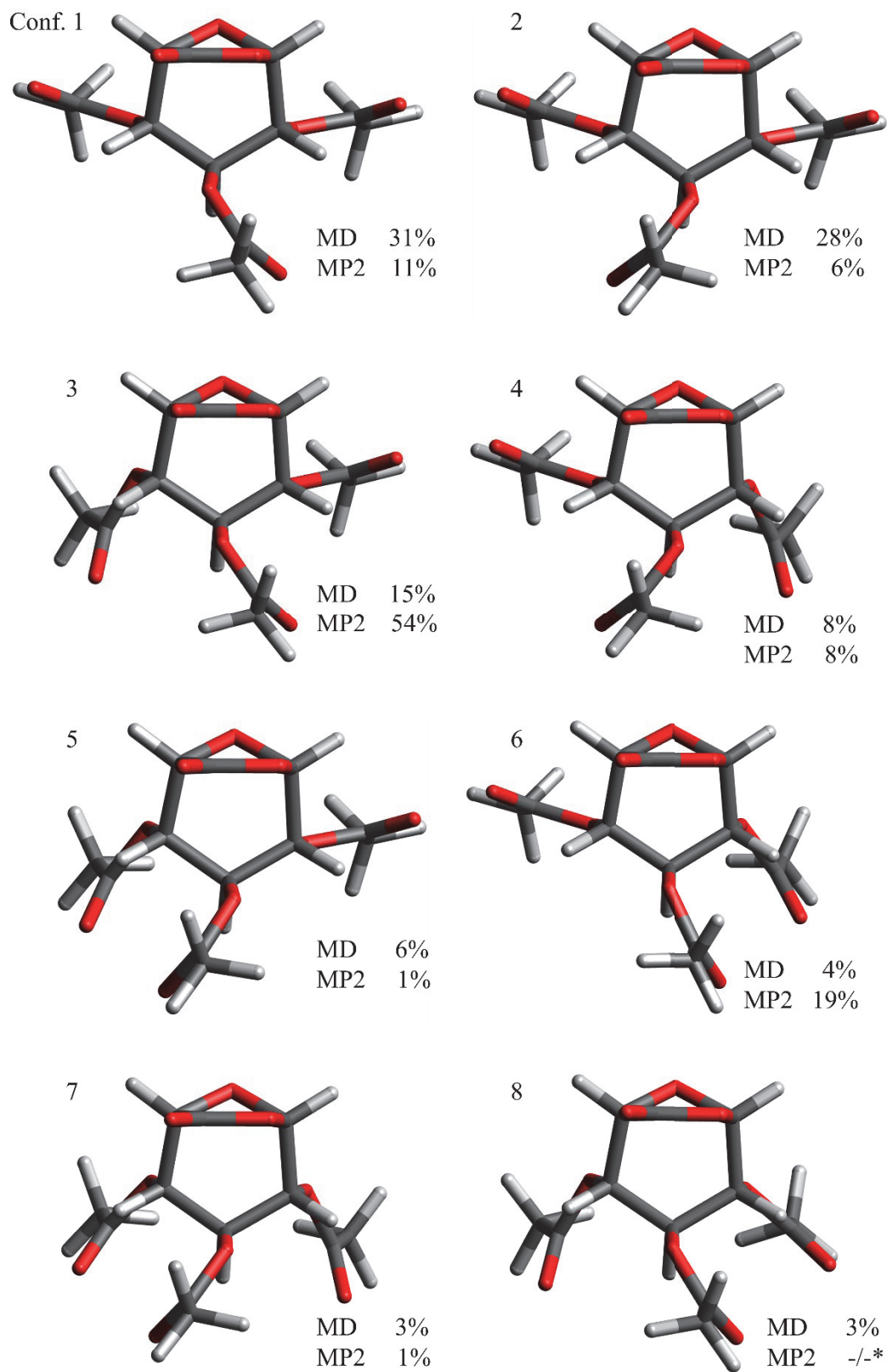
Figure 5.12. Graphical representation of the M05-2X/6-31G* optimized conformers of **60**, showing the relative position of the 2,3,4-*O*-acetyl groups and the relative abundances based on MD and MP2/aug-cc-pVTZ//M05-2X/6-31G* computations. (*: not a local minimum.)

As such, the small electronic effects influencing the conformational behavior of **60**, as indicated by the QM computations, were not sufficiently captured in the molecular dynamics approach.

Table 5.7. Summary of experimental and theoretical ^3J values (back-extracted from MD or Boltzmann-weighted QM results) for tri-*O*-acetyl-D-glucorono-6,1-lactone **60**.

(Hz)	exp.[a]	MD	DFT[c]	DFT/*ab initio*[d]
$^3J_{C6,H1}$	4.5[c]	5.9	6.2	6.2
$^3J_{C1',H2}$	4.5	3.4	3.4	3.5
$^3J_{C3',H3}$	n.d.[b]	4.3	3.4	3.4
$^3J_{C5',H4}$	4.3	3.7	2.9	2.9

a) measured in CDCl$_3$. b) not determined due to insufficient signal. c) M05-2X/6-311+G**//M05-2X/6-31G* d) MP2/aug-cc-pVTZ//M05-2X/6-31G*

To evaluate the MD and QM models of **60** discussed above, the back-calculated coupling constants from the three different models were compared to the experimentally determined $^3J_{C(sp2)OCH}$ values corresponding to the φ_{2-4} and θ dihedral angles. The results were summarized in Table 5.7. The coupling constant for $^3J_{C3',H3}$ could not be determined experimentally, due to insufficient signal. For the 2- and 4-acetyl groups, the theoretical coupling constants for $^3J_{C1',H2}$ and $^3J_{C5',H4}$ were not within the range of the experimentally determined values, after accounting for experimental error, similar to the data for the acetyl groups of *per*-acetylated monosaccharides α-**58** and α-59.

As can be seen in Table 5.7, both the MD and QM models predicted the coupling constant for $^3J_{C6,H1}$ – which corresponds to the θ angle – to be significantly larger than the experimentally determined value. In addition to slight variations between the experimental and computationally predicted dihedral angle, a prominent reason for this deviation is likely that the Karplus equation, as described in Chapter 4, was not adequately parameterized to describe the

Karplus relationship of the lactone-acetal bound H-1, and the different electronic structure along the coupling pathway.

Notably, the theoretical coupling constants determined using the GLYCAM06 force field were a closer match for the experimentally determined values than those back-calculated from the QM models. This could be a result of the static QM structures not fully capturing the flexibility of the acetyl groups. In particular, the QM model would not capture the relative shallow- or steepness of the energy landscape around the determined local minima in the QM models.

Taken together, the conformational analyses of compounds **58** – **60** indicated that while the Karplus equations discussed in Chapter 4 could be applied to other carbohydrate derivatives in chloroform, their modeling with the GLYCAM06 force field model was only partially successful. The results indicated that use of this approach should be carefully validated against QM computations and experimental data, where possible, for each individual molecule of interest outside of the scope of the original GLYCAM06 publication. Additionally, future work should explore the conformational analysis of per-acetylated di- or tri-saccharides derived from glucose and other carbohydrates, to further explore how well these compounds are modeled using the GLYCAM06 force field. In particular, the reason for the failure in applying the methodology to D-galactose derivate 59 deserved additional study, as it was in contrast to the apparent fit of the MD derived conformational model of acetylated derivatives of D-glucose. Here, the investigation of per-acetylated derivatives of other monosaccharides could be insightful.

Synthesis of 6,6'-linked ester disaccharides. To address the question of the influence of an ester functional group on the linkage between two monosaccharide units, a model compound had to be prepared. Initially, synthetic work focused on the synthesis of 6,6'-linked ester disaccharides, which were investigated first due to their potentially higher stability, compared to the acetal-ester in a potential 1,6 linkage. As established in Chapter 3, an oxidative esterification was envisioned to provide convenient access to 6,6'-ester linked disaccharides from 6-unprotected monosaccharide precursors. The synthesis of a selectively 6-unprotected

monosaccharide precursor was achieved for D-glucose in three steps on the basis of literature

procedures, as depicted in Figure 5.13.[208] Perbenzylation of free D-glucose yielded benzyl

2,3,4,6-tetra-*O*-benzyl-*β*-D-glucopyranoside 62 in 64% yield, followed by selective

debenzylation-acetylation at the 6-position mediated by $ZnCl_2$ to give benzyl 6-*O*-acetyl-2,3,4-tri-

O-benzyl-*β*-D-glucopyranoside 63. In the last step, benzyl 2,3,4-tri-O-benzyl-*β*-D-

glucopyranoside 64 was readily obtained from crude 63, through deacetylation in methanol with a

catalytic amount of sodium, in 57% yield over two steps and after recrystallization from ethanol.

This three-step synthetic pathway could be carried out on a multi-gram scale and it was found that

sufficient purity (>95% based on ^{1}H NMR) could be reached without the need for column

chromatography, contrary to the description in the literature.[208]
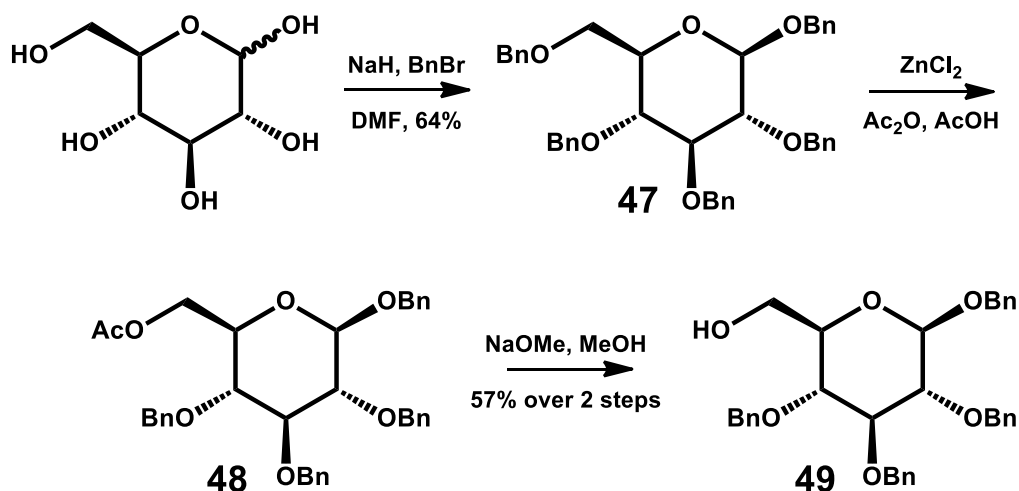
Figure 5.13. Synthesis of the 6-unprotected precursor **64** from D-glucose in 3 steps and 36% overall yield.[208]

As described in Chapter 3, the reaction of **64** under the established oxidative

esterification conditions with TEMPO/CaCl₂/Oxone did not yield the desired 6,6'-linked

disaccharide, due to competing side reactions. Fortuitously, the reaction in anhydrous acetonitrile

and with TCCA as a soluble terminal oxidant did yield the desired benzyl 2,3,4-tri-*O*-benzyl-*β*-D-

glucopyranosyl-(6→6')-(benzyl 2,3,4-tri-*O*-benzyl-*β*-D-glucopyranuronate) **65**, albeit in

relatively low 26% yield after column chromatography. Based on analysis of the observed $^3J_{HH}$

couplings in the ^1H NMR spectrum, **65** was determined to retain the $^4C_1$ conformation for both

monosaccharide units.
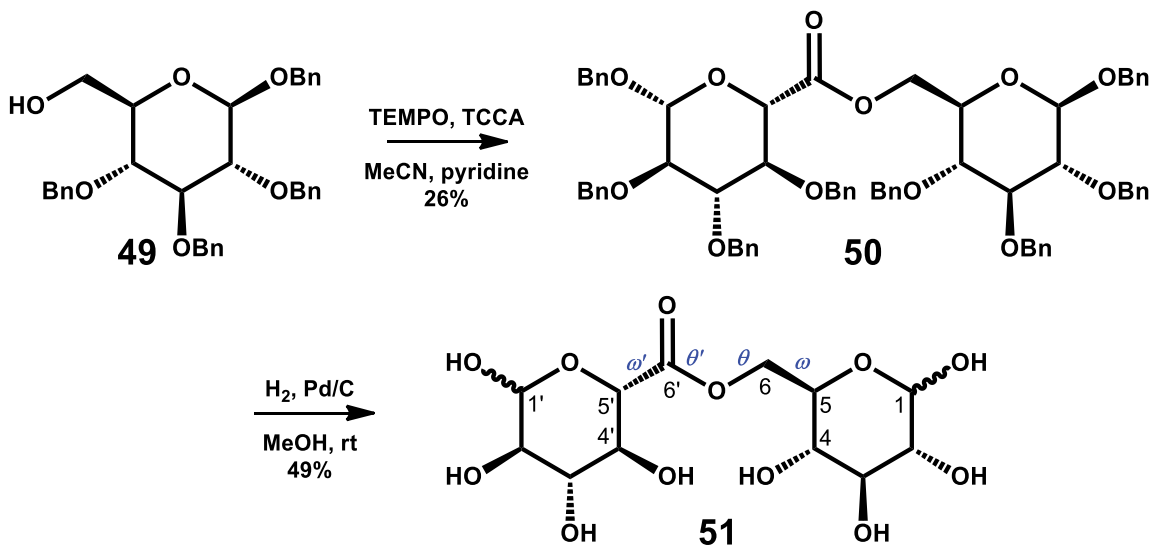
Figure 5.14. Oxidative esterification of **64** and subsequent debenzylation leading to the desired
6,6'-ester linked glucose dimer **66**.

In the final step, the reductive elimination of **65** with hydrogen gas and catalytic Pd/C

afforded the desired D-glucopyranosyl-6,6'-D-glucopyranuronate **66** in 49% yield, after column

chromatography with DCM:MeOH (gradient elution 95:5-7:3).
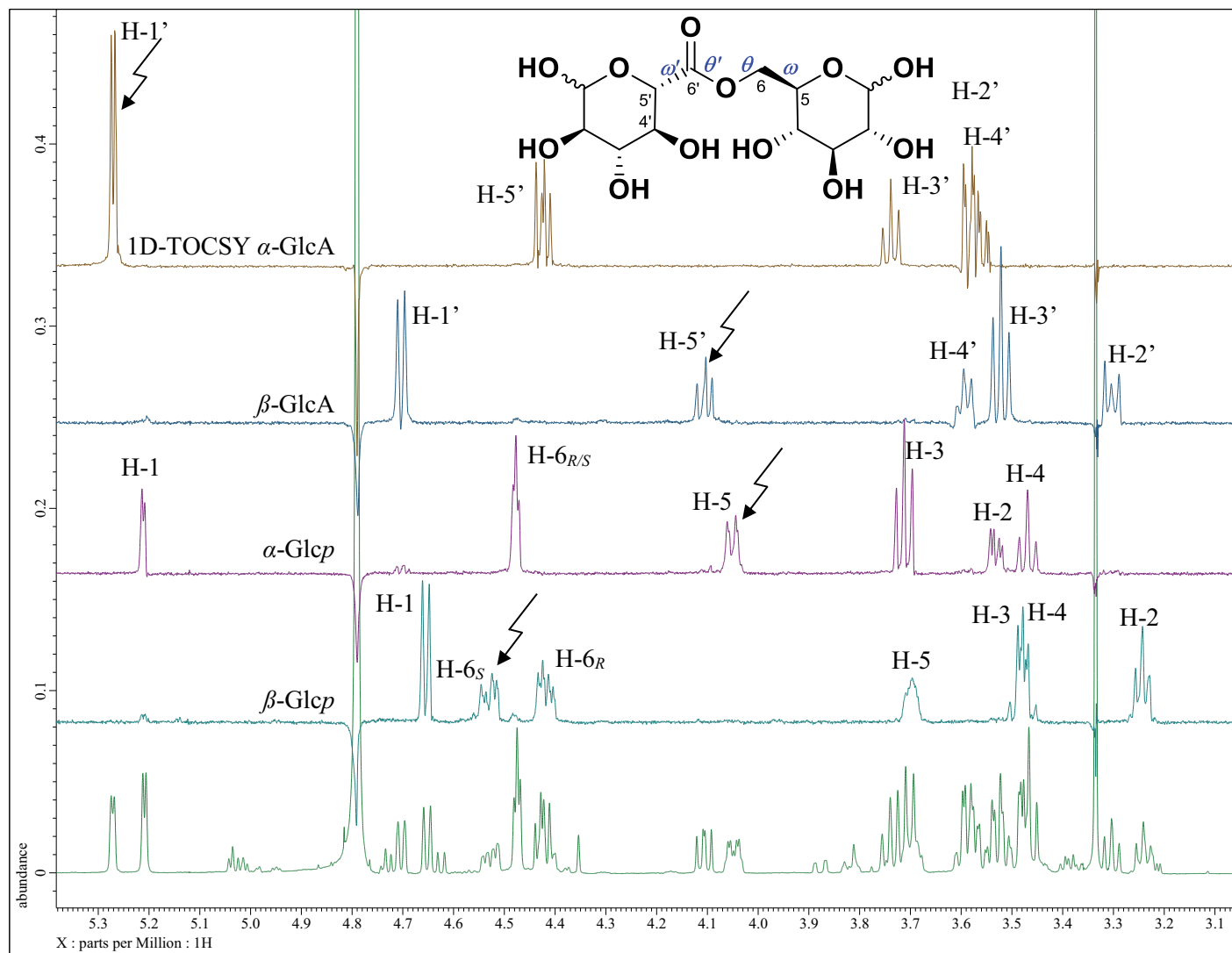
Figure 5.15. Overlay of ¹H NMR (bottom) and 1D TOCSY spectra of the four spin systems present in *αα/αβ/βα/ββ*-**66**.

The ^{1}H NMR spectrum of the purified **66** in D$_2$O indicated the presence of several different sugar units, as was expected due to the different anomers combinations. Using 1D TOCSY experiments, the spin systems corresponding to both α- and β-D-glucopyranuronate (α/β-GlcA) and α- and β-D-glucopyranosyl (α/β-Glc$p$) could be elucidated, as shown in Figure 5.15. The proton signals of H-6$_{R/S}$ of both α/β-Glc$p$ were found to be shifted significantly upfield, when compared to free α/β-D-glucose, which was indicative of the ester linkage. The assignment of the respective proton signals could be achieved from a 2D COSY experiment and the corresponding carbon signals were assigned from HMQC correlations. (See Appendix C for their spectra and chemical shift assignments.) The coupling constants of all four spin systems were indicative of $^4C_1$ ring conformation for **66**.

Additionally, an HMBC experiment allowed for the confirmation of the ester linkage: As shown in Figure 5.16, a total of four carbonyl carbon signals appeared in the ^{13}C spectrum. Based on the two-bond correlations to H-5 of the glucuronates, these could be assigned pairwise to the α-GlcA and β-GlcA subunits, respectively. Notably, the HMBC revealed three-bond correlations from both α-Glc$p$-H-6$_{R/S}$ and β-Glc$p$-H-6$_{R/S}$ (assignments by analogy to **46**) to α-GlcA-C-6. The same was the case for β-GlcA-C-6. Additionally, the signals of α/β-GlcA-H-5 appeared to be two overlapping doublets. Taken together, these observations revealed that the four identified spin systems were present in duplicate. Thus it was concluded that all four possible anomeric pairs of **66**, namely $\alpha\alpha$-**66**, $\alpha\beta$-**66**, $\beta\alpha$-**66** and $\beta\beta$-**66**, were present in solution and the 1D TOCSY spectra resulted from the overlap of two virtually identical spin systems, that only differed in the chemical shift of H-5 of the α/β-GlcA subunits, as seen in Figure 5.15 and Figure 5.16.
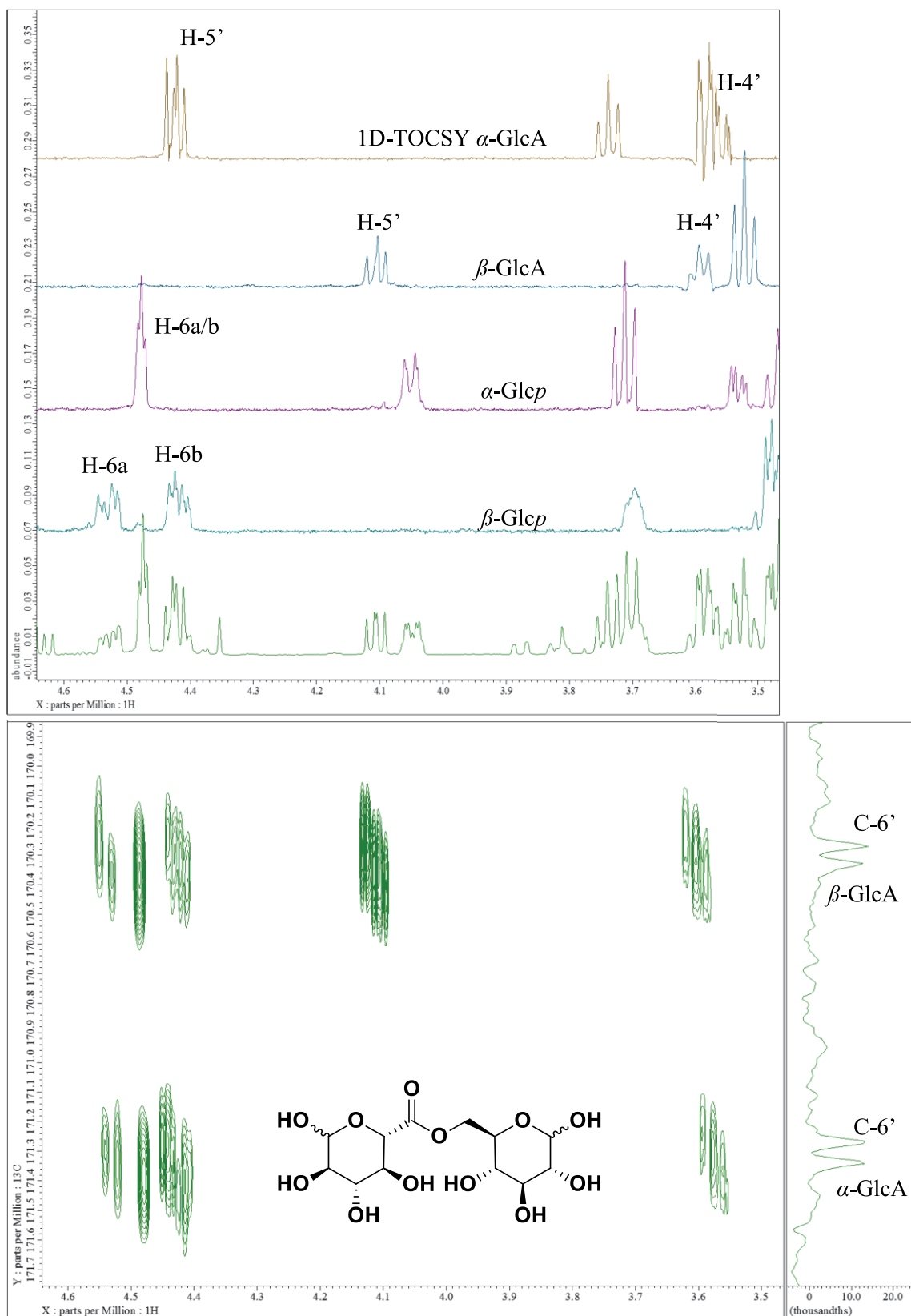
Figure 5.16. Overlay of 1D TOCSY spectra and magnified 2D HMBC spectrum of Compound **66** showing the 2- and 3-bond correlations of the ester linkage.

The complexity of the NMR spectrum of **66**, with a mixture of 4 diastereomers present due to the two anomeric centers, could have been reduced by fixation of the anomeric position, for example by starting the synthesis from methyl-α-D-glucopyranoside. However, as work from this laboratory and others has shown, methylation of the anomeric hydroxyl can significantly alter the dihedral distribution of the ω and θ angles in glucose.[150,207,209] To allow for the elucidation of the conformational effect of the ester functional group on the linkage between the two monosaccharides, the aforementioned methylation was omitted in order to avoid confounding changes to the conformational behavior of **66**.
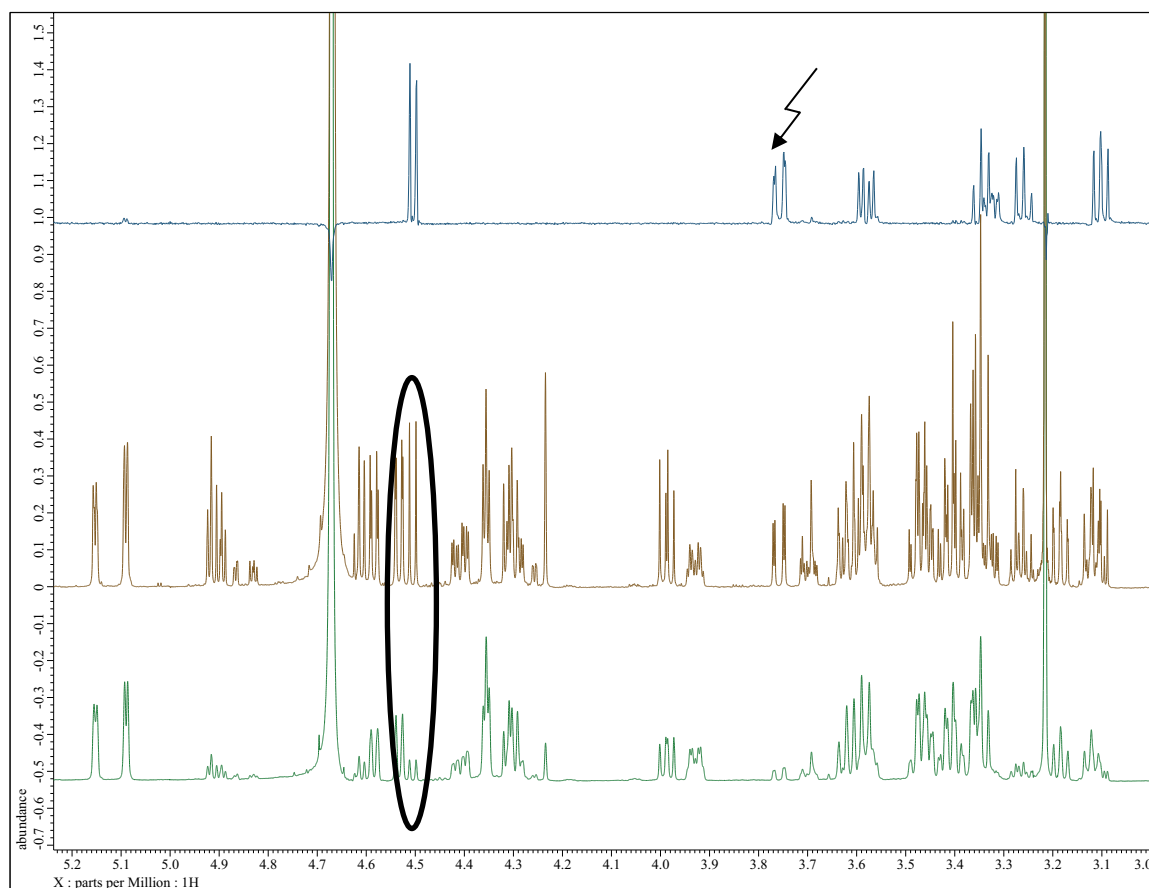
Figure 5.17. Evidence of ester hydrolysis. Overlay of the ^{1}H NMR spectrum of **66**, immediately after preparation of the NMR sample in D$_2$O (bottom), after 24 h at RT (middle), and the 1D TOCSY spectrum proving the identity of free ß-D-glucose.

Additional measurements of the ^{1}H NMR spectrum of the NMR sample of **66**, 24 h after preparation and storage at RT, indicated the increased abundance of other anomeric signals in the spectrum, as highlighted in Figure 5.17. One of these could be clearly identified as free *ß*-D-glucose through 1D TOCSY experiments. This proved the relative sensitivity of **66** to hydrolysis, possibly due to small amounts of acid or base in the NMR sample. Although no thorough experiments were performed on the stability of **66** under different acidic or basic conditions, these findings would suggest the relative instability of the ester linkage in **66**.

Synthetic route to analogs of 66 and 1,6'-linked ester disaccharides. The synthetic route to **66** starting from D-glucose, as outlined above, is also potentially viable for the preparation of the mannose analog of **66** from D-mannose or other 6-unprotected 1,2,3,4-tetra-*O*-benzylated monosaccharides. However, for multiple reasons including those discussed above related to the stability of the 6,6'-ester linkage, these analogs were not explored further in the present work. For the formation of a possible 1,6'-linked ester disaccharide, the epoxide opening with a carboxylic acid was explored initially, on the basis of literature precedence.[210] For this pathway, tri-*O*-benzyl-D-glucal **67**, accessible from commercially available tri-*O*-acetyl-D-glucal, was reacted with dimethyldioxirane, formed *in situ* from acetone and Oxone®, to yield 1,2-anhydro-3,4,6-tri-*O*-benzyl-*α*-D-glucopyranose **68**. The corresponding carboxylic acid could be obtained by oxidation of **64** with potassium dichromate to yield benzyl 2,3,4,6-tetra-O-benzyl-*β*-D-glucopyranuronic acid **69** according to literature procedures.[211] In the reaction of **68** with **69** in DCM, however, although product formation could be detected by ESI-MS to a small degree, it was not observed in significant enough amounts to be isolated and purified.

While other routes toward and the conformation of 1,6'-linked ester disaccharides were not explored further in in this work, the synthesis of 1,6-linked ester disaccharides could be achieved by the reaction of benzylated glucuronic chloride with 2,3,4,6-tetra-*O*-benzyl-*α/ß*-D-glucopyranose or using 2-(acylthio)-3-nitropyridine ester derivatives of glucuronic acid or

trichloroacetimidates to activate the carboxylic acid or alcohol, respectively, as described previously in the literature.[200-203]

Conformational analysis of D-glucopyranosyl-6,6'-D-glucopyranuronate (66). To establish a model of the conformational behavior of **66**, the ester disaccharide was modeled *in silico* using the 'extended' GLYCAM06 force field, modified as described in Chapter 4, for *αα*-**66** and *ßß*-**66** over 500 ns and using the TIP3P water solvent model. The conformational regions that were determined from the respective MD trajectories, as described previously, as well as the relevant dihedral angle histograms summarizing the conformations of the ester-linkage are summarized in **Table 5.8** and **Table 5.9**, and **Figure 5.18** and Figure 5.19 below.

The ester-linkage between the monosaccharide units of D-glucopyranosyl-6,6'-D-glucopyranuronate **66** can be described by 4 dihedral angles: ω (C4-C5-C6-O6) , θ (C5-C6-O6-C6'), θ' (C6-O6-C6'-C5'), and ω' (O6-C6'-C5'-C4'). The MD simulations of the two diastereomers *αα*-66 and *ßß*-66 were quite similar, with only small deviations in the overall distribution of the relevant dihedral angle conformations of the linkage between the two monosaccharide units. As such, the anomeric configuration was predicted to have a relatively small influence on the overall shape of the ester cross-linkage. Because of this, the mixed anomeric diastereomers *αß*-66 and *ßα*-66, albeit found to be present in solution based on the NMR analysis, were not modeled computationally, as their conformational analysis was expected to closely match that of the two *αα*- and *ßß*-isomers.

Table 5.8. Summary of the conformer regions of α-D-glucopyranosyl-6,6'-α-D-glucopyranuronate $\alpha\alpha$-**66** established based on its MD simulation.

Conformer #	C4-C5-C6-O6 ω / °	C5-C6-O6-C6' θ / °	C6-O6-C6'-C5' θ' / °	O6-C6'-C5'-C4' ω' / °	Count	% abundance
1	58	180	180	-97	14307	**29.9%**
2	58	180	180	90	3369	7.0%
3	58	-106	180	-97	7069	**14.8%**
4	58	-106	180	90	862	1.8%
5	58	103	180	-97	3489	7.3%
6	58	103	180	90	2502	5.2%
7	-168	180	180	-97	3206	6.7%
8	-168	180	180	90	1914	4.0%
9	-168	-106	180	-97	1624	3.4%
10	-168	-106	180	90	1096	2.3%
11	-168	103	180	-97	1213	2.5%
12	-168	103	180	90	441	0.9%
13	-73	180	180	-97	2235	4.7%
14	-73	180	180	90	1307	2.7%
15	-73	-106	180	-97	1374	2.9%
16	-73	-106	180	90	279	0.6%
17	-73	103	180	-97	702	1.5%
18	-73	103	180	90	893	1.9%
					47882	96% coverage

Table 5.9. Summary of the conformer regions of *ß*-D-glucopyranosyl-6,6'-*ß*-D-glucopyranuronate *ßß*-**66** established based on its MD simulation.

Conformer #	C4-C5-C6-O6 $\omega\,/\,°$	C5-C6-O6-C6' $\theta\,/\,°$	C6-O6-C6'-C5' $\theta'\,/\,°$	O6-C6'-C5'-C4' $\omega'\,/\,°$	Count	% abundance
1	58	180	180	-97	16709	34.6%
2	58	180	180	90	3283	6.8%
3	58	-106	180	-97	8223	17.0%
4	58	-106	180	90	966	2.0%
5	58	103	180	-97	6745	14.0%
6	58	103	180	90	3321	6.9%
7	-168	180	180	-97	1752	3.6%
8	-168	180	180	90	609	1.3%
9	-168	-106	180	-97	1549	3.2%
10	-168	-106	180	90	318	0.7%
11	-168	103	180	-97	727	1.5%
12	-168	103	180	90	214	0.4%
13	-73	180	180	-97	1572	3.3%
14	-73	180	180	90	594	1.2%
15	-73	-106	180	-97	803	1.7%
16	-73	-106	180	90	159	0.3%
17	-73	103	180	-97	447	0.9%
18	-73	103	180	90	278	0.6%
					48269	97% coverage
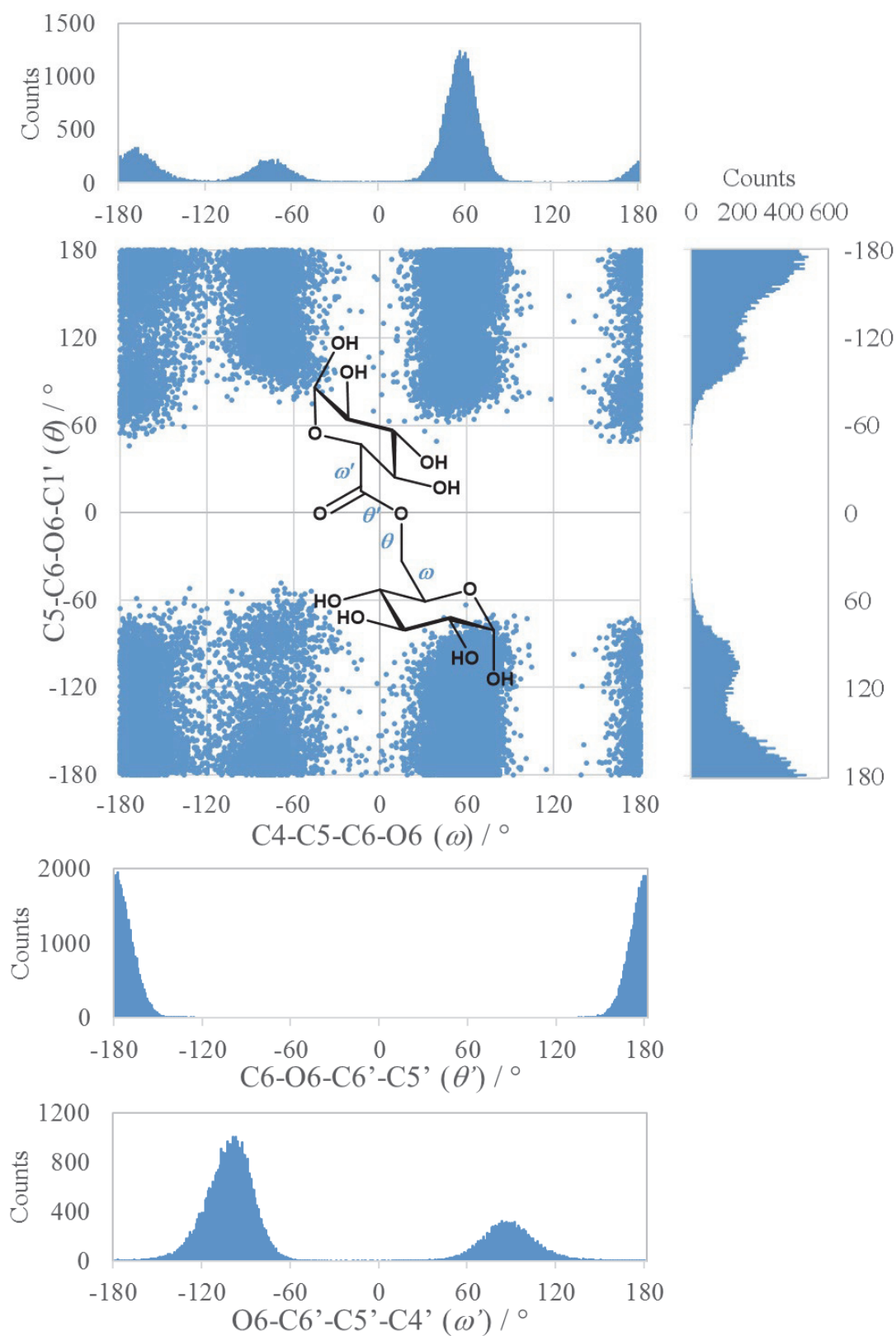
Figure 5.18. Summary of the relevant dihedral angle distributions of the ester linkage between the monosaccharide units of α-D-glucopyranosyl-6,6'-α-D-glucopyranuronate αα-**66** based on its MD simulation.
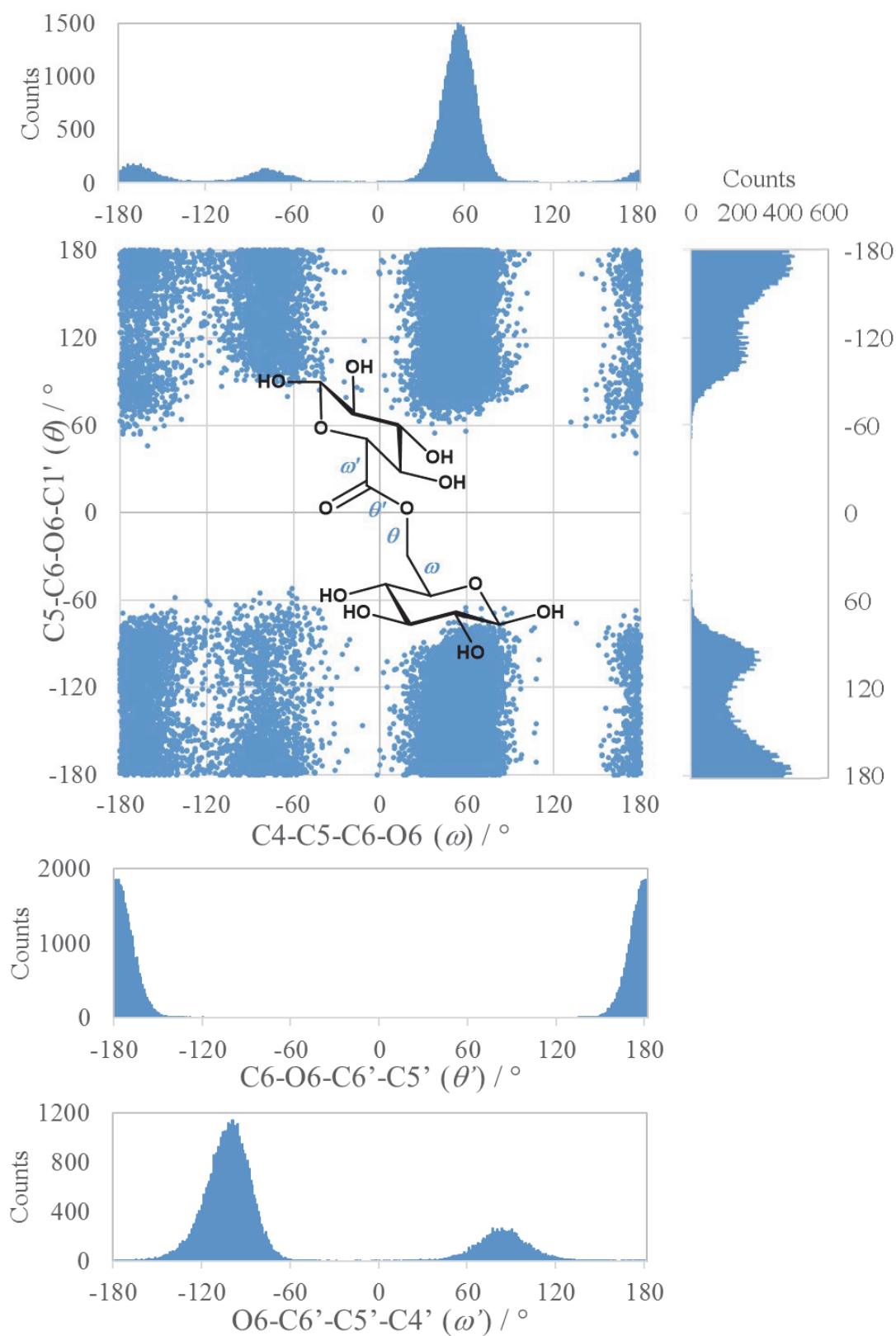
Figure 5.19. Summary of the relevant dihedral angle distributions of the ester linkage between the monosaccharide units of *ß*-D-glucopyranosyl-6,6'-*ß*-D-glucopyranuronate *ßß*-**66** based on its MD simulation.

As previously discussed, the ester-linkage in **66** can be described by 4 dihedral angles, as it involves four bonds. In the case of both *αα*-**66** and *ββ*-**66**, conformer 1 ($\omega = 58°$, $\theta = 180°$, θ' = 180°, ω' = -97°) was found to be the dominant conformational region at 35% and 30%, respectively. For *αα*-**66**, ω was found to largely favor g^+ (58°) with 66% abundance over the *st* (-168°) conformation at 20%, with the remainder of 14% present as g^- (-73°). As such, the ω angle thus was predicted to behave similar to that of 6-acetyl group in 6-*O*-acetyl-*α*-D-glucopyranose *α*-**46**, as described in Chapter 4. For θ, a 55 % preference for the *st* (180°) conformation was predicted, with the g^+ (103°) and g^- (-106°) conformations contributing 19% and 26%, respectively. Meanwhile, the θ' angle was computed to entirely assume the *st* (180°) conformation due to the carbonyl on C6'. Likewise, the ω' angle was found to be bimodal, with the predominant conformer being g^- (-97°) at 74%, over the minor g^+ conformer (90°, 26%). For *ββ*-**66**, the ω angle was found to assume a slightly larger proportion of the g^+ conformation at 81%, in favor of both the *st* and g^- conformations at 11% and 8%, thus differing slightly *αα*-**66**, similar to the difference in the predicted conformational behavior of 6-acetyl-*β*-D-glucopyranose *β*-**46**,when compared to 6-acetyl-*α*-D-glucopyranose *α*-**46**. For θ, the dihedral angle distributions were predicted to be largely unchanged between *αα*-**66** and *ββ*-**66**, with *ββ*-**66** also displaying a large preference for the *st* conformation with 51%, and the g^+ and g^- conformations contributing 24% and 25% respectively. The θ' and ω' angles were predicted to be virtually identical for *ββ*-**66**, as compared to *αα*-**66**, with θ' predicted to be *st* (180°) exclusively and ω' split between g^- (-97°) at 80% and g^+ (90°) at 20%. Additionally, both monosaccharide units were predicted to adopt the $^4C_1$ conformer exclusively for both *αα*-**66** and *ββ*-**66**.

Table 5.10. Summary of the relevant experimental and theoretical ^3J values (calculated based on the MD trajectories) for D-glucopyranosyl-6,6'-D-glucopyranuronate **66**.

(Hz)	exp.[a]		MD
$^3J_{\alpha\text{-H5},\alpha\text{-H6b}}$	3.0	$^3J_{\alpha\text{-H5},\alpha\text{-H6}R}$	3.2[d]
$^3J_{\alpha\text{-H5},\alpha\text{-H6a}}$	3.0	$^3J_{\alpha\text{-H5},\alpha\text{-H6}S}$	2.4[d]
$^3J_{\beta\text{-H5},\beta\text{-H6b}}$	5.4	$^3J_{\beta\text{-H5},\beta\text{-H6}R}$	2.9[d]
$^3J_{\beta\text{-H5},\beta\text{-H6a}}$	5.7	$^3J_{\beta\text{-H5},\beta\text{-H6}S}$	2.0[d]
$^3J_{\text{C6'},\alpha\text{-H6}R}$	3.1[b]	$^3J_{\alpha\text{-C6'},\alpha\text{-H6}R}$	3.4
$^3J_{\text{C6'},\alpha\text{-H6}S}$	3.1[b]	$^3J_{\alpha\text{-C6'},\alpha\text{-H6}S}$	3.1
$^3J_{\text{C6'},\beta\text{-H6}R}$	-/-[c]	$^3J_{\beta\text{-C6'},\beta\text{-H6}R}$	3.5
$^3J_{\text{C6'},\beta\text{-H6}S}$	2.5	$^3J_{\beta\text{-C6'},\beta\text{-H6}S}$	3.2

a) measured in D_2O. b) average of α-H6a/b due to AB-mixing. c) not determined due to spectral overlap. d) calculated based on the Karplus equation for $^3J_{\text{H5,H6}R/S}$ as discussed in Chapter 4. See Appendix C for a summary of the results and equation (11) from Chapter 4.

To evaluate the MD models of D-glucopyranosyl-6,6'-D-glucopyranuronate **66** discussed above, the back-calculated coupling constants from the MD simulations were compared to the experimentally determined $^3J_{\text{C6'},\text{H6}R/S}$ and $^3J_{\text{H5,H6}}$ values corresponding to the θ and ω dihedral angles. The results were summarized in Table 5.10. In the case of $\alpha\alpha$-**66**, the $^3J_{\text{H5,H6}}$ coupling constants were accurately reproduced by the MD simulation for the ω angle, however this was not the case for $\beta\beta$-**66**. Here, the computationally determined coupling constants were significantly smaller than the experimentally determined values. As discussed above, ω was predicted to predominantly be in the g^+ conformational region from the MD simulation. Based on the experimental data for $^3J_{\text{H5,H6}}$ in β-Glc$p$, the contribution from the g^- and st conformers is likely underestimated in the theoretical model. To determine the accuracy of the models for the θ angle, the back-calculated $^3J_{\text{C}(sp2)\text{OCH}}$ values were compared to data from the J-HMBC experiment for **66**. Due to the parameters of the measurement, there was a lower resolution in the ^{13}C dimension than in the regular HMBC experiment, resulting in a lack of separation between the cross-peaks of, for example, $^3J_{\alpha\text{-C6'},\alpha\text{-H6}R}$ and $^3J_{\beta\text{-C6'},\alpha\text{-H6}R}$. As a result, the determined values were an average from both α-C6' and β-C6'. Additionally, the coupling constants for $^3J_{\text{C6'},\alpha\text{-H6}R/S}$ overlapped, due to

AB-mixing of α-H-6$_{R/S}$. As shown in Table 5.10, the theoretical values for the $^3J_{C(sp2)OCH}$ coupling constants matched the experimentally determined values reasonably well. As such, the established conformational models of $\alpha\alpha$-**66** and $\beta\beta$-**66** were likely a good approximation for the conformational behavior of the θ angle of the ester linkage.

Markedly, only to the ω and θ dihedral angles yielded experimentally determinable $^3J_{HH}$ and $^3J_{CH}$ data. In the case of θ', the use of a ^{13}C-enriched sample would be required to measure the relevant $^3J_{CC}$ coupling constant between C6 and C5'. However, based on previous knowledge of the preference for the *anti* conformer of the θ' angle in esters, together with the results presented herein in Chapter 4, it was considered reasonable to assume that the MD simulation is an accurate representation of the actual behavior of the C6-O6-C6'-C5' angle. Likewise, the description of the ω' angle with a Karplus-type relationship on the basis of an experimentally measurable nuclide would require the use of ^{17}O enrichment. As such, experimental evidence for the behavior for the ω' angle in solution was not obtainable. In its absence, the MD simulation was assumed to be a suitable representation, based on its reasonable representation of the ω and θ angles, as discussed above.

To obtain a better understanding of the overall shape of D-glucopyranosyl-6,6'-D-glucopyranuronate **66**, with regards to the impact of the ester functional group on the conformational behavior of the molecule, representative structures of the three most abundant conformational regions of $\alpha\alpha$-**66** and $\beta\beta$-**66**, as shown in Figure 5.20, were compared to the most abundant conformer of its ether-linked analog D-glucopyranosyl 6,6'-D-glucopyranose **70**. The 6,6'-ether linked **70** has been previously prepared by Haines and others, after its allose analog was (erroneously) implied as the structure of the hypoglycemic compound 'coyolosa', as isolated from *Acrocomia mexicana root*.[212-215]
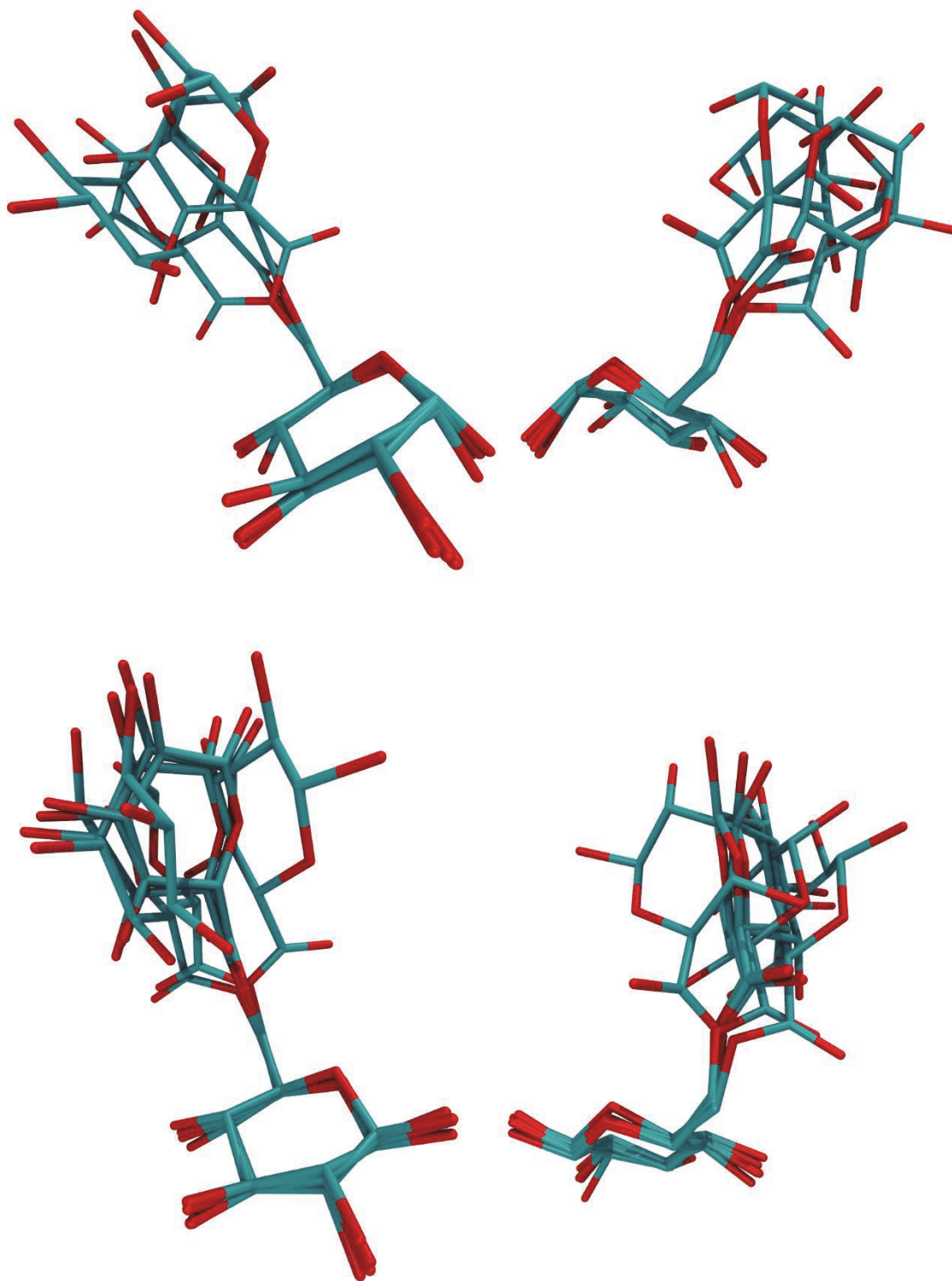
Figure 5.20. Overlay of the three most abundant conformational regions of *αα*-**66** (top) and *ββ*-**66** (bottom) based on their MD simulations shown from opposing viewpoints and with hydrogen atoms removed for clarity.

The MD simulations of *αα*/*ßß*-**70** were performed analogous to those for *αα*-**66** and *ßß*-**66**. The complete conformational space for both *αα*-**70** and *ßß*-**70** are summarized in Appendix C. The relevant dihedral angles of the ether-linkage and the graphical representation of the most abundant conformer of *ßß*-**70** are shown in Figure 5.21. From the comparison of the most abundant conformers of **66** and **70**, it could be observed that the change in the preferred conformation of the ω' angle for **66** (ω' = -97° in **66**, ω' = 58° in **70**) resulted in a drastic change of the orientation of the two monosaccharide units to one another, in that the preferred conformation places the two rings with the endocyclic oxygen pointed toward one another in **66**. In contrast, the two sugar rings were found to be facing in opposite directions in **70**. As such, the introduction of the ester functional group was predicted to significantly alter the overall shape of the disaccharide analog in solution, as a results of i) the reduced flexibility of the θ' and ω' dihedral angles and ii) the change in preferred conformation of ω' from g^+ in the ether-linked **70** to g^- in D-glucopyranosyl-6,6'-D-glucopyranuronate **66.**
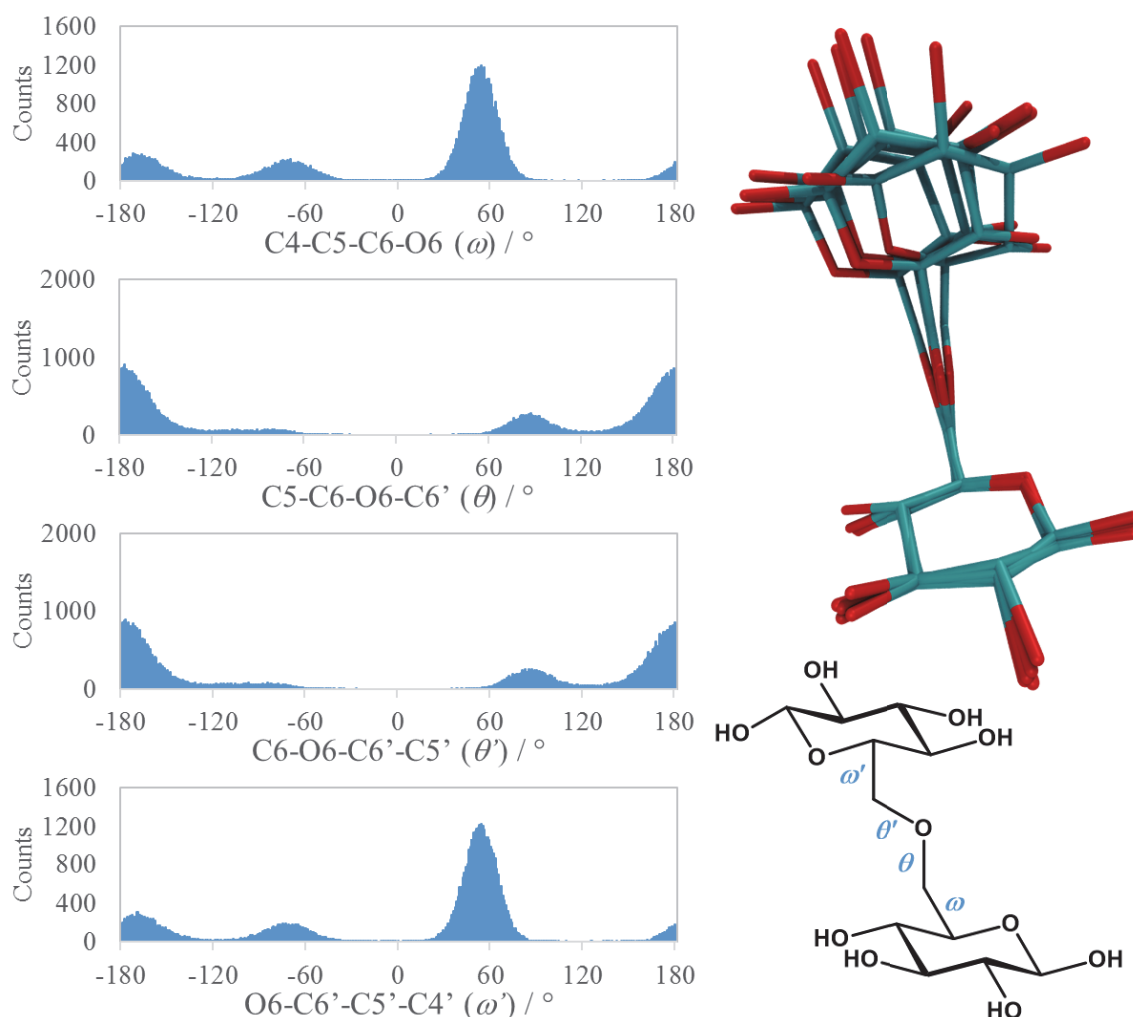
Figure 5.21. Dihedral angle distributions of the relevant linkage torsions and graphical representation most abundant conformer of *ß*-D-glucopyranosyl-6,6'-*ß*-D-glucopyranose **70**, based on its MD simulation. See Appendix C for complete description of conformational space.

Conclusions

In summary, the conformational analysis of compounds **58 – 60** and **66** revealed that the previously established Karplus equation, as described in Chapter 4, could be successfully applied to describe the θ dihedral angle in acetylated glucose and galactose derivatives and for the cross-linkage of 6,6'-ester linked disaccharide analogs in water and chloroform. However, it was also realized from **60** that the $^3J_{C(sp2)OCH}$ Karplus equation is not readily applicable to lactone-hemiacetals. Additionally, the difference between the experimentally determined and

computationally arrived coupling constants for the ω angle of **59** and *ßß*-**66** indicated that the 'extended' GLYCAM06 force field may not accurately capture all factors that influence the conformational behavior of the ω angle. Lastly, using the established conformational model of the model 6,6'-ester linked disaccharide analog **66**, it could be determined that the ester reduced the flexibility of the compound, with regards to the θ' and ω' dihedral angles. At the same time, this resulted in a change of the overall shape of the molecule, with regards to the orientation of the two monosaccharide units to one another, when compared to the 6,6'-ether linked analog **70**, which resulted in a 180° rotation of half of the molecule.

Chapter 6: Experimental and Methods Section

General Methods.

Sodium borate was purchased from EMScience, copper (II) tetrafluoroborate from Alfa Aesar, Naphthanol from Matheson Coleman & Bell and phenol from Mallinckrodt. 1-Hexanol was purchased from AlfaAesar. 2-Ethoxyethanol was obtained from Baker chemicals. 2-Phenoxyethanol was purchased from Eastman Chemical. Calcium chloride dihydrate was obtained from VWR. All other reagents were obtained from Sigma-Aldrich and used without further purifications. Solvents were distilled prior to use.

Column chromatography was performed on silica gel (Sorbent Technologies, 40-75 μm) and fractions analyzed with TLC run on equivalent mobile phase, or as otherwise noted, and analyzed through UV, $KMnO_4$ staining or charring with H_2SO_4/MeOH. Melting points (uncorrected) were determined using a Stanford Research Systems Digimelt MPA160.

^{1}H-NMR and ^{13}C-NMR spectra were acquired on a JEOL ECA-600 NMR-spectrometer (600 and 150 MHz, respectively). Structural assignments were corroborated by homo- and heteronuclear 2D NMR methods (COSY, HMQC, HMBC and TOCSY) where necessary. Chemical shifts are reported in parts per million (ppm, δ) relative to the residual protio solvent ($CDCl_3$, δ 7.26; CD_3OD, δ 3.31; D_2O, δ 4.79). ^{1}H NMR splitting patterns are designated as singlet (s), doublet (d), triplet (t), quartet (q), doublet of doublets (dd), doublet of doublets of doublets (ddd), doublet of triplets (dt), apparent triplet (apt t), and so forth. Splitting patterns that could not be visualized or easily interpreted were designated as broad (br) or multiplet (m). Coupling constants are reported in Hertz (Hz). Three-bond heteronuclear coupling constants were determined using a gradient-enhanced *J*-HMBC experiment with 8 scans over a 1638 x 512

data point matrix with an incrementally increasing coupling evolution time of $\tau = 0\text{-}260$ ms (in 20 ms increments) and a relaxation delay of 3s.[144] Data was fitted to $A = \sin(\pi \cdot {}^3J_{CH} \cdot \tau)$ using PSI-Plot to yield the coupling constants for the relevant three bond couplings.[145] Accurate mass measurements were performed on a JEOL AccuTOF mass spectrometer (Peabody, MA, USA) using either a DART ion source or an ESI ion source with polyethyleneglycol as an internal calibrant. GC/MS data was acquired using an Agilent Technologies 7890 A GC coupled to a 5975C inert XL MSD quadrupole mass spectrometer equipped with an EI source. ESI mass spectra were acquired on a Thermo-Finnegan TSQ ESI quadrupole mass spectrometer or a Varian 320 ESI triple quadrupole mass spectrometer.

Synthetic Methods.

Chapter 2: Diastereoselective Esterification.

The ^{1}H and ^{13}C NMR and high resolution mass spectral data for compounds **4**, **6**, **17 – 21**, **25**, **71**, **72**, **78 – 80**, **82 – 85** and **89** can be found in Appendices A + B. In addition, the spectral data for the remaining compounds listed hereafter may be found in the Supplemental Material to previously published research, which makes up a majority of the material discussed in Chapter 2.[216] It is accessible online at: http://www.arkat-usa.org/get-file/54871/

Synthesis of (±)-trans-2-substituted cyclohexanols.

(±)-trans-2-(p-tolylsulfanyl)cyclohexanol **4**. To a solution of cyclohexene oxide (9.88 g, 101 mmol) in THF (50 mL) was added *p*-thiocresol (13.5 g, 109 mmol), borax (4 g, 10.5 mmol) and water (50 mL). The reaction mixture was heated to 50 °C and stirred for 2 hours. Then, THF was evaporated and a NaOH solution. (5% w/v, 150 mL) was added and stirred for 30 min. The mixture was extracted with CH_2Cl_2 (4x75 mL) and the extracts were combined and dried over Na_2SO_4. Filtration and evaporation of the solvent yielded a yellow viscous liquid that crystallized at 4 °C overnight. The crude product was recrystallized from hexane to give the product as a white crystalline solid (20.3 g, 91%). mp 45-47 °C. ^{1}H NMR (600 MHz, CDCl$_3$): δ 7.35 (dt, 1.8 Hz, 7.8 Hz, 2H, Ar), 7.10 (br d, 7.8 Hz, 2H, Ar), 3.27 (dt, 4.2 Hz, 9.6 Hz, H-1), 3.04 (broad s, 1H,

OH), 2.66 (ddd, 4.2 Hz, 10.2 Hz, 12.0 Hz, H-2), 2.33 (s, 3H, Tolyl-CH$_3$), 2.07 (m, 2H, CH$_2$), 1.66 (m, 2H, CH$_2$), 1.26 (m, 4H, CH$_2$). ^{13}C NMR (150 MHz, CDCl$_3$): δ 138.28 (Ar-C$_q$), 134.83 (Ar-CH), 134.60 (Ar-CH), 129.94 (Ar-CH), 129.64 (Ar-CH), 128.33 (Ar-C$_q$), 71.70 (C1), 56.58 (C2), 33.66 (C6), 32.45 (C3), 26.12 (C5), 24.22 (C4), 21.05 (tolyl-CH$_3$). DART-HRMS: *m/z* calculated for C$_{13}$H$_{19}$OS [M + H]$^+$ 223.1152, found 223.1161; *m/z* calculated for C$_{13}$H$_{19}$OS [M + H − H$_2$O]$^+$ 205.1056, found 205.1042.

(±)-trans-2-(p-tolyloxy)cyclohexanol 6. To a solution of Na in absoluted ethanol (50 mL, 0.5 M) was added cyclohexene oxide (5.0 mL, 49.4 mmol) and *p*-cresol (5.36 g, 49.6 mmol) with stirring and the reaction was heated to 80 ºC with stirring for 24 hours. The yellow solution was then cooled, quenched with H$_2$O (10 mL) and neutralized using conc. HCl acid. The solution was then diluted with CH$_2$Cl$_2$ (50 mL) and transferred to a separatory funnel. The organic layer was separated and the aqueous layer washed with CH$_2$Cl$_2$ (20 mL). The combined organic layers (yellowish liquid) were washed with H$_2$O (30 mL) and sat. NaCl solution (30 mL) consecutively and then dried over Na$_2$SO$_4$. The drying agent was filtered off and the solvent evaporated to give a tan solid (10.02 g) The crude product was recrystallized from hexane and combined with a second crop of crystals from the filtrate to yield white needle-like crystals (7.24 g, 35.1 mmol, 71%). mp 84-87 ºC. ^{1}H NMR (600 MHz, CDCl$_3$): δ 7.08 (m, 2H, Ar), 6.85 (dt, 2.7 Hz, 8.4 Hz, 2H, Ar), 3.93 (ddd, 4.2 Hz, 8.4 Hz, 10.2 Hz, H-1), 3.70 (ddd, 4.8 Hz, 8.4 Hz, 10.8 Hz, H-2), 2.43 (broad s, 1H, OH), 2.29 (s, 3H, Tolyl-CH$_3$), 2.11 (m, 2H, CH$_2$), 1.74 (m, 2H, CH$_2$), 1.33 (m, 4H, CH$_2$). ^{13}C NMR (150 MHz, CDCl$_3$): δ 155.78 (Ar-C$_q$), 130.67 (Ar-C$_q$), 130.78 (2C, Ar-CH), 116.62 (2C, Ar-CH), 82.75 (C-1), 73.61 (C-2), 32.12, 29.34, 24.40, 24.01, 20.55 (tolyl-CH$_3$). DART-HRMS: *m/z* calculated for C$_{13}$H$_{19}$O$_2$ [M + H]$^+$ 207.1380, found 207.1373, *m/z* calculated for C$_{13}$H$_{17}$O [M + H − H$_2$O]$^+$ 189.1284, found 189.1278.

(±)-trans-2-(phenyloxy)cyclohexanol **7**. To a solution of Na in ethanol (10 , 0.4 M) was added cyclohexene oxide (1.0 mL, 9.9 mmol) and phenol (0.93 g, 10.2 mmol) with stirring and the reaction mixture was heated to gentle reflux with continued stirring for 24 hours. The

solution was then cooled and quenched with DI water (10 mL). Then, it was neutralized using

conc. HCl acid. The yellow liquid was diluted with CH_2Cl_2 (10 mL) and transferred to a

separatory funnel. The organic layer was separated and the aqueous layer washed with CH_2Cl_2

(2 x 10 mL). The combined organic layers (yellow liquid) were washed with sat. NaCl solution

(15 mL) and dried over Na_2SO_4. The drying agent was filtered off and the solvent evaporated to

give an off-white to yellow solid. The crude product was recrystallized from hexane to yield fine

white crystals (0.89 g, 4.6 mmol, 47%). mp 83-84 ºC. ^{1}H NMR (600 MHz, $CDCl_3$): δ 7.27 (m,

2H, Ar), 6.95 (m, 3H, Ar), 3.99 (ddd, 4.2 Hz, 8.4 Hz, 10.2 Hz, H-1), 3.71 (ddd, 4.8 Hz, 8.4 Hz,

10.8 Hz, H-2), 2.60 (broad s, 1H, OH), 2.15 (m, 1H, H-6a), 2.10 (m, 1H, H-3a), 1.74 (m, 2H,

CH_2), 1.43-1.24 (m, 4H, CH_2). ^{13}C NMR (150 MHz, $CDCl_3$): δ 157.93(Ar-C_q), 129.64 (2C, Ar-

CH), 121.36 (1C, Ar-CH), 116.45 (2C, Ar-CH), 82.29 (C-1), 73.55 (C-2), 32.12 (C-3), 29.28 (C-

6), 24.09, 24.02. DART-HRMS: *m/z* calculated for $C_{12}H_{17}O_2$ [M + H]$^+$ 193.1224, found

193.1245, *m/z* calculated for $C_{12}H_{15}O$ [M + H − H_2O]$^+$ 175.1118, found 175.1150.

(±)-trans-2-(napthalen-2-yloxy)cyclohexanol **9**. In a 100 mL round-bottom flask

equipped with reflux condenser was placed a previously prepared solution of NaOH in ethanol

(pH 14, 18 mL) to which was added cyclohexene oxide (2.0 mL, 20.0 mmol, Sigma) and 2-

naphthanol (2.95 g, 20.5 mmol, technical grade). The sandcolored suspension was stirred and

heated to about 90 ºC (oil bath temperature), which caused 2-naphthanol to dissolve and gave a

clear brown solution. Reaction progress was monitored by TLC (CH_2Cl_2). After consumption of

starting material, solution was allowed to cool to give a light-brown to yellow solution with off-

white solid. The suspension was then diluted with water (5 mL) and neutralized using conc. HCl.

The product was then extracted using CH_2Cl_2 (20 mL) and the aqueous layer washed twice with

CH_2Cl_2 (10 mL). The organic layers were combined and dried over Na_2SO_4. After filtration, the

solvent was removed to give a sandcolored solid, which was recrystallized from ethanol to yield

the product as fine white needle-shaped crystals (2.48 g, 52 %). mp 136-137 ºC. ^{1}H NMR (600

MHz, $CDCl_3$): δ (ppm) 7.74 (t, 6.6 Hz, 2H, Ar), 7.40 (d, 8.4 Hz, 1H, Ar), 7.42 (ddd, 1.2 Hz, 6.6

Hz, 7.8Hz, 1H, Ar), 7.32 (ddd, 1.2 Hz, 6.6 Hz, 7.8 Hz, 1H, Ar), 7.21 (br d, 2.4 Hz, 1H, Ar), 7.15 (dd, 2.4 Hz, 9.0 Hz, 1H, Ar), 4.15 (ddd, 4.8 Hz, 9.0 Hz, 10.8 Hz, H-1), 3.77 (ddd, 4.8 Hz, 8.4 Hz, 10.8 Hz, H-2), 2.24 (m, 1H, H-6), 2.12 (m, 1H, H-3), 2.00 (br s, OH), 1.77 (m, 2H, CH_2), 1.44 (m, 1H, CH_2), 1.40-1.29 (m, 3H, CH_2). ^{13}C NMR (150 MHz, $CDCl_3$): δ (ppm) 155.78 (Ar, C-O, C-7), 134.58 (Ar, C_q), 129.65 (Ar, CH), 129.31 (Ar, C_q), 127.70 (Ar, CH), 126.84 (Ar, CH), 126.47 (Ar, CH), 123.91 (Ar, CH), 119.66 (Ar, CH), 109.58 (Ar, CH), 82.36 (C-1), 73.55 (C-2), 32.20 (C-3), 29.20 (C-6), 24.10 (C-4), 24.01 (C-5). DART-HRMS: m/z calculated for $C_{16}H_{19}O_2$ $[M + H]^+$ 243.1380, found 243.1409. m/z calculated for $C_{16}H_{17}O$ $[M + H - H_2O]^+$ 225.1285, found 225.1278.

(±)-trans-2-(3,4,5-trimethoxyphenyloxy)cyclohexanol **11**. In a 100 mL round-bottom flask added cyclohexene oxide (1.50 mL, 14.8 mmol) and 3,4,5-trimethoxyphenol (2.69 g, 14.6 mmol) in a previously prepared solution of NaOH in EtOH (20 mL, pH = 14). A reflux condenser was attached and the reaction heated to reflux using an oilbath. The dark brown solution was heated for 6 hours, then allowed to cool to RT. The solution was diluted with H_2O (15 mL) and then extracted using CH_2Cl_2 (30 mL). The aqueous layer was washed using CH_2Cl_2 (2x10 mL) and the combined organic layers were dried over Na_2SO_4. The drying agent was filtered off and solvent removed using a rotavap to give a brown viscous oil which solidified after cooling. The crude product was recrystallized from hexane to yield off-white to tan crystals (3.38 g, 81%). mp 76-81 ºC. ^1H NMR (600 MHz, $CDCl_3$): δ (ppm) 6.19 (s, 2H, Ar), 3.90 (m, H-2), 3.82 (s, 6H, -OCH_3), 3.77 (s, 3H, -OCH_3), 3.68 (m, H-1), 2.59 (br s, OH), 2.10 (m, 2H, CH_2), 1.74 (m, 2H, CH_2), 1.38 (m, 1H, CH_2), 1.29 (m, 3H, CH_2). ^{13}C NMR (150 MHz, $CDCl_3$): δ (ppm) 154.47 (Ar-COC_{Cy}), 153.80 (2 C, Ar-$COCH_3$), 132.97 (Ar-$COCH_3$), 94.68 (2 C, Ar-CH), 83.25 (C-2), 73.57 (C-1), 61.10 (-OCH_3), 56.22 (2 C, -OCH_3), 32.15 (CH_2), 29.54 (CH_2), 24.09 (CH_2), 23.97 (CH_2). DART-HRMS: m/z calculated for $C_{15}H_{23}O_5$ $[M + H]^+$ 283.1540, found 283.1535.

(±)-trans-2-(p-tert-butyl-phenyloxy)cyclohexanol **13**. In a 100 mL round-bottom flask equipped with reflux condenser was placed a previously prepared solution of Na in ethanol (0.5 M, 20 mL) to which was added cyclohexene oxide (2.0 mL, 19.8 mmol) and *p-tert*-butylphenol (3.21 g, 21.4 mmol). The reaction mixture was heated to about 90 ºC (oil bath temperature), giving a clear solution. Reaction progress was monitored by TLC (CH_2Cl_2) and DART-HRMS. After consumption of starting material (2h45), solution was allowed to cool to give a light-yellow solution. The solution was then diluted with water (10 mL) and neutralized using conc. HCl, during which a white solid precipitated out. Then, CH_2Cl_2 (20 mL) was added to extract the product, giving two opaque colorless layers and the organic layer was separated. The aqueous layer was extracted with CH_2Cl_2 (2x12.5 mL). The organic layers were combined and dried over Na_2SO_4. After filtering off the drying agent, solvent was removed to give an off-white solid. The crude product was recrystallized twice from hexane to yield the product as fine white needle-shaped crystals (1.12 g, 23 %). mp 88-91 ºC. ^{1}H NMR (600 MHz, $CDCl_3$): δ (ppm) 7.28 (m, 2H, Ar), 6.87 (m, 2H, Ar), 3.95 (ddd, 4.8 Hz/9.0 Hz/10.2 Hz, 1H, H-2), 3.69 (m, 1H, H-1), 2.60 (br s, OH), 2.15 (m, 1H, CH_2), 2.09 (m, 1H, CH_2), 1.73 (m, 2H, CH_2), 1.42-1.24 (m, 4H, CH_2), 1.28 (s, 9H, tBu-CH_3). ^{13}C NMR (150 MHz, $CDCl_3$): δ (ppm) 155.62 (Ar, C_q), 144.14 (Ar, C_q), 126.42 (2C, Ar), 115.92 (2C, Ar), 82.43 (C-2), 73.61 (C-1), 34.18 (C_q, tBu), 32.09, 31.59 (3C, tBu), 29.40, 24.12, 24.03. DART-HRMS: *m/z* calculated for $C_{16}H_{25}O_2$ [M + H]$^+$ 249.1850, found 249.1835; *m/z* calculated for $C_{16}H_{23}O$ [M + H – H_2O]$^+$ 231.1744, found 231.1716; *m/z* calculated for $C_{32}H_{49}O_4$ [2M + H]$^+$ 497.3626, found 497.3634; *m/z* calculated for $C_{16}H_{24}O_2$ [M]$^{+•}$ 248.1776, found 248.1736.

(±)-trans-2-(2,6-dimethylphenyloxy)cyclohexanol **15**. To a solution of Na (0.1 g) in ethanol (10 mL) was added cyclohexene oxide (1.0 mL, 9.9 mmol) and 2,6-dimethylphenol (1.25 g, 10.2 mmol) with stirring and the reaction mixture was heated to gentle reflux for 24 hours. The solution was then cooled and quenched with DI water (10 mL) and neutralized using conc. HCl acid. The dark-brown liquid was then diluted with CH_2Cl_2 (10 mL) and transferred to a

separatory funnel. The organic layer was separated and the aqueous layer washed with CH_2Cl_2

(2 x 10 mL) until a nearly clear yellow aqueous layer remained. The combined organic layers

(dark-brown liquid) were washed with sat. NaCl solution (15 mL) and dried over Na_2SO_4. After

filtration, the solvent was evaporated to give a dark-brown liquid (2.0 g). The crude product was

purified via column chromatography (mob. phase 9:1 hexane:ethyl acetate) to yield a clear pale-

yellow liquid (1.52 g, 6.9 mmol, 80%). $R_f = 0.30$ (9:1 hexane:EtOAc). ^{1}H NMR (600 MHz,

$CDCl_3$): δ 6.99 (d, 7.8 Hz, 2H, *m*-Ar), 6.90 (dd, 7.2 Hz, 8.4 Hz, 1H, *p*-Ar), 3.79 (m, 2H, H-1, H-

2), 2.99 (broad s, 1H, OH), 2.29 (s, 6H, CH_3), 2.09 (m, 1H), 1.76 (m, 1H), 1.68 (m, 2H), 1.4-1.25

(m, 3H), 1.11 (tq, 3.6 Hz, 13.2 Hz, 1H). ^{13}C NMR (150 MHz, $CDCl_3$): δ 153.33 ($C_{q,Ar}$-O-C),

131.41 (2C, C_q), 129.09 (2C, *m*-Ar-CH), 123.65 (1C, *p*-Ar-CH), 84.81, 74.62, 32.25, 29.70,

24.34, 24.13, 17.49 (2C, CH_3). DART-HRMS: *m/z* calculated for $C_{14}H_{21}O_2$ [M + H]$^+$ 221.1537,

found 221.1513, *m/z* calculated for $C_{14}H_{19}O$ [M + H – H_2O]$^+$ 203.1431, found 203.1440; found

221.1513, *m/z* calculated for C14H24NO2 [M + NH$_4$]$^+$ 238.1807, found 238.1846.

(±)-trans-2-(cyclohexyloxy)cyclohexanol **17**. In a 100 mL round-bottom flask equipped

with reflux condenser was placed a previously prepared solution of Na in cyclohexanol (0.5 M,

20 mL) to which was added cyclohexene oxide (2.0 mL, 19.8 mmol). The reaction mixture was

heated to reflux. Reaction progress was monitored *via* TLC (CH_2Cl_2). After 24 h, solution was

allowed to cool and was then diluted with water (20 mL) and neutralized using conc. HCl. Then,

CH_2Cl_2 (10 mL) was added to extract the product and the sand colored organic layer was

separated. The brown-orange colored aqueous layer was extracted with CH_2Cl_2 (2x15 mL). The

organic layers were combined and washed with DI water (20 mL), then sat. NaCl solution (2x20

mL) and consequently dried over Na_2SO_4. After filtration, the solvent was removed under

reduced pressure to give a yellow liquid, from which cyclohexanol was removed using a rotavap

and oil pump vacuum. The remaining yellow oily liquid was separated using column

chromatography (mob. phase CH_2Cl_2) to give the desired product as a clear yellow oil (640.4 mg,

16 %). $R_f = 0.18$ (CH_2Cl_2). ^{1}H NMR (600 MHz, $CDCl_3$): δ (ppm) 3.34 (m, 2H, H-1, H-7), 3.08

(dt, 4.2 Hz, 10.2 Hz, 1H, H-2), 2.70 (broad s, OH), 2.0-1.9 (m, 3H), 1.82 (m, 1H), 1.68 (m, 4H), 1.51 (m, 1H), 1.3-1.1 (m, 10H). ^{13}C NMR (150 MHz, CDCl$_3$): δ (ppm) 81.39 (C-2), 75.90 (C-7), 73.82 (C-1), 34.22, 32.60, 32.03, 30.63, 25.76, 24.53, 24.51, 24.37, 24.09. DART-HRMS: *m/z* calculated for C$_{12}$H$_{23}$O$_2$ [M + H]$^+$ 199.1693, found 199.1692. *m/z* calculated for C$_{12}$H$_{21}$O [M + H – H$_2$O]$^+$ 181.1587, found 181.1615.

trans-2-(t-butoxy)cyclohexanol **19**. In a 100 mL RBF was combined Cu(BF$_4$)$_2$ (61.8 mg, 0.26 mmol), dichloromethane (20 mL), cyclohexene oxide (2.0 mL, 19.8 mmol) and freshly distilled *tert*-butanol (7.6 mL, 79.5 mmol). The resulting pale blue solution was stirred at rt. After the starting material was consumed (monitored by TLC, 90:10 hexane:ethyl acetate) after ~24 h, the reaction was quenched with DI water (20 mL), the layers separated and the aqueous extracted with dichloromethane (2x7 mL). The combined org. layers were washed with sat. NaCl soln. (2x20 mL) and dried over Na$_2$SO$_4$. After filtration, the solvent was evaporated to give a slightly milky liquid. TLC and DART-MS analysis showed the formation of multiple products (including a dimeric compound containing two cyclohexane rings). The desired product was isolated using column chromatography to give a clear viscous oil that solidified to form white needle-like crystals overnight at 4 ºC (0.60 g, 18% yield). mp 32-34 ºC. ^{1}H NMR (600 MHz, CDCl$_3$): δ (ppm) 3.30 (m, 1H, H-1), 3.19 (m, 1H, H-2), 2.55 (s, OH), 2.01 (m, 1H, H-6a), 1.90 (m, 1H, H-3a), 1.66 (m, 1H, H-4a), 1.65 (s, 1H, H-5a), 1.30-1.22 (m, 4H, H-3b,4b,5b,6b), 1.22 (s, 9H, CH$_3$). ^{13}C NMR (150 MHz, CDCl$_3$): δ (ppm) 76.57 (C-2), 74.08 (C-1), 73.97 (C$_q$, *t*Bu), 33.51 (C-3), 32.17 (C-6), 29.16 (3C, CH$_3$), 24.82 (C-5), 24.27 (C-4). DART-HRMS: *m/z* calculated for C$_{10}$H$_{21}$O$_2$ [M + H]$^+$ 173.1537, found 173.1525.

(±)-trans-2-(pyridin-2-ylthio)cyclohexanol **21**. In a 50 mL round-bottom flask equipped with a reflux condenser was placed 2-mercaptopyridine (1.22 g, 11.0 mmol) in a 1:1 mixture of THF:H$_2$O (10 mL) and added cyclohexene oxide (1.0 mL, 9.9 mmol) and sodium tetraborate (0.43 g, 1.1 mmol). The reaction mixture was heated to about 40 ºC, giving a yellow solution. After 2.5 h, the solution was allowed to cool and then extracted with CH$_2$Cl$_2$ (3x10 mL). The

combined yellow organic layers were washed with sat. $NaHCO_3$ soln. (15 mL) and dried over

Na_2SO_4. After filtering off the drying agent, solvent was removed to give a yellow oil, which was

purified using column chromatography (silica, 99:1 CH_2Cl_2:MeOH) to give a clear yellow oil

(0.68 g, 33%). R_f = 0.18 (99:1 CH_2Cl_2:MeOH). ^{1}H NMR (600 MHz, $CDCl_3$): δ (ppm) 8.33 (m,

1H, H-11), 7.48 (t, 6.9 Hz, 1H, H-9), 7.27 (dd, 0.6 Hz, 7.8 Hz, H-8), 7.00 (m, H-10), 6.12 (s, 1H,

OH), 3.50 (dt, 4.2 Hz, 10.2 Hz, H-2), 3.40 (dt, 3.9 Hz, 11.4 Hz, H-1), 2.19 (br d, 12.6 Hz, H-3a),

2.12 (br d, 13.2 Hz, H-6a), 1.74 (d, 6.6 Hz, 2H, H-4a,5a), 1.46 (br q, 12.6 Hz, H-6b), 1.37 (br q,

12.0 Hz, H-3b), 1.28 (q, 12.0 Hz, 2H, H4b,5b). ^{13}C NMR (150 MHz, $CDCl_3$): δ (ppm) 159.60

(C_q, C-7), 148.76 (C-11), 136.67 (C-9), 123.43 (C-8), 120.16 (C-10), 76.07 (C-2), 52.39 (C-1),

36.28 (C-3), 32.49 (C-6), 26.37, 24.25. DART-HRMS: *m/z* calculated for $C_{11}H_{16}NSO$ $[M + H]^+$

210.0948, found 210.0973. *m/z* calculated for $C_{11}H_{14}NS$ $[M + H - H_2O]^+$ 192.0842, found

192.0798.

  (±)-trans-2-(p-tolylsulfonyl)cyclohexanol **23**. Adapted from the literature.[86] In a 50 mL

round-bottom flask with a condenser attached, was placed *trans*-2-(p-tolylsulfanyl)-cyclohexanol

4 (1.99g, 8.97 mmol) and glacial acetic acid (4 mL). After hydrogen peroxide (4 mL, 30 wt%,

35.3 mmol) was added, the milky white mixture was heated to reflux for 5 hours, after which the

condenser was taken off and the clear-yellow solution heated without boiling. After another 1.5

hours, the gold-brown viscous liquid was allowed to cool to RT and left open overnight to

solidify and give a tan-colored solid cake, which was recrystallized from a minimum amount of

solvent (4:6 mixture of $CHCl_3$:hexane) to yield the product as pale-yellow crystals (1.40 g,

61.4%). mp 109-116 ºC. ^{1}H NMR (600 MHz, $CDCl_3$): δ 7.76 (d, 7.8Hz, 2H, Ar), 7.38 (d, 8.4

Hz, 2H, Ar), 3.88 (dt, 4.8Hz, 10.2 Hz, H-1), 3.83 (s, OH), 2.95 (ddd, 4.2Hz, 10.2Hz, 12.6Hz, H-

2), 2.46 (s, 3H, tolyl-CH_3), 2.12 (m, 1H, H-6), 1.89 (m, 1H, H-3), 1.70 (m, 2H, CH_2), 1.37-1.12

(m, 4H, H-3,H-6,CH_2). ^{13}C NMR (150 MHz, $CDCl_3$): δ 145.21 (Ar, C_q), 133.78 (Ar, C_q), 129.86

(Ar, 2C), 129.05 (Ar, 2C), 68.98 (C-2), 68.28 (C-1), 34.12 (C-6), 25.75, 24.56 (C-3), 23.58, 21.64 (tolyl-CH_3). DART-HRMS: *m/z* calculated for $C_{13}H_{19}SO_3$ [M + H]$^+$ 255.1050, found 255.1079.

(±)-trans-2-benzylcyclohexanol **25**. Adapted from the literature.[217] In a 50 mL 3-neck flask with condenser, dropping funnel and bubbler attached, placed magnesium ribbon pieces (0.61 g) and flushed with N_2. Added dry THF (18 mL), then slowly added benzyl bromide (1.2 mL in 8 mL dry THF) through the dropping funnel. Cooled on ice, then let stir at RT for 2h. To the slushy gray reaction mixture was added cyclohexene oxide (0.7 mL, in 5 mL THF) dropwise while cooling on ice. After ~15 min, allowed the dark gray colored reaction mixture to stir at rt overnight. Quenched with H_2O (20 mL), then filtered into a separatory funnel and extracted the aqueous with ethyl acetate (3x20 mL). The combined organic layers were washed with sat. NaCl solution (20 mL) and then dried over $MgSO_4$. After evaporation of solvent, a pale yellow oil was retained, which was separated via column chromatography (mob. phase gradient 9:1 – 8:2 hexane:ethyl acetate) to isolate the product as white needle-like crystals (78 mg, 6%) after evaporation of eluent. R_f = 0.18 (9:1 hexane:ethyl acetate). mp 73-75 ºC. ^{1}H NMR (600 MHz, CDCl$_3$): δ 7.27 (m, 2H), 7.18 (m, 3H), 3.29 (dt, 4.8 Hz, 9.6 Hz, H-1), 3.16 (dt, 13.8 Hz, 5.4 Hz, 1H, Benzyl-CH_2), 2.35 (m, 1H, Benzyl-CH_2), 1.97 (m, 1H), 1.71 (m, 1H), 1.63 (m, 1H), 1.57 (m, 1H), 1.50 (m, 1H, H-2), 1.43 (s, 1H, OH), 1.26 (m, 2H), 1.08 (m, 1H), 0.90 (m, 1H). ^{13}C NMR (150 MHz, CDCl$_3$): δ 140.84 ($C_{q,Ar}$), 129.50 (2C, Ar-CH), 128.26 (2C, Ar-CH), 125.83 (1C, Ar-CH), 74.65 (C-1), 47.13 (C-2), 39.10 (C-7), 35.93, 30.03, 25.51, 24.99. DART-HRMS: *m/z* calculated for $C_{13}H_{19}O$ [M + H]$^+$ 191.1431, found 191.1433, *m/z* calculated for $C_{13}H_{17}$ [M + H − H_2O]$^+$ 173.1325, found 173.1319; *m/z* calculated for $C_{13}H_{22}NO$ [M + NH_4]$^+$ 208.1701, found 208.1712; *m/z* calculated for $C_{26}H_{37}O_2$ [2M + H]$^+$ 381.2789, found 381.2769.

Acylation reactions. Racemic *trans*-2-substituted cyclohexanols **71** - **89** (0.2 mmol) were dissolved in solvent (CH_2Cl_2, 1 mL). If applicable, pyridine (0.8 μL, 0.01 mmol) was added immediately afterwards together with one equivalent of ProtonSponge® (21 mg, 0.1 mmol). The reaction was initiated by the addition of (±)-2-chloropropionyl chloride **3** or (±)-2-chloro-2-

phenylacetyl chloride **5** (0.1 mmol respectively). The reaction mixtures were stirred at rt for 24

hours and then evaporated to remove solvent (N$_2$ flow). The crude reaction mixtures were then

immediately taken up in CDCl$_3$ for ^{1}H NMR analysis. After this, the acylation product of the

reactions was isolated via column chromatography (mob. phase hexane:ethyl acetate or CH$_2$Cl$_2$,

see below) for full characterization.

(±)-(trans-2-(p-tolylsulfanyl)cyclohexyl) 2-chloropropanoate **71**. Mixture of

diastereomers (ratio of diastereomers determined using quartet signals for CH(CH$_3$)Cl at 4.30-

4.21 ppm). Isolated via column chromatography (R$_f$ = 0.41, 95:5 hexane:ethyl acetate). Clear

pale yellow oil. ^{1}H-NMR (600 MHz, CDCl$_3$): δ (ppm) 7.30 (m, 2H, Ar), 7.15 (m, 2H, Ar), 4.80

(dt, 4.2 Hz, 9.0 Hz, H-1), 4.30/4.26 (q, 10.2 Hz, 1H, CH(CH$_3$)Cl), 3.10 (*dt*, 4.2 Hz, 9.6 Hz, H-2),

2.32 (s, 3H, tolyl-CH$_3$), 2.05 (m, 2H, H-3a), 1.70 (m, 2H), 1.67/1.65 (d, 10.2 Hz, 3H,

CH(CH$_3$)Cl), 1.48-1.38 (m, 2H, H-6a,b), 1.38-1.23 (m, 2H, CH$_2$, H-3b). ^{13}C NMR (150 MHz,

CDCl$_3$): δ 169.47/169.33 (C=O), 137.63/137.61 (Ar-C$_q$), 133.54/133.45 (Ar, 2C), 130.10/130.05

(Ar-C$_q$), 129.73/129.70 (Ar, 2C), 76.39/76.26 (C-1), 53.07/52.78 (CH(CH$_3$)Cl), 50.24/50.17 (C-

2), 31.58/31.40 (C-6), 30.82/30.55 (C-3), 24.86/24.64, 23.42/23.27 (CH(CH$_3$)Cl), 21.69/21.54,

21.15 (tolyl-CH$_3$). DART-HRMS: *m/z* calculated for C$_{16}$H$_{21}$ClO$_2$S [M]$^{+•}$ 312.0951, found

312.0935; *m/z* calculated for C$_{13}$H$_{19}$S [M + H – HO$_2$C-CH(CH$_3$)Cl]$^+$ 205.1046, found 205.1016.

(±)-(trans-2-(p-tolyloxy)cyclohexyl) 2-chloropropanoate **72**. Mixture of diastereomers

(ratio of diastereomers determined using quartet signals for CH(CH$_3$)Cl at 4.30-4.26 ppm).

Isolated via column chromatography (R$_f$ = 0.37, 95:5 hexane:ethyl acetate). ^{1}H NMR (600 MHz,

CDCl$_3$): δ 7.06 (m, 2H, Ar), 6.84 (m, 2H, Ar), 5.02 (ddd, 4.2 Hz, 7.8 Hz, 9.6 Hz, H-1), 4.30/4.26

(q, 7.2 Hz, CH(CH$_3$)Cl), 4.19 (ddd, 4.2 Hz, 7.8 Hz, 9.0 Hz, H-2), 2.27 (s, 3H, tolyl-CH$_3$), 2.10 (m,

2H), 1.76 (m, 2H), 1.59/1.56 (d, 7.2 Hz, 3H, CH(CH$_3$)Cl), 1.55-1.24 (m, 4H). ^{13}C NMR (150

MHz, CDCl$_3$): δ 169.70 (C=O), 155.99 (Ar-C$_q$), 130.62 (Ar-C$_q$), 129.99 (2C, Ar-CH), 116.40

(2C, Ar-CH), 77.53 (C-2), 75.77 (C-1), 52.96 (CH(CH$_3$)Cl), 29.65, 29.30, 23.03, 22.88, 21.58

(CH(CH$_3$)Cl), 20.59 (tolyl-CH$_3$). DART-HRMS: *m/z* calculated for C$_{16}$H$_{22}$ClO$_3$ [M + H]$^+$

297.1252, found 297.1200, *m/z* calculated for $C_{13}H_{17}O$ [M + H – HO_2C-CH(CH₃)Cl]⁺ 189.1284, found 189.1257.

    (±)-(trans-2-(phenyloxy)cyclohexyl 2-chloropropanoate **73**. Mixture of diastereomers (ratio of diastereomers determined using quartet signals for CH(CH₃)Cl at 4.27/4.23 ppm). Isolated via column chromatography (R_f = 0.36, 95:5 hexane:ethyl acetate). Clear yellow oil. ¹H NMR (600 MHz, CDCl₃): δ (ppm) 7.25 (m, 2H, Ar), 6.93 (m, 3H, Ar), 5.03 (ddd, 4.8 Hz, 8.4 Hz, 9.6 Hz, H-1), 4.27 (m, H-2), 4.27/4.23 (q, 7.2 Hz, CH(CH₃)Cl), 2.27 (s, 3H, tolyl-CH₃), 2.10 (m, 2H), 1.76 (m, 2H), 1.57/1.53 (d, 7.2 Hz, 3H, CH(CH₃)Cl), 1.6-1.2 (m, 4H). ¹³C NMR (150 MHz, CDCl₃): δ 169.56 (C=O), 158.16 (Ar-C_q), 129.56 (2C, Ar-CH), 121.26 (C, Ar-CH), 116.32/116.19 (2C, Ar-CH), 77.13 (C-1), 75.79 (C-2), 52.93 (CH(CH₃)Cl), 29.65, 29.32, 23.02, 22.89, 21.54 (CH(CH₃)Cl). DART-HRMS: *m/z* calculated for $C_{15}H_{20}ClO_3$ [M + H]⁺ 283.1096, found 283.1096; *m/z* calculated for $C_{12}H_{15}O$ [M + H – HO_2C-CH(CH₃)Cl]⁺ 175.1118, found 175.1113.

    (±)-(trans-2-(napthalen-2-yloxy)cyclohexyl) 2-chloropropanoate **74**. Mixture of diastereomers (ratio of diastereomers determined using quartet signals for CH(CH₃)Cl at 4.30/4.24 ppm). Isolated via column chromatography (R_f = 0.28, 95:5 hexane:ethyl acetate). White solid. ¹H NMR (600 MHz, CDCl₃): δ (ppm) 7.74 (m, 3H, Ar), 7.44 (m, 1H, Ar), 7.34 (m, 1H, Ar), 7.25 (m, 1H, Ar), 7.15 (m, 1H, Ar), 5.12 (m, H-1), 4.45 (dt, 4.2 Hz, 9.0 Hz, 9.0 Hz, H-2), 4.30/4.24 (q, 6.6 Hz, CH(CH₃)Cl), 2.25 (m, 1H, H-3a), 2.14 (m, 1H, H-6a), 1.81 (m, 2H), 1.55/1.50 (d, 7.2 Hz, CH(CH₃)Cl), 1.67-1.38 (m, 4H). ¹³C NMR (150 MHz, CDCl₃): δ (ppm) 169.72/169.59 (C=O), 155.97/155.94 (C_Ar-O-C), 134.56 (Ar-C_q), 129.60 (Ar-CH), 129.26/129.23 (Ar-C_q), 127.71 (Ar-CH), 126.87/126.82 (Ar-CH), 126.49/126.44 (Ar-CH), 123.89/123.86 (Ar-CH), 119.64/119.54 (Ar-CH), 109.13/108.99 (Ar-CH), 77.41 (C-2), 75.99/75.69 (C-1), 52.88/52.76 (CH(CH₃)Cl), 29.70/29.59, 29.52/29.38, 23.24/23.13, 23.07/22.93, 21.51/21.48 (CH(CH₃)Cl). DART-HRMS: *m/z* calculated for $C_{19}H_{22}ClO_3$ [M + H]⁺ 333.1252, found 333.1292; *m/z* calculated for $C_{16}H_{17}O$ [M + H – HO_2C-CH(CH₃)Cl]⁺ 225.1274, found 225.1276.

(±)-(trans-2-(3,4,5-trimethoxyphenyloxy)cyclohexanol **75**. Mixture of diastereomers (ratio of diastereomers determined using quartet signals for CH(CH₃)Cl at 4.30/4.27 ppm). Isolated via column chromatography (R_f = 0.80, 1:1 hexane:ethyl acetate). Clear colorless oil. ^{1}H NMR (600 MHz, CDCl₃): δ (ppm) 6.20/6.19 (s, Ar, 2H), 5.0 (dt, 4.2 Hz, 8.4 Hz, 1H, H-2), 4.30/4.27 (q, 7.2 Hz, 1H, CH(CH₃)Cl), 4.18 (m, 1H, H-1), 3.81 (s, 6H, -OCH₃), 3.76 (s, 3H, -OCH₃) 2.06 (m, 2H, CH₂), 1.74 (m, 2H, CH₂), 1.59/1.57 (d, 6.6 Hz, 3H, CH(CH₃)Cl), 1.52 (m, 1H, CH₂), 1.40 (m, 3H, CH₂). ^{13}C NMR (150 MHz, CDCl₃): δ (ppm) 169.60/169.55 (C=O), 154.68/154.62 (C-O-C$_{Cy}$), 153.73 (Ar, 2C, C$_q$), 132.75 (Ar, C$_q$), 94.29/94.21 (Ar, 2C, CH), 77.54 (C-1), 75.27 (C-2), 61.06 (-OCH₃), 56.21 (2C, -OCH₃), 52.84/52.72 (CH(CH₃)Cl), 29.73/29.60, 29.17/29.00, 22.89/22.71, 22.80/22.61, 21.54/21.47 (CH(CH₃)Cl). DART-HRMS: *m/z* calculated for $C_{18}H_{26}ClO_6$ [M + H]$^+$ 373.1413, found 373.1453.

(±)-(trans-2-(p-tert-butyl-phenyloxy)cyclohexyl 2-chloropropanoate **76**. Mixture of diastereomers (ratio of diastereomers determined using quartet signals for CH(CH₃)Cl at 4.27/4.24 ppm). Isolated via column chromatography (R_f = 0.35, 95:5 hexane:ethyl acetate). Clear colorless oil. ^{1}H NMR (600 MHz, CDCl₃): δ (ppm) 7.26 (m, 2H, Ar), 6.86 (m, 2H, Ar), 5.02 (m, 1H, H-2), 4.27/4.24 (q, 6.6 Hz, 1H, CH(CH₃)Cl), 4.23 (m, 1H, H-1), 2.13 (m, 1H, CH₂), 2.07 (m, 1H, CH₂), 1.75 (m, 2H, CH₂), 1.56/1.53 (d, 6.6 Hz, 3H, CH(CH₃)Cl), 1.55-1.25 (m, 4H, CH₂), 1.28 (s, 9H, tBu-CH₃). ^{13}C NMR (150 MHz, CDCl₃): δ (ppm) 169.56 (C=O), 155.86 (C$_q$, Ar), 144.00 (C$_q$, Ar), 126.31 (Ar, 2C, CH), 115.87 (Ar, 2C, CH), 115.72 (Ar, C$_q$), 77.12 (C-1), 75.81 (C-2), 52.98 (CH(CH₃)Cl), 34.17 (C$_q$, tBu), 31.60 (tBu-CH₃), 29.66, 29.30, 22.99, 22.86, 21.55 (CH(CH₃)Cl). DART-HRMS: *m/z* calculated for $C_{19}H_{28}ClO_3$ [M + H]$^+$ 339.1722, found 339.1691; *m/z* calculated for $C_{16}H_{23}O$ [M + H – HO₂C-CH(CH₃)Cl]$^+$ 231.1744, found 231.1729.

(±)-(trans-2-(2,6-dimethylphenyloxy)cyclohexyl 2-chloropropanoate **77**. Mixture of diastereomers (ratio of diastereomers determined using quartet signals for CH(CH₃)Cl at 4.29/4.24 ppm). Isolated via column chromatography (R_f = 0.61, 9:1 hexane:ethyl acetate). Clear yellow oil. ^{1}H NMR (600 MHz, CDCl₃): δ (ppm) 6.97 (d, 7.2 Hz, 2H, *m*-Ar), 6.88 (t, 7.2 Hz,

1H, *p*-Ar), 5.06 (m, H-1), 4.29/4.24 (q, 7.2 Hz, CH(CH$_3$)Cl), 4.01 (ddd, 4.5 Hz, 8.4 Hz, 10.2 Hz,

1H, H-2), 2.28/2.27 (s, 6H, CH$_3$), 2.12 (m, 1H), 1.95 (m, 1H), 1.72 (m, 2H), 1.63/1.62 (d, 7.2

Hz, 3H, CH(CH$_3$)Cl), 1.52 (m, 1H), 1.40 (m, 2H), 1.21 (m, 1H). ^{13}C NMR (150 MHz, CDCl$_3$): δ

169.56 (C=O), 154.17 (Ar-C$_q$), 131.07 (2C, Ar-C$_q$), 129.04 (2C, Ar-CH), 123.43 (Ar-CH), 80.12

(C-2), 77.49 (C-1), 53.13 (CH(CH$_3$)Cl), 30.32, 29.91, 23.50 (2C), 21.73 (CH(CH$_3$)Cl), 17.36 (2C,

CH$_3$). DART-HRMS: *m/z* calculated for C$_{17}$H$_{24}$ClO$_3$ [M + H]$^+$ 311.1409, found 311.1397; *m/z*

calculated for C$_{14}$H$_{19}$O [M + H – HO$_2$C-CH(CH$_3$)Cl]$^+$ 203.1431, found 203.1441; *m/z* calculated

for C$_{17}$H$_{27}$ClNO$_3$ [M + NH$_4$]$^+$ 328.1679, found 328.1677.

(±)-(trans-2-(cyclohexyloxy)cyclohexyl 2-chloropropanoate **78**. Mixture of

diastereomers (ratio of diastereomers determined using quartet signals for CH(CH$_3$)Cl at

4.37/4.36 ppm). Isolated via column chromatography (R$_f$ = 0.42, CH$_2$Cl$_2$). Clear colorless oil.

^{1}H NMR (600 MHz, CDCl$_3$): δ (ppm) 4.72 (ddd, 4.2 Hz, 8.4 Hz, 9.6 Hz, 1H, H-2), 4.37/4.36 (q,

7.2 Hz, 1H, CH(CH$_3$)Cl), 3.35 (m, 2H, H-1, H-7), 2.01 (m, 1H), 1.95 (m, 1H), 1.81 (m, 2H), 1.69

(m, 3H), 1.68 (d, 7.2 Hz, 3H, CH(CH$_3$)Cl), 1.65 (m, 1H), 1.50 (m, 1H), 1.4-1.1 (m, 9H). ^{13}C

NMR (150 MHz, CDCl$_3$): δ 169.56/169.48 (C=O), 77.54 (C-2), 77.04, 76.60, 52.99

(CH(CH$_3$)Cl), 33.46, 32.87, 31.52, 29.76, 25.81, 24.32, 24.29, 23.57, 23.41, 21.70/21.66

(CH(CH$_3$)Cl). DART-HRMS: m/z calculated for C$_{15}$H$_{26}$ClO$_3$ [M + H]$^+$ 289.1565, found

289.1553; m/z calculated for C$_9$H$_{16}$ClO$_3$ [M + H – C$_6$H$_{10}$]$^+$ 207.0783, found 207.0774; *m/z*

calculated for C$_{12}$H$_{21}$O [M + H – HO$_2$C-CH(CH$_3$)Cl]$^+$ 181.1587, found 181.1569.

(±)-(trans-2-(tert-butoxy)cyclohexyl 2-chloropropanoate **79**. Mixture of diastereomers

(ratio of diastereomers determined using quartet signals for CH(CH$_3$)Cl at 4.36/4.34 ppm).

Isolated via column chromatography (R$_f$ = 0.23, 95:5 hexane:ethyl acetate). Clear pale yellow

oil. ^{1}H NMR (600 MHz, CDCl$_3$): δ (ppm) 4.64 (ddt, 4.2 Hz, 9.0 Hz, 9.0 Hz), 4.36/4.34 (q, 6.6

Hz, CH(CH$_3$)Cl), 3.48 (m, 1H), 2.01 (m, 1H), 1.86 (m, 1H), 1.7-1.6 (m, 2H), 1.69/1.68 (d, 7.2 Hz,

3H, CH(CH$_3$)Cl), 1.4-1.2 (m, 4H), 1.18/1.17 (9H, tBu). ^{13}C NMR (150 MHz, CDCl$_3$): δ 169.59

(C=O), 76.97, 73.93, 70.41, 53.05/52.76, 32.98, 29.43, 28.79/28.72, 23.12, 23.06, 21.89/21.52

(CH(CH$_3$)Cl). DART-HRMS: *m/z* calculated for C$_{13}$H$_{24}$ClO$_3$ [M + H]$^+$ 263.1409, found

263.1426; *m/z* calculated for C$_{10}$H$_{19}$O [M + H – C$_4$H$_8$]$^+$ 207.0783, found 207.0774.

(±)-trans-2-(pyridin-2-ylthio)cyclohexyl 2-chloropropanoate **80**. Mixture of

diastereomers (ratio of diastereomers determined using quartet signals for CH(CH$_3$)Cl at

4.18/4.17 ppm). Isolated via column chromatography (R$_f$ = 0.32, CH$_2$Cl$_2$). Clear yellow oil. ^{1}H

NMR (600 MHz, CDCl$_3$): δ (ppm) 8.41 (m, 1H, H-14), 7.45 (tt, 2.1 Hz, 7.5 Hz, 1H, H-12), 7.16

(t, 8.4 Hz, 1H, H-11), 6.97 (dd, 5.1 Hz, 7.5 Hz, 1H, H-13), 4.91 (m, 1H), 4.18/4.17 (q, 6.9 Hz,

CH(CH$_3$)Cl), 4.11/4.08 (dt, 4.2 Hz, 9.6 Hz, 1H), 2.25 (m, 1H), 2.08 (m, 1H), 1.77 (m, 1H), 1.71

(m, 1H), 1.65 (m, 2H), 1.52/1.51 (d, 7.2 Hz, 3H, CH(CH$_3$)Cl), 1.45 (m, 2H). ^{13}C NMR (150

MHz, CDCl$_3$): δ (ppm) 169.51/169.37 (C$_q$, C=O), 158.34 (C$_q$, C-10), 149.52/149.49 (C-14),

136.14/136.11 (H-12), 123.04/122.96 (H-11), 119.77 (H-13), 76.42/76.26, 53.00/52.80

(CH(CH$_3$)Cl), 45.77/45.61, 31.71/31.50, 30.83/30.68, 24.93/24.84, 23.38/23.31, 21.51/21.45

(CH(CH$_3$)Cl). DART-HRMS: *m/z* calculated for C$_{14}$H$_{19}$ClNSO$_2$ [M + H]$^+$ 300.0820, found

300.0802. *m/z* calculated for C$_{11}$H$_{15}$NS [M + H – HO$_2$C-CH(CH$_3$)Cl]$^+$ 192.0842, found

192.0798.

(±)-(trans-2-(p-tolylsulfonyl)cyclohexyl 2-chloropropanoate **81**. Mixture of

diastereomers (ratio of diastereomers determined using quartet signals for CH(CH$_3$)Cl at

4.03/4.00 ppm). Isolated via column chromatography (R$_f$ = 0.39, 8:2 hexane:ethyl acetate). Off-

white solid. ^{1}H NMR (600 MHz, CDCl$_3$): δ (ppm) 7.73 (d, 8.4 Hz, 2H), 7.36 (d, 7.8 Hz, 2H),

5.06 (dt, 4.8 Hz, 10.2 Hz, H-1), 4.03/4.00 (q, 7.2 Hz, CH(CH$_3$)Cl), 3.27 (ddd, 4.2 Hz, 9.6 Hz,

12.0 Hz, H-2), 2.44 (s, 3H, tolyl-CH$_3$), 2.21 (m, 1H), 2.11 (m, 1H), 1.84 (m, 1H), 1.73 (m, 1H),

1.59 (d, 7.2 Hz, 3H, CH(CH$_3$)Cl), 1.52 (m, 1H), 1.4-1.2 (m, 3H). ^{13}C NMR (150 MHz, CDCl$_3$): δ

168.84 (C=O), 144.91 (C$_{q,Ar}$-S), 135.59 (C$_q$), 129.94 (2C, Ar), 128.87 (2C, Ar), 71.78 (C-1),

65.32 (C-2), 53.03 (CH(CH$_3$)Cl), 31.05 (C-6), 25.16 (C-3), 23.98, 23.16, 21.74 (CH(CH$_3$)Cl),

21.65. DART-HRMS: *m/z* calculated for C$_{16}$H$_{22}$ClO$_4$S [M + H]$^+$ 345.0922, found 345.0938.

(±)-(trans-2-benzylcyclohexyl) 2-chloropropanoate **82**. Mixture of diastereomers (ratio of diastereomers determined using quartet signals for CH(CH$_3$)Cl at 4.28/4.23 ppm). Isolated via column chromatography (R$_f$ = 0.44, 95:5 hexane:ethyl acetate). Clear colorless oil. ^{1}H NMR (600 MHz, CDCl$_3$): δ (ppm) 7.21 (m, 2H, Ph), 7.12 (t, 7.8 Hz, 1H, *p*-Ar), 7.06 (m, 2H, Ph), 4.56 (m, 1H, H-1), 4.28/4.23 (q, 6.9 Hz, CH(CH$_3$)Cl), 2.86 (ddd, 3.6 Hz, 13.2 Hz, 29.4 Hz, 1H, H-7a), 2.22 (ddd, 2.4 Hz, 9.0 Hz, 12.0 Hz, H-7b), 1.96 (m, 1H), 1.88-1.65 (m, 6H), 1.65-1.50 (m, 1H), 1.40-0.93 (m, 4H). ^{13}C NMR (150 MHz, CDCl$_3$): δ 169.81 (C=O), 140.16 (Ar-C$_q$), 129.33/129.28 (2C, Ar-CH), 128.31 (2C, Ar-CH), 126.00 (Ar-CH), 78.73/78.67 (C-1), 52.98/52.88 (CH(CH$_3$)Cl), 43.86/43.66 (C-2), 38.87/38.71 (C-7), 31.58/31.44, 30.02/29.98, 25.01, 24.49, 21.60/21.46 (CH(CH$_3$)Cl). DART-HRMS: *m/z* calculated for C$_{16}$H$_{22}$ClO$_2$ [M + H]$^+$ 281.1303, found 281.1303; *m/z* calculated for C$_{13}$H$_{17}$ [M + H – HO$_2$C-CH(CH$_3$)Cl]$^+$ 173.1325, found 173.1297; *m/z* calculated for C$_{16}$H$_{25}$ClNO$_2$ [M + NH$_4$]$^+$ 298.1564, found 298.1574.

(±)-(trans-2-methylcyclohexyl) 2-chloropropanoate **83**. Mixture of diastereomers (ratio of diastereomers determined using doublet signals for CH(CH$_3$)Cl at 1.68/1.67 ppm). Isolated via column chromatography (R$_f$ = 0.35, 95:5 hexane:ethyl acetate). ^{1}H NMR (600 MHz, CDCl$_3$): δ 4.45 (m, H-1), 4.37/4.36 (q, 7.2 Hz, CH(CH$_3$)Cl), 1.97 (m, 1H), 1.75 (m, 2H), 1.68/1.67 (d, 6.9 Hz, CH(CH$_3$)Cl), 1.64-1.55 (m, 2H), 1.35-1.20 (m, 3H), 1.07 (m, 1H), 0.91 (d, 6.6 Hz, 2H, Cy-CH$_3$), 0.89 (d, 6.6 Hz, 1H, Cy-CH$_3$). ^{13}C NMR (150 MHz, CDCl$_3$): δ 169.84 (C=O), 80.36/80.24 (C-1), 53.12/52.89 (CHClCH$_3$), 37.31/37.20, 34.74, 33.51, 31.48, 25.35/25.27, 24.68, 21.70/21.48 (CHClCH$_3$). DART-HRMS: *m/z* calculated for C$_{10}$H$_{18}$ClO$_2$ [M + H]$^+$ 205.0990, found 205.1040.

(±)-(trans-2-(p-tolylsulfanyl)cyclohexyl 2-chloro-2-phenylethanoate **84**. Mixture of diastereomers (ratio of diastereomers determined using signal for H-2 at 3.05/2.99 ppm). Isolated via column chromatography (R$_f$ = 0.58, 95:5 hexane:ethyl acetate). Clear pale yellow oil. ^{1}H NMR (600 MHz, CDCl$_3$): δ (ppm) 7.51/7.42 (m, 2H, Ph), 7.37/7.33 (m, 3H, Ph), 7.32/7.17 (dt, 2.4 Hz, 7.8 Hz, 2H, Tol), 7.12/7.05 (br d, 7.8 Hz, 2H, Tol), 5.31/5.10 (s, 1H, CHClPh), 4.79/4.75 (dt, 4.2 Hz, 8.4 Hz, H-1), 3.05/2.99 (ddd, 4.2 Hz, 9.0 Hz, 10.2 Hz, H-2), 2.34/2.31 (s, 3H, tolyl-

CH$_3$), 2.11/2.05 (m, 1H), 1.93 (m, 1H), 1.65/1.58 (m, 2H), 1.5-1.2 (m, 4H). ^{13}C NMR (150 MHz, CDCl$_3$): δ 167.57 (C=O), 137.67 (C$_q$), 136.17 (C$_q$), 133.55 (2C, Tol), 130.26 (C$_q$), 129.76/129.67 (2C, Tol), 129.30/129.21 (Ph), 128.88/128.80 (2C, Ph), 128.22/127.99 (2C, Ph), 77.38/76.35 (C-1), 59.52/59.37 (CHClPh), 50.06 (C-2), 31.33, 30.44, 24.71, 23.20, 21.22 (tolyl-CH$_3$). DART-HRMS: *m/z* calculated for C$_{21}$H$_{24}$ClSO$_2$ [M + H]$^+$ 374.1107, found 374.1101; *m/z* calculated for C$_{13}$H$_{17}$S [M + H – HO$_2$C-CHClPh]$^+$ 205.1046, found 205.1036.

(±)-(trans-2-(p-tolyloxy)cyclohexyl 2-chloro-2-phenylethanoate **85**. Mixture of diastereomers (ratio of diastereomers determined using signal for H-2 at 4.18/4.08 ppm). Isolated via column chromatography (R$_f$ = 0.32, 95:5 hexane:ethyl acetate). Clear yellow oil. ^{1}H NMR (600 MHz, CDCl$_3$): δ (ppm) 7.41 (m, 2H, Ph), 7.27 (m, 3H, Ph), 7.07/6.99 (m, 8.4 Hz, 2H, Tol), 6.80/6.65 (dt, 8.4 Hz, 2.4 Hz, 2H, Tol), 5.30/5.23 (s, 1H, CHClPh), 5.02 (m, 1H, H-1), 4.18/4.08 (ddd, 9.6 Hz, 8.4 Hz, 4.2 Hz, 1H, H-2), 2.30/2.27 (s, 3H, tolyl-CH$_3$), 2.10 (m, 1H), 1.99 (m, 1H), 1.73 (m, 1H), 1.64 (m, 1H), 1.55-1.24 (m, 4H). ^{13}C NMR (150 MHz, CDCl$_3$): δ 167.78 (C=O), 155.87 (C$_q$-O-C, Tol), 136.09/135.85 (C$_q$, Ar), 130.62/130.46 (C$_q$, Ar), 130.01/129.88 (2C, Tol-CH), 129.19/129.13 (1C, Ph-CH), 128.87/128.78 (2C, Ph-CH), 127.98 (2C, Ph-CH), 116.37/116.30 (2C, Tol-CH), 76.48 (C-2), 76.15 (C-1), 59.48/59.42 (CHClPh), 31.69, 29.64/29.48, 29.18, 22.99, 22.89, 22.77, 20.63 (tolyl-CH$_3$). DART-HRMS: *m/z* calculated for C$_{21}$H$_{24}$ClO$_3$ [M + H]$^+$ 359.1409, found 359.1419; *m/z* calculated for C$_{13}$H$_{17}$O [M + H – HO$_2$C-CH(CH$_3$)Cl]$^+$ 189.1274, found 189.1246.

(±)-(trans-2-(2,6-dimethylphenyloxy)cyclohexyl 2-chloro-2-phenylethanoate **86**. Mixture of diastereomers (ratio of diastereomers determined using signal for H-1 at 5.11/5.05 ppm). Isolated via column chromatography (R$_f$ = 0.54, 9:1 hexane:ethyl acetate). Pale yellow oil. ^{1}H NMR (600 MHz, CDCl$_3$): δ (ppm) 7.5-7.3 (m, 5H, Ph-CH), 7.0-6.8 (m, 3H, Ph(CH$_3$)$_2$-CH), 5.30/5.13 (s, CH(Ph)Cl), 5.11/5.05 (ddd, 4.8 Hz, 8.4 Hz, 10.2 Hz, H-1), 3.94 (m, H-2), 2.26/2.15 (s, 6H, CH$_3$), 2.13/2.02 (m, 1H), 1.94/1.81 (m, 1H), 1.70/1.61 (m, 2H), 1.55-1.10 (m, 4H). ^{13}C NMR (150 MHz, CDCl$_3$): δ 167.75(C=O), 154.30 (Ar-C$_q$), 131.18/131.01 (2C, Ar-C$_q$),

129.25/129.17 (Ph), 129.05/128.95 (2C, Ph(CH$_3$)$_2$), 128.90/128.79 (2C, Ph), 128.22/127.93 (2C, Ph), 123.47/123.37 (Ph(CH$_3$)$_2$), 80.07/79.86 (C-2), 78.19/77.59 (C-1), 59.60/59.29, 30.37/30.01, 29.77/29.64, 23.47/23.41, 23.36/23.31, 17.34/17.28 (2C, CH$_3$). DART-HRMS: *m/z* calculated for C$_{22}$H$_{26}$ClO$_3$ [M + H]$^+$ 373.1565, found 373.1553; *m/z* calculated for C$_{14}$H$_{19}$O [M + H – HO$_2$C-CH(CH$_3$)Cl]$^+$ 203.1431, found 203.1440; *m/z* calculated for C$_{14}$H$_{16}$ClO$_2$ [M + H – HOPh(CH$_3$)$_2$]$^+$ 251.0834, found 251.0851; *m/z* calculated for C$_{22}$H$_{29}$ClNO$_3$ [M + NH$_4$]$^+$ 390.1836, found 390.1880.

(±)-(trans-2-(cyclohexyloxy)cyclohexyl 2-chloro-2-phenylethanoate **87**. Mixture of diastereomers (ratio of diastereomers determined using signal for H-2 at 4.78/4.74 ppm). Isolated via column chromatography (R$_f$ = 0.48, CH$_2$Cl$_2$). Clear colorless oil. ^{1}H NMR (600 MHz, CDCl$_3$): δ (ppm) 7.49 (m, 2H, Ph), 7.36 (m, 3H, Ph), 5.32/5.32 (s, CHPhCl), 4.78/4.74 (m, 1H, H-2), 3.33/3.29 (m, 1H), 3.25/3.16 (m, 1H), 2.1-1.0 (m, 18H). ^{13}C NMR (150 MHz, CDCl$_3$): δ 167.78/167.73 (C=O), 136.20/136.13 (C$_q$, Ph), 129.27/129.18 (Ph), 128.91/128.82 (2C, Ph), 128.10/128.04 (2C, Ph), 78.15/77.84 (C-2), 76.92/76.87, 76.23/76.12, 59.59/59.55, 33.43/33.25, 32.68/32.39, 31.57/31.34, 29.92/29.47, 25.81/25.71, 24.38/24.32, 23.55/23.38, 23.43/23.23. DART-HRMS: *m/z* calculated for C$_{20}$H$_{28}$ClO$_3$ [M + H]$^+$ 351.1722, found 351.1738.

(±)-(trans-2-(p-tolylsulfonyl)cyclohexyl 2-chloro-2-phenylethanoate **88**. Mixture of diastereomers (ratio of diastereomers determined using signal for H-1 at 5.05/4.94 ppm). Isolated via column chromatography (F12-13: R$_f$ = 0.27, F15-16: R$_f$ = 0.31, 8:2 hexane:ethyl acetate). Clear colorless oil. ^{1}H NMR (600 MHz, CDCl$_3$): δ (ppm) 7.8-7.2 (m, 9 H, Ar), 5.09/4.62 (s, CHClPh), 5.05/4.94 (dt, 4.5 Hz, 9.9 Hz, H-1), 3.29/3.18 (ddd, 4.8 Hz, 9.0 Hz, 10.8 Hz, H-2), 2.49/2.42 (s, 3H, tolyl-CH$_3$), 2.31/2.13 (m, 2H), 1.92-1.64 (m, 2H), 1.64-0.8 (m, 4H). ^{13}C NMR (150 MHz, CDCl$_3$): δ 167.29/166.83 (C=O), 144.87/144.83 (C$_{q,Ar}$-S), 136.50/135.34 (C$_q$), 135.78/135.23 (C$_q$), 130.00/129.88, 129.43/129.31, 128.95/128.80, 128.72/128.40, 127.75, 72.44/72.33 (C-1), 65.44/64.90 (C-2), 59.20/58.36 (CH(CH$_3$)Cl), 30.64/30.53, 25.12/24.36, 23.93/23.74, 23.05/22.91, 21.77/21.75. DART-HRMS: *m/z* calculated for C$_{21}$H$_{24}$ClO$_4$S [M + H]$^+$

407.1079, found 407.1084; *m/z* calculated for $C_{21}H_{27}ClNO_4S$ [M + NH_4]$^+$ 424.1344, found

424.1308; *m/z* calculated for $C_{13}H_{17}O_2S$ [M + H – $HO_2CCHCl(C_6H_5)$]$^+$ 237.0944, found

237.0943; *m/z* calculated for $C_{42}H_{47}Cl_2O_8S_2$ [M + H – $HO_2CCHCl(C_6H_5)$]$^+$ 813.2084, found

813.1933.

(±)-trans-2-(methyl)cyclohexyl 2-chloro-2-phenylethanoate **89**. Mixture of diastereomers

(ratio of diastereomers determined using signal for CH(Ph)Cl at 5.34/5.33 ppm). Isolated via

column chromatography (R_f = 0.54, 95:5 hexane:ethyl acetate). Clear yellow oil. ^{1}H NMR (600

MHz, CDCl$_3$): δ (ppm) 7.19 (m, 2H, Ph), 7.35 (m, 3H, Ph), 5.34/5.33 (s, CH(Ph)Cl), 4.46/4.43

(dt, 4.2 Hz, 10.2 Hz, H-1), 1.98/1.85 (m, 1H), 1.73 (m, 1H), 1.68 (m, 1H), 1.62-1.45 (m, 2H),

1.35-1.11 (m, 3H), 1.03 (m, 1H), 0.86/0.63 (d, 6.6 Hz, 3H, CH$_3$). ^{13}C NMR (150 MHz, CDCl$_3$):

δ (ppm) 168.15 (C_q, C=O), 136.27/136.06 (C_q, Ph), 129.25/129.22 (Ph), 128.85/128.82 (2C, Ph),

127.99/127.97 (2C, Ph), 81.02/80.92 (C-1), 59.76/59.45 (CH(Ph)Cl), 37.25/37.11, 33.43,

31.50/31.12, 25.22/25.16, 24.67/24.56, 18.37/18.03 (CH$_3$). DART-HRMS: *m/z* calculated for

$C_{15}H_{20}ClO_2$ [M + H]$^+$ 267.1147, found 267.1139; *m/z* calculated for C_7H_{13} [M + H – HO_2C-

CH(Ph)Cl]$^+$ 97.1012, found 97.1017; *m/z* calculated for $C_{15}H_{23}ClNO_2$ [M + NH_4]$^+$ 284.1417,

found 284.1370.

Chapter 3: Oxidative Esterification.

The ^{1}H and ^{13}C NMR and high-resolution mass spectral data for compounds **90 – 96**

characterized hereafter can be found in Appendices A+B.

General procedure for oxidative esterification of primary alcohols. The respective

primary alcohol (1.0 mmol) was added to a suspension of Oxone® (400.0 mg, 1.3 mmol),

CaCl2 · 2 H_2O (73.5 mg, 0.5 mmol) and TEMPO (1.6 mg, 0.01 mmol) in dichloromethane (2

mL). The reaction was initiated by the addition of 0.1 mL DI water. The reaction mixture was

stirred at rt for the indicated times or until TLC or GC/MS showed consumption of the starting

material and then filtered. After evaporation of the solvent using a rotavap, the crude reaction

mixtures were separated via column chromatography (mob. phase hexane:ethyl acetate, as noted)

to yield the desired ester dimers.

Hexyl hexanoate **90**.[218] Isolated via column chromatography (R_f = 0.38, 98:2

hexane:ethyl acetate). Clear colorless oil. ^{1}H-NMR (600 MHz, $CDCl_3$): δ (ppm) 4.03 (t, 6.6 Hz,

2H), 2.26 (t, 7.5 Hz, 2H), 1.59 (m, 4H), 1.28 (m, 10 H), 0.86 (dt, 2.4 Hz, 6.9 Hz, 6H). ^{13}C NMR

(150 MHz, $CDCl_3$): δ (ppm) 174.04 (C=O), 64.43 (C-O), 34.42, 31.50, 31.39, 28.68, 25.66,

24.77, 22.60, 22.39, 14.03, 13.95. HRMS: *m/z* calculated for $C_{12}H_{25}O_2$ [M + H]$^+$ 201.1849, found

201.1823; *m/z* calculated for $C_{24}H_{49}O_4$ [M + H]$^+$ 401.3626, found 401.3581; analytical data

matched those previously reported.

Propyl propanoate **91**.[219] Isolated by distilling off the more volatile aldehyde

sideproduct. Clear colorless oil. ^{1}H-NMR (600 MHz, $CDCl_3$): δ (ppm) 4.00 (t, 6.9 Hz, 2H), 2.29

(q, 7.6 Hz, 2H), 1.63 (m, 2H), 1.11 (t, 7.5 Hz, 3H), 0.91 (t, 7.2 Hz, 3H). ^{13}C NMR (150 MHz,

$CDCl_3$): δ (ppm) 174.74 (C=O), 65.99 (C-O), 27.70, 22.08, 10.47, 9.26. HRMS: *m/z* calculated

for $C_6H_{13}O_2$ [M + H]$^+$ 117.0911, found 117.0895; analytical data matched those previously

reported.

Dodecyl dodecanoate **92**.[220] Isolated via column chromatography (R_f = 0.65 (95:5

hexane:ethyl acetate), 98:2 hexane:ethyl acetate). Clear colorless oil. ^{1}H-NMR (600 MHz,

$CDCl_3$): δ (ppm) 4.05 (t, 6.6 Hz, 2H), 2.28 (t, 7.5 Hz, 2H), 1.61 (quint, 4H), 1.25 (m, 34 H), 0.88

(t, 7.2 Hz, 6H). ^{13}C NMR (150 MHz, $CDCl_3$): δ (ppm) 174.10 (C=O), 64.48 (C-O), 34.50, 32.00,

29.77, 29.74, 29.72, 29.69 (2C), 29.66, 29.62, 29.56, 29.43 (2C), 29.37, 29.35, 29.25, 28.74,

26.03, 25.12, 22.77 (2C), 14.19 (2C). HRMS: *m/z* calculated for $C_{12}H_{25}O_2$ [M + H]$^+$ 369.3728, found 369.3767; *m/z* calculated for $C_{12}H_{28}O_2N$ [M + NH$_4$]$^+$ 386.3993, found 386.4015; *m/z* calculated for $C_{24}H_{49}O_4$ [2M + H]$^+$ 737.7382, found 737.7208; analytical data matched those previously reported.

Phenylethyl 2-phenylacetate **93**.[221] Isolated via column chromatography (R_f = 0.43, 95:5→9:1 hexane:ethyl acetate). Clear bright yellow oil with rose odor. ^{1}H-NMR (600 MHz, CDCl$_3$): δ (ppm) 7.4-7.1 (m, 10H, Ph-CH), 4.32 (t, 6.9 Hz, 2H, CH$_2$-O), 3.61 (s, 2H, CH$_2$-C(=O)O), 2.92 (t, 6.9 Hz, 2H, CH$_2$-Ph). ^{13}C NMR (150 MHz, CDCl$_3$): δ (ppm) 171.61 (C=O), 137.84 (Cq, Ar), 134.09 (Cq, Ar), 129.40 (2C, CH, Ar), 129.03 (2C, CH, Ar), 128.67 (2C, CH, Ar), 128.58 (2C, CH, Ar), 127.16 (CH, Ar), 126.64 (CH, Ar), 65.45 (CH$_2$-O), 41.54 (CH$_2$-C(=O)O), 35.14 (CH$_2$-Ph). HRMS: *m/z* calculated for $C_{16}H_{17}O_2$ [M + H]$^+$ 241.1224, found 241.1198; *m/z* calculated for $C_8H_9^+$ 105.0699, found 105.0690; analytical data matched those previously reported.

Cyclohexylmethyl cyclohexanecarboxylate **94**.[222] Isolated via column chromatography (R_f = 0.30, 98:2 hexane:ethyl acetate). Clear colorless oil. ^{1}H-NMR (600 MHz, CDCl$_3$): δ (ppm) 3.84 (d, 6.6 Hz, 2H), 2.27 (tt, 3.6 Hz, 11.4 Hz, 1H), 1.91-1.85 (m, 2H), 1.75-1.55 (m, 9H), 1.42 (br dq, 2.7 Hz, 6.0 Hz, 2H), 1.29-1.09 (m, 6H), 0.98-0.90 (m, 2H). ^{13}C NMR (150 MHz, CDCl$_3$): δ (ppm) 176.29 (C=O), 69.33 (C-O), 43.41, 37.25, 29.75 (2C), 29.19 (2C), 26.46, 25.87, 25.78 (2C), 25.56 (2C). HRMS: *m/z* calculated for $C_{14}H_{25}O_2$ [M + H]$^+$ 225.1849, found 225.1827; *m/z* calculated for $C_{28}H_{49}O_4$ [2M + H]$^+$ 449.3625, found 449.3534; analytical data matched those previously reported.

2-Ethoxyethyl 2-ethoxyacetate **95**. Isolated via column chromatography (R_f = 0.43 (2:1 hexane:ethyl acetate), 9:1→2:1 hexane:ethyl acetate). Clear colorless oil. ^{1}H-NMR (600 MHz, CDCl$_3$): δ (ppm) 4.30 (m, 2H), 4.11 (s, 2H), 3.64 (m, 2H), 3.60 (q, 7.0 Hz, 2H), 3.53 (7.0 Hz, 2H), 1.25 (t, 6.9 Hz, 3H), 1.21 (t, 6.9 Hz, 3H). ^{13}C NMR (150 MHz, CDCl$_3$): δ (ppm) 170.58 (C=O), 68.14, 67.93, 67.17, 66.61, 63.87, 15.05, 14.97. HRMS: *m/z* calculated for $C_8H_{17}O_4$ [M +

H]$^+$ 177.1121, found 177.1105; *m/z* calculated for $C_8H_{20}NO_4$ [M + NH$_4$]$^+$ 194.1387, found 194.1377.

2,2-Dimethylpropyl pivalate **96**.[96] Isolated by distilling off pivaldehyde sideproduct (bp 75 °C). Clear colorless oil. ^{1}H-NMR (600 MHz, CDCl$_3$): δ (ppm) 3.74 (s, 2H), 1.21 (s, 9H), 0.94 (s, 9H). ^{13}C NMR (150 MHz, CDCl$_3$): δ (ppm) 178.63 (C=O), 73.69 (C-O), 39.04 (C_q), 31.58 (C_q), 27.33 (3C), 26.52 (3C). HRMS: *m/z* calculated for $C_{10}H_{21}O_2$ [M + H]$^+$ 173.1536, found 173.1580; *m/z* calculated for $C_{20}H_{41}O_4$ [2M + H]$^+$ 345.2999, found 345.3034; *m/z* calculated for $C_{10}H_{22}O_2$ [M + 2H]$^{2+}$ 87.0805, found 87.0789; analytical data matched those previously reported.

Chapter 4: Development of a C(*sp*2)OCH Karplus equation.

^{1}H and ^{13}C NMR analyses and ESI-HRMS spectra of the compounds described hereafter are included in the Appendices A&B.

Trimethylsilyl 2,3,4,6-tetra-O-trimetylsilyl-α/β-D-glucopyranose **54**. Scaled up from the literature.[141] In a 2-neck flask flushed with N$_2$, glucose (2.02 g, 11.2 mmol) was added followed by dichloromethane (20 mL), hexamethyldisilazane (7.5 mL, 35.8 mmol, 3.2 equiv), and TMSOTf (400 µL, 2.2 mmol, 0.2 equiv) to give a white suspension. While stirring under N$_2$ overnight at rt, the solution turned clear-colorless. The solvent was evaporated *in vacuo* and the residue was redissolved in hexane (50 mL) and washed with DI water (3x12 mL). The combined aqueous layers were extracted with hexane (10 mL). The combined organic layers were washed with brine (30 mL), then dried with sodium sulfate. After filtration and evaporation, a clear colorless liquid (6.04 g, 99%, *α:β* 61:39) was obtained and was used without further purification. R$_f$ (9:1 hex:EtOAc) 0.85. ^{1}H NMR (600 MHz, CDCl$_3$): δ 5.00 (d, 3.0 Hz, *α*-1), 4.45 (d, 7.2 Hz, *β*-1), 3.77 (t, 9.0 Hz, 1H), 3.75-3.64 (m, 2H-*α*, 1H-*β*), 3.60 (dd, 6.0 Hz, 10.8 Hz, *β*), 3.44-3.37 (m, 1H-*α*, 2H-*β*), 3.33 (dd, 3.0 Hz, 9.0 Hz, *α*-2), 3.24-3.19 (m, 2H, *β*), 0.16 (s, 9H, *α*-Si(CH$_3$)$_3$), 0.16 (s, 9H, *β*-Si(CH$_3$)$_3$), 0.15 (s, 9H, *α*-Si(CH$_3$)$_3$), 0.15 (s, 9H, *β*-Si(CH$_3$)$_3$), 0.14 (s, 9H, *β*-Si(CH$_3$)$_3$), 0.14 (s, 9H, *α*-Si(CH$_3$)$_3$), 0.14 (s, 9H, *β*-Si(CH$_3$)$_3$), 0.12 (s, 9H, *α*-Si(CH$_3$)$_3$), 0.10 (s, 9H, *α*-Si(CH$_3$)$_3$), 0.10 (s, 9H, *β*-Si(CH$_3$)$_3$). ^{13}C NMR (150 MHz, CDCl$_3$): δ 98.24 (*β*-1), 93.97 (*α*-1),

78.51 (β), 77.61 (β), 76.97 (β), 74.26 (α), 74.10 (β), 72.53 (α), 72.35 (α), 72.05 (α), 62.40 (α),

62.38 (β), 1.47 (β), 1.42 (β), 1.36 (α), 1.05 (α), 1.02 (β), 0.55 (α), 0.53 (α), 0.27 (α), -0.15 (β), -

0.37 (β). HRMS (DART-MS): *m/z* calculated for $C_{21}H_{52}O_6Si_5$ [M]$^{•+}$ 540.2610, found 540.2862;

m/z calculated for $C_{15}H_{33}O_4Si_3$ [M − 2 x TMS-OH]$^{•+}$ 361.1681, found 361.1650. All analytical

data matched those previously reported.[141]

Trimethylsilyl 6-O-acetyl-2,3,4-tris-O-trimethylsilyl-α/β-D-glucopyranoside **55** *and*

acetyl 6-acetyl-2,3,4-tris-O-trimethylsilyl-α/β-D-glucopyranoside **56**. Based on literature

procedures.[142] In a 100 mL round bottom flask, per-TMS-D-glucose (1.194 mg, 2.2 mmol) and

added pyridine (4.3 mL), acetic anhydride (3.2 mL) and acetic acid (273 µL, 2.2 equiv). Stirred

the clear solution for 7 days at room temperature to give a clear slightly yellow reaction mixture.

Diluted with dichloromethane (100 mL) and washed with 0.5 M HCl solution (2x150 mL),

backextracting the combined aqueous layers with dichloromethane (25 mL). After washing with

sat. Na_2CO_3 solution (100 mL), dried organic layers over Na_2SO_4. After filtration, evaporated

solvent to yield a colorless clear oil which was separated via column chromatography (95:5 →

9:1 hexane:ethyl acetate) to yield tetramethylsilyl 6-acetyl-2,3,4-tetramethylsilyl-*α/β*-D-glucose

(0.47 g, 42%) and acetyl 6-acetyl-2,3,4-tetramethylsilyl-*α/β*-D-glucose (0.17 g, 16%).

Trimethylsilyl 6-O-acetyl-2,3,4-tris-O-trimethylsilyl-α/β-D-glucopyranoside **55***:* clear colorless

oil. R*f* (9:1 hex:EtOAc) 0.59/0.49. *α:β* 77:23. ^{1}H NMR (600 MHz, CDCl$_3$): δ 5.02 (d, 3.0 Hz,

α-1), 4.46 (d, 7.8 Hz, *β-1*), 4.34 (dd, 1.5 Hz, 11.7 Hz, *β-6a*), 4.30 (dd, 2.4 Hz, 12.0 Hz, *α*-6a),

4.06 (dd, 4.8 Hz, 12.0 Hz, *α*-6b), 4.00 (ddd, 1.8 Hz, 4.8 Hz, 12.0 Hz, *β-6b*), 3.91 (ddd, 2.4 Hz,

4.8 Hz, 9.6 Hz, *α*-5), 3.79 (app. t, 9.0 Hz, *α*-3), 3.45 (app. t, 9.0 Hz, *α*-4), 3.41-3.38 (m, 3H, *β-*

5,4,3), 3.37 (dd, 3.0 Hz, 9.6 Hz, *α*-2), 2.09 (s, 3 H, *α*-Ac), 2.06 (s, 3H, *β*-Ac), 0.16 (s, 9 H, *β*-

TMS), 0.16 (s, 9 H, *α*-TMS), 0.16 (s, 9 H, *β*-TMS), 0.15 (s, 9 H, *α*-TMS), 0.14 (s, 9 H, *α*-TMS),

0.14 (s, 9 H, *β*-TMS), 0.13 (s, 2 x 9 H, *α*-TMS + *β*-TMS). ^{13}C NMR (150 MHz, CDCl3): δ 171.1

(*α*), 94.1 (*α*), 74.1 (*α*), 74.0 (*α*), 72.5 (*α*), 70.0 (*α*), 64.0 (*α*), 21.1 (*α*), 1.4 (*α*), 1.0 (*α*), 0.6 (*α*), 0.2

(α). HRMS (DART-MS): *m/z* calculated for $C_{20}H_{50}NO_7Si_4$ [M + NH$_4$]$^+$ 528.2664, found 528.2854. *Acetyl 6-O-acetyl-2,3,4-tris-O-trimethylsilyl-α/β-D-glucopyranoside* **56**: clear colorless oil. R$_f$ (9:1 hex:EtOAc) 0.29/0.24. α:β 77:23. ^{1}H NMR (600 MHz, CDCl$_3$): δ 6.08 (d, 3.6 Hz, α-1), 5.43 (d, 7.2 Hz, β-1), 4.34 (dd, 2.4 Hz, 12.0 Hz, β-6a), 4.32 (dd, 2.4 Hz, 12.0 Hz, α-6a), 4.04 (dd, 5.4 Hz, 12.0 Hz, α-6b), 4.02 (dd, 5.4 Hz, 12.0 Hz, β-6b), 3.81 (ddd, 2.4 Hz, 4.8 Hz, 10.2 Hz, α-5), 3.74 (app. t, 9.0 Hz, α-3), 3.57 (dd, 3.0 Hz, 9.0 Hz, α-2), 3.53 (m, 2H, α-4, β-5), 3.45 (m, 3H, β-2, β-3, β-4), 2.12 (s, 3H, β-Ac), 2.10 (s, 3 H, α-Ac), 2.08 (s, 3 H, α-Ac), 2.07 (s, 3 H, β-Ac), 0.16 (s, 9 H, β-TMS), 0.16 (s, 9 H, α-TMS), 0.16 (s, 9 H, α-TMS), 0.15 (s, 18 H, 2x β-TMS), 0.12 (s, 9 H, α-TMS). ^{13}C NMR (150 MHz, CDCl$_3$): δ 170.9, 170.9, 169.6, 169.3, 94.5, 92.2, 78.1, 74.9, 74.7, 74.1, 72.4, 72.3, 71.7, 71.6, 63.5, 63.3, 21.2, 20.8, 20.7, 1.1, 1.0, 0.8, 0.7, 0.7, 0.0. HRMS (DART-MS): *m/z* calculated for $C_{19}H_{44}NO_8Si_3$ [M + NH$_4$]$^+$ 498.2375, found 498.2520. All analytical data matched those previously reported.[142]

6-O-Acetyl-α/β-D-glucopyranose **46**. Adapted from the literature.[142] To the TMS-derivate **55** (85 mg, 0.17 mmol) in a round bottom flask flushed with nitrogen was added dry methanol (3 mL) and DOWEX 50WX8 resin (0.50 g) and stirred at RT. After 10 min, TLC showed **55** to be fully consumed. The reaction mixture was then filtered at 15 min and evaporated. The obtained yellow to orange clear oil was dried under high vacuum overnight (29 mg, 0.13 mmol, 78%). α:β 42:58. ^{1}H NMR (600 MHz, D$_2$O): δ 5.18 (d, 4.2 Hz, α-1), 4.62 (d, 7.8 Hz, β-1), 4.37 (dd, 2.4 Hz, 12.3 Hz, β-6$_S$), 4.31 (dd, 2.4 Hz, 12.0 Hz, α-6$_S$), 4.27 (dd, 4.8 Hz, 12.0 Hz, α-6$_R$), 4.21 (dd, 5.7 Hz, 12.3 Hz, β-6$_R$), 3.99 (ddd, 2.4 Hz, 4.5 Hz, 10.2 Hz, α-5), 3.68 (t, 9.6 Hz, α-3), 3.63 (ddd, 2.4 Hz, 4.8 Hz, 9.9 Hz, β-5), 3.50 (dd, 3.9 Hz, 9.9 Hz, α-2), 3.47-3.41 (m, α-4, β-4, β-3), 3.22 (apt t, 9.0 Hz, β-2), 2.09 (s, β-CH$_3$), 2.09 (s, α-CH$_3$). ^{13}C NMR (150 MHz, D$_2$O): δ 174.17, 174.14, 96.04 (β-1), 92.18 (α-1), 75.54, 74.02 (β-2), 73.36 (β-5), 72.60 (α-3), 71.41 (α-2), 69.60, 69.52, 69.12 (α-5), 63.49 (2C, α-6, β-6), 20.23, 20.21. HRMS (ESI-MS): *m/z* calculated for $C_8H_{14}O_7Na$ [M + Na]$^+$ 245.0637, found 245.0653.

Acetyl 6-O-acetyl-α/β-D-glucopyranoside **47**. Adapted from the literature.[142] To the TMS-derivate **56** (90.8 mg, 0.19 mmol) in a round bottom flask flushed with nitrogen was added dry methanol (3 mL) and DOWEX 50WX8 resin (0.50 g) and stirred at RT. After 10 min, TLC showed **56** to be fully consumed and the reaction mixture was filtered and evaporated. The obtained yellow to orange clear oil was dried under high vacuum overnight (45.2 mg, 0.17 mmol, 89%). *α:β* 24:76. ^{1}H NMR (600 MHz, D_2O:MeOD-d_4 2:1): δ 6.03 (d, 3.6 Hz, *α*-1), 5.48 (d, 8.4 Hz, *β*-1), 4.35 (dd, 2.1 Hz, 12.3 Hz, *β*-6$_R$), 4.29 (dd, 2.4 Hz, 12.0 Hz, *α*-6$_R$), 4.22 (dd, 4.8 Hz, 12.0 Hz, *α*-6$_S$), 4.21 (dd, 5.6 Hz, 12.0 Hz, *β*-6$_S$), 3.87 (ddd, 2.4 Hz, 5.6 Hz, 10.2 Hz, *α*-5), 3.71 (t, 9.6 Hz, *α*-3), 3.70 (ddd, 2.4 Hz, 4.8 Hz, 9.9 Hz, *β*-5), 3.65 (dd, 3.9 Hz, 9.9 Hz, *α*-2), 3.51 (t, 9.9 Hz, *β*-3), 3.45 (t, 9.6 Hz, *α*-4), 3.43 (t, 9.6 Hz, *β*-4), 3.41 (t, 9.6 Hz, *β*-2), 2.16 (s, *α*-CH$_3$).2.15 (s, *β*-CH$_3$), 2.07 (s, *α*-CH$_3$), 2.07 (s, *β*-CH$_3$). ^{13}C NMR (150 MHz, D_2O:MeOD-d_4 2:1): δ 174.98 (C=O, *α*-6Ac), 174.95 (C=O, *β*-1-Ac), 173.75 (C=O, *α*-1-Ac), 173.42 (C=O, *β*-1-Ac), 95.29 (*β*-1), 93.29 (*α*-1), 76.72 (*β*-3), 75.62 (*β*-5), 74.09 (*α*-3), 73.28 (*β*-2), 72.92 (*α*-5), 71.49 (*α*-2), 70.59 (*β*-4), 70.55 (*α*-4), 64.55 (*α*-6), 64.36 (*β*-6), 21.49, 21.49, 21.33, 21.33. HRMS (DART-MS): *m/z* calculated for $C_{10}H_{16}O_8Na$ [M + Na]$^+$ 287.0743, found 287.0709.

Mixture containing 2,6-diacetyl-α/β-D-glucopyranose **48** *and 3,6-diacetyl-α/β-D-glucopyranose* **49**. Heating of a solution of **47** (25 mg) in D_2O:MeOD-d4 (0.6 mL, 2:1 by volume) to 40 °C for 14 h overnight induced acetyl migration to form a mixture containing *β*-**47** (due to the slower acetyl migration from *β*-**47** compared to *α*-**47**), *α*-**48**, *β*-**48**, *α*-**49**, *β*-**49** and *α*-**46**, *β*-**46**, as determined by 1D-TOCSY experiments (see Appendix A for spectra and assignments of chemical shifts). The ratio of the compounds was determined by ^{1}H NMR to be 1:0.48:0.30:0.32:0.13:0.17:0.37, respectively.

Methyl-α/β-D-glucopyranuronate **50**. In a flame-dried round bottom flask, added D-glucurono-6,3-lactone (0.688 g, 3.90 mmol), dry methanol (4 mL) and a small piece of sodium. The suspension was stirred at room temperature for 4 hours to yield an orange-amber clear solution. After evaporation to give an orange sticky syrup, NMR showed 84% conversion to the

desired methyl ester. The product was isolated using column chromatography (100% ethyl acetate, dry loading) to give the desired product as a white crystalline solid (71%). R$_f$ (EtOAc) 0.2. *α:β* 60:40. ^{1}H NMR (600 MHz, D$_2$O): δ 5.26 (d, 3.6 Hz, *α*-1), 4.69 (d, 8.4 Hz, *β*-1), 4.38 (d, 10.2 Hz, *β* -5), 4.07 (d, 9.6 Hz, *α*-5), 3.81 (s, *α*-CH$_3$), 3.81 (s, *β*-CH$_3$), 3.73 (t, 9.3 Hz, *α*-3), 3.60-3.55 (m, 3H, *α*-2, *α*-4, *β*-4), 3.51 (t, 9.3 Hz, *β*-3), 3.29 (apt t, 8.7 Hz, *β*-2). ^{13}C NMR (150 MHz, D$_2$O): δ 171.99 (*β*-C=O), 171.05 (*α*-C=O), 96.20 (*β*-1), 92.44 (*α*-1), 75.13 (*β*-3), 74.64 (*α*-5), 73.68 (*β*-2), 72.30 (*α*-3), 71.48, 71.28, 71.05, 70.66 (*β*-5), 53.10 (CH$_3$), 53.07 (CH$_3$). HRMS (DART-MS): *m/z* calculated for C$_7$H$_{12}$O$_7$Na [M + Na]$^+$ 231.0481, found 231.0501.

(Tetrahydropyran-2-yl)-methyl acetate **53**. Tetrahydropyran-2-yl methanol (2.0 g, 17.2 mmol) was dissolved in pyridine (20 mL) and DMAP (50 mg, 0.4 mmol, 0.05 eq) was added. The reaction mixture was cooled to 0 °C and acetic anhydride (10 ml, 105.8 mmol) was added dropwise. The mixture was allowed to slowly reach room temperature and stirred for another 5 h. The product was obtained by distillation as a clear colorless liquid (1.87 g, 11.8 mmol, 69%). b.p. 205 °C ^{1}H NMR (600 MHz, CDCl$_3$): δ 4.03 (dd, 3.6 Hz, 12.0 Hz, H-6$_S$), 3.97 (m, H-1a), 3.95 (dd, 6.9 Hz, 11.7 Hz, H-6$_R$), 3.50 (m, H-5), 3.40 (dt, 2.4 Hz, 11.4 Hz, H-1b), 2.04 (s, 3H, CH$_3$), 1.82 (m, 1H), 1.5 (m, 4H), 1.29 (m, H-4a). ^{13}C NMR (150 MHz, CDCl$_3$): δ 171.15 (C-7, C=O), 75.47 (C-5), 68.46 (C-1), 67.58 (C-6), 27.83 (C-4), 25.77, 23.01, 21.01 (CH$_3$). HRMS (DART-MS): *m/z* calculated for C$_8$H$_{15}$O$_3$ [M + H]$^+$ 159.1016, found 159.0842; *m/z* calculated for C$_6$H$_{11}$O [M + H – HOAc]$^+$ 99.0805, found 99.0669.

Chapter 5: Synthesis and Conformational Analysis of carbohydrate esters

NMR analyses and ESI-HRMS spectra of the compounds described hereafter are included in the Appendices A&B.

Synthesis of acetylated carbohydrate derivatives.

Acetyl-2,3,4,6-tetra-O-acetyl-α/ß-D-glucopyranoside **58**. Based on literature procedures.[205] In a 100 ml RBF, dissolved D-glucose (2.00 g, 11.1 mmol) in acetic anhydride (30 mL) and cooled to 0°C. Iodine (140 mg, 0.6 mmol) was added and the reaction mixture stirred

for 2 hours. Acetic anhydride was then removed in *vacuo*. DCM (40 mL) was added to dissolve the yellow solid and the organic layer was washed with $Na_2S_2O_3$ (2 x 15 mL), dried with $MgSO_4$, and concentrated in vacuo to give the desired product as a colorless solid (4.12 g, 10.6 mmol, 95%). *α:ß* 75:25. ^{1}H NMR (600 MHz, CDCl$_3$): δ 6.33 (d, 3.7 Hz, α, H-1), 5.47 (t, 9.6 Hz, H-3), 5.14 (t, 9.6 Hz, H-4), 5.10 (dd, 3.6 Hz, 10.2 Hz, H-2), 4.27 (dd, 3.6 Hz, 12.6 Hz, H-6$_R$), 4.12 (ddd, 2.1 Hz, 3.6 Hz, 10.8 Hz, H-5), 4.09 (dd, 2.1, Hz, 12.3 Hz, H-6$_S$), 2.18 (s, 3H, COC**H$_3$**), 2.10 (s, 3H, COC**H$_3$**), 2.04 (s, 3H, COC**H$_3$**), 2.03 (s, 3H, COC**H$_3$**), 2.02 (s, 3H, COC**H$_3$**). ^{13}C NMR (150 MHz, CDCl$_3$): δ 170.73, 170.33, 169.75, 169.48, 168.84, 89.14 (C-1), 69.90 (2C, C-3, C-5), 69.27 (C-2), 67.95 (C-4), 61.53 (C-6), 20.97, 20.79, 20.75, 20.65, 20.54. HRMS (DART-MS): *m/z* calculated for $C_{16}H_{26}NO_{11}$ [M + NH$_4$]$^+$ 408.1500, found 408.1450; *m/z* calculated for $C_{14}H_{19}O_9$ [M + H – HOAc]$^+$ 331.1024, found 331.1065; *m/z* calculated for $C_{14}H_{19}O_9$ [M + H – 2 HOAc]$^+$ 271.0812, found 271.0848; *m/z* calculated for $C_{14}H_{19}O_9$ [M + H – 3 HOAc]$^+$ 211.0601, found 211.0614; *m/z* calculated for $C_{14}H_{19}O_9$ [M + H – 4 HOAc]$^+$ 211.0601, found 211.0614.

Acetyl-2,3,4,6-tetra-O-acetyl-α/ß-D-galactopyranoside **59**. Based on literature procedures.[205] In a 100 ml RBF, dissolved D-galactose (2.00 g, 11.1 mmol) in acetic anhydride (30 mL) and cooled to 0°C. Iodine (140 mg, 0.6 mmol) was added and the reaction mixture stirred for 2 hours. Acetic anhydride was then removed in *vacuo*. DCM (40 mL) was added to dissolve the yellow solid and the organic layer was washed with $Na_2S_2O_3$ (2 x 15 mL), dried with $MgSO_4$, and concentrated in vacuo to give the desired product as a colorless solid (3.73 g, 9.6 mmol, 86%) *α:ß* 87:13. ^{1}H NMR (600 MHz, CDCl$_3$): δ 6.35 (d, 2.4 Hz, H-1), 5.48 (m, H-3), 5.31 (m, 2H, H-2, H-4), 4.32 (dt, 1.2 Hz, 6.6 Hz, H-5), 4.07 (m, 2H, H-6$_{R/S}$), 2.14 (s, 3H, COC**H$_3$**), 2.14 (s, 3H, COC**H$_3$**), 2.02 (s, 3H, COC**H$_3$**), 2.00 (s, 3H, COC**H$_3$**), 1.98 (s, 3H, COC**H$_3$**). ^{13}C NMR (150 MHz, CDCl$_3$): δ 170.44, 170.20 (2C), 169.95, 169.00, 89.77 (C-1), 68.82 (C-5), 67.48, 67.41, 66.49, 61.31 (C-6). HRMS (DART-MS): *m/z* calculated for $C_{16}H_{26}NO_{11}$ [M + NH$_4$]$^+$ 408.1500, found 408.1430; *m/z* calculated for $C_{14}H_{19}O_9$ [M + H – HOAc]$^+$ 331.1024, found 331.1028.

2,3,4,6-Tetra-O-acetyl-α-D-glucopyranuronate **61**. Adapted from the literature.[206] In a

100 ml RBF, dissolved D-glucoronic acid (2.00 g, 10.3 mmol) in acetic anhydride (30 mL) and

cooled to 0°C. Iodine (140 mg, 0.6 mmol) was added and the reaction mixture stirred for 2 hours.

Acetic anhydride was removed in *vacuo*. DCM (40 mL) was added to dissolve the yellow solid

and the organic layer was washed with $Na_2S_2O_3$ (2 x 15 mL), dried with $MgSO_4$, and

concentrated in vacuo to give the desired product as an off-white solid (3.58g, 8.9 mmol, 86%).

α:β 12:88. ^1H NMR (600 MHz, $CDCl_3$): δ 5.80 (d, 4.8 Hz, H-1), 5.30 (m, 2H, H-4, H-3), 5.14

(apt t, 4.8 Hz, H-2), 4.24 (d, 5.4 Hz, H-5), 2.12 (s, 3H, COC**H₃**), 2.05 (s, 3H, COC**H₃**), 2.04 (s,

3H, COC**H₃**), 2.03 (s, 3H, COC**H₃**). ^{13}C NMR (150 MHz, $CDCl_3$): δ 170.09, 169.88, 169.37,

169.06, 91.37 (C-1), 72.43 (C-5), 71.82 (C-3), 70.14 (C-2), 68.62 (C-4), 20.85, 20.64 (2C), 20.60

[only *β* denoted for ^{13}C]. HRMS (DART-MS): *m/z* calculated for $C_{14}H_{22}NO_{11}$ $[M + NH_4]^+$

380.1187, found 380.1175; *m/z* calculated for $C_{12}H_{15}O_9$ $[M + H - HOAc]^+$ 303.0711, found

303.0684; *m/z* calculated for $C_{10}H_{11}O_7$ $[M + H - 2 HOAc]^+$ 243.0499, found 243.0436.

2,3,4-Tri-O-acetyl-β-D-glucopyranurono-6,1-lactone **60**. Based on literature

procedures.[206] 2,3,4,6-Tetra-O-acetyl-α-D-glucopyranuronate **61** (3.58 g, 11.5 mmol) was

dissolved in anhydrous DCM (70 mL) under N_2 and $SnCl_4$ (3.2 mL, 27.4 mmol, 2.4 eq) was

added. The reaction mixture was stirred overnight. DCM (70 mL) and $NaHCO_3$ (175 mL) were

added to the reaction mixture and it was stirred for another 1.5h, before filtering through Celite.

The organic layer was separated and washed with saturated $NaHCO_3$ (4 x 90 mL), dried over

Na_2SO_4, and concentrated in *vacuo*. After recrystallization from methanol, the product was

obtained as colorless crystals (0.56 g, 2.4 mmol, 21%). ^1H NMR (600 MHz, $CDCl_3$): δ 5.91 (apt

t, $J_{1,2}$ 1.5 Hz, $J_{1,3}$ 1.5 Hz, H-1), 4.94 (apt quint, $J_{3,1}$ 1.5 Hz, $J_{3,2}$ 1.5 Hz, $J_{3,4}$ 1.5 Hz, $J_{3,5}$ 1.5 Hz, H-3),

4.80 (apt q, $J_{4,2}$ 1.4 Hz, $J_{4,3}$ 1.4 Hz, $J_{4,5}$ 1.4 Hz, H-4), 4.77 (apt q, $J_{2,1}$ 1.6 Hz, $J_{2,3}$ 1.6 Hz, $J_{2,4}$ 1.6

Hz, H-2), 4.59 (apt t, $J_{5,4}$ 1.8 Hz, $J_{5,3}$ 1.8 Hz, H-5), 2.17 (s, 6H, 2 COCH₃), 2.09 (s, 3h, COCH₃).

^{13}C NMR (150 MHz, $CDCl_3$): δ 169.6, 169.5, 168.7 (2C), 168.0 (C-6), 100.6 (C-1), 71.3 (C-5),

69.2 (C-3), 66.3 (C-4), 66.1 (C-2), 20.9, 20.8 (2C). HRMS (DART-MS): *m/z* calculated for

$C_{12}H_{18}NO_9$ [M + NH$_4$]$^+$ 320.0976, found 320.0958; *m/z* calculated for $C_{12}H_{15}O_9$ [M + H]$^+$

303.0711, found 303.0692; *m/z* calculated for $C_{10}H_{11}O_7$ [M + H – 2 HOAc]$^+$ 243.0499, found

243.0447; *m/z* calculated for $C_8H_7O_5$ [M + H – 2 HOAc]$^+$ 183.0288, found 183.0243.

Synthesis of 6,6'-ester-linked disaccharides.

Benzyl-2,3,4,6-tetra-O-benzyl-β-D-glucopyranoside **62**. Based on literature

procedures.[208] In a 3-neck flask with gas adapter and dropping funnel, added glucose (4.13 g,

22.9 mmol) and DMF under N$_2$ atmosphere. Stirred the suspension at RT. Added portion of

NaH (2.6 g, 108.3 mmol), then stirred at RT for 30 minutes. Then added benzyl bromide (8.8 ml,

74.1 mmol) dropwise while cooling on ice. Left to stir on ice for 10 minutes after addition, then

at RT for 2.5 h. Added a second portion of NaH (2.5 g, 104.2 mmol) and, after stirring for 30

min at RT, added benzyl bromide (8.8 mL, 74.1 mmol) dropwise while cooling the reaction

mixture on ice. After stirring for another 2.5 h at RT, added a last portion of NaH (2.0 g, 83.3

mmol) and, after stirring for another 30 min, benzyl bromide (6.4 mL, 53.9 mmol) was added

dropwise with cooling. The tan-yellow suspension was then allowed to stir at room temperature

overnight. The reaction was quenched with 7 mL methanol and the bulk of DMF was evaporated

using a rotavap under reduced pressure. The mixture was diluted with 150 mL dichloromethane

and 100 mL DI water. After separation, the organic layer was washed with 3x150 mL DI water.

After backextraction of the combined aqueous layers with 50 mL dichloromethane, the combined

organic layers were washed with 2x100 mL sat. NaCl solution and dried over Na2SO4. After

filtration, the bright yellow solution was evaporated to give a yellow liquid which was

crystallized from methanol (approx. 230 mL) to give the product as fine white needle-like crystals

(9.21 g, 14.6 mmol, 64%). ^{1}H NMR (600 MHz, CDCl$_3$): δ 7.40-7.15 (m, 25 H, Bn-CH), 5.00-

4.50 (m, 10H, Bn-CH$_2$), 4.52 (d, 7.8 Hz, H-1), 3.77 (dd, 1.8 Hz, 10.8 Hz, H-6a), 3.71 (dd, 5.1 Hz,

11.1 Hz, H-6b), 3.65 (t, 9.0 Hz, H-3), 3.62 (t, 9.0 Hz, H-4), 3.53 (t, 8.4 Hz, H-2), 3.48 (ddd, 1.8

Hz, 4.8 Hz, 9.0 Hz, H-5). ^{13}C NMR (150 MHz, CDCl$_3$): δ 138.69, 138.49, 138.29, 138.20,

137.58, 128.49 (4C), 128.47 (4C), 128.43 (2C), 128.28 (2C), 128.04 (4C), 127.97 (2C), 127.85

(4C), 127.74, 127.70 (2C), 102.71 (C-1), 84.83 (C-3), 82.40 (C-2), 77.99 (C-4), 75.81, 75.10, 75.00 (2C, C-5), 73.59, 71.25, 69.04 (C-6). HRMS (DART-MS): *m/z* calculated for $C_{41}H_{46}NO_6$ [M + NH$_4$]$^+$ 648.3320, found 648.3272.

Benzyl-6-O-acetyl-2,3,4-tri-O-benzyl-β-D-glucopyranoside **63**. Based on literature procedures.[208] In a 3-neck flask with gas adapter, placed $ZnCl_2$ (10.7g, 78.2 mmol) and heated under vacuum to drive off residual water. After cooling under N_2, added a mixture of acetic acid:acetic anhydride (62 mL, 1:5) and stirred with cooling on an icebath. To this, added benzyl 2,3,4,6-tetra-O-benzyl-β-D-glucopyranoside 62 (as a solution in acetic acid:acetic anhydride (1:5, 62 mL). Allowed the reaction mixture to come to RT slowly over the course of 90 minutes. After another hour of stirring at RT, the clear yellow reaction mixture was poured into approximately 300 mL of an ice-water mixture to precipitate the benzyl 6-O-acetyl-2,3,4-tri-O-benzyl-β-D-glucopyranoside as a white solid (6.2 g after drying). The crude compound was used without purification in the subsequent reaction. ^{1}H NMR (600 MHz, CDCl$_3$): δ 7.40-7.21 (m, 20H, Bn-CH), 5.02-4.92 (m, 3H, Bn-CH$_2$), 4.84–4.49 (m, 6H, 5x CH$_2$-Bn, H-1), 4.35 (dd, 1.2 Hz, 11.7 Hz, 1H, H-6a), 4.24 (dd, 4.3 Hz, 11.7 Hz, H-6b), 3.67 (t, 8.3 Hz, H-3), 3.61–3.48 (m, 3H, H-2, H-4, H-5), 2.05 (s, 3H, COCH$_3$). ^{13}C NMR (150 MHz, CDCl$_3$): δ 170.6 (C=O), 138.3, 138.1, 137.6, 137.0, 128.4, 128.3, 128.2, 128.0, 127.9, 127.8, 127.7, 127.6, 102.2 (C-1), 84.5 (C-3), 82.0 (C-5), 77.2 (C-2), 75.6 (CH$_2$), 74.8 (CH$_2$), 74.7 (CH$_2$), 72.7 (C-4), 71.0 (CH$_2$), 63.0 (C-6), 20.8 (CH$_3$).

Benzyl-2,3,4-tri-O-benzyl-β-D-glucopyranoside **64**. Based on literature procedures.[208] In a 250 mL round-bottom flask, dissolved sodium metal (0.3 g) in dry methanol (70 mL). To this, crude benzyl 6-O-acetyl-2,3,4-tri-O-benzyl-β-D-glucopyranoside **63** was added and stirred at RT for 5 h, at which point TLC (2:1 hexane:ethyl acetate) indicated complete conversion of the starting material. The clear yellow reaction mixture was poured onto approximately 280 mL of ice-cold water to give a milky white suspension, which was allowed to settle overnight. After cooling on ice, the white solid product was filtered and washed with additional ice-cold wchaater

to give benzyl 2,3,4-tri-O-benzyl-β-D-glucopyranoside (4.5 g, 57% over two steps). The product

was of sufficient purity as determined by ^{1}H NMR, when compared to material recrystallized

from ethanol. ^{1}H NMR (600 MHz, CDCl$_3$): δ 7.38-7.26 (m, 20H, Bn-CH), 4.95 (d, 10.8 Hz, Bn-

CH$_2$), 4.93 (d, 11.4 Hz, Bn-CH$_2$), 4.92(d, 12.0 Hz, Bn-CH$_2$), 4.86 (d, 10.8 Hz, Bn-CH$_2$), 4.80 (d,

10.8 Hz, Bn-CH$_2$), 4.72 (d, 10.8 Hz, Bn-CH$_2$), 4.69 (d, 12.0 Hz, Bn-CH$_2$), 4.63 (d, 10.8 Hz, Bn-

CH$_2$), 4.57 (d, 7.8 Hz, H-1), 3.87 (dd, 3.0 Hz, 12.0 Hz, H-6a), 3.70 (dd, 7.2 Hz, 12.0 Hz, H-6b),

3.67 (t, 9.0 Hz, H-3), 3.57 (t, 9.3 Hz, H-4), 3.48 (dd, 8.1 Hz, 9.3 Hz, H-2), 3.36 (ddd, 3.0 Hz, 4.8

Hz, 9.6 Hz, H-5). ^{13}C NMR (150 MHz, CDCl$_3$): δ 138.59, 138.39, 138.05, 137.36, 128.59 (4 C),

128.50 (2 C), 128.47 (2 C), 128.24 (2 C), 128.17 (2 C), 128.04 (4 C), 127.98 (2 C), 127.80,

127.76, 102.93 (C-1), 84.63 (C-3), 82.43 (C-2), 77.65 (C-4), 75.81 (CH$_2$), 75.16 (CH$_2$), 75.14 (C-

5), 75.09 (CH$_2$), 71.77 (CH$_2$), 62.17 (C-6). HRMS (DART-MS): *m/z* calculated for C$_{34}$H$_{40}$NO$_6$

[M + NH$_4$]$^+$ 558.2851, found 558.2884.

Benzyl-2,3,4-tri-O-benzyl-β-D-glucopyranosyl-(6→6')-(benzyl 2,3,4-tri-O-benzyl-β-D-glucopyranuronate) **65**. Adapted from the literature.[94] In a scintillation vial, combined benzyl

2,3,4-tri-O-benzyl-β-D-glucopyranoside **64** (200 mg, 0.37 mmol), pyridine (60 µL, 0.74 mmol,

2.0 equiv.), TEMPO (3 mg, 0.02 mmol, 5 mol%) and then dissolved in anhydrous acetonitrile (1

mL). In a separate vial, dissolved TCCA (94 mg, 0.40 mmol, 1.1 equiv) in anhydrous acetonitrile

(1 mL) and slowly added the clear solution to the reaction mixture over the course of several

minutes. Stirred for 90 minutes hours, then quenched with saturated NaHCO$_3$ (5 mL) to give a

pale yellow suspension, which was stirred for another 5 minutes. The crude reaction mixture was

then filtered and the retained solids washed with saturated NaHCO$_3$ (3 mL) and DCM (4 mL).

The organic layer was separated and the aqueous layer etracted with DMC (3 x 4 mL). The

combined organic layers were dried over Na2SO4 to give a clear pale yellow solution, which was

evaporated with a rotavap to give a yellow sticky oil. The desired product was isolated via

column chromatography (95:5 to 8:2 hexane: EtOAc gradient elution) to yield a colorless oil

which solidified under high vacuum (51.2 mg, 0.05 mmol, 27%). R$_f$ 0.86 (8:2 hexane:EtOAc).

^{1}H NMR (600 MHz, CDCl$_3$): δ 7.33-7.18 (m, 40H, Bn-CH), 4.94 (d, 11.4 Hz, 2H, Bn-CH$_2$), 4.91 (d, 10.8 Hz, Bn-CH$_2$), 4.89 (d, 10.8 Hz, Bn-CH$_2$), 4.87 (d, 11.4 Hz, Bn-CH$_2$), 4.84 (d, 10.8 Hz, Bn-CH$_2$), 4.79 (d, 12.0 Hz, Bn-CH$_2$), 4.78 (13.8 Hz, Bn-CH$_2$), 4.78 (d, 10.8 Hz, Bn-CH$_2$), 4.77 (d, 10.8 Hz, Bn-CH$_2$), 4.70 (d, 10.8 Hz, Bn-CH$_2$), 4.70 (d, 10.8 Hz, Bn-CH$_2$), 4.69 (d, 10.8 Hz, Bn-CH$_2$), 4.59 (d, 12.0 Hz, Bn-CH$_2$), 4.58 (d, 10.8 Hz, Bn-CH$_2$), 4.57 (d, 8.1 Hz, H-1'), 4.55 (d, 12.3 Hz, Bn-CH$_2$), 4.53 (dd, 1.8 Hz, 12.0 Hz, H-6*proS*), 4.49 (d, 8.4 Hz, H-1), 4.33 (dd, 5.1 Hz, 11.7 Hz, H-6*proR*), 3.95 (t, 8.4 Hz, H-5'), 3.92 (t, 8.4 Hz, H-4'), 3.66 (t, 8.7 Hz, H-3'), 3.65 (t, 8.7 Hz, H-3), 3.60 (dd, 9.0 Hz, H-4), 3.58 (apt t, 8.4 Hz, H-2'), 3.54 (ddd, 1.8 Hz, 4.8 Hz, 9.4 Hz, H-5), 3.51 (dd, 7.8 Hz, 9.0 Hz, H-2). ^{13}C NMR (150 MHz, CDCl$_3$): δ 168.34 (C=O, C-6'), 138.51, 138.44, 138.37, 138.25, 138.00, 137.84, 137.20, 137.05, 128.6 – 127.7 (40C, Bn-CH), 102.87 (C-1'), 102.39 (H-1), 84.59 (C-3), 83.89 (C-3'), 82.39 (C-2), 82.01 (C-2'), 79.30 (C-4'), 77.83 (C-4), 75.83 (2C), 75.31, 75.11, 75.05 (2C), 74.92 (C-5'), 72.80 (C-5), 71.35, 71.06, 64.35 (C-6). HRMS (ESI-MS): *m/z* calculated for C$_{61}$H$_{61}$O$_{12}$Na [M + Na – C$_7$H$_7$]$^+$ 1009.4133, found 1009.4240.

Glucopyranosyl-6,6' glucopyranuronate **66**. In a 50 mL three-neck round bottom flask, under nitrogen gas atmosphere, added Pd/C (14 mg) in ethyl acetate (2.5 mL) and rinsed the flask walls with methanol (1 mL). To this, **65** (83.9 mg, 77 µmol) dissolved in methanol (2 mL) was added. Evaporated and filled the flask with nitrogen gas thrice, then repeated with hydrogen gas thrice, before attaching a double-walled balloon with hydrogen gas and stirring the reaction mixture overnight. Checked for completion by TLC (95:5 DCM:MeOH). After 24 h, removed the hydrogen gas atmosphere and replaced with nitrogen. After filtration of the crude product mixture, the flask was rinsed with methanol (1mL). Washed the filter cake with an additional amount of methanol (5 mL). The combined filtrates were evaporated using a rotavap and the product was separated using column chromatography (dryloading, silica, DCM:MeOH 95:5 → 7:3) to yield a clear colorless crystalline solid (13.7 mg, 38 µmol, 49%) after evaporation and drying under vacuum overnight. R$_f$ 0.45 (7:3 DCM:MeOH). For ^{1}H and ^{13}C NMR (600 MHz,

150 MHz, D$_2$O) assignment, see tabular representation in Appendix A. HRMS (ESI-MS): *m/z*

calculated for C$_{12}$H$_{20}$O$_{12}$Na [M + Na]$^+$ 379.0847, found 379.0939.

Attempted epoxide opening with carboxylate nucleophile.

Tri-O-benzyl-glucal **67**. Based on literature procedures.[223] 3,4,6-tri-*O*-acetyl-D-glucal

(2.00 g, 7.3 mmol) was dissolved in MeOH (5 mL) and KCN (9.9 mg, 0.14 mmol) was added.

The reaction was stirred for 3 h, and another portion of KCN (9.7 mg, 0.14 mmol) was added.

After an additional three hours, TLC indicated that the reaction was complete, and the mixture

was concentrated to a yellow oil. To the crude oil was added anhydrous DMF (20 mL) and the

solution was cooled to 0 °C. Sodium hydride (1.25 g, 60% dispersion in mineral oil, 31.2 mmol,

4.3 equiv.) was added carefully and the mixture was stirred at 0 °C for 30 minutes. Then benzyl

bromide (3.0 mL, 25.6 mmol, 3.5 equiv.) was added dropwise, and the mixture was allowed to

warm to room temperature overnight. The bright-yellow mixture was quenched with methanol (1

ml). The phases were separated and the aqueous phase was extracted with hexane (3 × 6 mL).

The combined organic extracts were dried over Na$_2$SO$_4$, filtered and concentrated in *vacuo* to

give a clear yellow oil that solidified overnight (3.06 g). Recrystallization of the crude product

from a mixture of MeOH/H$_2$O (1:1, 12 mL) afforded the product as off-white crystals (1.99 g, 4.8

mmol, 65%). ^{1}H NMR (600 MHz, CDCl$_3$): δ 7.34-7.23 (m, 15H, Bn-CH), 6.43 (d, 7.2 Hz, H-1),

4.87 (dd, 2.7 Hz, 6.3 Hz, H-2), 4.83 (d, 11.7 Hz), 4.64 (d, 11.7 Hz), 4.63 (d, 11.7 Hz), 4.60-4.54

(m, 3H, Bn-CH$_2$), 4.21 (m, H-3), 4.06 (ddd, 2.4 Hz, 4.8 Hz, 8.4 Hz, H-5), 3.86 (dd, 6.0 Hz, 8.4

Hz, H-4), 3.81 (dd, 4.8 Hz, 10.8 Hz, H-6a), 3.76 (dd, 3.0 Hz, 10.8 Hz, H-6b). ^{13}C NMR (150

MHz, CDCl$_3$): δ 144.82 (C-1), 138.43, 138.27, 138.09, 128.50 (4C), 128.48 (2C), 128.00 (2C),

127.88 (2C), 127.83 (3C), 127.75 (2C), 100.04 (C-2), 76.85 (C-5), 75.83 (C-3), 74.49 (C-4),

73.85, 73.60, 70.56, 68.62 (C-6). HRMS (DART-MS): *m/z* calculated for C$_{20}$H$_{21}$O$_3$ [M + H -

HOBn]$^+$ 309.1486, found 309.1503; *m/z* calculated for C$_{40}$H$_{41}$O$_6$ [2M + H - 2HOBn]$^+$ 617.2898,

found 617.2869.

1,2-Anhydro-3,4,6-tri-O-benzyl-a-D-glucopyranose **68**. Adapted from the literature.[224]

Added tri-O-benzyl-D-glucal (1.5 g, 3.6 mmol) in a mixture of DCM (15 mL), acetone (3 mL)

and sat. aq. $NaHCO_3$ solution (25 mL). Stirred the mixture vigorously and cooled on an ice bath.

To this, added a solution of Oxone (4.45 g in 20 mL DI water) dropwise over 10 minutes. Stirred

on ice for another 40 min, then at RT for 4 hours. Separated layers and extracted the milky

organic layer with DCM (2x15 mL). The combined organic layers were dried over Na_2SO_4 and

then concentrated to give a white solid, which was recrystallized from hexane (5 mL) to yield the

desired product as white solid (1.31 g, 3.0 mmol, 84%). ^{1}H NMR (600 MHz, $CDCl_3$): δ (ppm)

7.4-7.1 (m, 15H), 4.98 (br d, 1.8 Hz, H-1), 4.80 (d, 11.4 Hz, 2H, Benzyl-CH_2), 4.69 (d, 11.4 Hz,

Benzyl-CH_2), 4.61 (d, 12.6 Hz, Benzyl-CH_2), 4.58 (d, 10.8 Hz, Benzyl-CH_2), 4.52 (d, 12.0 Hz,

Benzyl-CH_2), 3.97 (dd, 0.9 Hz, 8.1 Hz, 1H), 3.74 (m, 2H), 3.65 (m, 2H), 3.06 (d, 2.4 Hz, H-2).

^{13}C NMR (150 MHz, $CDCl_3$): δ (ppm) 138.25 (Cq), 138.00 (Cq), 137.58 (Cq), 128.65 (2C),

128.48 (2C), 128.44 (2C), 128.08 (2C), 127.97 (2C), 127.90 (3C), 127.80, 127.77, 79.03, 77.61

(C-1), 74.66 (Benzyl-CH_2), 74.30, 73.65 (Benzyl-CH_2), 72.36 (Benzyl-CH_2), 69.50, 68.28 (C-6),

52.65 (C-2). HRMS: *m/z* calculated for $C_{27}H_{29}O_5$ $[M + H]^+$ 433.2010, found 433.2; *m/z*

calculated for $C_{27}H_{32}NO_5$ $[M + NH_4]^+$ 450.2280, found 450.2286; *m/z* calculated for $C_{20}H_{21}O_4$ [M

+ H - HOBn]$^+$ 325.1435, found 325.1466; *m/z* calculated for $C_{13}H_{13}O_3$ $[M + H - 2\ HOBn]^+$

217.0860, found 217.0866.

Benzyl-2,3,4,6-tri-O-benzyl-β-D-glucopyranuronic acid **69**. Based on literature

procedures.[211] In a 3-neck round bottom flask attached with a reflux condenser and dropping-

funnel, dissolved benzyl 2,3,4-tetra-*O*-benzyl-*β*-D-glucopyranoside **64** (500 mg, 0.9 mmol) in 10

mL acetone and heated to approximately 55 °C. Then, added a solution of potassium dichromate

(444 mg, 1.5 mmol, 1.6 eq) in sulfuric acid (3 mL, 3M) dropwise to the solution. Heated the

reaction for 1 h until it had turned from orange/brown to a pale green solution with a dark green

residue. After allowing it to cool, the reaction mixture was poured into water (100 mL) and

extracted with DCM (2x50 mL). The combined organic layers were washed with water (50 mL)

and sat. NaCl solution (50 mL) and dried over Na_2SO_4. After filtration and evaporation of

solvent, the crude product was obtained as a milky yellow viscous solid, which crystallized into

an off-white solid upon standing. The pure product was obtained after column chromatography

(6:1 toluene:MeOH) as an off-white solid (0.48 g, 0.86 mmol, 93%). R_f 0.31 (4:1

toluene:MeOH). ^{1}H NMR (600 MHz, $CDCl_3$): δ (ppm) 7.4-7.1 (m, 20H), 4.95-4.55 (m, 9H, 8 x

Bn-CH_2, H-1), 4.0-3.8 (m, 2H), 3.70-3.45 (m, 3H), 3.36 (m, H-5). ^{13}C NMR (150 MHz, $CDCl_3$):

δ (ppm) 138.37 (2C, Cq), 138.20 (Cq), 137.02 (Cq), 128.6-127.7 (20C), 102.64, 83.61, 81.70,

79.15, 75.14, 75.1-74.9 (4C, Bn-CH_2), 74.59. HRMS (DART-MS): *m/z* calculated for $C_{34}H_{33}O_7$

$[M - H]^-$ 553.2231, found 553.2004; *m/z* calculated for $C_{27}H_{27}O_7$ $[M - C_7H_7]^-$ 463.1762, found

463.1692.

Computational Methods.

Chapter 2: Diastereoselective Esterification.

Quantum Mechanical Calculations. Computations were performed using the

Gaussian09 software package.[135] Transition state geometries for the ester formation were

optimized at the B3LYP/6-31G* level of theory using tight optimization criteria on ultrafine

integration grid and used implicit PCM solvent correction for dichloromethane for **4**, **6** and **27**

with **3** and the acyl-pyridinium intermediate of **3**. Molecular orbitals representing the HOMO of

the transition state structures were visualized using the cubegen utility of Gaussian09 from the

respective checkpoint files.[135]

Chapter 4: Development of a C(*sp2*)OCH Karplus equation

Conformer search. The initial conformer search for compounds **46**, **47**, **48**, **49** and **50**

was performed using the Spartan14 software suite.[134,225] The input geometry was restrained to the

preferred chair conformation, with twist and boat conformations excluded. The conformer

distribution was computed using MAXCYCLES = 1000 and MAXCONFORMERS = 20000 with

100% conformers kept at the HF/6-31G*//AM1 level of theory (implicit solvent model used).

The lowest energy conformer fitting the above criteria was chosen as the starting geometry for the molecular dynamics computations.

Molecular Dynamics. Molecular dynamics simulations of compounds **46**, **47**, **48, 49** and **50** were run using the Amber14 software suite and the GLYCAM06 force field, which has been specially parameterized to the flexible behavior of carbohydrate molecules, while the MD simulation of **53** was performed with the Generalized Amber Force Field (gaff).[146,157,226] Input files were generated on the basis of .pdb files from Spartan14 conformer search using the format taken from the Glycam webtool Carbohydrate Builder.[227] Simulations were performed using explicitly modeled solvent environment with the TIP3P water model (or $CHCl_3$ in the case of **53**) and periodic boundary conditions of 8 Å.[148] Minimization and heating were both performed using a commonly used two-step procedure, with the initial minimization and heating step, respectively, affecting only solvent molecules by using positional restraints on the carbohydrate molecule. The production runs were performed over 500 ns in order to sufficiently sample the available conformational space.[146,147] The MD simulation input parameters used have been reproduced in the Appendix. All MD runs were monitored for successful equilibration prior to and stability during the production run based on energy and pressure data extracted using the existing process_mdout.perl and process_minout.perl scripts. Graphical representations of a representative sample can be found in the Appendix. Extraction of dihedral angle values using vmd from the MD trajectories was preceded by editing of the .prmtop and .mdcrd files to remove water molecules using the CPPTRAJ utility.[228,229]

Parameter expansion for the GLYCAM06 force field. The GLYCAM06 force filed was expanded to include torsion parameter terms for Os-Cg-Os-C and H2-Cg-Os-C for the 1-acetyl linkage in **47** and Os-Cg-C –O , Os-C –Cg-Os and Os-C Cg-H1 to parameterize the 6-ester-linkage and allow for the use of the carbohydrate specific force field use with methyl *α/β*-D-glucopyranuronate **50**. The 1-acetyl linkage could be modeled using substitutions with existing parameters for Cg-Cg-Os-C and H1-Cg-Os-C, respectively. This resulted in a mean error of 1.15

kcal/mol or 14.8% of the highest rotational barrier compared to QM calculations for a test set of α/β-**47** and tetrahydropyran-2-yl acetate, which was considered sufficient on the basis of similar errors in the original GLYCAM06 publication.[146] Detailed results may be found in Appenix C. The procedure for the parameterization of the 6-ester-linkage was adapted from the GLYCAM06 publication and used two model compounds, namely methyl methoxyacetate and methyl tetrahydropyran-2-acetate. The necessary Molecular Mechanics computations were performed using Amber14 over 2000 cycles of steepest descent algorithm, followed by up to 4000 cycles following the conjugate gradient algorithm – using dihedral angle constraints to obtain the same geometry as in the DFT calculations. Related input files and results of the parameter fitting are replicated in the Appendix, together with the developed torsion parameters. The resulting systemic mean error of 0.37 kcal/mol compared to QM calculations compares favorably to that obtained for the carboxylate functional group in the original GLYCAM06 paper.[146]

Atomic charge generation. The atomic charges supplied with GLYCAM06 were adjusted for **46**, **48** and **49** based on established procedures to account for the acetyl group derivation by modifying the charge of the bonded glycan carbon by +0.008.[230] In the absence of preexisting atomic charges for acetyl 6-acetyl-*α/β*-D-glucopyranoside **47** and methyl *α/β*-D-glucopyranuronate 50 in the GLYCAM06 force field parameters, they were derived using the two-stage RESP fit protocol, as established by Cornell *et al.*.[154] After an initial RESP fit based on Gaussian esp calculations (using HF/6-31G* and the undocumented iop(6/33=2) option and pop=chelpg) on a preoptimized HF/6-31G* geometry and the espgen and respgen utilities of AmberTools16, a 50 ns MD simulation was run with the initial atomic charges in explicit solvent (TIP3P or CHCl3 box).[226] Then, 100 representative geometries were extracted from the MD trajectory (every 50th of 5000 stored geometries) and reoptimized at the HF/6-31G* level of theory, followed by a second RESP fit as described above which was averaged across all 100 conformers to give final values for the atomic charges for both anomers of **47** and **50**, respectively , and **53**. Final charges are reproduced in Appendix C. The Gaussian input files

were prepared using a modified version of a python script described by Reisbick and Willoughby.[231]

Quantum Mechanical Calculations. Computations were performed using the Gaussian09 software package.[135] Geometries were optimized at the M05-2X/6-31G* level of theory using tight optimization criteria on ultrafine integration grid and used implicit PCM solvent correction for water. The M05-2X Minnesota functional was chosen for this study, as it was found by Csonka *et al.* and others to give better energetics for carbohydrates than the commonly used B3LYP functional, provided a higher density DFT grid was used.[232-234] Additionally, Bally *et al.* found that reoptimization of geometry optimizations performed using the 6-31G* basis set with larger basis sets generally changed calculated coupling constants very little (rms change below 0.15Hz) and if the 'mixed' option is invoked, geometry reoptimization was found to have even less of an effect.[151] The inclusion of diffuse functions (+) did not give notably better results, but increases time requirement more than 3-fold. Thus, 6-31G* was chosen as the basis set for the current study as a good compromise between accuracy and computational expense. In their study, Bally *et al.* also found no improvement upon adding implicit solvent model, however as this might not be the case with water and carbohydrates, implicit PCM solvent correction was included.[151] Higher level energies were calculated at the M05-2X/6-311+G** level, again using the implicit PCM solvent correction, as this basis set was found to give more accurate representation of relative energies for carbohydrates, than calculations based on 6-31G*(PCM) alone.[233] Gibbs Free Energies were calculated using thermal corrections from frequency calculations at the M05-2X/6-31G* level of theory. Relative abundances of the conformers were calculated using the Boltzmann distribution of the relative Gibbs Free Energies. Torsional angle scans were performed using relaxed geometry scans using the above optimization criteria to obtain +/- 10/20° isomers. Fermi contact value calculations were performed using GIAO-NMR calculations (FConly, mixed) at the M052X/6-311G**[u+1s] level of theory and implicit PCM solvent correction for water. The larger basis set was modified

to include polarization orbitals, but no diffuse functions, as Bally *et al*. found them not to add additional value in NMR calculations, while the increased valence functions improved rms error (6-311G(d,p) vs 6-31G(d,p)) at little additional computational cost.[151] The use of 'FCOnly' calculates only the Fermi contact term, saving significant computation time over the 'spinspin' option. As others have found, this is often the preferred option because the spin−orbit terms are negligible or cancel out for $^3J_{CH}$, thus leaving the Fermi contact term as the only relevant contribution.[151,152]

Chapter 5: Synthesis and Conformational Analysis of carbohydrate esters

Molecular Dynamics. Molecular dynamics simulations of compounds **58**, **59**, **60** and *αα/ββ*-**66** were performed in the same manner as described for Chapter 4. Simulations were run with explicit solvent models that matched the NMR experiment (TIP3P or CHCL3 solvent models).[148,226] The production runs were performed over 500 ns in order to sufficiently sample the available conformational space.[146,147]

Atomic charge generation. The atomic charges for compounds **58**, **59**, **60**, *αα/ββ*-**66** and *αα/ββ*-**70** were derived using the two-stage RESP fit protocol, as established by Cornell *et al.* and discussed above for Chapter 4.[154] Final charges and initial molecular geometries are reproduced in Appendix C.

Quantum Mechanical Calculations. Computations were performed using the Gaussian09 software package.[135] Molecular geometries representative of the established conformational regions of **60** were optimized at the M05-2X/6-31G* level of theory in the manner described previously.[232] All local minima were verified using vibrational frequency analysis. Single point energy calculations were performed at either the M05-2X/6-311+G** or MP2/aug-cc-pVTZ levels of theory.[235,236] The reasoning for the choice of methods/functionals and basis sets are discussed previously in the section on Chapter 4. Gibbs Free Energies were calculated using thermal corrections from frequency calculations at the M05-2X/6-31G* level of

theory. Relative abundances of the conformers were calculated using the Boltzmann distribution

of the relative Gibbs Free Energies

REFERENCES

1.　In *IUPAC. Compendium of Chemical Terminology, 2nd ed. (the "Gold Book")*; McNaught, A. D. W., A., Ed.; Blackwell Scientific Publications: Oxford, 1997.

2.　Freese, E.; Sheu, C. W.; Galliers, E.: Function of Lipophilic Acids as Antimicrobial Food Additives. *Nature* **1973**, *241*, 321-325, DOI: 10.1038/241321a0.

3.　Nes, I. F.; Eklund, T.: The effect of parabens on DNA, RNA and protein synthesis in Escherichia coli and Bacillus subtilis. *J. Appl. Bacteriol.* **1983**, *54*, 237-242, DOI: 10.1111/j.1365-2672.1983.tb02612.x.

4.　Schnaar, R. L.: Glycolipid-mediated cell–cell recognition in inflammation and nerve regeneration. *Arch. Biochem. Biophys.* **2004**, *426*, 163-172, DOI: 10.1016/j.abb.2004.02.019.

5.　Kabanov, D. S.; Prokhorenko, I. R.: Structural analysis of lipopolysaccharides from Gram-negative bacteria. *Biochemistry (Moscow)* **2010**, *75*, 383-404, DOI: 10.1134/s0006297910040012.

6.　Steimle, A.; Autenrieth, I. B.; Frick, J.-S.: Structure and function: Lipid A modifications in commensals and pathogens. *International Journal of Medical Microbiology* **2016**, *306*, 290-301, DOI: 10.1016/j.ijmm.2016.03.001.

7.　Raetz, C. R. H.; Guan, Z.; Ingram, B. O.; Six, D. A.; Song, F.; Wang, X.; Zhao, J.: Discovery of new biosynthetic pathways: the lipid A story. *J. Lipid Res.* **2009**, *50*, S103-S108, DOI: 10.1194/jlr.R800060-JLR200.

8.　Daniotti, J. L.; Lardone, R. D.; Vilcaes, A. A.: Dysregulated Expression of Glycolipids in Tumor Cells: From Negative Modulator of Anti-tumor Immunity to Promising Targets

for Developing Therapeutic Agents. *Front. Oncol.* **2015**, *5*, 300-310, DOI: 10.3389/fonc.2015.00300.

9.   Fischer, E.; Speier, A.: Darstellung der Ester. *Berichte der deutschen chemischen Gesellschaft* **1895**, *28*, 3252-3258, DOI: 10.1002/cber.189502803176.

10.   Neises, B.; Steglich, W.: Simple Method for the Esterification of Carboxylic Acids. *Angew. Chem. Int. Ed.* **1978**, *17*, 522-524, DOI: 10.1002/anie.197805221.

11.   Köpnick, H.; Schmidt, M.; Brügging, W.; Rüter, J.; Kaminsky, W. *Polyesters*. In *Ullmann's Encyclopedia of Industrial Chemistry*; Wiley-VCH Verlag GmbH & Co. KGaA: 2000, 10.1002/14356007.a21_227.

12.   Pfeffer, P. E.; Silbert, L. S.: Esterification by alkylation of carboxylate salts. Influence of steric factors and other parameters on reaction rates. *J. Org. Chem.* **1976**, *41*, 1373-1379, DOI: 10.1021/jo00870a018.

13.   Moore, G. G.; Foglia, T. A.; McGahan, T. J.: Preparation of hindered esters by the alkylation of carboxylate salts with simple alkyl halides. *J. Org. Chem.* **1979**, *44*, 2425-2429, DOI: 10.1021/jo01328a019.

14.   Min, B.-H.; Kim, D.-S.; Park, H.-S.; Jun, C.-H.: Pd/C-Catalyzed Carbonylative Esterification of Aryl Halides with Alcohols by Using Oxiranes as CO Sources. *Chem. Eur. J.* **2016**, *22*, 6234-6238, DOI: 10.1002/chem.201600570.

15.   Perkowski, A. J.; Nicewicz, D. A.: Direct Catalytic Anti-Markovnikov Addition of Carboxylic Acids to Alkenes. *J. Am. Chem. Soc.* **2013**, *135*, 10334-10337, DOI: 10.1021/ja4057294.

16.   Tang, S.; Yuan, J.; Liu, C.; Lei, A.: Direct oxidative esterification of alcohols. *Dalton Transactions* **2014**, *43*, 13460-13470, DOI: 10.1039/C4DT01133C.

17.   Claisen, L.; Claparède, A.: Condensationen von Ketonen mit Aldehyden. *Berichte der deutschen chemischen Gesellschaft* **1881**, *14*, 2460-2468, DOI: 10.1002/cber.188101402192.

18. Hauser, C. R.; Hudson, B. E. *The Acetoacetic Ester Condensation and Certain Related Reactions*. In *Organic Reactions*; John Wiley & Sons, Inc.: 2004, 10.1002/0471264180.or001.09.

19. Guo, J.; Ye, X.-S.: Protecting Groups in Carbohydrate Chemistry: Influence on Stereoselectivity of Glycosylations. *Molecules* **2010**, *15*, 7235, DOI: 10.3390/molecules15107235.

20. Mojaverian, P.; Swanson, B. N.; Ferguson, R. K.: Enalapril, a new nonsulfhydryl angiotensin converting enzyme inhibitor, does not potentiate morphine analgesia. *Eur. J. Pharmacol.* **1984**, *98*, 303-306, DOI: 10.1016/0014-2999(84)90607-1.

21. Patchett, A. A.: The chemistry of enalapril. *Brit. J. Clin. Pharmaco.* **1984**, *18*, 201S-207S, DOI: 10.1111/j.1365-2125.1984.tb02599.x.

22. Loll, P. J.; Picot, D.; Garavito, R. M.: The structural basis of aspirin activity inferred from the crystal structure of inactivated prostaglandin H2 synthase. *Nat. Struct. Mol. Biol.* **1995**, *2*, 637-643, DOI: 10.1038/nsb0895-637.

23. Aich, U.; Campbell, C. T.; Elmouelhi, N.; Weier, C. A.; Sampathkumar, S. G.; Choi, S. S.; Yarema, K. J.: Regioisomeric SCFA Attachment to Hexosamines Separates Metabolic Flux from Cytotoxicity and MUC1 Suppression. *ACS Chem. Biol.* **2008**, *3*, 230-240, DOI: 10.1021/cb7002708.

24. Pasteur, L.: Recherches sur les relations qui peuvent exister entre la forme cristalline, la composition chimique et le sens de la polarisation rotatoire. *Annales de Chimie et de Physique* **1848**, *24*, 442-459.

25. Kauffman, G. B. M., Robin D.: Pasteur's Resolution of Racemic Acid: A Sesquicentennial Retrospect and a New Translation. *The Chemical Educator* **1998**, *3*, 1-4, DOI: 10.1007/s00897980257a.

26. van't Hoff, J. H.: Voorstel tot Uitbreiding der Tegenwoordige in de Scheikunde gebruikte Structuurformules in de Ruimte, benevens een daarmee samenhangende Opmerking

omtrent het Verband tusschen Optisch Actief Vermogen en chemische Constitutie van Organische Verbindingen (Proposal for the Extension of Current Chemical Structural Formulas into Space, together with Related Observation on the Connection between Optically Active Power and the Chemical Constitution of Organic Compounds). **1874**, *pamphlet published by the author*.

27.   van't Hoff, J. H.: Sur les formules de structure dans l'espace (Concerning the structural formulas in space). *Archives neerlandaises des sciences exactes et naturelles* **1874**, *9*, 445-454.

28.   Le Bel, J. A.: Sur les relations qui existent entre les formules atomiques des corps organiques et le pouvoir rotatoire de leurs dissolutions (On the relations that exist between the atomic formulas of organic substances and the rotatory power of their solutions). *Bull. Soc. Chim. Paris* **1874**, *22*, 337-347.

29.   Mason, S.: The origin of chirality in nature. *Trends Pharmacol. Sci.* **1986**, *7*, 20-23, DOI: 10.1016/0165-6147(86)90235-X.

30.   Blackmond, D. G.: The Origin of Biological Homochirality. *CSH Perspect. Biol.* **2010**, *2*, a002147, DOI: 10.1101/cshperspect.a002147.

31.   Bijvoet, J. M.; Peerdeman, A. F.; van Bommel, A. J.: Determination of the Absolute Configuration of Optically Active Compounds by Means of X-Rays. *Nature* **1951**, *168*, 271-272, DOI: 10.1038/168271a0.

32.   Cahn, R. S.; Ingold, C.; Prelog, V.: Specification of Molecular Chirality. *Angew. Chem. Int. Ed.* **1966**, *5*, 385-415, DOI: 10.1002/anie.196603851.

33.   Corey, E. J.; Ensley, H. E.: Preparation of an optically active prostaglandin intermediate via asymmetric induction. *J. Am. Chem. Soc.* **1975**, *97*, 6908-6909, DOI: 10.1021/ja00856a074.

34. Ensley, H. E.; Parnell, C. A.; Corey, E. J.: Convenient synthesis of a highly efficient and recyclable chiral director for asymmetric induction. *J. Org. Chem.* **1978**, *43*, 1610-1612, DOI: 10.1021/jo00402a037.

35. Whitesell, J. K.; Chen, H. H.; Lawrence, R. M.: trans-2-Phenylcyclohexanol. A powerful and readily available chiral auxiliary. *J. Org. Chem.* **1985**, *50*, 4663-4664, DOI: 10.1021/jo00223a055.

36. Evans, D. A.; Bartroli, J.; Shih, T. L.: Enantioselective aldol condensations. 2. Erythro-selective chiral aldol condensations via boron enolates. *J. Am. Chem. Soc.* **1981**, *103*, 2127-2129, DOI: 10.1021/ja00398a058.

37. Evans, D. A.; Ennis, M. D.; Mathre, D. J.: Asymmetric alkylation reactions of chiral imide enolates. A practical approach to the enantioselective synthesis of .alpha.-substituted carboxylic acid derivatives. *J. Am. Chem. Soc.* **1982**, *104*, 1737-1739, DOI: 10.1021/ja00370a050.

38. Pasteur, L.: Mémoire sur la fermentation de l'acide tartrique (On the fermentation of tartaric acid). *C.R. Hebd. Seances Acad. Sci. Paris* **1858**, *46*, 615-618.

39. Robinson, D. E. J. E.; Bull, S. D.: Kinetic resolution strategies using non-enzymatic catalysts. *Tetrahedron: Asymmetry* **2003**, *14*, 1407-1446, DOI: 10.1016/S0957-4166(03)00209-X.

40. Vedejs, E.; Jure, M.: Effizienz in der nichtenzymatischen kinetischen Racematspaltung. *Angew. Chem.* **2005**, *117*, 4040-4069, DOI: 10.1002/ange.200460842.

41. Vedejs, E.; Jure, M.: Efficiency in Nonenzymatic Kinetic Resolution. *Angew. Chem. Int. Ed.* **2005**, *44*, 3974-4001, DOI: 10.1002/anie.200460842.

42. Arseniyadis, S.; Valleix, A.; Wagner, A.; Mioskowski, C.: Kinetic resolution of amines: a highly enantioselective and chemoselective acetylating agent with a unique solvent-induced reversal of stereoselectivity. *Angew. Chem. Int. Ed. Engl.* **2004**, *43*, 3314-3317, DOI: 10.1002/anie.200453956.

43. Arseniyadis, S. S., P.V.; Valleix, A.; Mathew, S.P.; Blackmond, D.G.; Wagner, A.; Mioskowski, C.: Tuning the Enantioselective N-Acetylation of Racemic Amines: A Spectacular Salt Effect. *J. Am. Chem. Soc.* **2005**, *127*, 6138-6139, DOI: 10.1021/ja051302+.

44. Leclercq, L.; Suisse, I.; Agbossou-Niedercorn, F.: Kinetic Resolution of Racemic Secondary Alcohols Mediated by N-Methylimidazole in the Presence of Optically Active Acyl Chlorides. *Eur. J. Org. Chem.* **2010**, *2010*, 2696-2700, DOI: 10.1002/ejoc.200901075.

45. Shiina, I.; Nakata, K.; Ono, K.; Sugimoto, M.; Sekiguchi, A.: Kinetic resolution of the racemic 2-hydroxyalkanoates using the enantioselective mixed-anhydride method with pivalic anhydride and a chiral acyl-transfer catalyst. *Chem. Eur. J.* **2010**, *16*, 167-172, DOI: 10.1002/chem.200902257.

46. Krasnov, V. P.; Gruzdev, D. A.; Levit, G. L.: Nonenzymatic Acylative Kinetic Resolution of Racemic Amines and Related Compounds. *Eur. J. Org. Chem.* **2012**, *2012*, 1471-1493, DOI: 10.1002/ejoc.201101489.

47. Li, X.; Jiang, H.; Uffman, E. W.; Guo, L.; Zhang, Y.; Yang, X.; Birman, V. B.: Kinetic resolution of secondary alcohols using amidine-based catalysts. *J. Org. Chem.* **2012**, *77*, 1722-1737, DOI: 10.1021/jo202220x.

48. Harada, S.; Kuwano, S.; Yamaoka, Y.; Yamada, K.; Takasu, K.: Kinetic resolution of secondary alcohols catalyzed by chiral phosphoric acids. *Angew. Chem. Int. Ed. Engl.* **2013**, *52*, 10227-10230, DOI: 10.1002/anie.201304281.

49. Kawabata, T.; Nagato, M.; Takasu, K.; Fuji, K.: Nonenzymatic kinetic resolution of racemic alcohols through an "induced fit" process. *J. Am. Chem. Soc.* **1997**, *119*, 3169-3170, DOI: 10.1021/Ja963275g.

50. Yamada, S.; Misono, T.; Iwai, Y.: Kinetic resolution of sec-alcohols by a new class of pyridine catalysts having a conformation switch system. *Tetrahedron Lett.* **2005**, *46*, 2239-2242, DOI: 10.1016/j.tetlet.2005.02.019.

51. Lee, S. Y.; Murphy, J. M.; Ukai, A.; Fu, G. C.: Nonenzymatic dynamic kinetic resolution of secondary alcohols via enantioselective acylation: synthetic and mechanistic studies. *J. Am. Chem. Soc.* **2012**, *134*, 15149-15153, DOI: 10.1021/ja307425g.

52. Dalaigh, C. O.; Hynes, S. J.; Maher, D. J.; Connon, S. J.: Kinetic resolution of sec-alcohols using a new class of readily assembled (S)-proline-derived 4-(pyrrolidino)-pyridine analogues. *Org. Biomol. Chem.* **2005**, *3*, 981-984, DOI: 10.1039/b419335k.

53. Yang, D. J., G.-S.; Yip, Y.-C.; Wong, M.-K.: Diastereoselective Epoxidation of Cyclohexene Derivatives by Dioxiranes Generated in Situ. Importance of Steric and Field Effects. *J. Org. Chem.* **1999**, *64*, 1635-1639, DOI: 10.1021/jo9821978.

54. Orendt, A. M. R., S.W.; Rainier, J.D.: The Role of Asynchronous Bond Formation in the Diastereoselective Epoxidation of Cyclic Enol Ethers: A Density Functional Theory Study. *J. Org. Chem.* **2006**, *71*, 5565-5573, DOI: 10.1021/jo060502g.

55. Wright, S. W.; Choi, C.; Chung, S.; Boscoe, B. P.; Drozda, S. E.; Mousseau, J. J.; Trzupek, J. D.: Reversal of Diastereoselection in the Conjugate Addition of Cuprates to Unsaturated Lactams. *Org. Lett.* **2015**, 10.1021/acs.orglett.5b02533, DOI: 10.1021/acs.orglett.5b02533.

56. Turlington, M. P., L.: Reverse the Diastereoselectivity of the Rh(I)-Catalyzed Pauson-Khand Cycloaddition. *Org. Lett.* **2011**, *13*, 4332-4335, DOI: 10.1021/ol201670c.

57. Shengule, S. R.; Ryder, G.; Willis, A. C.; Pyne, S. G.: Highly diastereoselective N-acyliminium ion cyclization reactions of a tethered furan. *Tetrahedron* **2012**, *68*, 10280-10285, DOI: 10.1016/j.tet.2012.10.014.

58. Ellwood, A. R.; Mortimer, A. J.; Goodman, J. M.; Porter, M. J.: Reversal of facial selectivity in a thia-Claisen rearrangement by incorporation of a vinylic bromine substituent. *Org. Biomol. Chem.* **2013**, *11*, 7530-7539, DOI: 10.1039/c3ob41580e.

59. Kalck, P.; Urrutigoity, M.: Asymmetric catalysis induced by the substrate itself. *Coord. Chem. Rev.* **2004**, *248*, 2193-2200, DOI: 10.1016/j.ccr.2004.05.001.

60. Guan, Y.; López-Alberca, M. P.; Lu, Z.; Zhang, Y.; Desai, A. A.; Patwardhan, A. P.; Dai, Y.; Vetticatt, M. J.; Wulff, W. D.: Catalytic Asymmetric Synthesis of Alkynyl Aziridines: Both Enantiomers of cis-Aziridines from One Enantiomer of the Catalyst. *Chem. Eur. J.* **2014**, *20*, 13894-13900, DOI: 10.1002/chem.201404587.

61. Matsukawa, Y.; Dileep Kumar, J. S.; Yoneyama, Y.; Katagiri, T.; Uneyama, K.: Reversed diastereoselectivity in the ring-opening reaction of (S)-TFPO with a chiral aminoacetonitrile Schiff base. *Tetrahedron: Asymmetry* **2000**, *11*, 4521-4528, DOI: 10.1016/S0957-4166(00)00431-6.

62. Chaubey, N. R.; Wadawale, A. P.; Ghosh, S. K.: Practical synthesis of diastereoisomers by a temperature-guided reversal of diastereoselectivity in the desymmetrization of meso-bridged anhydrides with a chiral oxazolidin-2-one. *Tetrahedron: Asymmetry* **2013**, *24*, 1212-1217, DOI: 10.1016/j.tetasy.2013.07.027.

63. Chughtai, J. H. G., J.M.; Harris, S.G.; Parsons, S.; Rankin, D.W.H.; Schwalbe, C.H.: New Homochiral Ketoalcohols from Aldol Reactions of (+)-Isomenthone and Reversal of Diastereoselectivity. *Tetrahedron Lett.* **1997**, *38*, 9043-9046, DOI: 10.1016/S0040-4039(97)10430-0.

64. Storch, G.; Trapp, O.: Temperature-Controlled Bidirectional Enantioselectivity in a Dynamic Catalyst for Asymmetric Hydrogenation. *Angew. Chem. Int. Ed.* **2015**, *54*, 3580-3586, DOI: 10.1002/anie.201412098.

65.   Evans, S.; Omkaram, N.; Scheffer, J. R.; Trotter, J.: Stereoselectivity reversal of a photochemical reaction in the solid state. *Tetrahedron Lett.* **1985**, *26*, 5903-5906, DOI: 10.1016/S0040-4039(00)98257-1.

66.   Lu, B. Z.; Senanayake, C.; Li, N.; Han, Z.; Bakale, R. P.; Wald, S. A.: Control of Diastereoselectivity by Solvent Effects in the Addition of Grignard Reagents to Enantiopure t-Butylsulfinimine: Syntheses of the Stereoisomers of the Hydroxyl Derivatives of Sibutramine. *Org. Lett.* **2005**, *7*, 2599-2602, DOI: 10.1021/ol0507017.

67.   Toueg, J. P., J.: Dramatic Solvent Effect on the Diastereoselectivity of Michael Addition: Study toward the synthesis of ABC Ring System of Hexacyclinic Acid. *Org. Lett.* **2008**, *10*, 45-48, DOI: 10.1021/ol702566c.

68.   Node, M.; Hashimoto, D.; Katoh, T.; Ochi, S.; Ozeki, M.; Watanabe, T.; Kajimoto, T.: Asymmetric Michael Addition of a Recyclable Chiral Amine: Inversion of Stereoselectivity Caused by the Difference of Ethereal Solvents. *Org. Lett.* **2008**, *10*, 2653-2656, DOI: 10.1021/ol8007793.

69.   Garzan, A.; Jaganathan, A.; Salehi Marzijarani, N.; Yousefi, R.; Whitehead, D. C.; Jackson, J. E.; Borhan, B.: Solvent-dependent enantiodivergence in the chlorocyclization of unsaturated carbamates. *Chem. Eur. J.* **2013**, *19*, 9015-9021, DOI: 10.1002/chem.201300189.

70.   Lazny, R.; Nodzewska, A.; Tomczuk, I.: Spontaneous and diastereoselective aldol reactions of cyclic β-amino ketones in the presence of water. *Tetrahedron Lett.* **2011**, *52*, 5680-5683, DOI: 10.1016/j.tetlet.2011.08.107.

71.   Lazny, R.; Ratkiewicz, A.; Nodzewska, A.; Wysocka, J.: A DFT study of the origins of the stereoselectivity in the aldol reaction of bicyclic amino ketones in the presence of water. *Tetrahedron Lett.* **2012**, *53*, 5871-5874, DOI: 10.1016/j.tetlet.2012.08.070.

72.   Cainelli, G.; Giacomini, D.; Panunzio, M.; Zarantonello, P.: Reversal of diastereoselectivity in the addition of C-nucleophiles to N-trimethylsilyl imines via

Grignard derived organo copper-boron trifluoride reagents. *Tetrahedron Lett.* **1992**, *33*, 7783-7786, DOI: 10.1016/0040-4039(93)88045-K.

73.   Lindsay, H. A.; Salisbury, C. L.; Cordes, W.; McIntosh, M. C.: Unusual Reagent Control of Diastereoselectivity in the 1,2-Addition of Hard Carbon Nucleophiles to C6-Heteroatom Substituted Cyclohexenones. *Org. Lett.* **2001**, *3*, 4007-4010, DOI: 10.1021/ol016673j.

74.   Ordóñez, M.; Hernández-Fernández, E.; Rojas-Cabrera, H.; Labastida-Galván, V.: Reversal of diastereoselectivity in the benzylation of the lithium enolates of phosphonopropanoamides by changing the base equivalents. *Tetrahedron: Asymmetry* **2008**, *19*, 2767-2770, DOI: 10.1016/j.tetasy.2008.11.028.

75.   Rajendiran, C.; Nagarajan, P.; Naidu, A.; Dubey, P. K.: Reversal Diastereoselectivity Between the Organomagnesium and Organolithium Reagents on Chiral N-Tert-Butylsulfinylaldimines for the Preparation of Chiral Amines. *Synth. Commun.* **2014**, *44*, 2936-2942, DOI: 10.1080/00397911.2014.909487.

76.   Yamamoto, Y.; Maruyama, K.: Concerning reversal of diastereoselectivity in the BF3 promoted addition of crotyl—organometallic compounds to aldehydes. *J. Organomet. Chem.* **1985**, *284*, C45-C48, DOI: 10.1016/0022-328X(85)80039-5.

77.   Awandi, D.; Henin, F.; Muzart, J.; Pete, J.-P.: Reversal of diastereoselectivity in protonation of chiral photodienols. *Tetrahedron: Asymmetry* **1991**, *2*, 1101-1104, DOI: 10.1016/S0957-4166(00)82006-6.

78.   Panek, J. S.; Beresis, R.: Double stereodifferentiation in the Lewis acid-promoted addition of chiral (E)-crotylsilanes with (S)-2-(benzyloxy)propanal. Effect of Lewis acid on reaction diastereoselection. *J. Org. Chem.* **1993**, *58*, 809-811, DOI: 10.1021/jo00056a005.

79. Sanji, T.; Mitsugi, H.; Tanaka, M.; Fujiyama, H.; Sakurai, H.: Lewis base induced reversal of diastereoselectivity in the addition of alcohols to chiral silylenes. *Organometallics* **2006**, *25*, 6159-6161, DOI: 10.1021/om060671r.

80. Martinez-Castaneda, A.; Rodriguez-Solla, H.; Concellon, C.; del Amo, V.: Switching diastereoselectivity in proline-catalyzed aldol reactions. *J. Org. Chem.* **2012**, *77*, 10375-10381, DOI: 10.1021/jo3020352.

81. Sreenithya, A. S., R.B.: Noninnocent Role of N-Methyl Pyrrolidinone in Thiazolidinethione-Promoted Asymmetric Aldol Reactions. *Org. Lett.* **2012**, *14*, 5752-5755, DOI: 10.1021/ol302761n.

82. Ivšić, T.; Novak, J.; Došlić, N.; Hameršak, Z.: One catalyst for both enantiomers: uncovering the inversion of enantioselectivity in cinchona-mediated desymmetrization of glutaric meso-anhydrides. *Tetrahedron* **2012**, *68*, 8311-8317, DOI: 10.1016/j.tet.2012.07.035.

83. Wang, X.-N.; Hsung, R. P.; Qi, R.; Fox, S. K.; Lv, M.-C.: A Highly Stereoselective Addition of Lithiated Ynamides to Ellman-Davis Chiral N-tert-Butanesulfinyl Imines. *Org. Lett.* **2013**, *15*, 2514-2517, DOI: 10.1021/ol400989x.

84. Samoshin, A. V. V., J.; Curtis, M.; Samoshin, V.V.; Franz, A.H.: The first example of amine-induced reversal of diastereoselectivity in acylation of some trans-2-substituted cyclohexanols. *ARKIVOC* **2012**, *8*, 27-35, DOI: 10.3998/ark.5550190.0013.803.

85. Lide, D. R. In *CRC Handbook of Chemistry and Physics, 97th Edition*; CRC Press: Boca Raton, FL, 2016.

86. Lambert, J. B.; Beadle, B. M.; Kuang, K. Y.: Phenylsulfonyl as a beta participating group. *J. Org. Chem.* **1999**, *64*, 9241-9246, DOI: 10.1021/Jo991536+.

87. Nenaidenko, V. G.; Balenkova, E. S.: New Synthetic Capabilities of Sulfonium Salts. *Russ. J. Org. Chem.* **2003**, *39*, 291-330, DOI: 10.1023/a:1025525327399.

88.   Rao, K. V. R.; Caiveau, N.; David, R.; Shalayel, I.; Milet, A.; Vallée, Y.: Theoretical Study, Synthesis, and Reactivity of Five-Membered-Ring Acyl Sulfonium Cations. *Eur. J. Org. Chem.* **2015**, *2015*, 6125-6129, DOI: 10.1002/ejoc.201500749.

89.   Higuchi, T.; Gensch, K.-H.: Acylation through a Sulfonium Ion Intermediate. Coupled Conversion of a Carboxylic Acid to an Acid Anhydride during Oxidation of a Thioether to a Sulfoxide1. *J. Am. Chem. Soc.* **1966**, *88*, 3874-3875, DOI: 10.1021/ja00968a045.

90.   Tirado-Rives, J.; Jorgensen, W. L.: Performance of B3LYP Density Functional Methods for a Large Set of Organic Molecules. *J. Chem. Theory Comput.* **2008**, *4*, 297-306, DOI: 10.1021/ct700248k.

91.   Gaspa, S.; Porcheddu, A.; De Luca, L.: Metal-Free Oxidative Cross Esterification of Alcohols via Acyl Chloride Formation. *Adv. Synth. Catal.* **2016**, *358*, 154-158, DOI: 10.1002/adsc.201500912.

92.   Pradhan, P. P.; Bobbitt, J. M.; Bailey, W. F.: Oxidative Cleavage of Benzylic and Related Ethers, Using an Oxoammonium Salt. *J. Org. Chem.* **2009**, *74*, 9524-9527, DOI: 10.1021/jo902144b.

93.   Gaspa, S.; Porcheddu, A.; De Luca, L.: Metal-Free Direct Oxidation of Aldehydes to Esters Using TCCA. *Org. Lett.* **2015**, *17*, 3666-3669, DOI: 10.1021/acs.orglett.5b01579.

94.   Abramovich, A.; Toledo, H.; Pisarevsky, E.; Szpilman, A. M.: Organocatalytic Oxidative Dimerization of Alcohols to Esters. *Synlett* **2012**, *23*, 2261-2265, DOI: 10.1055/s-0032-1317018.

95.   Murahashi, S.; Naota, T.; Ito, K.; Maeda, Y.; Taki, H.: Ruthenium-catalyzed oxidative transformation of alcohols and aldehydes to esters and lactones. *J. Org. Chem.* **1987**, *52*, 4319-4327, DOI: 10.1021/jo00228a032.

96.   Morita, K.; Nishiyama, Y.; Ishii, Y.: Selective dimerization of aldehydes to esters catalyzed by zirconocene and hafnocene complexes. *Organometallics* **1993**, *12*, 3748-3752, DOI: 10.1021/om00033a053.

97.	Moriyama, K.; Takemura, M.; Togo, H.: Selective Oxidation of Alcohols with Alkali Metal Bromides as Bromide Catalysts: Experimental Study of the Reaction Mechanism. *J. Org. Chem.* **2014**, *79*, 6094-6104, DOI: 10.1021/jo5008064.

98.	Srimani, D.; Balaraman, E.; Gnanaprakasam, B.; Ben-David, Y.; Milstein, D.: Ruthenium Pincer-Catalyzed Cross-Dehydrogenative Coupling of Primary Alcohols with Secondary Alcohols under Neutral Conditions. *Adv. Synth. Catal.* **2012**, *354*, 2403-2406, DOI: 10.1002/adsc.201200438.

99.	Merbouh, N.; Bobbitt, J. M.; Brueckner, C.: Oxoammonium Salts. 9. Oxidative Dimerization of Polyfunctional Primary Alcohols to Esters. An Interesting β Oxygen Effect. *J. Org. Chem.* **2004**, *69*, 5116-5119, DOI: 10.1021/jo049461j.

100.	Craig, J. C.; Horning, E. C.: Preparation of Esters by Hemiacetal Oxidation. *J. Org. Chem.* **1960**, *25*, 2098-2102, DOI: 10.1021/jo01082a007.

101.	Bolm, C.; Magnus, A. S.; Hildebrand, J. P.: Catalytic Synthesis of Aldehydes and Ketones under Mild Conditions Using TEMPO/Oxone. *Org. Lett.* **2000**, *2*, 1173-1175, DOI: 10.1021/ol005792g.

102.	Tao, X.; Cao, X.; Yu, W.; Zhang, J.: Oxidation of Alcohols under Mild Conditions Using Oxone/CaCl2/TEMPO. *Chinese J. Org. Chem.* **2010**, *30*, 250-253.

103.	Widmalm, G.: A perspective on the primary and three-dimensional structures of carbohydrates. *Carbohydr. Res.* **2013**, *378*, 123-132, DOI: 10.1016/j.carres.2013.02.005.

104.	Widmalm, G. *General NMR spectroscopy of carbohydrates and conformational analysis in solution*. In *Comprehensive Glycoscience*; Kamerling, J. P., Ed.; Elsevier Ltd.: 2007; Vol. 2, p 101-132.

105.	Mazzanti, A.; Casarini, D.: Recent trends in conformational analysis. *Wiley Interdiscip. Rev.: Comput. Mol. Sci.* **2012**, *2*, 613-641, DOI: 10.1002/wcms.96.

106. Frank, M. *Conformational analysis of carbohydrates - a historical overview*. In *Bioinformatics for Glycobiology and Glycomics*; John Wiley & Sons Ltd.: 2009, 10.1002/9780470029619.ch18, p 337-357.

107. Gerbst, A. G.; Grachev, A. A.; Shashkov, A. S.; Nifantiev, N. E.: Computation techniques in the conformational analysis of carbohydrates. *Russ. J. Bioorg. Chem.* **2007**, *33*, 24-37, DOI: 10.1134/S1068162007010037.

108. Grachev, A. A.; Gerbst, A. G.; Shashkov, A. S.; Nifantiev, N. E.: Application of modern NMR techniques for conformational analysis of oligo- and polysaccharides. *Russ. Chem. Rev.* **2009**, *78*, 717-736, DOI: 10.1070/RC2009v078n08ABEH004061.

109. Karplus, M.: Vicinal proton coupling in nuclear magnetic resonance. *J. Am. Chem. Soc.* **1963**, *85*, 2870-2871, DOI: 10.1021/ja00901a059.

110. Karplus, M.; Anderson, D. H.; Farrar, T. C.; Gutowsky, H. S.: Valence-bond interpretation of electron coupled proton-proton magnetic interactions measured via deuterium substitution. *J. Chem. Phys.* **1957**, *27*, 597-598, DOI: 10.1063/1.1743784.

111. Ramsey, N. F.: Electron coupled interactions between nuclear spins in molecules. *Phys. Rev.* **1953**, *91*, 303-307, DOI: 10.1103/PhysRev.91.303.

112. Haasnoot, C. A. G.; de Leeuw, F. A. A. M.; de Leeuw, H. P. M.; Altona, C.: Interpretation of vicinal proton-proton coupling constants by a generalized Karplus relation. Conformational analysis of the exocyclic C4′-C5′ bond in nucleosides and nucleotides: Preliminary Communication. *Recl. Trav. Chim. Pays-Bas* **1979**, *98*, 576-577, DOI: 10.1002/recl.19790981206.

113. Haasnoot, C. A. G.; de Leeuw, F. A. A. M.; Altona, C.: The relationship between proton-proton NMR coupling constants and substituent electronegativities—I. *Tetrahedron* **1980**, *36*, 2783-2792, DOI: 10.1016/0040-4020(80)80155-4.

114. Haasnoot, C. A. G.; de Leeuw, F. A. A. M.; de Leeuw, H. P. M.; Altona, C.: The relationship between proton–proton NMR coupling constants and substituent

electronegativities. II—conformational analysis of the sugar ring in nucleosides and nucleotides in solution using a generalized Karplus equation. *Organ. Magnet. Res.* **1981**, *15*, 43-52, DOI: 10.1002/mrc.1270150111.

115.   Toukach, F. V.; Ananikov, V. P.: Recent advances in computational predictions of NMR parameters for the structure elucidation of carbohydrates: methods and limitations. *Chem. Soc. Rev.* **2013**, *42*, 8376-8415, DOI: 10.1039/c3cs60073d.

116.   Coxon, B. *Chapter 3 Developments in the Karplus Equation as they Relate to the NMR Coupling Constants of Carbohydrates*. In *Adv. Carbohydr. Chem. Biochem.*; Academic Press: 2009; Vol. 62, p 17-82.

117.   Minch, M. J.: Orientational dependence of vicinal proton-proton NMR coupling constants: The Karplus relationship. *Concepts Magn. Reson.* **1994**, *6*, 41-56, DOI: 10.1002/cmr.1820060104.

118.   Altona, C. *Vicinal coupling constants and conformation of biomolecules*. In *Encyclopedia of NMR*; John Wiley & Sons, Ltd: 2007, DOI: 10.1002/9780470034590.emrstm0587.

119.   Grimmer, C. D.; Slabber, C. A.: Conformational analysis: 3JHCOC and 3JHCCC Karplus relationships for methylene 1H nuclei. *Magn. Reson. Chem.* **2015**, *53*, 590-595, DOI: 10.1002/mrc.4264.

120.   Munzarová, M. L.; Sklenář, V.: Three-Bond Sugar−Base Couplings in Purine versus Pyrimidine Nucleosides: A DFT Study of Karplus Relationships for 3JC2/4-H1' and 3JC6/8-H1' in DNA. *J. Am. Chem. Soc.* **2002**, *124*, 10666-10667, DOI: 10.1021/ja026502p.

121.   Tafazzoli, M.; Ghiasi, M.: New Karplus equations for 2JHH, 3JHH, 2JCH, 3JCH, 3JCOCH, 3JCSCH, and 3JCCCH in some aldohexopyranoside derivatives as determined using NMR spectroscopy and density functional theory calculations. *Carbohydr. Res.* **2007**, *342*, 2086-2096, DOI: 10.1016/j.carres.2007.05.032.

122. Tvaroška, I.; Hricovíni, M.; Petráková, E.: An attempt to derive a new Karplus-type equation of vicinal proton-carbon coupling constants for COCH segments of bonded atoms. *Carbohydr. Res.* **1989**, *189*, 359-362, DOI: 10.1016/0008-6215(89)84112-6.

123. Suardíaz, R.; Pérez, C.; García de la Vega, J. M.; Fabián, J. S.; Contreras, R. H.: Theoretical Karplus relationships for vicinal coupling constants around χ1 in Valine. *Chem. Phys. Lett.* **2007**, *442*, 119-123, DOI: 10.1016/j.cplett.2007.05.049.

124. Aydin, R.; Günther, H.: 13C, 1H spin–spin coupling. X—Norbornane: A reinvestigation of the karplus curve for 3J(13C, 1H). *Magn. Reson. Chem.* **1990**, *28*, 448-457, DOI: 10.1002/mrc.1260280513.

125. De Marco, A.; Llinas, M.: Complete assignment of carbon signals in a stereospecific peptide via selective and single off-resonance Proton decoupling experiments. Analysis of the carbon-13 nuclear magnetic resonance spectrum of alumichrome at 67.88 MHz. *Biochemistry* **1979**, *18*, 3846-3854, DOI: 10.1021/bi00585a003.

126. Houseknecht, J. B.; Lowary, T. L.; Hadad, C. M.: Improved Karplus Equations for 3JC1,H4 in Aldopentofuranosides: Application to the Conformational Preferences of the Methyl Aldopentofuranosides. *J. Phys. Chem. A* **2003**, *107*, 372-378, DOI: 10.1021/jp026610y.

127. Anderson, J. E.; Ijeh, A. I.: Eclipsed ground-state conformations for methoxycyclohexanes with adjacent methyl-group substitution. An NMR criterion and molecular mechanics calculations. *J. Chem. Soc. Perk. Trans. 2* **1994**, 10.1039/P29940001965, 1965-1967, DOI: 10.1039/P29940001965.

128. Mulloy, B.; Frenkiel, T. A.; Davies, D. B.: Long-range carbon—proton coupling constants: Application to conformational studies of oligosaccharides. *Carbohydr. Res.* **1988**, *184*, 39-46, DOI: 10.1016/0008-6215(88)80004-1.

129. Cloran, F.; Carmichael, I.; Serianni, A. S.: Density Functional Calculations on Disaccharide Mimics: Studies of Molecular Geometries and Trans-O-glycosidic

3JCOCH and 3JCOCC Spin-Couplings. *J. Am. Chem. Soc.* **1999**, *121*, 9843-9851, DOI: 10.1021/ja984384t.

130.   Cloran, F.; Carmichael, I.; Serianni, A. S.: 13C−H and 13C−13C Spin Coupling Behavior in Aldofuranosyl Rings from Density Functional Theory. *J. Phys. Chem. A* **1999**, *103*, 3783-3795, DOI: 10.1021/jp9905676.

131.   Stenutz, R.; Carmichael, I.; Widmalm, G.; Serianni, A. S.: Hydroxymethyl Group Conformation in Saccharides: Structural Dependencies of 2JHH, 3JHH, and 1JCH Spin−Spin Coupling Constants. *J. Org. Chem.* **2002**, *67*, 949-958, DOI: 10.1021/jo010985i.

132.   González-Outeiriño, J.; Nasser, R.; Anderson, J. E.: Conformation of Acetate Derivatives of Sugars and Other Cyclic Alcohols. Crystal Structures, NMR Studies, and Molecular Mechanics Calculations of Acetates. When Is the Exocyclic C−O Bond Eclipsed? *J. Org. Chem.* **2005**, *70*, 2486-2493, DOI: 10.1021/jo048295c.

133.   Turney, T.; Pan, Q.; Sernau, L.; Carmichael, I.; Zhang, W.; Wang, X.; Woods, R. J.; Serianni, A. S.: O-Acetyl Side-Chains in Monosaccharides: Redundant NMR Spin-Couplings and Statistical Models for Acetate Ester Conformational Analysis. *J. Phys. Chem. B* **2017**, *121*, 66-77, DOI: 10.1021/acs.jpcb.6b10028.

134.   Wavefunction Inc.; Wavefunction, Inc.: Irvine, CA.

135.   Frisch, M. J.; Trucks, G. W.; Schlegel, H. B.; Scuseria, G. E.; Robb, M. A.; Cheeseman, J. R.; Scalmani, G.; Barone, V.; Mennucci, B.; Petersson, G. A.; Nakatsuji, H.; Caricato, M.; Li, X.; Hratchian, H. P.; Izmaylov, A. F.; Bloino, J.; Zheng, G.; Sonnenberg, J. L.; Hada, M.; Ehara, M.; Toyota, K.; Fukuda, R.; Hasegawa, J.; Ishida, M.; Nakajima, T.; Honda, Y.; Kitao, O.; Nakai, H.; Vreven, T.; Montgomery Jr., J. A.; Peralta, J. E.; Ogliaro, F.; Bearpark, M. J.; Heyd, J.; Brothers, E. N.; Kudin, K. N.; Staroverov, V. N.; Kobayashi, R.; Normand, J.; Raghavachari, K.; Rendell, A. P.; Burant, J. C.; Iyengar, S. S.; Tomasi, J.; Cossi, M.; Rega, N.; Millam, N. J.; Klene, M.; Knox, J. E.; Cross, J. B.;

Bakken, V.; Adamo, C.; Jaramillo, J.; Gomperts, R.; Stratmann, R. E.; Yazyev, O.; Austin, A. J.; Cammi, R.; Pomelli, C.; Ochterski, J. W.; Martin, R. L.; Morokuma, K.; Zakrzewski, V. G.; Voth, G. A.; Salvador, P.; Dannenberg, J. J.; Dapprich, S.; Daniels, A. D.; Farkas, Ö.; Foresman, J. B.; Ortiz, J. V.; Cioslowski, J.; Fox, D. J.; Gaussian, Inc.: Wallingford, CT, USA, 2009.

136.   Kennedy, J. F.; Kumar, H.; Panesar, P. S.; Marwaha, S. S.; Goyal, R.; Parmar, A.; Kaur, S.: Enzyme-catalyzed regioselective synthesis of sugar esters and related compounds. *J. Chem. Technol. Biotechnol.* **2006**, *81*, 866-876, DOI: 10.1002/jctb.1473.

137.   Therisod, M.; Klibanov, A. M.: Facile enzymatic preparation of monoacylated sugars in pyridine. *J. Am. Chem. Soc.* **1986**, *108*, 5638-5640, DOI: 10.1021/ja00278a053.

138.   Adinolfi, M.; Barone, G.; Iadonisi, A.; Schiattarella, M.: An easy approach for the acetylation of saccharidic alcohols. Applicability for regioselective protections. *Tetrahedron Lett.* **2003**, *44*, 4661-4663, DOI: 10.1016/S0040-4039(03)01072-4.

139.   Brecker, L.; Mahut, M.; Schwarz, A.; Nidetzky, B.: In situ proton NMR study of acetyl and formyl group migration in mono-O-acyl D-glucose. *Magn. Reson. Chem.* **2009**, *47*, 328-332, DOI: 10.1002/mrc.2395.

140.   Ishihara, K.; Kurihara, H.; Yamamoto, H.: An extremely simple, convenient, and selective method for acetylating primary alcohols in the presence of secondary alcohols. *J. Org. Chem.* **1993**, *58*, 3791-3793, DOI: 10.1021/jo00067a005.

141.   Joseph, A. A.; Verma, V. P.; Liu, X.-Y.; Wu, C.-H.; Dhurandhare, V. M.; Wang, C.-C.: TMSOTf-Catalyzed Silylation: Streamlined Regioselective One-Pot Protection and Acetylation of Carbohydrates. *Eur. J. Org. Chem.* **2012**, *2012*, 744-753, DOI: 10.1002/ejoc.201101267.

142.   Witschi, M. A.; Gervay-Hague, J.: Selective Acetylation of per-O-TMS-Protected Monosaccharides. *Org. Lett.* **2010**, *12*, 4312-4315, DOI: 10.1021/ol101751d.

143. Bollenback, G. N.; Long, J. W.; Benjamin, D. G.; Lindquist, J. A.: The synthesis of aryl-D-glucopyranosiduronic acids. *J. Am. Chem. Soc.* **1955**, *77*, 3310-3315, DOI: 10.1021/ja01617a047.

144. Willker, W.; Leibfritz, D.: Determination of heteronuclear long-range H,X coupling constants from gradient-selected HMBC spectra. *Magn. Reson. Chem.* **1995**, *33*, 632-638, DOI: 10.1002/mrc.1260330804.

145. Poly Software International Inc.; 8.02a ed.; Poly Software International, Inc.: Pearl River, NY, 2005.

146. Kirschner, K. N., Yongye, A.B., Tschampel, S.M., Daniels, C.R., Foley, B.L, Woods, R.J.: GLYCAM06: A Generalizable Biomolecular Force Field. Carbohydrates. *J. Comput. Chem.* **2008**, *29*, 622-655, DOI: 10.1002/jcc.20820.

147. Seo, M.; Castillo, N.; Ganzynkowicz, R.; Daniels, C. R.; Woods, R. J.; Lowary, T. L.; Roy, P.-N.: Approach for the Simulation and Modeling of Flexible Rings: Application to the α-D-Arabinofuranoside Ring, a Key Constituent of Polysaccharides from Mycobacterium tuberculosis. *J. Chem. Theory Comput.* **2008**, *4*, 184-191, DOI: 10.1021/ct700284r.

148. Jorgensen, W. L.; Chandrasekhar, J.; Madura, J. D.; Impey, R. W.; Klein, M. L.: Comparison of simple potential functions for simulating liquid water. *J. Chem. Phys.* **1983**, *79*, 926-935, DOI: 10.1063/1.445869.

149. Pereira, C. S.; Kony, D.; Baron, R.; Muller, M.; van Gunsteren, W. F.; Hunenberger, P. H.: Conformational and dynamical properties of disaccharides in water: a molecular dynamics study. *Biophys. J.* **2006**, *90*, 4337-4344, DOI: 10.1529/biophysj.106.081539.

150. Watson, A. H., S.; Franz, A.H.: 6-O-(α-D-glucopyranosyl)-α/β-D-glucopyranose (isomaltose) or 6-O-(α-D-galactopyranosyl)-α/β-D-glucopyranose (melibiose) core. *in preparation*.

151. Bally, T.; Rablen, P. R.: Quantum-Chemical Simulation of 1H NMR Spectra. 2. Comparison of DFT-Based Procedures for Computing Proton–Proton Coupling Constants in Organic Molecules. *J. Org. Chem.* **2011**, *76*, 4818-4830, DOI: 10.1021/jo200513q.

152. Bagno, A.; Rastrelli, F.; Saielli, G.: Predicting 13C NMR Spectra by DFT Calculations. *J. Phys. Chem. A* **2003**, *107*, 9964-9973, DOI: 10.1021/jp0353284.

153. McNaught, A. D.: Nomenclature of carbohydrates. *Carbohydr. Res.* **1997**, *297*, 1-92, DOI: 10.1016/S0008-6215(97)83449-0.

154. Cornell, W. D.; Cieplak, P.; Bayly, C. I.; Kollmann, P. A.: Application of RESP charges to calculate conformational energies, hydrogen bond energies, and free energies of solvation. *J. Am. Chem. Soc.* **1993**, *115*, 9620-9631, DOI: 10.1021/ja00074a030.

155. Blomqvist, J.; Ahjopalo, L.; Mannfors, B.; Pietilä, L. O.: Studies on aliphatic polyesters I: Ab initio, density functional and force field studies of esters with one carboxyl group. *J. Mol. Struc. - THEOCHEM* **1999**, *488*, 247-262, DOI: 10.1016/S0166-1280(99)00038-X.

156. McAliley, J. H.; Bruce, D. A.: Development of Force Field Parameters for Molecular Simulation of Polylactide. *J. Chem. Theory Comput.* **2011**, *7*, 3756-3767, DOI: 10.1021/ct200251x.

157. Wang, J.; Wolf, R. M.; Caldwell, J. W.; Kollman, P. A.; Case, D. A.: Development and testing of a general amber force field. *J. Comput. Chem.* **2004**, *25*, 1157-1174, DOI: 10.1002/jcc.20035.

158. Allinger, N. L.: Conformational analysis. 130. MM2. A hydrocarbon force field utilizing V1 and V2 torsional terms. *J. Am. Chem. Soc.* **1977**, *99*, 8127-8134, DOI: 10.1021/ja00467a001.

159. Brandley, B. K.; Schnaar, R. L.: Cell-surface carbohydrates in cell recognition and response. *J. Leukocyte Biol.* **1986**, *40*, 97-111.

160. Zhao, Y.-Y.; Takahashi, M.; Gu, J.-G.; Miyoshi, E.; Matsumoto, A.; Kitazume, S.; Taniguchi, N.: Functional roles of N-glycans in cell signaling and cell adhesion in cancer. *Cancer Science* **2008**, *99*, 1304-1310, DOI: 10.1111/j.1349-7006.2008.00839.x.

161. Cobb, B. A.; Kasper, D. L.: Coming of age: carbohydrates and immunity. *Eur. J. Immunol.* **2005**, *35*, 352-356, DOI: 10.1002/eji.200425889.

162. Bard, F.; Chia, J.: Cracking the Glycome Encoder: Signaling, Trafficking, and Glycosylation. *Trends Cell Biol.* **2016**, *26*, 379-388, DOI: 10.1016/j.tcb.2015.12.004.

163. Werz, D. B.; Ranzinger, R.; Herget, S.; Adibekian, A.; von der Lieth, C.-W.; Seeberger, P. H.: Exploring the Structural Diversity of Mammalian Carbohydrates ("Glycospace") by Statistical Databank Analysis. *ACS Chem. Biol.* **2007**, *2*, 685-691, DOI: 10.1021/cb700178s.

164. Mattos, L. C. d.: Structural diversity and biological importance of ABO, H, Lewis and secretor histo-blood group carbohydrates. *Rev. Bras. Hemtol. Hemoter.* **2016**, *38*, 331-340.

165. Cumpstey, I.; Ramstadius, C.; Akhtar, T.; Goldstein, I. J.; Winter, H. C.: Non-Glycosidically Linked Pseudodisaccharides: Thioethers, Sulfoxides, Sulfones, Ethers, Selenoethers, and Their Binding to Lectins. *Eur. J. Org. Chem.* **2010**, *2010*, 1951-1970, DOI: 10.1002/ejoc.200901481.

166. Cumpstey, I.: Neodisaccharide diglycosyl compounds: Ethers, thioethers and selenoethers. A survey of their synthesis and biological activity. *CR Chem.* **2011**, *14*, 274-285, DOI: 10.1016/j.crci.2010.05.004.

167. Lairson, L. L. H., B.; Davies, G.J.; Withers, S.G.: Glycosyltransferases: Structures, Functions, and Mechanisms. *Annu. Rev. Biochem* **2008**, *77*, 521-555, DOI: 10.1146/annurev.biochem.76.061005.092322.

168. Bojarová, P.; Křen, V.: Glycosidases: a key to tailored carbohydrates. *Trends Biotechnol.*, *27*, 199-209, DOI: 10.1016/j.tibtech.2008.12.003.

169. Sharon, N.; Lis, H.: History of lectins: from hemagglutinins to biological recognition molecules. *Glycobiology* **2004**, *14*, 53R-62R, DOI: 10.1093/glycob/cwh122.

170. Ghazarian, H.; Idoni, B.; Oppenheimer, S. B.: A glycobiology review: Carbohydrates, lectins and implications in cancer therapeutics. *Acta Histochemica* **2011**, *113*, 236-247, DOI: 10.1016/j.acthis.2010.02.004.

171. Xu, D. E., J.D.: Demystifying Heparan Sulfate–Protein Interactions. *Annu. Rev. Biochem* **2014**, *83*, 129-157, DOI: 10.1146/annurev-biochem-060713-035314.

172. Hileman, R. E.; Fromm, J. R.; Weiler, J. M.; Linhardt, R. J.: Glycosaminoglycan-protein interactions: definition of consensus sites in glycosaminoglycan binding proteins. *BioEssays* **1998**, *20*, 156-167, DOI: 10.1002/(SICI)1521-1878(199802)20:2<156::AID-BIES8>3.0.CO;2-R.

173. Matsui, H.; Sasaki, M.; Takemasa, E.; Kaneta, T.; Chiba, S.: Kinetic Studies on the Substrate Specificity and Active Site of Rabbit Muscle Acid α-Glucosidase. *J. Biochem.* **1984**, *96*, 993-1004.

174. Chiba, S.: Molecular Mechanism in α-Glucosidase and Glucoamylase. *Biosci. Biotechnol. Biochem.* **1997**, *61*, 1233-1239, DOI: 10.1271/bbb.61.1233.

175. Bock, K.; Defaye, J.; Driguez, H.; Bar-Guilloux, E.: Conformations in solution of alpha,alpha-trehalose, alpha-D-glucopyranosyl alpha-D-mannopyranoside, and their 1-thioglycosyl analogs, and a tentative correlation of their behaviour with respect to the enzyme trehalase. *Eur. J. Biochem.* **1983**, *131*, 595-600, DOI: 10.1111/j.1432-1033.1983.tb07304.x.

176. Catelani, G.; D'Andrea, F.; Guazzelli, L.; Griselli, A.; Testi, N.; Chiacchio, M. A.; Legnani, L.; Toma, L.: Synthesis and conformational analysis of a simplified inositol-model of the Streptococcus pneumoniae 19F capsular polysaccharide repeating unit. *Carbohydr. Res.* **2017**, *443-444*, 29-36, DOI: 10.1016/j.carres.2017.03.012.

177.   Cheetham, N. W. H.; Dasgupta, P.; Ball, G. E.: NMR and modelling studies of disaccharide conformation. *Carbohydr. Res.* **2003**, *338*, 955-962, DOI: 10.1016/S0008-6215(03)00069-7.

178.   Darré, L.; Ivani, I.; Dans, P. D.; Gómez, H.; Hospital, A.; Orozco, M.: Small Details Matter: The 2′-Hydroxyl as a Conformational Switch in RNA. *J. Am. Chem. Soc.* **2016**, 10.1021/jacs.6b09471, DOI: 10.1021/jacs.6b09471.

179.   Hoog, C.; Landersjo, C.; Widmalm, G.: Oligosaccharides display both rigidity and high flexibility in water as determined by 13C NMR relaxation and 1H,1H NOE spectroscopy: evidence of anti-φ and anti-ψ torsions in the same glycosidic linkage. *Chem. Eur. J.* **2001**, *7*, 3069-3077, DOI: 10.1002/1521-3765(20010716)7:14<3069::AID-CHEM3069>3.0.CO;2-A.

180.   Landstroem, J.; Widmalm, G.: Glycan flexibility: insights into nanosecond dynamics from a microsecond molecular dynamics simulation explaining an unusual nuclear Overhauser effect. *Carbohydr. Res.* **2010**, *345*, 330-333, DOI: 10.1016/j.carres.2009.11.003.

181.   Taniguchi, T.; Nakano, K.; Baba, R.; Monde, K.: Analysis of Configuration and Conformation of Furanose Ring in Carbohydrate and Nucleoside by Vibrational Circular Dichroism. *Org. Lett.* **2017**, *19*, 404-407, DOI: 10.1021/acs.orglett.6b03626.

182.   Vogel, P.: Monosaccharide and disaccharide mimics: new molecular tools for biology and medicine. *Chimia* **2001**, *55*, 359-365.

183.   Vichasilp, C.; Nakagawa, K.; Sookwong, P.; Higuchi, O.; Luemunkong, S.; Miyazawa, T.: Development of high 1-deoxynojirimycin (DNJ) content mulberry tea and use of response surface methodology to optimize tea-making conditions for highest DNJ extraction. *LWT - Food Sci. Technol.* **2012**, *45*, 226-232, DOI: 10.1016/j.lwt.2011.09.008.

184. Joubert, P. H.; Venter, H. L.; Foukaridis, G. N.: The effect of miglitol and acarbose after an oral glucose load: a novel hypoglycaemic mechanism? *Brit. J. Clin. Pharmaco.* **1990**, *30*, 391-396, DOI: 10.1111/j.1365-2125.1990.tb03789.x.

185. Rosner, H.; Google Patents: 2004.

186. Parella, T.; Espinosa, J. F.: Long-range proton–carbon coupling constants: NMR methods and applications. *Prog. Nucl. Magn. Reson. Spectrosc.* **2013**, *73*, 17-55, DOI: 10.1016/j.pnmrs.2013.07.001.

187. Xiong, X.; Chen, Z.; Cossins, B. P.; Xu, Z.; Shao, Q.; Ding, K.; Zhu, W.; Shi, J.: Force fields and scoring functions for carbohydrate simulation. *Carbohydr. Res.* **2015**, *401*, 73-81, DOI: 10.1016/j.carres.2014.10.028.

188. Sabesan, S.; Neira, S.; Davidson, F.; Duus, J. O.; Bock, K.: Synthesis, Enzymic, and NMR Studies of Novel Sialoside Probes: Unprecedented, Selective Neuraminidase Hydrolysis of and Inhibition by C-6-(methyl)-Gal Sialosides. *J. Am. Chem. Soc.* **1994**, *116*, 1616-1634, DOI: 10.1021/ja00084a003.

189. Vidal, P.; Vauzeilles, B.; Bleriot, Y.; Sollogoub, M.; Sinay, P.; Jimenez-Barbero, J.; Espinosa, J. F.: Conformational behaviour of glycomimetics: NMR and molecular modelling studies of the C-glycoside analogue of the disaccharide methyl beta-D-galactopyranosyl-(1-->3)-beta-D-glucopyranoside. *Carbohydr. Res.* **2007**, *342*, 1910-1917, DOI: 10.1016/j.carres.2007.04.017.

190. Asensio, J. L.; Cañada, F. J.; García-Herrero, A.; Murillo, M. T.; Fernández-Mayoralas, A.; Johns, B. A.; Kozak, J.; Zhu, Z.; Johnson, C. R.; Jiménez-Barbero, J.: Conformational Behavior of Aza-C-Glycosides: Experimental Demonstration of the Relative Role of the exo-anomeric Effect and 1,3-Type Interactions in Controlling the Conformation of Regular Glycosides. *J. Am. Chem. Soc.* **1999**, *121*, 11318-11329, DOI: 10.1021/ja9922734.

191. Denton, R. W.; Cheng, X.; Tony, K. A.; Dilhas, A.; Hernandez, J. J.; Canales, A.; Jimenez-Barbero, J.; Mootoo, D. R.: C-Disaccharides as probes for carbohydrate recognition - investigation of the conformational requirements for binding disaccharide mimetics of sialyl Lewis X. *Eur. J. Org. Chem.* **2007**, 645-654, DOI: 10.1002/ejoc.200600825.

192. Duus, J. O.; Bock, K.; Ogawa, S.: An NMR spectroscopic and conformational study of 12 pseudo-disaccharides (D-glucopyranosyl-5a-carba-D- and -L-glucopyranoses). *Carbohydr. Res.* **1994**, *252*, 1-18, DOI: 10.1016/0008-6215(94)90002-7.

193. Peri, F.; Jimenez-Barbero, J.; Garcia-Aparicio, V.; Tvaroska, I.; Nicotra, F.: Synthesis and conformational analysis of novel N(OCH3)-linked disaccharide analogues. *Chem. Eur. J.* **2004**, *10*, 1433-1444, DOI: 10.1002/chem.200305587.

194. Chung, I.-M.; Kim, S. H.; Ahn, Y. S.; Ahmad, A.: Glucuronopyranosyl polyglucopyranosyl constituent from the fruits of Lycium chinense. *Asian J. Chem.* **2012**, *24*, 3206-3208.

195. Vila, F. C.; Colombo, R.; de Lira, T. O.; Yariwake, J. H.: HPLC microfractionation of flavones and antioxidant (radical scavenging) activity of Saccharum officinarum L. *J. Braz. Chem. Soc.* **2008**, *19*, 903-908, DOI: 10.1590/S0103-50532008000500014.

196. Li, X.; Yao, S.; Tu, B.; Li, X.; Jia, C.; Song, H.: Determination and comparison of flavonoids and anthocyanins in Chinese sugarcane tips, stems, roots and leaves. *J. Sep. Sci.* **2010**, *33*, 1216-1223, DOI: 10.1002/jssc.200900567.

197. Baddeley, T. C.; Wardell, J. L.: Synthesis of Per- and Poly-Substituted Trehalose Derivatives: Studies of Properties Relevant to Their Use as Excipients for Controlled Drug Release. *J. Carbohydr. Chem.* **2009**, *28*, 198-221, DOI: 10.1080/07328300902887672.

198.   Alcock, R.; Blair, J. A.; O'Mahony, D. J.; Raoof, A.; Quirk, A. V.: Modifying the release of leuprolide from spray dried OED microparticles. *J. Controlled Release* **2002**, *82*, 429-440, DOI: 10.1016/S0168-3659(02)00165-7.

199.   Kondratenko, R. M.; Baltina, L. A.; Mustafina, S. R.; Vasil'eva, E. V.; Ismagilova, A. F.; Vasil'eva, N. G.; Tolstikov, G. A.: Transformations of Glycyrrhizic Acid: XV. Synthesis of Triterpene Saponins with Monosaccharide Residues Attached through Ester Bonds. *uss. J. Bioorg. Chem.* **2003**, *29*, 601-605, DOI: 10.1023/B:RUBI.0000008903.65076.93.

200.   Schmidt, R. R.; Rücker, E.: Stereoselective glycosidations of uronic acids. *Tetrahedron Lett.* **1980**, *21*, 1421-1424, DOI: 10.1016/S0040-4039(00)92735-7.

201.   Schmidt, R. R.; Michel, J.: Reduction of 1-O-acyl-α-D-glucopyranoses to α-glucosides and to 1,5-anhydroglucitol. *J. Org. Chem.* **1981**, *46*, 4787-4788, DOI: 10.1021/jo00336a034.

202.   Barrett, A. G. M.; Bezuidenhoudt, B. C. B.: A convenient stereoselective synthesis of α-glycosyl esters. *Heterocycles* **1989**, *28*, 209-212, DOI: 10.3987/COM-88-S106.

203.   Barrett, A. G. M.; Lee, A. C.: Redox glycosidation: stereoselective syntheses of (1→6) linked disaccharides via thionoester intermediates. *J. Org. Chem.* **1992**, *57*, 2818-2824, DOI: 10.1021/jo00036a012.

204.   Brown, J. A.; Fry, S. C.: The preparation and susceptibility to hydrolysis of novel O-galacturonoyl derivatives of carbohydrates. *Carbohydr. Res.* **1993**, *240*, 95-106, DOI: 10.1016/0008-6215(93)84175-6.

205.   Mukhopadhyay, B.; Kartha, K. P. R.; Russell, D. A.; Field, R. A.: Streamlined Synthesis of Per-O-acetylated Sugars, Glycosyl Iodides, or Thioglycosides from Unprotected Reducing Sugars1. *J. Org. Chem.* **2004**, *69*, 7758-7760, DOI: 10.1021/jo048890e.

206.   Tosin, M.; Murphy, P. V.: Synthesis of α-Glucuronic Acid and Amide Derivatives in the Presence of a Participating 2-Acyl Protecting Group. *Org. Lett.* **2002**, *4*, 3675-3678, DOI: 10.1021/ol026629j.

207. Nishida, Y.; Hori, H.; Ohrui, H.; Meguro, H.: 1H NMR Analyses of Rotameric Distribution of C5-C6 bonds of D-Glucopyranoses in Solution. *J. Carbohydr. Chem.* **1988**, *7*, 239-250, DOI: 10.1080/07328308808058917.

208. Lu, W.; Navidpour, L.; Taylor, S. D.: An expedient synthesis of benzyl 2,3,4-tri-O-benzyl-β-d-glucopyranoside and benzyl 2,3,4-tri-O-benzyl-β-d-mannopyranoside. *Carbohydr. Res.* **2005**, *340*, 1213-1217, DOI: 10.1016/j.carres.2005.02.013.

209. Thibaudeau, C.; Stenutz, R.; Hertz, B.; Klepach, T.; Zhao, S.; Wu, Q.; Carmichael, I.; Serianni, A. S.: Correlated C−C and C−O Bond Conformations in Saccharide Hydroxymethyl Groups: Parametrization and Application of Redundant 1H−1H, 13C−1H, and 13C−13C NMR J-Couplings. *J. Am. Chem. Soc.* **2004**, *126*, 15668-15685, DOI: 10.1021/ja0306718.

210. Timmers, C. M.; Van Straten, N. C. R.; Van der Marel, G. A.; Van Boom, J. H.: An expeditious route to Streptococci and Enterococci glycolipids via ring-opening of 1,2-anhydrosugars with protic acids. *J. Carbohydr. Chem.* **1998**, *17*, 471-487, DOI: 10.1080/07328309808002906.

211. Fügedi, P.: Synthesis of 4-O-(α-L-Rhamnopyranosyl-D-Glucopyranuronic Acid. *J. Carbohydr. Chem.* **1987**, *6*, 377-398, DOI: 10.1080/07328308708057927.

212. Haines, A. H.: Synthesis of 6,6'-ether linked disaccharides from d-allose, d-galactose, d-glucose and d-mannose; evidence on the structure of coyolosa. *Org. Biomol. Chem.* **2004**, *2*, 2352-2358, DOI: 10.1039/B407468H.

213. Haines, A. H.: Evidence on the structure of coyolosa. Synthesis of 6,6′-ether linked hexoses. *Tetrahedron Lett.* **2004**, *45*, 835-837, DOI: 10.1016/j.tetlet.2003.11.033.

214. Pérez G, S.; Pérez G, R. M.; Pérez G, C.; Zavala S, M. A.; Vargas S, R.: Coyolosa, a new hypoglycemic from Acrocomia mexicana. *Pharm. Acta Helv.* **1997**, *72*, 105-111, DOI: 10.1016/S0031-6865(96)00019-2.

215. Takahashi, H.; Fukuda, T.; Mitsuzuka, H.; Namme, R.; Miyamoto, H.; Ohkura, Y.; Ikegami, S.: Development of a Novel Sugar Linkage: 6,6′-Ether-Connected Sugars. *Angew. Chem. Int. Ed.* **2003**, *42*, 5069-5071, DOI: 10.1002/anie.200352388.

216. Hackbusch, S.; Franz, A. H.: Acylation of trans-2-substituted cyclohexanols: the impact of substituent variation on the pyridine-induced reversal of diastereoselectivity. *ARKIVOC* **2015**, *vii*, 172-194, DOI: 10.3998/ark.5550190.p009.321.

217. Al Hazmi, A. M.; Sheikh, N. S.; Bataille, C. J. R.; Al-Hadedi, A. A. M.; Watkin, S. V.; Luker, T. J.; Camp, N. P.; Brown, R. C. D.: trans-2-Tritylcyclohexanol as a Chiral Auxiliary in Permanganate-Mediated Oxidative Cyclization of 2-Methylenehept-5-enoates: Application to the Synthesis of trans-(+)-Linalool Oxide. *Org. Lett.* **2014**, *16*, 5104-5107, DOI: 10.1021/ol502454r.

218. Yamamoto, N.; Obora, Y.; Ishii, Y.: Iridium-Catalyzed Oxidative Methyl Esterification of Primary Alcohols and Diols with Methanol. *J. Org. Chem.* **2011**, *76*, 2937-2941, DOI: 10.1021/jo2003264.

219. Khusnutdinov, R. I.; Shchadneva, N. A.; Baiguzina, A. R.; Lavrentieva, Y. Y.; Dzhemilev, U. M.: Generation of alkyl hypochlorites in oxidation of alcohols with carbon tetrachloride catalyzed by vanadium and manganese compounds. *Russ. Chem. Bull.* **2002**, *51*, 2074-2079, DOI: 10.1023/A:1021668011691.

220. Nguyen, H.-P.; Znifeche, S.; Baboulène, M.: An Improved Greener Esterification of Fatty Alcohols Using a Renewable Acid–Ionic Liquid Couple as Catalyst–Solvent. *Synth. Commun.* **2004**, *34*, 2085-2093, DOI: 10.1081/SCC-120037923.

221. Sølvhøj, A.; Madsen, R.: Dehydrogenative Coupling of Primary Alcohols To Form Esters Catalyzed by a Ruthenium N-Heterocyclic Carbene Complex. *Organometallics* **2011**, *30*, 6044-6048, DOI: 10.1021/om200928b.

222. Hon, Y.-S.; Wong, Y.-C.; Chang, C.-P.; Hsieh, C.-H.: Tishchenko reactions of aldehydes promoted by diisobutylaluminum hydride and its application to the macrocyclic lactone formation. *Tetrahedron* **2007**, *63*, 11325-11340, DOI: 10.1016/j.tet.2007.08.074.

223. Buda, S.; Gołębiowska, P.; Mlynarski, J.: Application of the 2-Nitrobenzyl Group in Glycosylation Reactions: A Valuable Example of an Arming Participating Group. *Eur. J. Org. Chem.* **2013**, *2013*, 3988-3991, DOI: 10.1002/ejoc.201300123.

224. Cheshev, P.; Marra, A.; Dondoni, A.: Direct epoxidation of d-glucal and d-galactal derivatives with in situ generated DMDO. *Carbohydr. Res.* **2006**, *341*, 2714-2716, DOI: 10.1016/j.carres.2006.09.003.

225. Shao, Y.; Molnar, L. F.; Jung, Y.; Kussmann, J.; Ochsenfeld, C.; Brown, S. T.; Gilbert, A. T. B.; Slipchenko, L. V.; Levchenko, S. V.; O'Neill, D. P.; DiStasio Jr, R. A.; Lochan, R. C.; Wang, T.; Beran, G. J. O.; Besley, N. A.; Herbert, J. M.; Yeh Lin, C.; Van Voorhis, T.; Hung Chien, S.; Sodt, A.; Steele, R. P.; Rassolov, V. A.; Maslen, P. E.; Korambath, P. P.; Adamson, R. D.; Austin, B.; Baker, J.; Byrd, E. F. C.; Dachsel, H.; Doerksen, R. J.; Dreuw, A.; Dunietz, B. D.; Dutoi, A. D.; Furlani, T. R.; Gwaltney, S. R.; Heyden, A.; Hirata, S.; Hsu, C.-P.; Kedziora, G.; Khalliulin, R. Z.; Klunzinger, P.; Lee, A. M.; Lee, M. S.; Liang, W.; Lotan, I.; Nair, N.; Peters, B.; Proynov, E. I.; Pieniazek, P. A.; Min Rhee, Y.; Ritchie, J.; Rosta, E.; David Sherrill, C.; Simmonett, A. C.; Subotnik, J. E.; Lee Woodcock Iii, H.; Zhang, W.; Bell, A. T.; Chakraborty, A. K.; Chipman, D. M.; Keil, F. J.; Warshel, A.; Hehre, W. J.; Schaefer Iii, H. F.; Kong, J.; Krylov, A. I.; Gill, P. M. W.; Head-Gordon, M.: Advances in methods and algorithms in a modern quantum chemistry program package. *Phys. Chem. Chem. Phys.* **2006**, *8*, 3172-3191, DOI: 10.1039/B517914A.

226. Case, D. A. B., R.M; Botello-Smith, W.; Cerutti, D.S.; Cheatham III, T.E.; Darden, T.A.; Duke, R.E.; Giese, T.J.; Gohlke, H.; Goetz, A.W.; Homeyer, N.; Izadi, S.; Janowski, P.; Kaus, J.; Kovalenko, A.; Lee, T.S.; LeGrand, S.; Li, P.; Lin, C.; Luchko, T.; Luo, R.;

Madej, B.; Mermelstein, D.; Merz, K.M.; Monard, G.; Nguyen, H.; Nguyen, H.T.; Omelyan, I.; Onufriev, A.; Roe, D.R.; Roitberg, A.; Sagui, C.; Simmerling, C.L.; Swails, J.; Walker, R.C.; Wang, J.; Wolf, R.M.; Wu, X.; Xiao, L.; York D.M. and Kollman P.A. University of California, San Francisco, 2016.

227. Woods Group (2005-2016) *GLYCAM Web. Carbohydrate Builder.* Complex Carbohydrate Research Center, University of Georgia, Athens, GA. (http://glycam.org).

228. Humphrey, W.; Dalke, A.; Schulten, K.: VMD: visual molecular dynamics. *J. Mol. Graph.* **1996**, *14*, 33-38, DOI: 10.1016/0263-7855(96)00018-5.

229. Roe, D. R.; Cheatham, T. E.: PTRAJ and CPPTRAJ: Software for Processing and Analysis of Molecular Dynamics Trajectory Data. *J. Chem. Theory Comput.* **2013**, *9*, 3084-3095, DOI: 10.1021/ct400341p.

230. Foley, L. In *Help for GLYCAM-Web. Adding chemical derivatives to GLYCAM residues*; Woods, R. J., Ed. 2016; Vol. 2016.

231. Reisbick, S.; Willoughby, P.: Generation of Gaussian 09 Input Files for the Computation of ^{1}H and ^{13}C NMR Chemical Shifts of Structures from a Spartan'14 Conformational Search. *Protocol Exchange* **2014**, 10.1038/protex.2014.015, DOI: 10.1038/protex.2014.015.

232. Zhao, Y.; Schultz, N. E.; Truhlar, D. G.: Design of Density Functionals by Combining the Method of Constraint Satisfaction with Parametrization for Thermochemistry, Thermochemical Kinetics, and Noncovalent Interactions. *J. Chem. Theory Comput.* **2006**, *2*, 364-382, DOI: 10.1021/ct0502763.

233. Csonka, G. I.; French, A. D.; Johnson, G. P.; Stortz, C. A.: Evaluation of Density Functionals and Basis Sets for Carbohydrates. *J. Chem. Theory Comput.* **2009**, *5*, 679-692, DOI: 10.1021/ct8004479.

234. Marianski, M.; Supady, A.; Ingram, T.; Schneider, M.; Baldauf, C.: Assessing the Accuracy of Across-the-Scale Methods for Predicting Carbohydrate Conformational

Energies for the Examples of Glucose and α-Maltose. *J. Chem. Theory Comput.* **2016**, *12*, 6157-6168, DOI: 10.1021/acs.jctc.6b00876.

235.   Møller, C.; Plesset, M. S.: Note on an Approximation Treatment for Many-Electron Systems. *Physical Review* **1934**, *46*, 618-622, DOI: 10.1103/PhysRev.46.618.

236.   Kendall, R. A.; Jr., T. H. D.; Harrison, R. J.: Electron affinities of the first-row atoms revisited. Systematic basis sets and wave functions. *J. Chem. Phys.* **1992**, *96*, 6796-6806, DOI: 10.1063/1.462569.

APPENDIX A. NMR SPECTRAL DATA
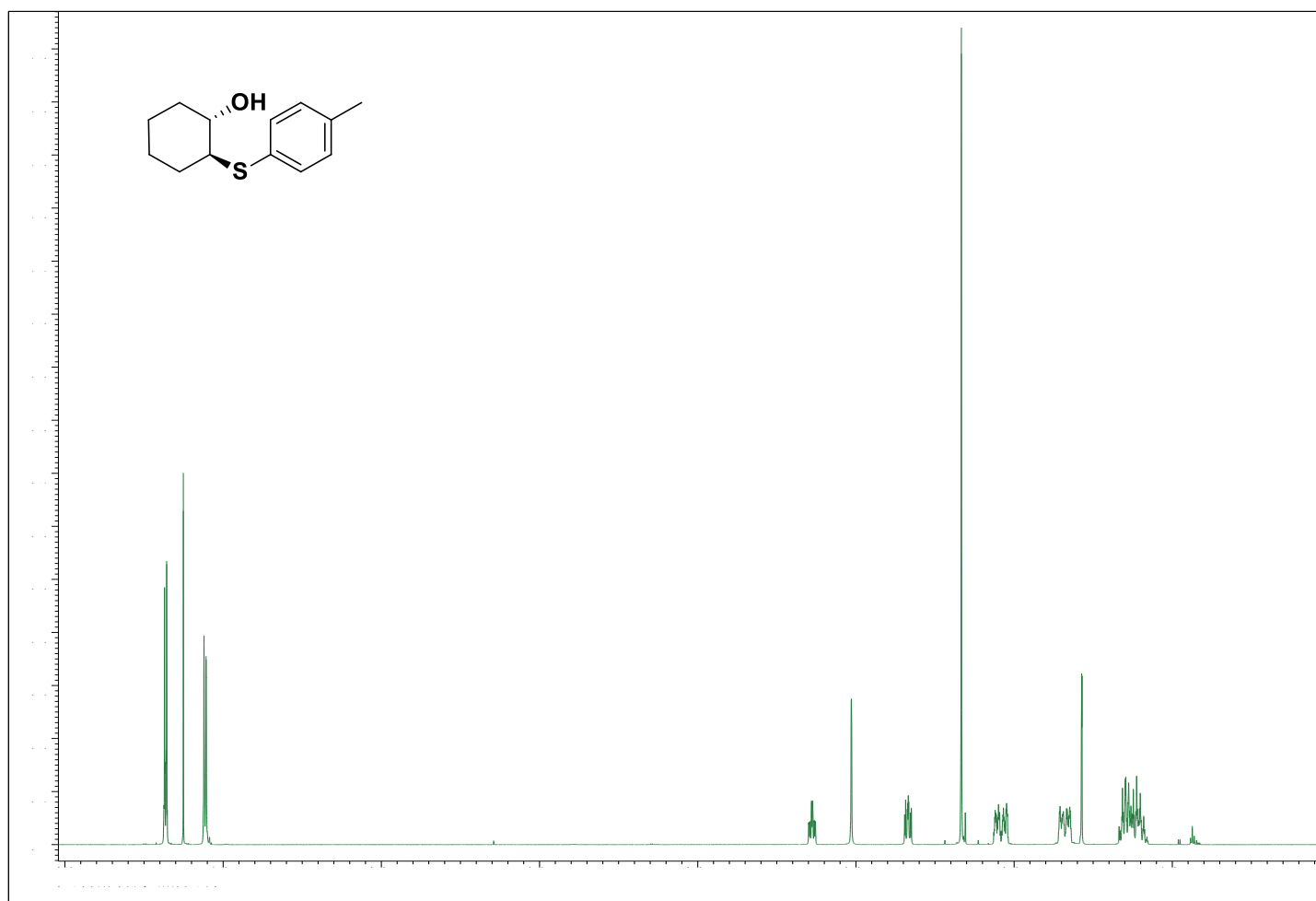
^{1}H NMR of **4** [(±)-*trans*-2-(*p*-tolylsulfanyl)cyclohexanol]
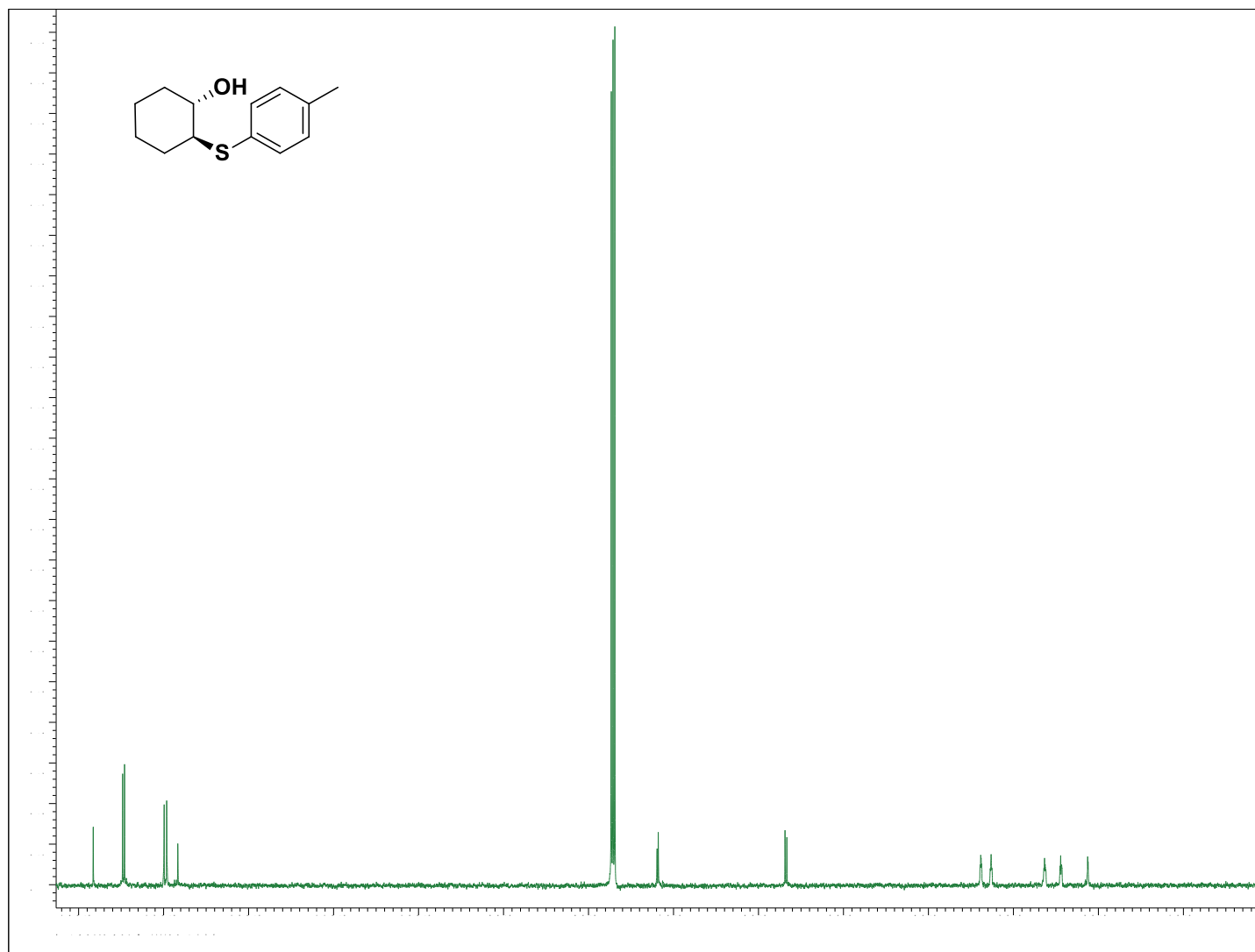
^{13}C NMR of **4** [(±)-*trans*-2-(*p*-tolylsulfanyl)cyclohexanol]
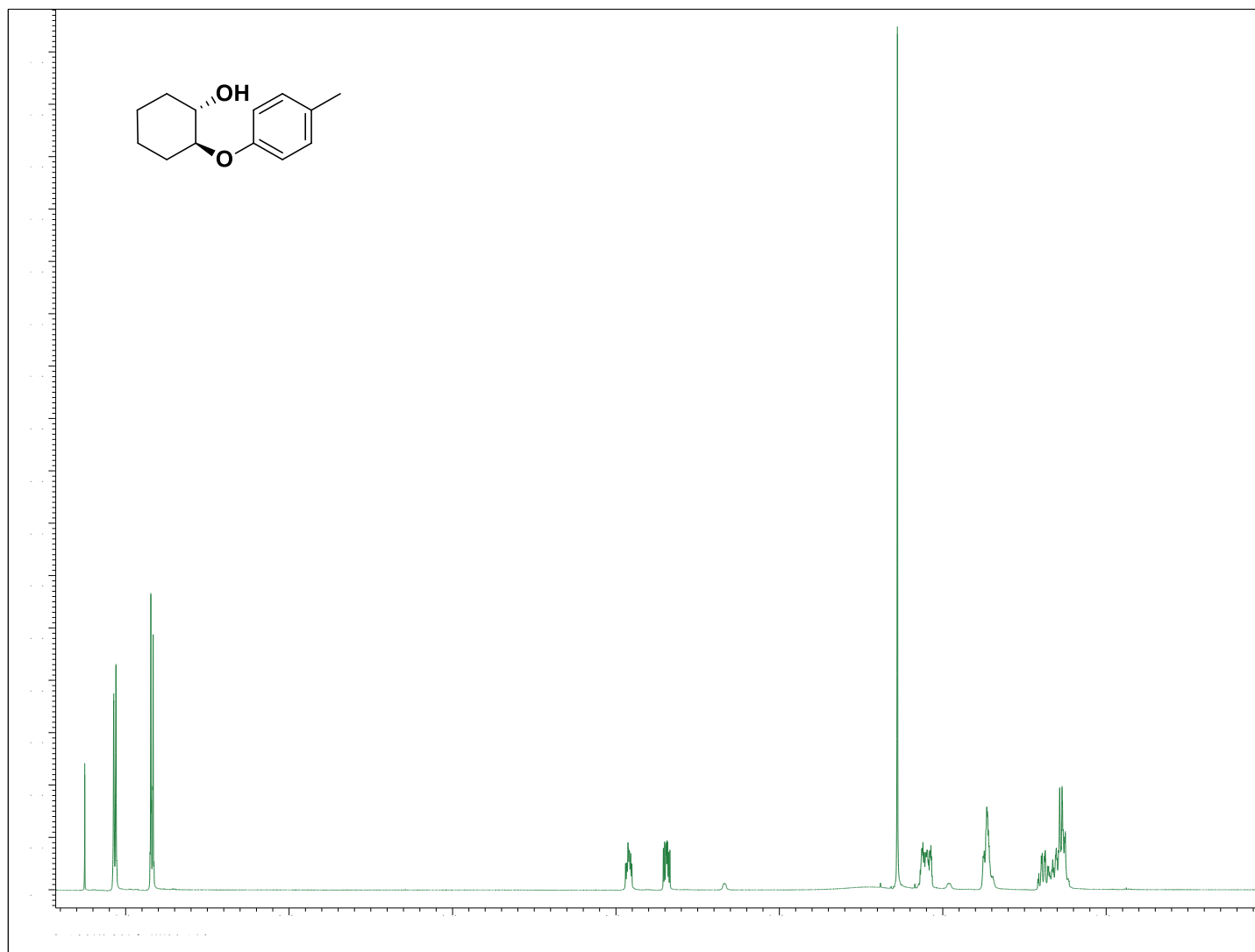
^{1}H NMR of **6** [(±)-*trans*-2-(*p*-tolyloxy)cyclohexanol]
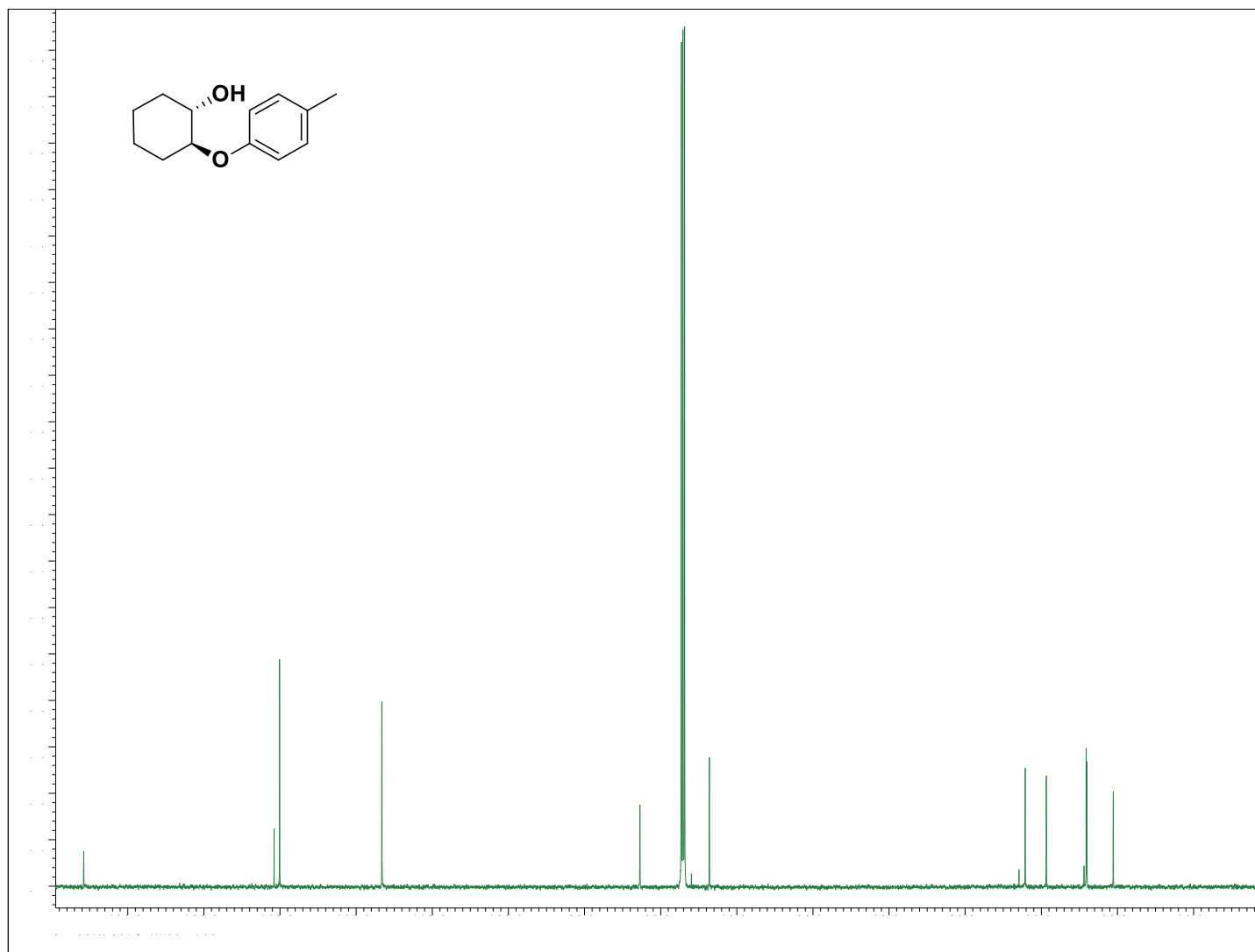
^{13}C NMR of **6** [(±)-*trans*-2-(*p*-tolyloxy)cyclohexanol]
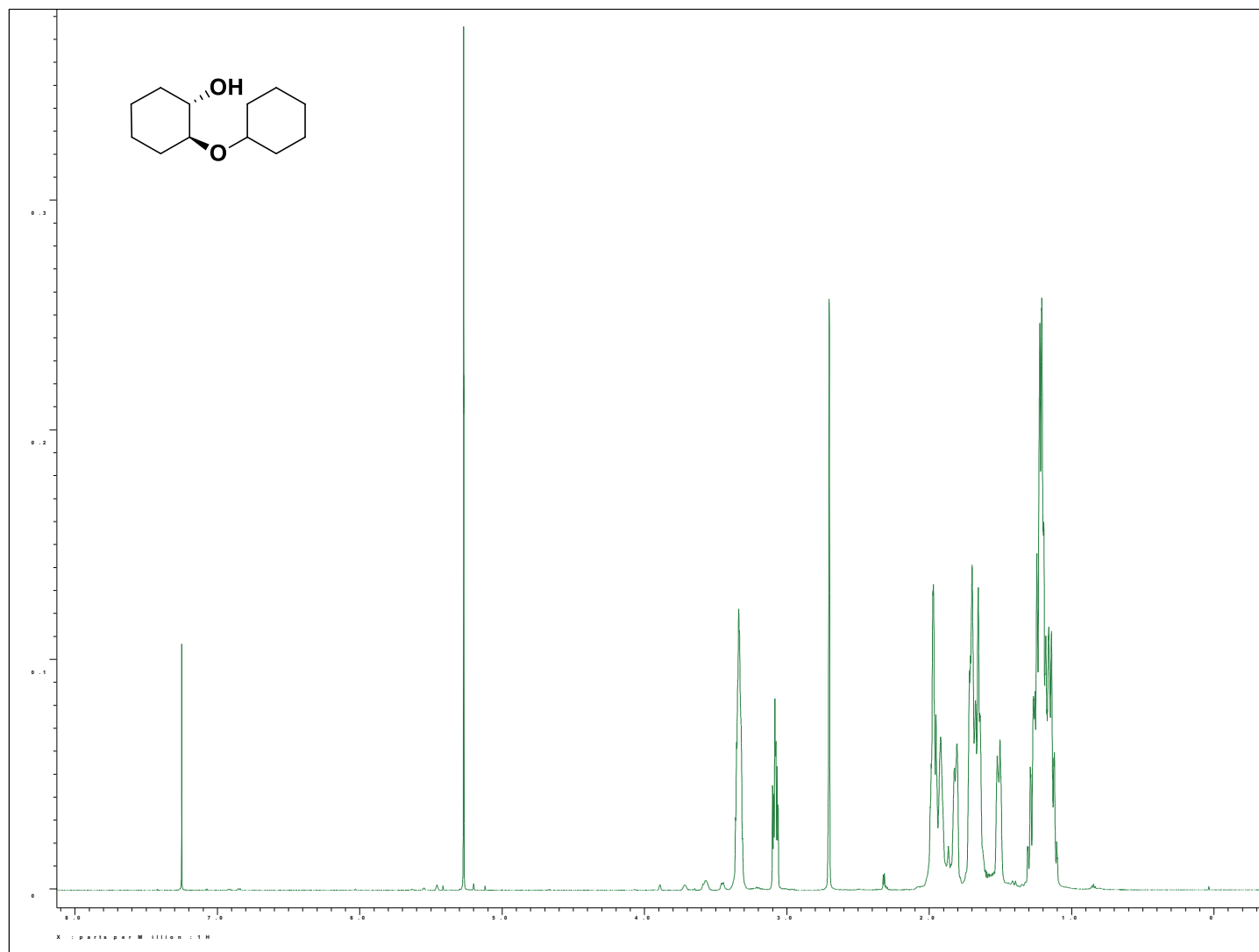
^{1}H NMR of **17** [(±)-*trans*-2-(cyclohexyloxy)cyclohexanol]
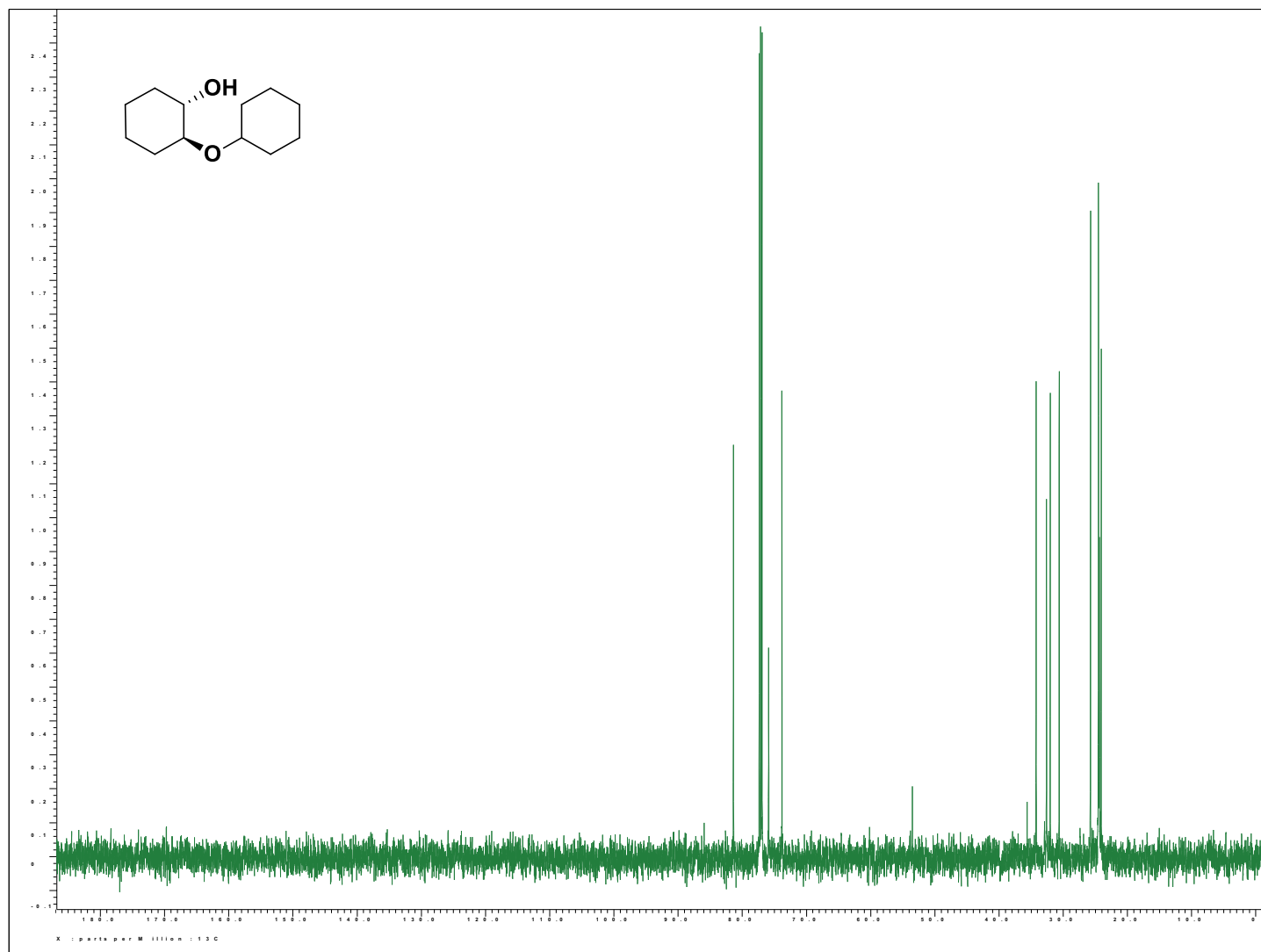
^{13}C NMR of **17** [(±)-*trans*-2-(cyclohexyloxy)cyclohexanol]
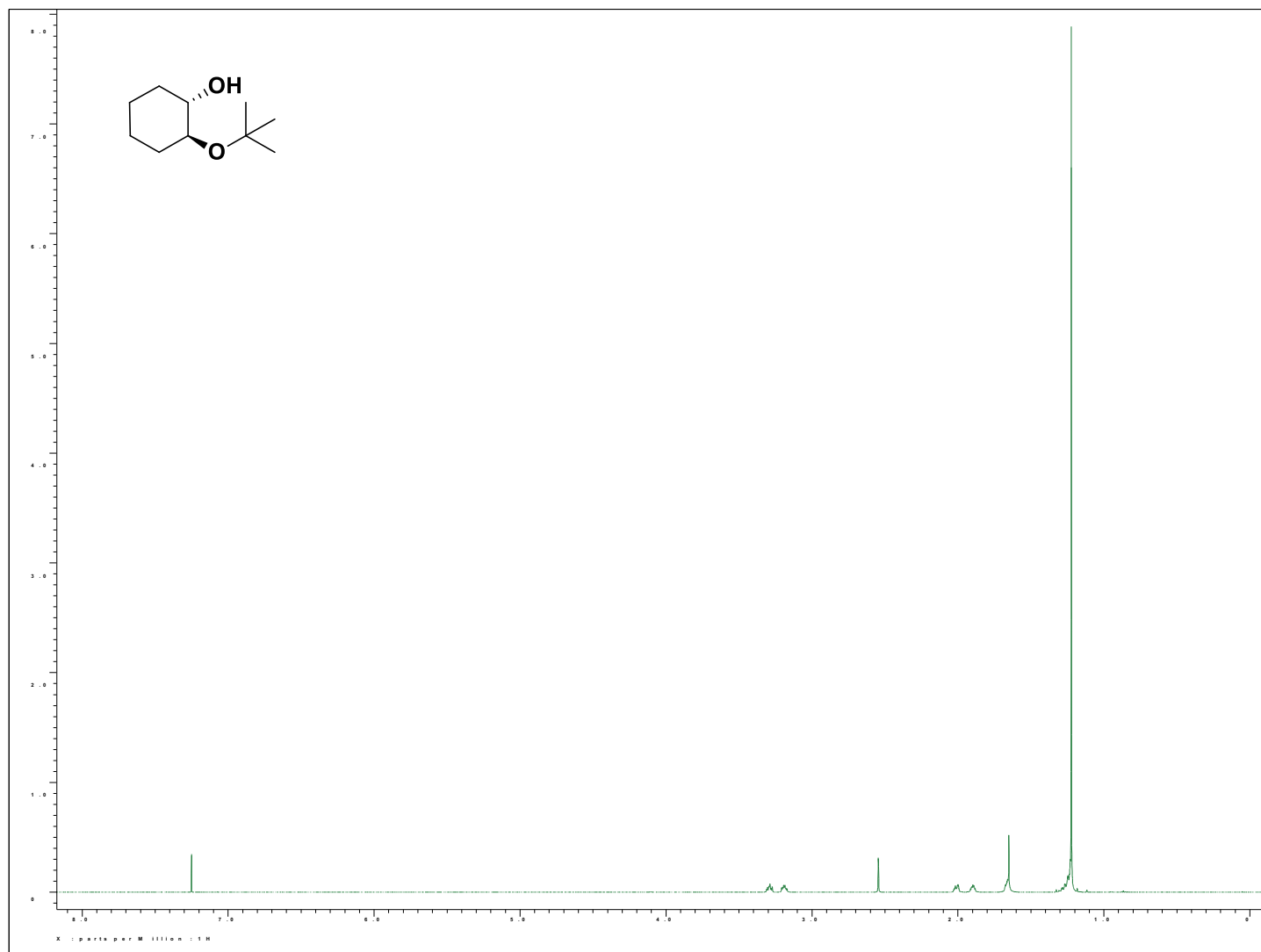
^{1}H NMR of **19** [(±)-*trans*-2-(*t*-butoxy)cyclohexanol]
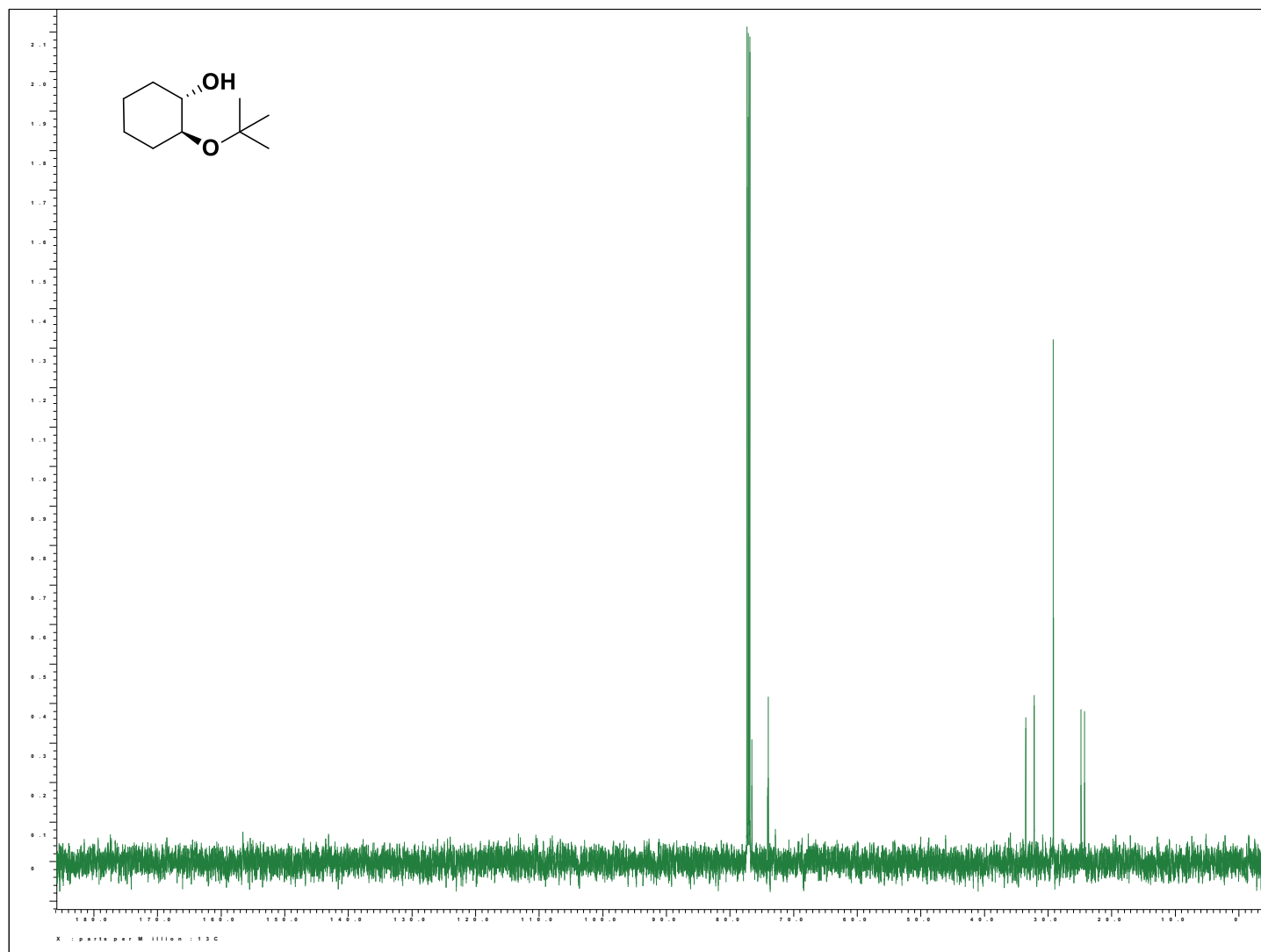
^{13}C NMR of **19** [(±)-*trans*-2-(*t*-butoxy)cyclohexanol]
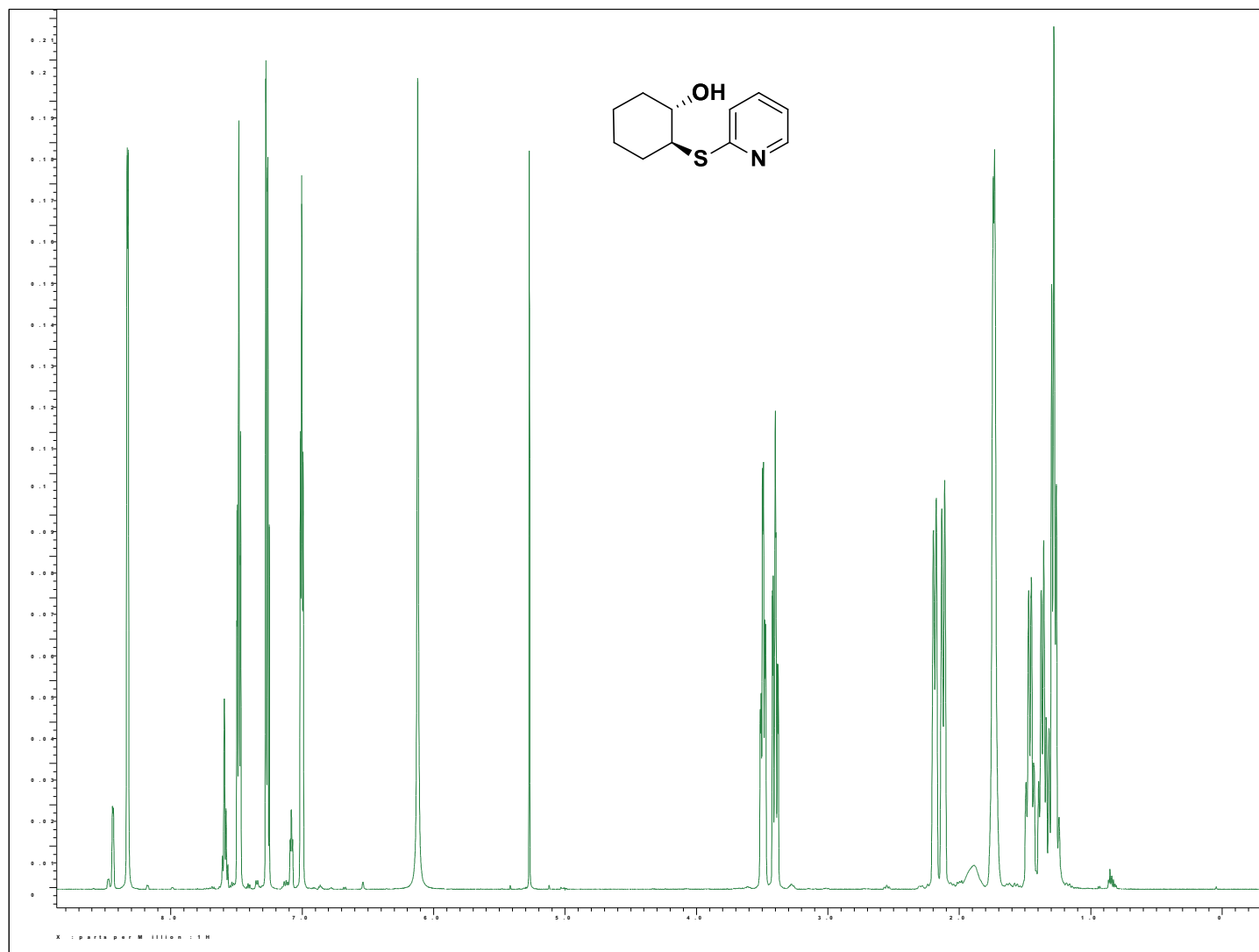
^{1}H NMR of **21** [(±)-*trans*-2-(pyridine-2-ylthio)cyclohexanol]
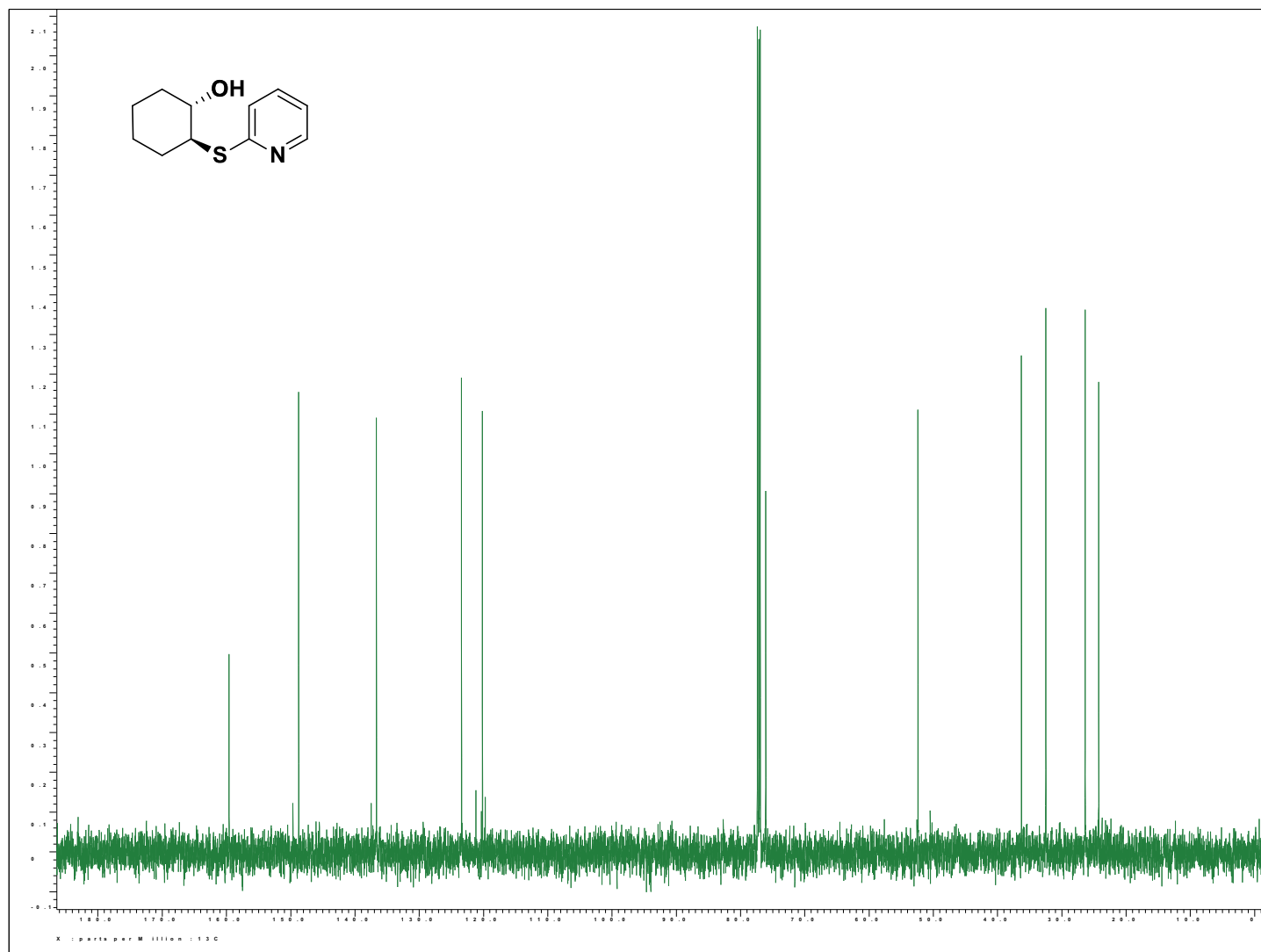
^{13}C NMR of **21** [(±)-*trans*-2-(pyridine-2-ylthio)cyclohexanol]
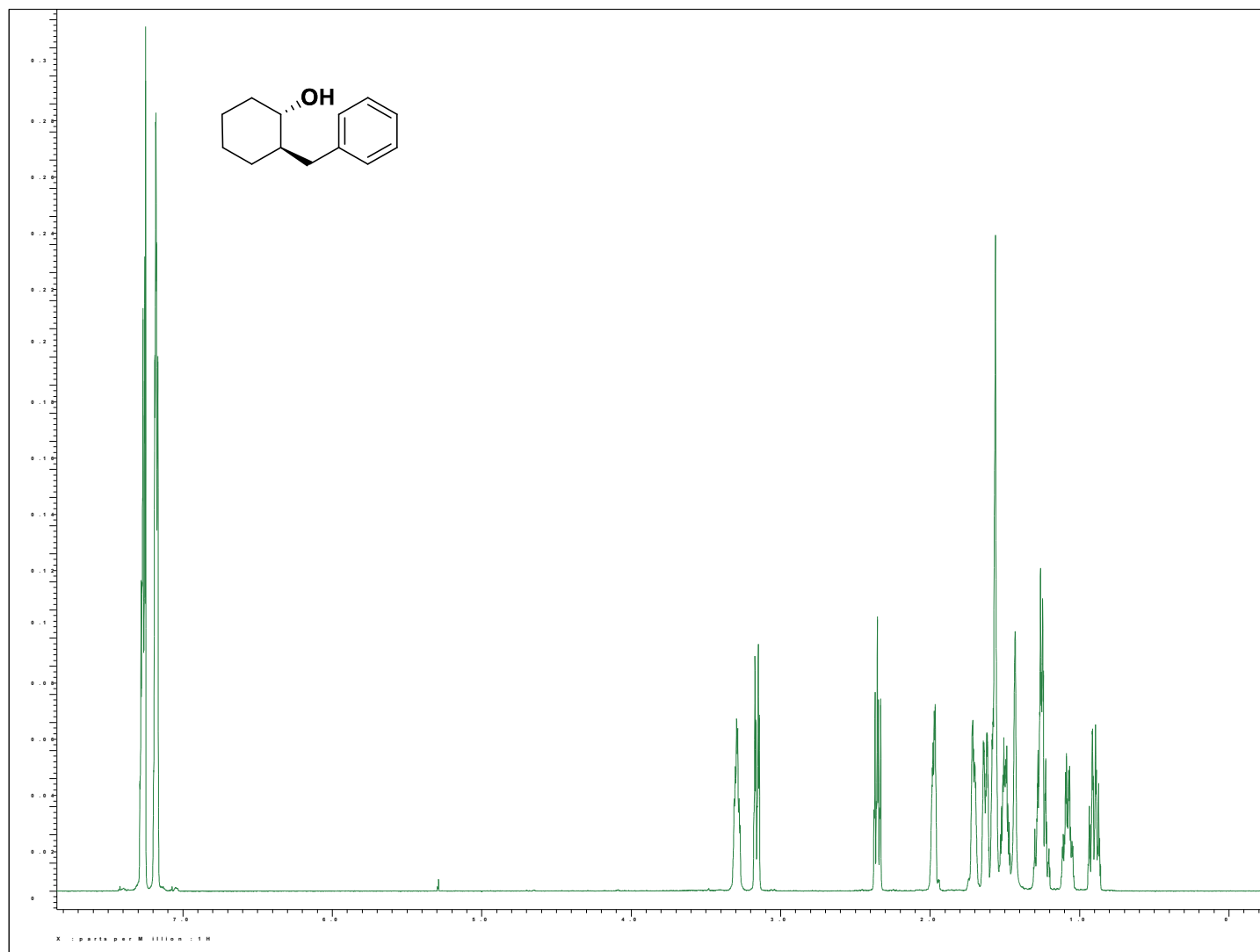
^{1}H NMR of **25** [(±)-*trans*-2-(benzyl)cyclohexanol]
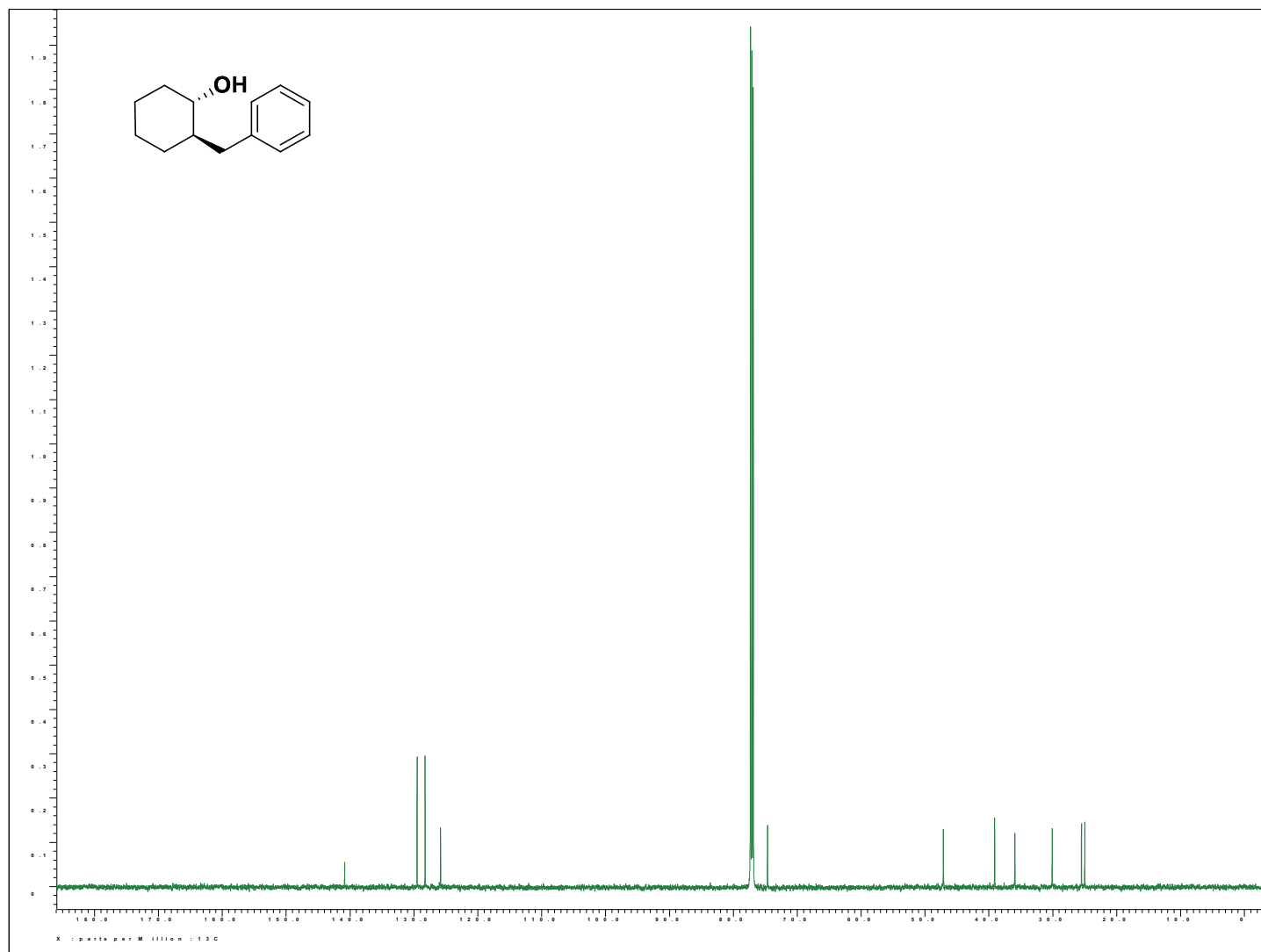
¹³C NMR of **25** [(±)-*trans*-2-(benzyl)cyclohexanol]

¹H NMR of **71** [(±)-(*trans*-2-(*p*-tolylsulfanyl)cyclohexyl) 2-chloropropanoate]
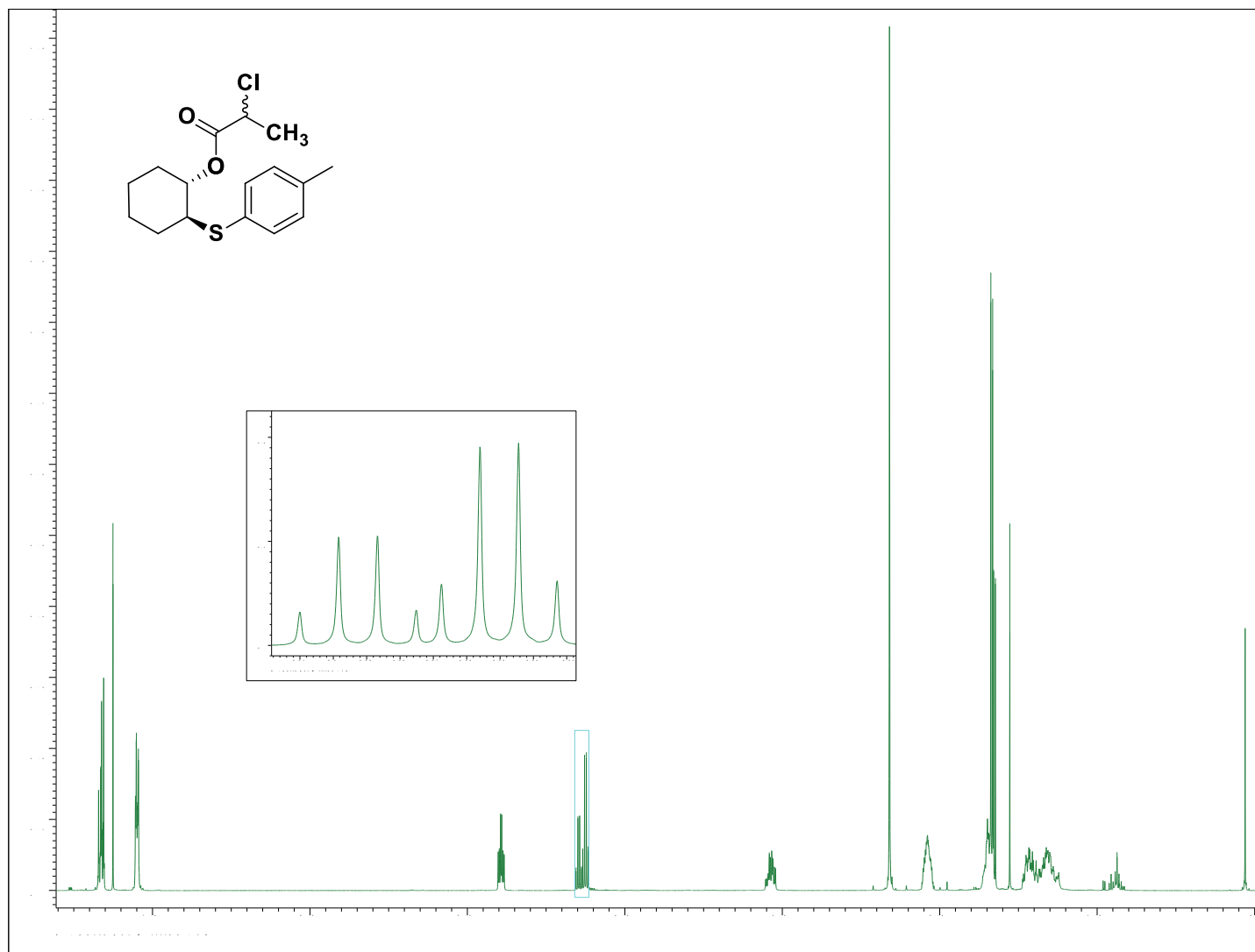
^{13}C NMR of **71** [(±)-(*trans*-2-(*p*-tolylsulfanyl)cyclohexyl) 2-chloropropanoate]

^{1}H NMR of **72** [(±)-(*trans*-2-(*p*-tolyloxy)cyclohexyl) 2-chloropropanoate]
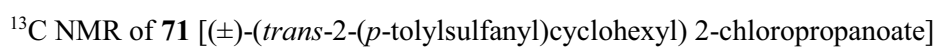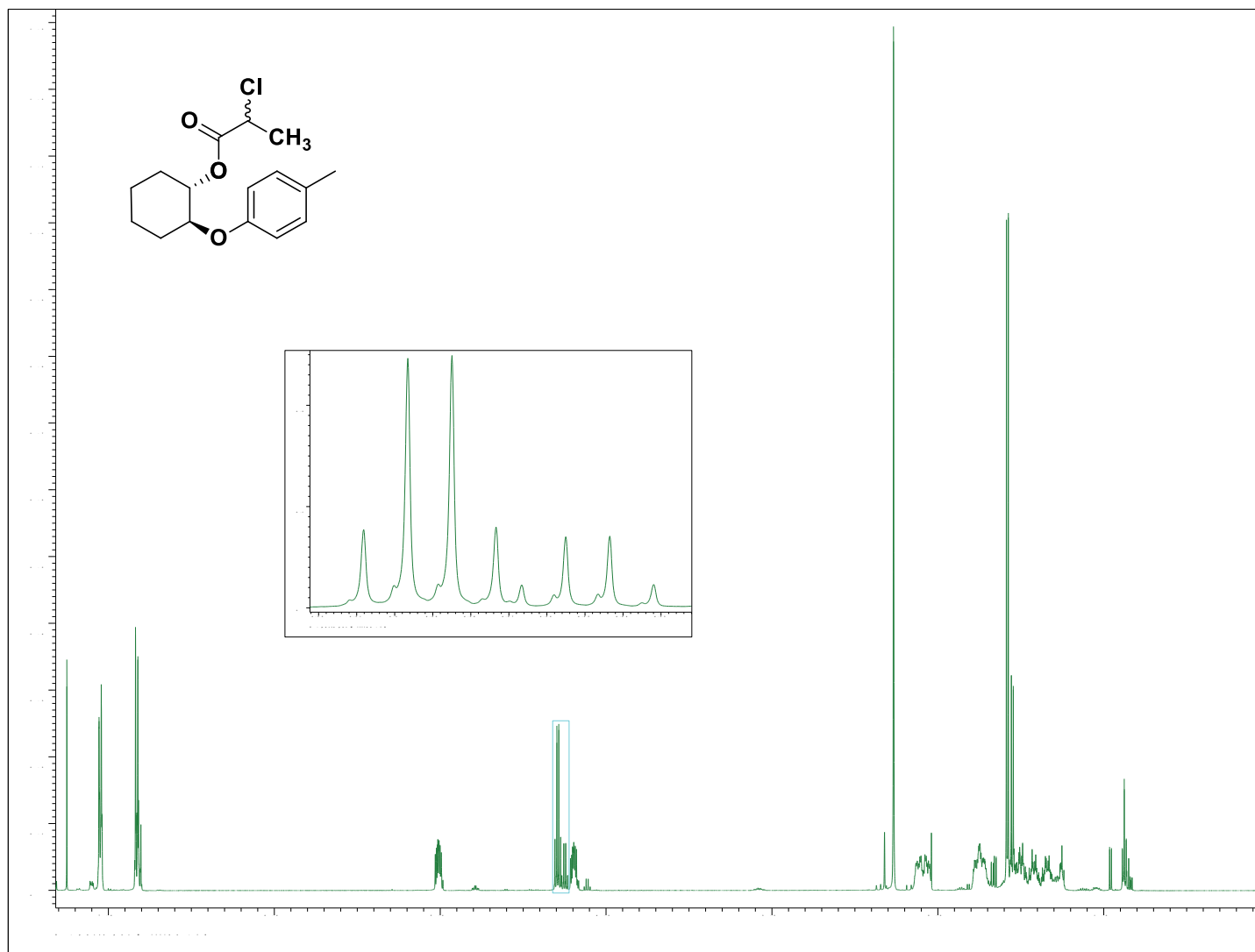
^{13}C NMR of **72** [(±)-(*trans*-2-(*p*-tolyloxy)cyclohexyl) 2-chloropropanoate]
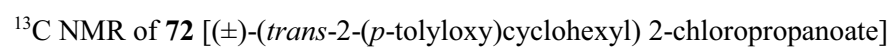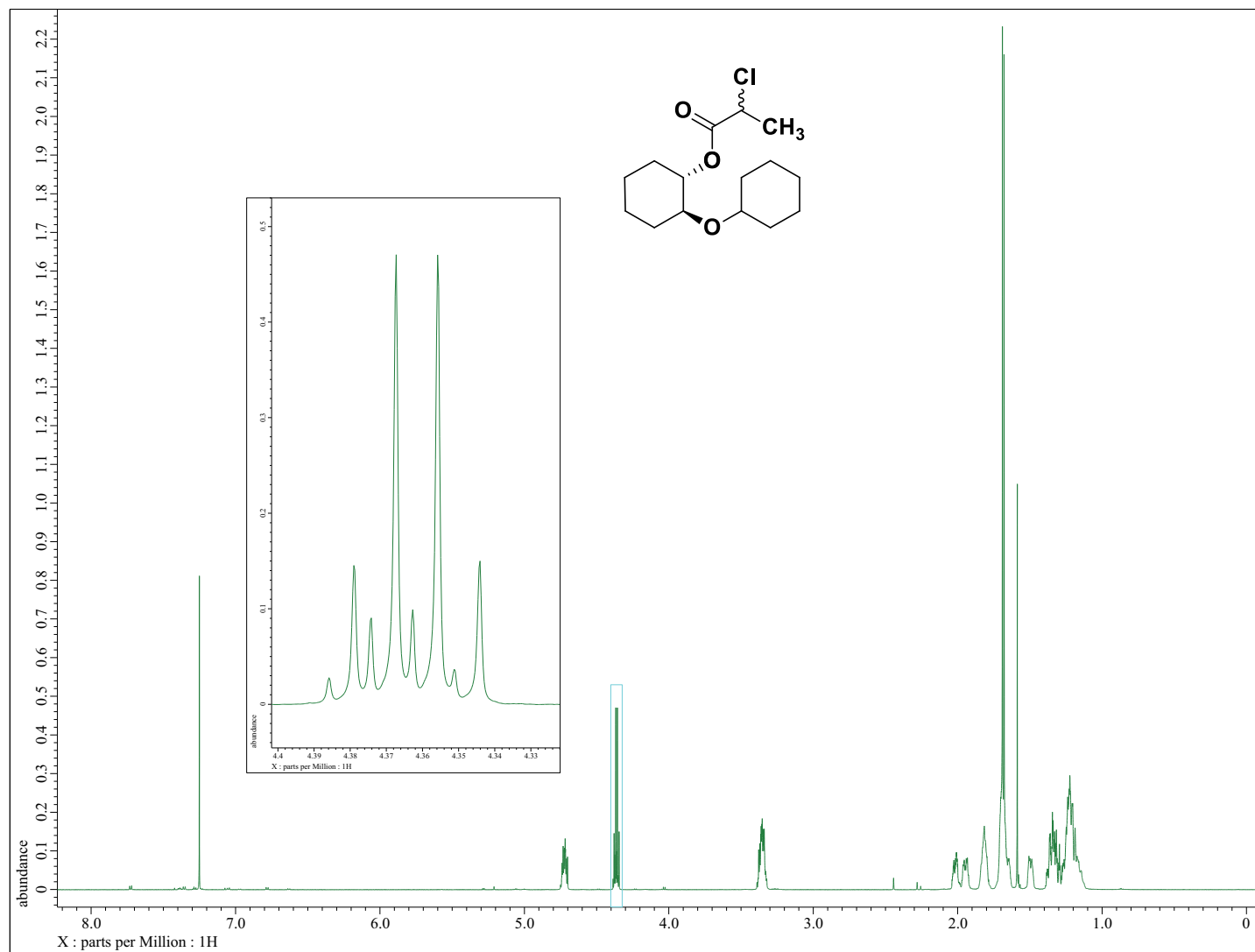
^{1}H NMR of **78** [(±)-(*trans*-2-(cyclohexyloxy)cyclohexyl 2-chloropropanoate]
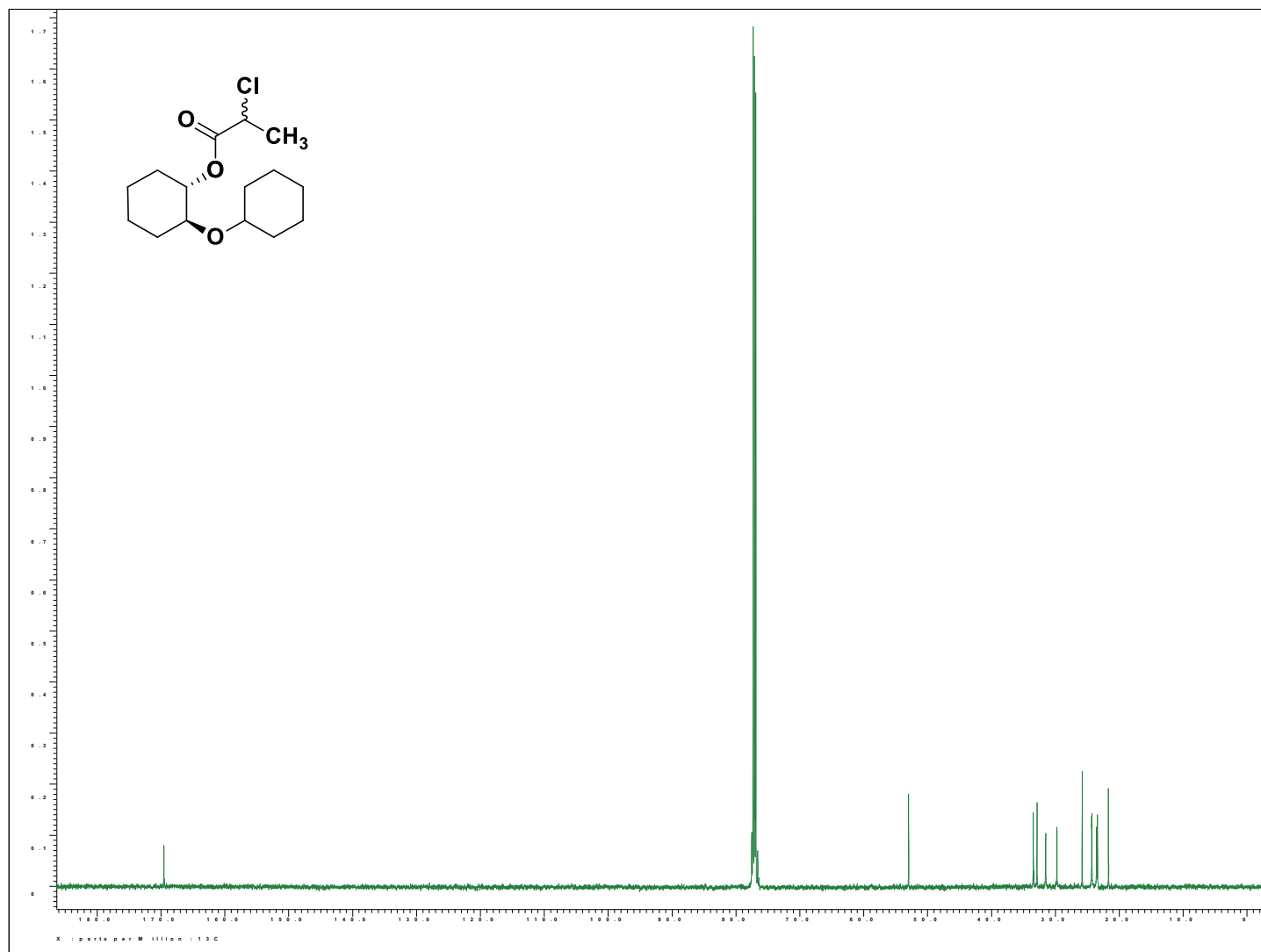
^{13}C NMR of **78** [(±)-(*trans*-2-(cyclohexyloxy)cyclohexyl 2-chloropropanoate]
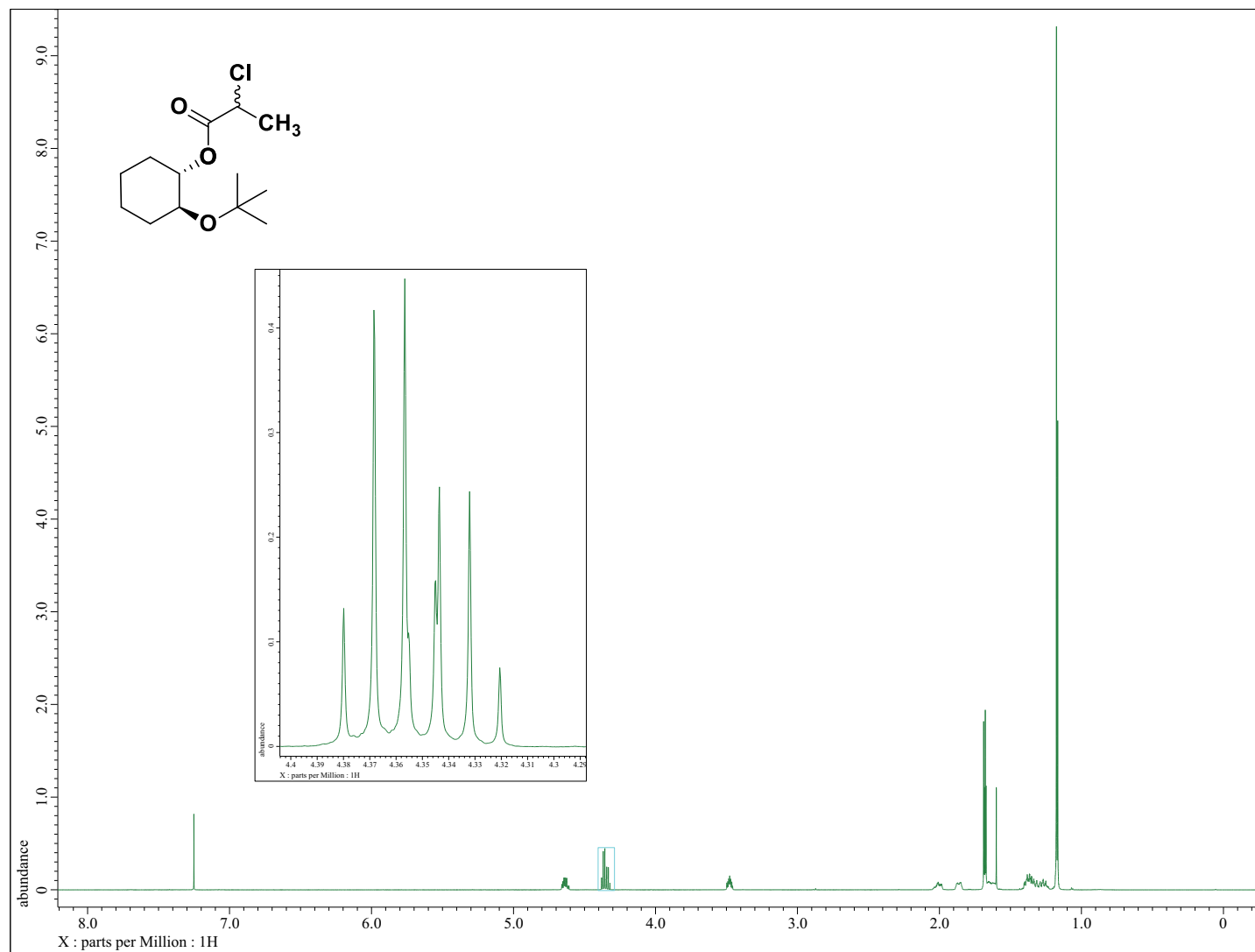
^{1}H NMR of **79** [(±)-(*trans*-2-(*tert*-butoxy)cyclohexyl 2-chloropropanoate]
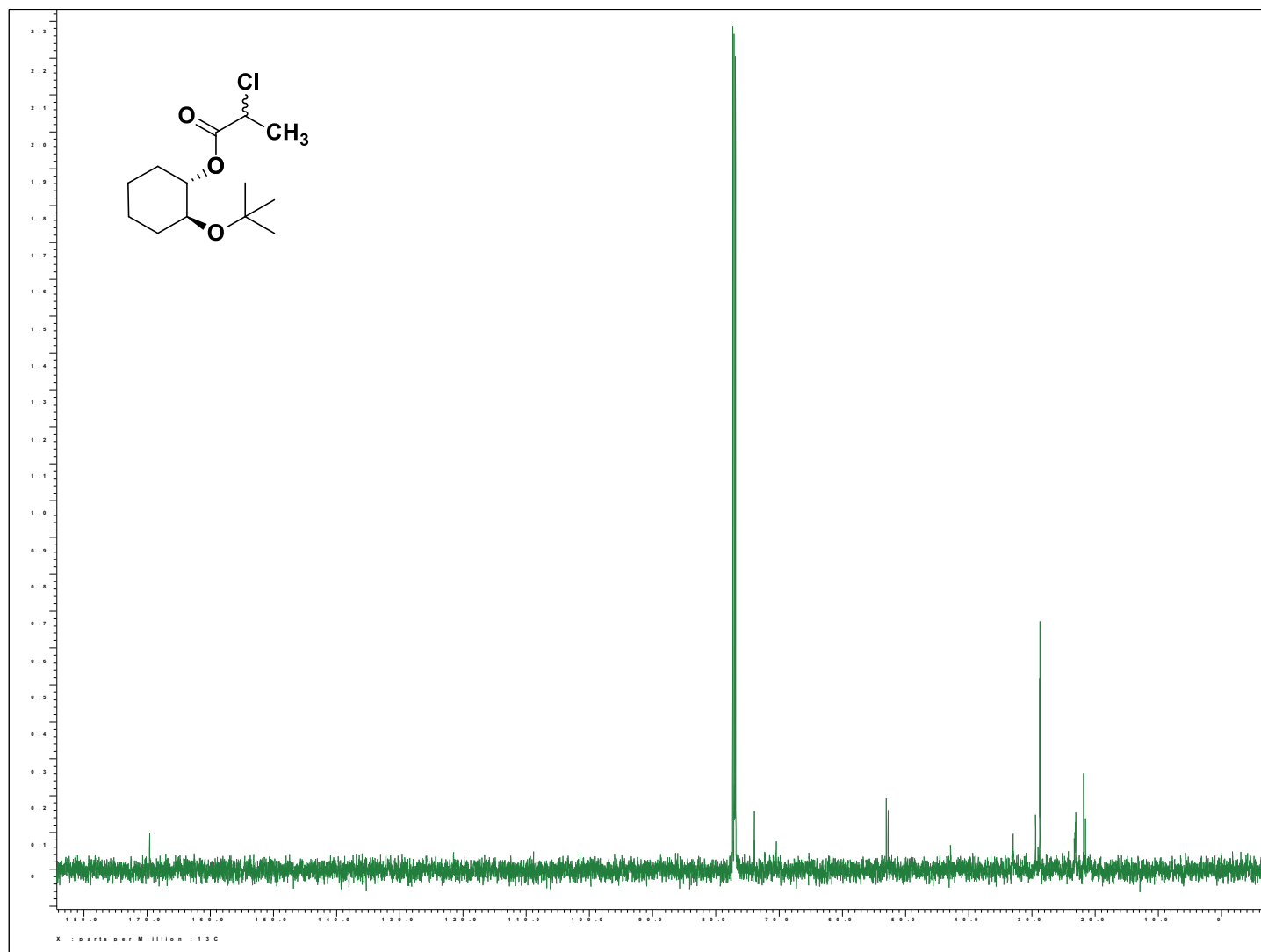
^{13}C NMR of **79** [(±)-(*trans*-2-(*tert*-butoxy)cyclohexyl 2-chloropropanoate]
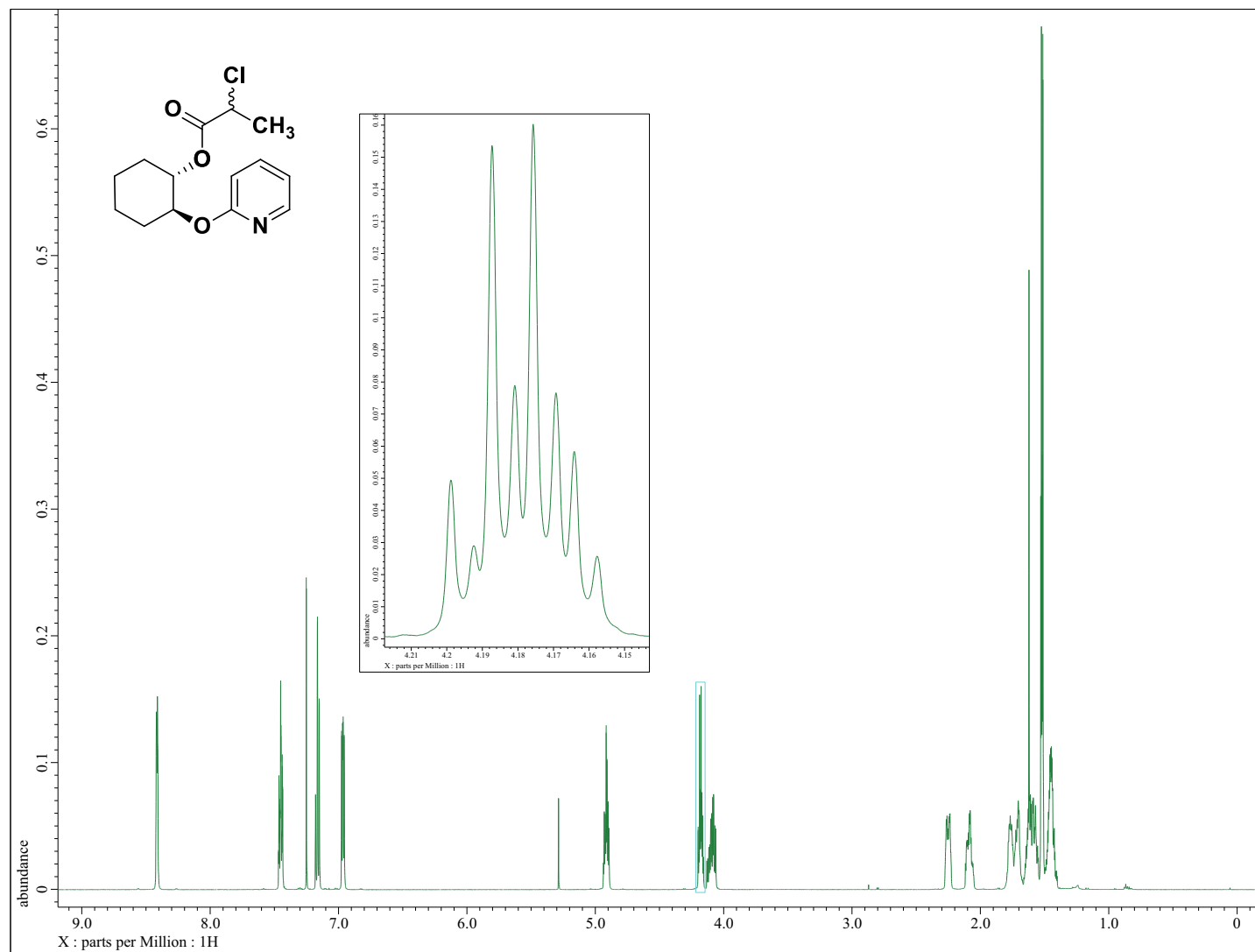
^{1}H NMR of **80** [(±)-*trans*-2-(pyridin-2-ylthio)cyclohexyl 2-chloropropanoate]
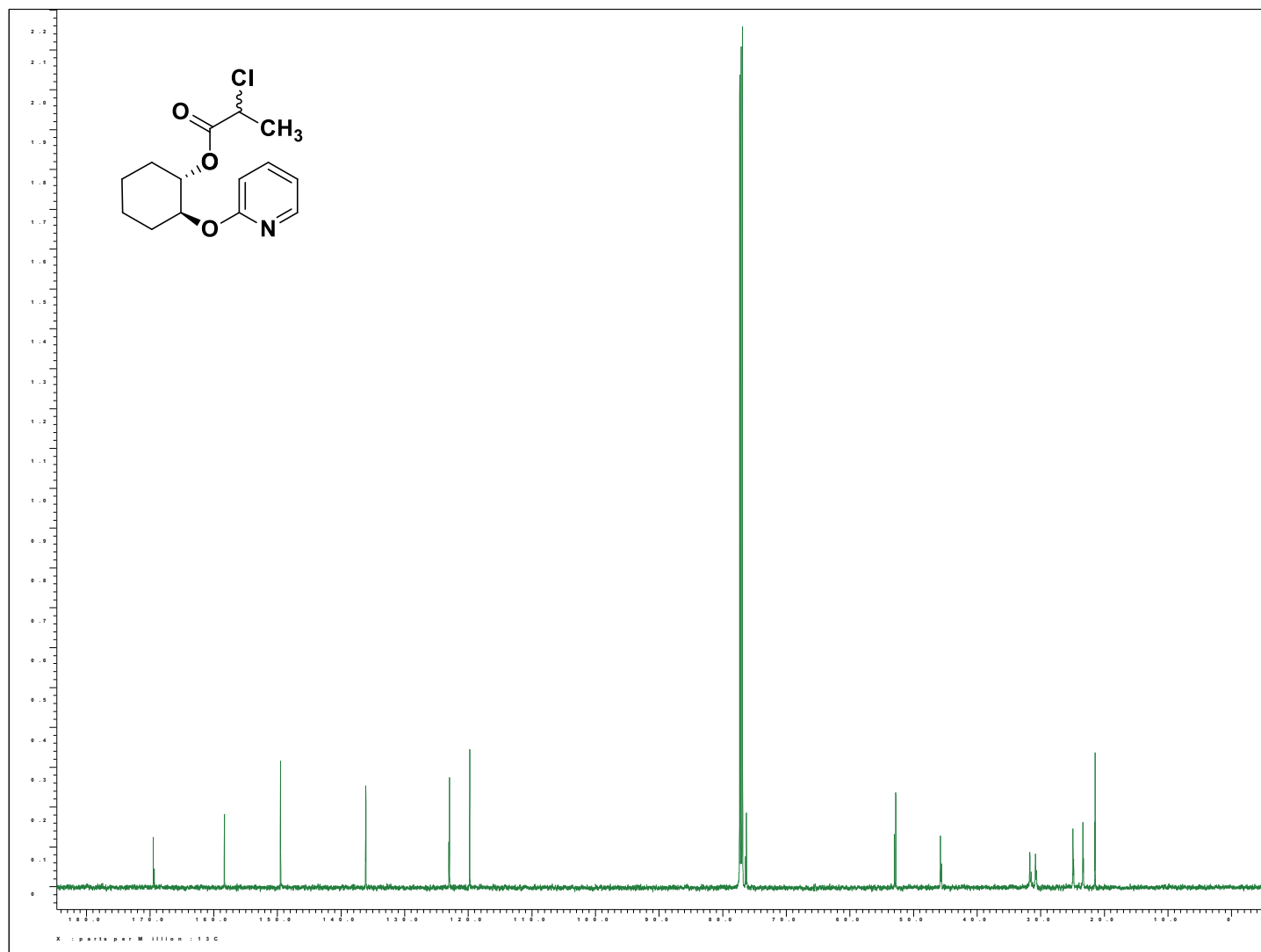
^{13}C NMR of **80** [(±)-*trans*-2-(pyridin-2-ylthio)cyclohexyl 2-chloropropanoate]
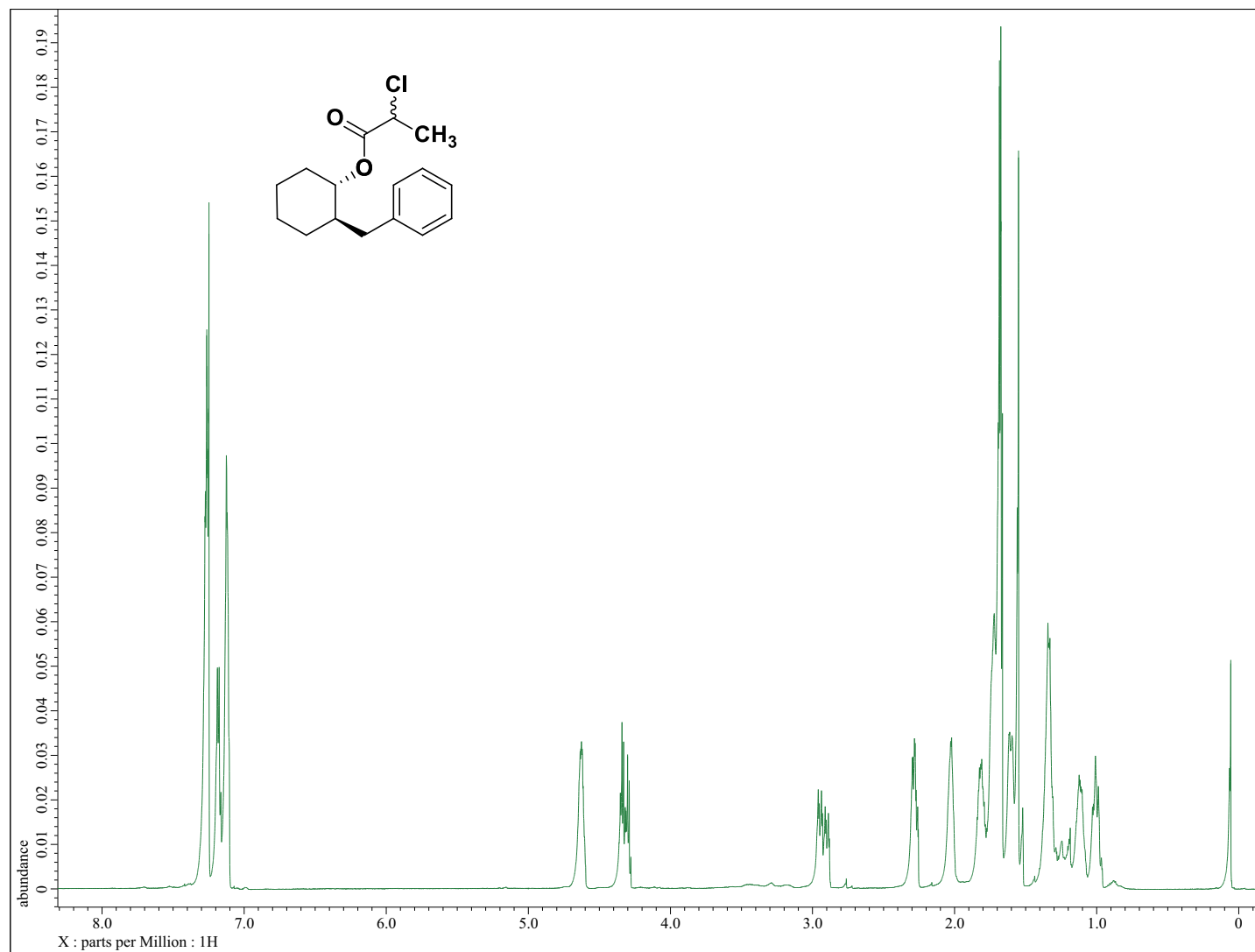
^{1}H NMR of **82** [(±)-(*trans*-2-benzylcyclohexyl) 2-chloropropanoate]
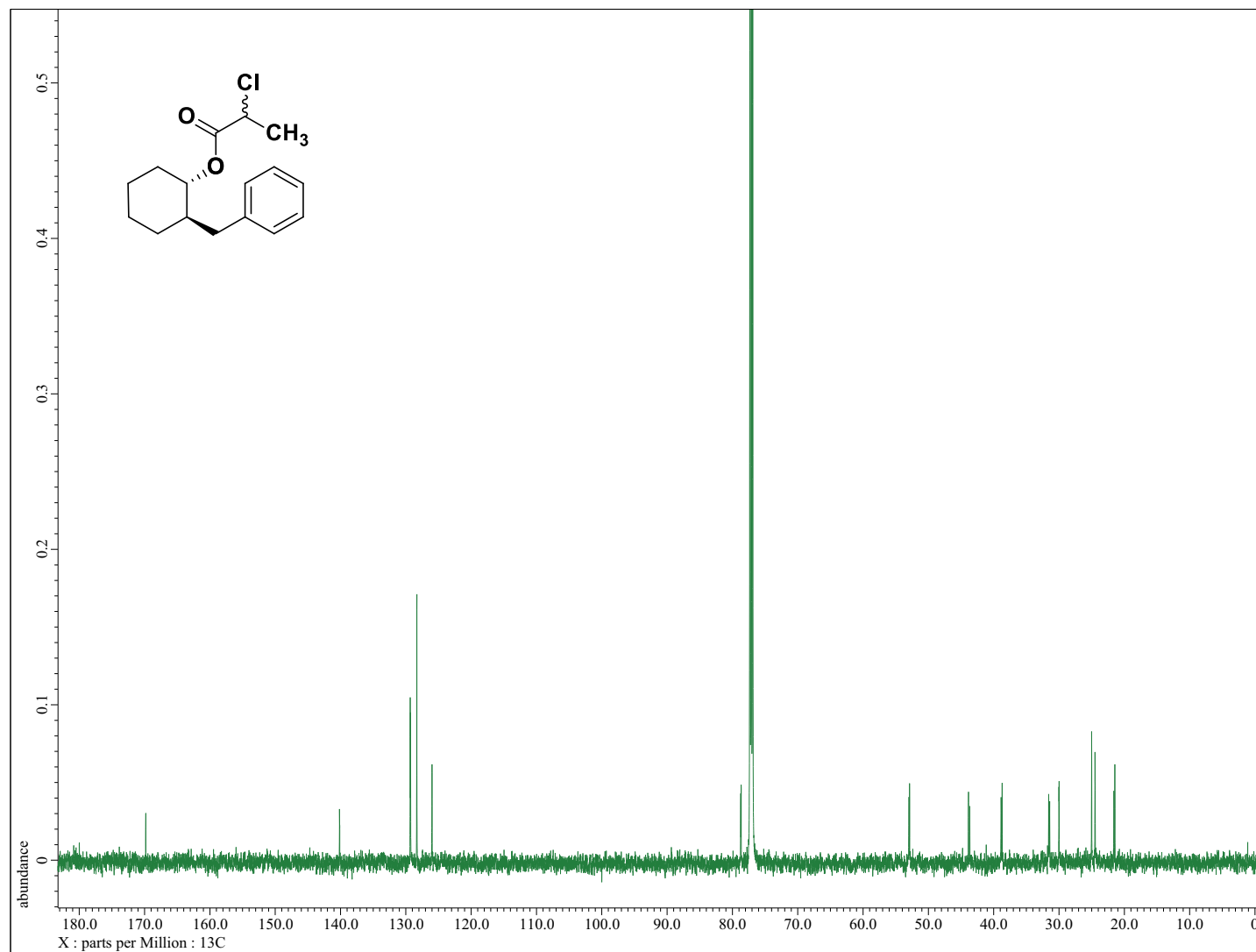
^{13}C NMR of **82** [(±)-(*trans*-2-benzylcyclohexyl) 2-chloropropanoate]
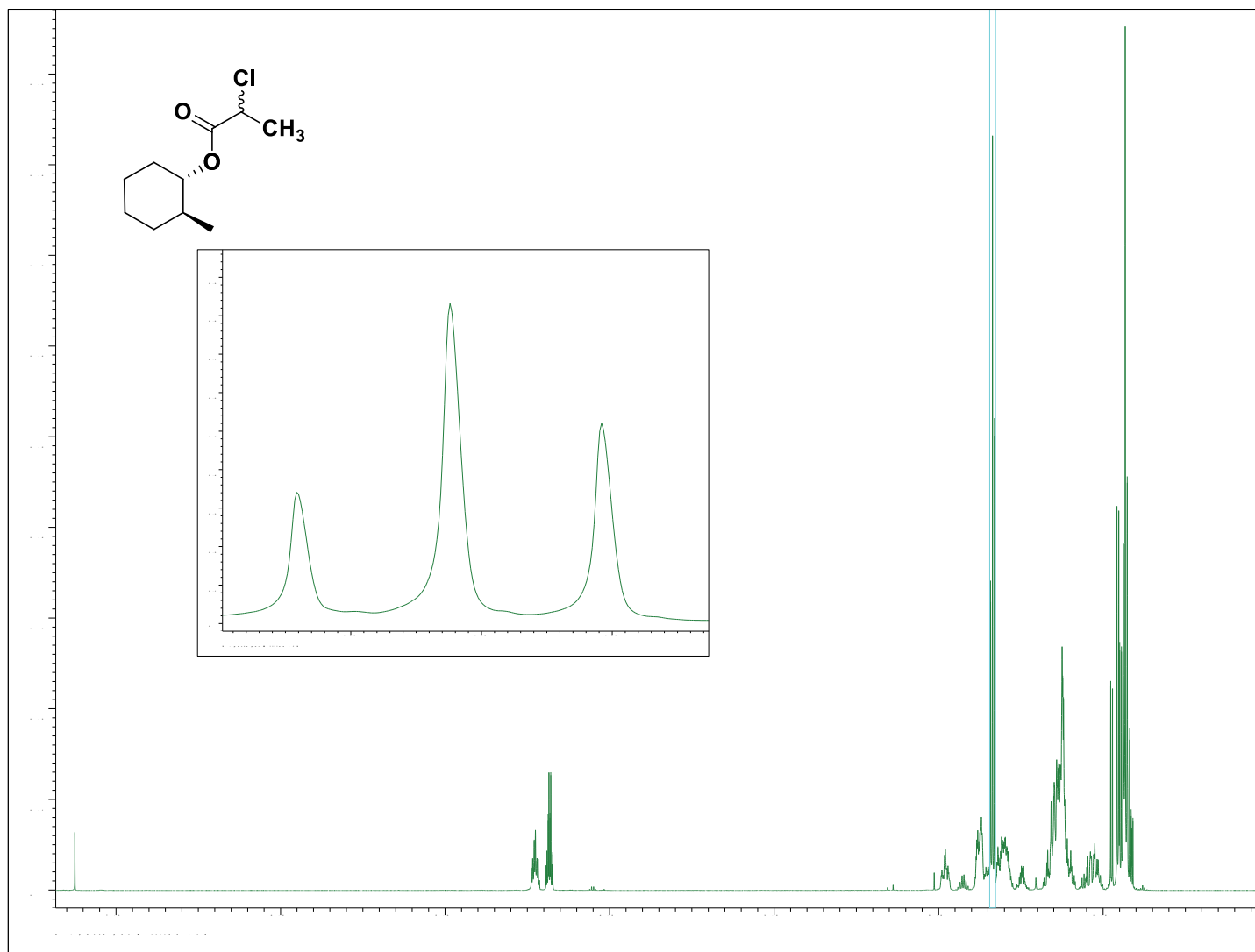
^{1}H NMR of **83** [(±)-(*trans*-2-methylcyclohexyl) 2-chloropropanoate]
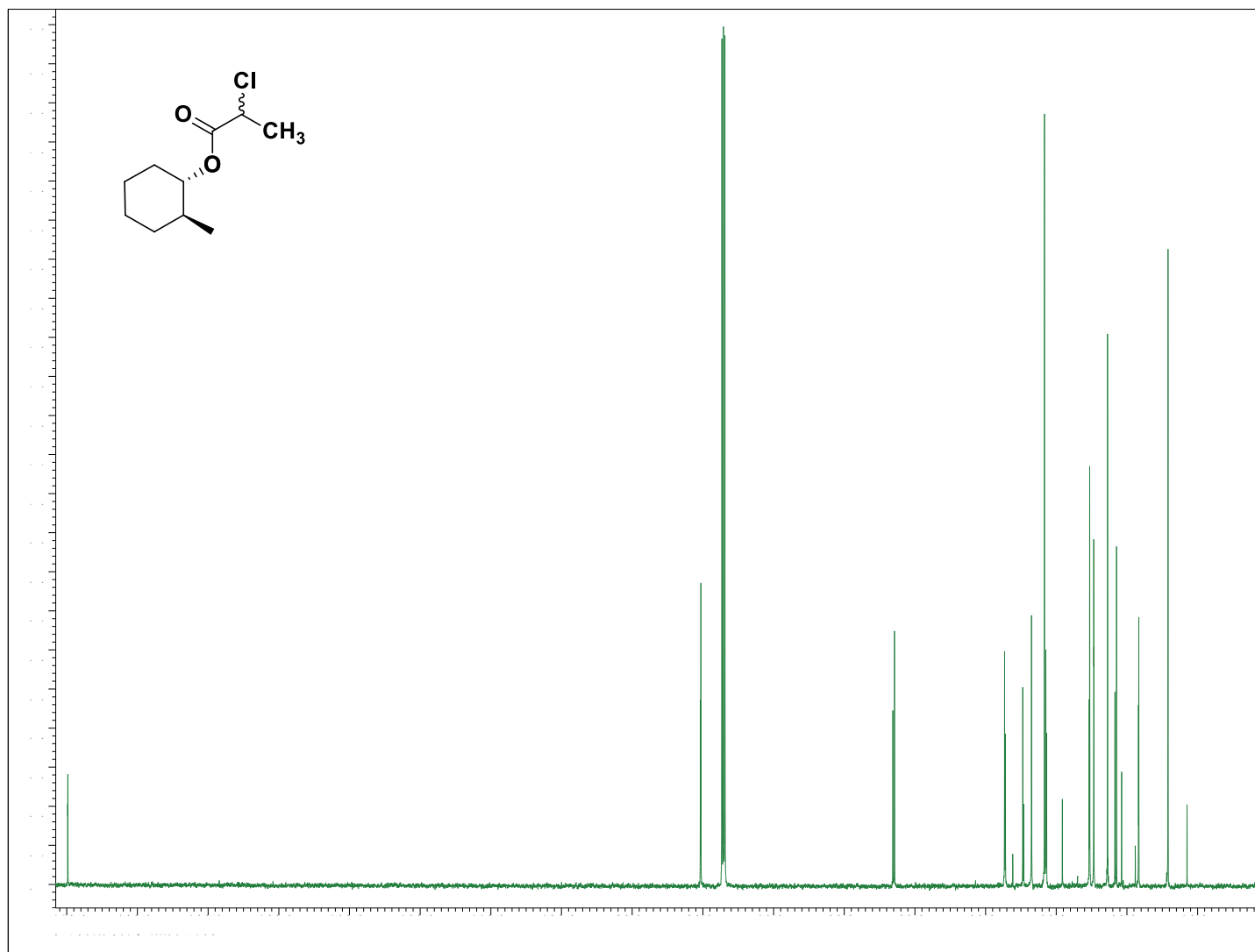
^{13}C NMR of **83** [(±)-(*trans*-2-methylcyclohexyl) 2-chloropropanoate]
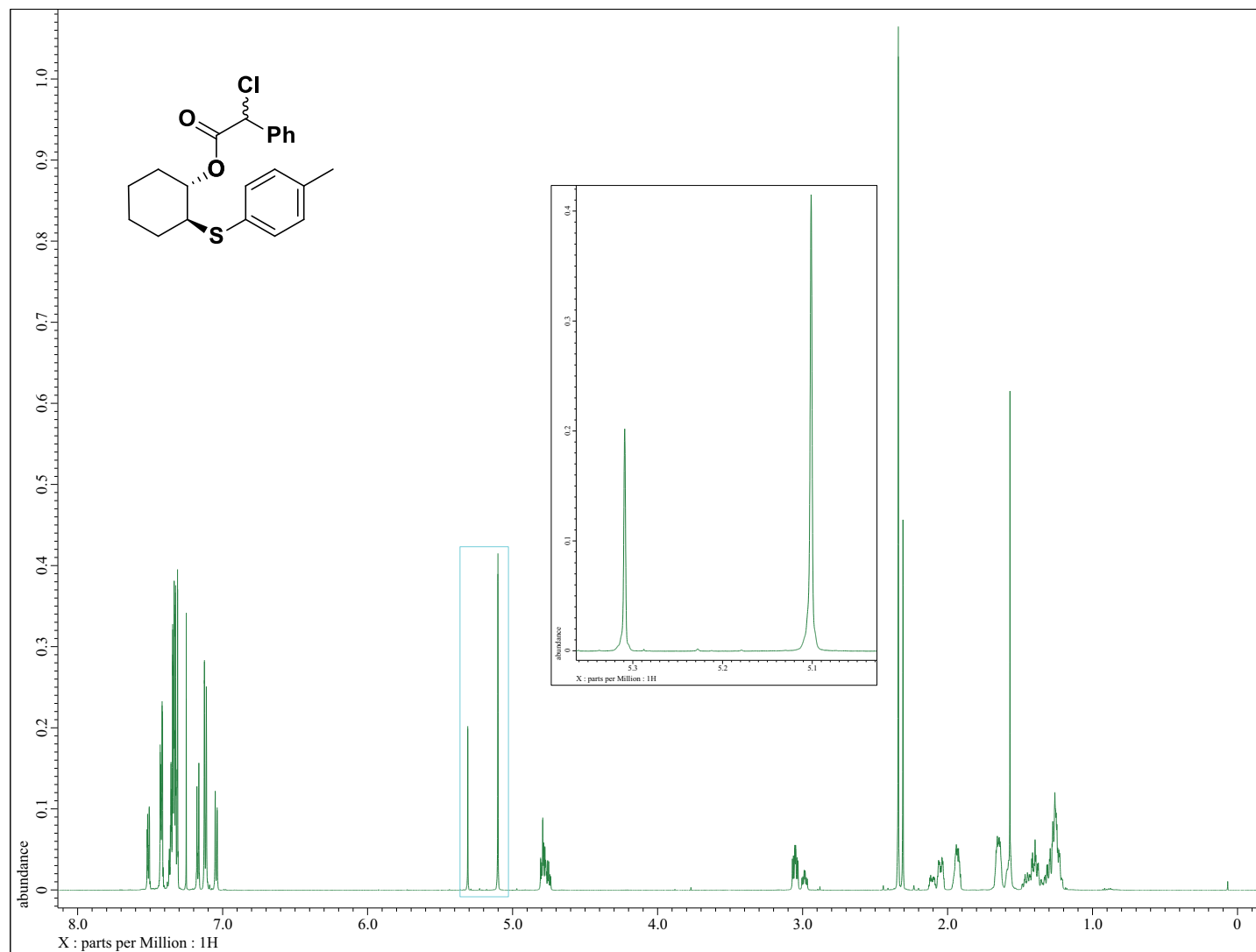
^{1}H NMR of **84** [(±)-(*trans*-2-(*p*-tolylsulfanyl)cyclohexyl 2-chloro-2-phenylethanoate]
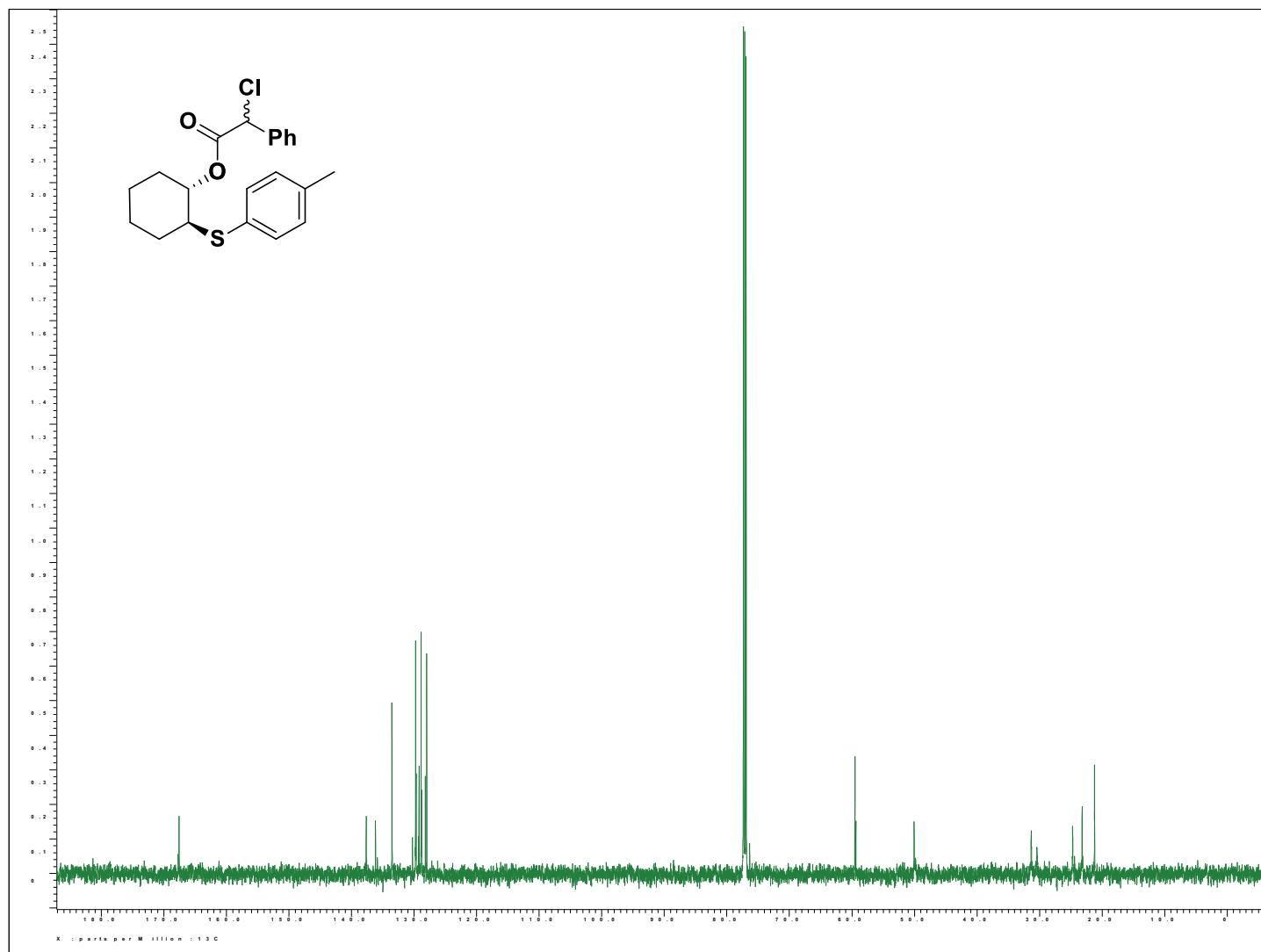
^{13}C NMR of **84** [(±)-(*trans*-2-(*p*-tolylsulfanyl)cyclohexyl 2-chloro-2-phenylethanoate]
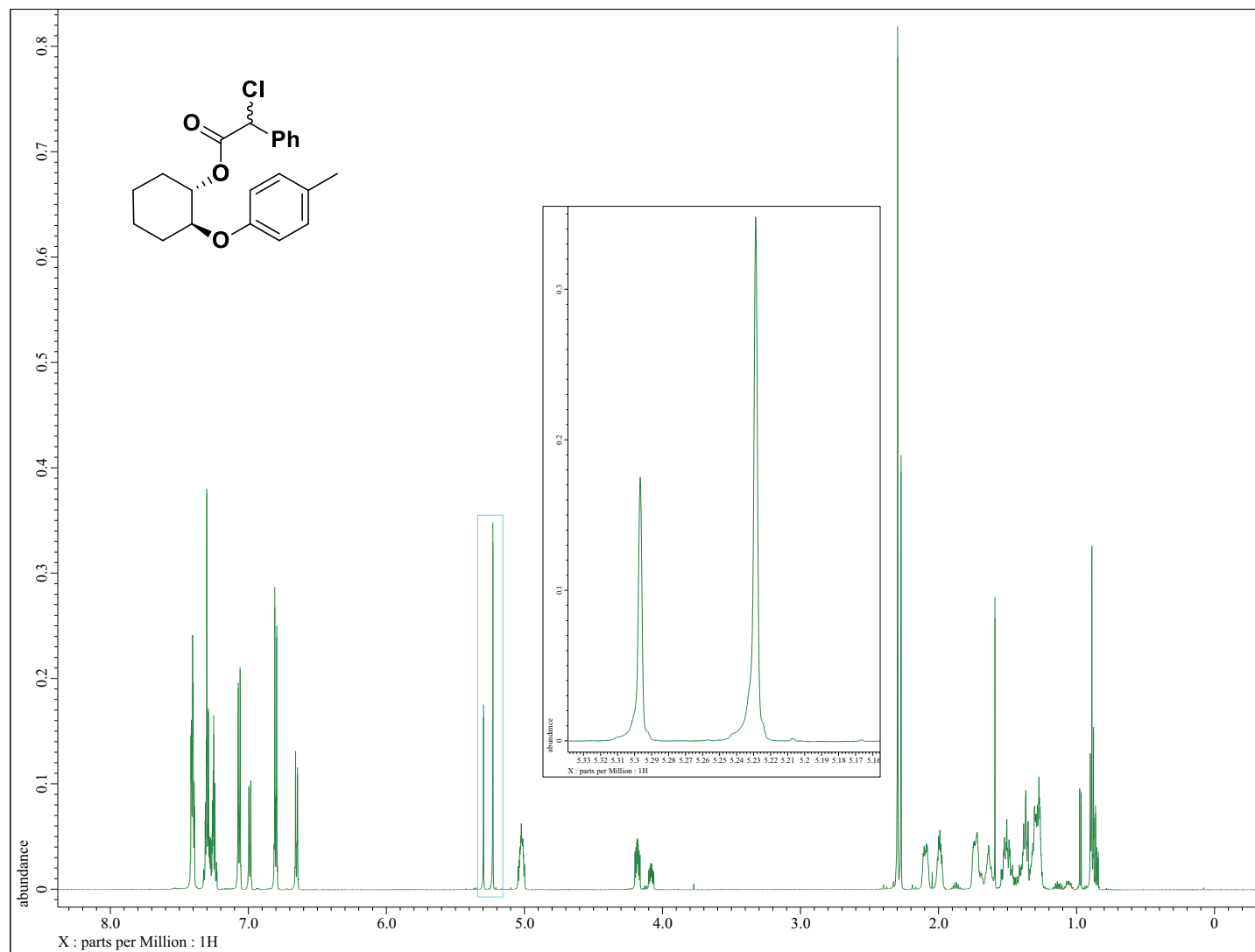
^{1}H NMR of **85** [(±)-(*trans*-2-(*p*-tolyloxy)cyclohexyl 2-chloro-2-phenylethanoate]
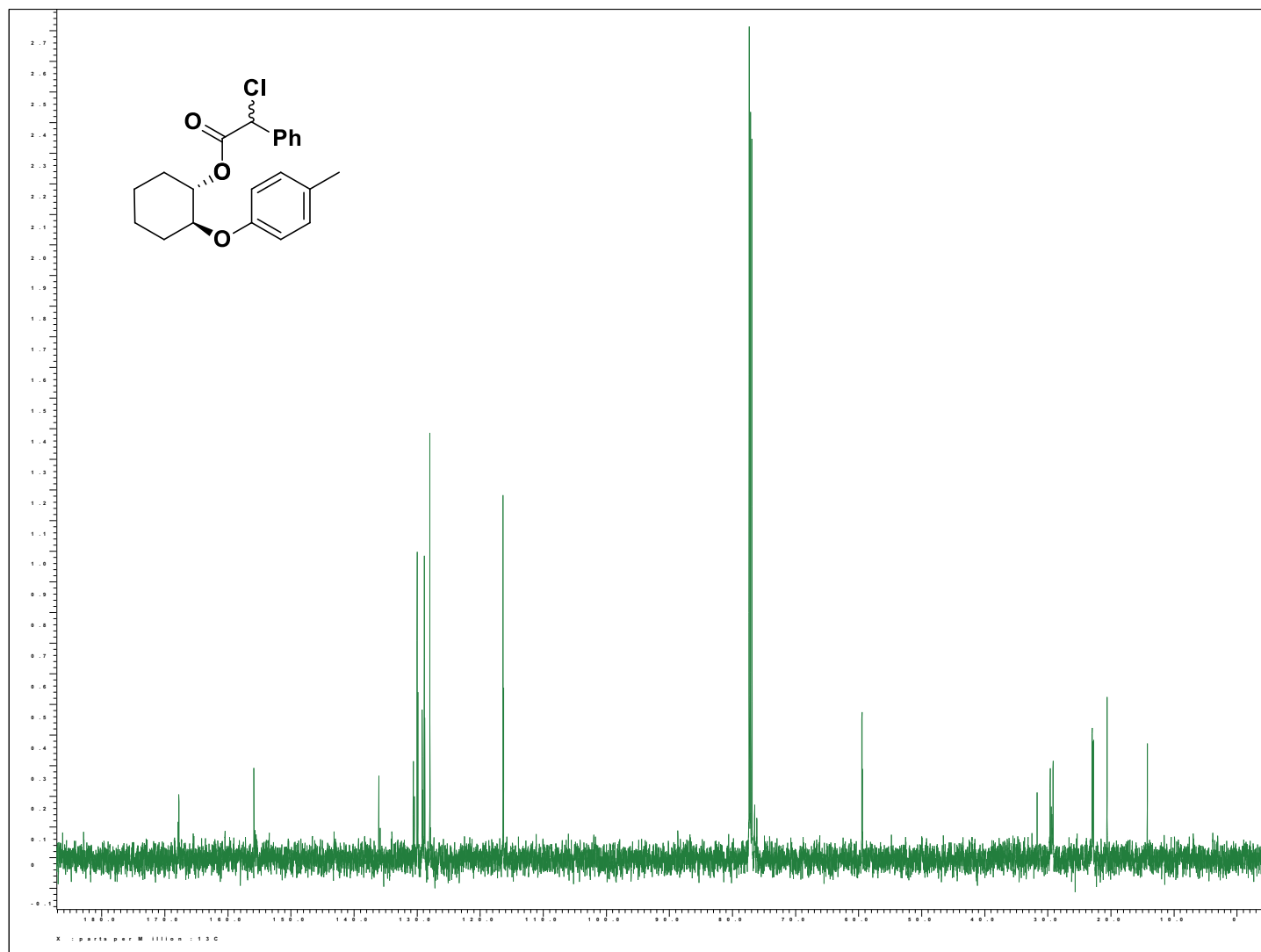
^{13}C NMR of **85** [(±)-(*trans*-2-(*p*-tolyloxy)cyclohexyl 2-chloro-2-phenylethanoate]
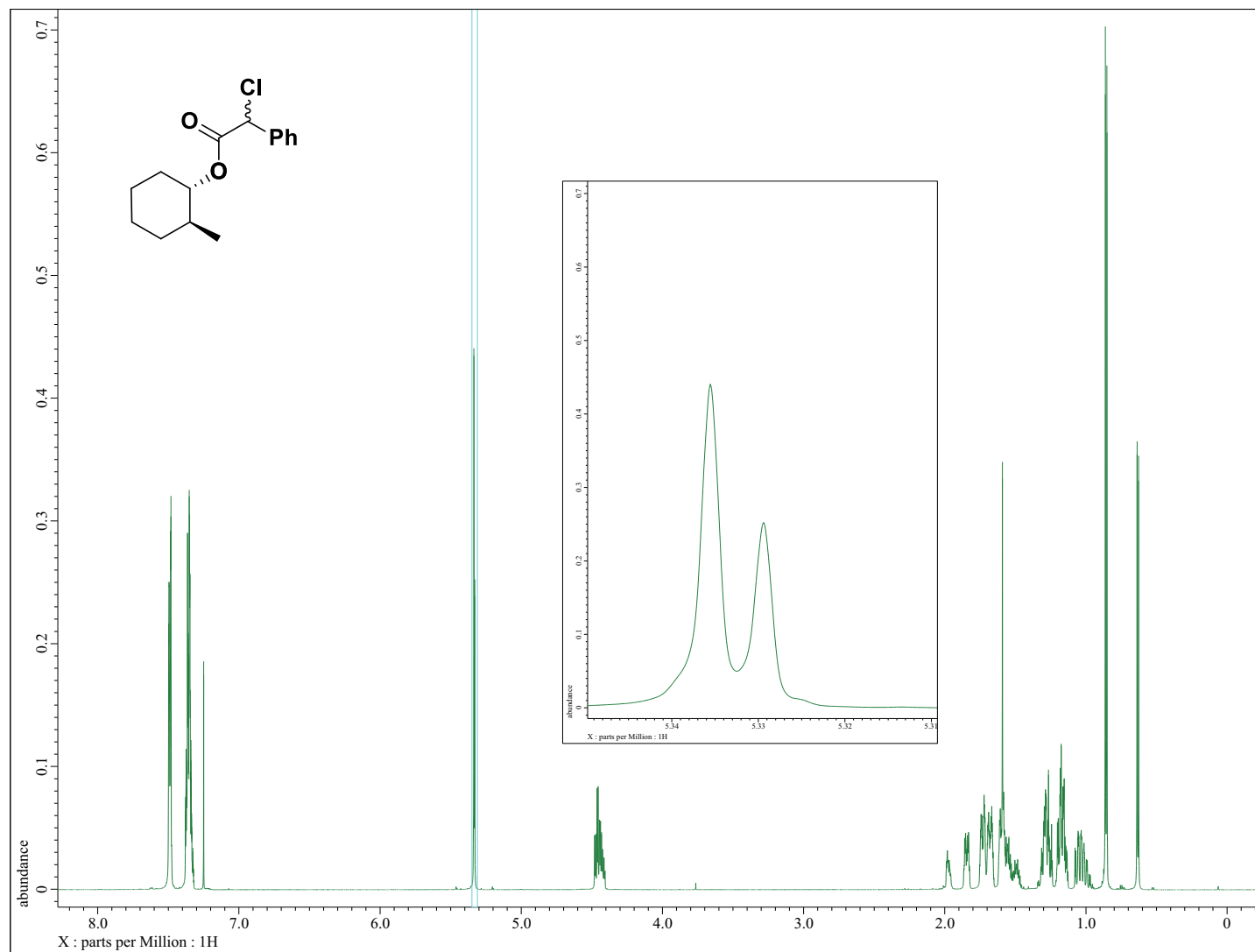
^{1}H NMR of **89** [(±)-*trans*-2-(methyl)cyclohexyl 2-chloro-2-phenylethanoate]
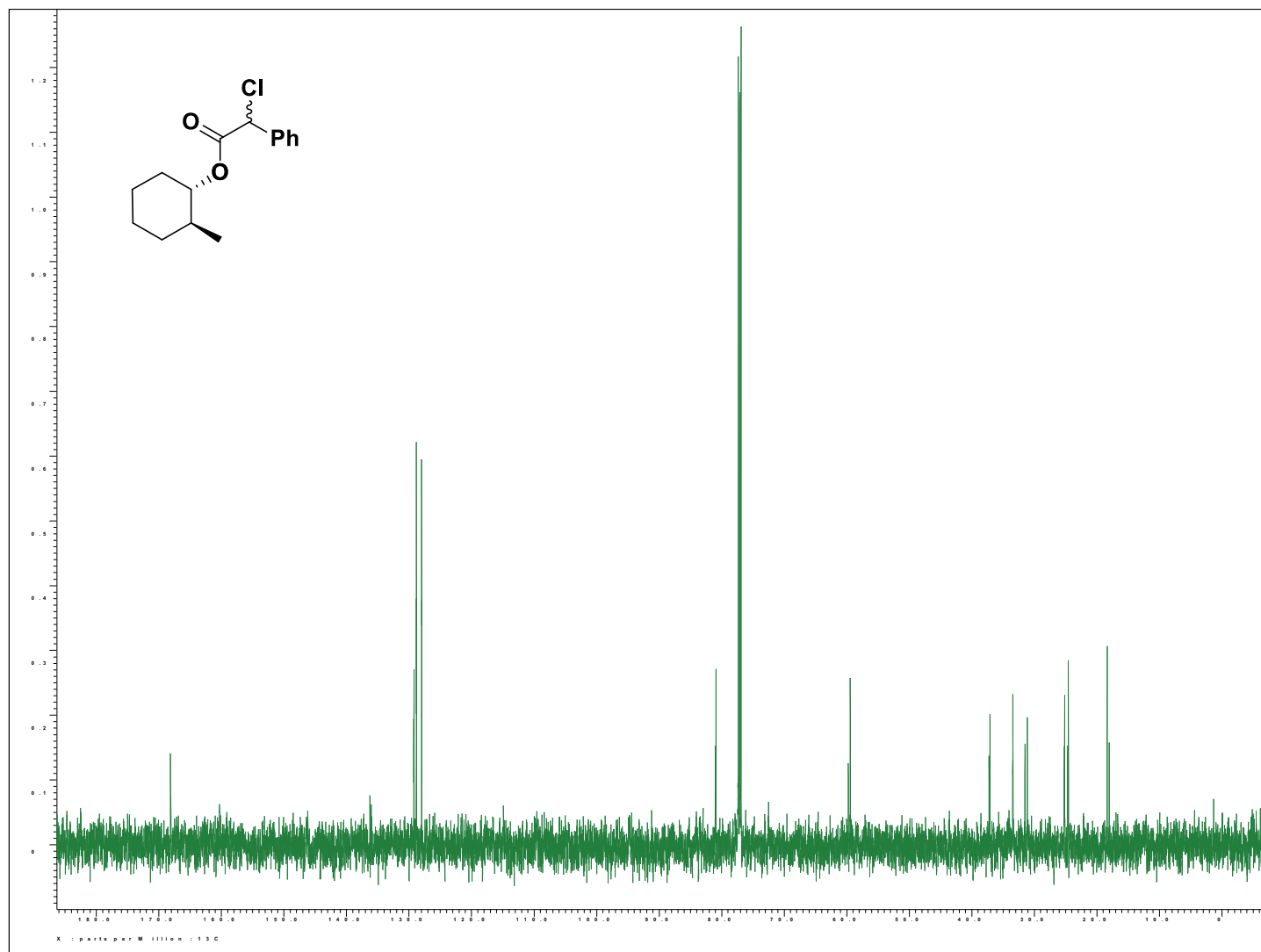
^{13}C NMR of **89** [(±)-*trans*-2-(methyl)cyclohexyl 2-chloro-2-phenylethanoate]
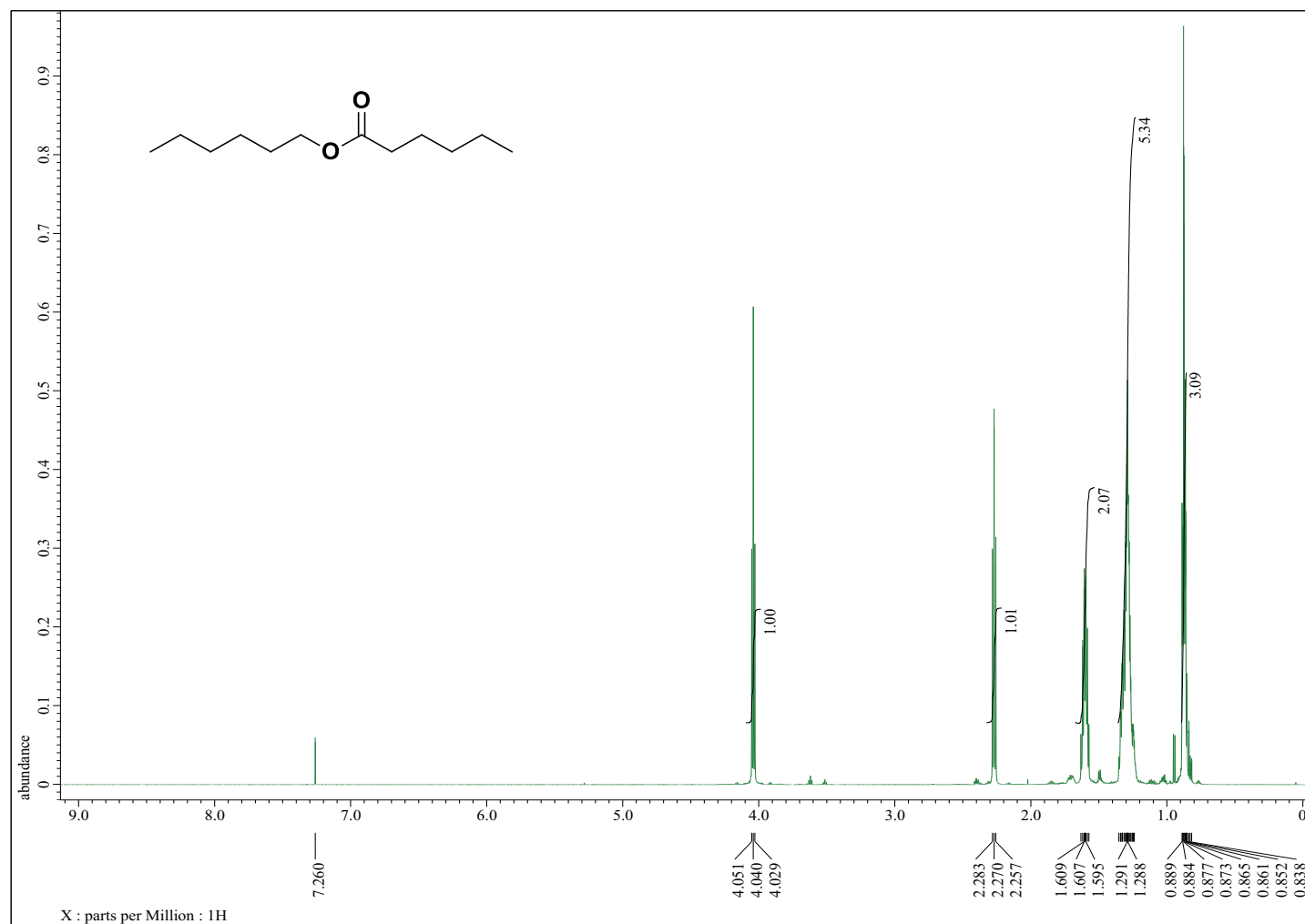
^{1}H NMR of Compound **90** [hexyl hexanoate]

^{13}C NMR of Compound **90** [hexyl hexanoate]

X : parts per Million : 13C

174.042

77.317
77.097
76.887

64.430

34.422
31.502
31.387
28.678
25.662
24.771
22.598
22.387
14.028
13.952

abundance

^{1}H NMR of Compound **91** [propyl propanoate]

abundance

X : parts per Million : 1H

4.031 4.020 4.008

2.335 2.322 2.310 2.297
1.654 1.643 1.631 1.619
1.155 1.142 1.129 1.117
0.941 0.929 0.916

1.02   1.00   1.00

1.55   1.53
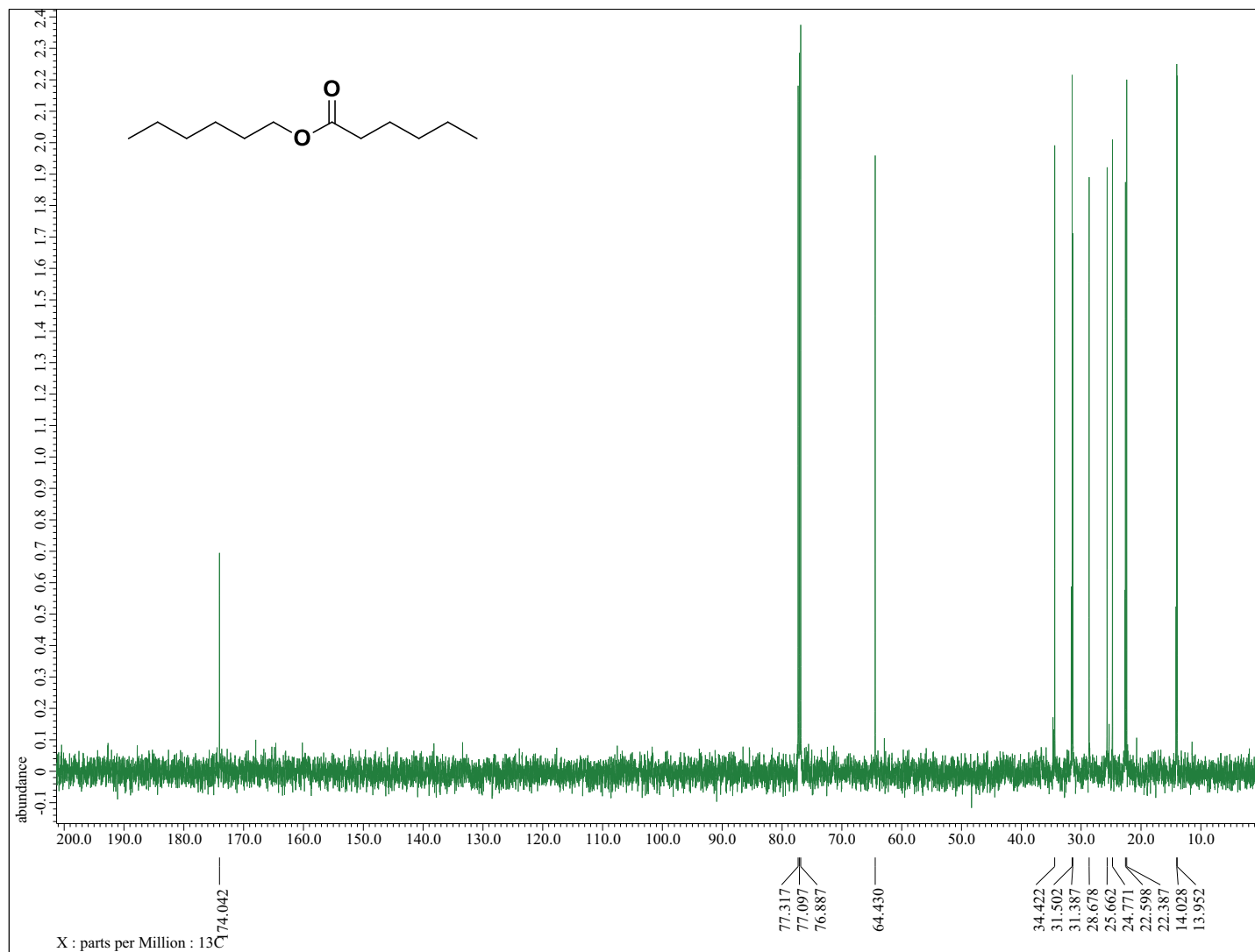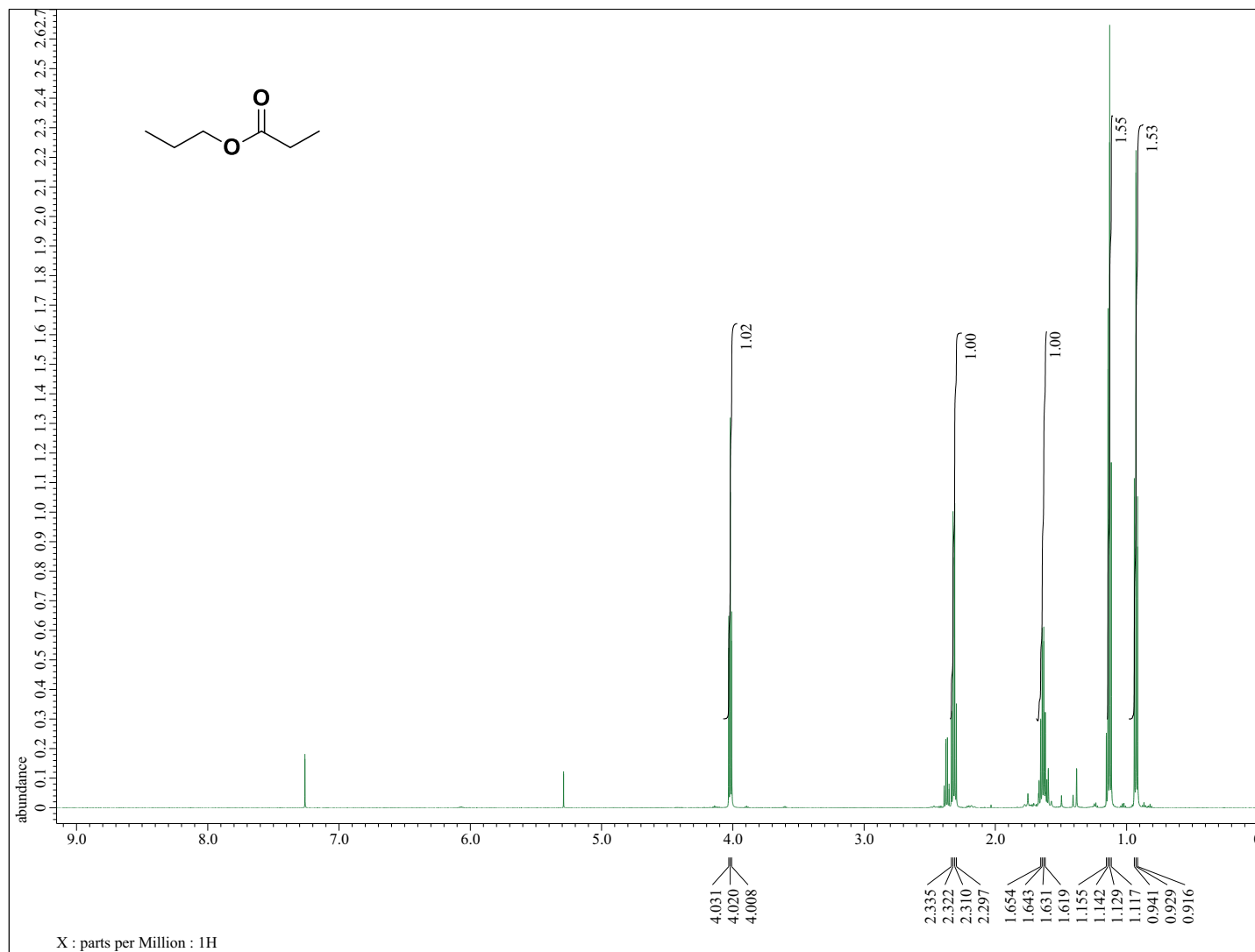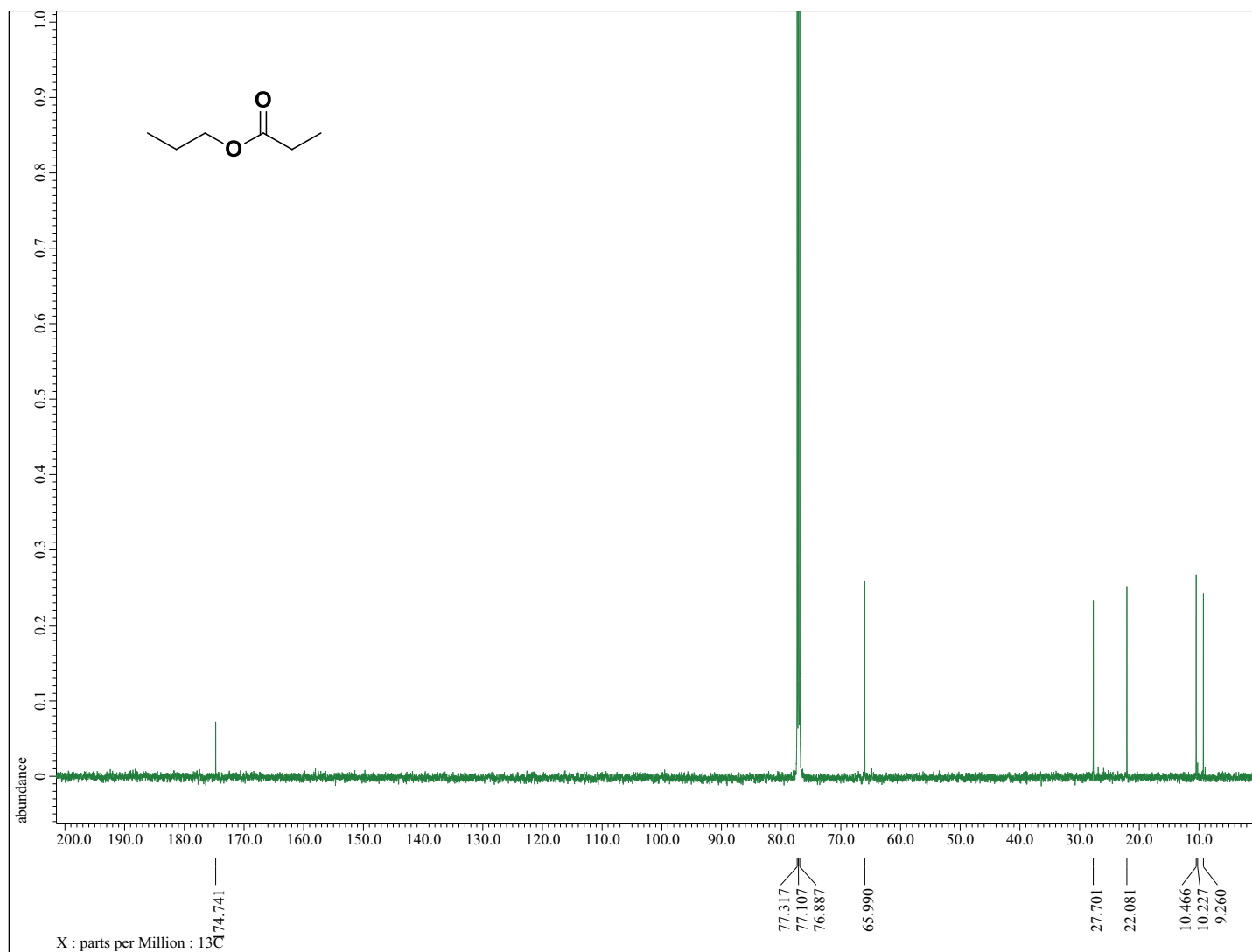
^{13}C NMR of Compound **91** [propyl propanoate]
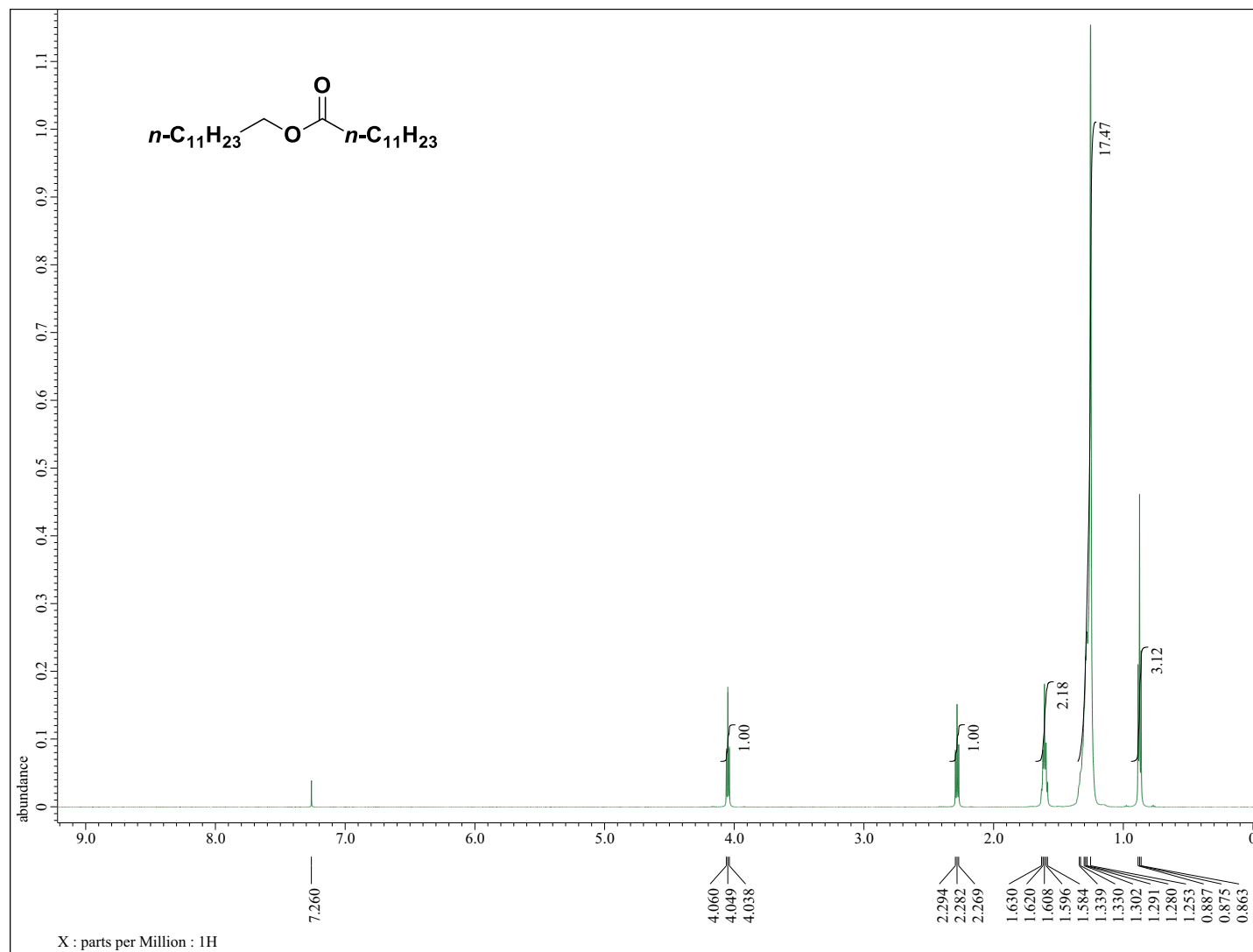
^{1}H NMR of Compound **92** [dodecyl dodecanoate]
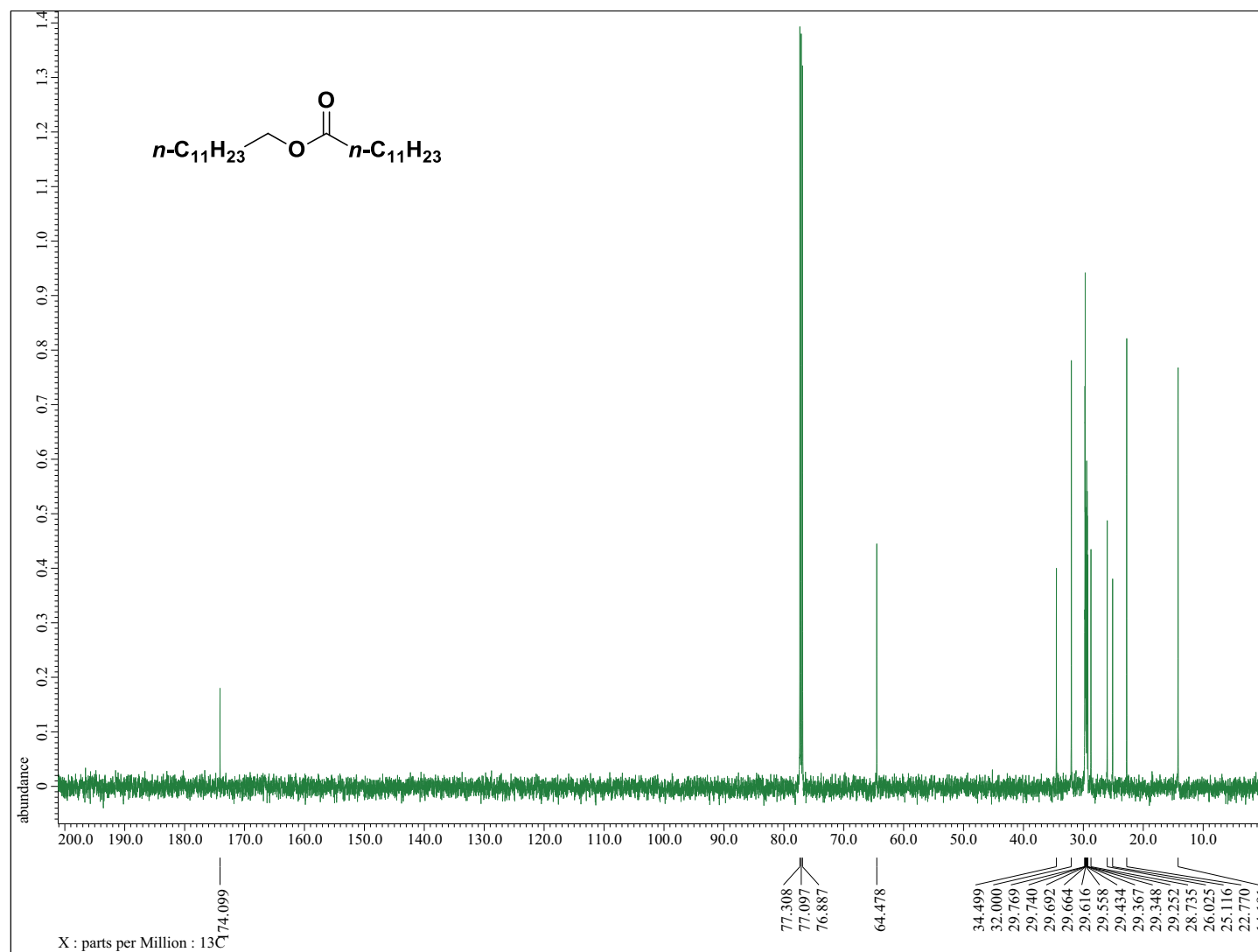
^{13}C NMR of Compound **92** [dodecyl dodecanoate]
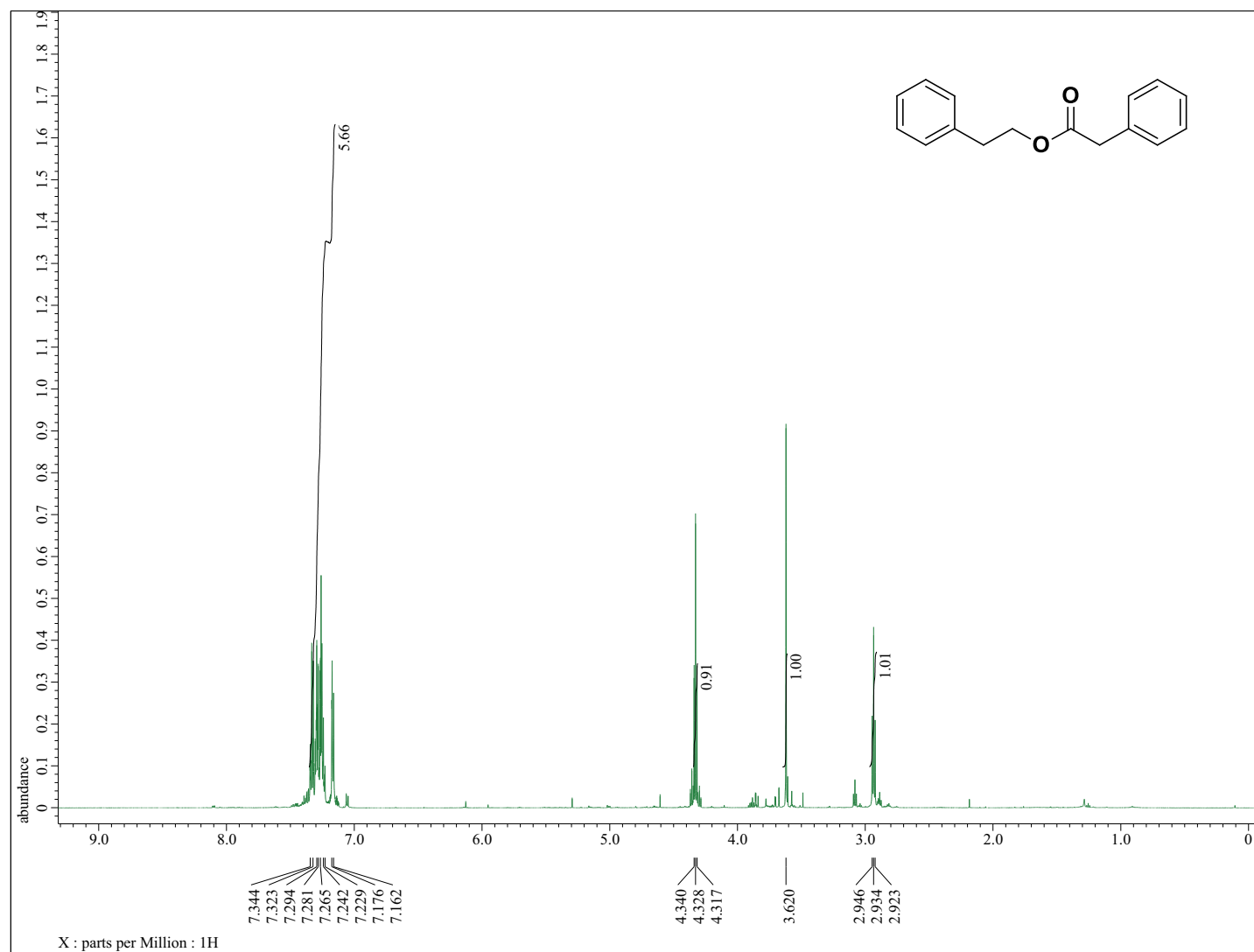
^{1}H NMR of Compound **93** [phenethyl 2-phenylacetate]
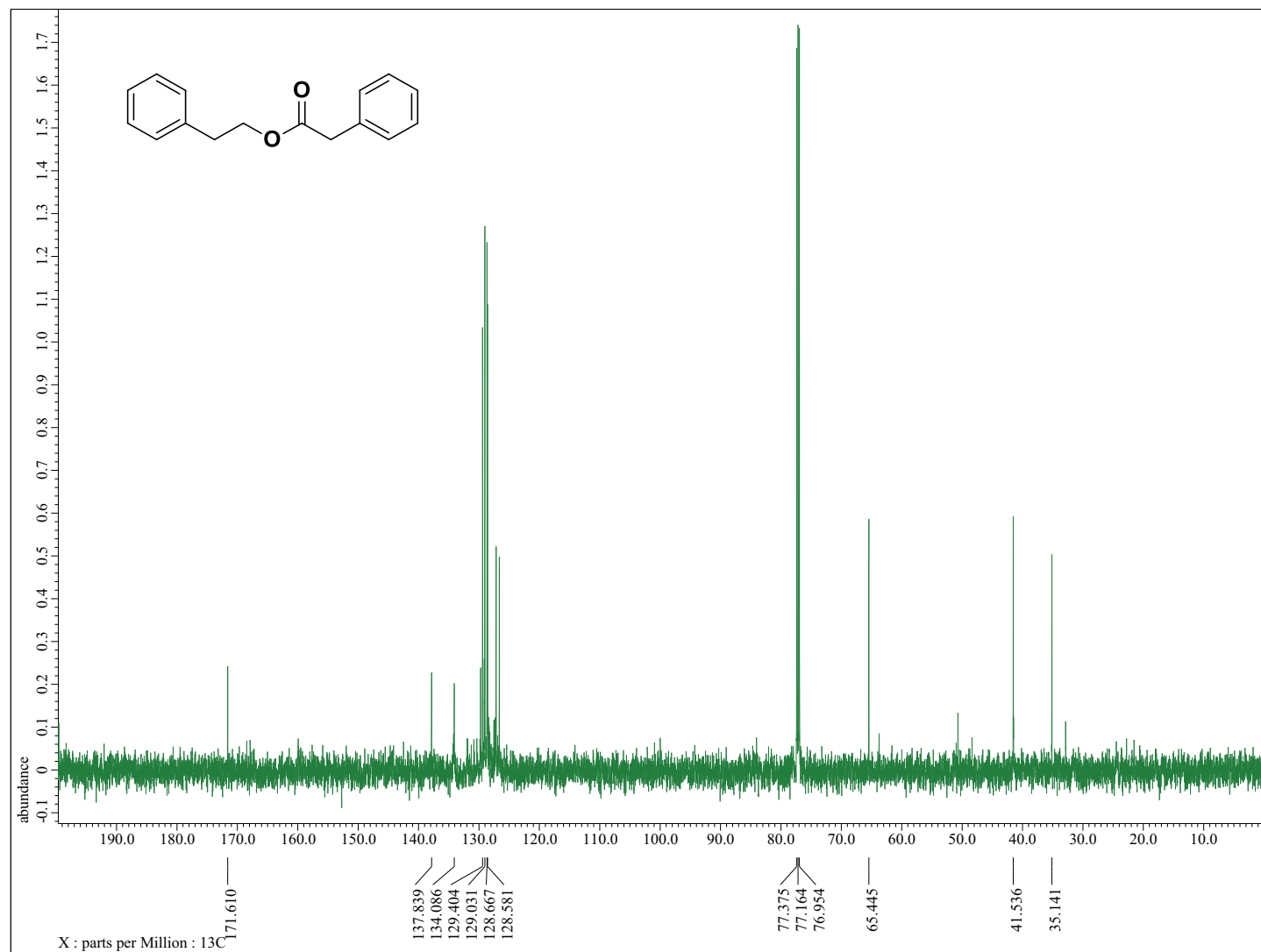
^{13}C NMR of Compound **93** [phenethyl 2-phenylacetate]
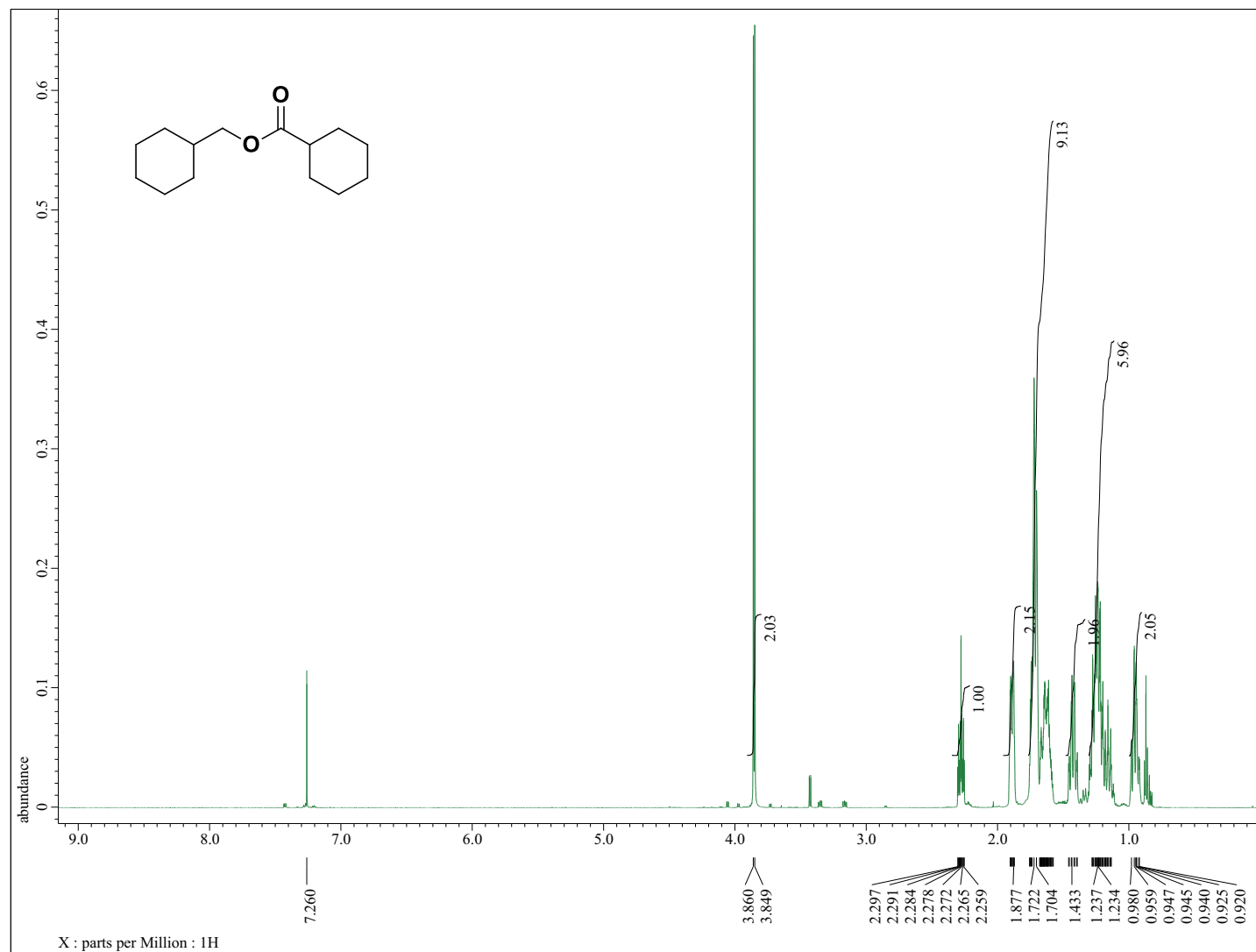
^{1}H NMR of Compound **94** [cyclohexylmethyl cyclohexanecarboxylate]
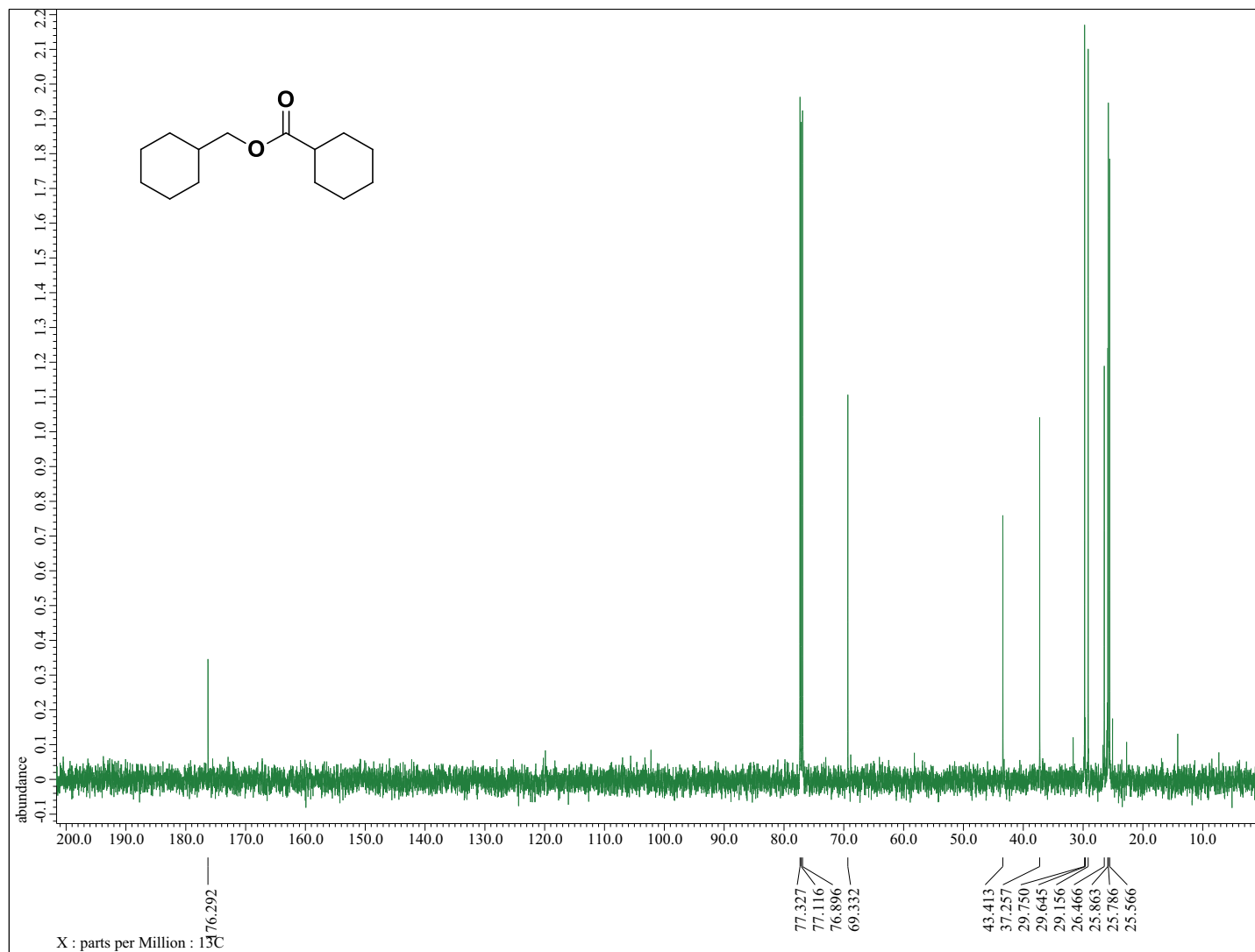
^{13}C NMR of Compound **94** [cyclohexylmethyl cyclohexanecarboxylate]
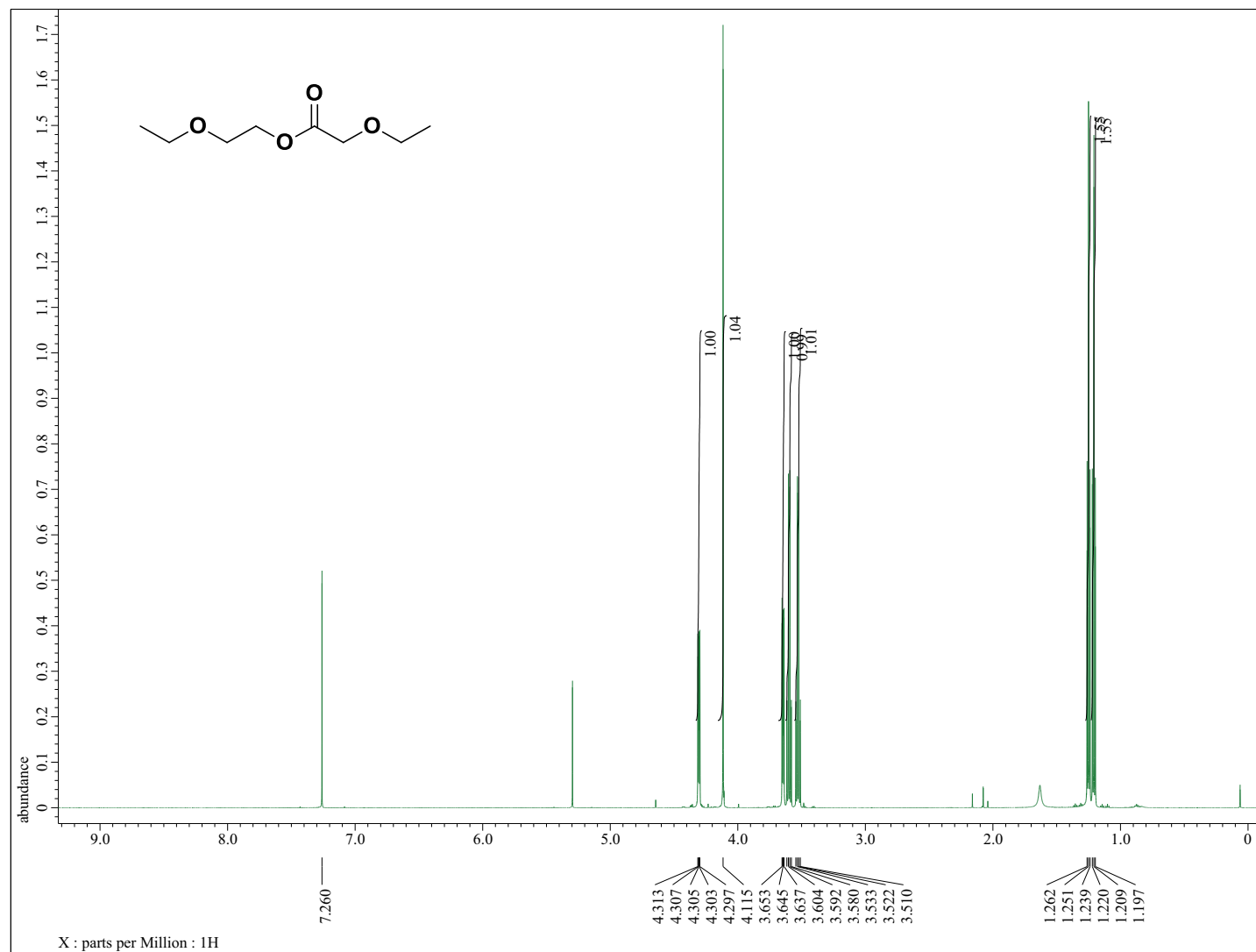
^{1}H NMR of Compound **95** [2-ethoxyethyl 2-ethoxyacetate]

^{13}C NMR of Compound **95** [2-ethoxyethyl 2-ethoxyacetate]

170.700

77.317
77.107
76.887
68.250
68.039
67.283
66.728
63.989

15.158
15.072

abundance

X : parts per Million : 13C
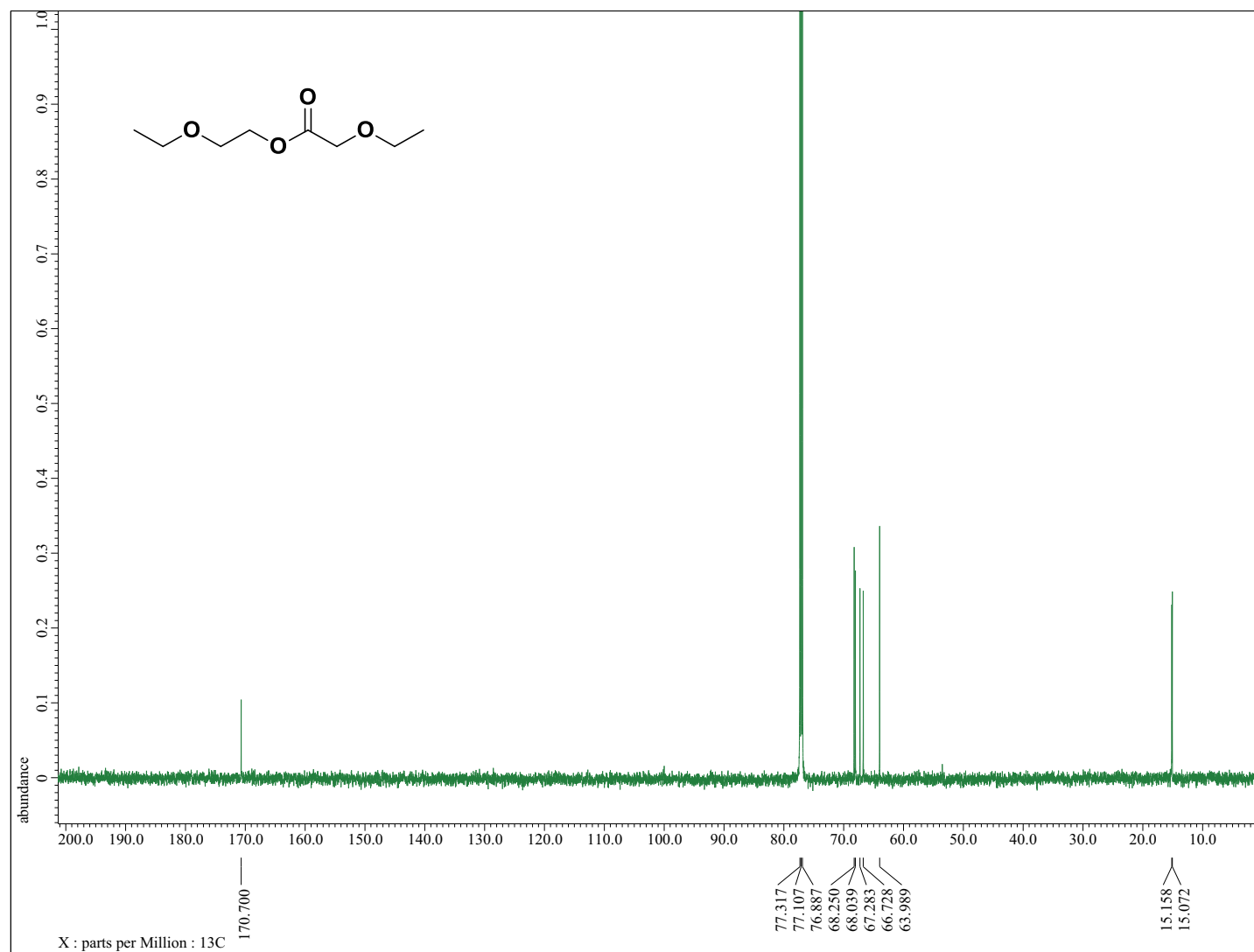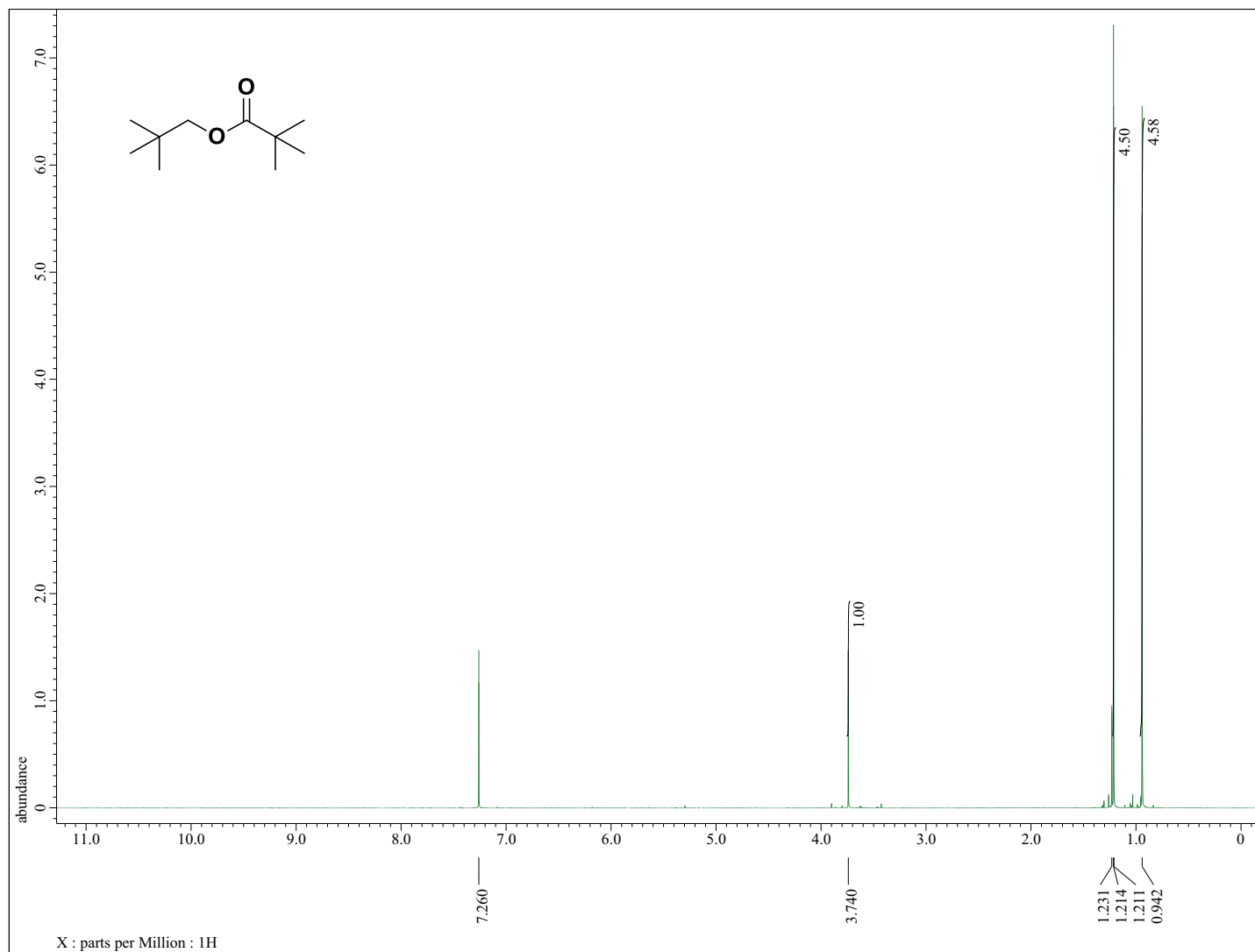
^{1}H NMR of Compound **96** [2,2-dimethylpropyl pivalate]

X : parts per Million : 1H

abundance

7.260

3.740

1.231
1.214
1.211
0.942

4.50

4.58

1.00
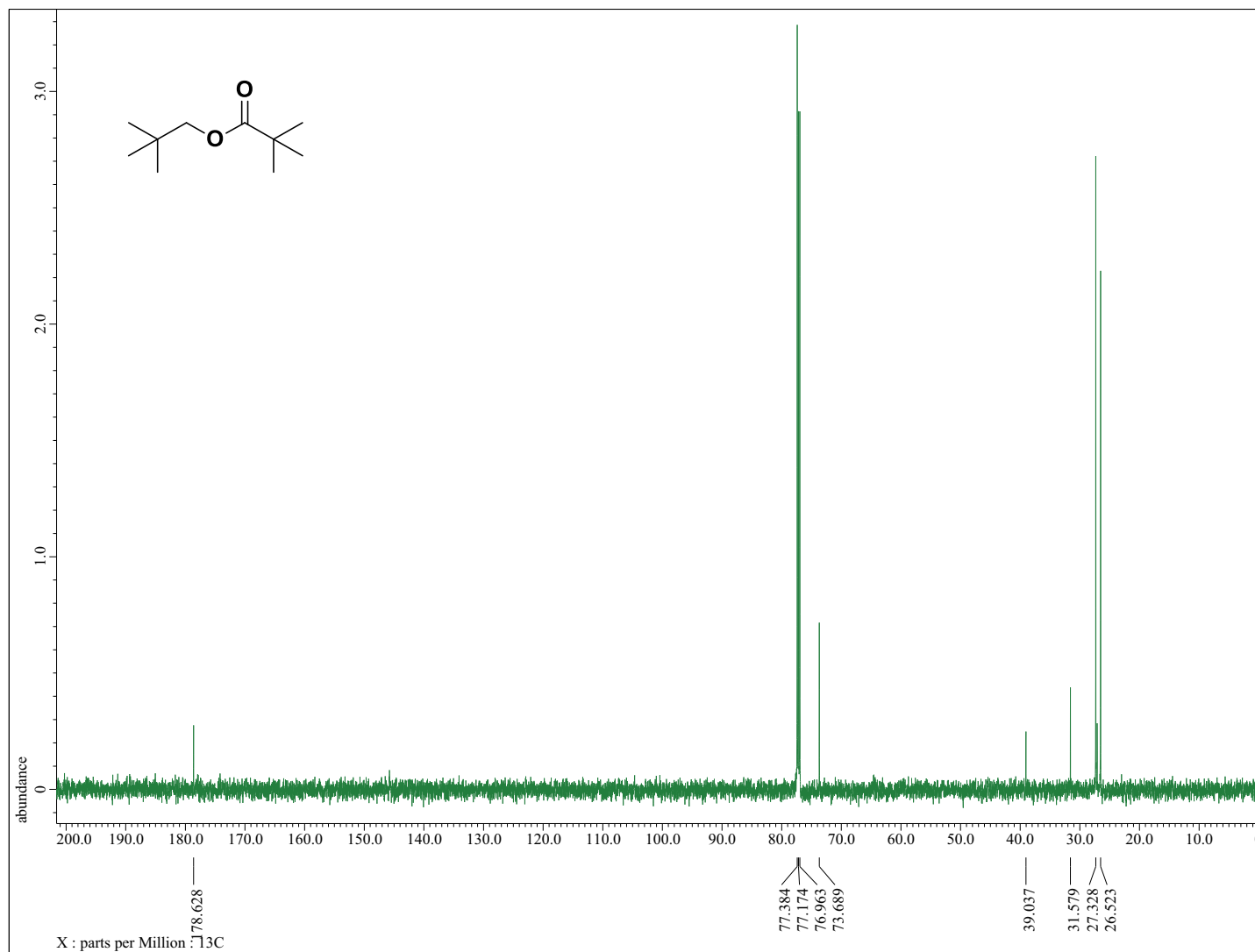
^{13}C NMR of Compound **96** [2,2-dimethylpropyl pivalate]
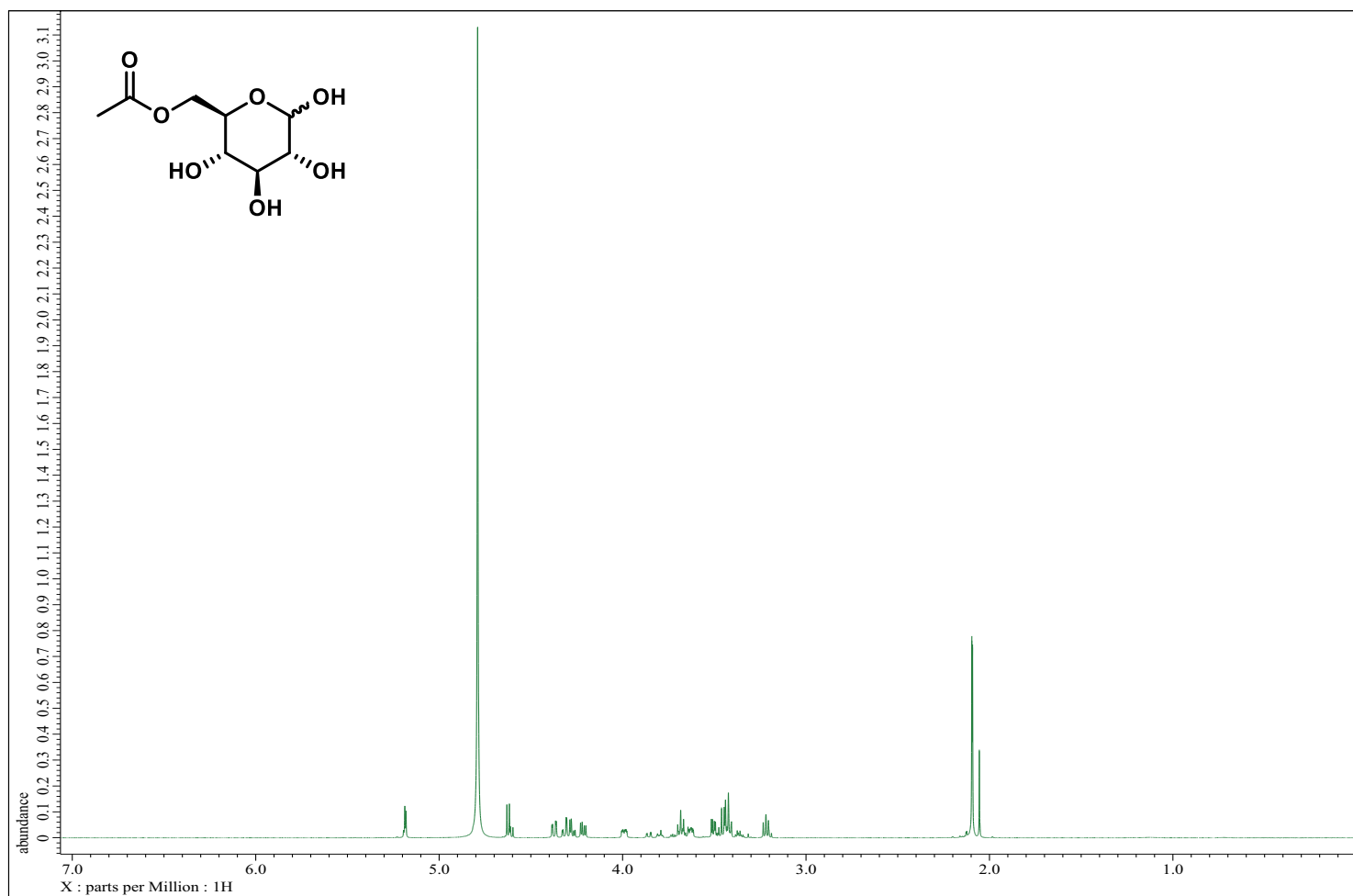
^{1}H NMR of **46** [6-*O*-Acetyl-*α*/*ß*-D-glucopyranose]
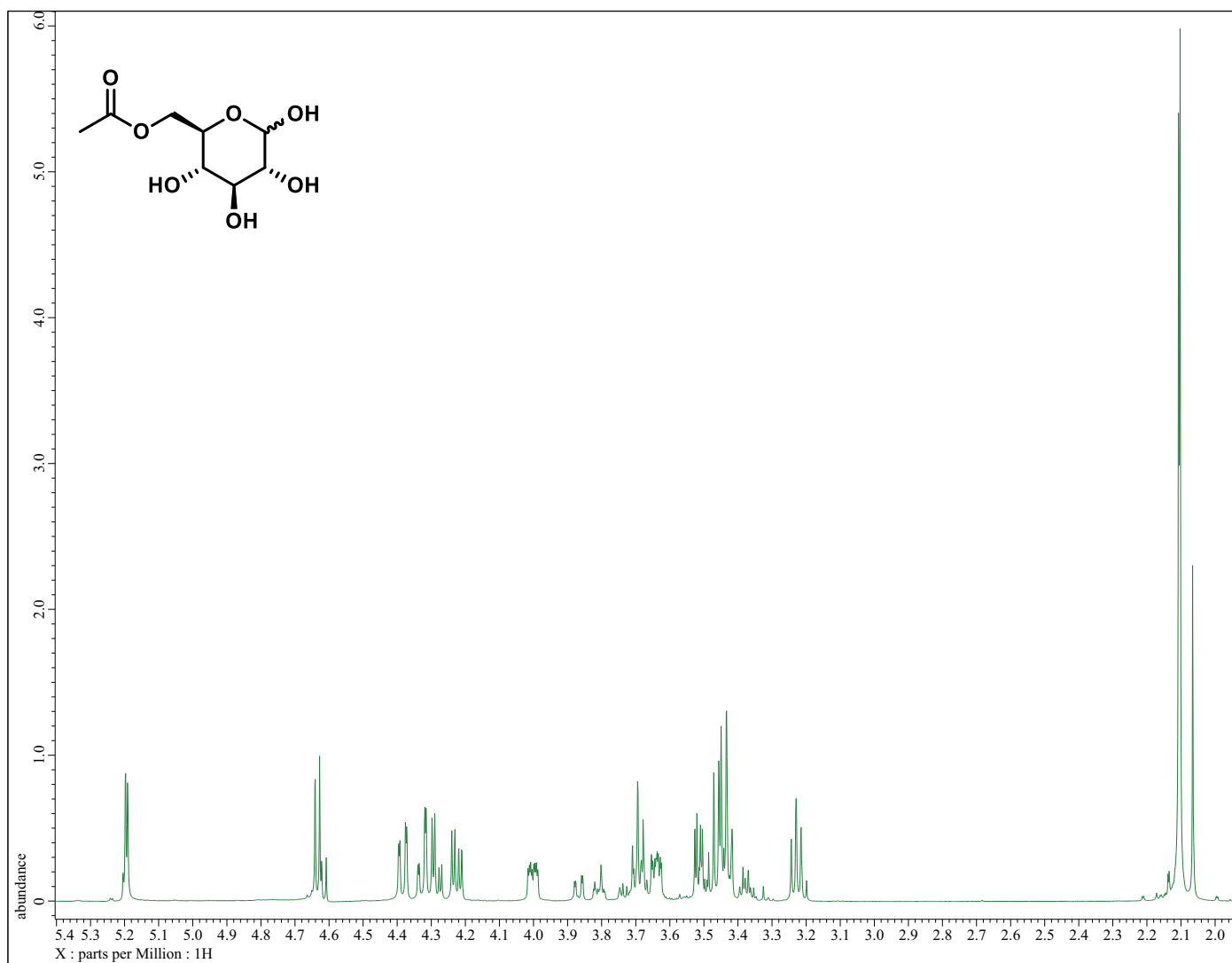
H$_2$O-Presaturation ^{1}H NMR of Compound **46** expanded to show relevant range
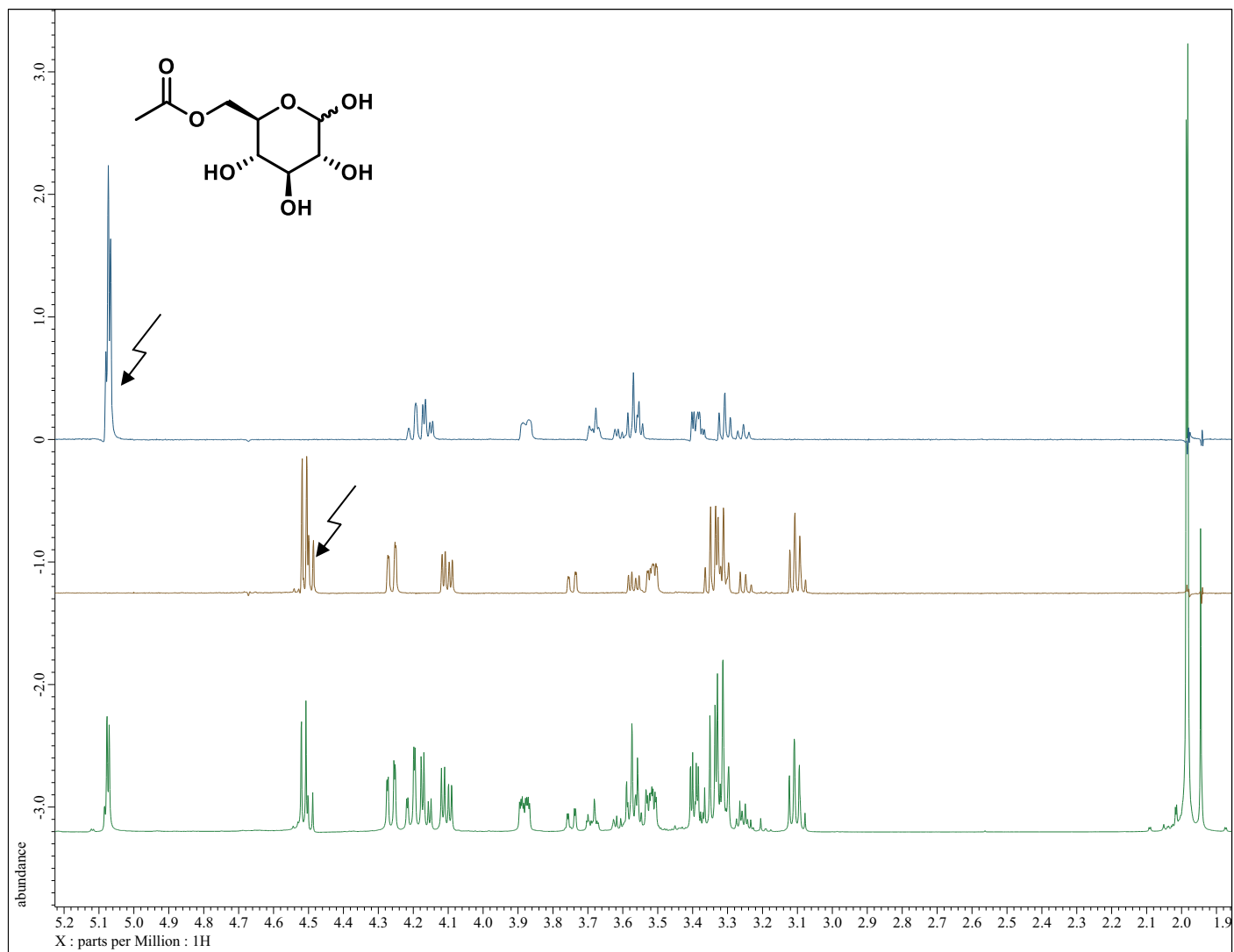
H₂O-Presaturation ¹H NMR of Compound **46** overlaid with 1D TOCSY data for *α*-**1** (top) and *ß*-**1** (middle)
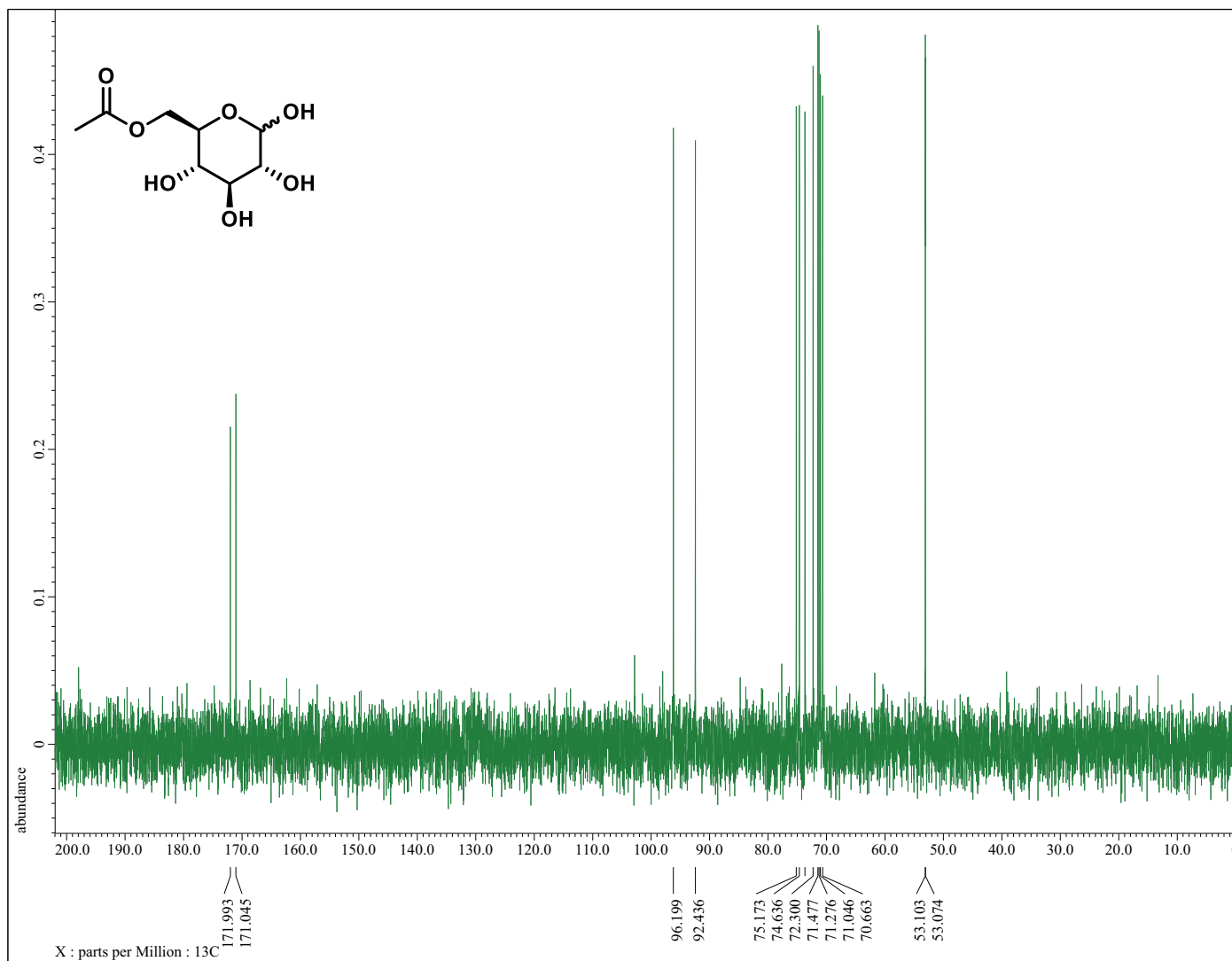
¹³C NMR of **46** [6-*O*-Acetyl-*α*/*β*-D-glucopyranose]
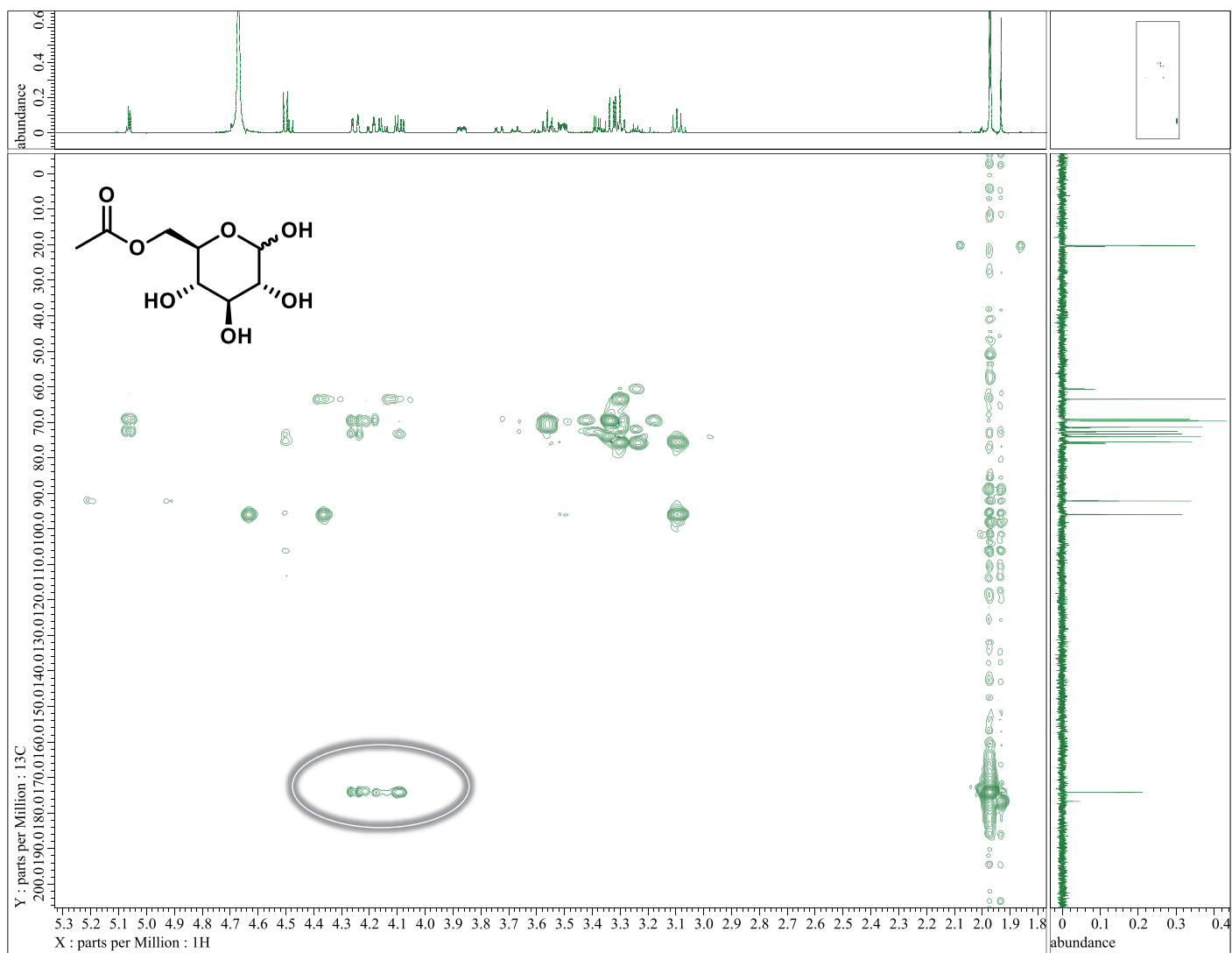
HMBC NMR of Compound **46** highlighting area of cross-peaks used in determination of $^3J_{CH}$
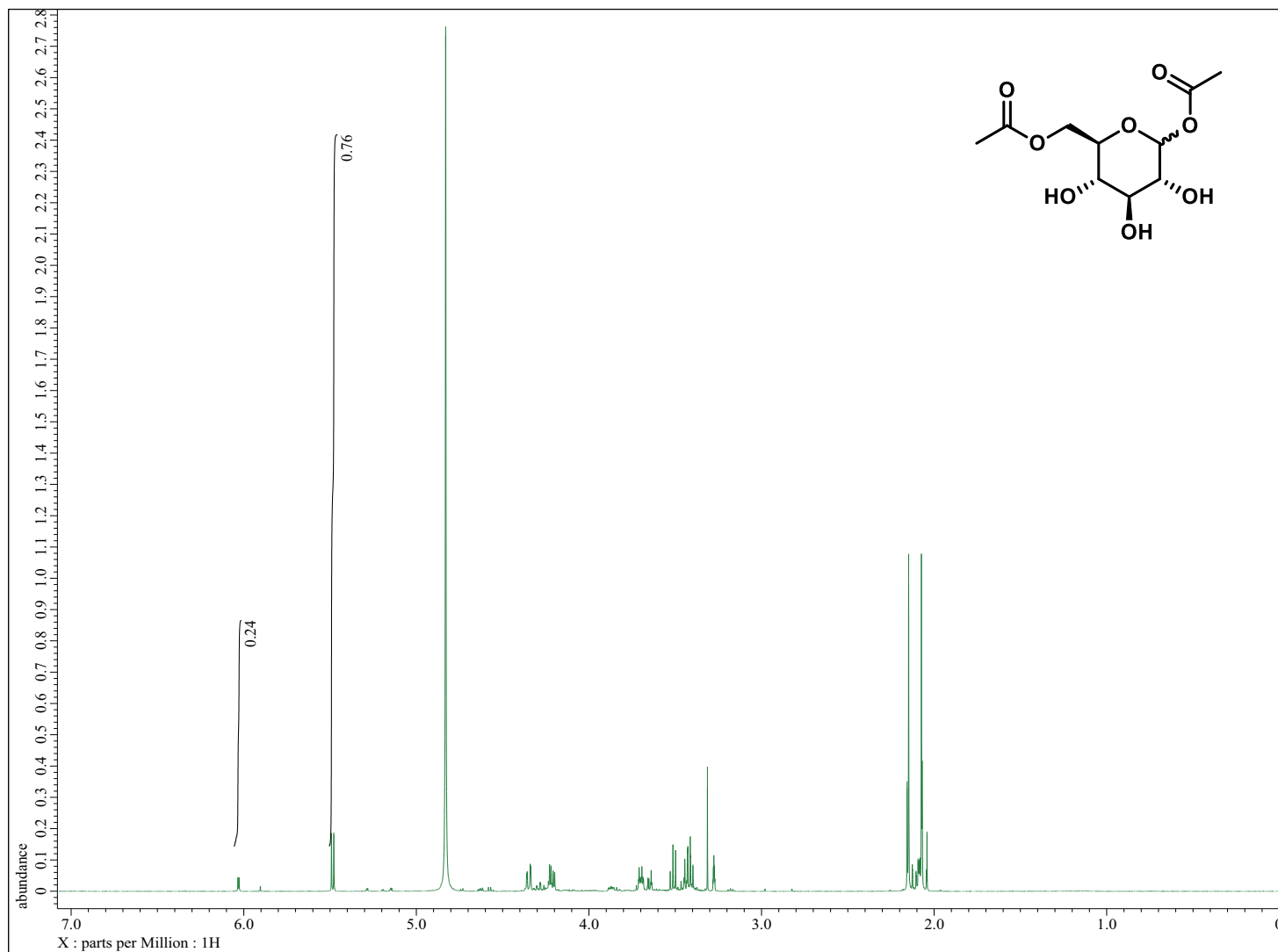
^{1}H NMR of **47** [Acetyl-6-*O*-acetyl-*α*/*β*-D-glucopyranoside]
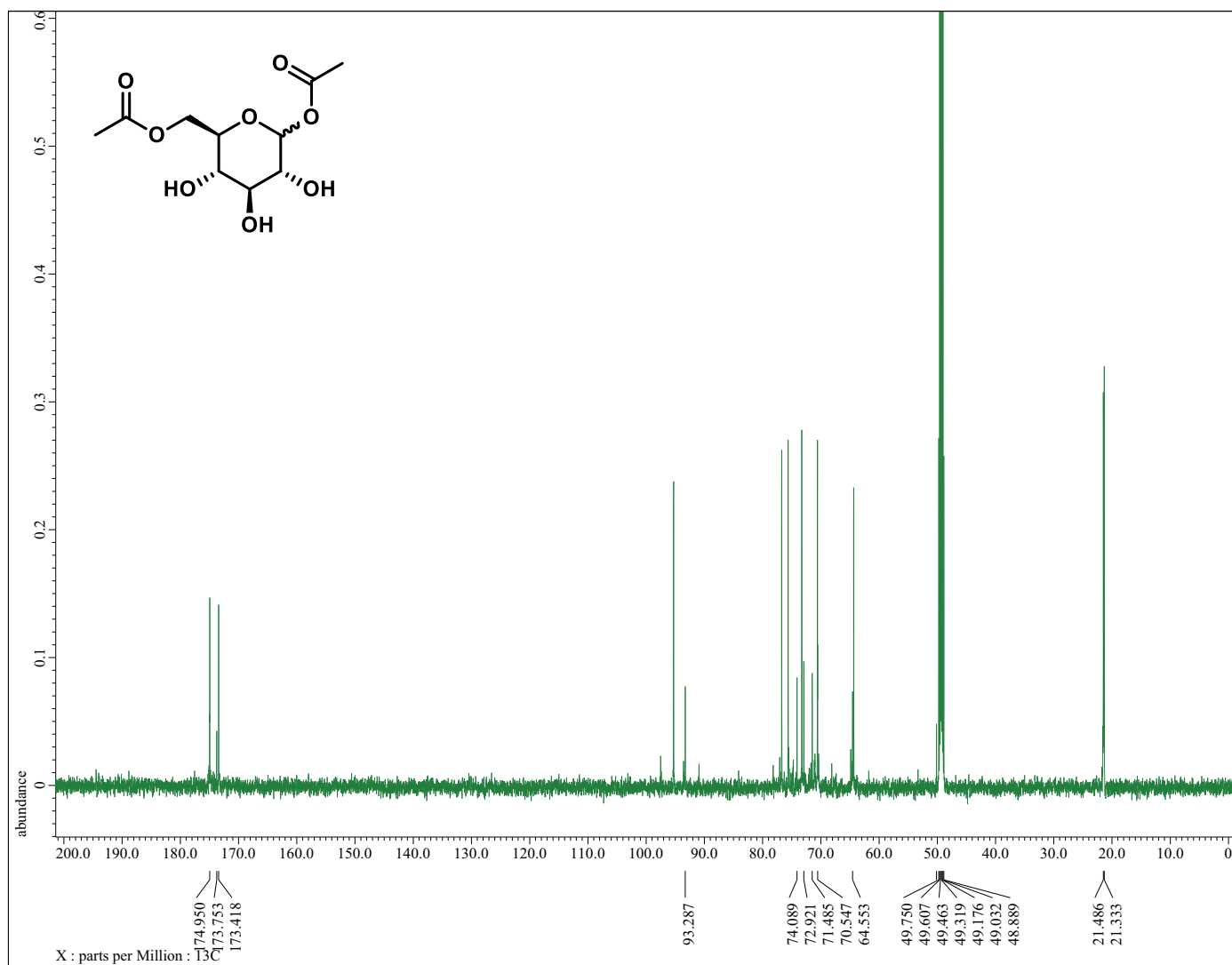
^{13}C NMR of **47** [Acetyl-6-*O*-acetyl-*α*/*β*-D-glucopyranoside]
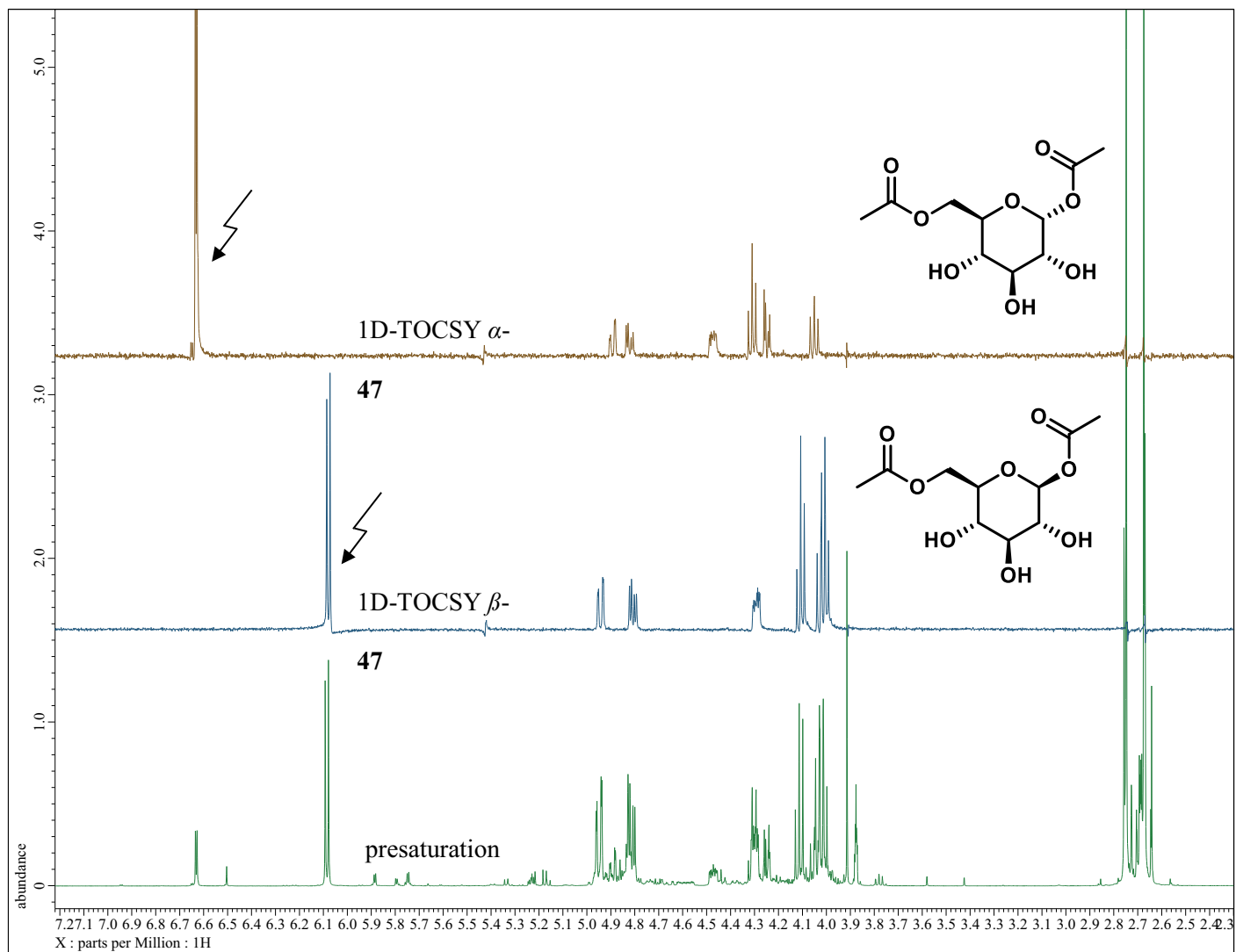
Overlay of 1D-TOCSY and H_2O-presaturation ^1H NMR experiments of Compound **47**
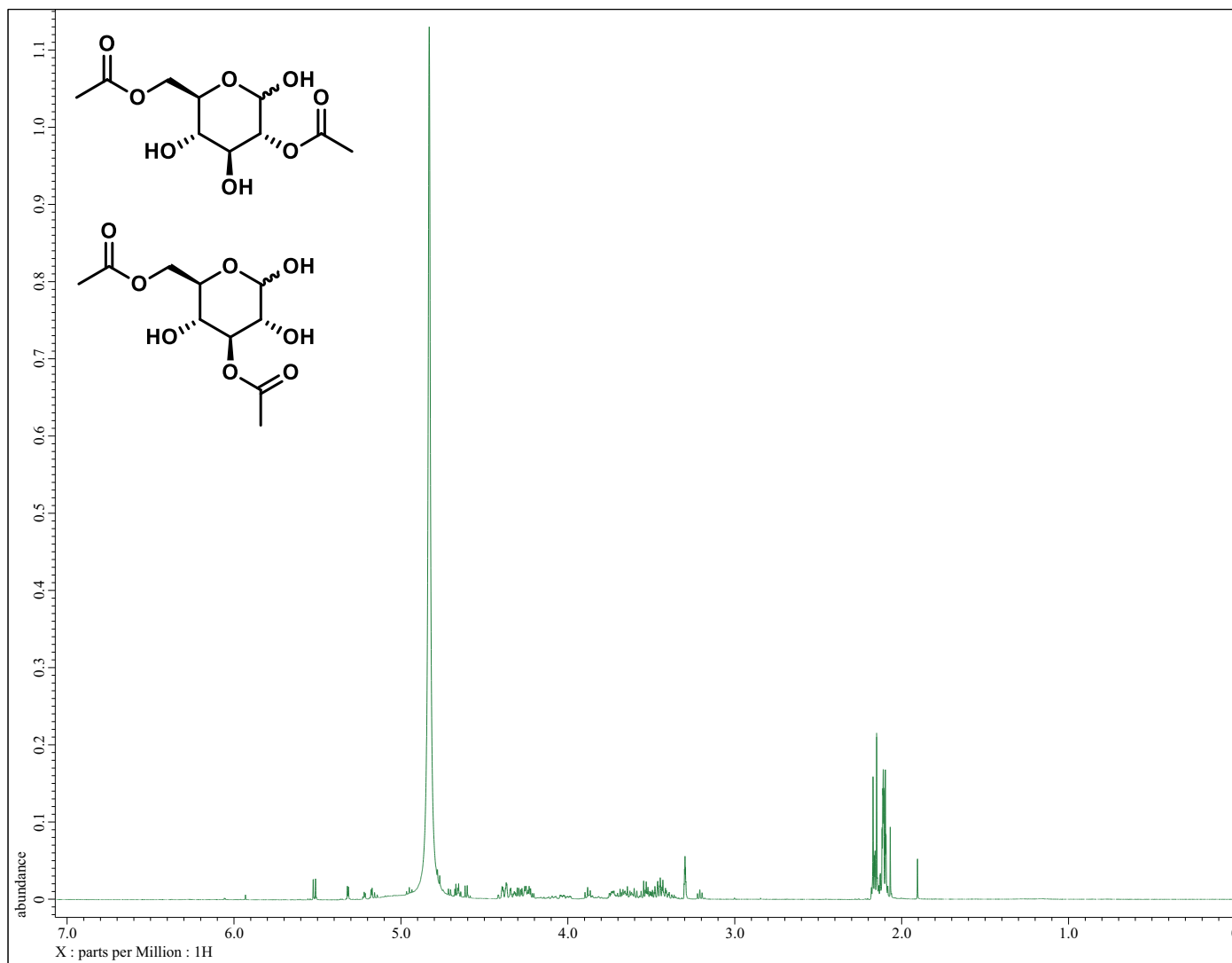
^{1}H NMR of the mixture containing *α/ß*-**48** [2,6-di-*O*-acetyl-*α/ß*-D-glucopyranose] and *α/ß*-**49** [3,6-di-*O*-acetyl-*α/ß*-D-glucopyranose]
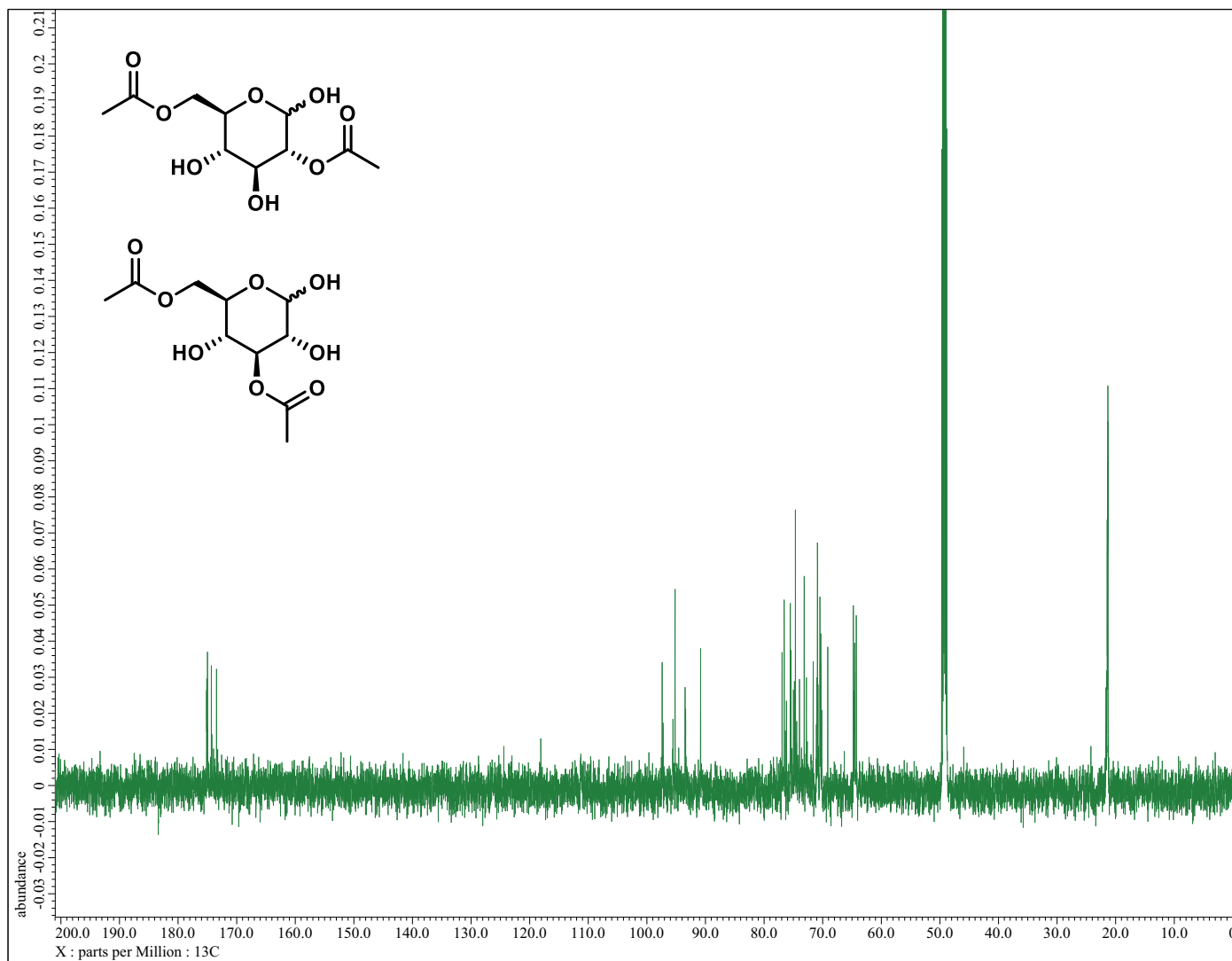
^{13}C NMR of the mixture containing *α*/*ß*-**48** [2,6-di-*O*-acetyl-*α*/*ß*-D-glucopyranose] and *α*/*ß*-**49** [3,6-di-*O*-acetyl-*α*/*ß*-D-glucopyranose]
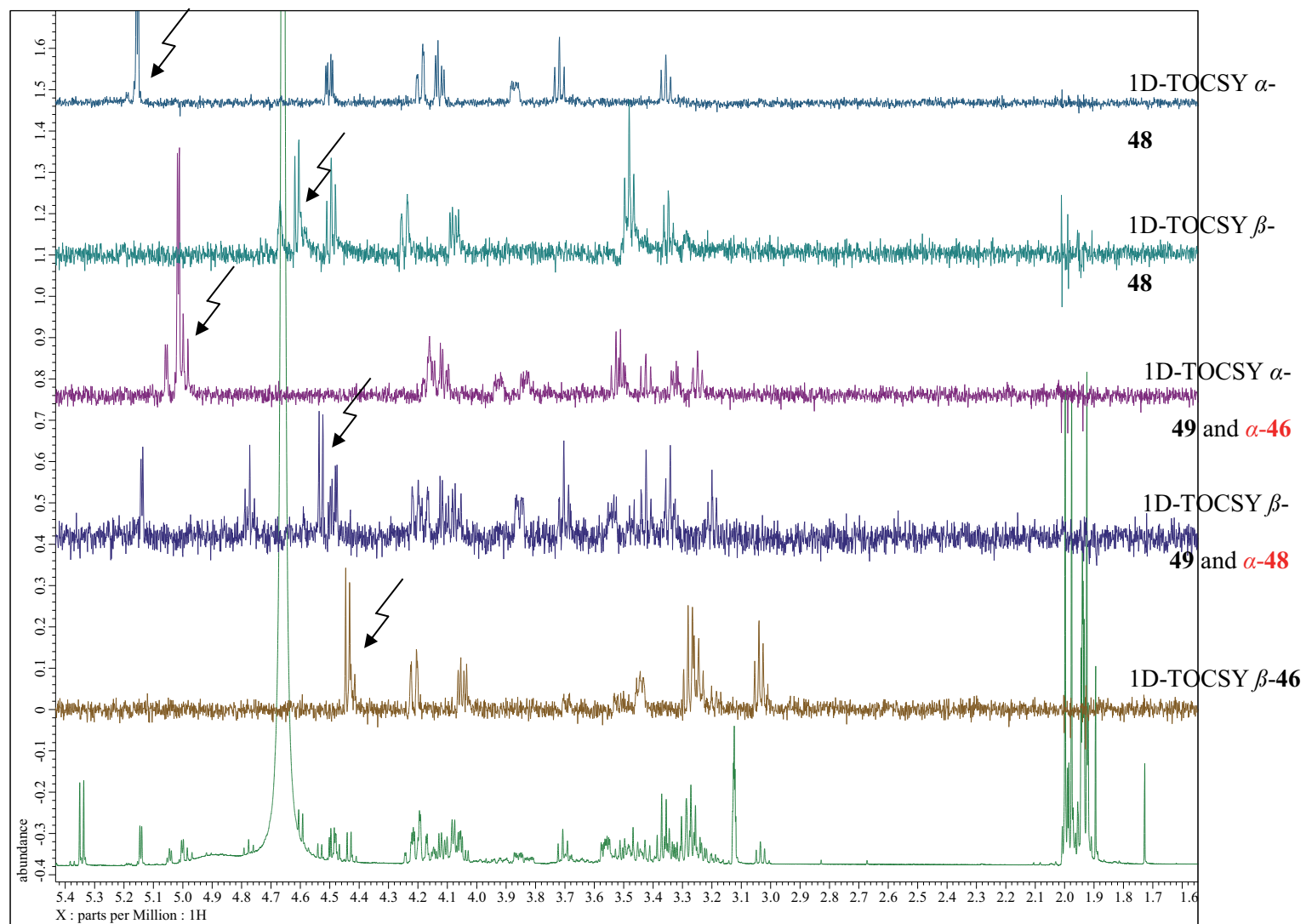
^{1}H NMR (bottom) and 1D TOCSY (500 ns mixing time) overlays for the mixture containing *α/β*-**48** and *α/β*-**49**
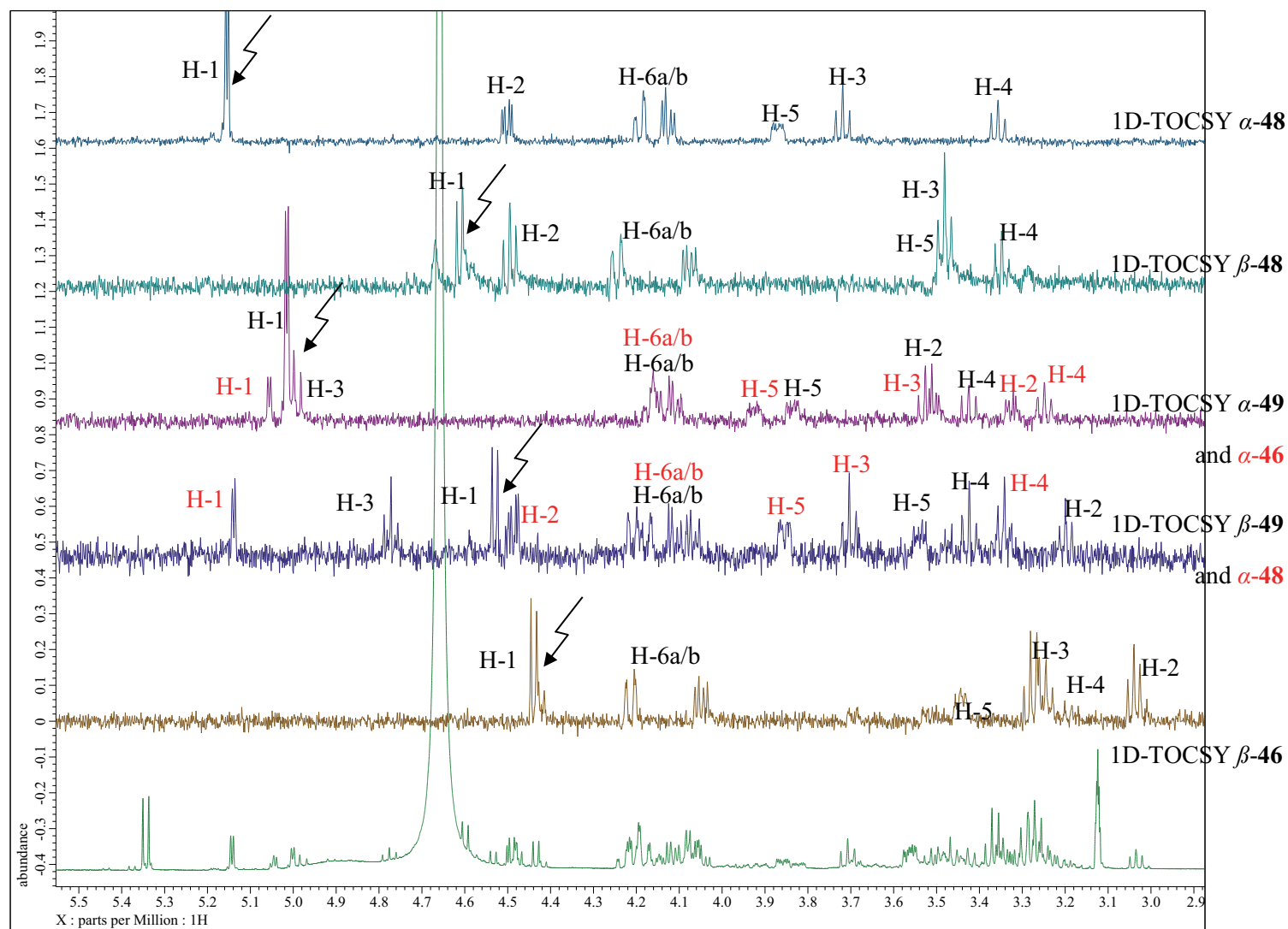
1D TOCSY overlays for the mixture containing *α/β*-**48** and *α/β*-**49** magnified to show assignment of hydrogens on pyranose ring

¹H NMR of **50** [Methyl-*α*/*ß*-D-glucopyranuronate]

5.264
5.258
4.790
4.697
4.684
4.390
4.373
4.075
4.059
3.806
3.743
3.727
3.712
3.591
3.535
3.512
3.497
3.306
3.291
3.277

abundance

X : parts per Million : 1H
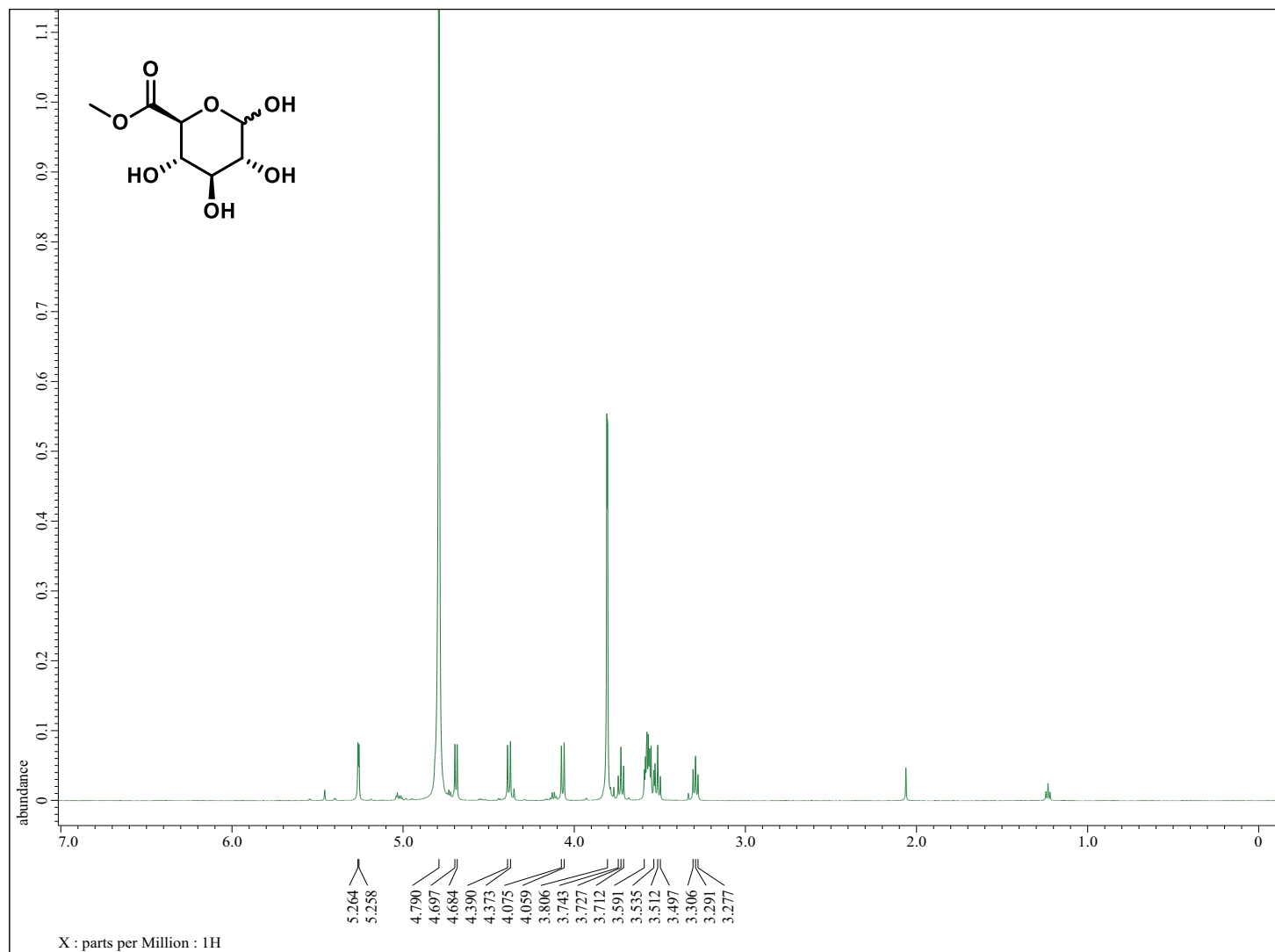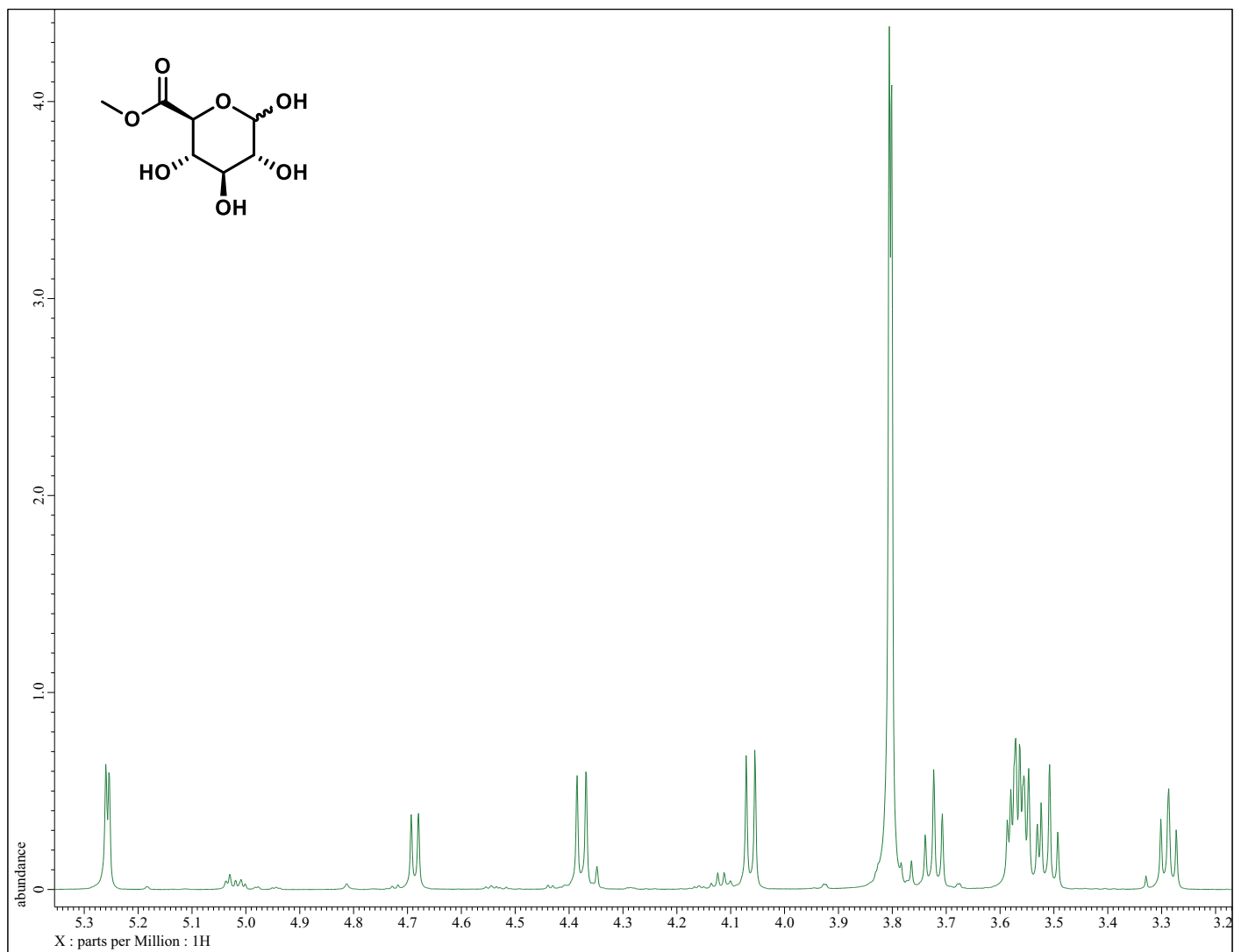
Expanded view of H$_2$O-presaturation ^{1}H NMR of Compound **50**
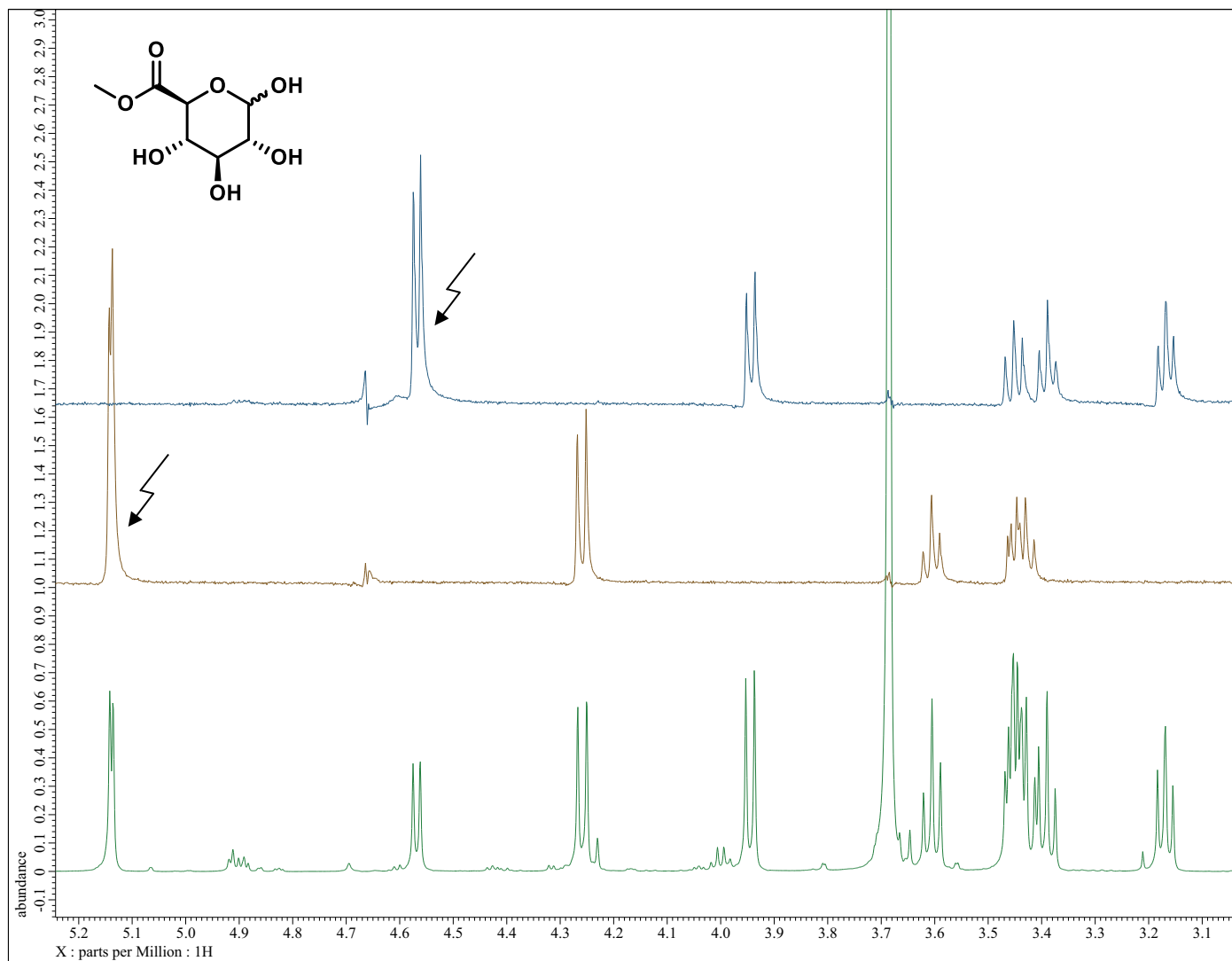
H₂O-Presaturation ¹H NMR of Compound **50** overlaid with 1D TOCSY spectra for *α*-**50** (middle) and *β*-**50** (top)
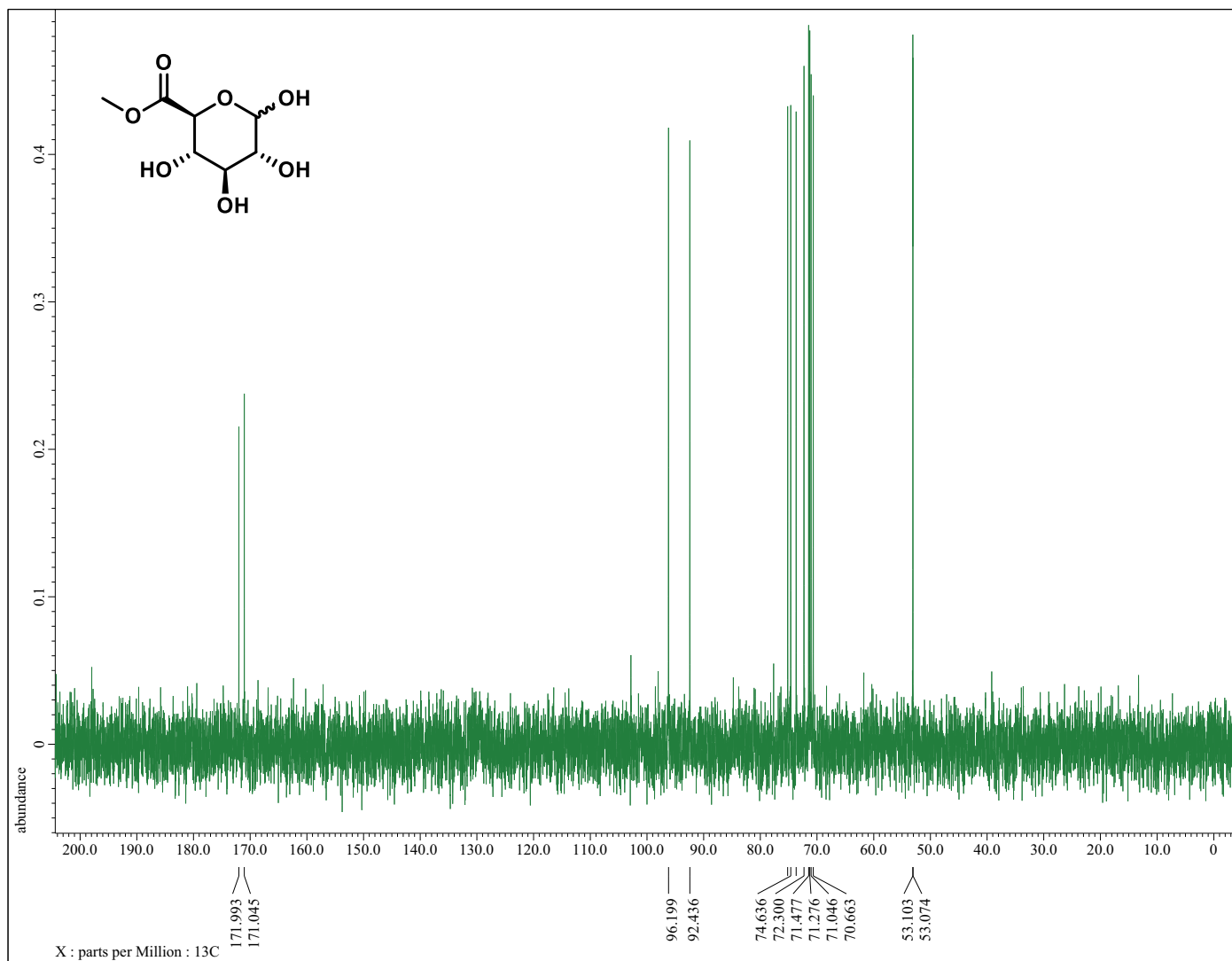
^{13}C NMR of **50** [Methyl-*α*/*β*-D-glucopyranuronate]
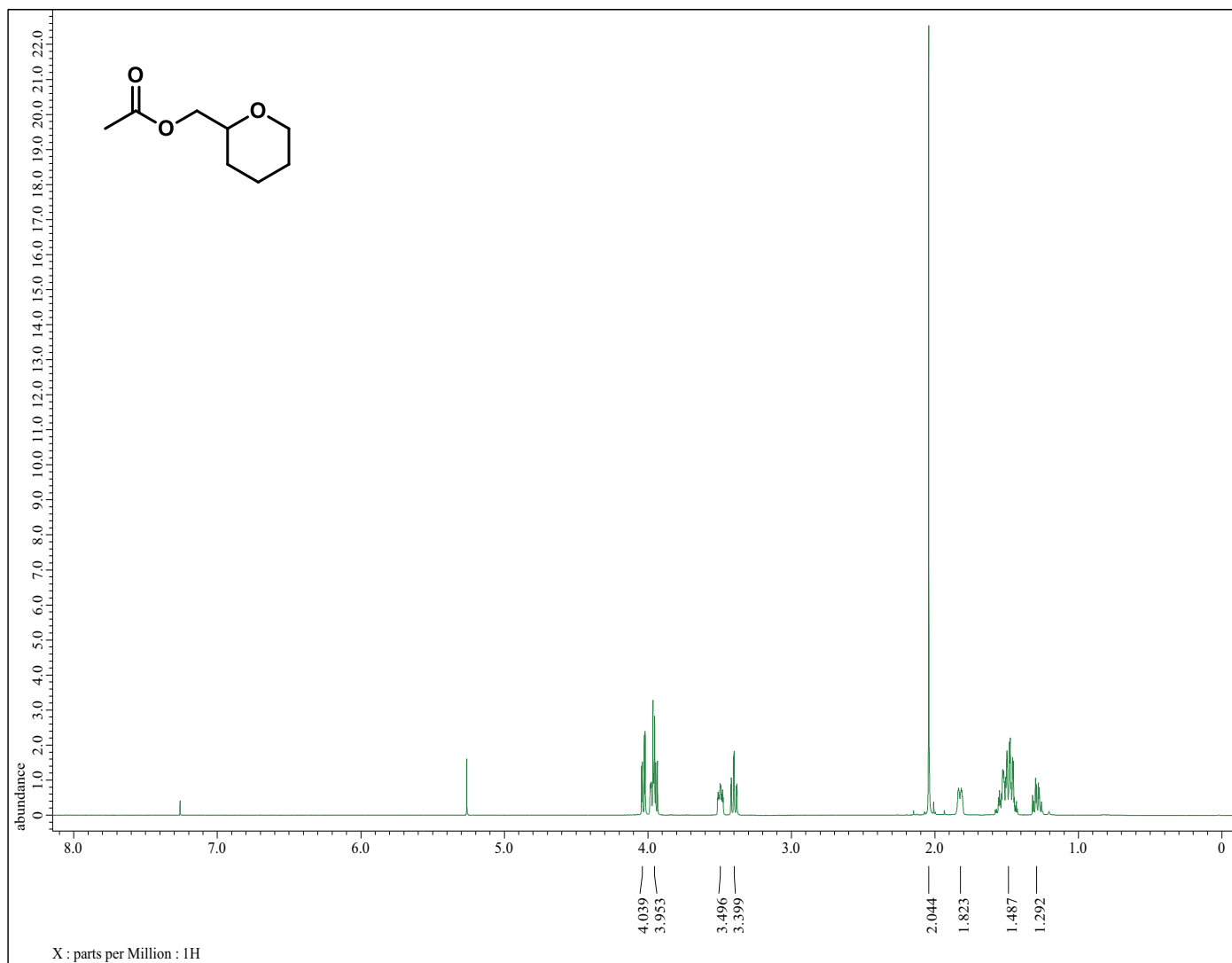
^{1}H NMR of **53** [(Tetrahydropyran-2-yl)-methyl acetate]
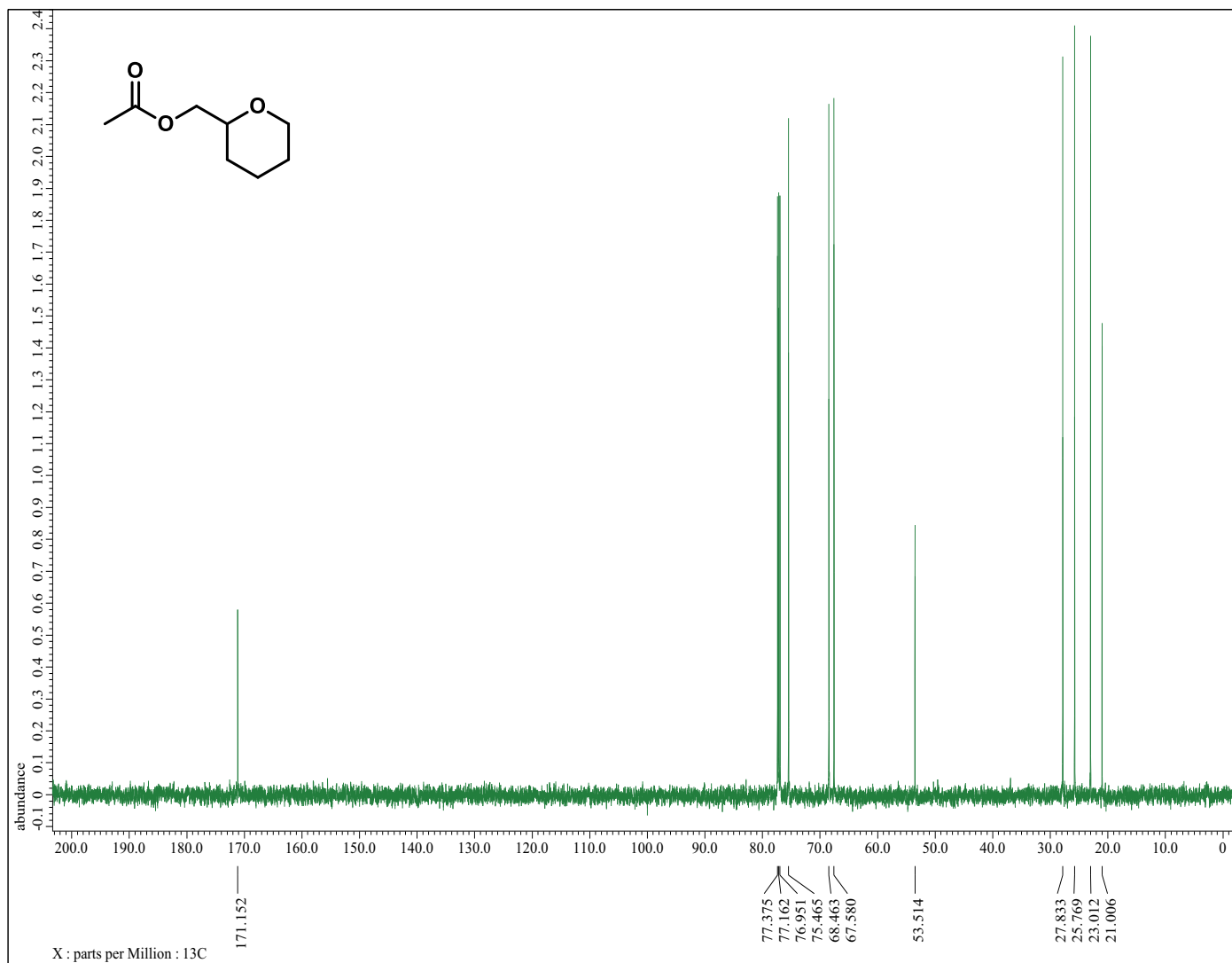
^{13}C NMR of **53** [(Tetrahydropyran-2-yl)-methyl acetate]
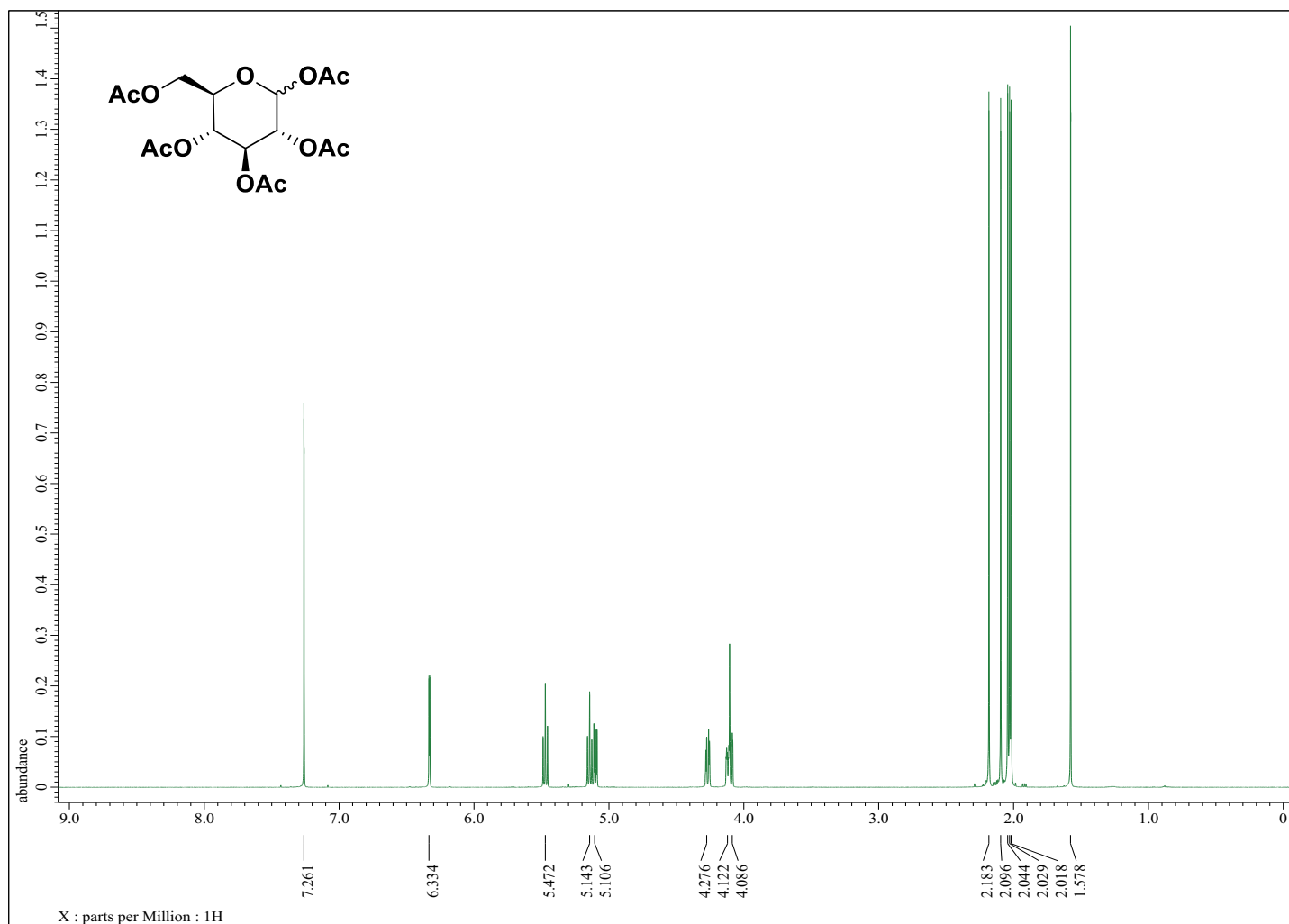
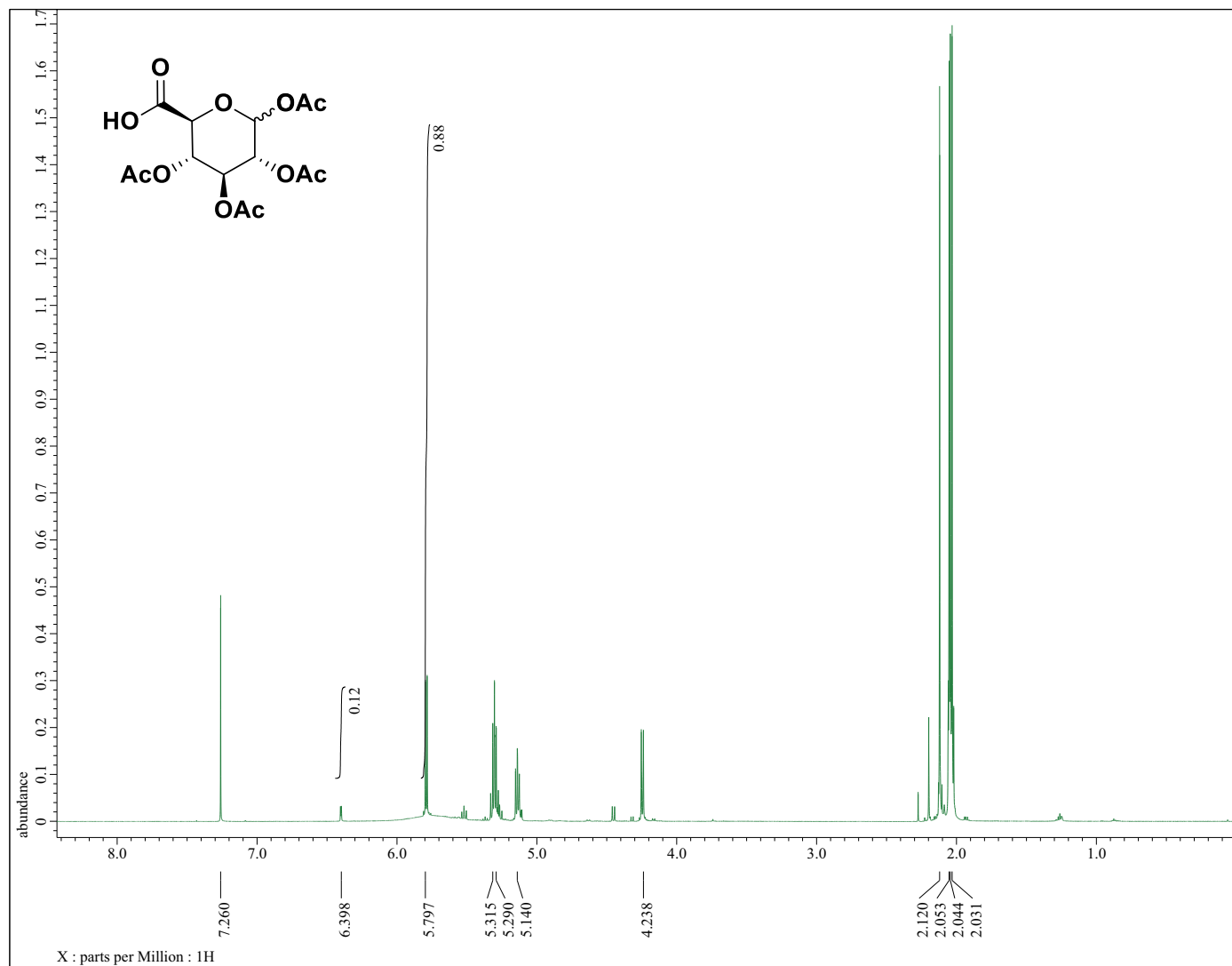^{1}H NMR of Compound **58** [Acetyl-2,3,4,6-tetra-*O*-acetyl-*α*/*ß*-D-glucopyranoside]
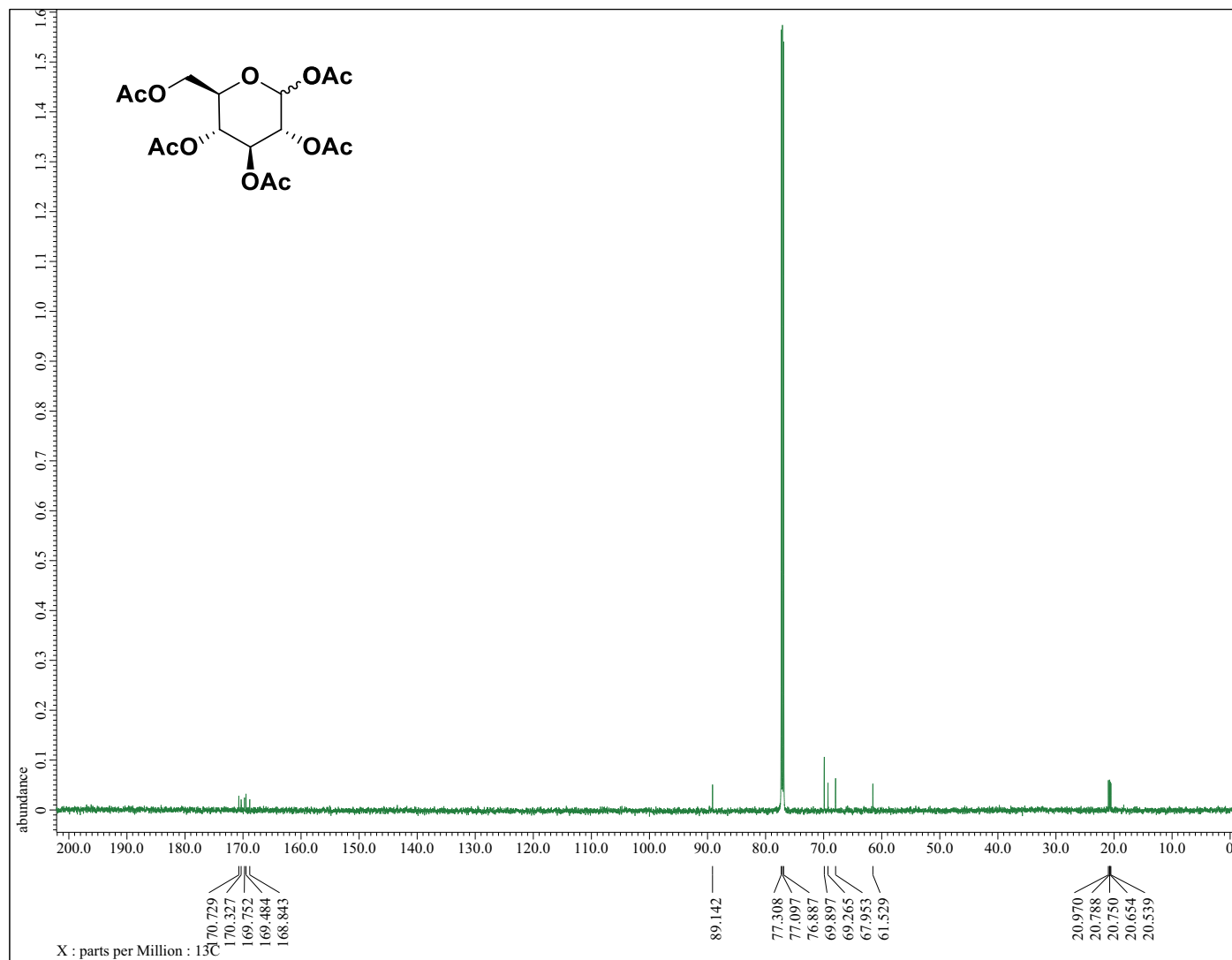
^{13}C NMR of Compound **58** [Acetyl-2,3,4,6-tetra-*O*-acetyl-*α*/*ß*-D-glucopyranoside]
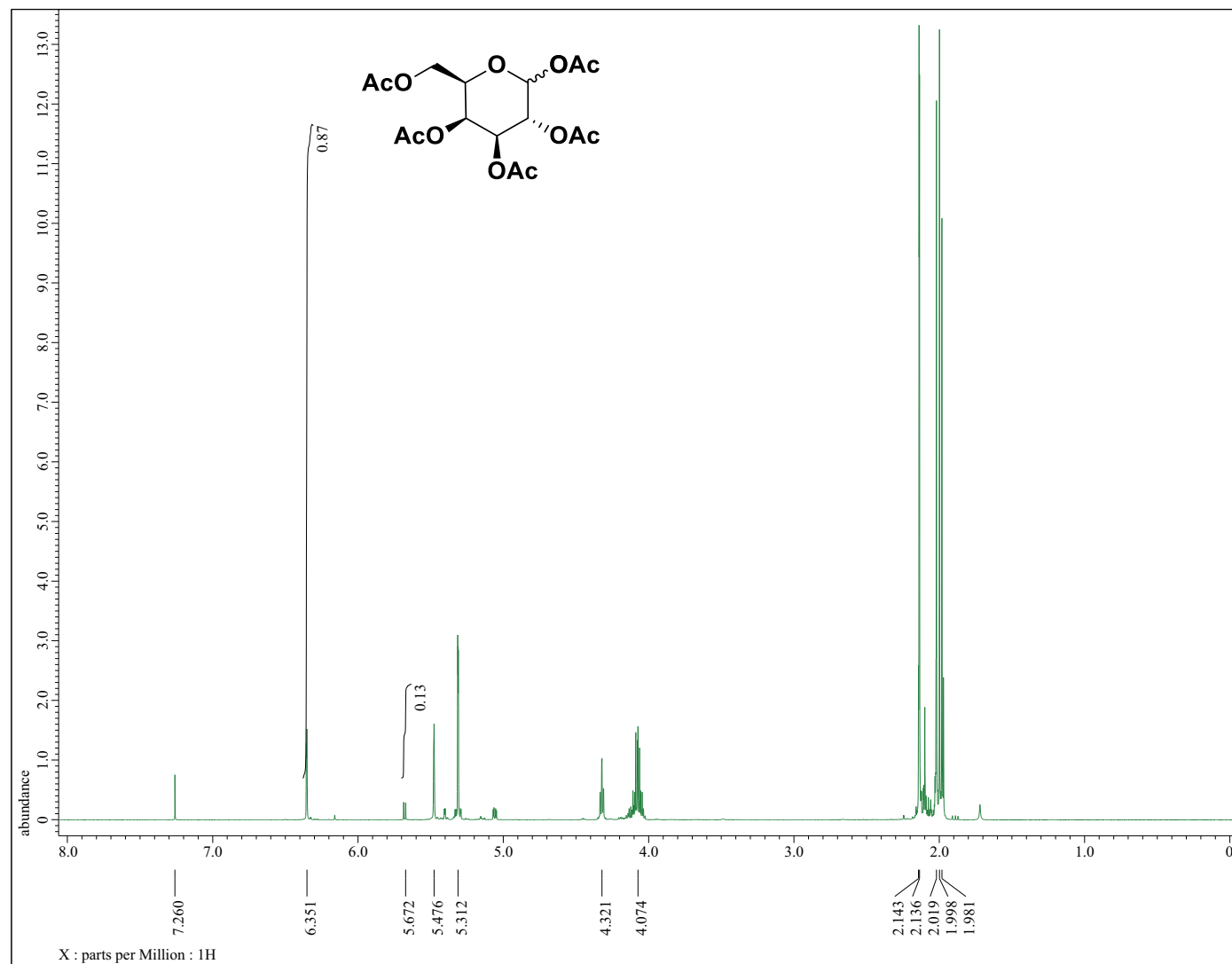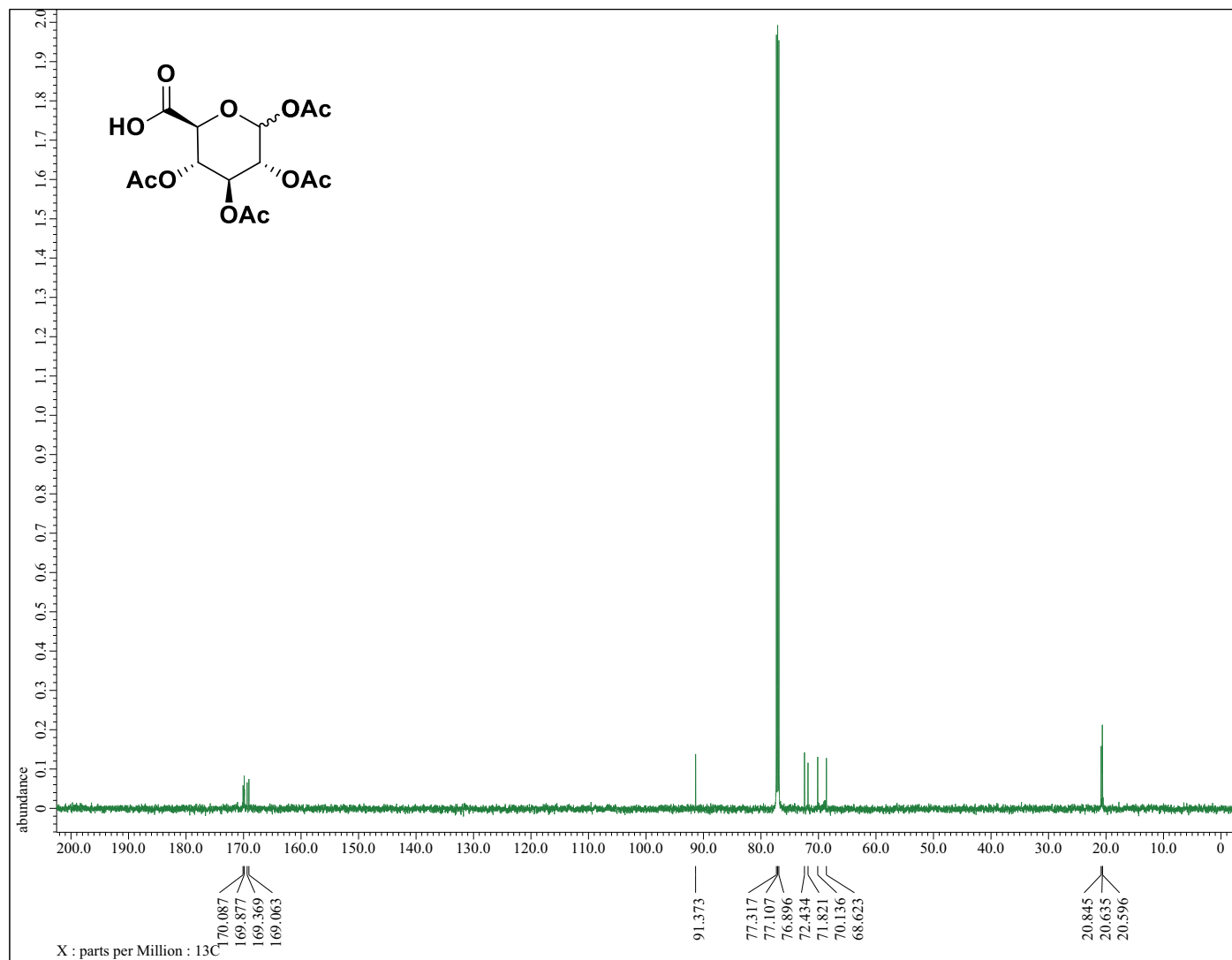
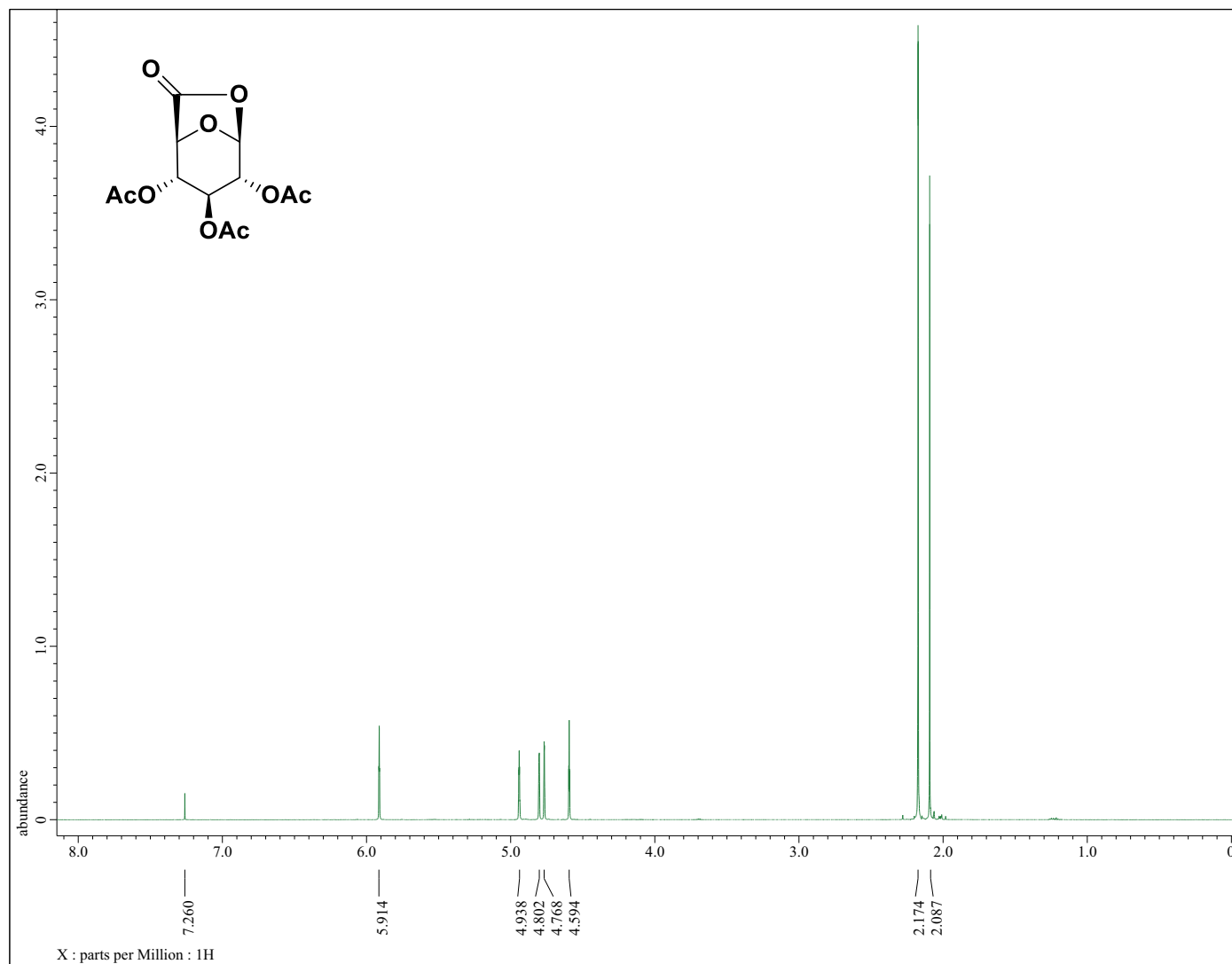^{1}H NMR of Compound **59** [Acetyl-2,3,4,6-tetra-*O*-acetyl-*α*/*β*-D-galactopyranoside]
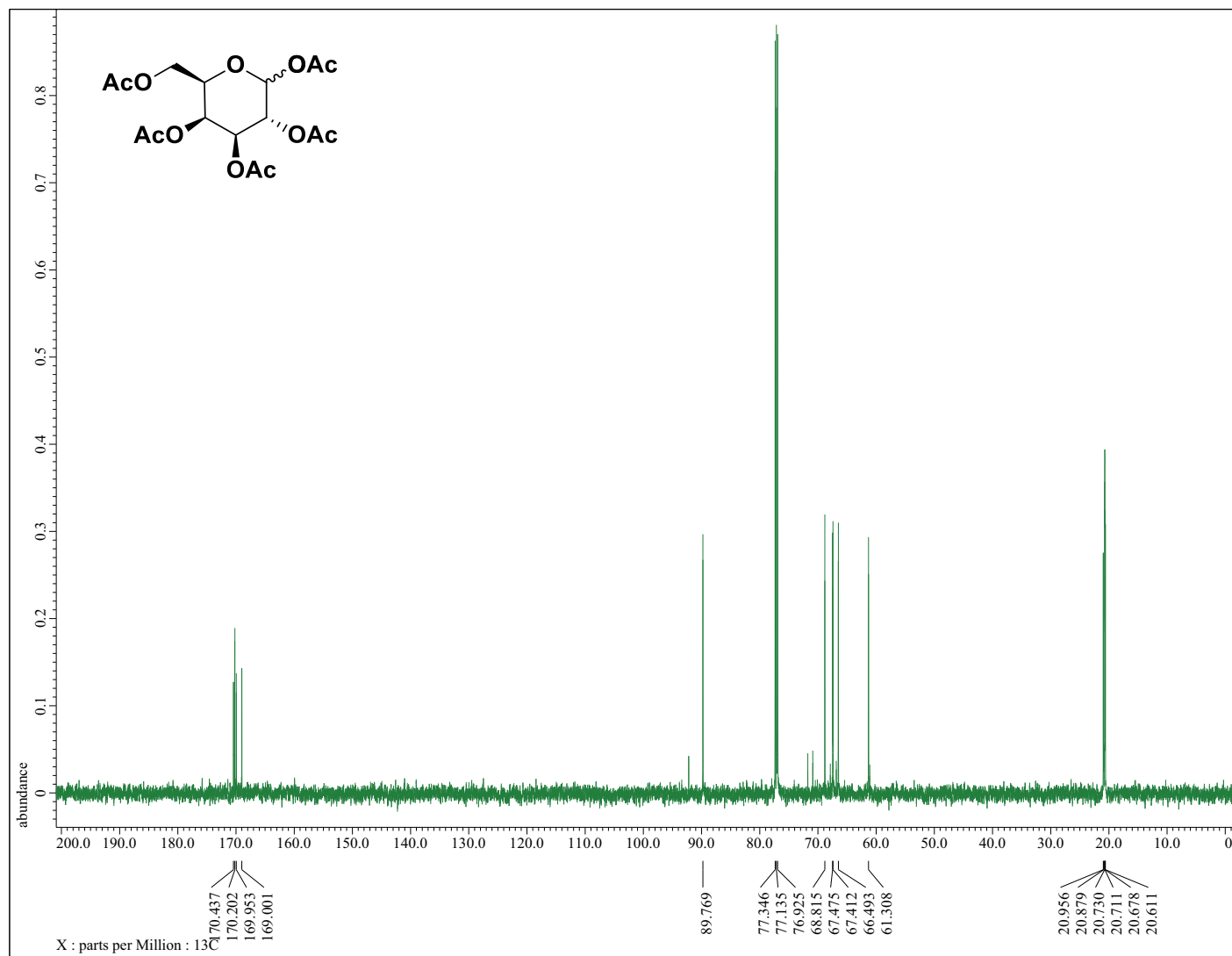
^{13}C NMR of Compound **59** [Acetyl-2,3,4,6-tetra-*O*-acetyl-*α*/*ß*-D-galactopyranoside]
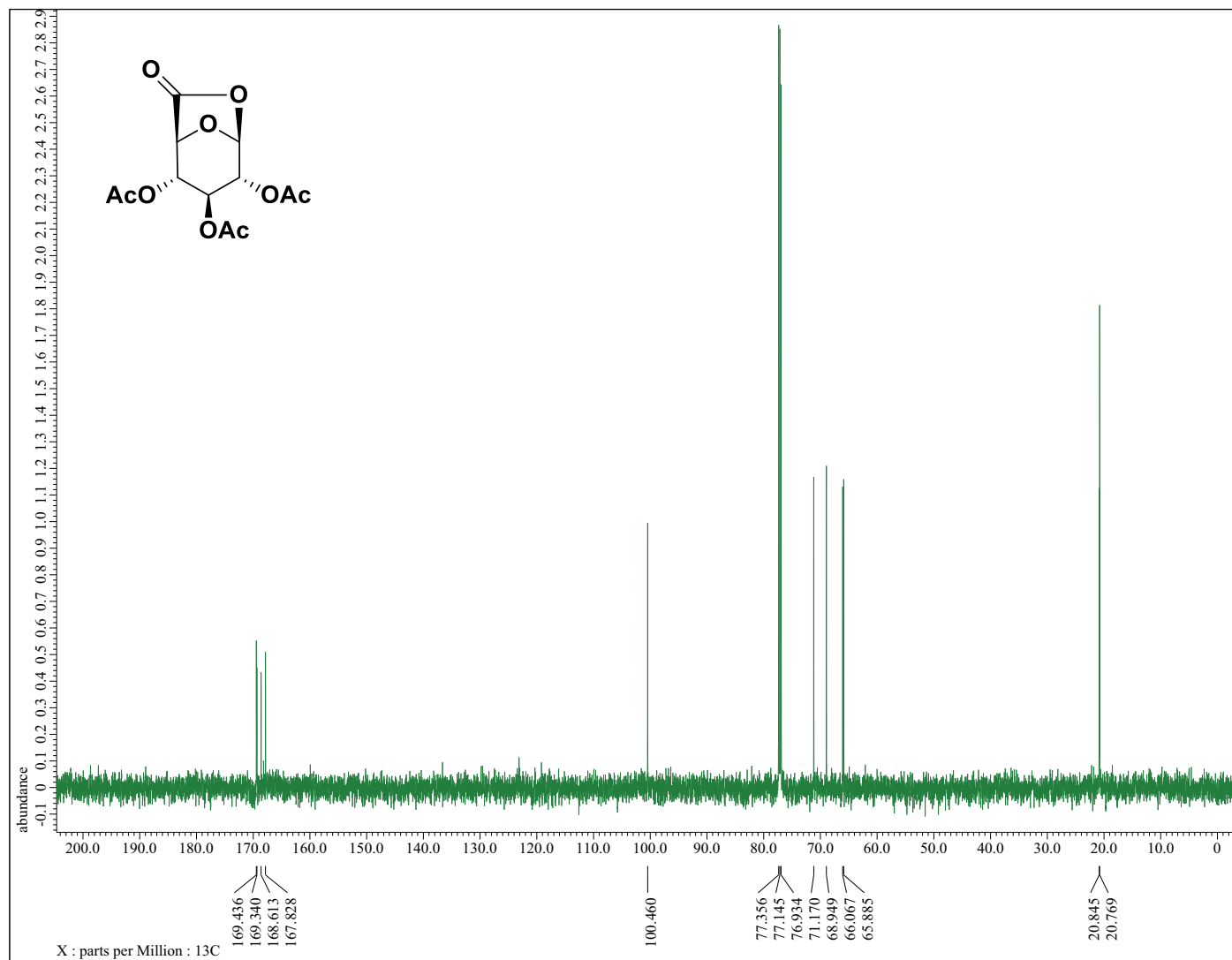
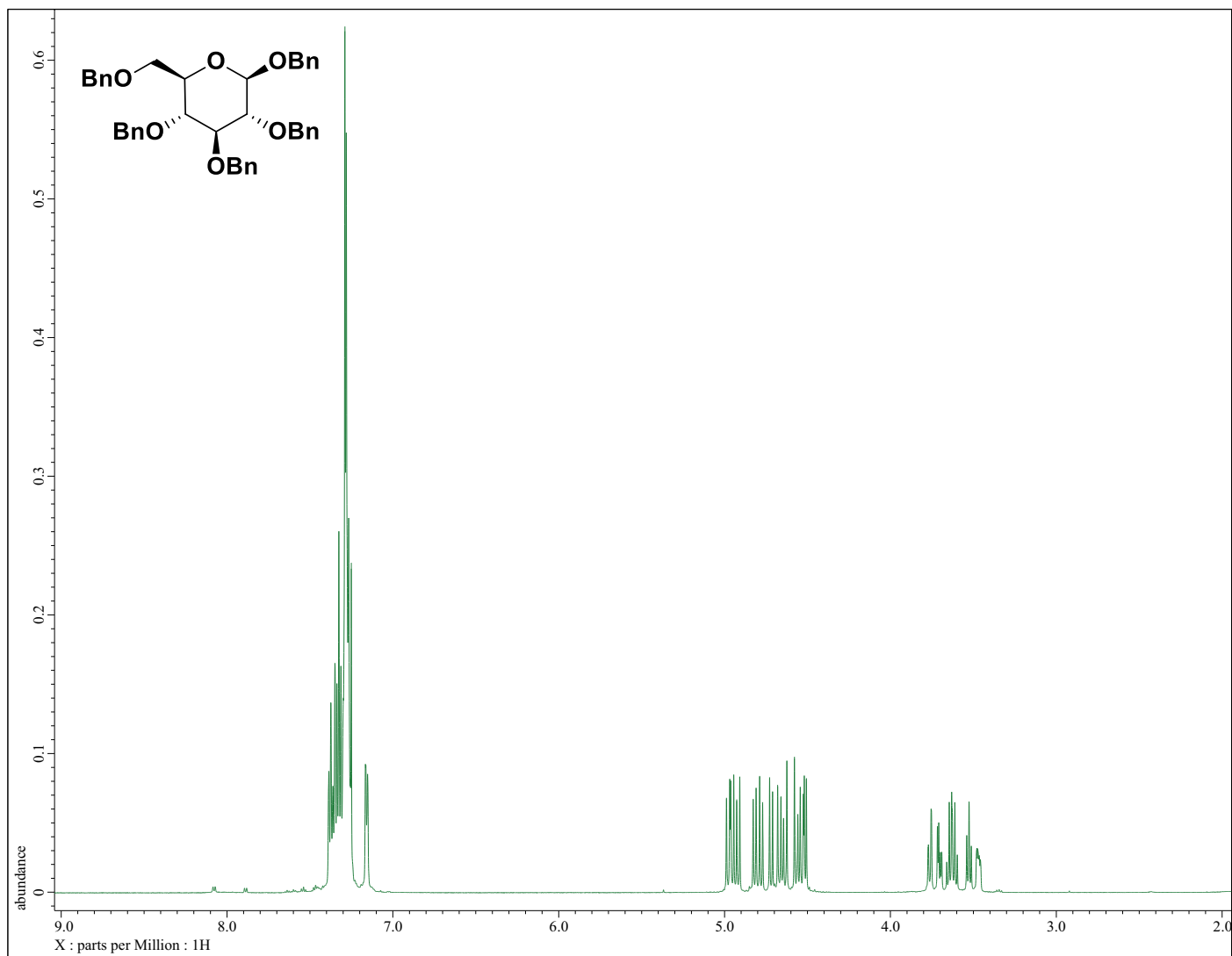¹H NMR of Compound **61** [1,2,3,4-Tetra-*O*-acetyl-*α*/*ß*-D-glucopyranuronic acid]

^{13}C NMR of Compound **61** [1,2,3,4-Tetra-*O*-acetyl-*α*/*β*-D-glucopyranuronic acid]
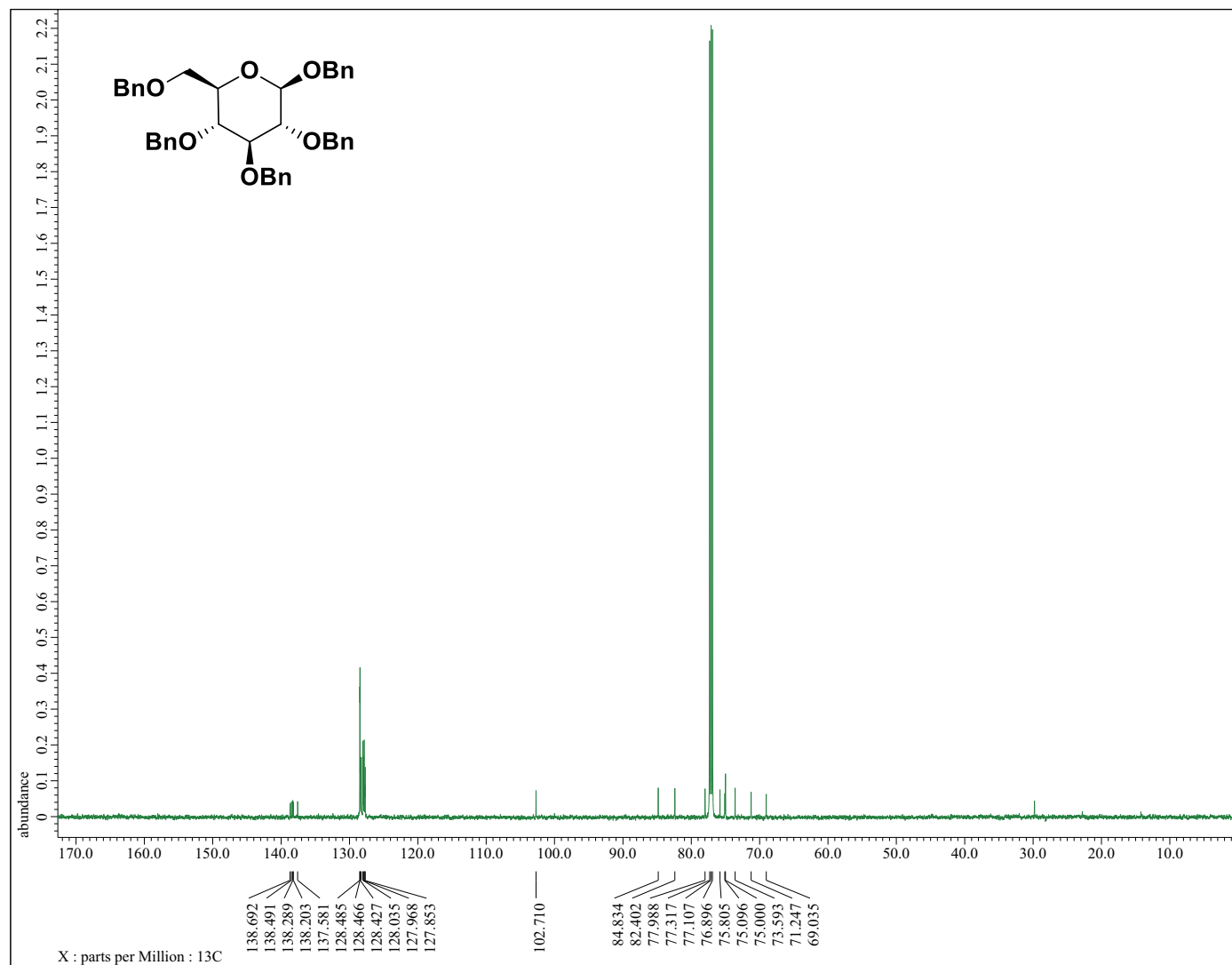
^{1}H NMR of Compound **60** [2,3,4-Tri-*O*-acetyl-D-glucurono-6,1-lactone]

^{13}C NMR of Compound **60** [2,3,4-Tri-*O*-acetyl-D-glucurono-6,1-lactone]

^{1}H NMR of Compound **62** [Benzyl-2,3,4,6-tetra-*O*-benzyl-*β*-D-glucopyranoside]

abundance

X : parts per Million : 13C

138.692
138.491
138.289
138.203
137.581
128.485
128.466
128.427
128.035
127.968
127.853

102.710

84.834
82.402
77.988
77.317
77.107
76.896
75.805
75.096
75.000
73.593
71.247
69.035

^{13}C NMR of Compound **62** [Benzyl-2,3,4,6-tetra-*O*-benzyl-*β*-D-glucopyranoside]
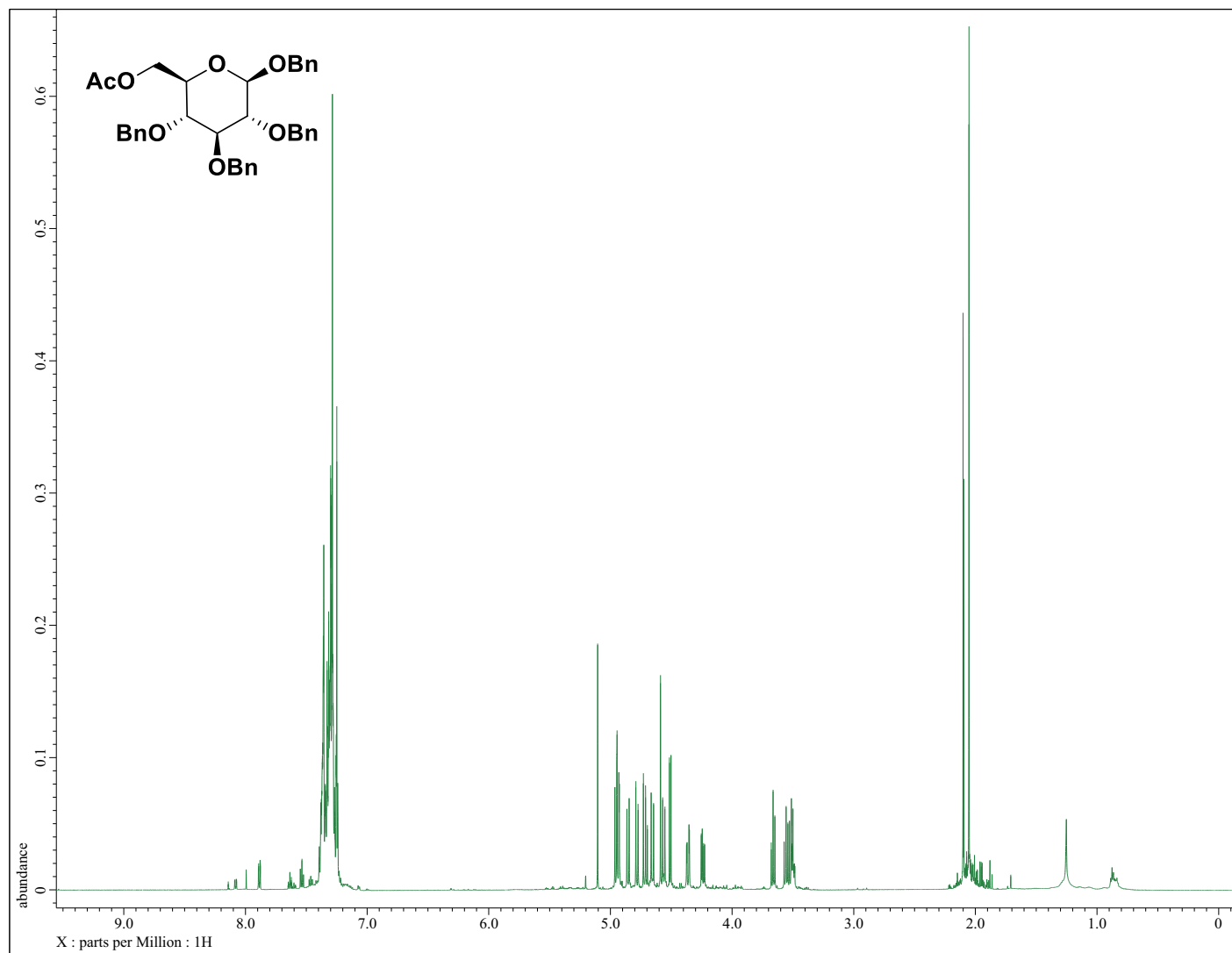
^{1}H NMR of Compound **63** [Benzyl-6-*O*-acetyl-2,3,4-tri-*O*-benzyl-*β*-D-glucopyranoside]

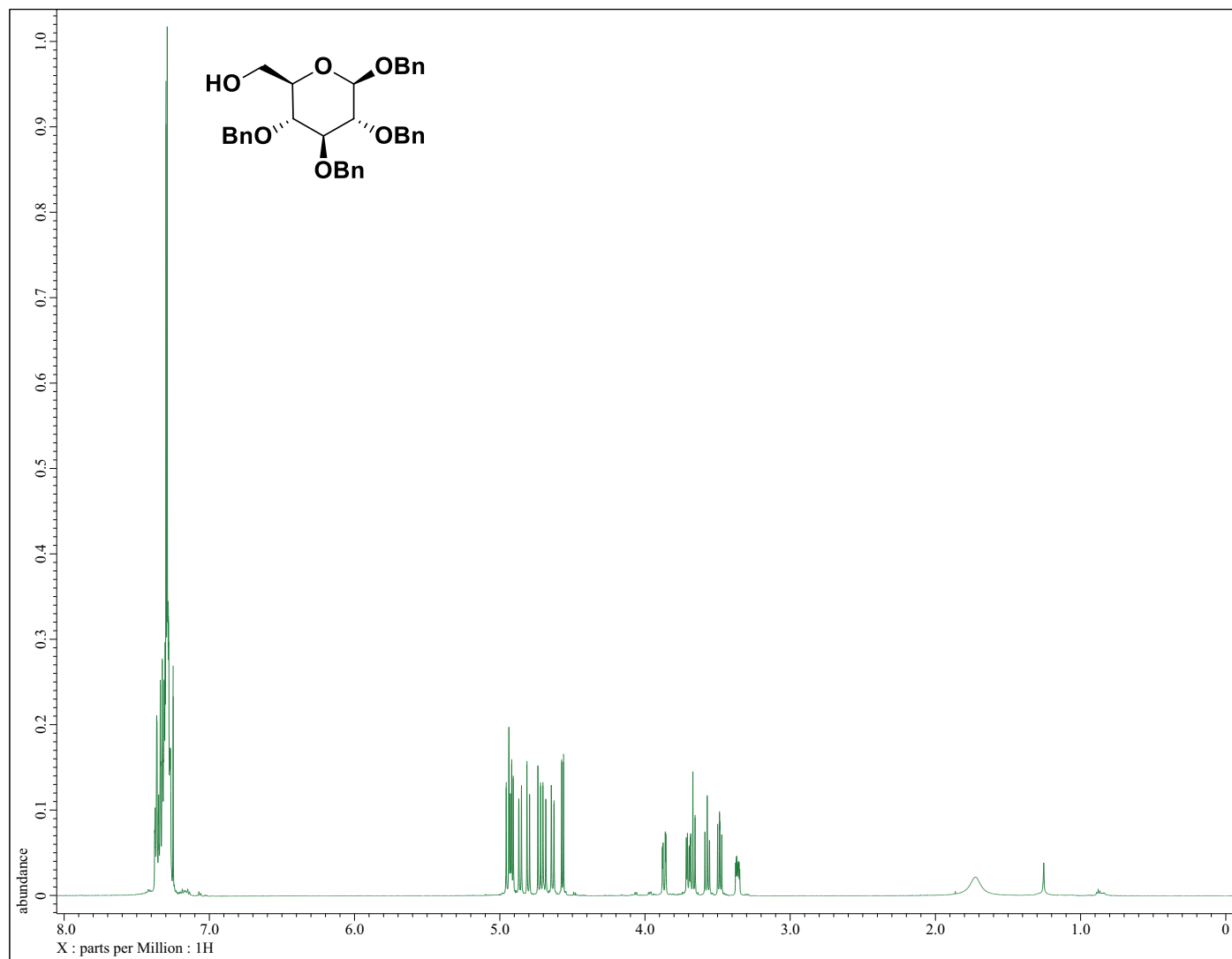^{1}H NMR of Compound **64** [Benzyl-2,3,4-tri-*O*-benzyl-*β*-D-glucopyranoside]

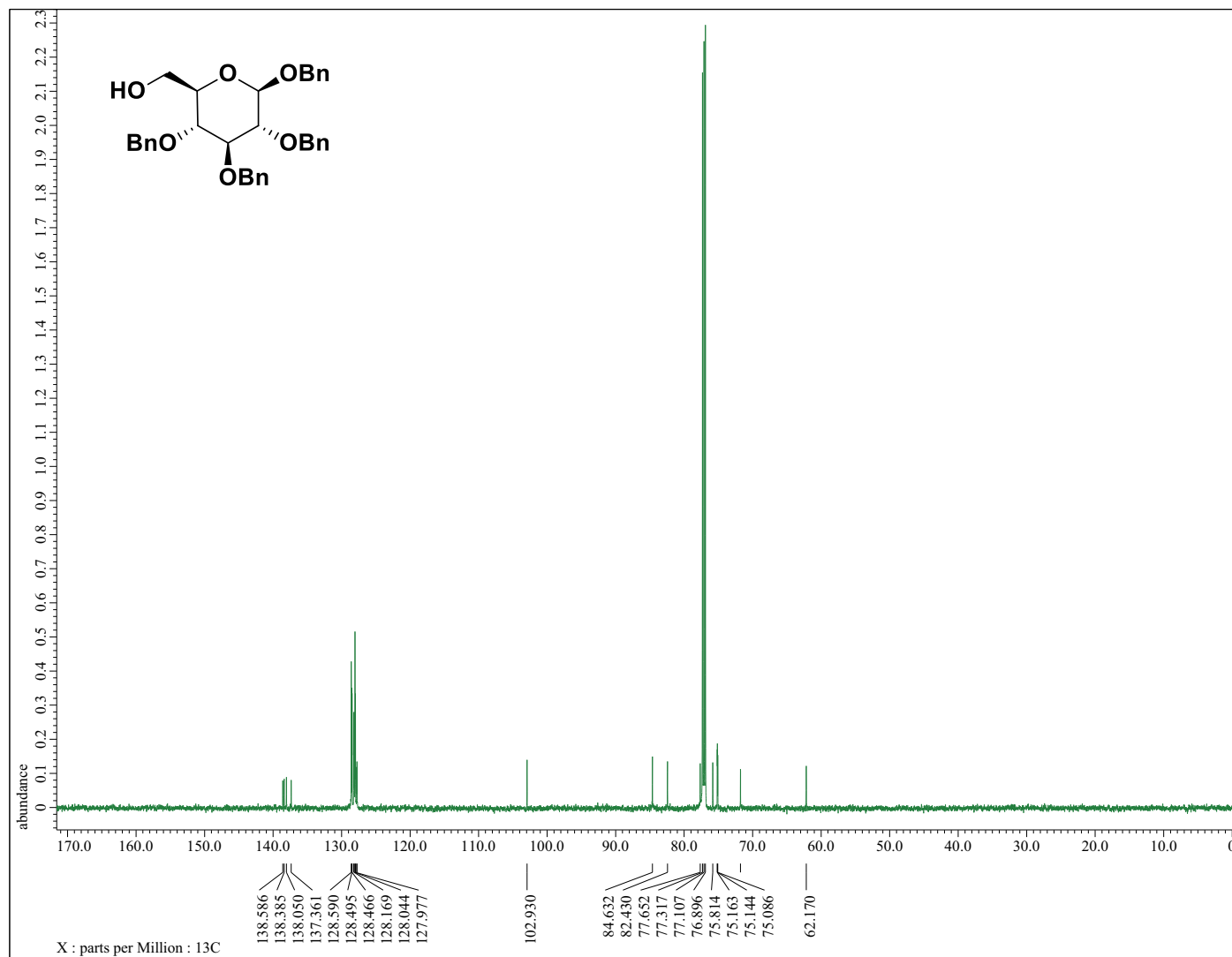^{13}C NMR of Compound **64** [Benzyl-2,3,4-tri-*O*-benzyl-*β*-D-glucopyranoside]
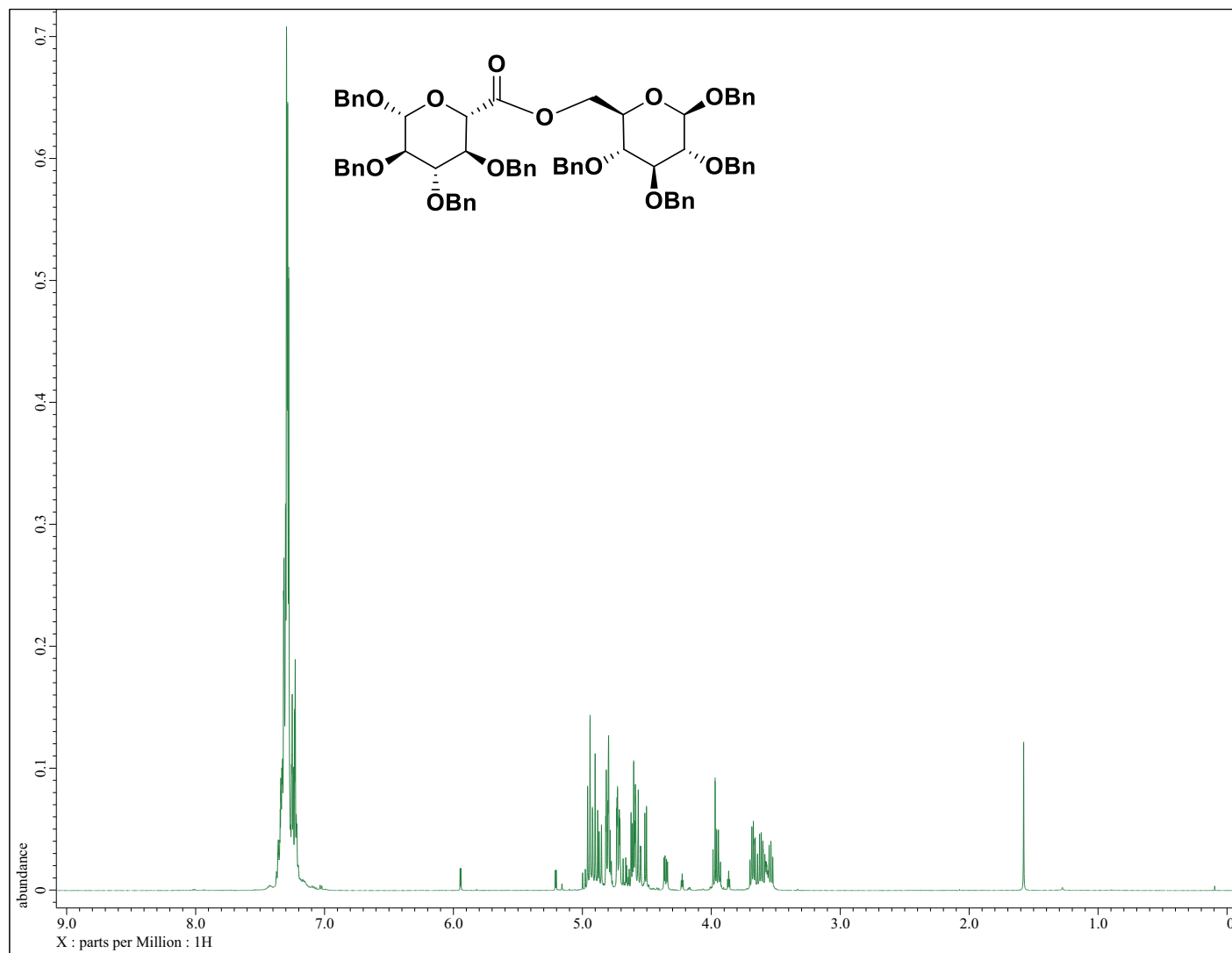
^{1}H NMR of Compound **65** [Benzyl-2,3,4-tri-O-benzyl-*β*-D-glucopyranosyl-(6→6')-(benzyl-2,3,4-tri-O-benzyl-*β*-D-glucopyranuronate)]
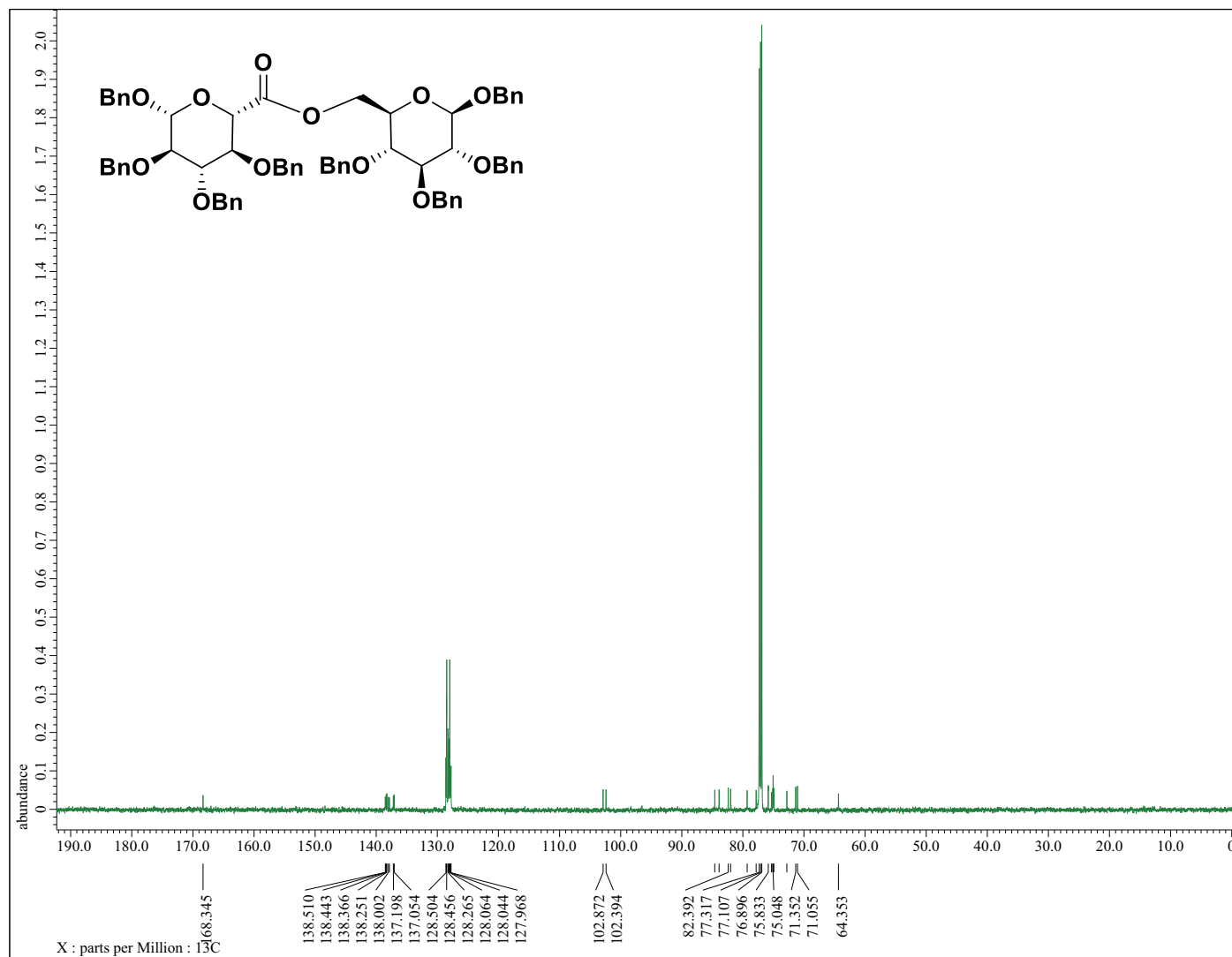
^{13}C NMR of Compound **65** [Benzyl-2,3,4-tri-O-benzyl-*β*-D-glucopyranosyl-(6→6')-(benzyl-2,3,4-tri-O-benzyl-*β*-D-glucopyranuronate)]

311
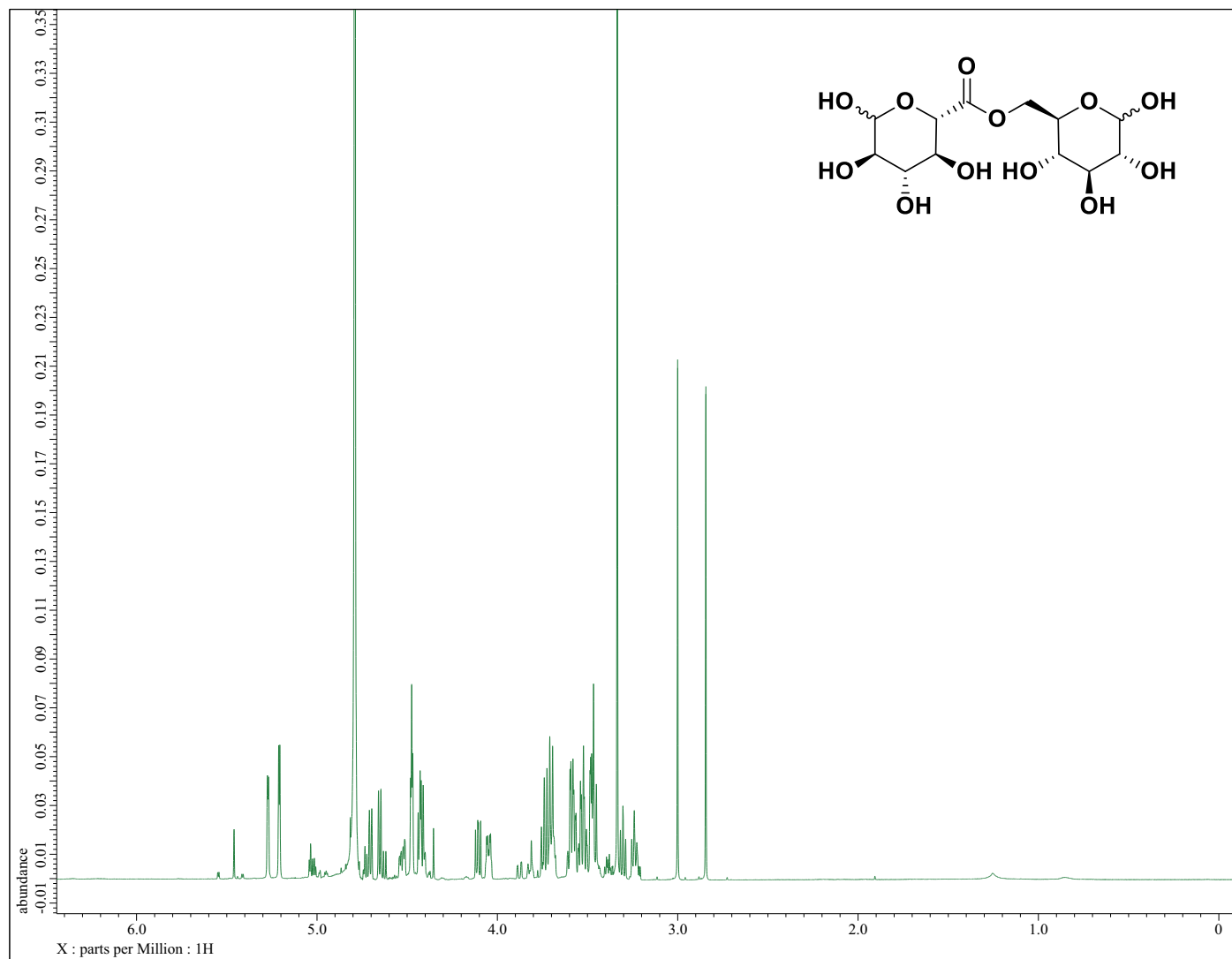
^{1}H NMR of Compound **66** [*α*/*ß*-D-Glucopyranosyl-(6→6')-*α*/*ß*-glucopyranuronate]

Magnified ^{1}H NMR of Compound **66** [*α/ß*-D-Glucopyranosyl-(6→6')-*α/ß*-glucopyranuronate]
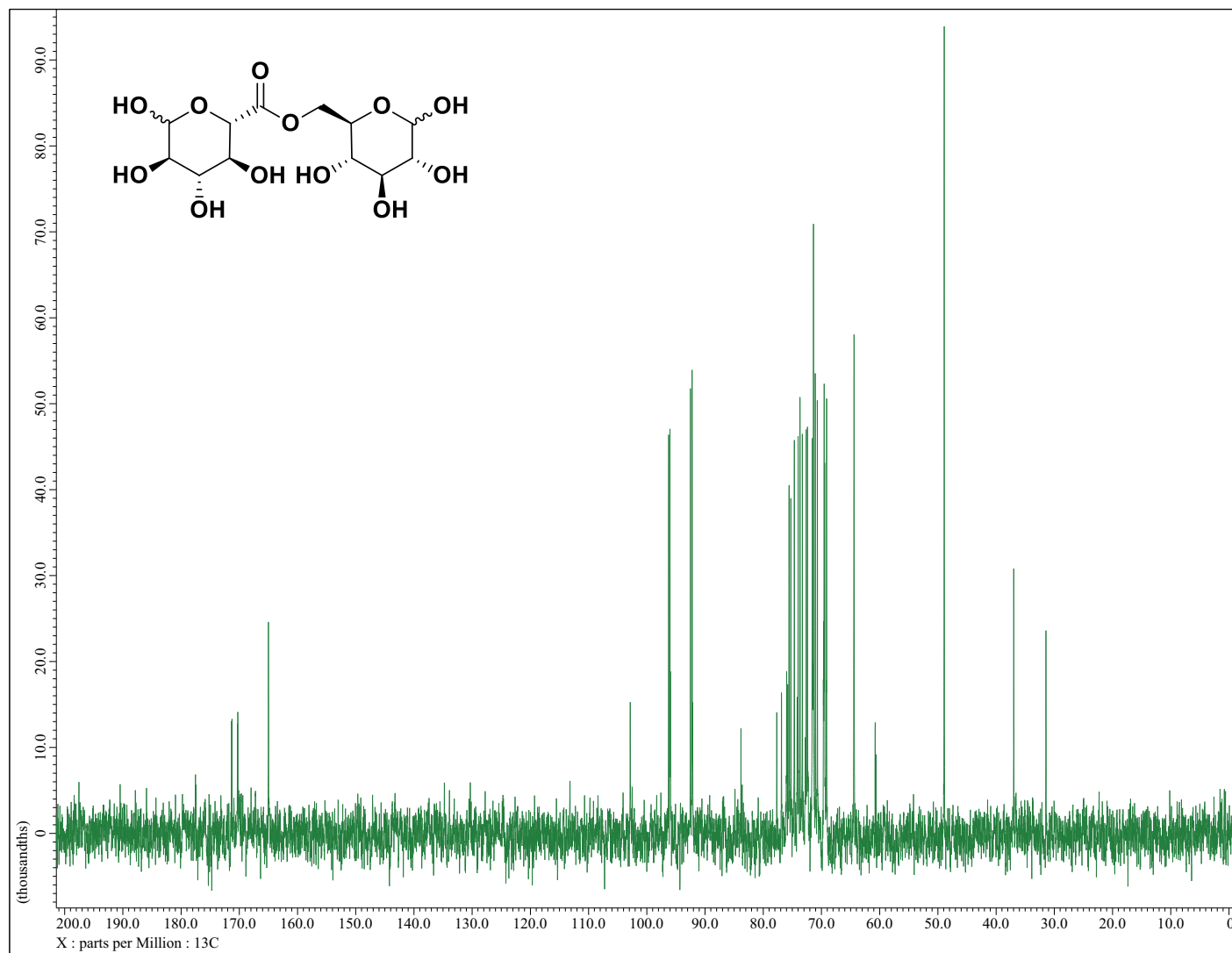
^{13}C NMR of Compound **66** [*α/ß*-D-Glucopyranosyl-(6→6')-*α/ß*-glucopyranuronate]
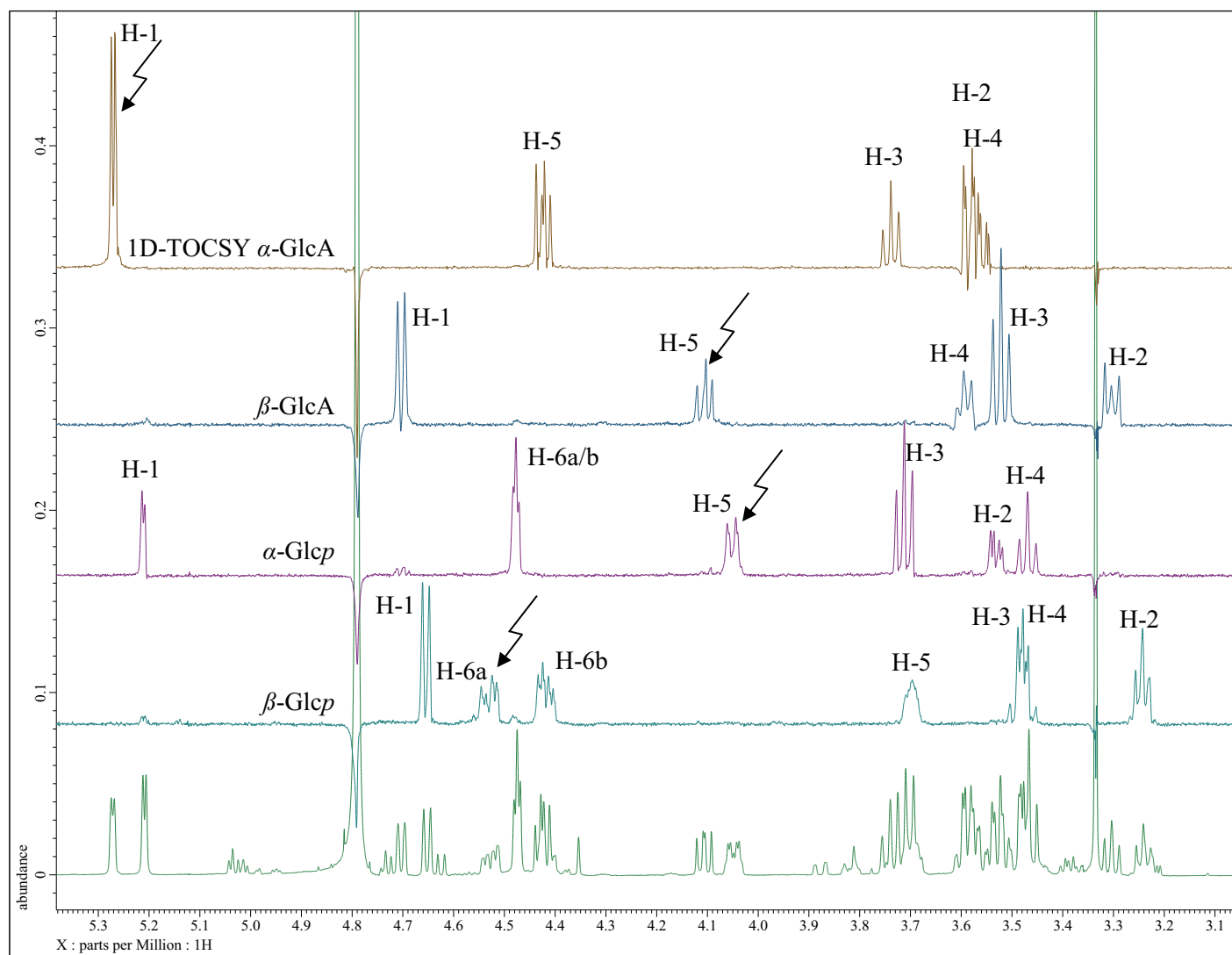
Overlay of ^{1}H NMR (bottom) and 1D TOCSY spectra (500 ms mixing time) of the four spin systems present in Compound **66**.
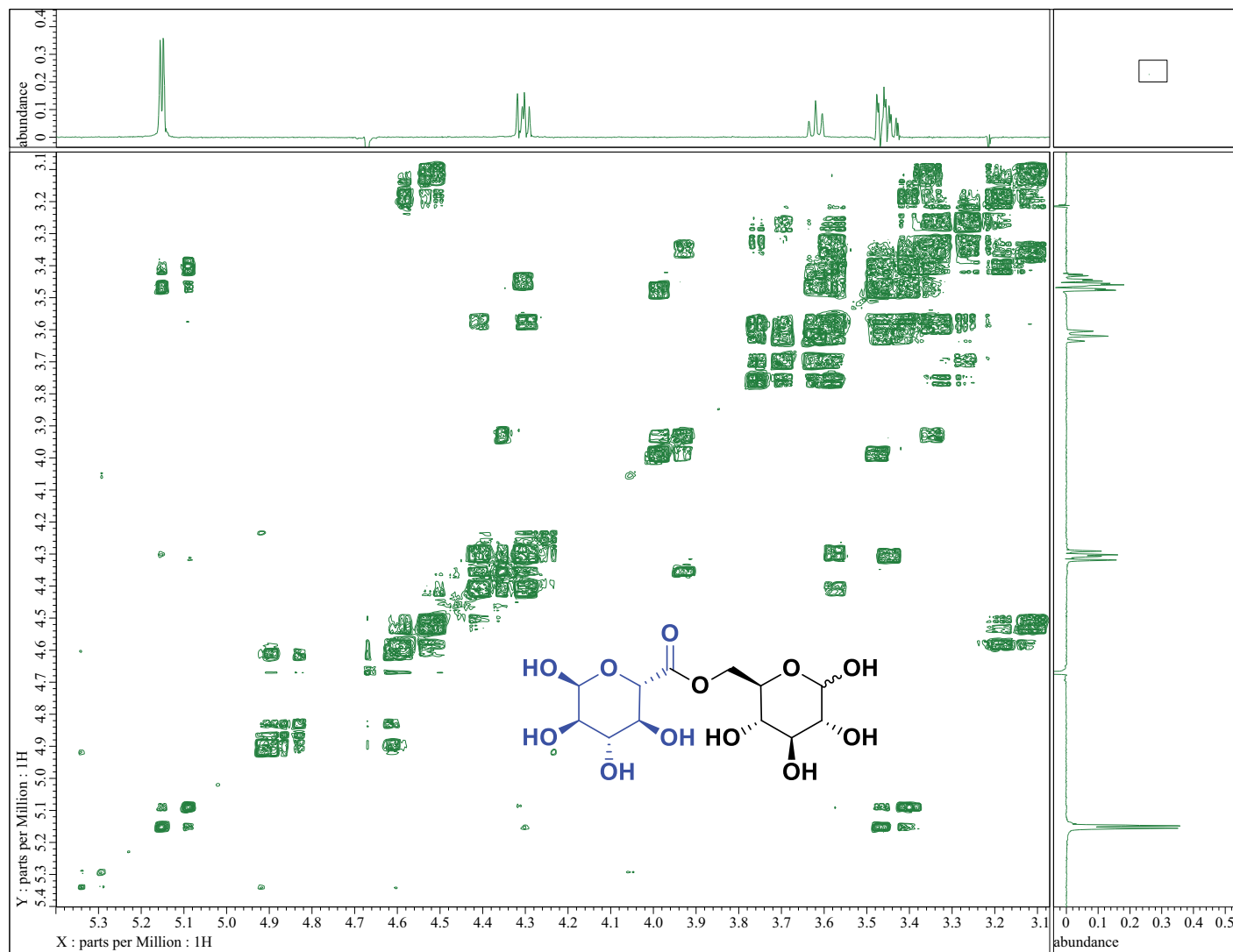
Magnified 2D COSY spectrum and 1D projection of TOCSY of *α*-GlcA of Compound **66**.
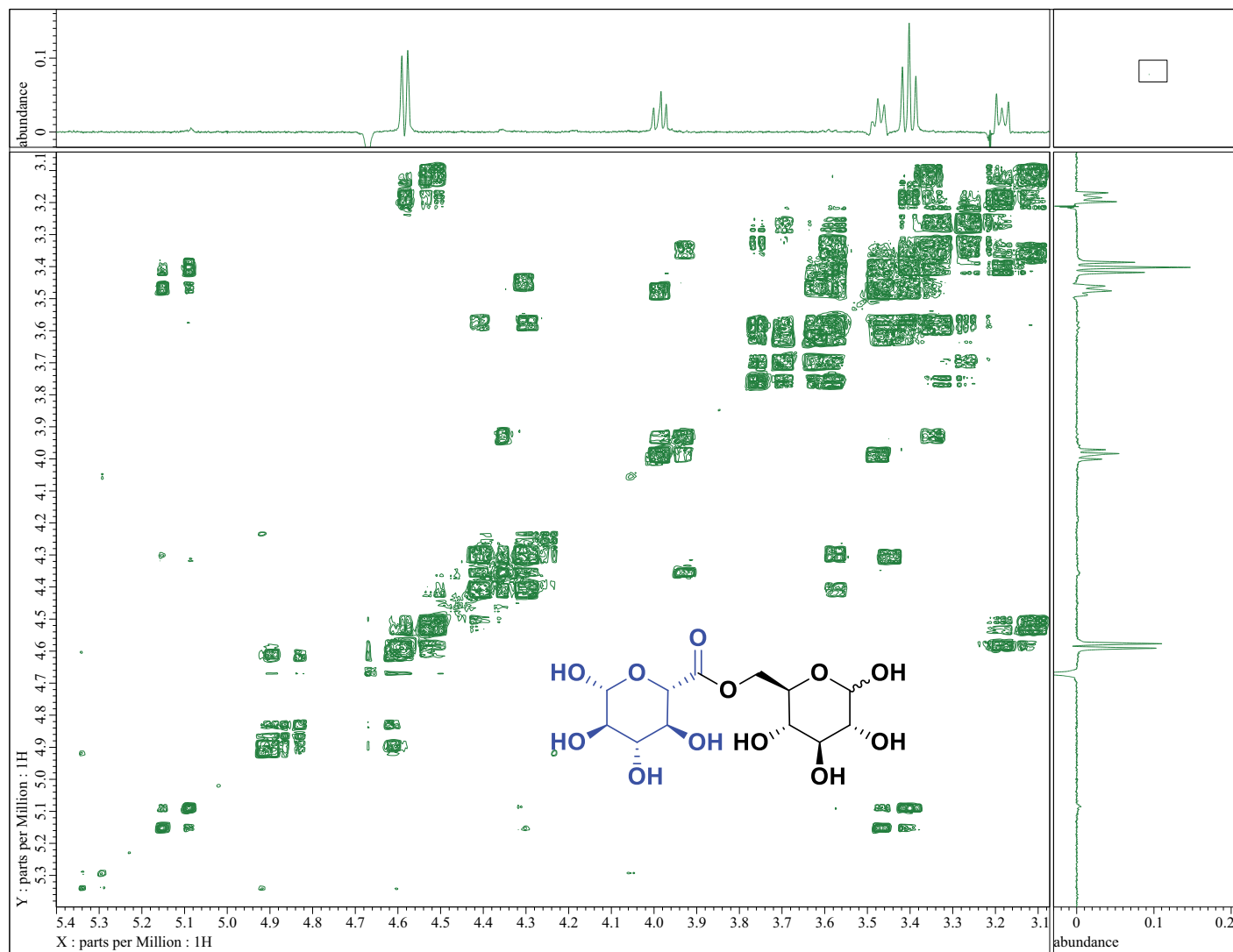
Magnified 2D COSY spectrum with 1D projection of TOCSY of *ß*-GlcA of Compound **66**.
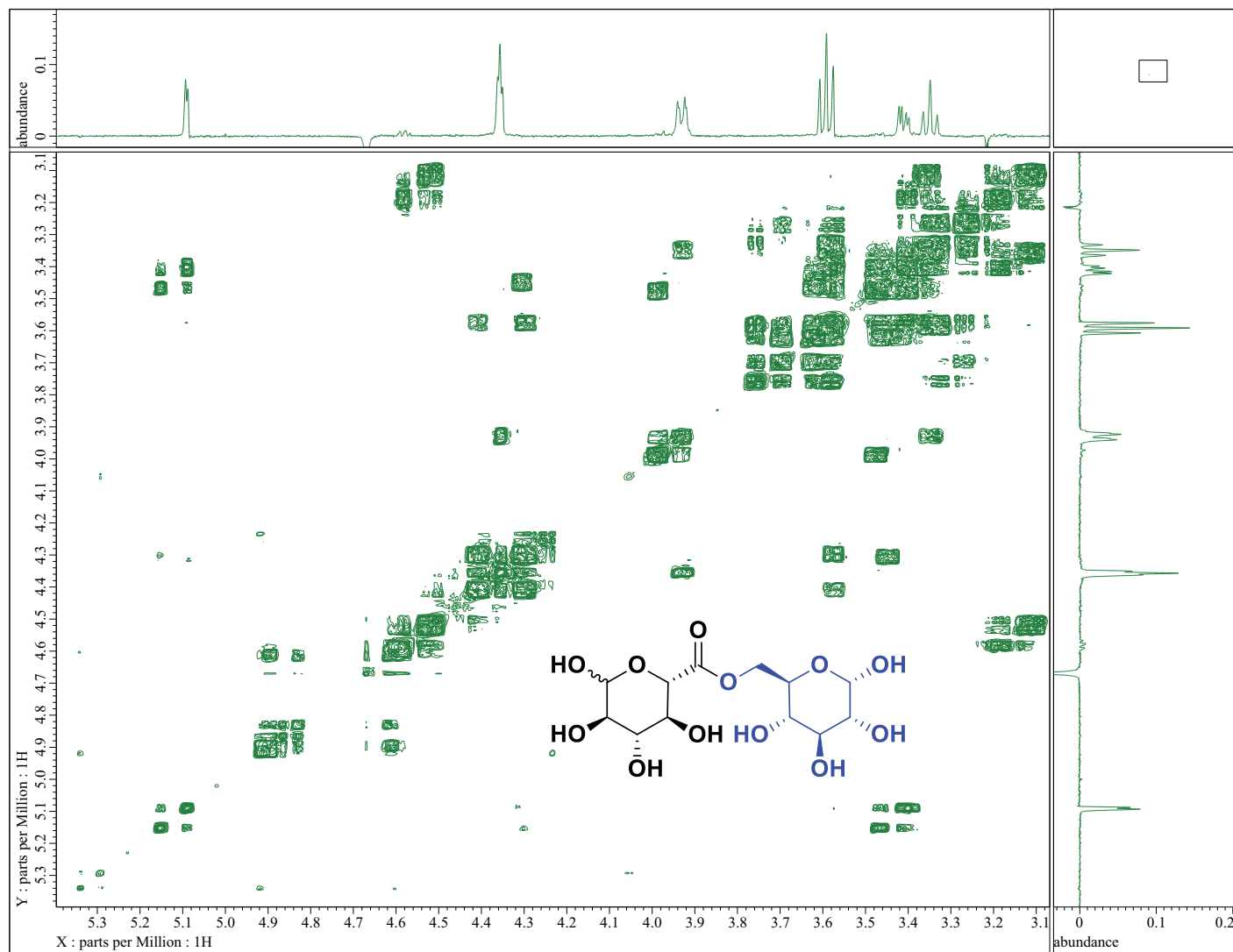
Magnified 2D COSY spectrum with 1D projection of TOCSY of *α*-Glc*p* of Compound **66**.
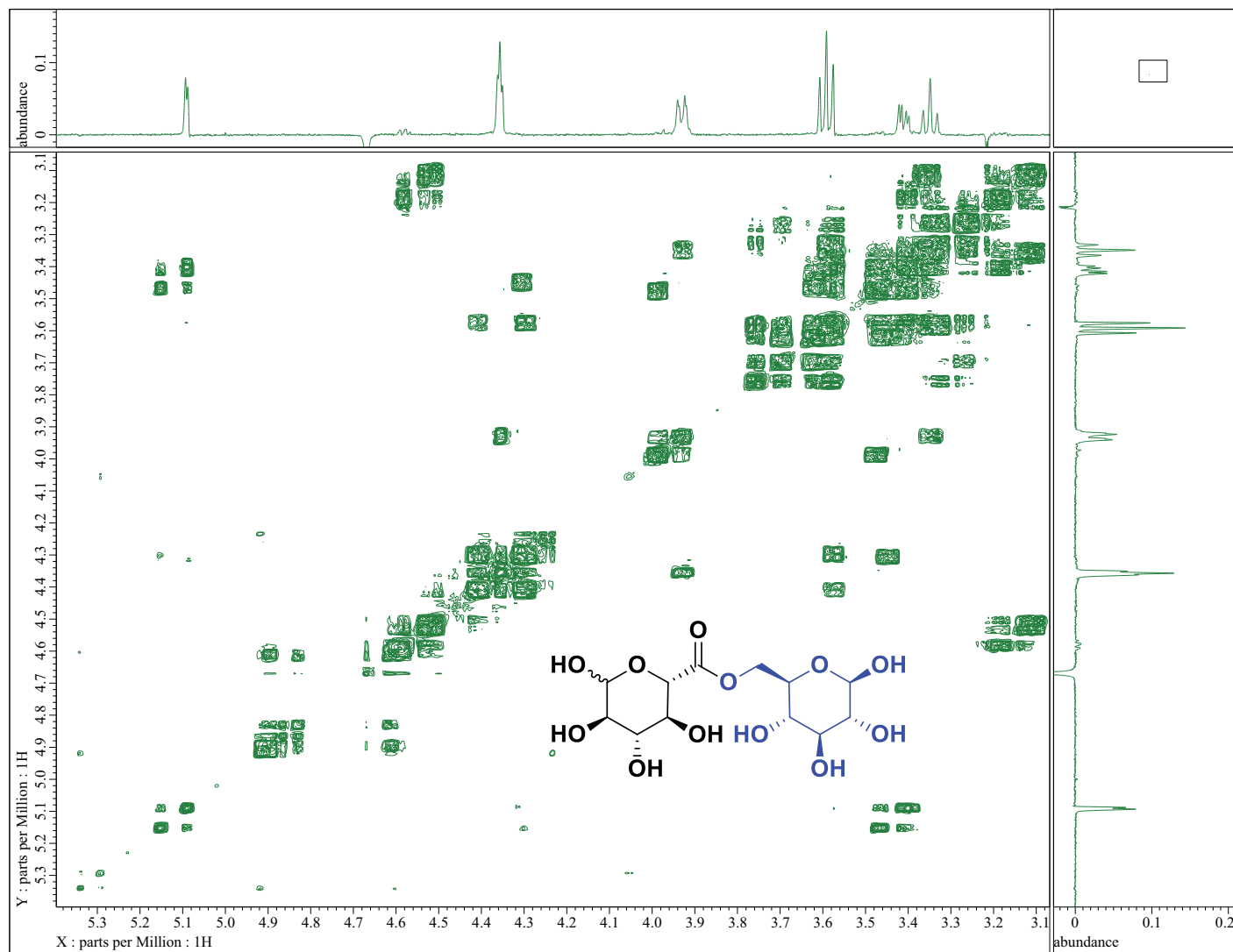
Magnified 2D COSY spectrum with 1D projection of TOCSY of *ß*-Glc*p* of Compound **66**.
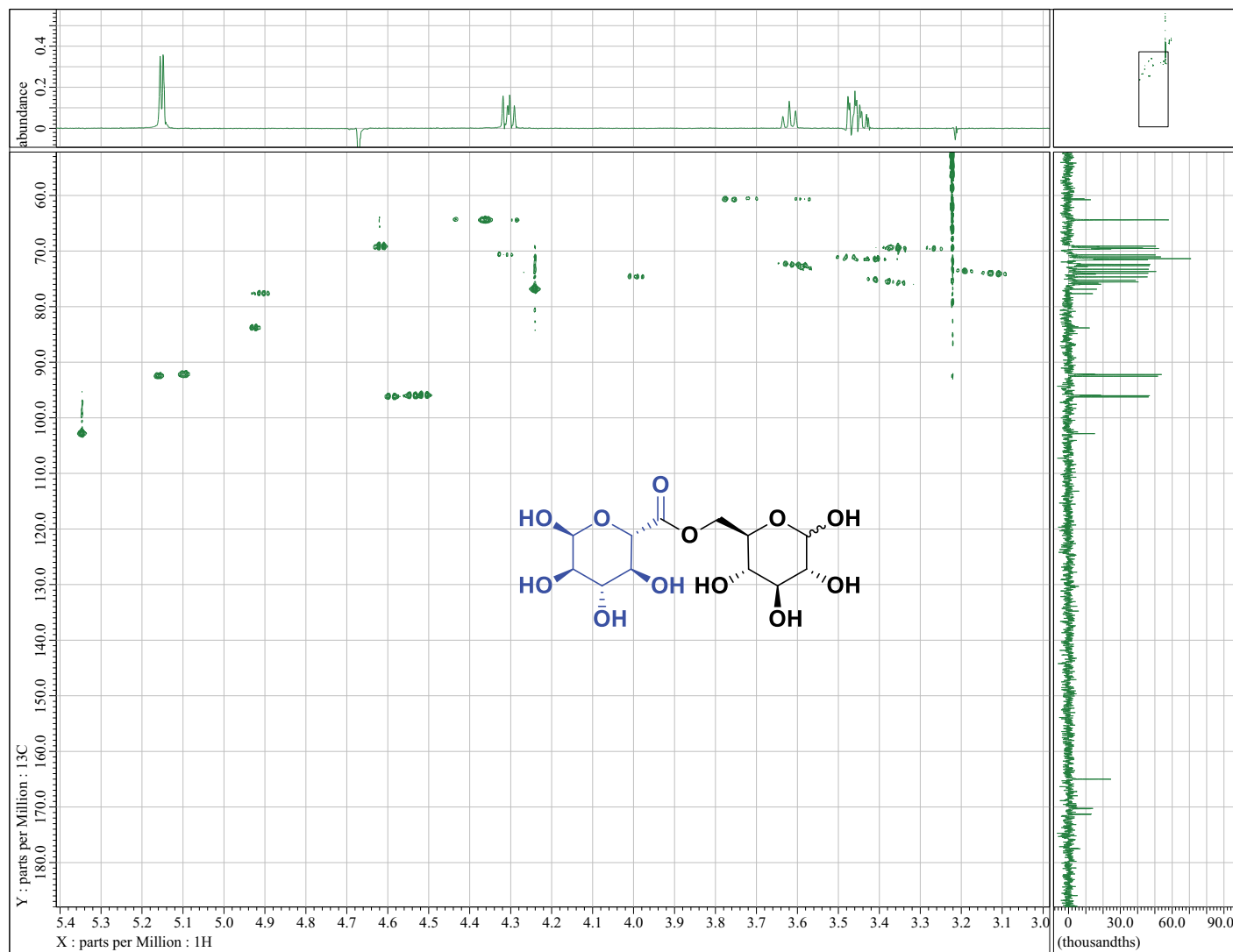
2D HMQC spectrum with 1D projection of TOCSY of *α*-GlcA of Compound **66**.
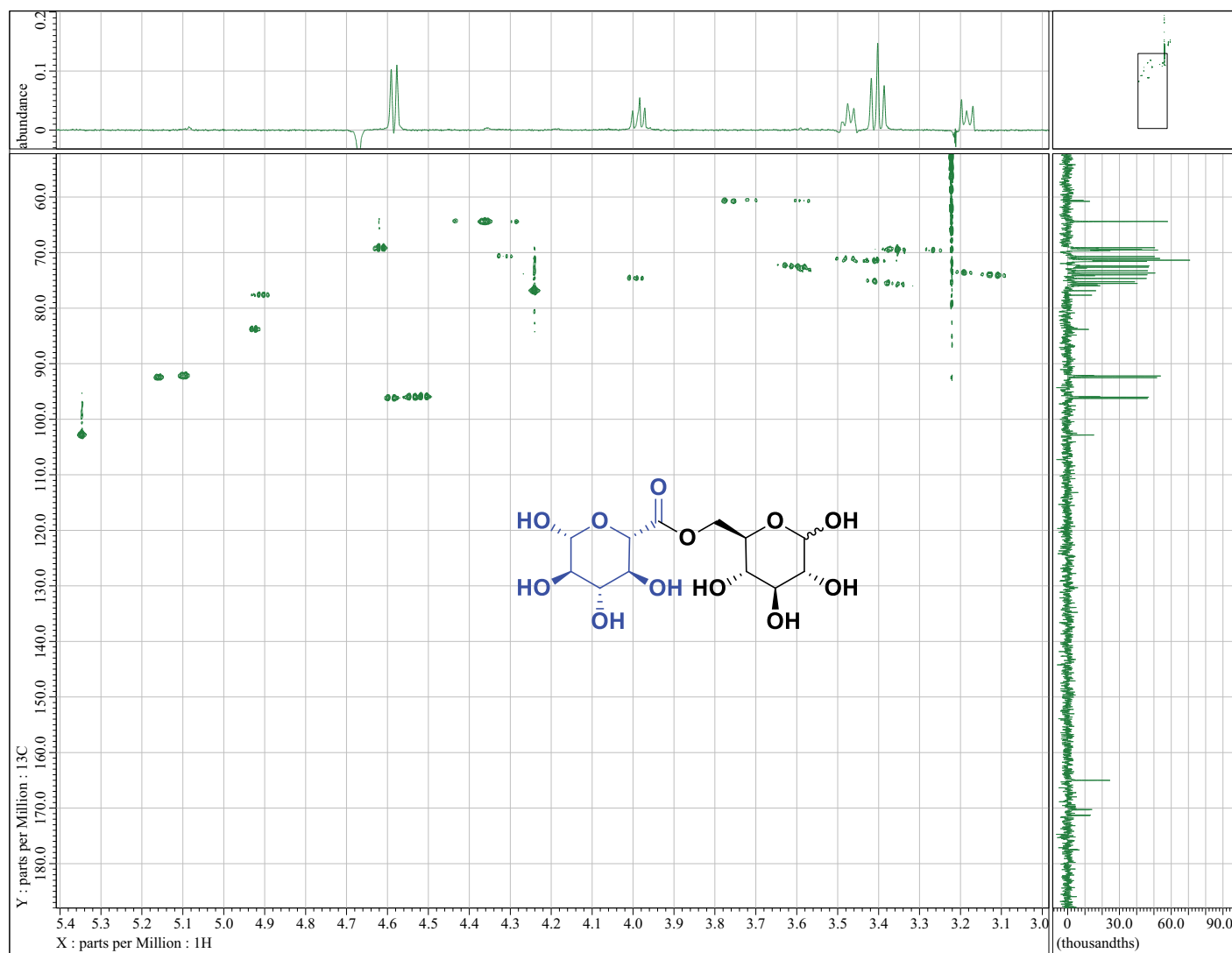
2D HMQC spectrum with 1D projection of TOCSY of *ß*-GlcA of Compound **66**.
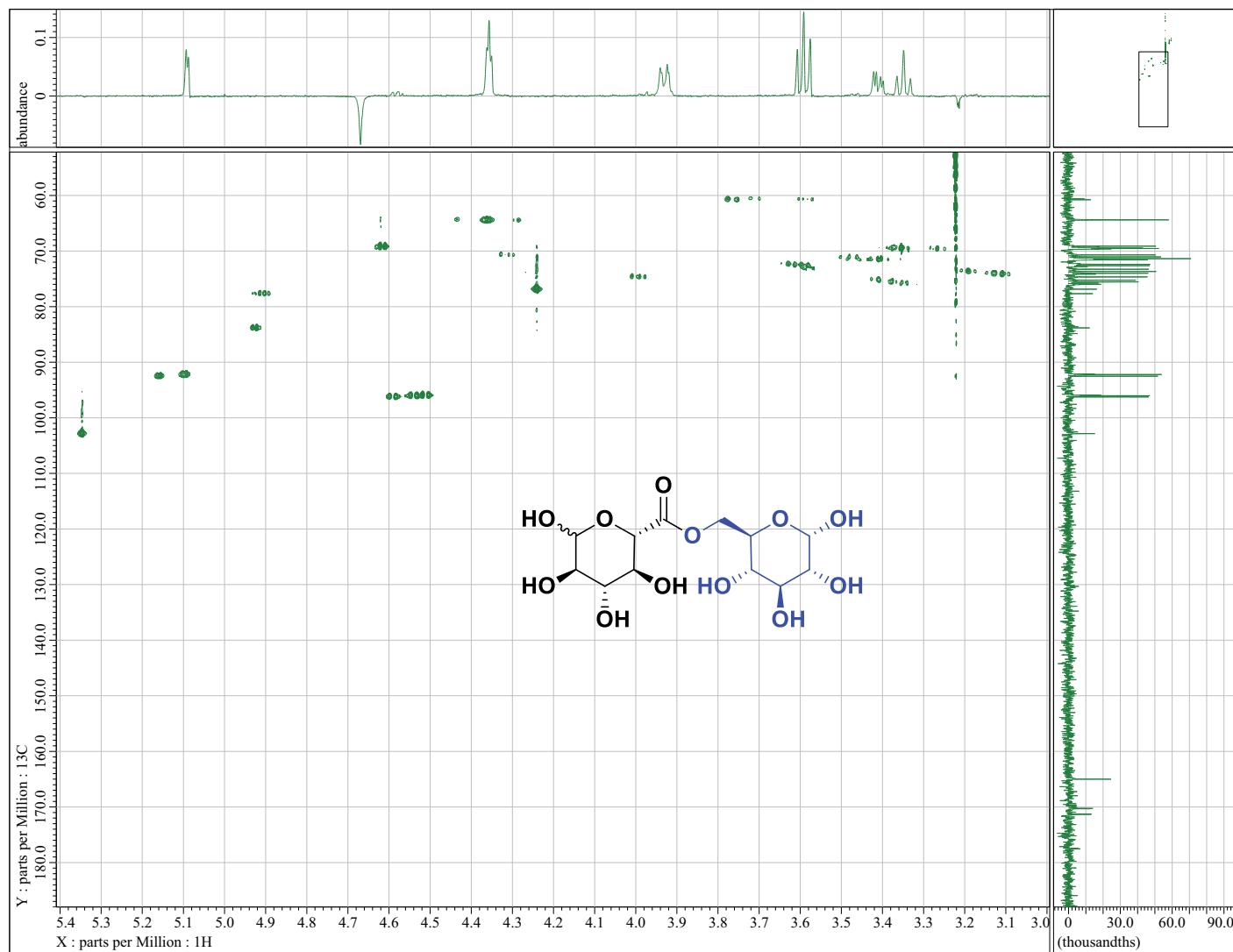
2D HMQC spectrum with 1D projection of TOCSY of *α*-Glc*p* of Compound **66**.
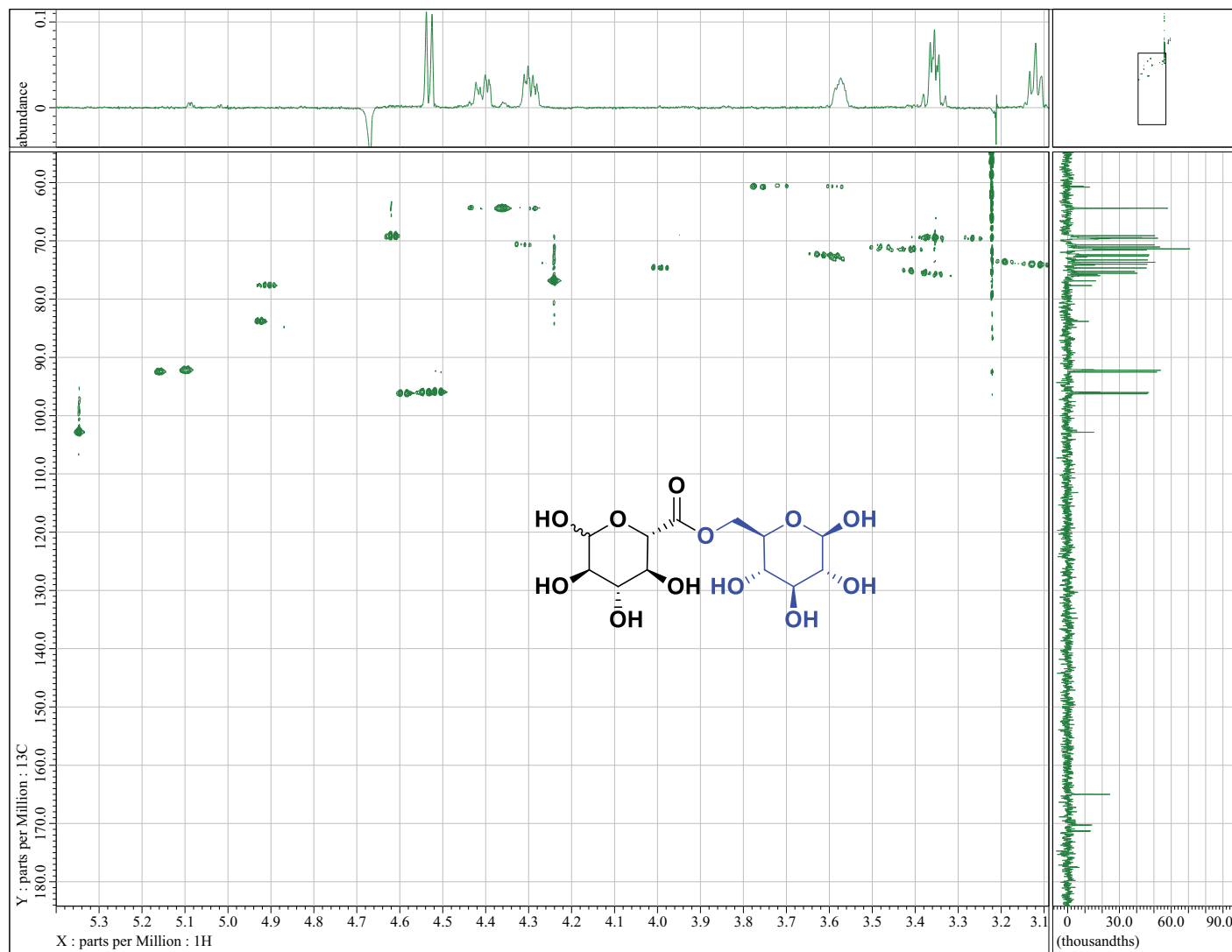
2D HMQC spectrum with 1D projection of TOCSY of *ß*-Glc*p* of Compound **66**.
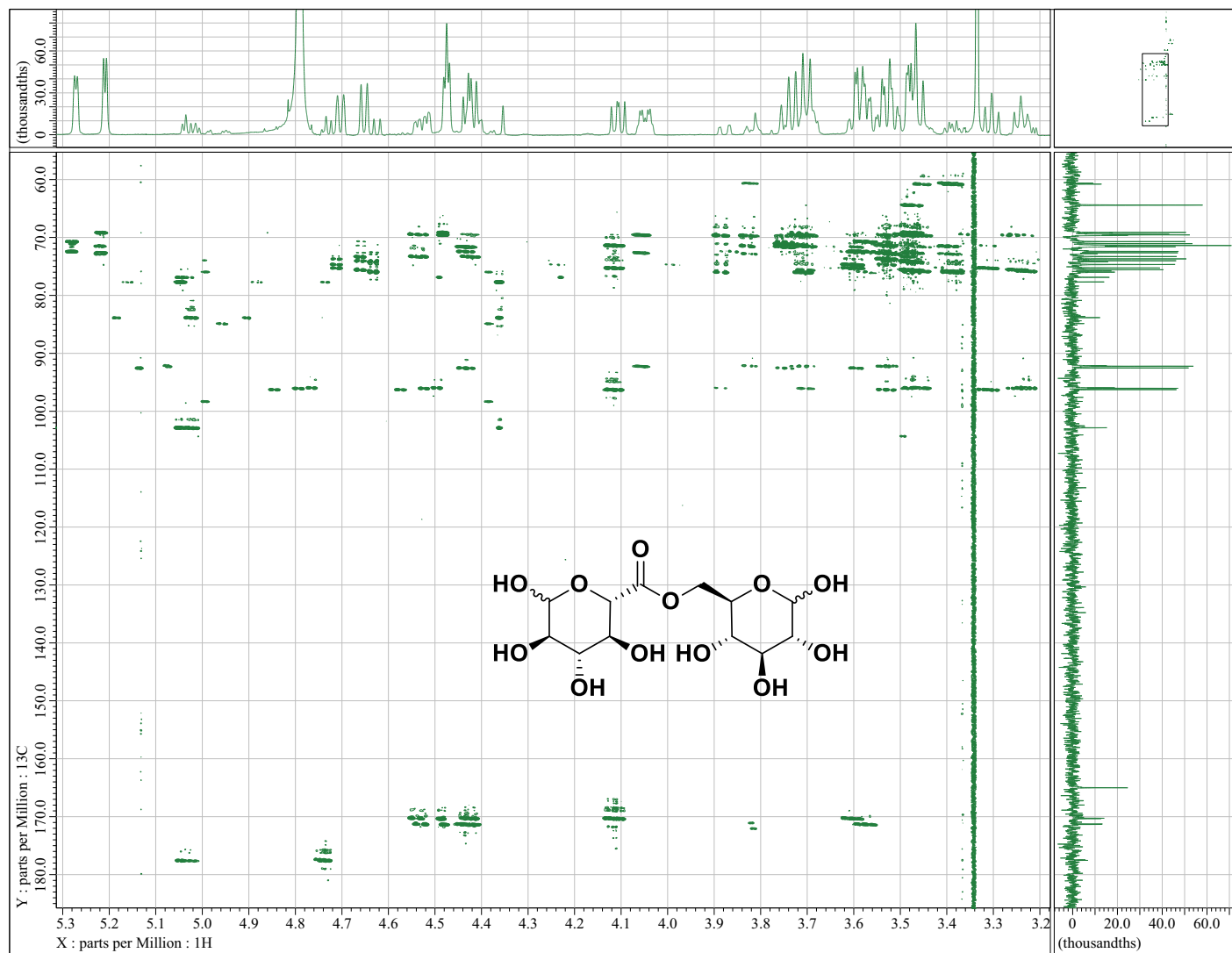
2D HMBC spectrum of Compound **66**.
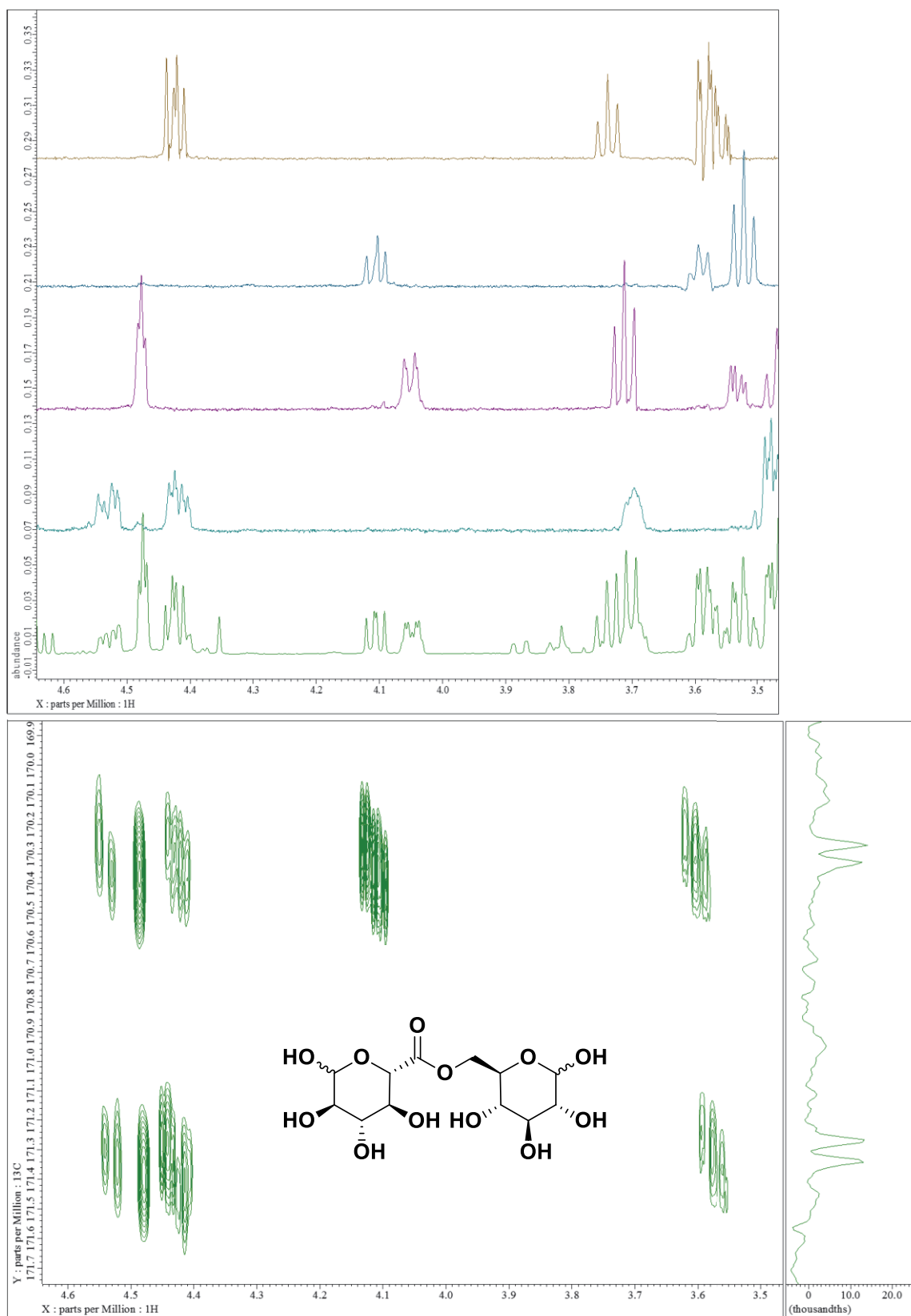
Overlay of 1D TOCSY spectra and magnified 2D HMBC spectrum of Compound **66** showing the 2- and 3-bond correlations of the ester linkage.

Tabular representation of the chemical shift assignments and coupling constants for the four monosaccharide units of **66**.

δ / ppm	α-GlcA	ß-GlcA	α-Glc	ß-Glc
H-1	5.28 (d, 4.2 Hz)	4.71 (d, 8.4 Hz)	5.21 (d, 3.0 Hz)	4.67 (d, 7.8 Hz)
H-2	3.59 (dd, 3.0 Hz, 10.2 Hz)	3.30 (t, 8.1 Hz)	3.53 (dd, 3.6 Hz, 10.2 Hz)	3.24 (t, 8.1 Hz)
H-3	3.74 (t, 9.6 Hz)	3.59 (t, 9.6 Hz)	3.71 (t, 9.3 Hz)	3.48 (m)
H-4	3.55 (dd, 2.1 Hz, 9.9 Hz)	3.52 (t, 9.0 Hz)	3.47 (t, 9.9 Hz)	3.48 (m)
H-5	4.42 (d, 9.6 Hz)	4.11 (d, 8.7 Hz)	4.06 (ddd, 3.0 Hz, 6.0 Hz, 9.6 Hz)	3.69 (m)
H-6a	-/-	-/-	4.48 (d, 3.3 Hz, AB-mixing)	4.53 (dd, 5.7 Hz, 12.3 Hz)
H-6b	-/-	-/-	4.48 (d, 3.3 Hz, AB-mixing)	4.42 (dd, 5.4 Hz, 12.0 Hz)
C-1	92.5	96.2	92.2	96.0
C-2	71.1	73.7	71.4	74.0
C-3	72.3	73.4	72.7	75.7
C-4	71.4	71.1	69.4	69.5
C-5	70.7	74.7	69.1	72.6
C-6	171.25/171.35	170.25/170.35	64.4	64.4

BnO

O

BnO''

OBn

16.44

1.04

2.03

5.02

1.01

1.00

3.05

abundance

9.0   8.0   7.0   6.0   5.0   4.0   3.0   2.0   1.0   0

6.431
6.419

4.824
4.652
4.645
4.633
4.626
4.584
4.568
4.565
4.545
4.064
3.874
3.864
3.860
3.849
3.821
3.803
3.774
3.769
3.756

X : parts per Million : 1H
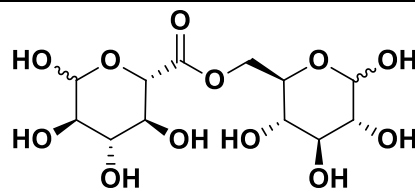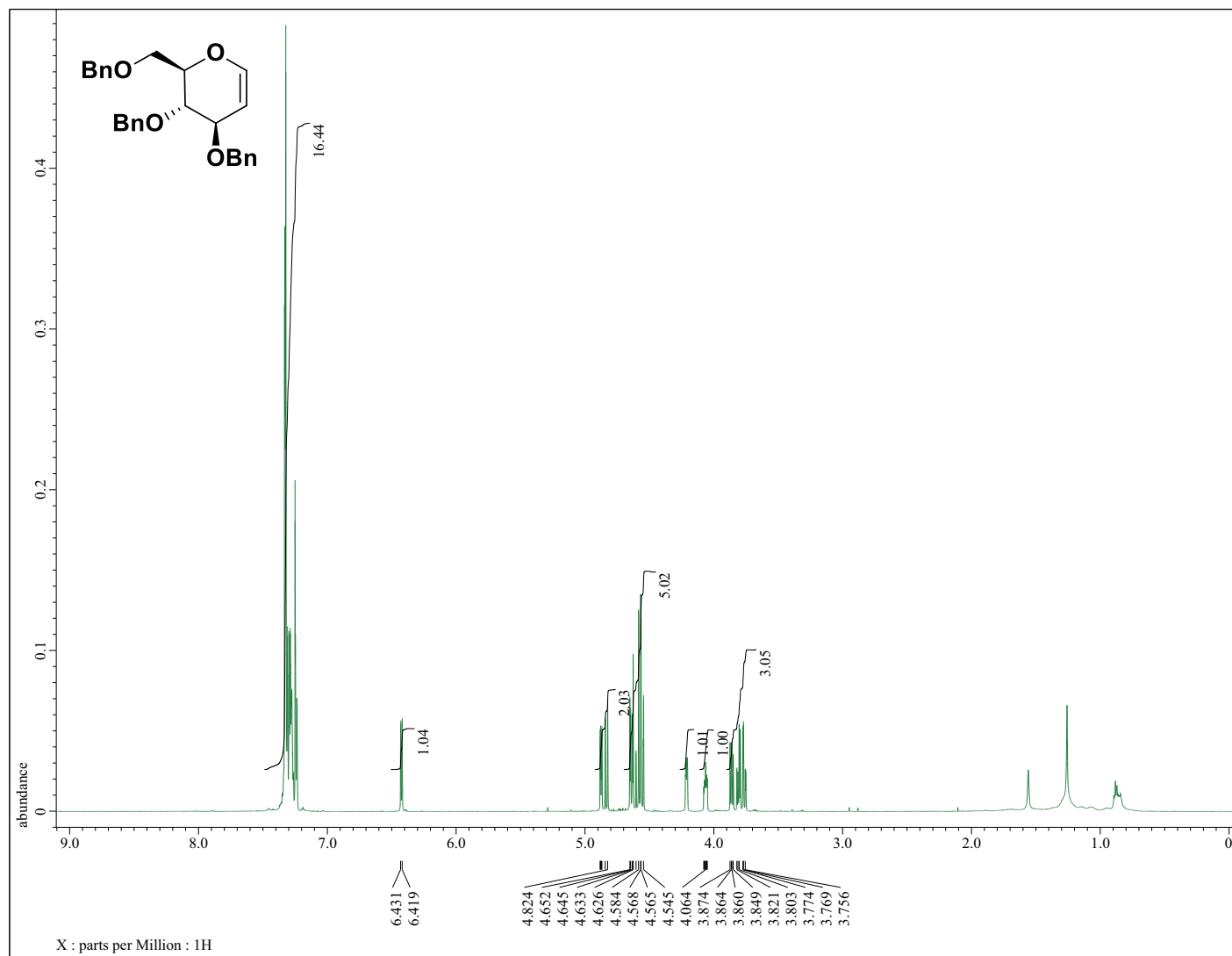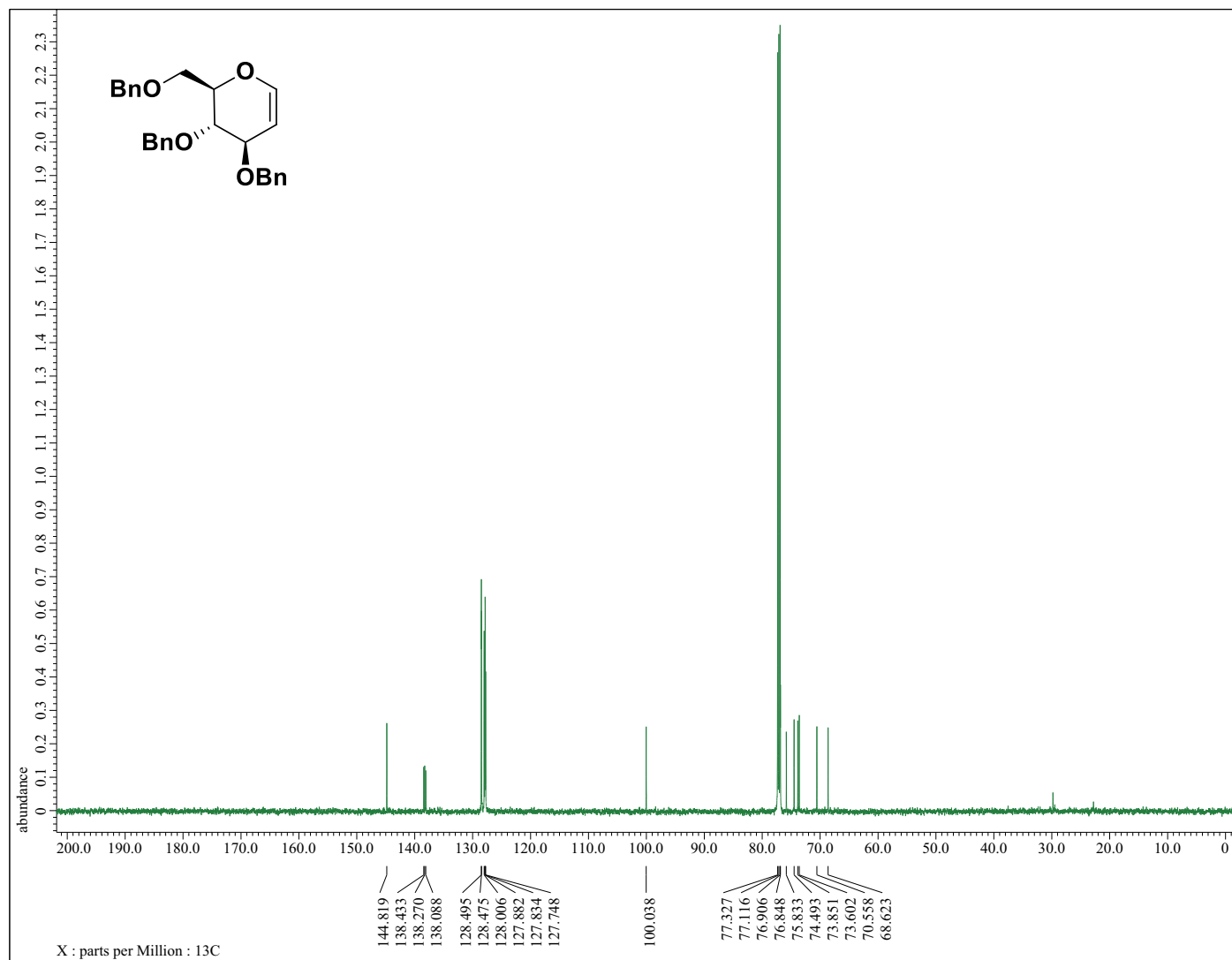
¹H NMR of Compound **67** [3,4,6-Tri-*O*-benzyl-D-glucal]

^{13}C NMR of Compound **67** [3,4,6-Tri-*O*-benzyl-D-glucal]

abundance

X : parts per Million : 13C

144.819
138.433
138.270
138.088
128.495
128.475
128.006
127.882
127.834
127.748
100.038
77.327
77.116
76.906
76.848
75.833
74.493
73.851
73.602
70.558
68.623

^{1}H NMR of Compound **68** [1,2-Anhydro-3,4,6-tri-*O*-benzyl-*α*-D-glucopyranose]

138.251
138.002
137.581
128.648
128.475
128.437
128.083
127.968
127.901
127.767

79.031
77.605
77.317
77.097
76.887
74.656
74.301
73.650
72.358
69.495
68.279

52.653

X : parts per Million : 13C

abundance

^{13}C NMR of Compound **68** [1,2-Anhydro-3,4,6-tri-*O*-benzyl-*α*-D-glucopyranose]

^{1}H NMR of Compound **69** [Benzyl-2,3,4-tri-*O*-benzyl-*β*-D-glucopyranuronic acid]

APPENDIX B. MASS SPECTRAL DATA
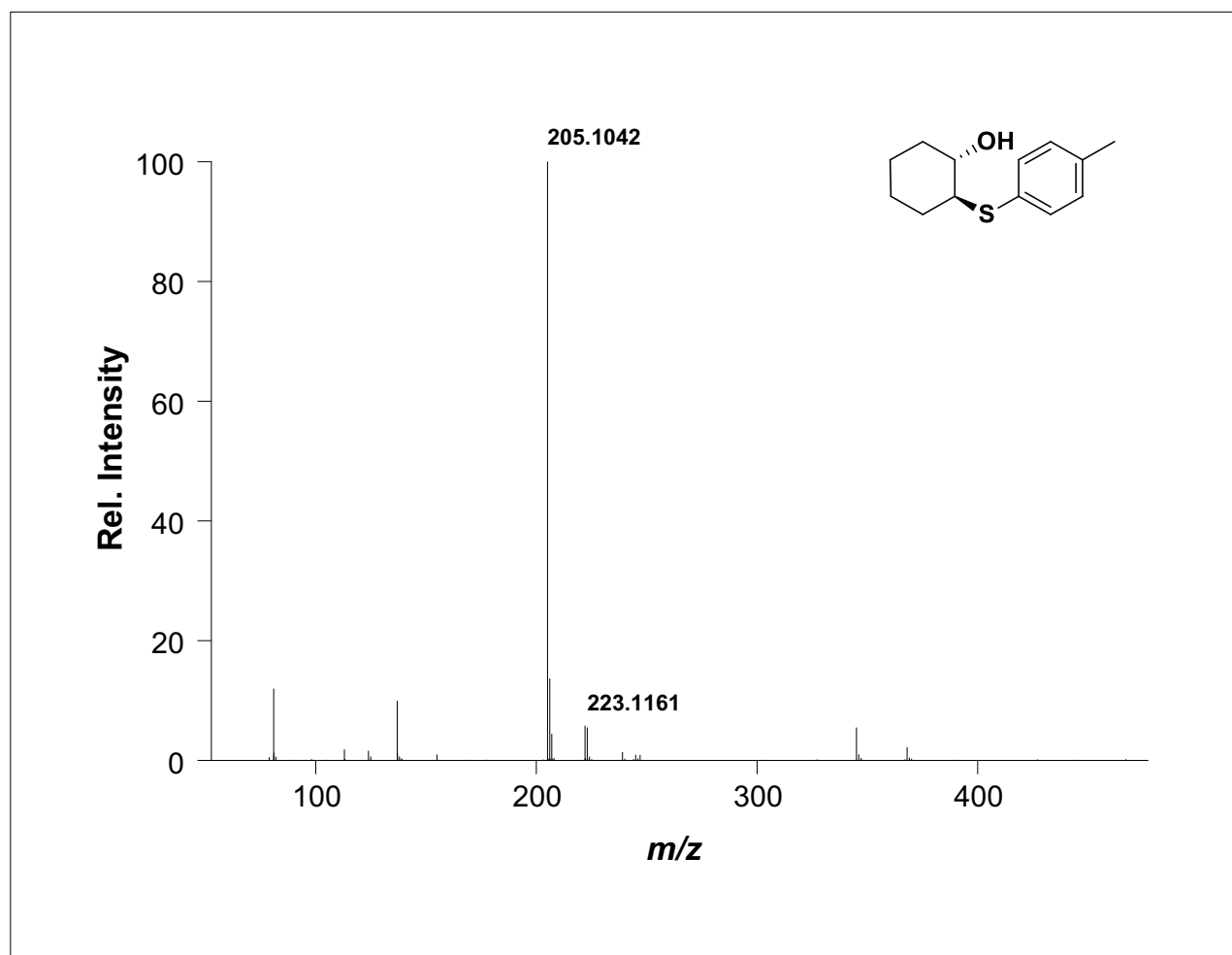
DART-HRMS of **4** [(±)-*trans*-2-(*p*-tolylsulfanyl)cyclohexanol]
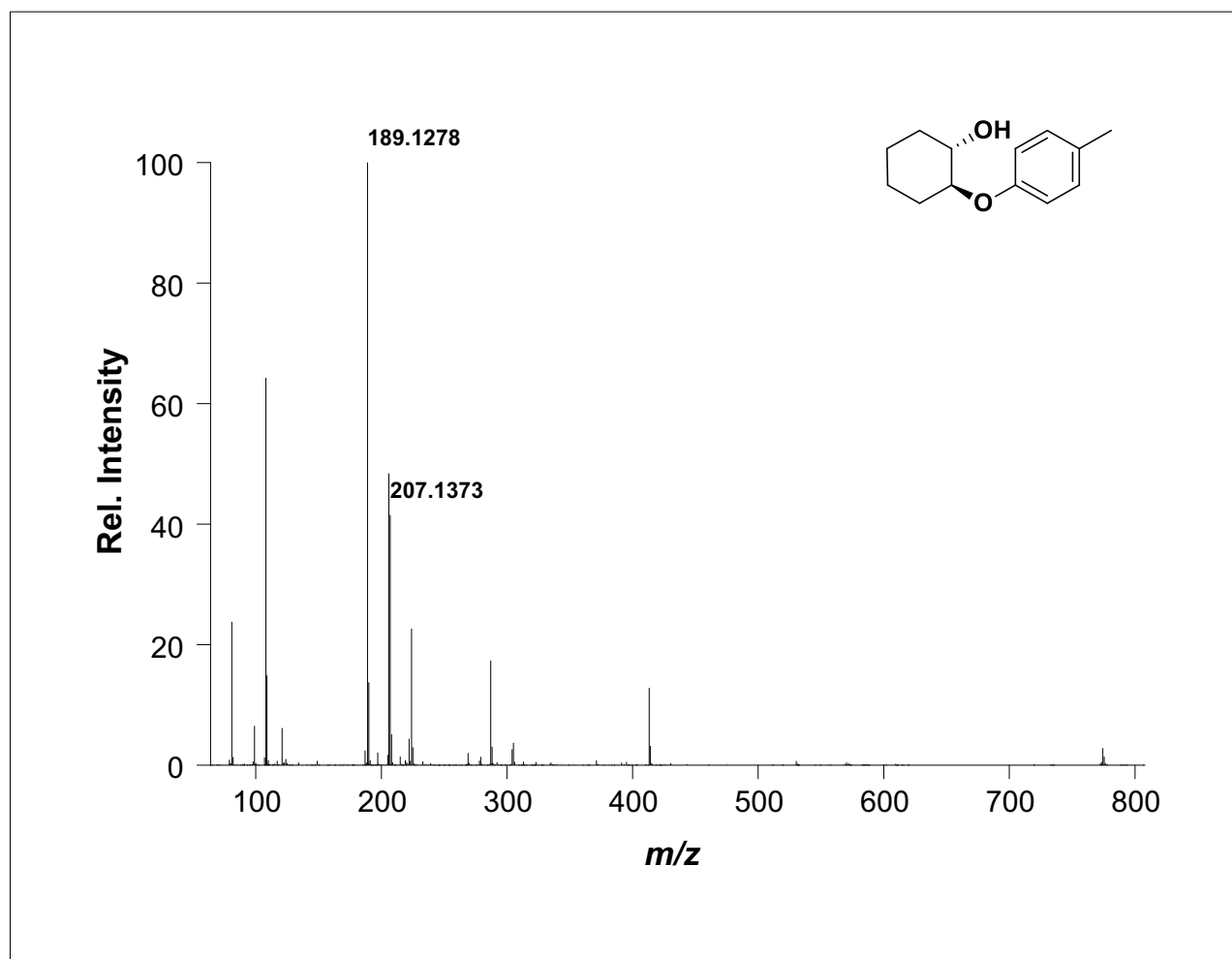
DART-HRMS of **6** [(±)-*trans*-2-(*p*-tolyloxy)cyclohexanol]
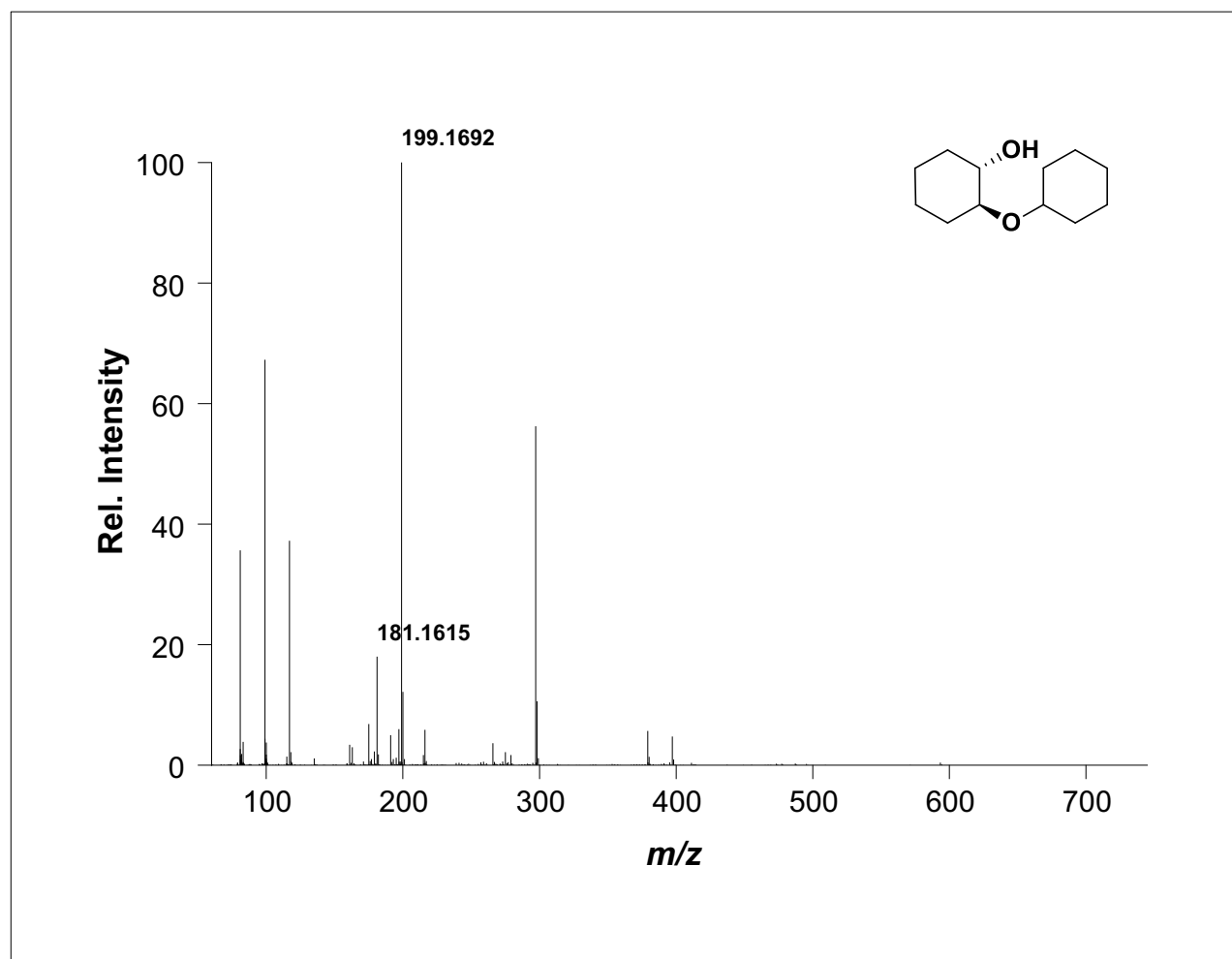
DART-HRMS of **17** [(±)-*trans*-2-(cyclohexyloxy)cyclohexanol]

DART-HRMS of **19** [(±)-*trans*-2-(*t*-butoxy)cyclohexanol]

210.0973

192.0798

Rel. Intensity

100

80

60

40

20

0

100   200   300   400   500   600

m/z
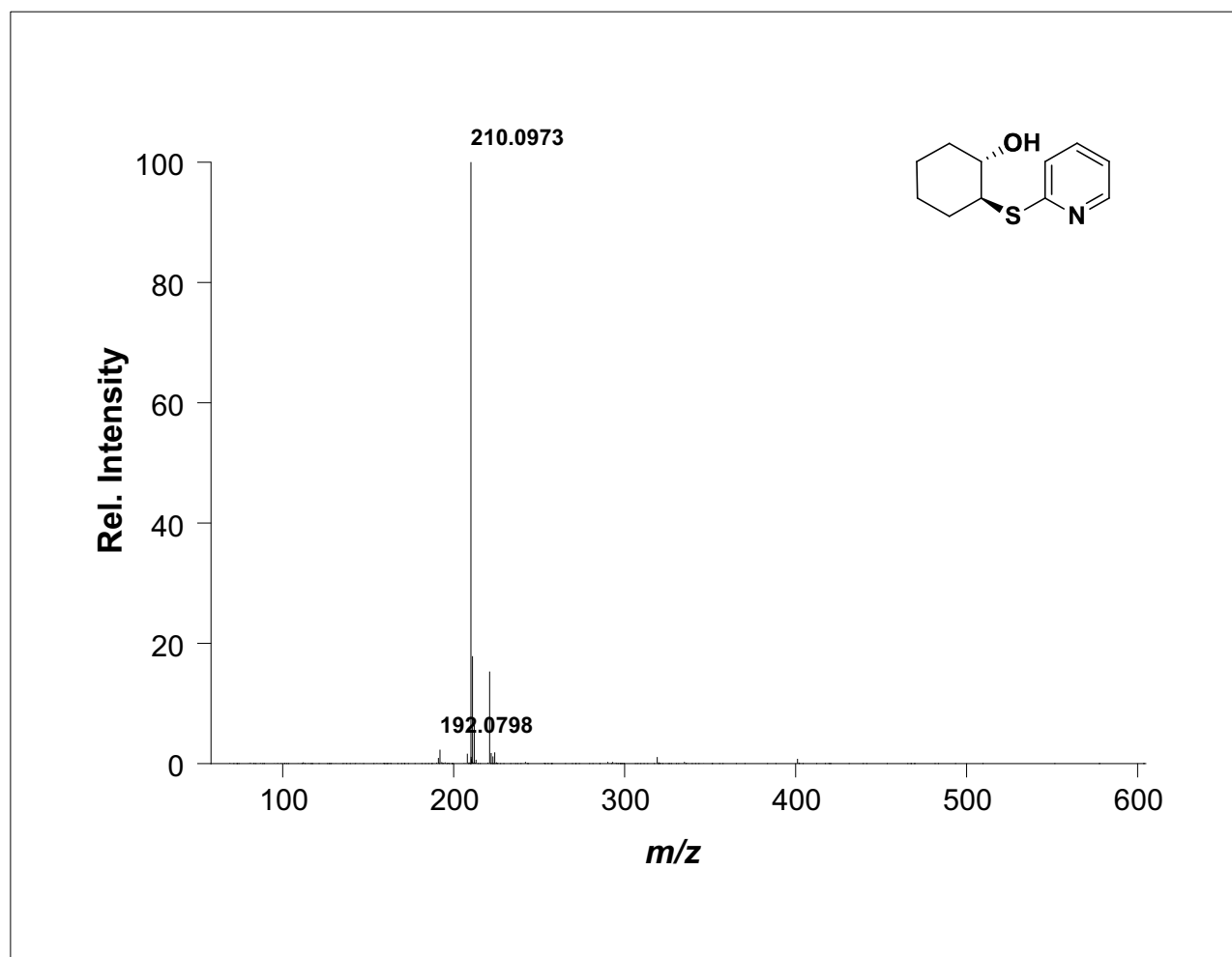
DART-HRMS of **21** [(±)-*trans*-2-(pyridine-2-ylthio)cyclohexanol]
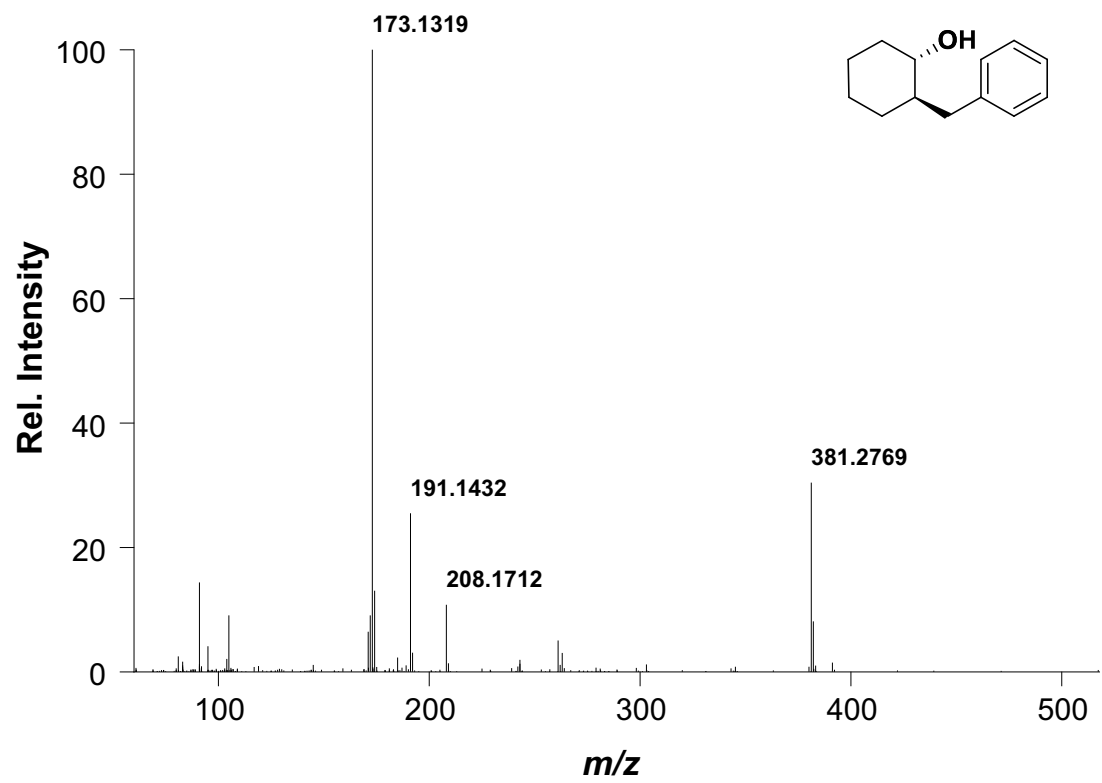
DART-HRMS of **25** [(±)-*trans*-2-(benzyl)cyclohexanol]
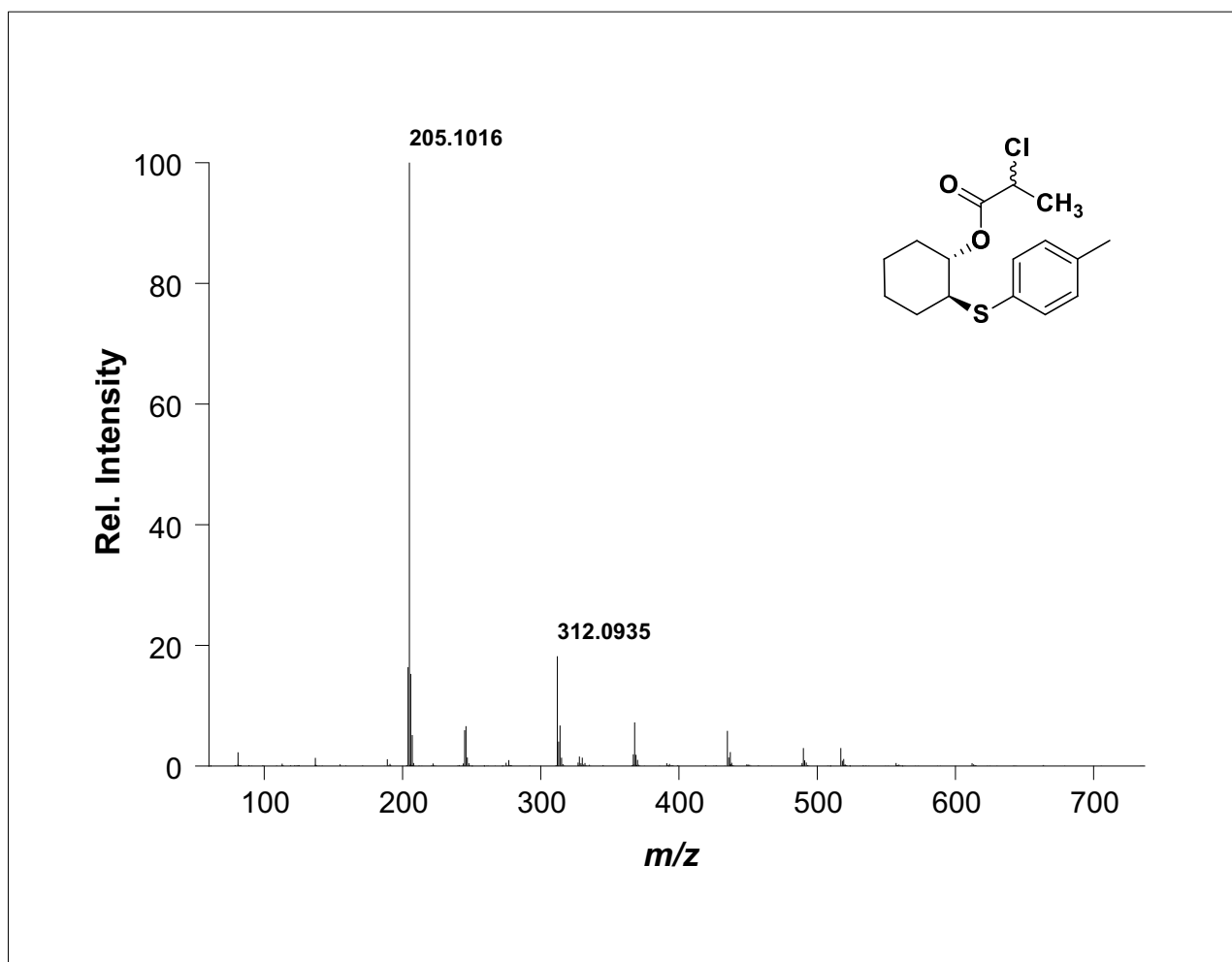
DART-HRMS of **71** [(±)-(*trans*-2-(*p*-tolylsulfanyl)cyclohexyl) 2-chloropropanoate]
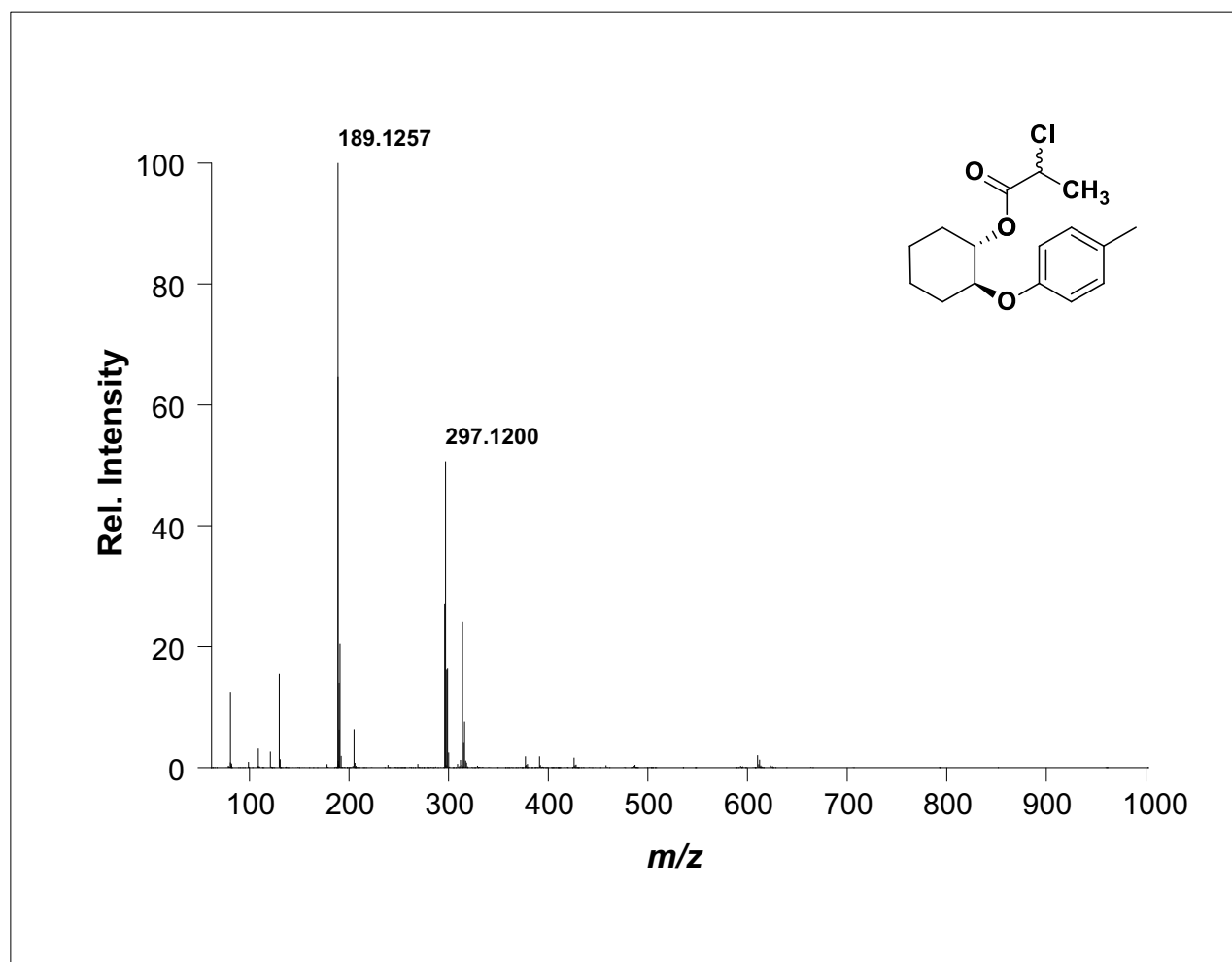
DART-HRMS of **72** [(±)-(*trans*-2-(*p*-tolyloxy)cyclohexyl) 2-chloropropanoate]
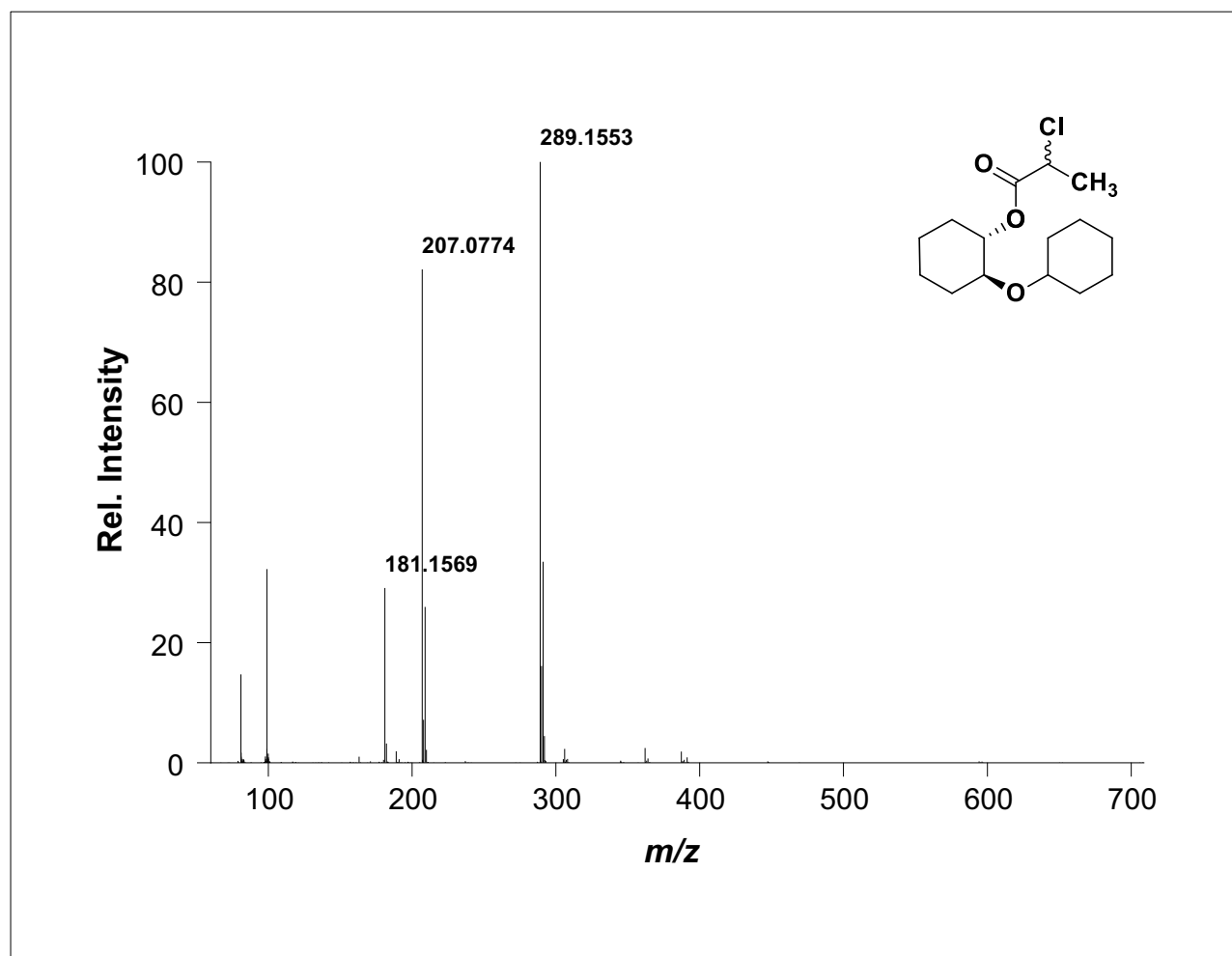
DART-HRMS of **78** [(±)-(*trans*-2-(cyclohexyloxy)cyclohexyl 2-chloropropanoate]
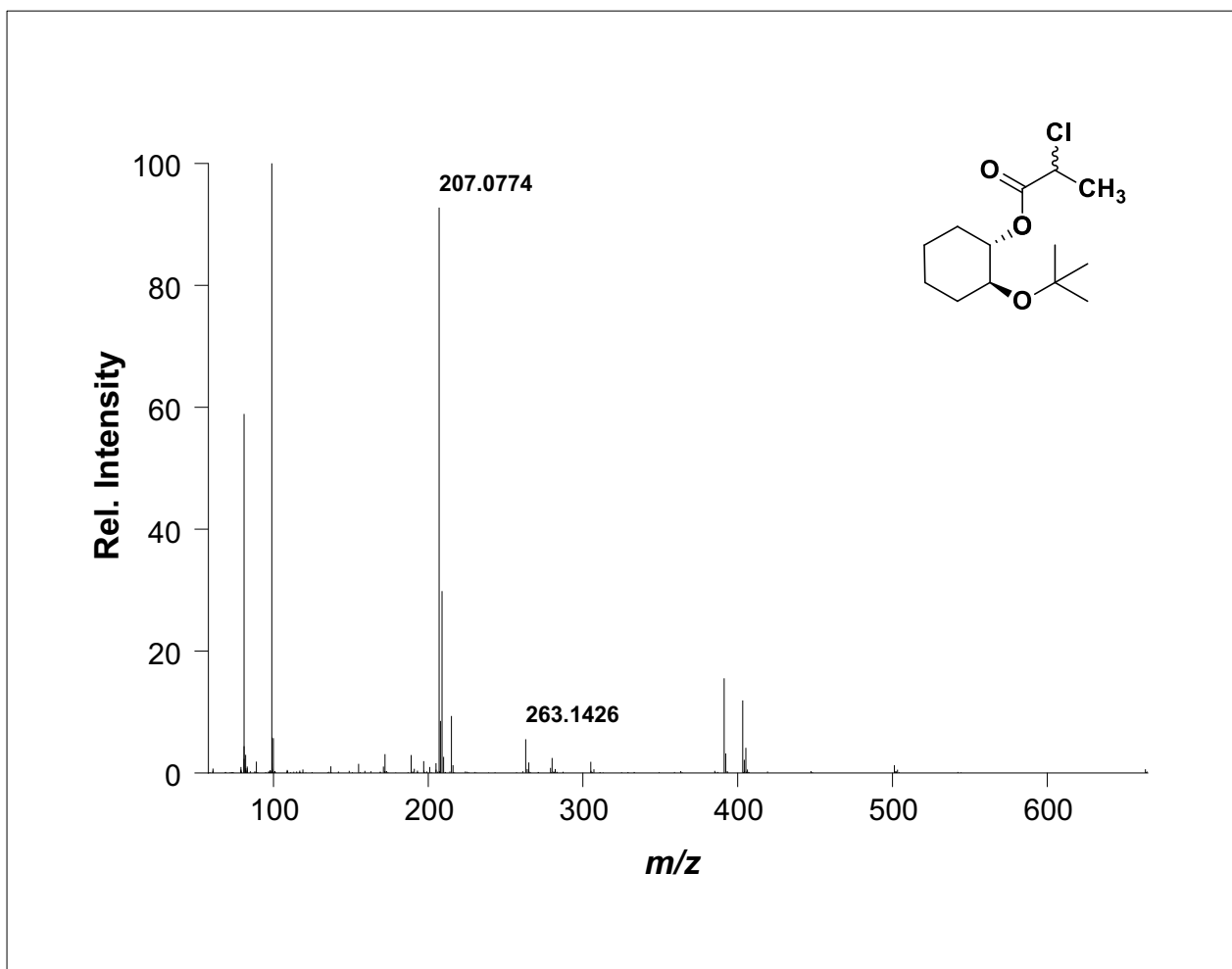
DART-HRMS of **79** [(±)-(*trans*-2-(*tert*-butoxy)cyclohexyl 2-chloropropanoate]
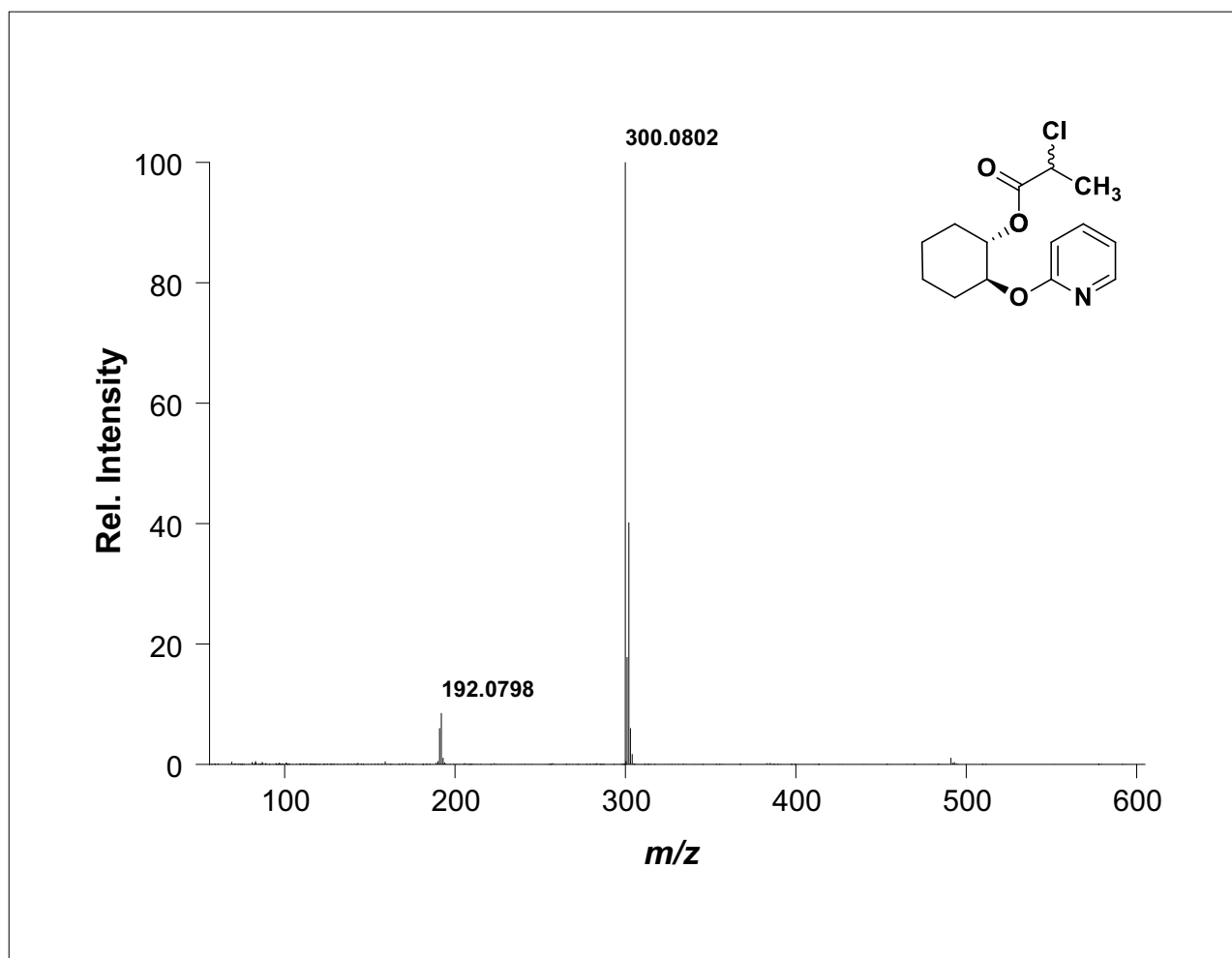
DART-HRMS of **80** [(±)-*trans*-2-(pyridin-2-ylthio)cyclohexyl 2-chloropropanoate]
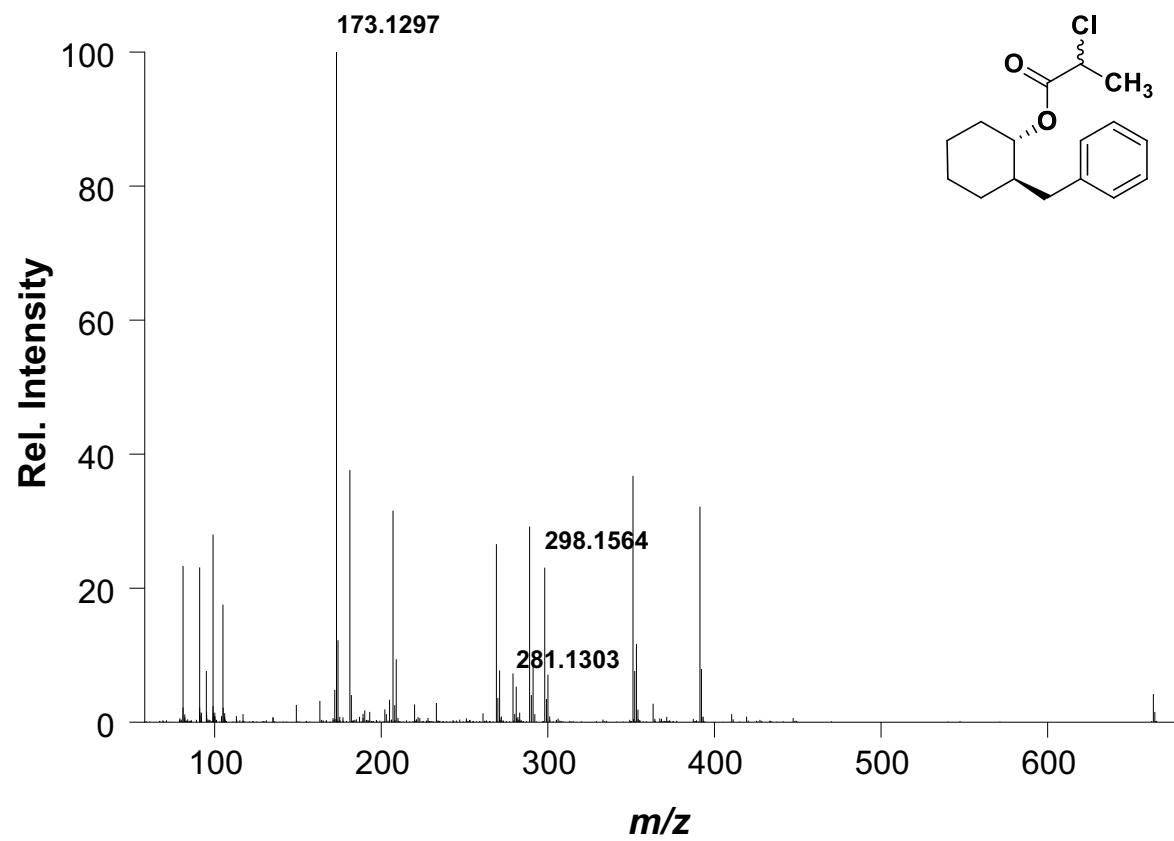
DART-HRMS of **82** [(±)-(*trans*-2-benzylcyclohexyl) 2-chloropropanoate]
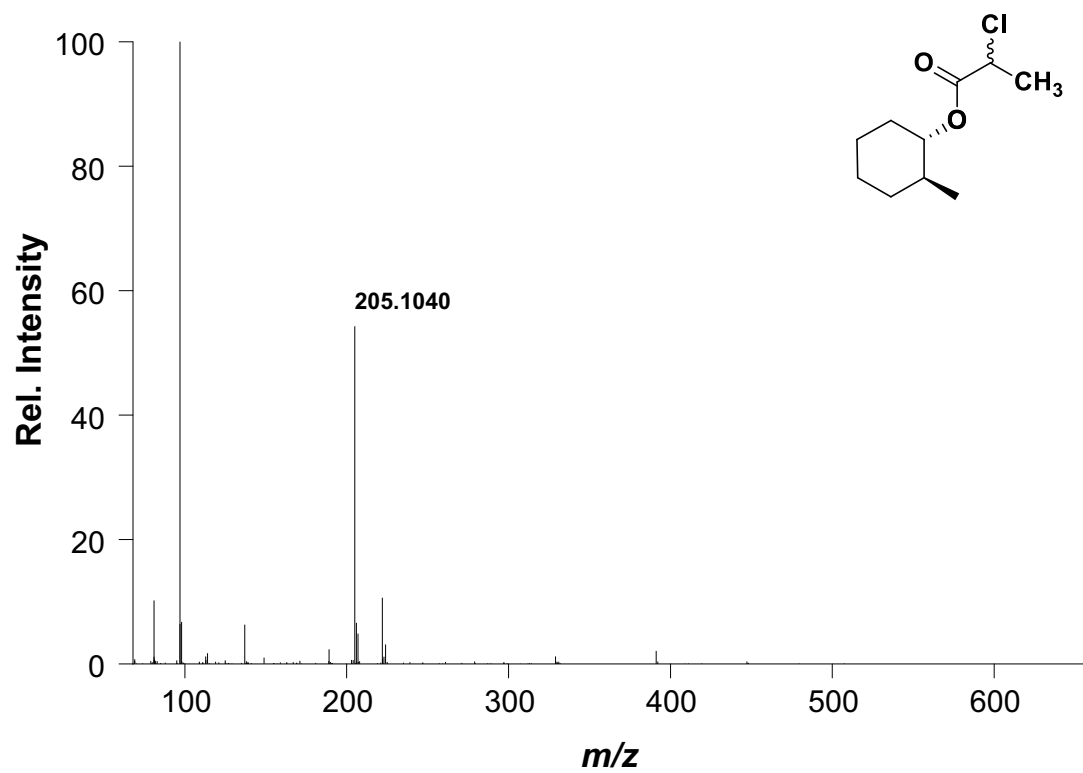
DART-HRMS of **83** [(±)-(*trans*-2-methylcyclohexyl) 2-chloropropanoate]
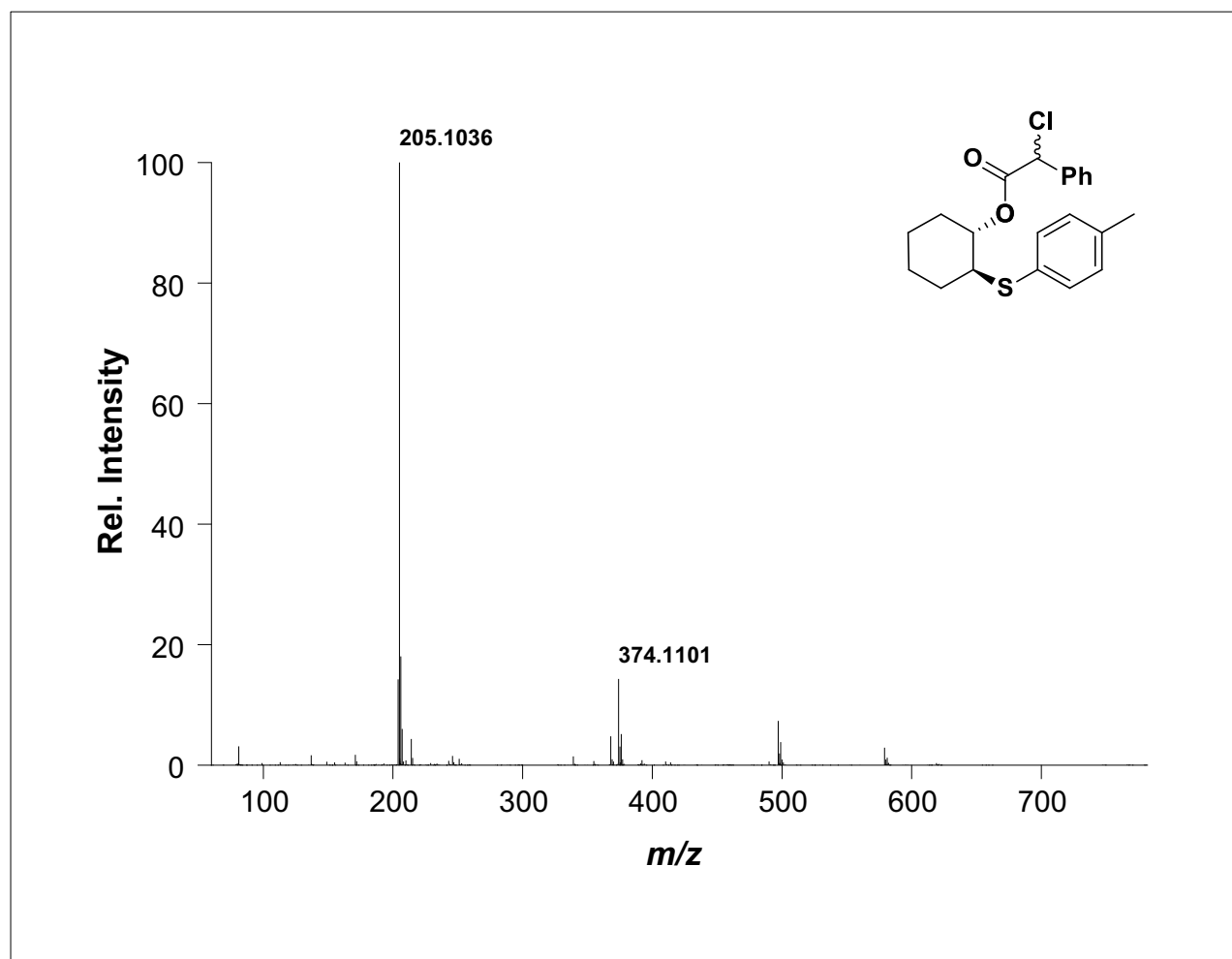
DART-HRMS of **84** [(±)-(*trans*-2-(*p*-tolylsulfanyl)cyclohexyl 2-chloro-2-phenylethanoate]
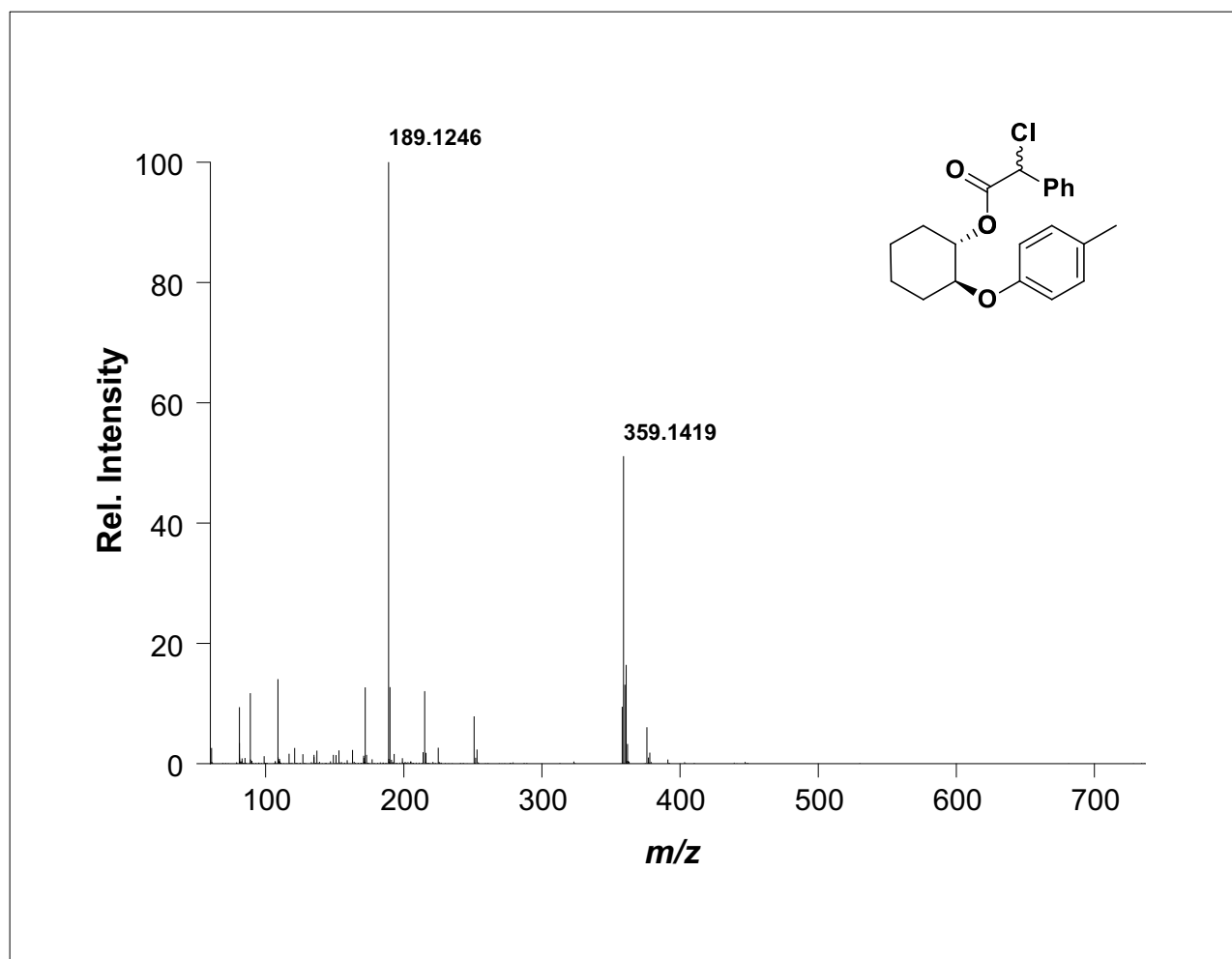
DART-HRMS of **85** [(±)-(*trans*-2-(*p*-tolyloxy)cyclohexyl 2-chloro-2-phenylethanoate]
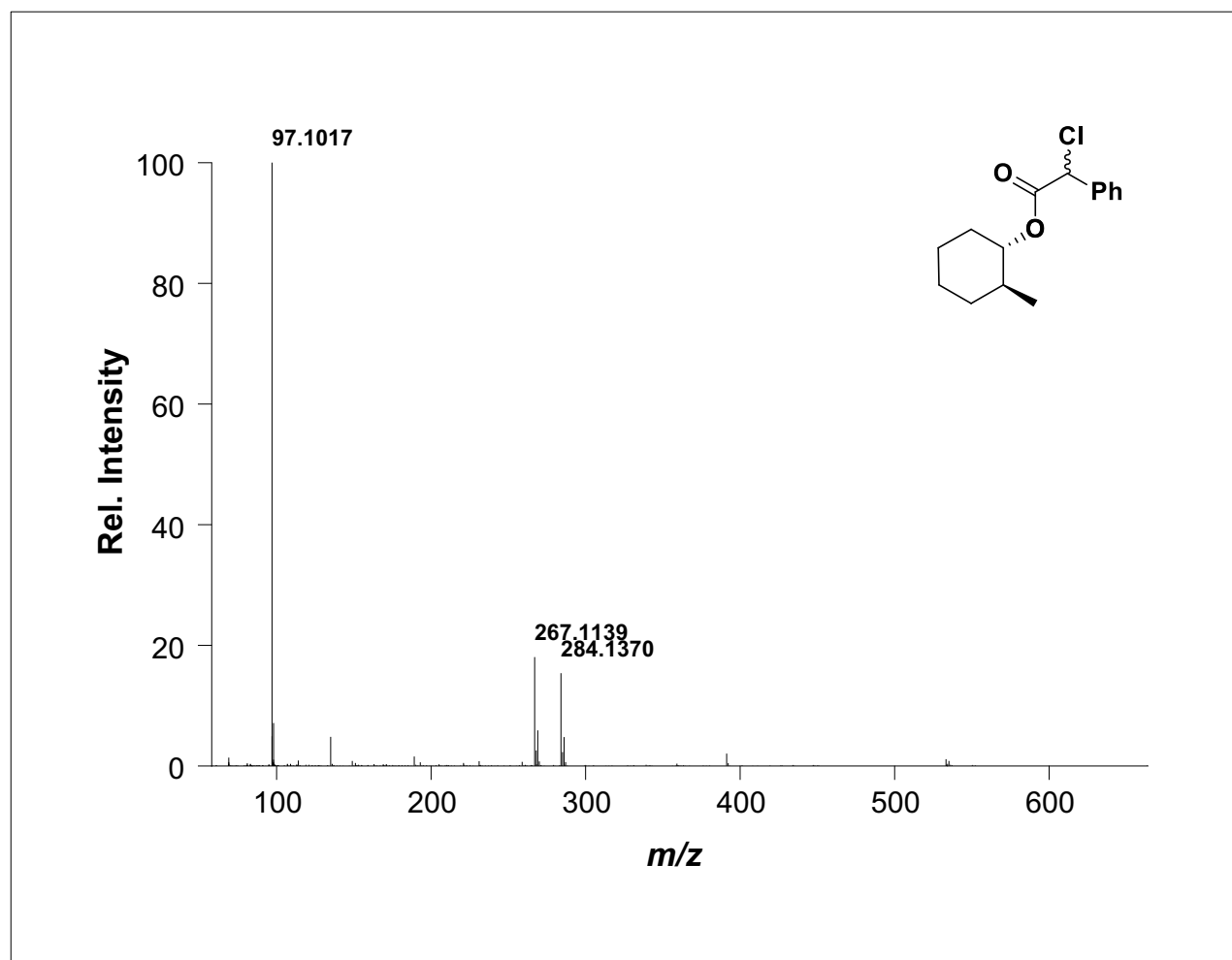
DART-HRMS of **89** [(±)-*trans*-2-(methyl)cyclohexyl 2-chloro-2-phenylethanoate]
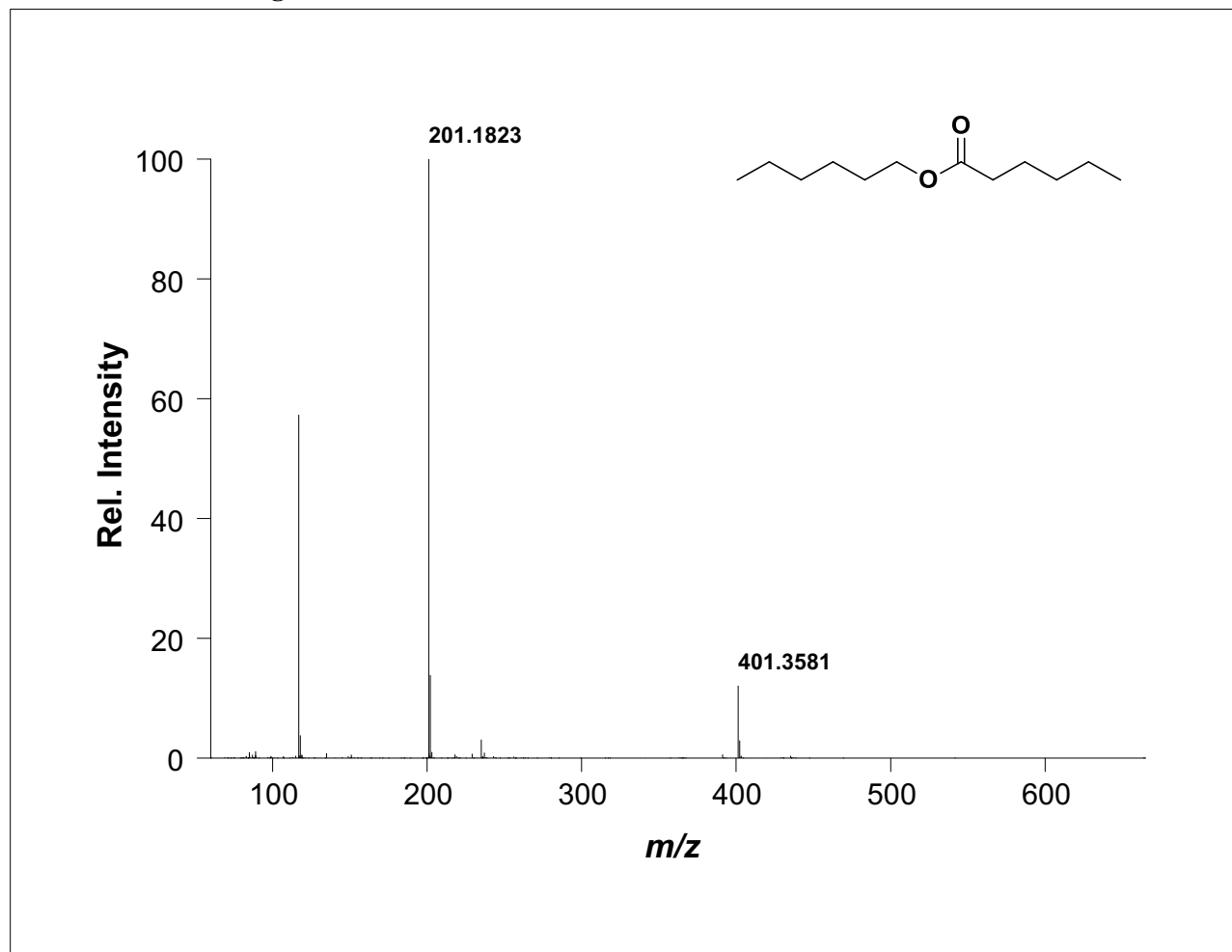
DART-HRMS of Compound 90 [hexyl hexanoate]
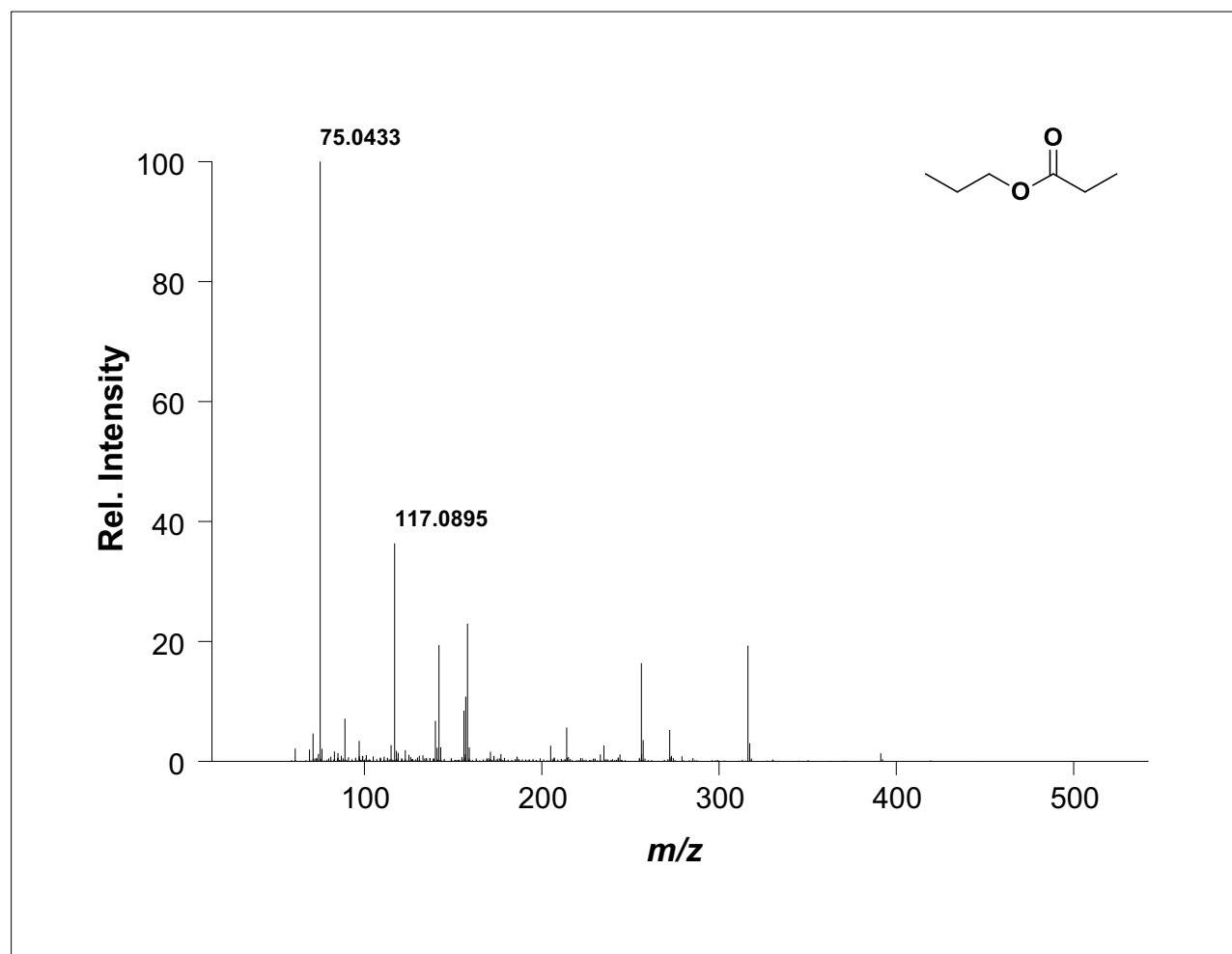
DART-HRMS of Compound 91 [propyl propanoate]
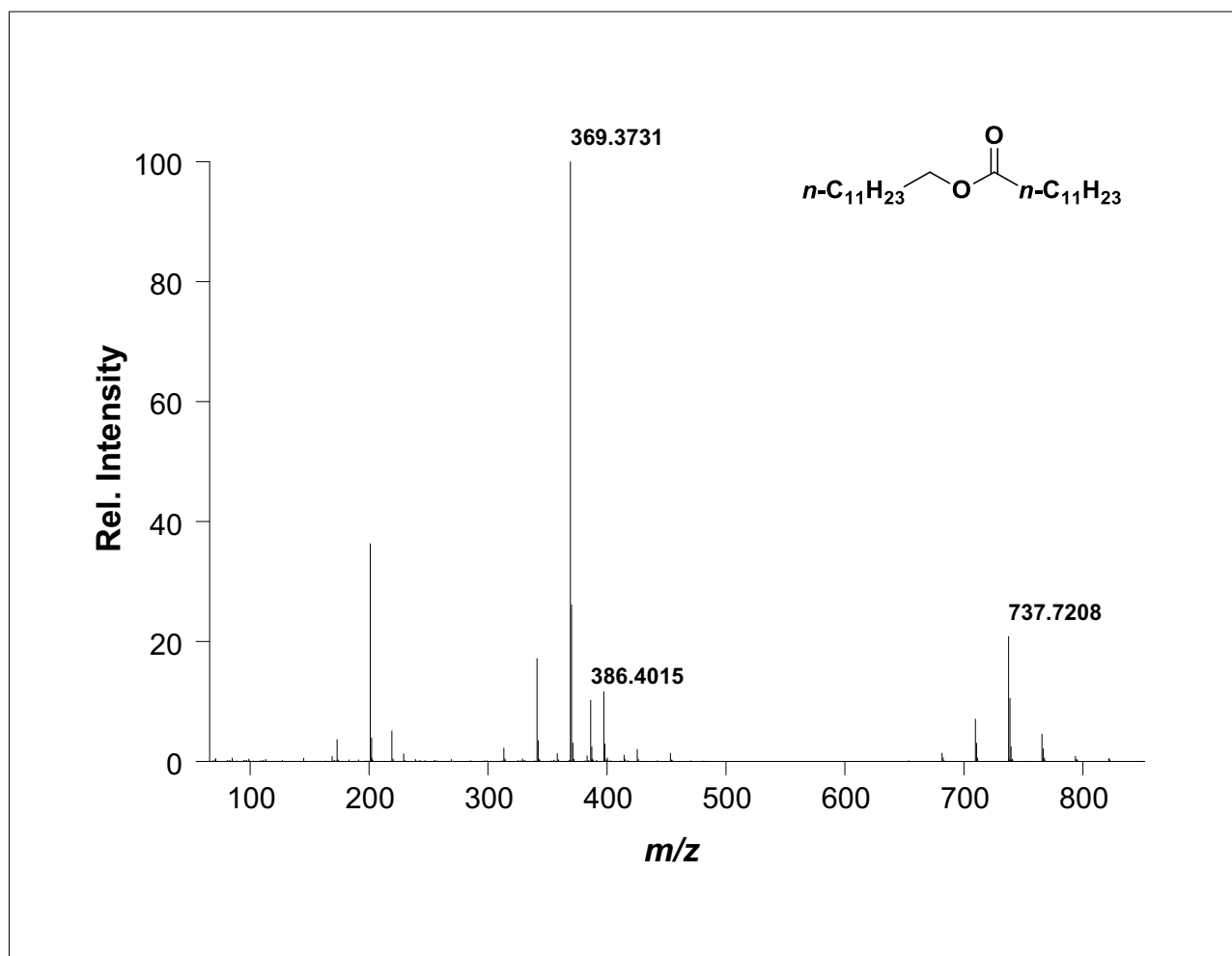
DART-HRMS of Compound 92 [dodecyl dodecanoate]
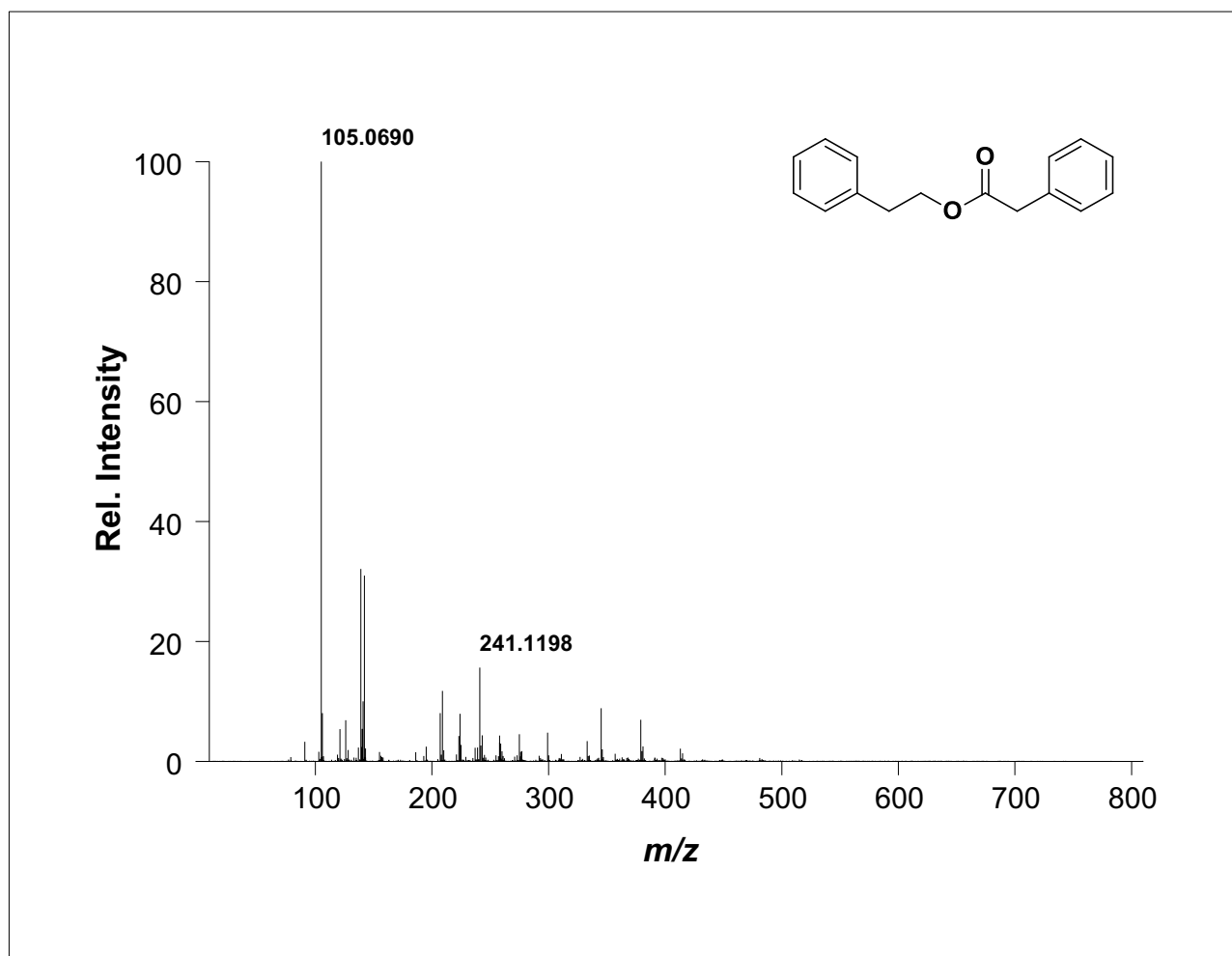
DART-HRMS of Compound 93 [phenethyl 2-phenylacetate]
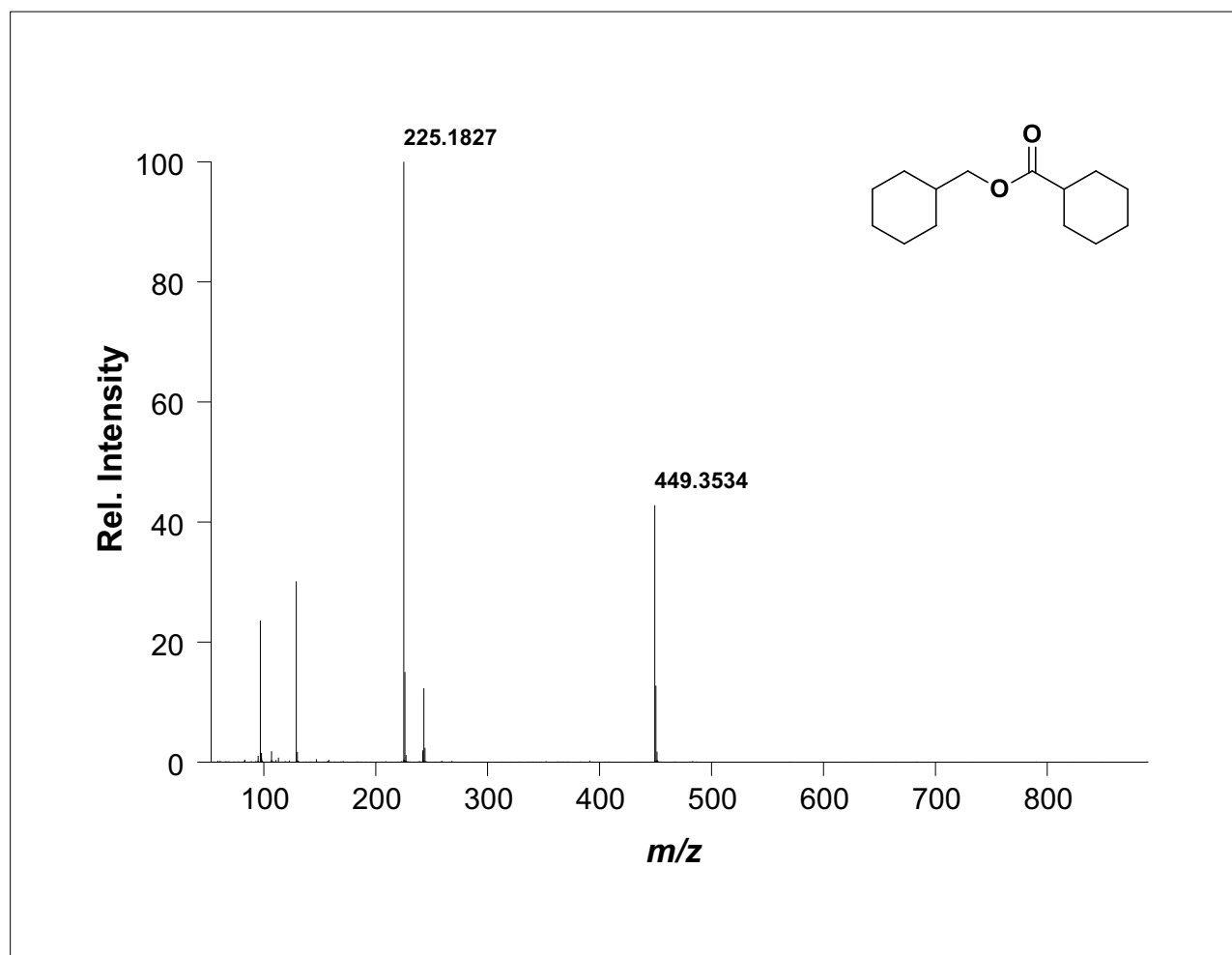
DART-HRMS of Compound 94 [cyclohexylmethyl cyclohexanecarboxylate]
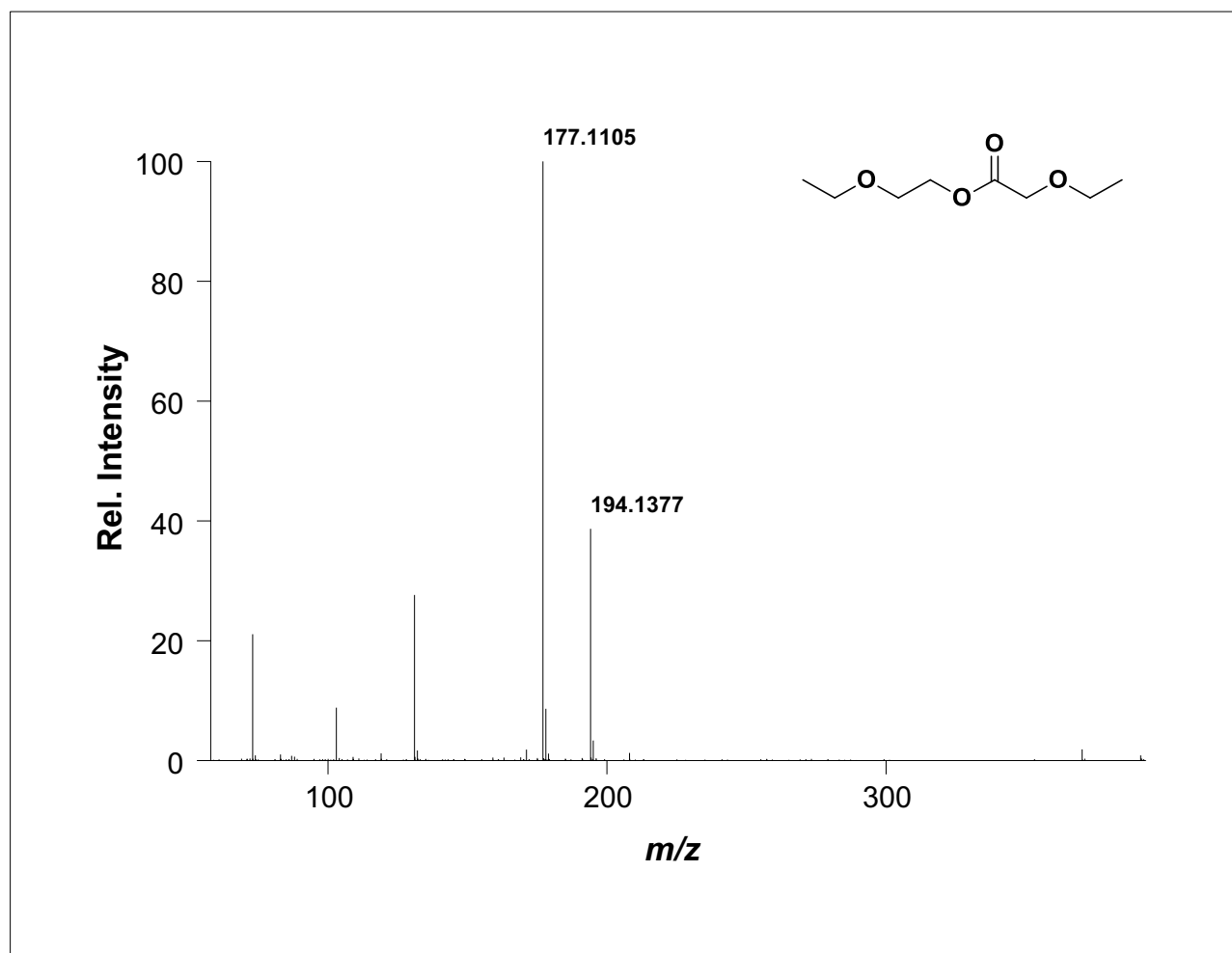
DART-HRMS of Compound 95 [2-ethoxyethyl 2-ethoxyacetate]
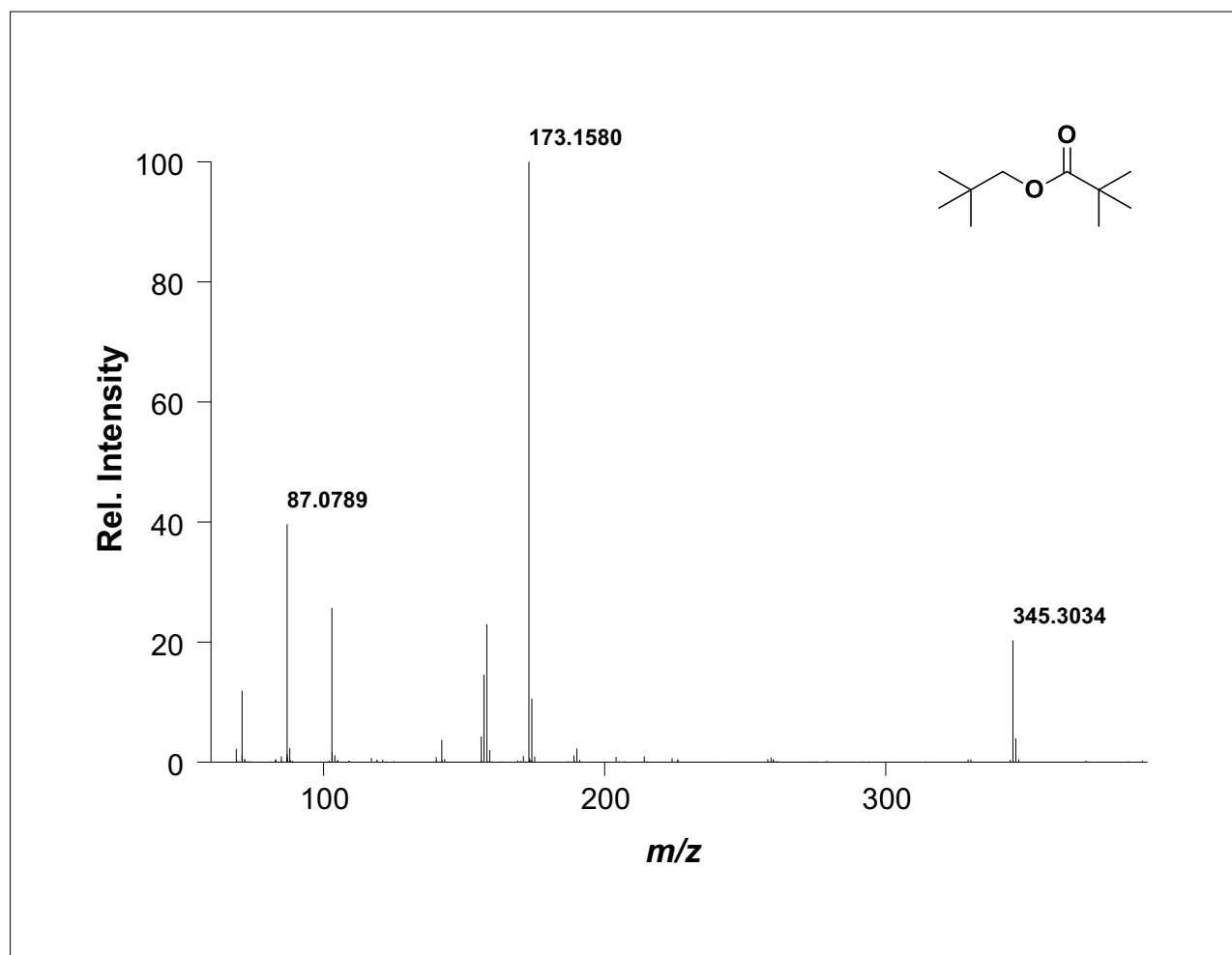
DART-HRMS of Compound 96 [2,2-dimethylpropyl pivalate]
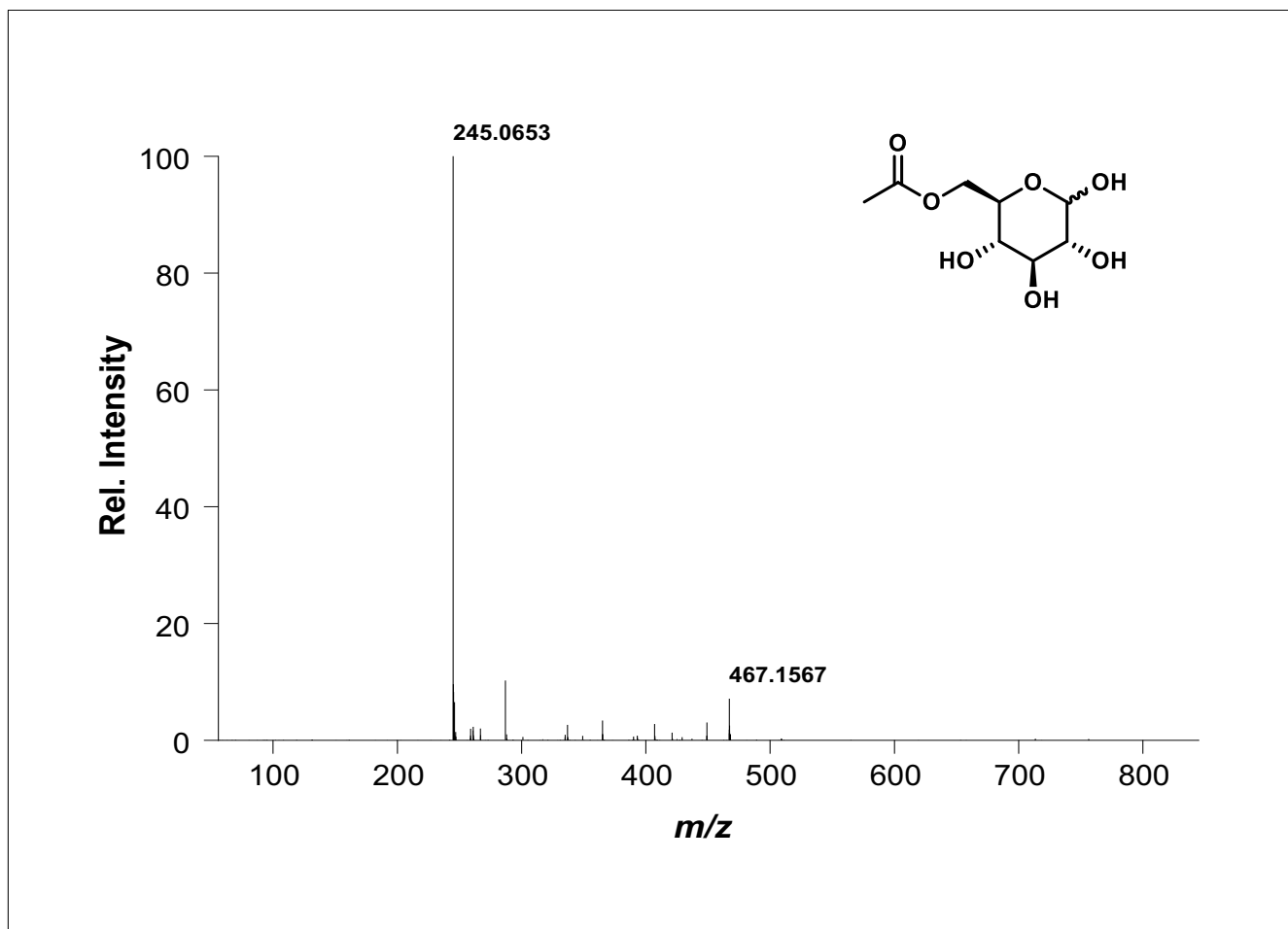
ESI-HRMS of Compound **46** [6-*O*-Acetyl-*α*/*ß*-D-glucopyranose]
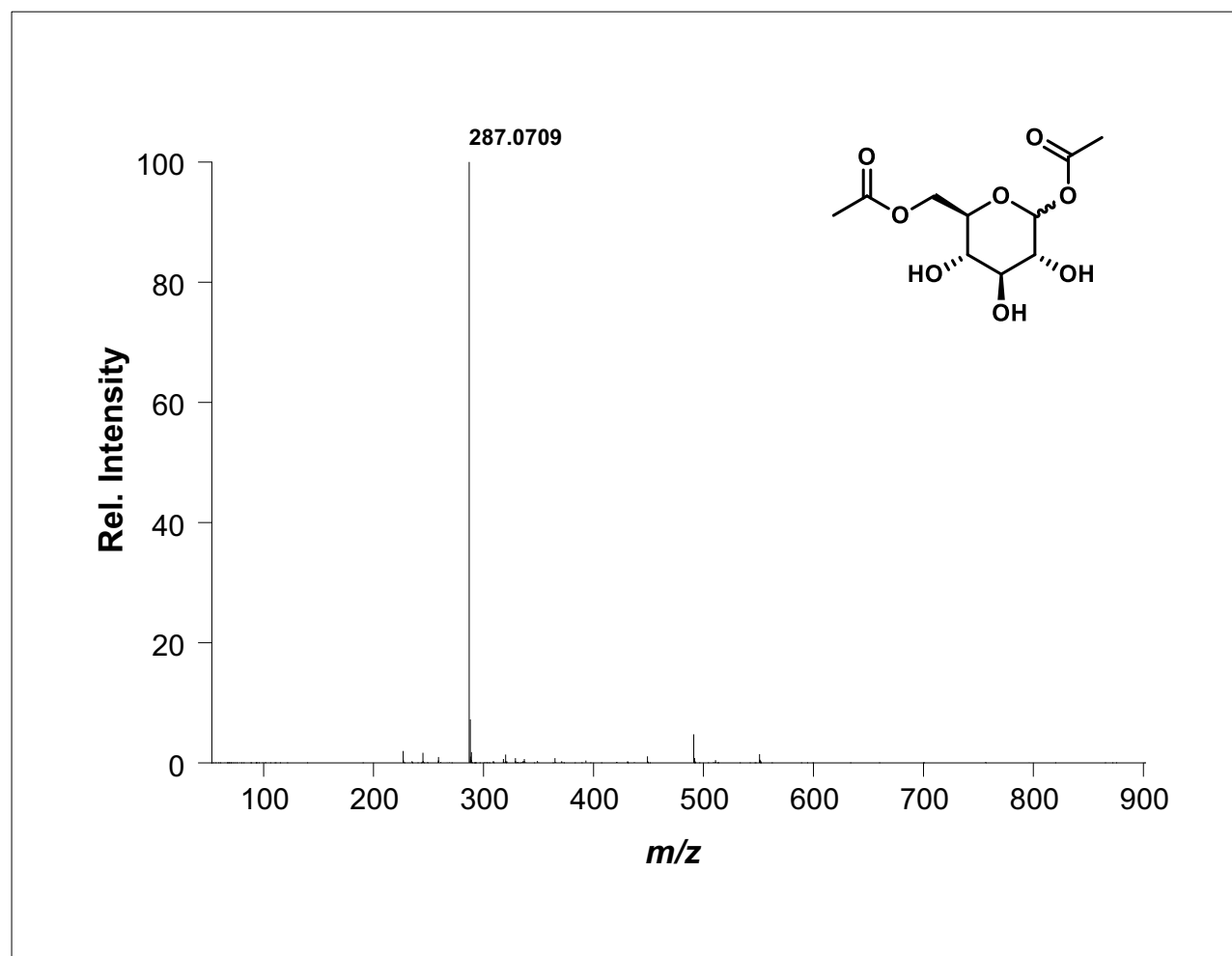
ESI-HRMS of Compound **47** [Acetyl-6-*O*-acetyl-*α*/*ß*-D-glucopyranoside]
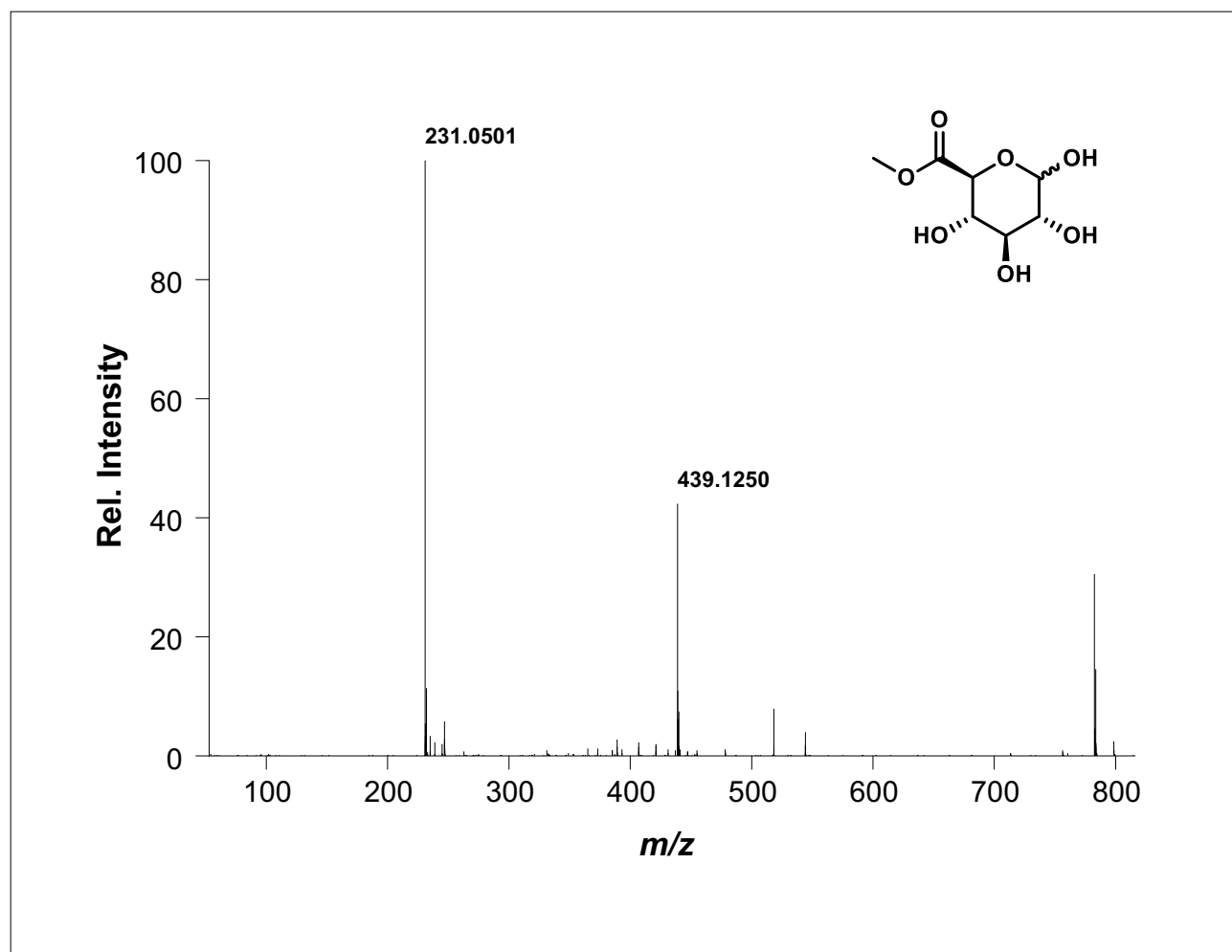
ESI-HRMS of Compound **50** [Methyl-*α*/*ß*-D-glucopyranuronate]
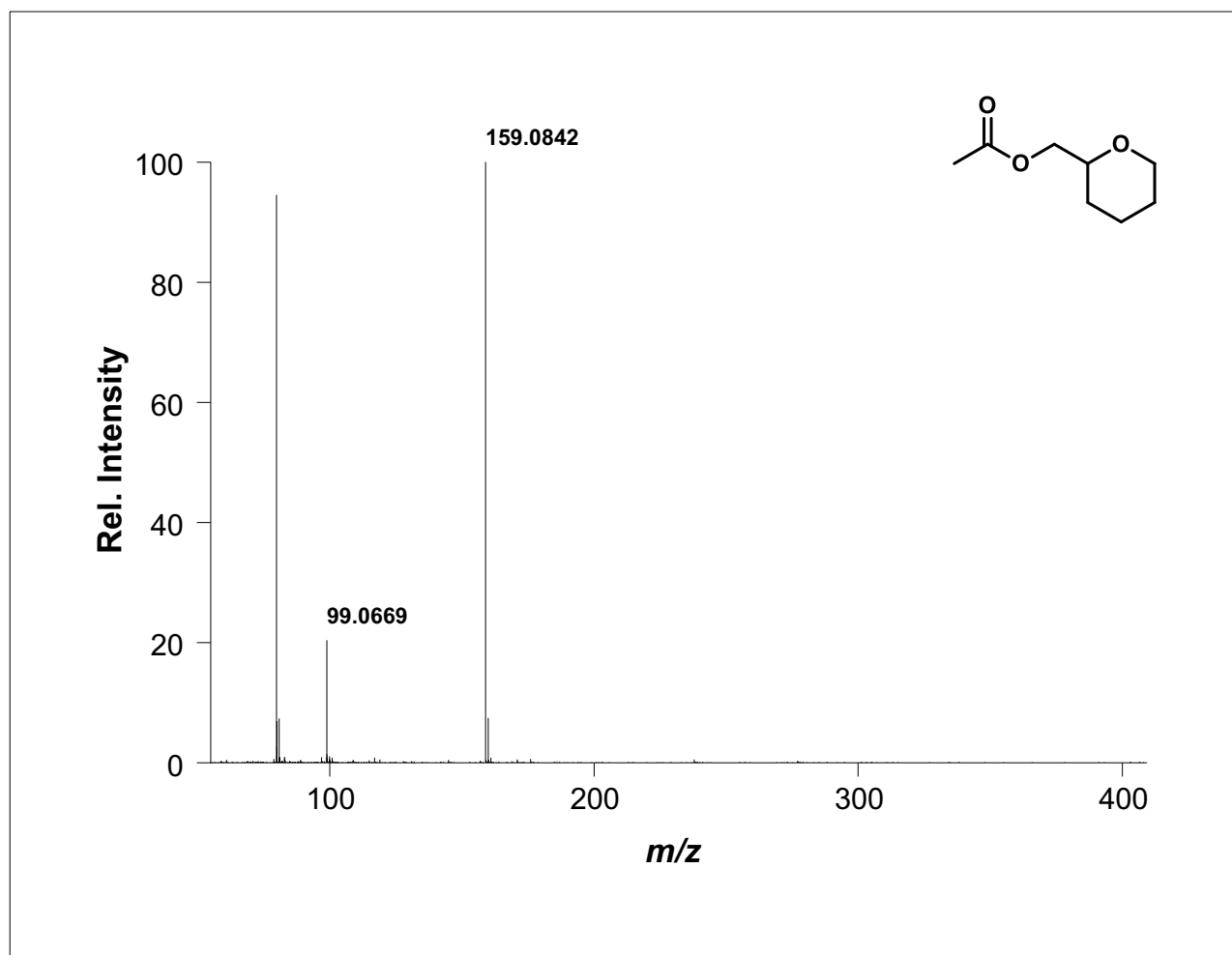
ESI-HRMS of Compound **53** [(Tetrahydropyran-2-yl)-methyl acetate]
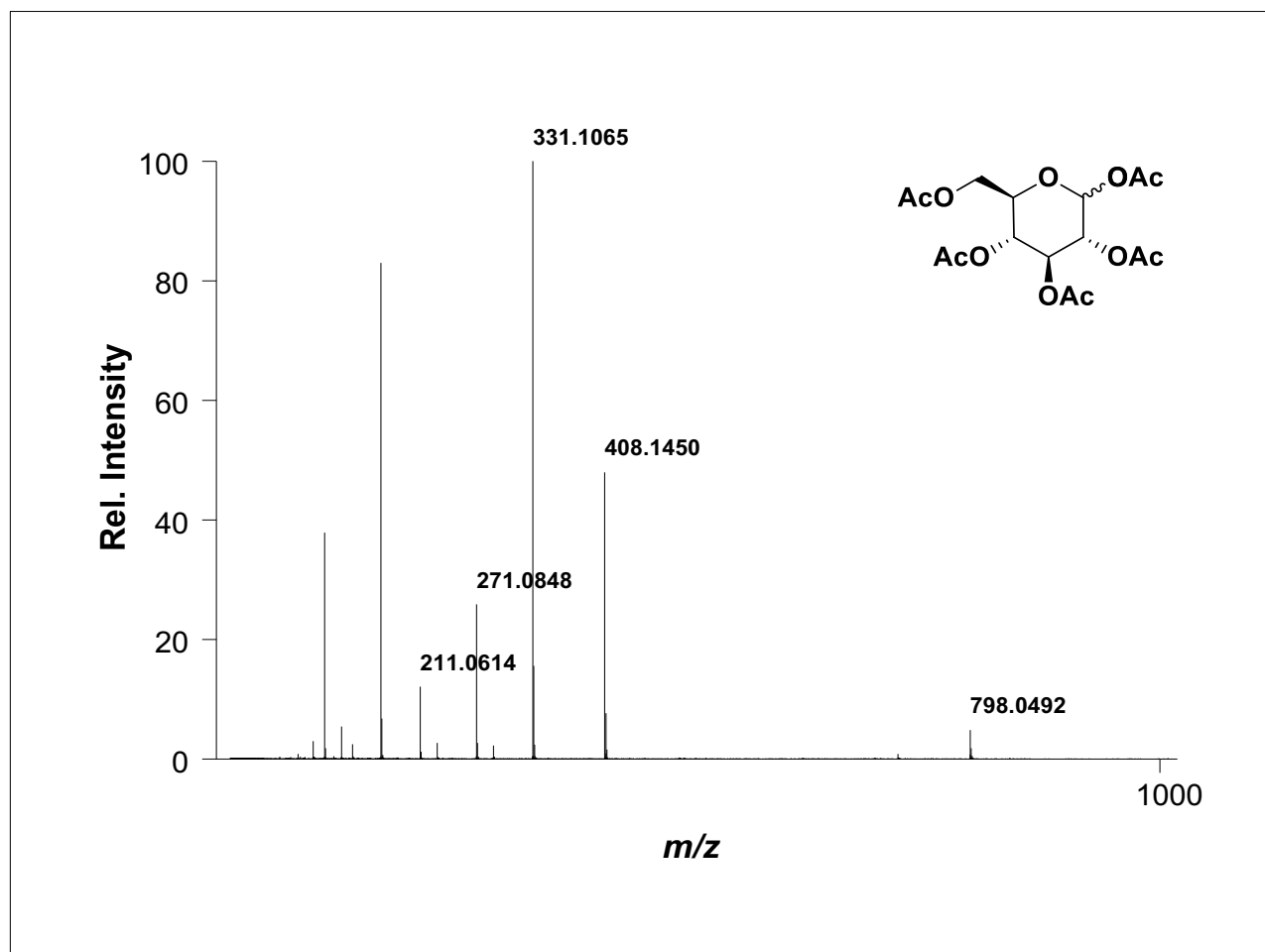
DART-HRMS of Compound **58** [Acetyl-2,3,4,6-tetra-*O*-acetyl-*α*/*ß*-D-glucopyranoside]
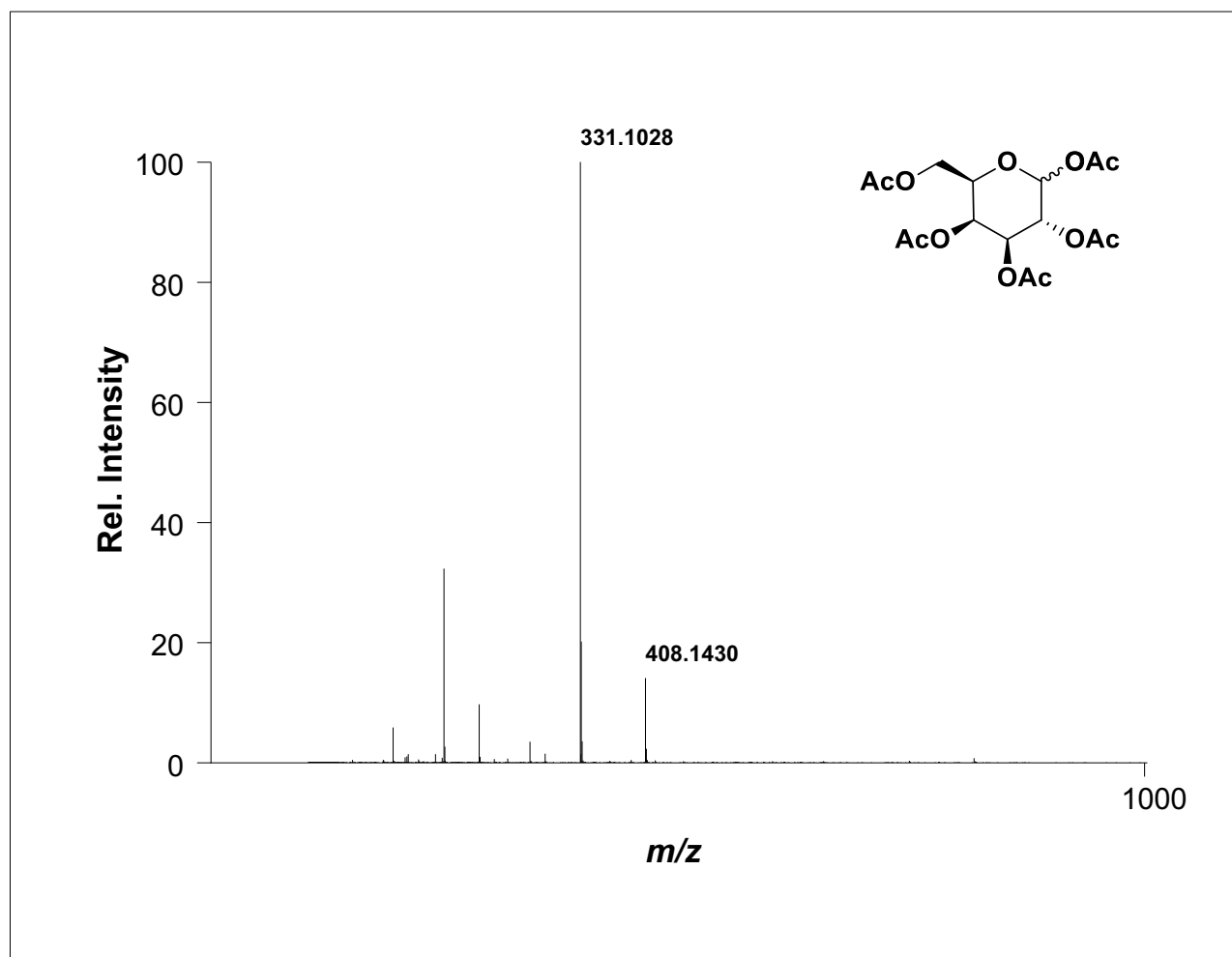
DART-HRMS of Compound **59** [Acetyl-2,3,4,6-tetra-*O*-acetyl-*α*/*ß*-D-galactopyranoside]
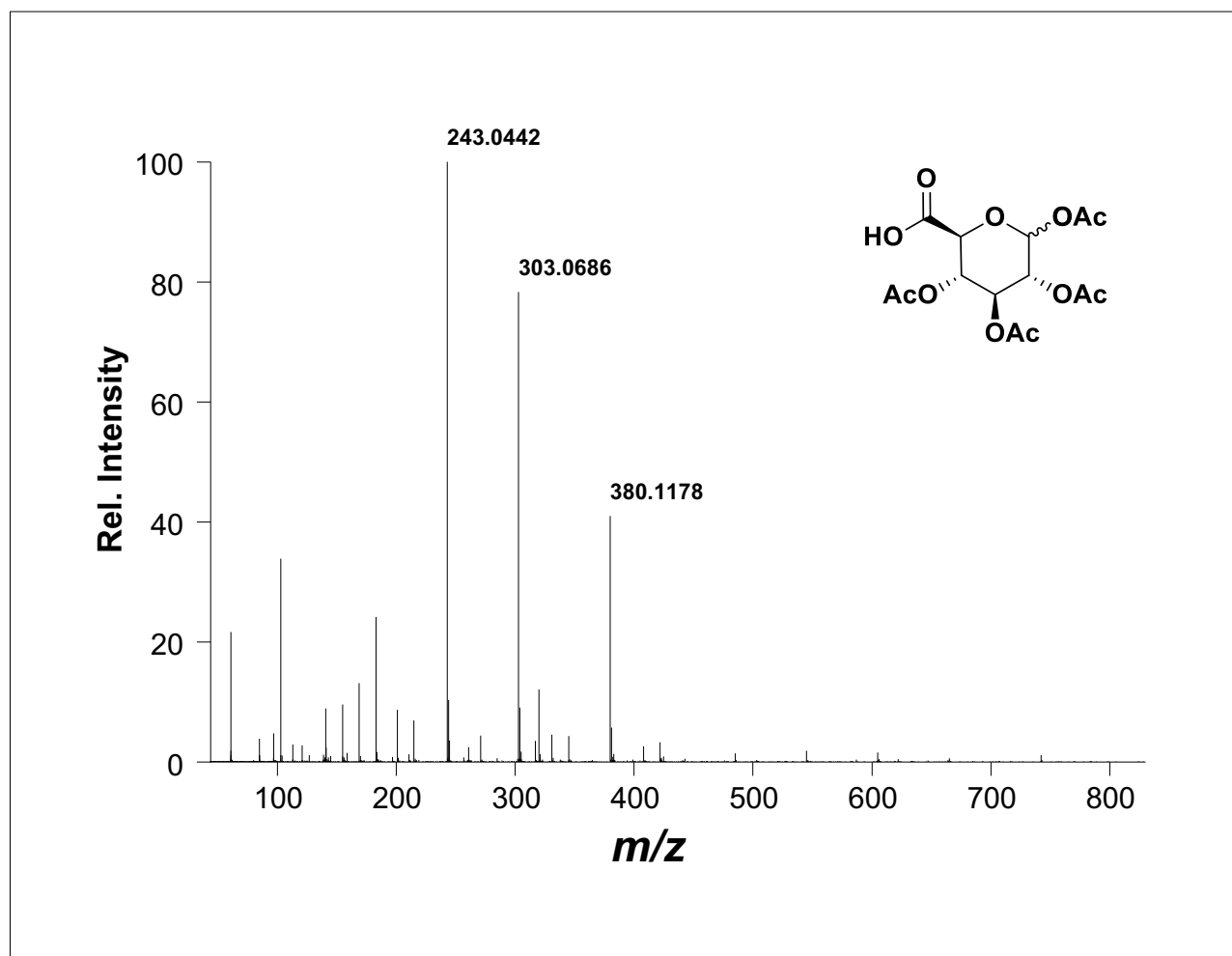
DART-HRMS of Compound **61** [1,2,3,4-Tetra-*O*-acetyl *α/ß*-D-glucopyranuronic acid]
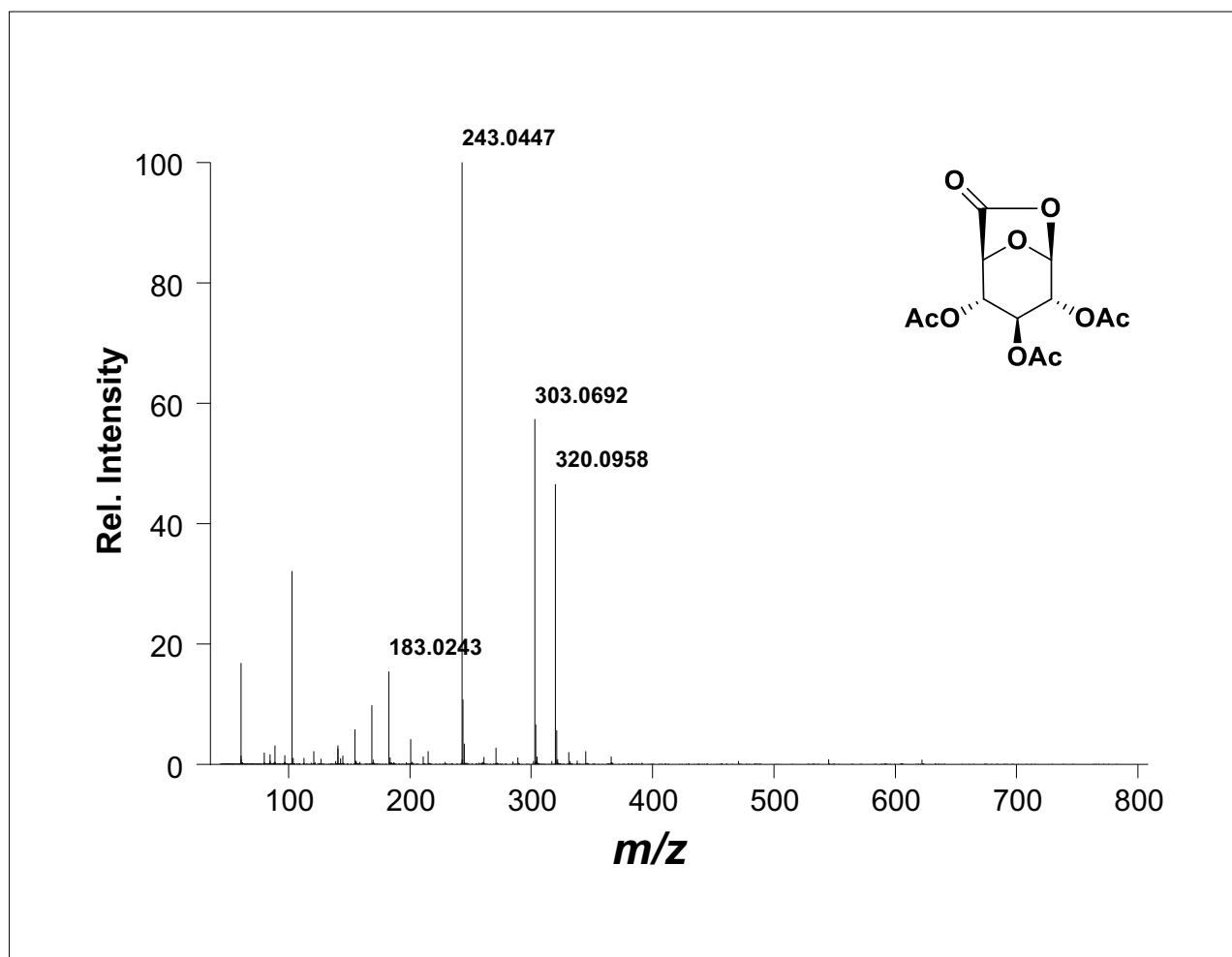
DART-HRMS of Compound **60** [2,3,4-Tri-*O*-acetyl-D-glucurono-6,1-lactone]
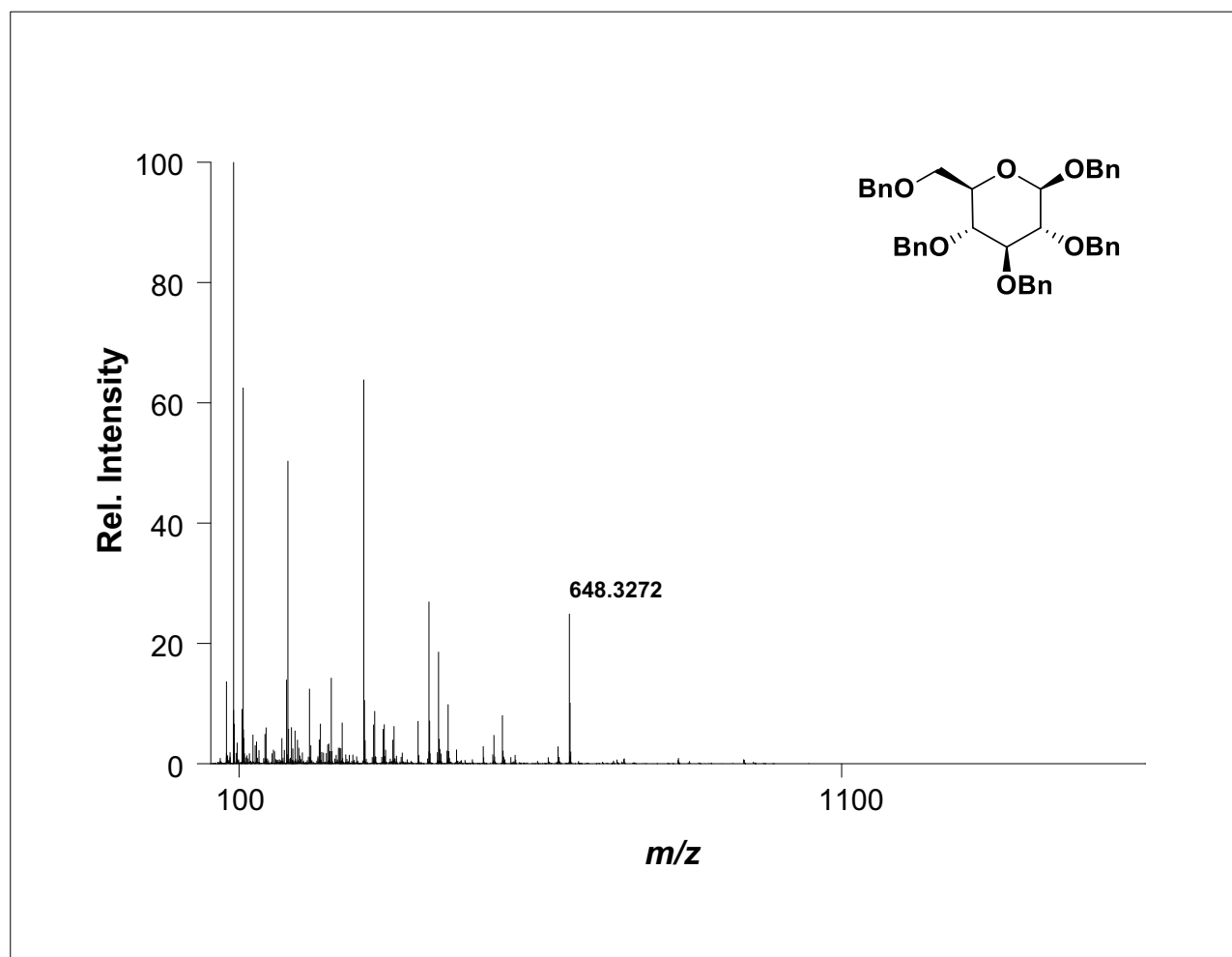
DART-HRMS of Compound **62** [Benzyl-2,3,4,6-tetra-*O*-benzyl-*β*-D-glucopyranoside]

DART-HRMS of Compound **64** [Benzyl-2,3,4-tri-*O*-benzyl-*β*-D-glucopyranoside]

ESI-HRMS of Compound **65** [Benzyl-2,3,4-tri-*O*-benzyl-*β*-D-glucopyranosyl-(6→6')-(benzyl-2,3,4-tri-*O*-benzyl-*β*-D-glucopyranuronate)]
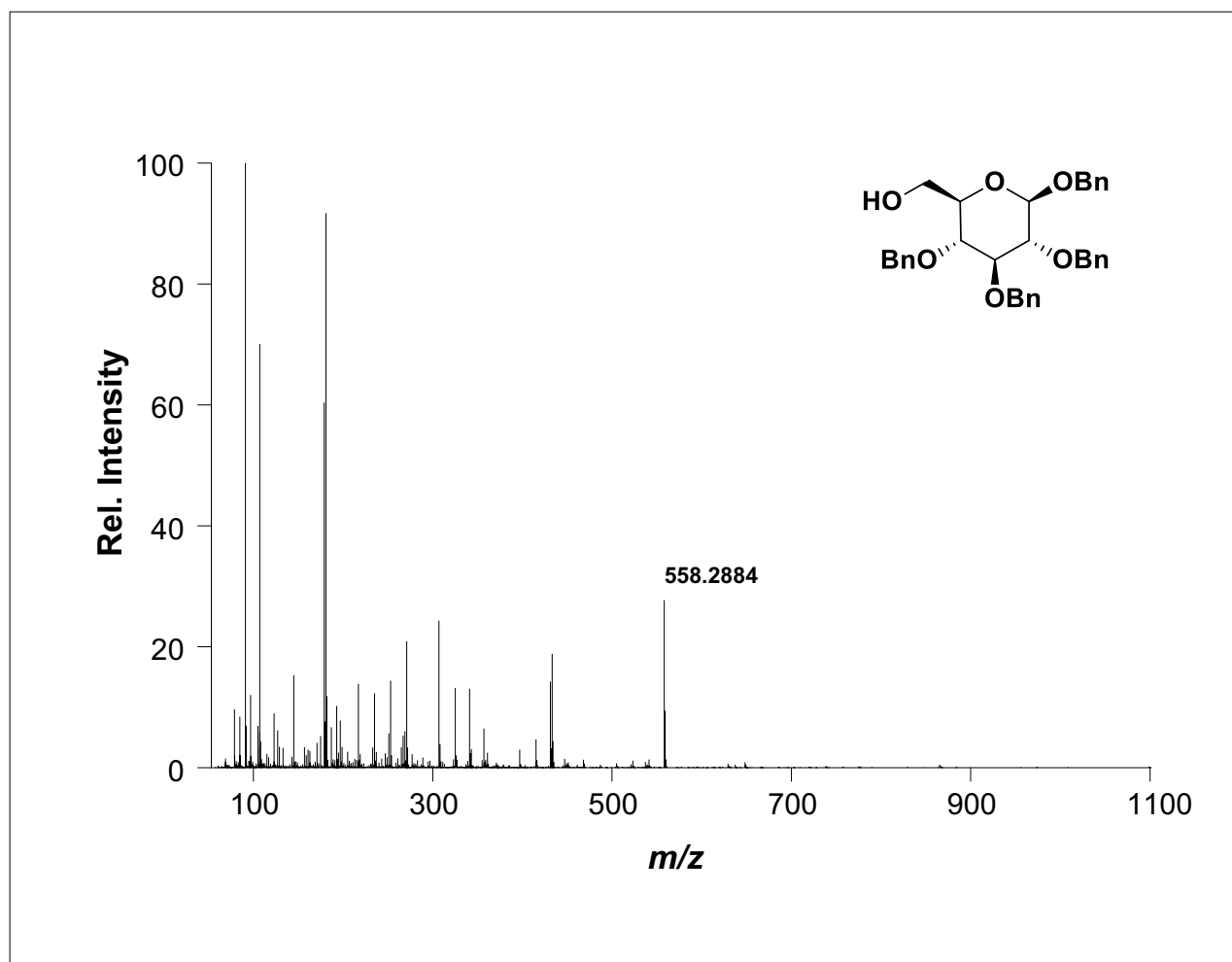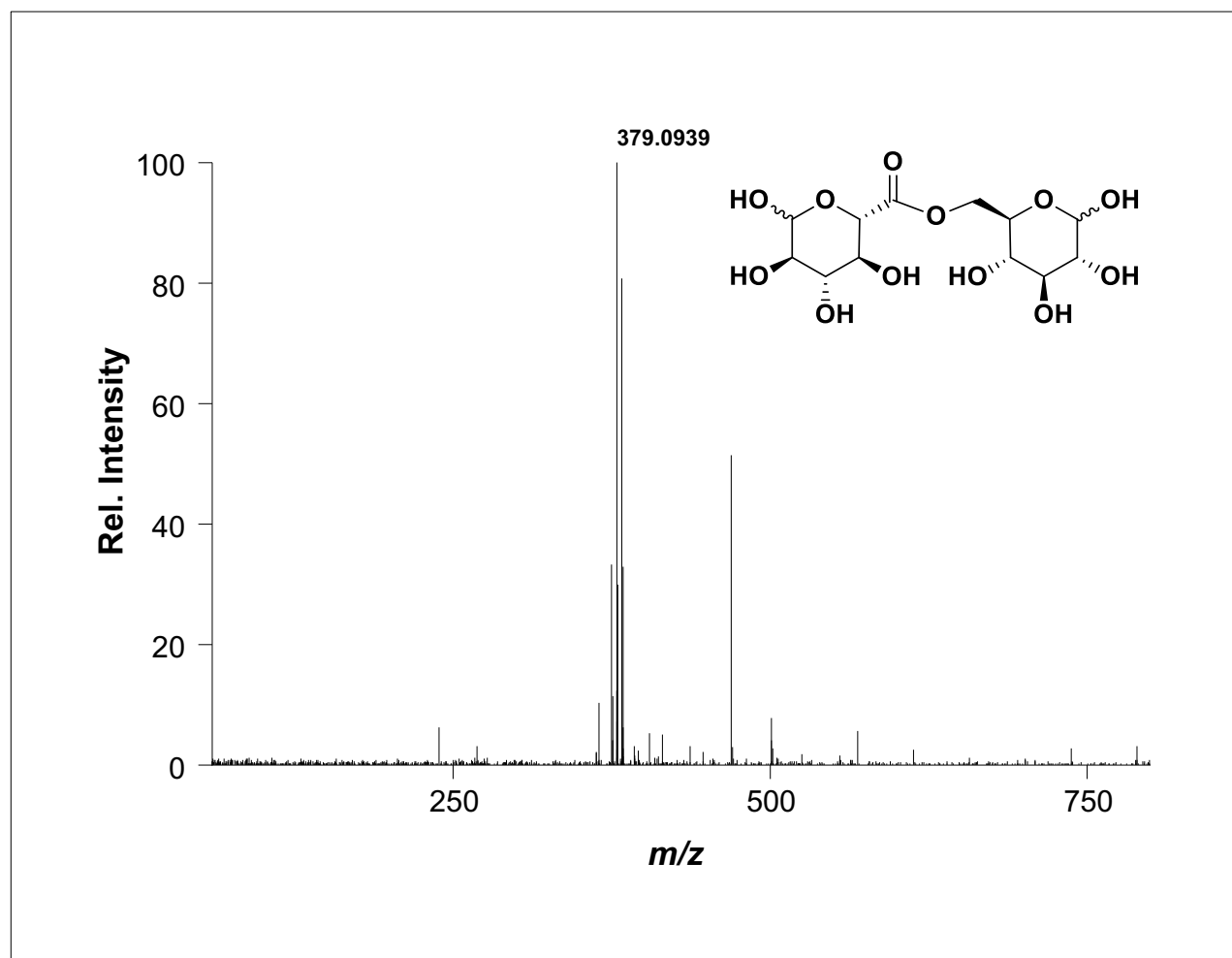
ESI-HRMS of Compound **66** [*α/ß*-D-Glucopyranosyl-(6→6')-*α/ß*-glucopyranuronate]
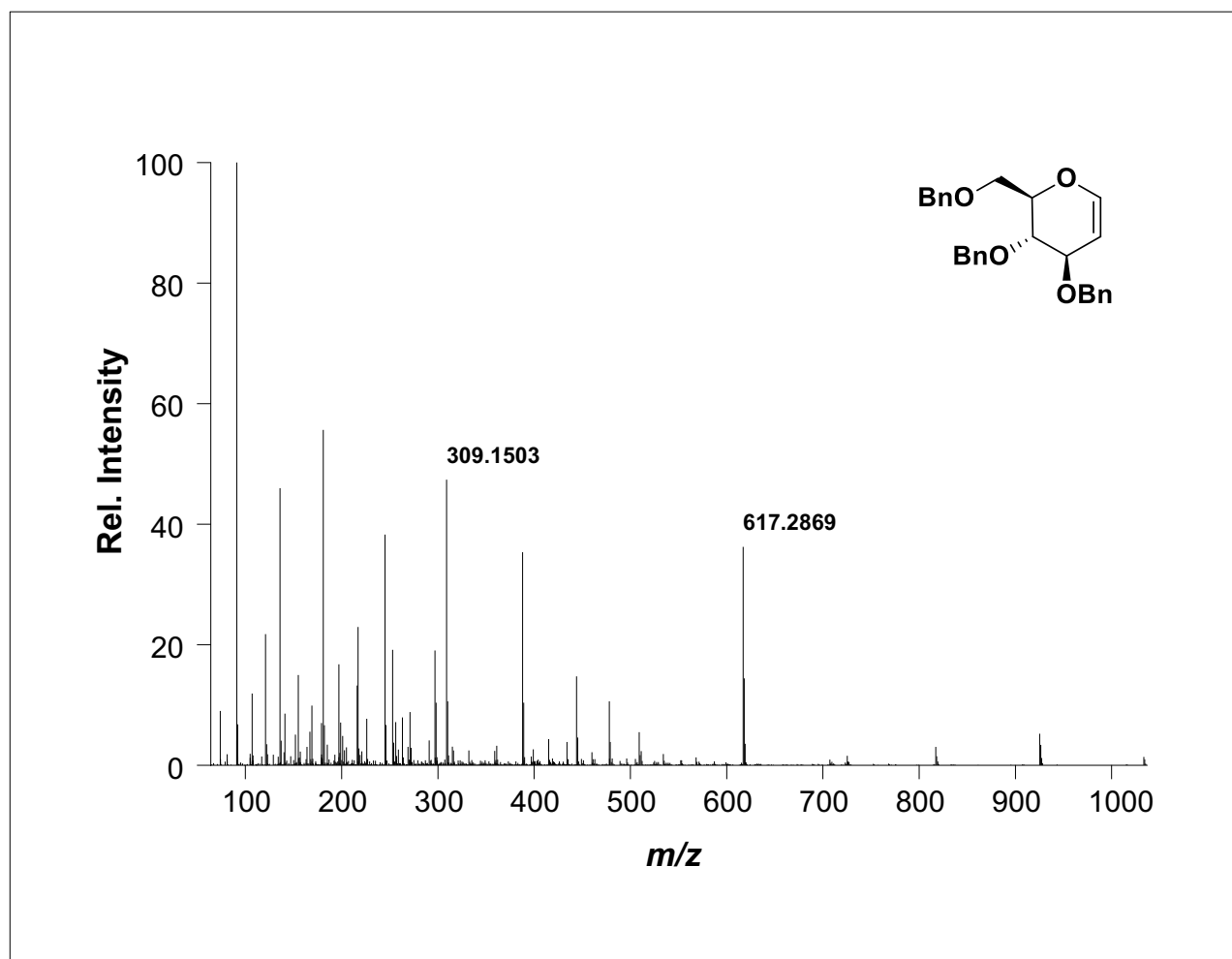
DART-HRMS of Compound **67** [3,4,6-Tri-*O*-benzyl-D-glucal]
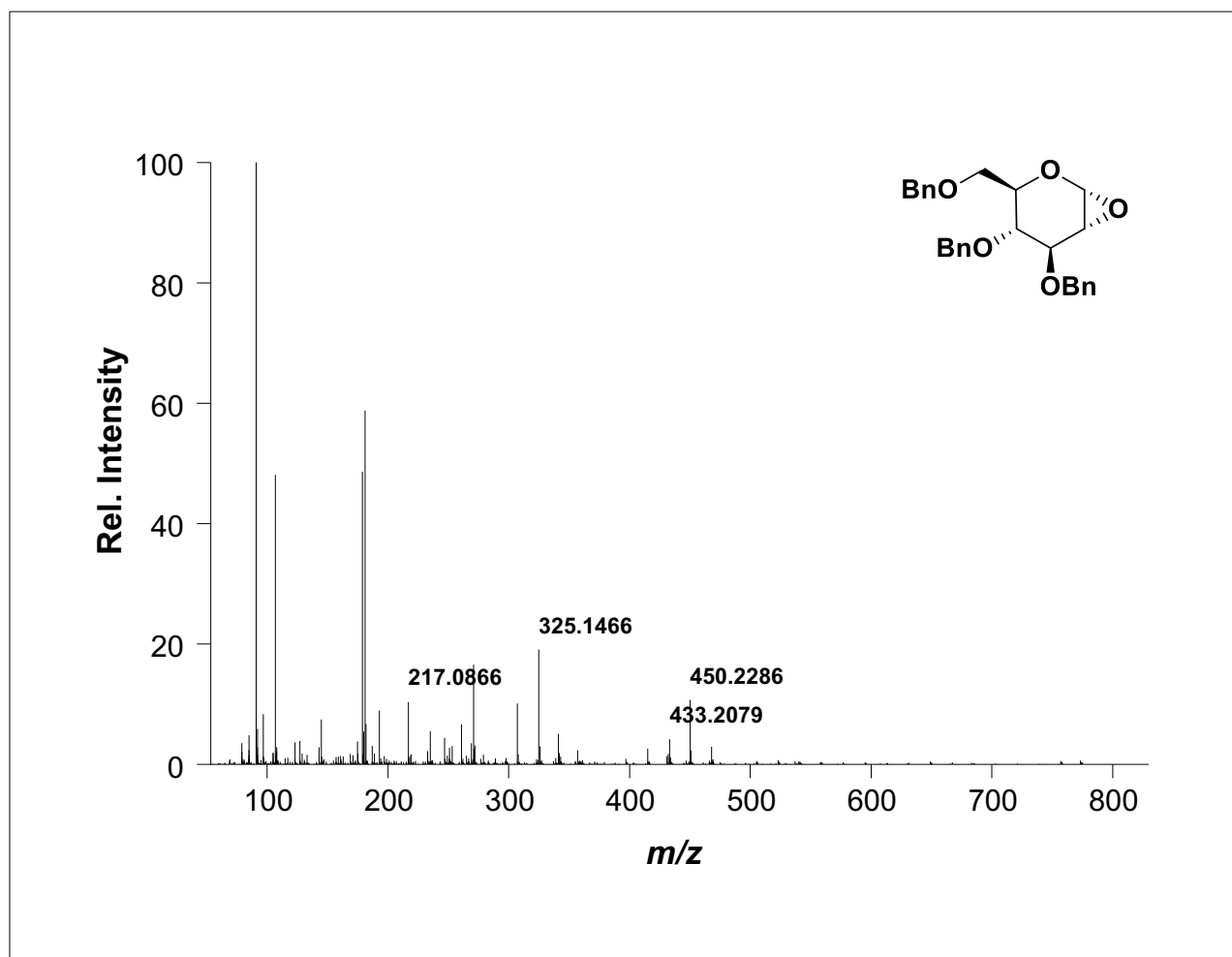
DART-HRMS of Compound **68** [1,2-Anhydro-3,4,5-tri-*O*-benzyl-α-D-glucopyranose]
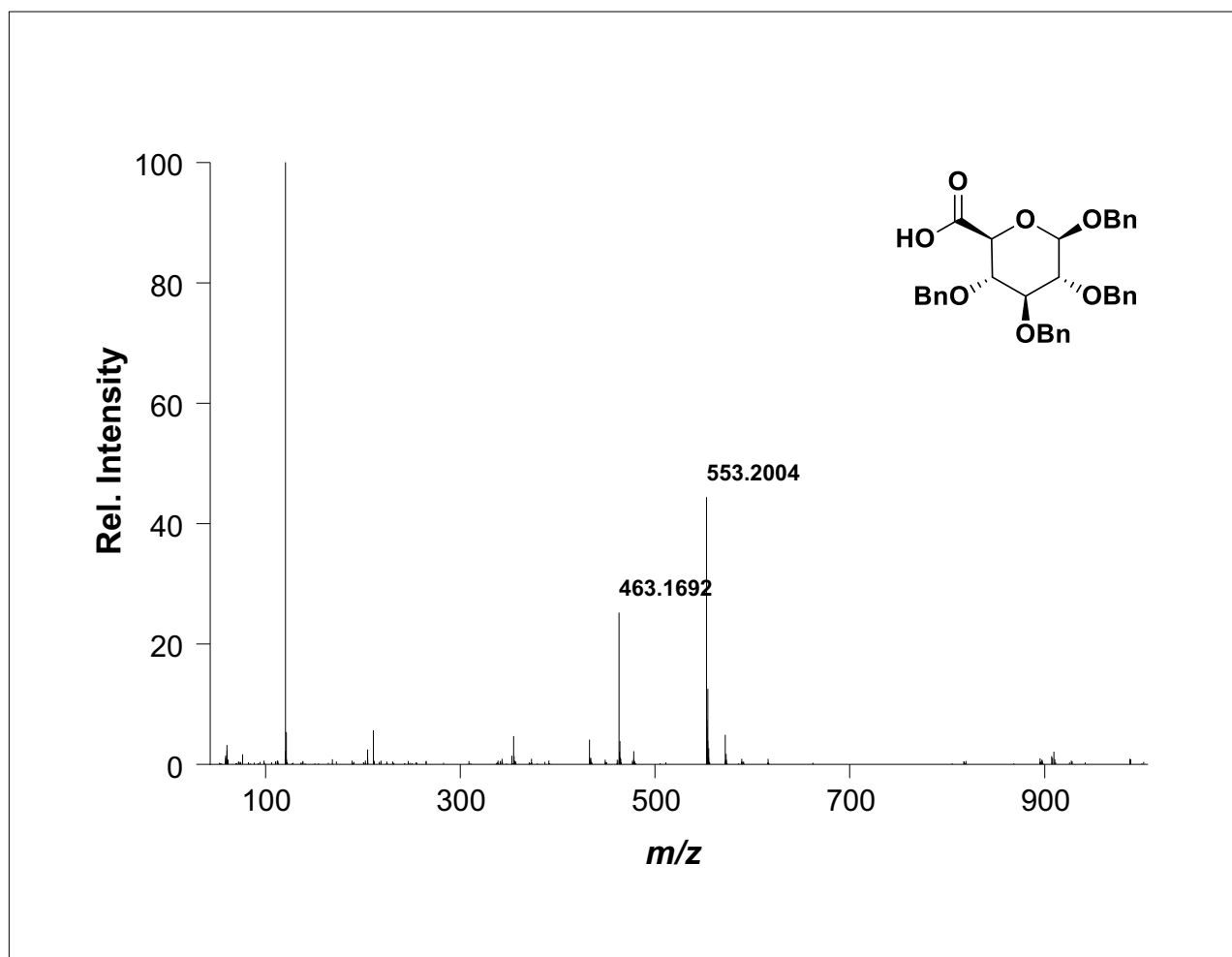
DART-HRMS of Compound **69** [Benzyl-2,3,4-tri-*O*-benzyl-*β*-D-glucopyranuronic acid]

APPENDIX C. COMPUTATIONAL DATA
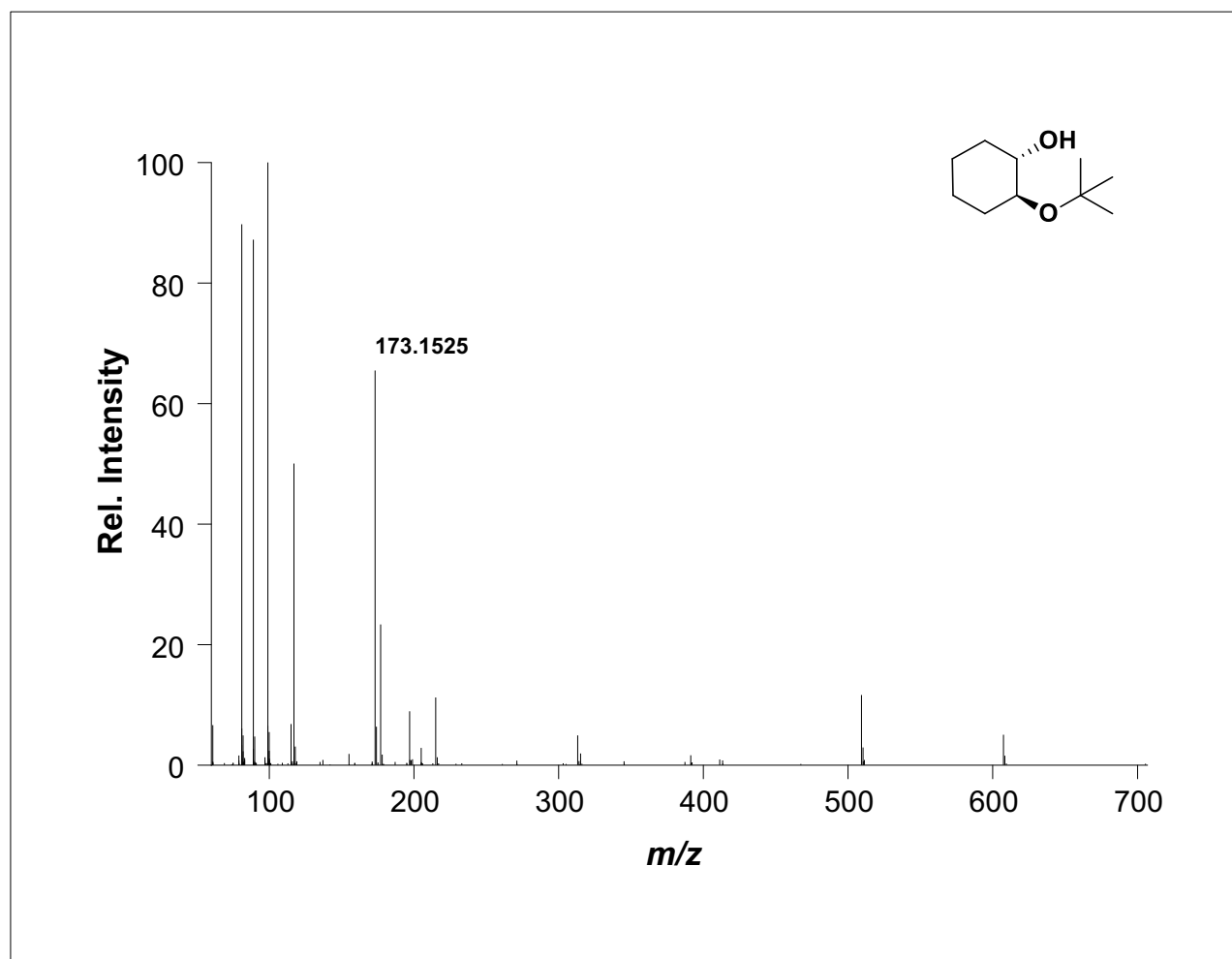
Chapter 2: Diasteroselective Esterification.

HOMO representation of acyl chloride and acyl pyridinium transition state structures for compounds 4, 6 and 27.

(catalyzed reaction with acyl pyridinium on left, uncatalyzed reaction on right)**:**

2-Methyl (*R*,*R*,*R*,*R*)-(a,a)
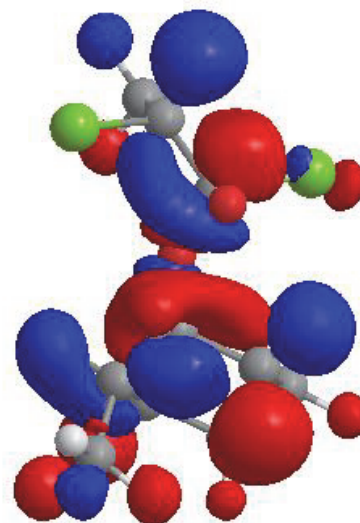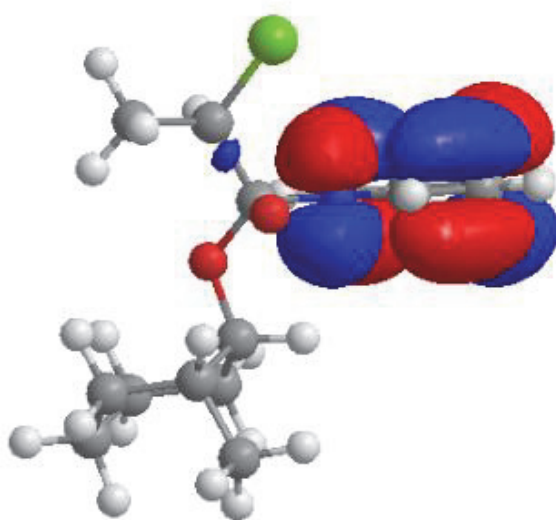
2-Methyl (*R*,*R*,**R**,*R*)-(e,e)
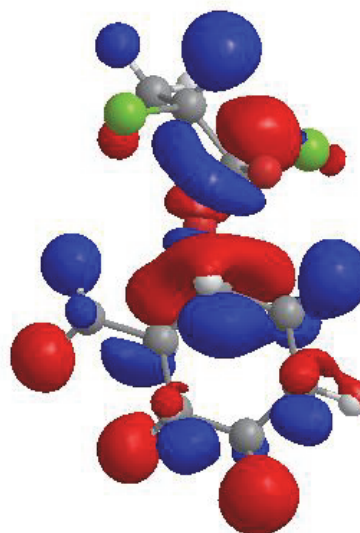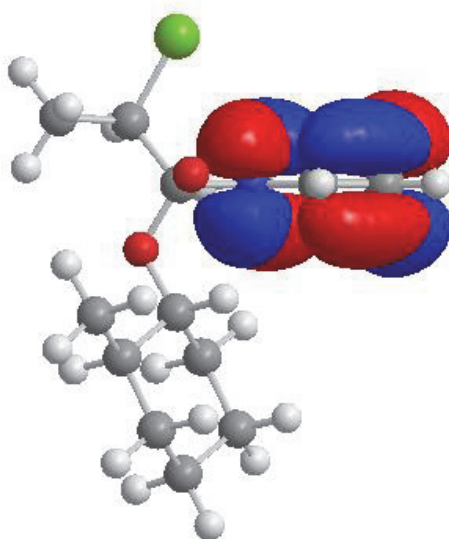
2-Methyl (*R*,*R*,***R***,*S*)-(a,a)
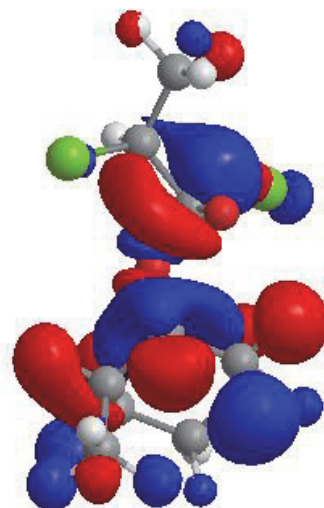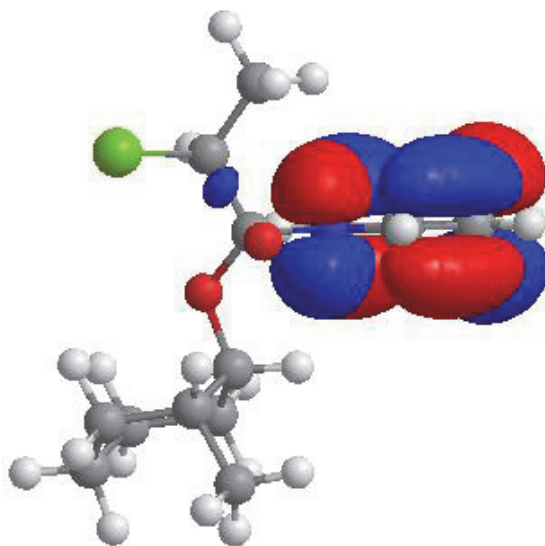
2-Methyl (*R*,*R*,***R***,*S*)-(e,e)
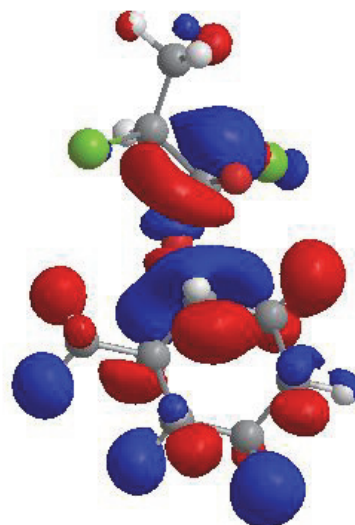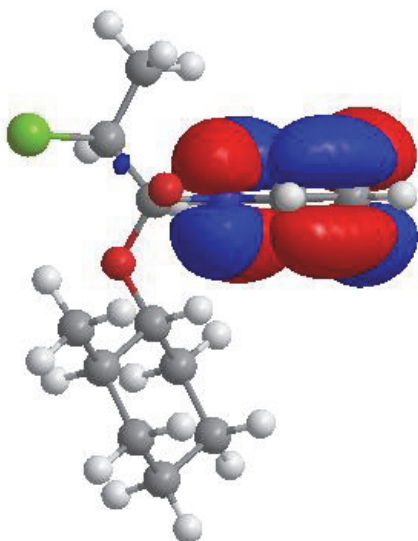
2-Methyl (*R*,*R*,***S***,*R*)-(a,a)
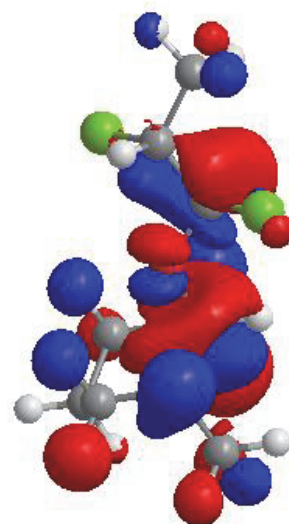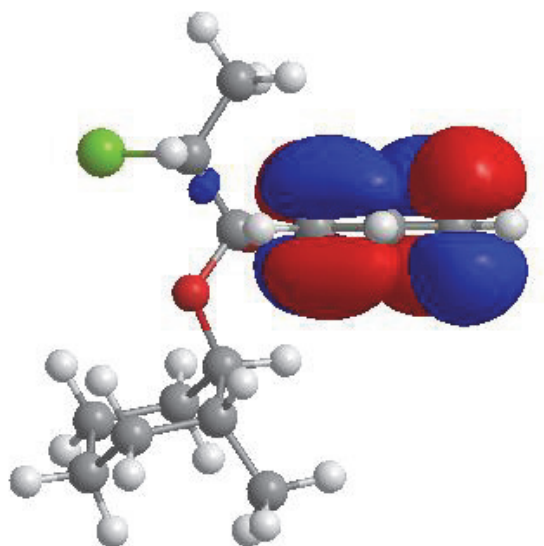
2-Methyl (*R*,*R*,***S***,*R*)-(e,e)
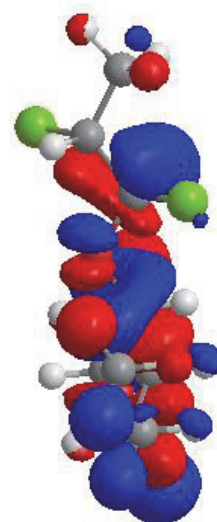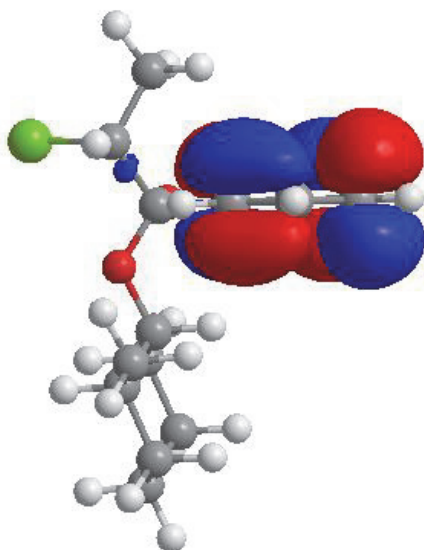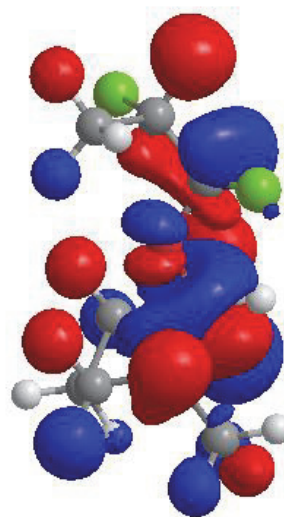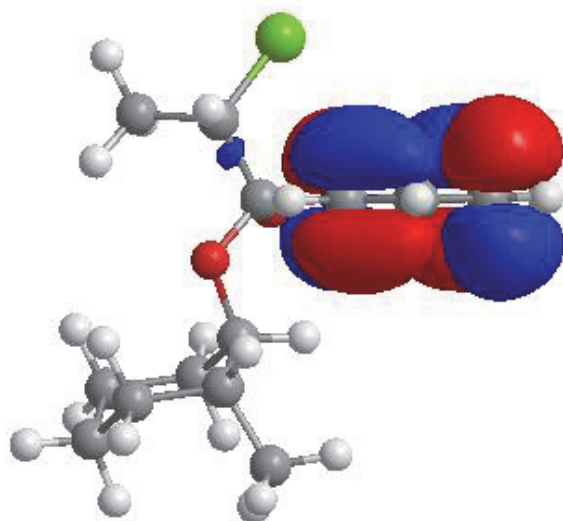
2-Methyl (*R*,*R*,*S*,*S*)-(a,a)

2-Methyl (*R*,*R*,*S*,*S*)-(e,e)
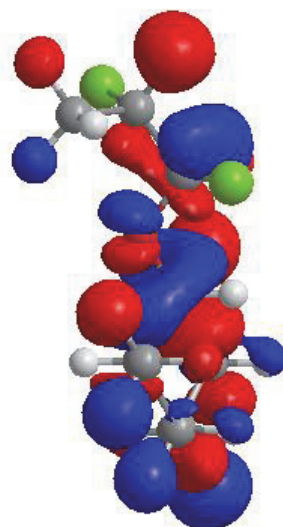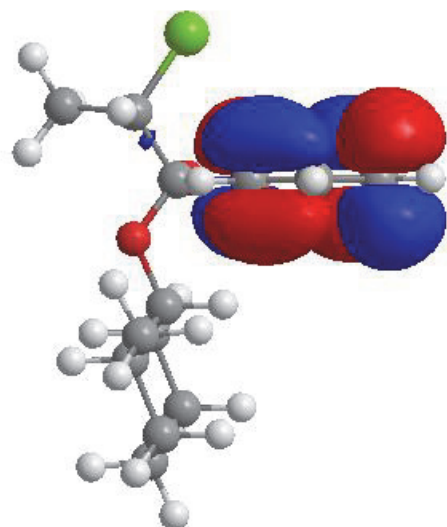
2-OTol (*R*,*R*,***R***,*R*)-(a,a)
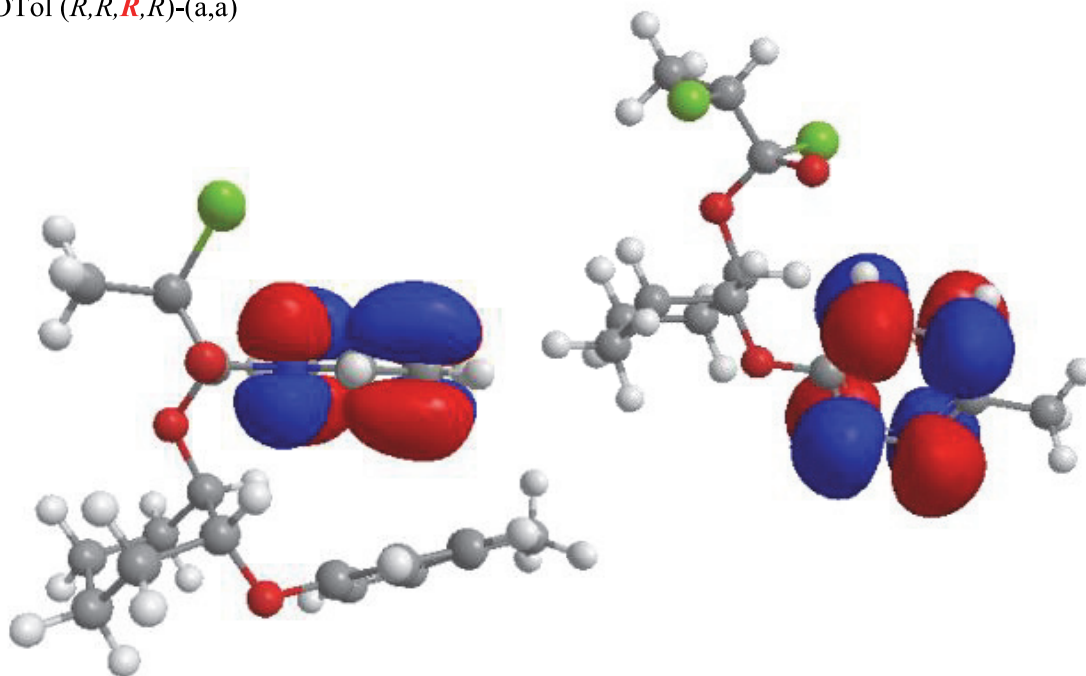
2-OTol (*R*,*R*,***R***,*R*)-(e,e)
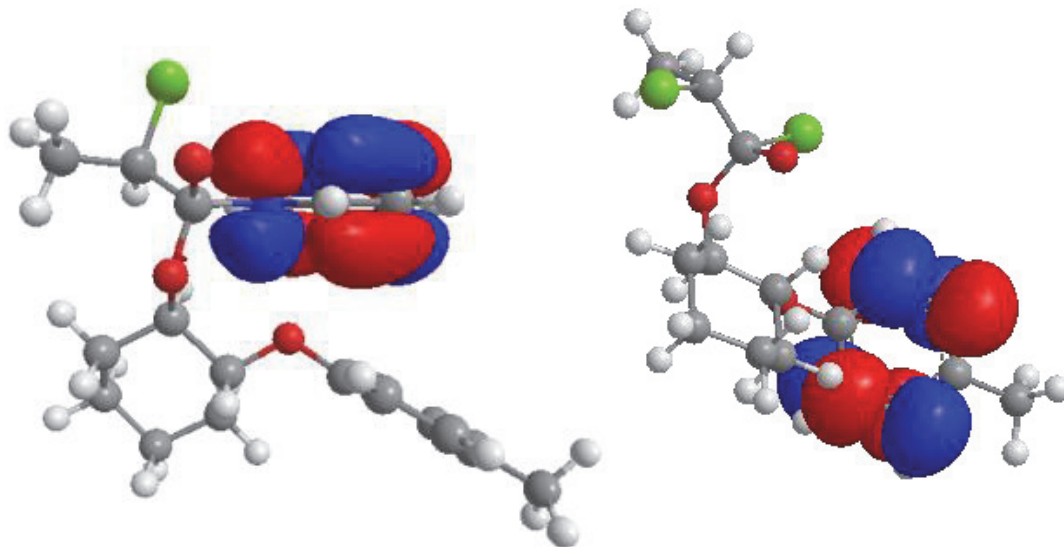
2-OTol (*R*,*R*,***R***,*S*)-(a,a)
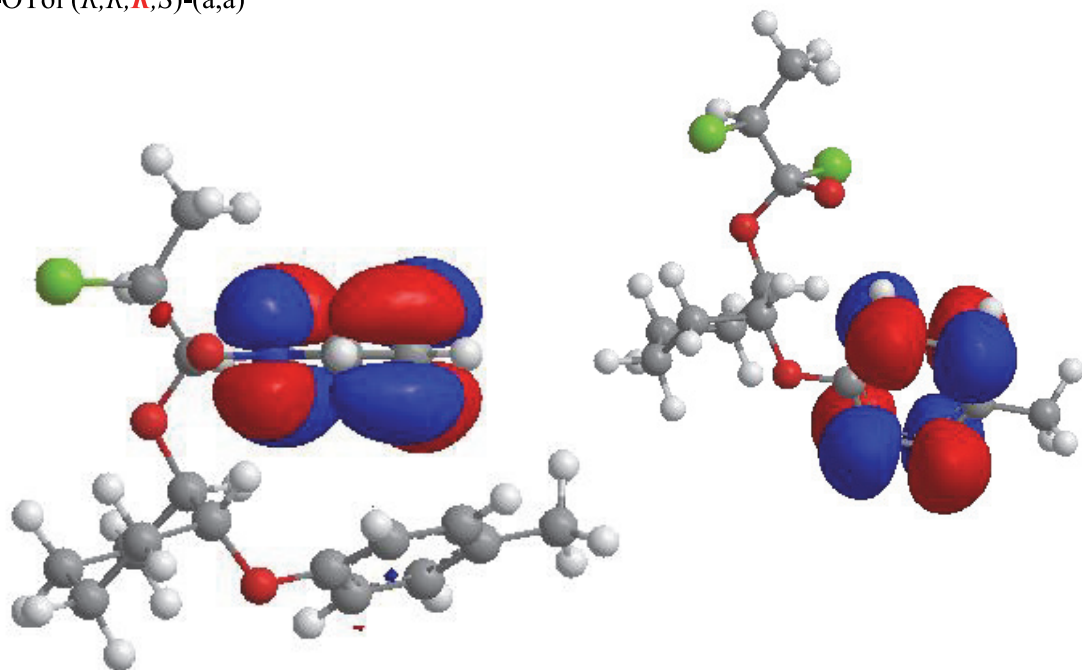
2-OTol (*R*,*R*,***R***,*S*)-(e,e)
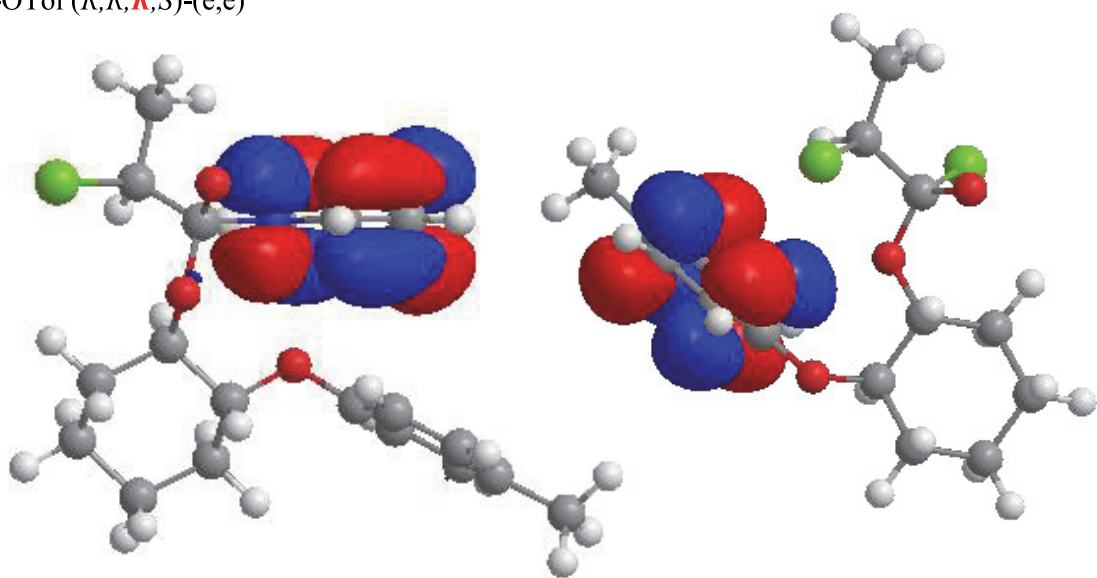
2-OTol (*R*,*R*,***S***,*R*)-(a,a)
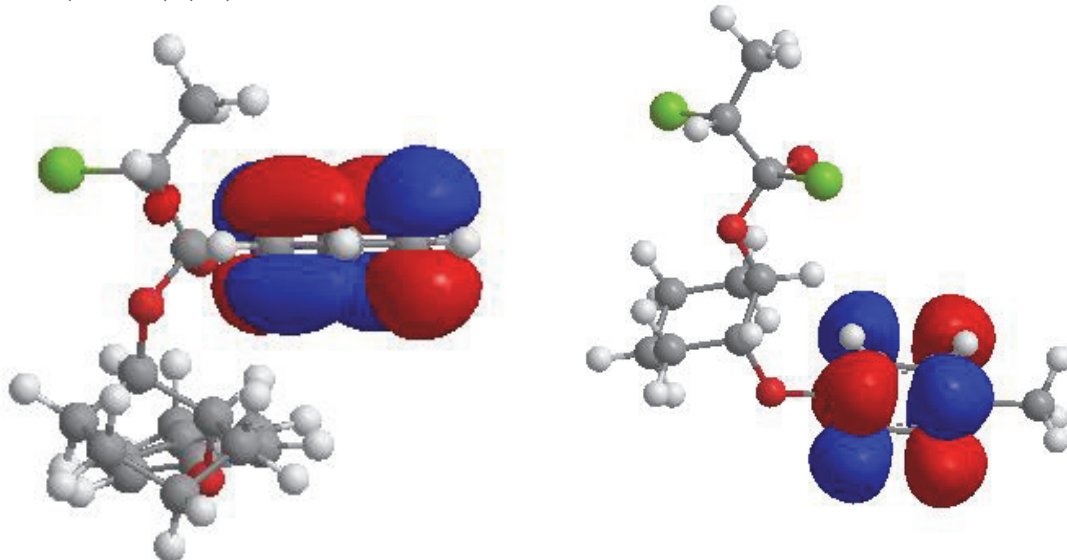
2-OTol (*R*,*R*,***S***,*R*)-(e,e)
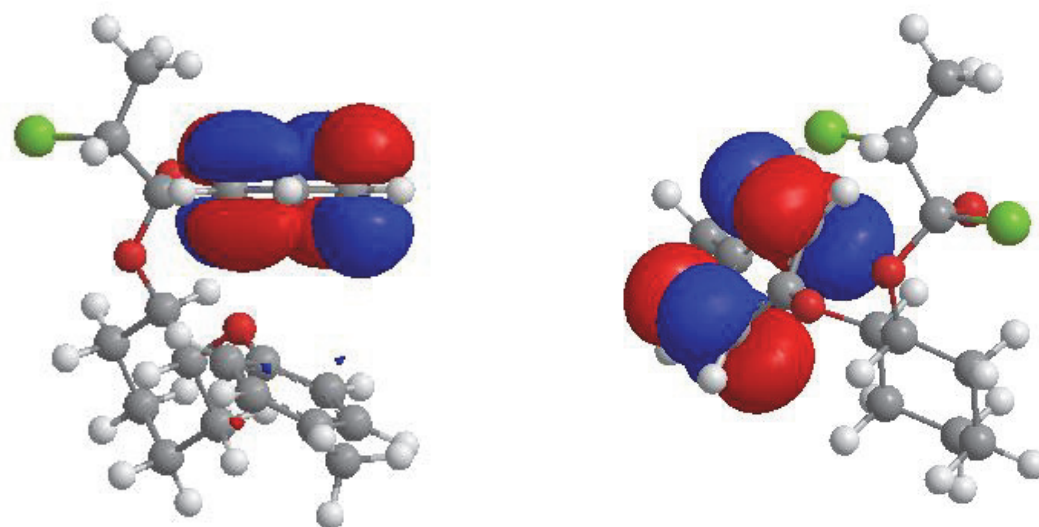
2-OTol (*R*,*R*,***S***,*S*)-(a,a)
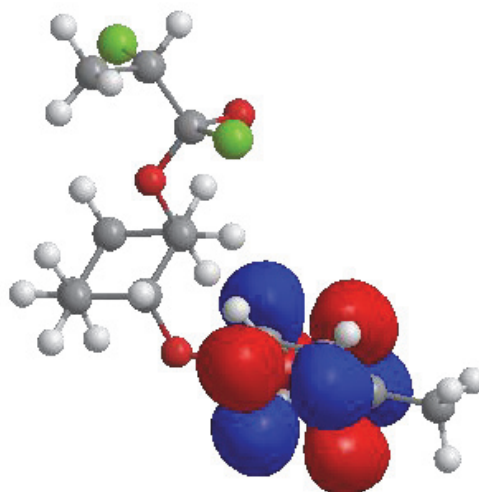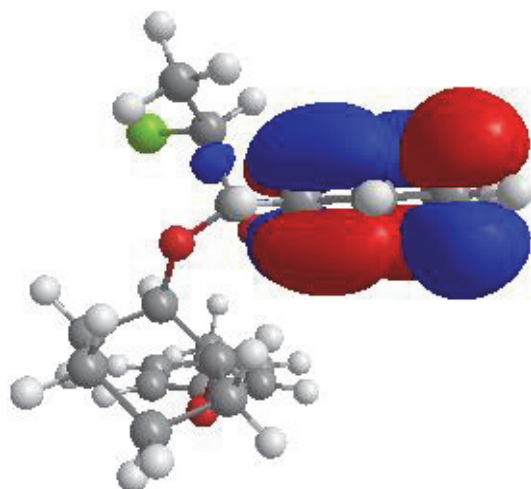
2-OTol (*R*,*R*,***S***,*S*)-(e,e)
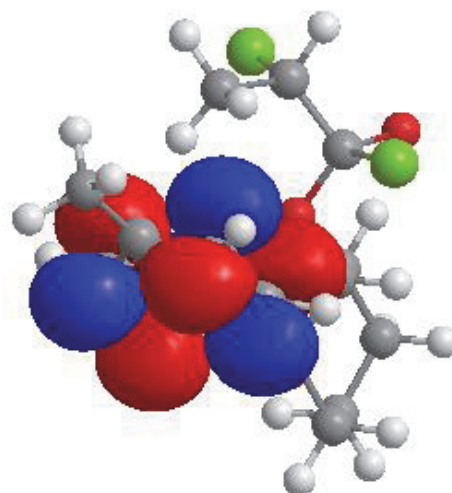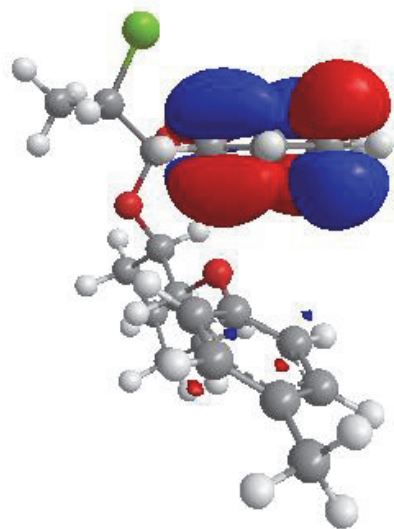
2-STol (*R*,*R*,***R***,*R*)-(a,a)
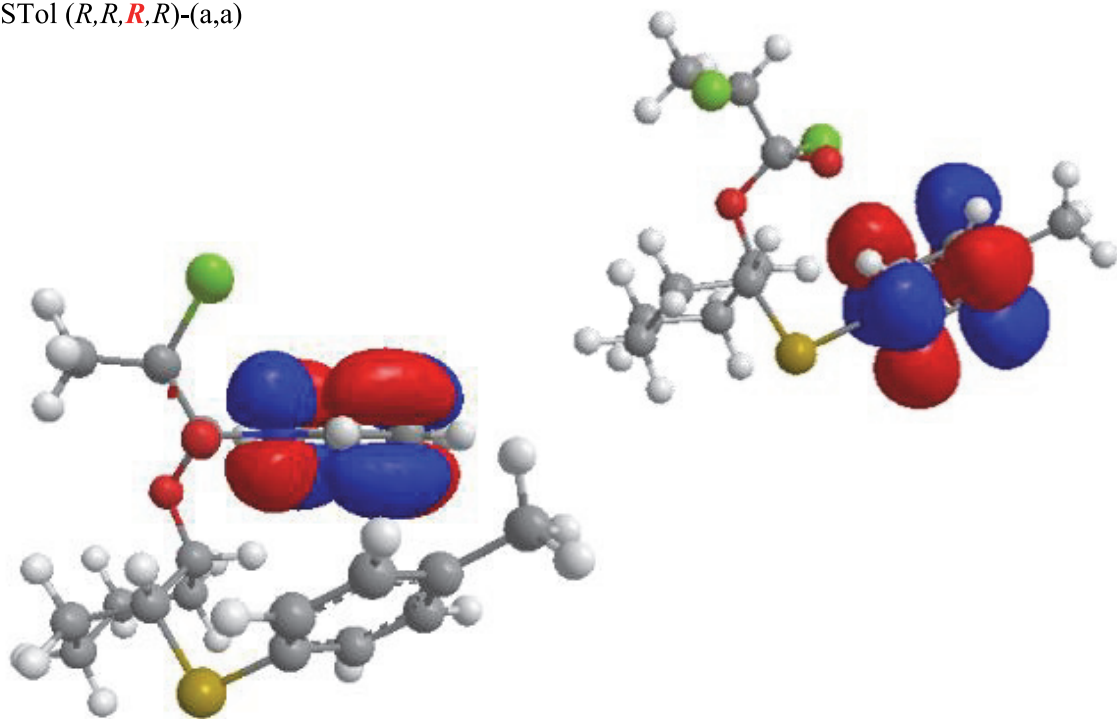
2-STol (*R*,*R*,***R***,*R*)-(e,e)
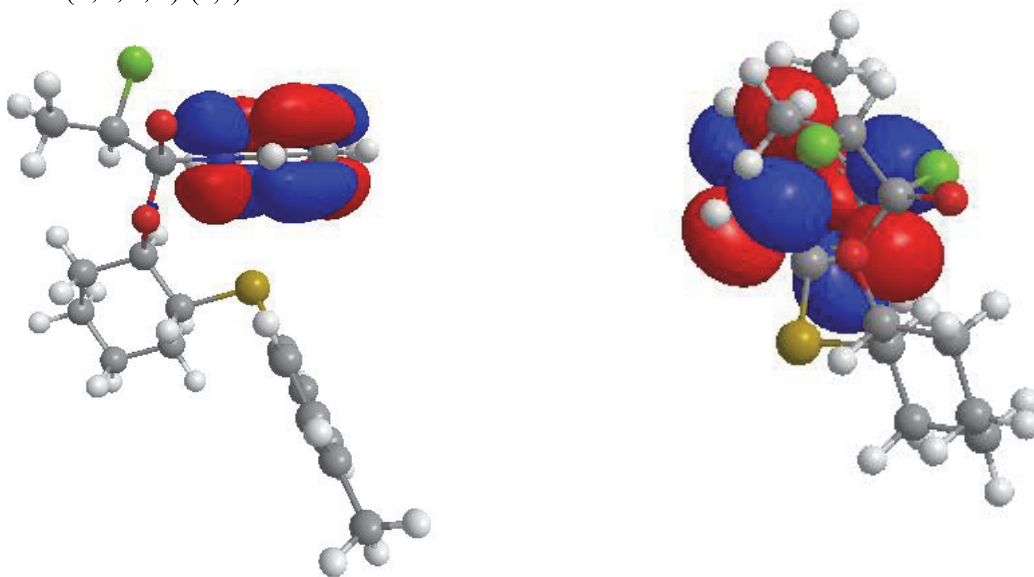
2-STol (*R*,*R*,***R***,*S*)-(a,a)
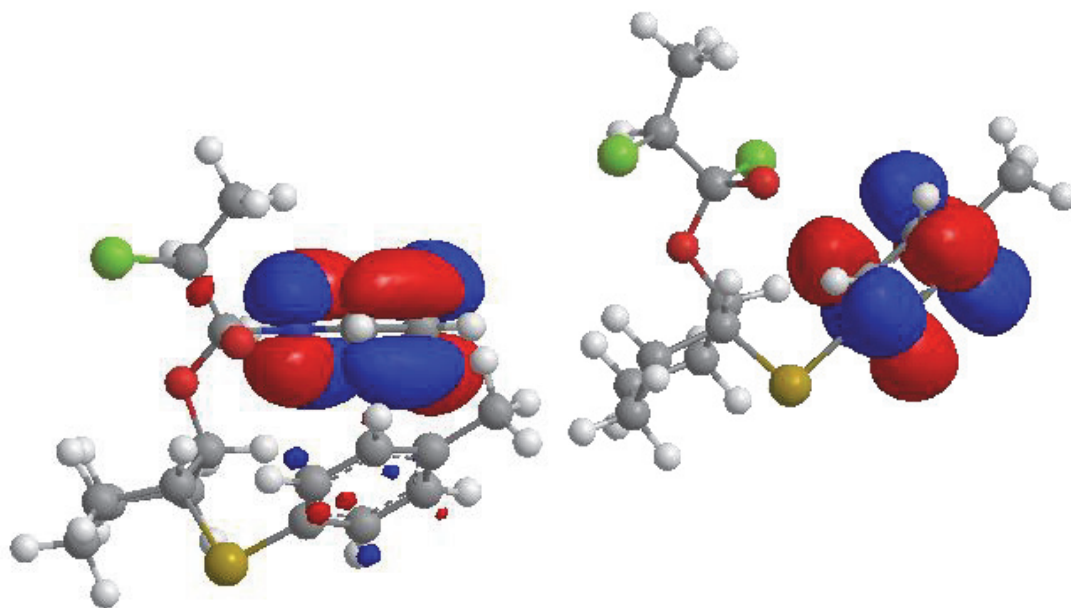
2-STol (*R*,*R*,***R***,*S*)-(e,e)
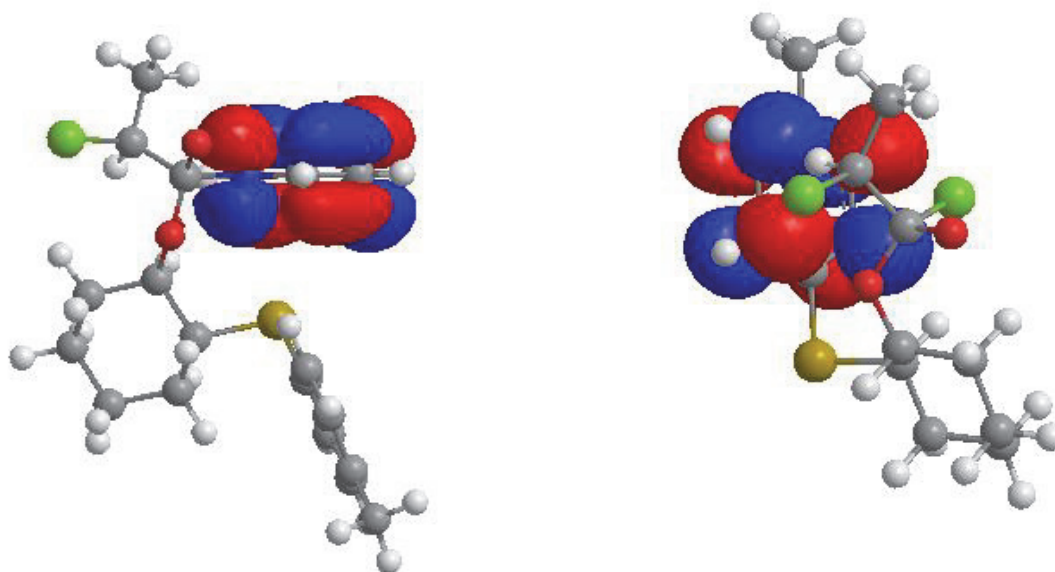
2-STol (*R*,*R*,***S***,*R*)-(a,a)
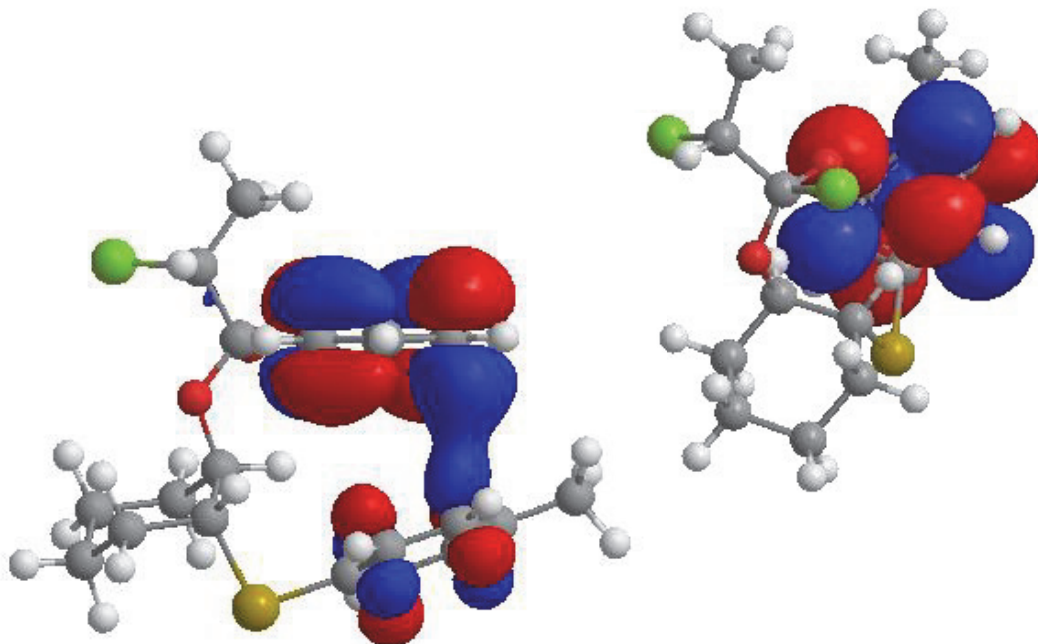
2-STol (*R*,*R*,***S***,*R*)-(e,e)
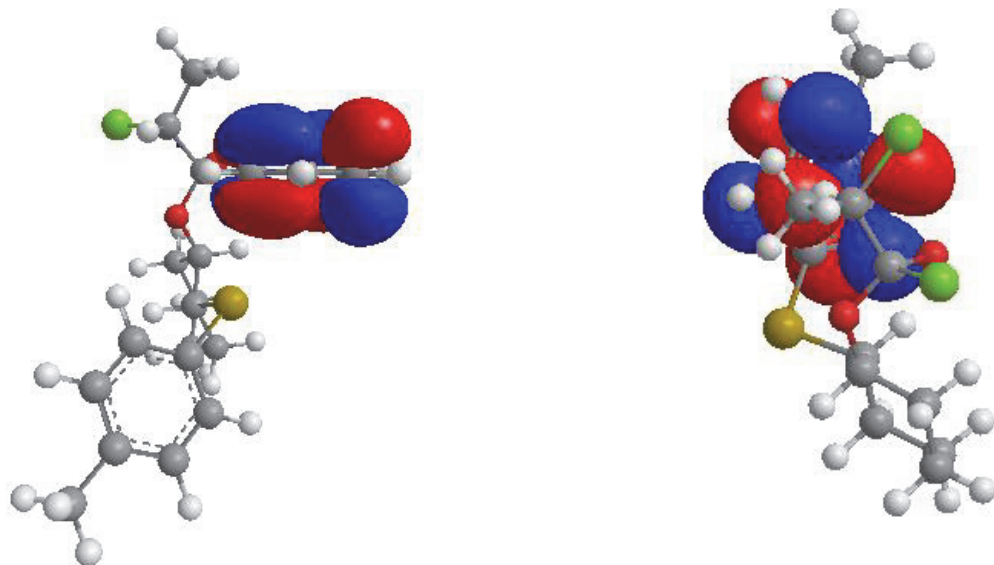
2-STol (*R*,*R*,***S***,*S*)-(a,a)
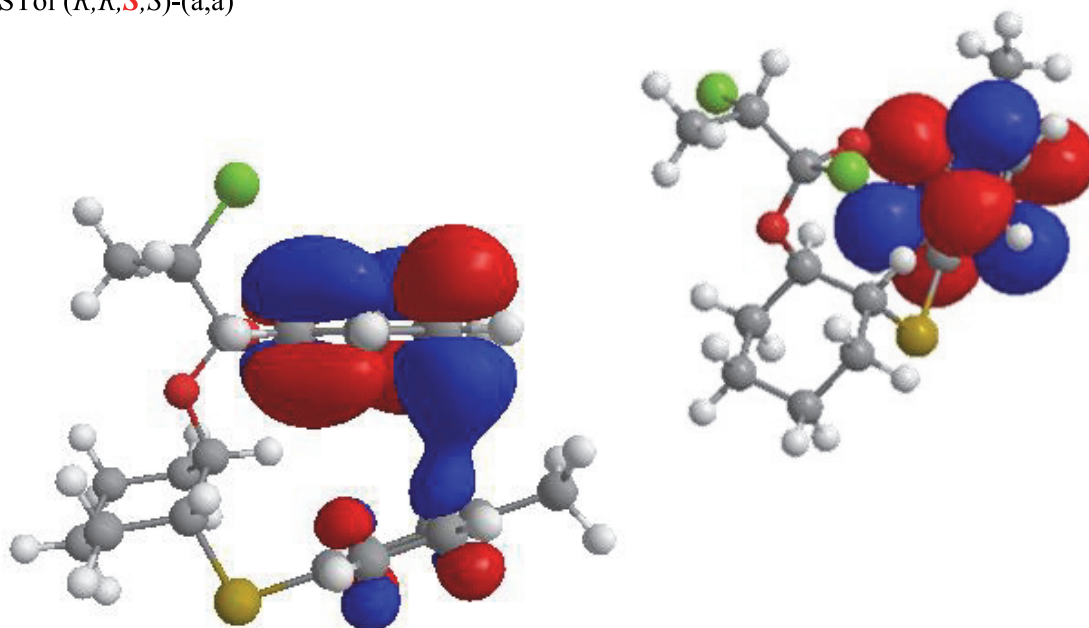
2-STol (*R*,*R*,***S***,*S*)-(e,e)
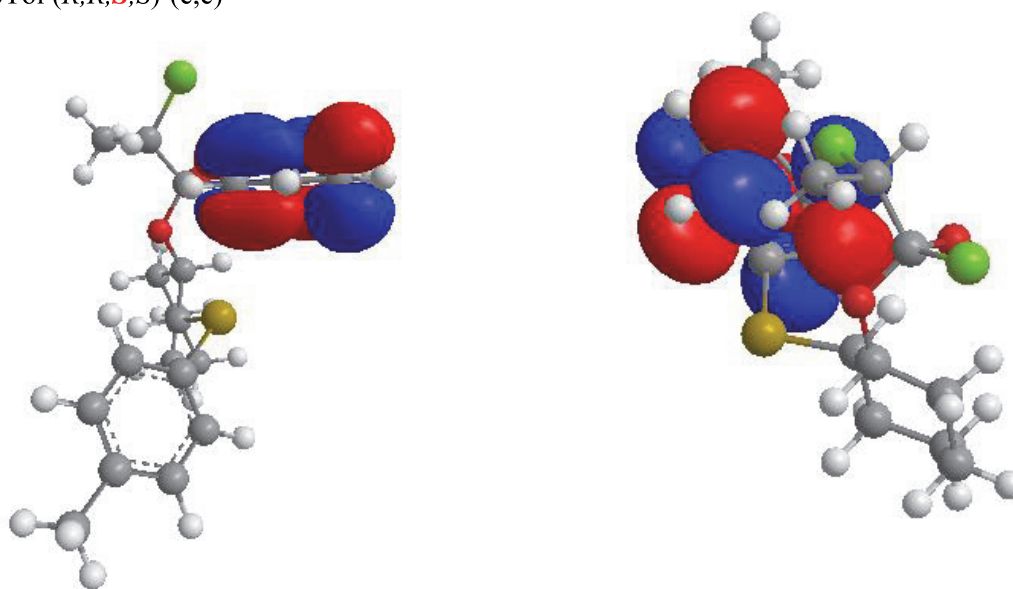
Chapter 4: Development of a Karplus Equation for $^3J_{\mathrm{C}(sp2)\mathrm{OCH}}$.

Molecular Dynamics parameters.

Minimization.

```
Step 1: Minimize with solute held fixed
                  &cntrl
                  imin=1,
              maxcyc=2000,
                ncyc=1000,
                ntpr=100,
                  ntb=1,
                  ntr=1,
                cut=10.0,
                    /
            Hold the sugar fixed
                  500.0
                  RES 1
                   END
                   END

        Step 2: Minimize entire system
                  &cntrl
                  imin=1,
              maxcyc=4500,
                ncyc=1000,
                  ntb=1,
                  ntr=0,
                cut=10.0,
                    /
```

Heating.

```
    Step 1: Heat with weak constraints on solute for 20ps
                      &cntrl
                      imin=0,
                      ntx=1,
                    irest=0,
                      ntb=1,
                      ntr=1,
                  nstlim=10000,
                    dt=0.002,
                      ntf=2,
```

```
                              ntc=2,
                           tempi=0.0,
                          temp0=300.0,
                            cut=8.0,
                             ntb=1,
                             ntt=3,
                         gamma_ln=1.0,
                            ig=-1,
                 ntpr=100, ntwx=100, ntwr=1000
                               /
           Keep sugar fixed with weak restraints
                            10.0
                           RES 1
                            END
                            END


    Step 2: Heat for 100ps with full system without constraints
                          &cntrl
                  imin=0, irest=1, ntx=7,
                ntb=2, pres0=1.0, ntp=1,
                          taup=2.0
                           ntr=0,
                        nstlim=50000,
                          dt=0.002,
                           ntf=2,
                           ntc=2,
                         tempi=300.0,
                         temp0=300.0,
                           cut=8.0,
                    ntt=3, gamma_ln=1.0,
                           ig=-1,
                 ntpr=100, ntwx=100, ntwr=1000
                              /
```

Production run.

```
                   Production 500ns
                        &cntrl
                        imin=0,
                    irest=0, ntx=1,
                   nstlim=500000000,
                        dt=0.001,
                         ntf=2,
                         ntc=2,
                       temp0=300.0,
```

```
ntpr=10000, ntwx=10000, ntwr=100000,
                ntxo=2,
                cut=8.0,
      ntb=2, pres0=1.0, ntp=1, taup=2.0,
                ntt=3,
            gamma_ln=1.0,
                ig=-1,
                  /
```

GLYCAM Parameter fitting results for 1-acetyl linkage

1Ac.frcmod parameters:

```
Os-Cg-Os-C  1   -0.01    0.0           -3        SCEE=1.0 SCNB=1.0ᵇ

            1    0.04    0.0           -2        SCEE=1.0 SCNB=1.0ᵇ

            1    0.12    0.0            1        SCEE=1.0 SCNB=1.0ᵇ

H2-Cg-Os-C  1    0.00    0.0            1        SCEE=1.0 SCNB=1.0ᵇ
```

Acetyl-6-*O*-acetyl-α-D-glucopyranoside

Torsion angle (°)	ΔQM (kcal/mol)	ΔMM (kcal/mol)
82.42	0.38	1.59
112.42	1.03	1.91
142.42	0.00	0.00
172.42	3.14	1.75
202.42	3.56	5.00
232.42	4.84	6.18
262.42	6.29	6.11
292.42	7.84	6.06
322.42	8.46	8.72
352.42	8.90	9.71
22.42	7.10	6.37
52.42	2.92	3.18
< Error >		0.85
% of maximum barrier		8.8/9.6

---

[b] Based on suggestions from GLYCAM community (GLYCAM-L@LISTSERV.UGA.EDU)

Acetyl-6-*O*-acetyl-*β*-D-glucopyranoside

Torsion angle (°)	ΔQM (kcal/mol)	ΔMM (kcal/mol)
64.46	3.88	1.04
94.46	5.41	4.04
124.46	8.90	7.70
154.46	6.56	7.26
184.46	5.20	5.17
214.46	4.36	5.47
244.46	0.63	0.43
274.46	0.00	0.00
304.46	2.59	1.57
334.46	8.31	5.78
4.46	10.99	7.48
34.46	7.07	3.21
	< Error >	1.53
	% of maximum barrier	19.9/13.9

(Tetrahydropyran-2-yl)-methyl acetate

Torsion angle (°)	ΔQM (kcal/mol)	ΔMM (kcal/mol)
279.1	0.00	0.00
309.1	2.99	1.87
339.1	8.57	5.79
9.1	10.13	6.79
39.1	6.07	3.56
69.1	4.04	3.91
99.1	5.92	6.99
129.1	6.88	7.35
159.1	4.86	4.93
189.1	1.56	0.96
219.1	0.77	0.01
249.1	0.37	0.09
	< Error >	1.09
	% of maximum barrier	14.9/10.8

Acetyl-6-*O*-acetyl-*α*-D-glucopyranoside
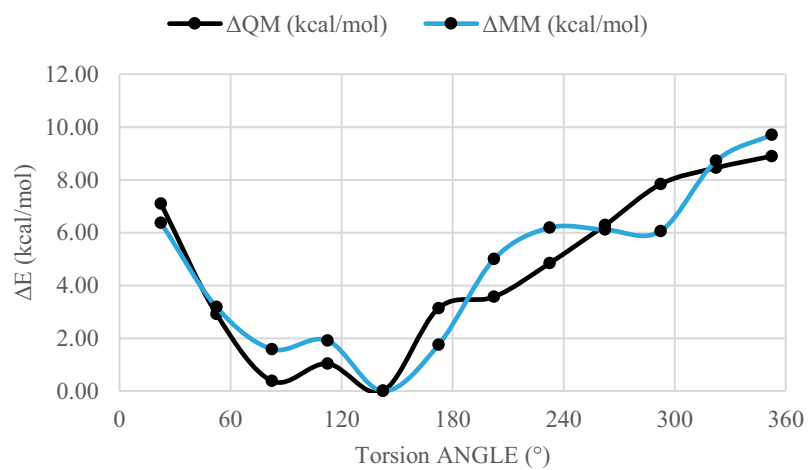
Acetyl-6-*O*-acetyl-*β*-D-glucopyranoside
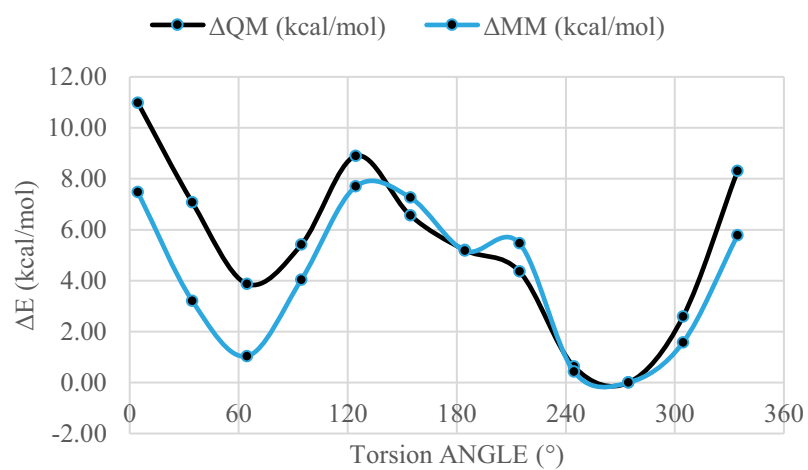
(Tetrahydropyran-2-yl)-methyl acetate
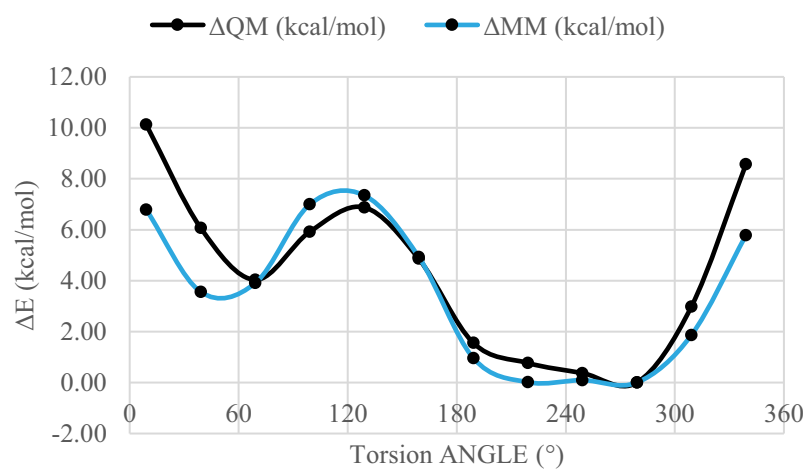
GLYCAM Parameter fitting results for 6-ester linkage

Minimization MM input

```
                    Minimize
                     &cntrl
                    imin=1,
              maxcyc=6000, ncyc=2000,
                     ntb=0,
                    cut=10.0,
                    nmropt=1,
                       /
                 &wt type='END',
                       /
        DISANG=methylmethoxyacetate_B3LYP_SPXX.RST
```

Example dihedral angle restraint input[c]

```
 # 15 atoms read from pdb file
methylmethoxyacetate_B3LYP_SP0.pdb.
 # 1 mma OCCO:  (1 mma O1)-(1 mma C2)-(1 mma C3)-(1 mma O2) 180.0
180.0
  &rst    iat =     2,     6,     7,     8,
       r1 = 178.97, r2 = 179.97, r3 = 179.97, r4 = 180.97,
       rk2 =   5000.0, rk3 =   5000.0,                      &end
```

Results:

MeDGlc.frcmod parameters:

```
        Os-Cg-C -O    1    0.04    0.0    -3.    SCEE=1.0 SCNB=1.0
                      1   -1.25    0.0    -2.    SCEE=1.0 SCNB=1.0
                      1    0.01    0.0     1.    SCEE=1.0 SCNB=1.0
        Os-C -Cg-Os   1    0.40    0.0     1.    SCEE=1.0 SCNB=1.0
        Os-C -Cg-H1   1    0.00    0.0     1.    SCEE=1.0 SCNB=1.0
```

---

[c] See http://ambermd.org/tutorials/advanced/tutorial4/ for a helpful tutorial on torsional restraints in AMBER.

methyl THP-2-carboxylate

Torsion angle (°)	ΔQM (kcal/mol)	ΔMM (kcal/mol)
14.89	0.19	0.28
44.89	0.33	0.19
74.89	0.48	0.94
104.89	0.37	1.68
134.89	0.36	1.31
164.89	0.25	0.47
194.89	0.00	0.00
224.89	0.12	0.46
254.89	0.82	1.96
284.89	1.68	2.74
314.89	1.84	2.47
344.89	1.01	1.46
14.89	0.19	0.28
	< Error >	0.57
	% of maximum barrier	20.7 / 30.8

methyl methoxyacetate

Torsion angle (°)	ΔQM (kcal/mol)	ΔMM (kcal/mol)
180.00	0.00	0.00
210.00	0.51	0.38
240.00	1.31	1.02
270.00	1.31	1.19
300.00	0.82	0.84
330.00	0.30	0.57
0.00	0.12	0.53
30.00	0.30	0.57
60.00	0.82	0.84
90.00	1.31	1.19
120.00	1.31	1.03
150.00	0.51	0.38
180.00	0.00	0.00
	< Error >	0.17
	% of maximum barrier	14.5 / 13.1

Average of both compounds

	< Error >	0.37
	% of maximum barrier	16.9 / 22.7

The above error and % of maximum barrier compare favorably to the results obtained for the carboxylate group (0.72 kcal/mol and 38.0%) in the original GLYCAM06 paper.[146]

Any correction to the torsion parameters to adjust the MM data to fit closer (lower) to the QM data in methyl THP-2-carboxylate would inevitably move it further away from the target QM values for methyl methoxyacetate (compare figures below). Thus, the established parameters above represent the best compromise on the basis of the mean <error> values for both compounds.

methyl THP-2-carboxylate
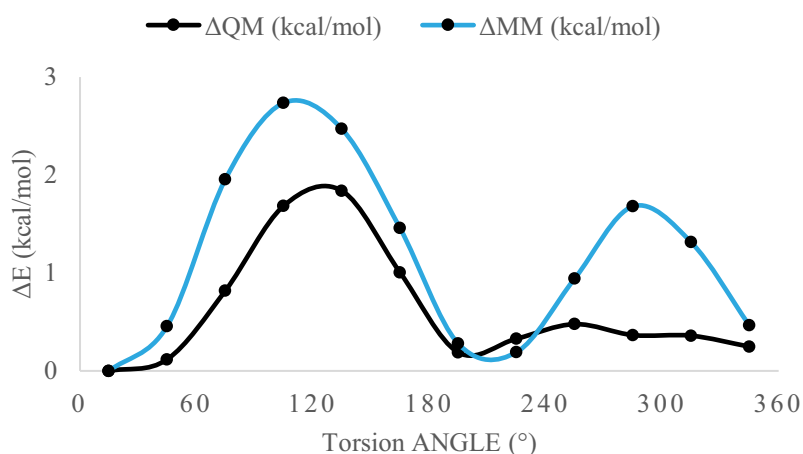
methyl methoxyacetate
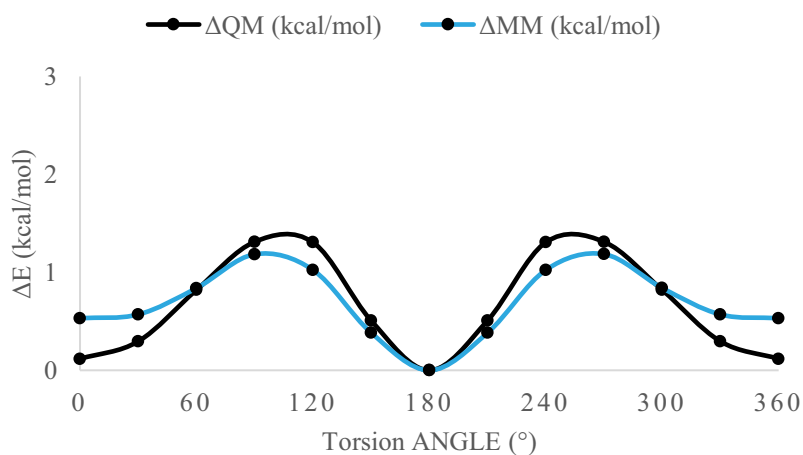
Atomic charges derived for _α/β_-47, _α/β_-50 and 53 based on procedure by Cornell et al.[154]

Acetyl-6-_O_-acetyl-_α_-D-glucopyranoside _α_-**2**

C5	Cg	0.187680
C4	Cg	0.256063
C3	Cg	0.267703
C2	Cg	0.210290
C1	Cg	0.655238
O5	Os	-0.582957
H1	H2	0.000000
H2	H1	0.000000
H3	H1	0.000000
H4	H1	0.000000
H5	H1	0.000000
C6	Cg	0.398599
H61	H1	0.000000
H62	H1	0.000000
O6	Os	-0.508444
CA3	C	0.736774
CA4	Cg	0.044833
HA4	Hc	0.000000
HA5	Hc	0.000000
HA6	Hc	0.000000
OA2	O	-0.600784
O4	Oh	-0.695237
HO4	Ho	0.435529
O3	Oh	-0.695870
HO3	Ho	0.446324
O2	Oh	-0.703122
HO2	Ho	0.441322
O1	Os	-0.465162
CA1	C	0.678461
CA2	Cg	0.056753
HA1	Hc	0.000000
HA2	Hc	0.000000
HA3	Hc	0.000000
OA1	O	-0.563995

Acetyl-6-*O*-acetyl-α-D-glucopyranoside *β*-**47**

```
C5    Cg     0.157695
C4    Cg     0.256866
C3    Cg     0.282844
C2    Cg     0.252268
C1    Cg     0.595842
O5    Os    -0.508318
H1    H2     0.000000
H2    H1     0.000000
H3    H1     0.000000
H4    H1     0.000000
H5    H1     0.000000
C6    Cg     0.391920
H61   H1     0.000000
H62   H1     0.000000
O6    Os    -0.506155
CA3   C      0.739965
CA4   Cg     0.042963
HA4   Hc     0.000000
HA5   Hc     0.000000
HA6   Hc     0.000000
OA2   O     -0.600621
O4    Oh    -0.701072
HO4   Ho     0.439388
O3    Oh    -0.710394
HO3   Ho     0.448685
O2    Oh    -0.726056
HO2   Ho     0.450433
O1    Os    -0.514949
CA1   C      0.723895
CA2   Cg     0.057891
HA1   Hc     0.000000
HA2   Hc     0.000000
HA3   Hc     0.000000
OA1   O     -0.573091
```

Methyl-α-D-glucoronate α-**50**

```
C5    Cg    0.203469
C4    Cg    0.240155
O5    Os   -0.625264
C1    Cg    0.598023
C2    Cg    0.205744
C3    Cg    0.411706
C6    C"    0.846180
H5    H1    0.000000
O62   Os   -0.483378
CM    Cg    0.306565
HM1   H1    0.000000
HM2   H1    0.000000
HM3   H1    0.000000
O61   O"   -0.604046
O4    Oh   -0.729197
H4    H1    0.000000
HO4   Ho    0.448741
O3    Oh   -0.747212
H3    H1    0.000000
HO3   Ho    0.446781
O2    Oh   -0.708367
H2    H1    0.000000
HO2   Ho    0.445286
O1    Oh   -0.712912
H1    H2    0.000000
HO1   Ho    0.457724
```

Methyl-*β*-D-glucoronate *β*-**50**

```
C5    Cg     0.162756
C4    Cg     0.280145
O5    Os    -0.575959
C1    Cg     0.550484
C2    Cg     0.300668
C3    Cg     0.291477
C6    C      0.851559
H5    H1     0.000000
O62   Os    -0.482506
CM    Cg     0.309702
HM1   H1     0.000000
HM2   H1     0.000000
HM3   H1     0.000000
O61   O     -0.605135
O4    Oh    -0.733893
H4    H1     0.000000
HO4   Ho     0.459403
O3    Oh    -0.731423
H3    H1     0.000000
HO3   Ho     0.460004
O2    Oh    -0.745306
H2    H1     0.000000
HO2   Ho     0.456490
O1    Oh    -0.704345
H1    H2     0.000000
HO1   Ho     0.455875
```

(Tetrahydropyran-2-yl)-methyl acetate **53**

```
C1   c3    0.223353
C2   c3    0.017711
C3   c3   -0.002925
C4   c3    0.003924
C5   c3    0.203133
O5   os   -0.443565
C6   c3    0.326198
O6   os   -0.510537
C1'  c     0.756385
C2'  c3    0.033436
O1'  o    -0.607115
H11  h1    0.000000
H12  h1    0.000000
H21  hc    0.000000
H22  hc    0.000000
H31  hc    0.000000
H32  hc    0.000000
H41  hc    0.000000
H42  hc    0.000000
H51  h1    0.000000
H61  h1    0.000000
H62  h1    0.000000
HM1  hc    0.000000
HM2  hc    0.000000
HM3  hc    0.000000
```

Representative example of Minimization and Heating convergence

Initial Restrained Minimization
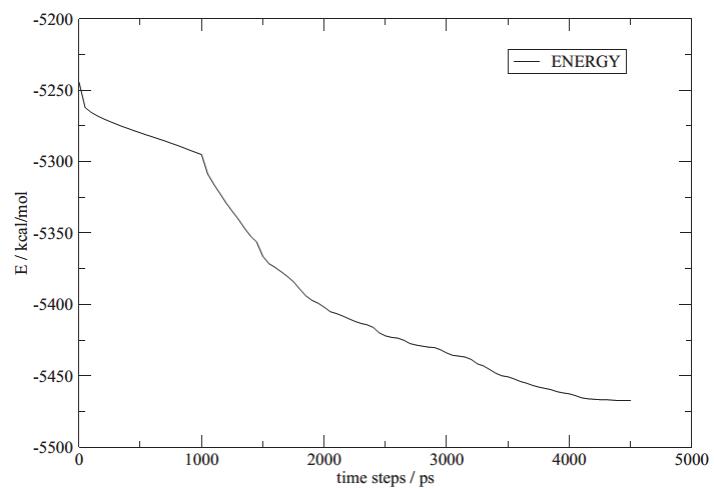
Full Minimization
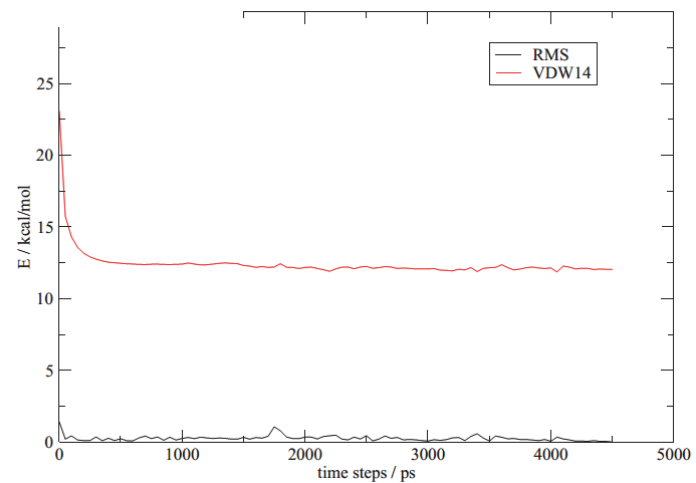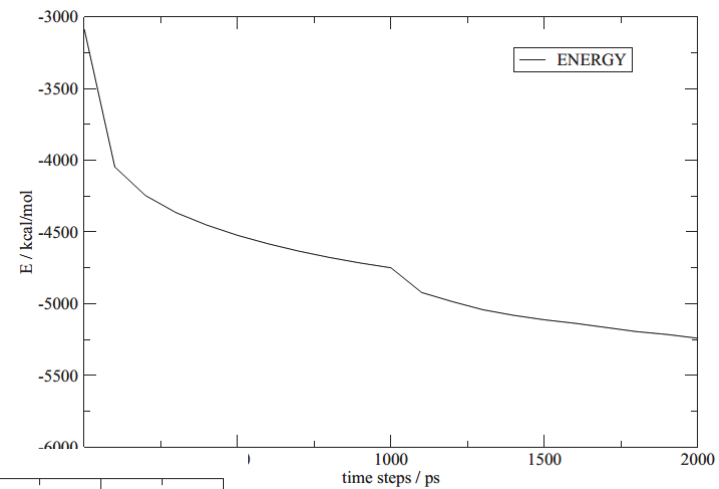
Heating. Energies should level out within the last 50 ps of the heating procedure, indicating a stable trajectory.
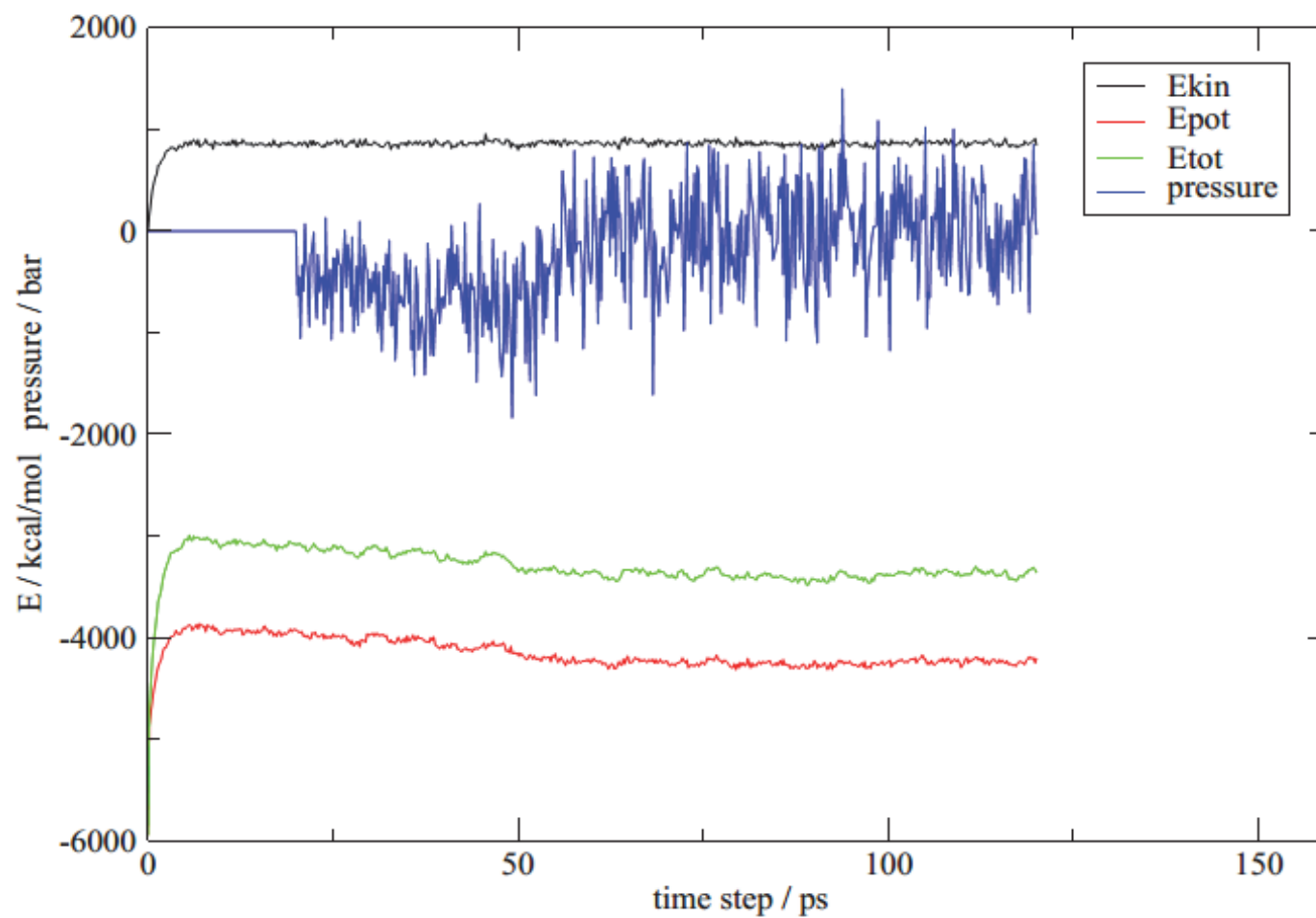
Production. Pressure will vary wildly, but median should be 1 atm. Energies should be stable throughout entire trajectory.
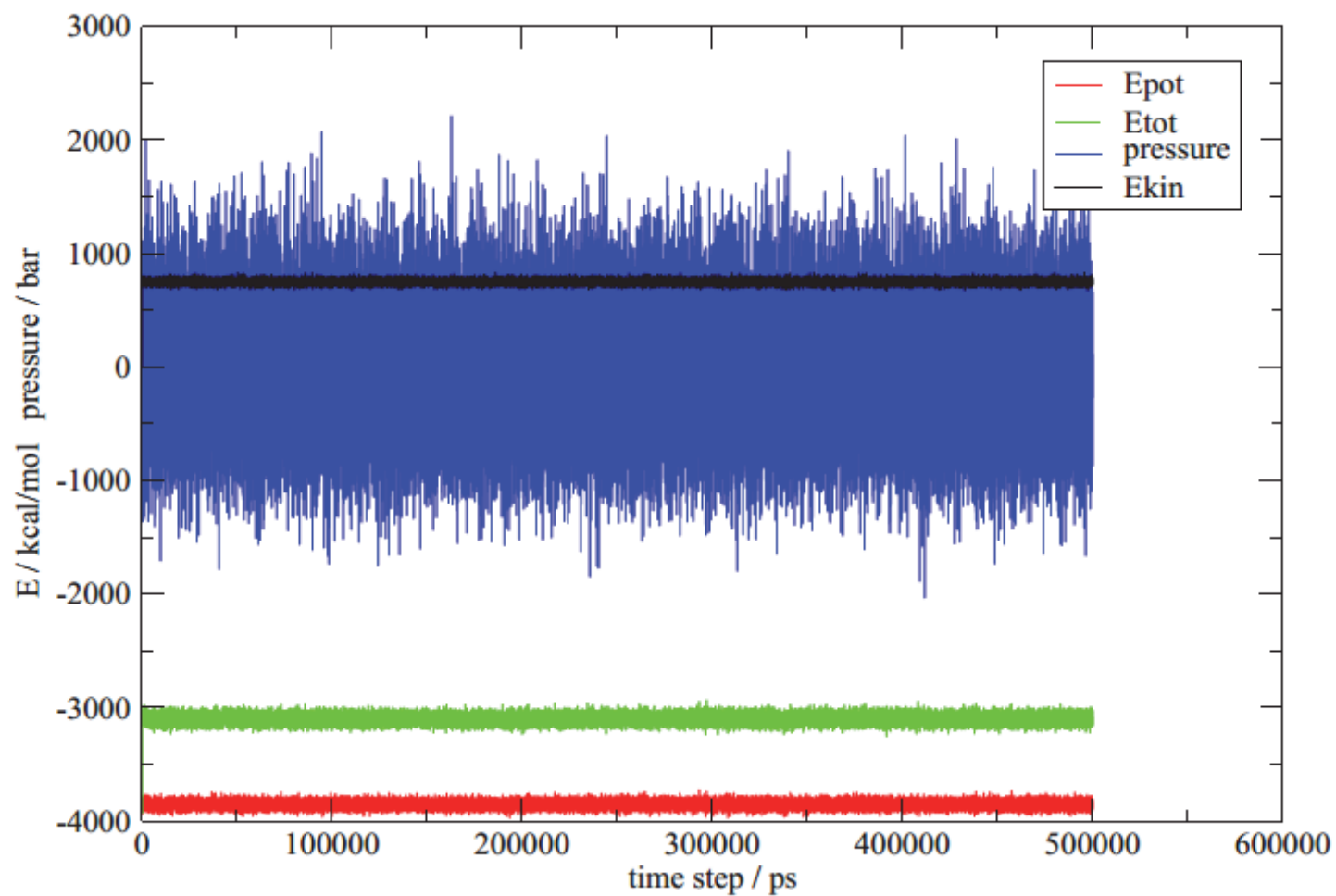
Summaries of conformational analysis for compounds *α/ß*-2, *α/ß*-7 and *α/ß*-8 based on MD simulations

Summary of the MD simulation for *α*-**47** showing population histograms and Ramachandran plot data for the relevant dihedral angles θ (C5-C6-O6-C1'), ω (C4-C5-C6-O6) and θ' (C6-O6-C1'-C2') on the 6-acetyl and φ (O5-C1-O1-C3') and ψ (C1-O1-C3'-C4') on the 1-acetyl linkage.

Summary of the MD simulation for *β*-**47** showing population histograms and Ramachandran plot data for the relevant dihedral angles *θ* (C5-C6-O6-C1'), *ω* (C4-C5-C6-O6) and *θ*' (C6-O6-C1'-C2') on the 6-acetyl and *φ* (O5-C1-O1-C3') and *ψ* (C1-O1-C3'-C4') on the 1-acetyl linkage.

Summary of the MD simulation for *α*-**48** showing population histograms and Ramachandran plot data for the relevant dihedral angles *θ* (C5-C6-O6-C1'), *ω* (C4-C5-C6-O6) and *θ* ' (C6-O6-C1'-C2') on the 6-acetyl and *φ* (C1-C2-O2-C3') and *ψ* (C2-O2-C3'-C4') on the 2-acetyl linkage.

Summary of the MD simulation for *β*-**48** showing population histograms and Ramachandran plot data for the relevant dihedral angles *θ* (C5-C6-O6-C1'), *ω* (C4-C5-C6-O6) and *θ* ' (C6-O6-C1'-C2') on the 6-acetyl and *φ* (C1-C2-O2-C3') and *ψ* (C2-O2-C3'-C4') on the 2-acetyl linkage.

Summary of the MD simulation for α-**49** showing population histograms and Ramachandran plot data for the relevant dihedral angles θ (C5-C6-O6-C1'), ω (C4-C5-C6-O6) and θ' (C6-O6-C1'-C2') on the 6-acetyl and φ (C2-C3-O3-C3') and ψ (C3-O3-C3'-C4') on the 3-acetyl linkage.

Summary of the MD simulation for *β*-**49** showing population histograms and Ramachandran plot data for the relevant dihedral angles *θ* (C5-C6-O6-C1'), *ω* (C4-C5-C6-O6) and *θ*' (C6-O6-C1'-C2') on the 6-acetyl and *φ* (C2-C3-O3-C3') and *ψ* (C3-O3-C3'-C4') on the 3-acetyl linkage.

Summary of the MD simulation for *α*-**57** showing population histograms and Ramachandran plot data for the relevant dihedral angles *θ* (C5-C6-O6-C1'), *ω* (C4-C5-C6-O6) and *θ* ' (C6-O6-C1'-C2') on the 6-acetyl and *φ* (C3-C4-O4-C3') and *ψ* (C4-O4-C3'-C4') on the 4-acetyl linkage.

Summary of the MD simulation for *β*-**57** showing population histograms and Ramachandran plot data for the relevant dihedral angles θ (C5-C6-O6-C1'), ω (C4-C5-C6-O6) and θ' (C6-O6-C1'-C2') on the 6-acetyl and φ (C3-C4-O4-C3') and ψ (C4-O4-C3'-C4') on the 4-acetyl linkage.

Summary of QM optimized conformers for 6-*O*-acetyl-*α*-D-glucose *α*-46 (M05-2X/6-31G*)

Conformer	ω / ° C4-C5-C6-O6		θ / ° C5-C6-O6-C1'		θ' / ° C6-O6-C1'-C2'	
#	QM	MD	QM	MD	QM	MD
1	55	58	-178	180	180	180
2	58	58	103	103	-174	180
3	60	58	-96	-106	-175	180
4	-58	-73	-178	180	-179	180
5	-63	-73	96	103	-172	180
6	-46	-73	-70	-106	174	180
7	-173	-168	179	180	180	180
8	-177	-168	82	103	180	180
9	-175	-168	-105	-106	174	180

Summary of QM optimized conformers for 6-*O*-acetyl-*β*-D-glucose *β*-46 (M05-2X/6-31G*)

Conformer	ω / ° C4-C5-C6-O6		θ / ° C5-C6-O6-C1'		θ' / ° C6-O6-C1'-C2'	
#	QM	MD	QM	MD	QM	MD
1	55	58	-178	180	180	180
2	58	58	102	103	-174	180
3	60	58	-96	-106	-175	180
4	-58	-73	-177	180	-179	180
5	-63	-73	96	103	-172	180
6	-45	-73	-70	-106	174	180
7	-173	-168	179	180	180	180
8	-177	-168	82	103	180	180
9	-174	-168	-103	-106	175	180

Summary of data for Karplus equation derived for the H5-C5-C6-H6$_{R/S}$ linkage in carbohydrates on the basis of α/β-D-glucose (M052X/6-311G**[u+1s]//M05-2X/6-31G*)

The coupling constants were computed analogous to **46** as described in the Methods section on the basis of DFT optimized geometries from the MD trajectories. The resulting data are plotted together with the Karplus equation (fitted using PSI-Plot) below:
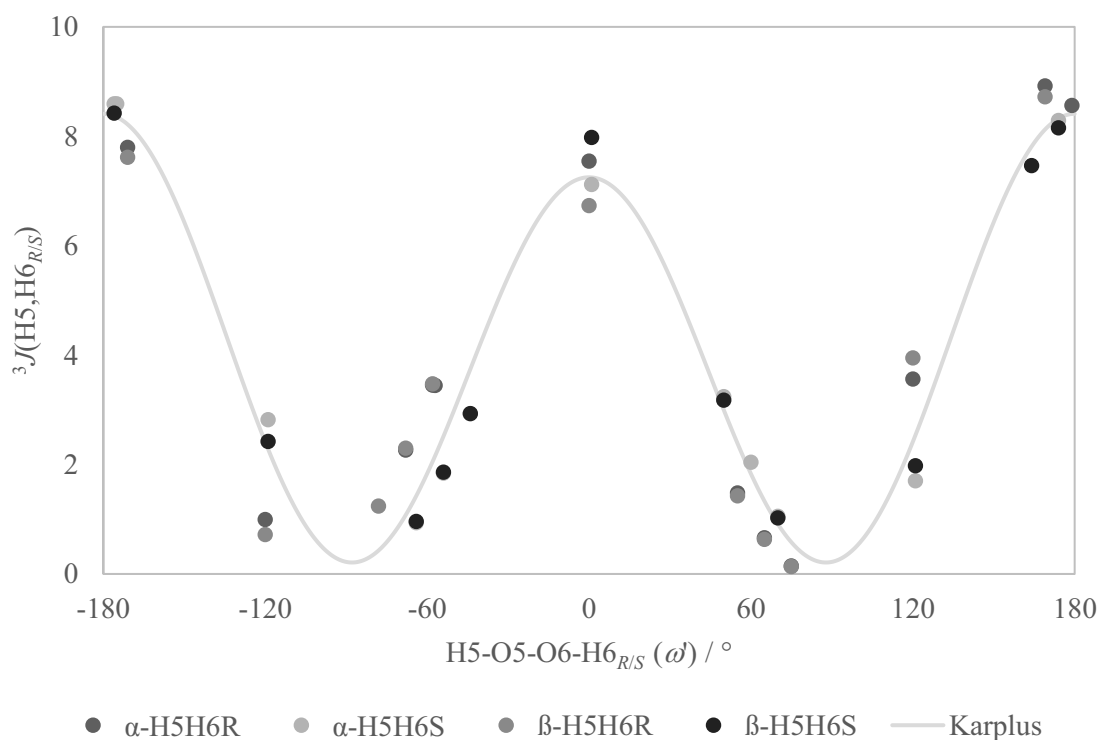
$$^{3}J_{\text{H5,H6}R/S} \text{ / Hz} = 7.61 \cdot \cos^{2} \omega' - 0.58 \cdot \cos \omega' + 0.22 \qquad (11)$$

$$r^{2} = 0.966, \text{ rms} = 0.80$$

Chapter 5: Synthesis and Conformational Analysis of cabohydrate esters

Starting geometries used for MD simulations and atomic charges derived for 58, 59, 60,

***αα/ββ*-66 and *αα/ββ*-70. based on two-step RESP procedure, as described by Cornell et al.[154]**

Acetyl 2,3,4,6-tetra-*O*-acetyl-*α*-D-glucopyranoside **58**:

Name	Type	X	Y	Z	Charge
C1	Cg	1.611	−1.360	−0.335	0.699734
C2	Cg	1.384	0.107	−0.696	0.205001
C3	Cg	0.303	0.726	0.170	0.259889
C4	Cg	−0.936	−0.158	0.125	0.307031
C5	Cg	−0.590	−1.597	0.493	0.137605
O5	Os	0.422	−2.079	−0.396	−0.586643
C6	Cg	−1.788	−2.519	0.383	0.421152
C7	C	3.458	−1.521	1.170	0.634133
C8	Cg	3.810	−1.607	2.625	0.074199
O7	O	4.239	−1.525	0.250	−0.545164
O1	Os	2.117	−1.427	1.006	−0.453410
C9	C	3.511	0.774	−1.466	0.688758
C10	Cg	4.763	1.499	−1.079	0.062060
O8	O	3.320	0.177	−2.496	−0.554937
O2	Os	2.582	0.849	−0.479	−0.489211
C11	C	−0.422	2.987	0.404	0.644632
C12	Cg	−0.783	4.207	−0.390	0.060522
O9	O	−0.527	2.863	1.600	−0.541734
O3	Os	0.014	2.002	−0.413	−0.404821
C13	C	−2.908	1.069	0.650	0.659236
C14	Cg	−3.829	1.414	1.779	0.068857
O10	O	−3.009	1.440	−0.495	−0.544837
O4	Os	−1.900	0.277	1.085	−0.483231
C15	C	−3.693	−1.771	−0.834	0.708601
C16	Cg	−4.198	−1.480	−2.216	0.055021
O11	O	−4.285	−1.519	0.190	−0.590556

```
O6    Os   -2.456   -2.316   -0.871   -0.491892
H1    H1    2.318   -1.823   -1.014    0.000000
H2    H1    1.098    0.162   -1.746    0.000000
H3    H1    0.645    0.857    1.196    0.000000
H4    H1   -1.364   -0.119   -0.875    0.000000
H5    H1   -0.224   -1.640    1.522    0.000000
H6S   H1   -1.449   -3.552    0.402    0.000000
H6R   H1   -2.480   -2.330    1.198    0.000000
H8    Hc    3.284   -2.445    3.082    0.000000
H9    Hc    4.884   -1.730    2.730    0.000000
H10   Hc    3.486   -0.694    3.127    0.000000
H11   Hc    5.383    1.644   -1.959    0.000000
H12   Hc    4.524    2.452   -0.610    0.000000
H13   Hc    5.295    0.879   -0.355    0.000000
H14   Hc   -0.939    5.045    0.283    0.000000
H15   Hc   -1.704    3.991   -0.934    0.000000
H16   Hc   -0.004    4.432   -1.117    0.000000
H17   Hc   -3.263    1.947    2.544    0.000000
H18   Hc   -4.641    2.031    1.408    0.000000
H19   Hc   -4.217    0.492    2.212    0.000000
H20   Hc   -3.842   -0.483   -2.490    0.000000
H21   Hc   -5.284   -1.473   -2.209    0.000000
H21   Hc   -3.812   -2.200   -2.934    0.000000
```

Acetyl 2,3,4,6-tetra-*O*-acetyl-*α*-D-galactopyranoside **59**:
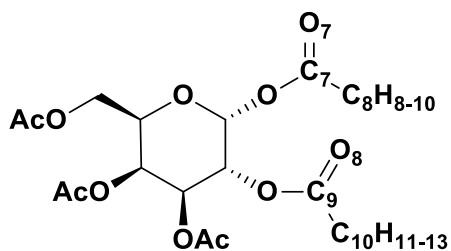
Name	Type	X	Y	Z	Charge
C1	Cg	1.579	-1.220	-0.627	0.728023
C2	Cg	1.376	0.295	-0.543	0.203118
C3	Cg	0.353	0.619	0.523	0.209252
C4	Cg	-0.929	-0.160	0.251	0.347599
C5	Cg	-0.630	-1.645	0.123	0.129308
O5	Os	0.382	-1.886	-0.858	-0.627098
C6	Cg	-1.841	-2.427	-0.363	0.443331
C7	C	3.457	-1.836	0.717	0.619543
C8	Cg	3.841	-2.334	2.079	0.075667
O7	O	4.217	-1.597	-0.190	-0.544930
O1	Os	2.116	-1.675	0.626	-0.439366
C9	C	3.499	1.109	-1.170	0.683092
C10	Cg	4.786	1.665	-0.641	0.058409
O8	O	3.258	0.836	-2.320	-0.553458
O2	Os	2.604	0.917	-0.168	-0.481086
C11	C	-0.471	2.567	1.563	0.653693
C12	Cg	-0.845	3.999	1.327	0.054590
O9	O	-0.649	1.943	2.580	-0.545639
O3	Os	0.088	2.022	0.455	-0.396772
C13	C	-2.488	1.176	-0.954	0.603154
C14	Cg	-2.956	1.521	-2.334	0.082976
O10	O	-2.950	1.600	0.080	-0.527254
O4	Os	-1.471	0.286	-1.000	-0.441431
C15	C	-4.025	-1.548	0.029	0.698990
C16	Cg	-4.984	-1.177	1.121	0.058117
O11	O	-4.178	-1.307	-1.145	-0.576947
O6	Os	-2.927	-2.155	0.534	-0.514885
H1	H1	2.264	-1.477	-1.428	0.000000
H2	H1	1.049	0.661	-1.514	0.000000
H3	H1	0.737	0.364	1.510	0.000000
H4	H1	-1.647	0.019	1.048	0.000000
H5	H1	-0.302	-2.017	1.096	0.000000
H6S	H1	-2.102	-2.125	-1.372	0.000000

```
H6R   H1   -1.638   -3.495   -0.328   0.000000
H8    Hc    3.300   -3.253    2.300   0.000000
H9    Hc    4.912   -2.505    2.111   0.000000
H10   Hc    3.557   -1.590    2.824   0.000000
H11   Hc    4.591    2.448    0.090   0.000000
H12   Hc    5.319    0.852   -0.145   0.000000
H13   Hc    5.382    2.043   -1.466   0.000000
H14   Hc   -1.025    4.488    2.280   0.000000
H15   Hc   -1.761    4.008    0.734   0.000000
H16   Hc   -0.065    4.512    0.767   0.000000
H17   Hc   -3.435    0.638   -2.757   0.000000
H18   Hc   -2.106    1.786   -2.961   0.000000
H19   Hc   -3.667    2.340   -2.281   0.000000
H20   Hc   -5.982   -1.076    0.705   0.000000
H21   Hc   -4.666   -0.211    1.520   0.000000
H22   Hc   -4.964   -1.910    1.923   0.000000
```

2,3,4-Tri-*O*-acetyl-D-glucurono-6,1-lactone **60**:
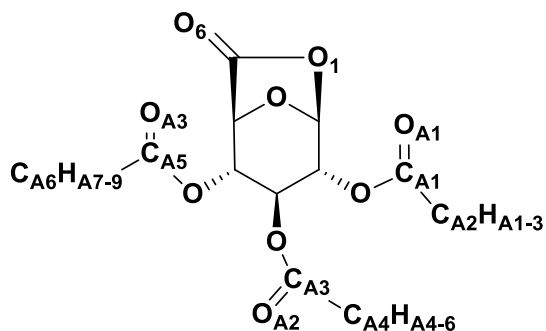
Name	Type	X	Y	Z	Charge
C5	Cg	-1.210	-1.779	0.721	0.378932
C4	Cg	-0.417	-0.547	1.147	0.183201
C3	Cg	-0.220	0.411	-0.042	0.500268
C2	Cg	-0.051	-0.310	-1.392	0.239315
C1	Cg	-0.864	-1.600	-1.447	0.643829
O5	Os	-0.531	-2.416	-0.354	-0.557304
O1	Os	-2.252	-1.285	-1.277	-0.501907
H1	H2	-0.726	-2.146	-2.373	0.000000
O2	Os	1.304	-0.730	-1.562	-0.573868
H2	H1	-0.341	0.370	-2.190	0.000000
O3	Os	-1.399	1.207	-0.130	-0.553209
H3	H1	0.658	1.020	0.137	0.000000
O4	Os	0.843	-1.047	1.599	-0.532444
H4	H1	-0.919	-0.007	1.948	0.000000
C6	C	-2.521	-1.358	0.052	0.618099
H5	H	-1.359	-2.480	1.535	0.000000
CA5	C	1.582	-0.193	2.343	0.771400
CA3	C	2.180	0.236	-1.922	0.748907
CA1	C	-1.387	2.564	0.047	0.670948
O6	O	-3.588	-1.136	0.538	-0.520663
OA2	O	-2.440	3.137	-0.020	-0.553339
OA3	O	1.222	0.933	2.591	-0.581259
OA1	O	1.852	1.391	-2.059	-0.578113
CA4	Cg	-0.065	3.235	0.304	0.082537
HA4	Hc	0.622	3.060	-0.524	0.000000
HA5	Hc	0.388	2.852	1.220	0.000000
HA6	Hc	-0.257	4.299	0.405	0.000000
CA6	Cg	2.863	-0.833	2.786	0.051013
HA7	Hc	3.426	-1.158	1.911	0.000000
HA8	Hc	2.640	-1.716	3.385	0.000000
HA9	Hc	3.441	-0.120	3.365	0.000000

```
CA2   Cg    3.559   -0.322   -2.100    0.063657
HA1   Hc    3.537   -1.120   -2.841    0.000000
HA2   Hc    3.896   -0.753   -1.156    0.000000
HA3   Hc    4.231    0.469   -2.413    0.000000
```

α-D-Glucopyranosyl 6,6'-*α*-D-glucopyranuronate *αα*-**66**:
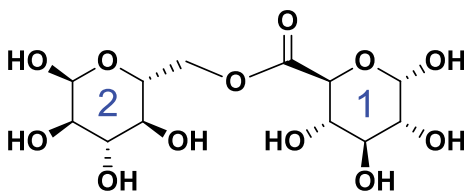
Name	Type	X	Y	Z	Charge
C21	Cg	-3.733	-1.122	1.238	0.560066
C22	Cg	-5.031	-0.564	0.628	0.232662
C23	Cg	-4.751	0.103	-0.726	0.380373
O23	Oh	-5.877	0.840	-1.174	-0.735215
C24	Cg	-3.594	1.107	-0.591	0.210948
O24	Oh	-3.245	1.647	-1.852	-0.708805
C25	Cg	-2.361	0.364	-0.052	0.254872
O25	Os	-2.659	-0.206	1.228	-0.587548
C26	Cg	-1.204	1.333	0.174	0.339380
O26	Os	-0.011	0.525	0.133	-0.495278
O21	Oh	-3.334	-2.229	0.463	-0.717212
O22	Oh	-6.008	-1.572	0.485	-0.700711
C11	Cg	3.253	-1.599	-0.790	0.593358
C12	Cg	4.614	-0.898	-0.984	0.214674
C13	Cg	4.849	0.126	0.137	0.408358
O13	Oh	6.033	0.827	-0.197	-0.738560
C14	Cg	3.647	1.079	0.234	0.216003
O14	Oh	3.902	1.910	1.349	-0.708300
C15	Cg	2.365	0.247	0.435	0.231674
O15	Os	2.195	-0.673	-0.644	-0.625818
C16	C	1.150	1.146	0.453	0.844118
O16	O	1.138	2.343	0.762	-0.607266
O11	Oh	3.196	-2.369	0.388	-0.716998
O12	Oh	5.593	-1.921	-0.934	-0.705912
H21	H2	-3.869	-1.395	2.323	0.000000
H22	H1	-5.486	0.182	1.340	0.000000
H23	H1	-4.489	-0.683	-1.490	0.000000
H43	Ho	-6.642	0.255	-1.088	0.441496
H24	H1	-3.892	1.937	0.107	0.000000
H44	Ho	-4.064	1.979	-2.244	0.437394
H25	H1	-2.059	-0.455	-0.763	0.000000
H61	H1	-1.159	2.085	-0.656	0.000000
H62	H1	-1.275	1.842	1.169	0.000000

```
H41   Ho   -2.480   -2.529    0.799    0.456978
H42   Ho   -5.598   -2.310    0.011    0.439675
H11   H2    2.970   -2.215   -1.690    0.000000
H12   H1    4.639   -0.385   -1.983    0.000000
H13   H1    4.989   -0.406    1.120    0.000000
H33   Ho    6.124    1.540    0.449    0.443246
H14   H1    3.562    1.695   -0.703    0.000000
H34   Ho    3.198    2.576    1.380    0.440518
H15   H1    2.407   -0.313    1.412    0.000000
H31   Ho    4.047   -2.818    0.484    0.459569
H32   Ho    6.453   -1.481   -0.970    0.442256
```

ß-D-Glucopyranosyl 6,6'-*ß*-D-glucopyranuronate *ßß*-**66**:
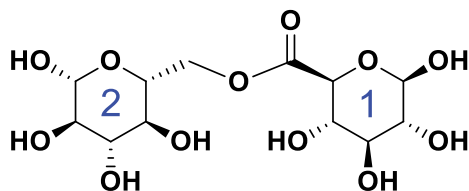

```
Name Type    X        Y        Z       Charge
C21  Cg     3.842    0.307   -1.146    0.502973
C22  Cg     3.589    1.165    0.087    0.299822
C23  Cg     3.299    0.261    1.265    0.279559
O23  Oh     2.949    1.039    2.393   -0.723127
C24  Cg     2.153   -0.674    0.909    0.257077
O24  Oh     1.973   -1.538    2.017   -0.711832
C25  Cg     2.485   -1.446   -0.369    0.223590
O25  Os     2.725   -0.521   -1.423   -0.544999
C26  Cg     1.385   -2.382   -0.819    0.359915
O26  Os     0.166   -1.656   -1.094   -0.500984
O21  Oh     4.034    1.182   -2.210   -0.695860
O22  Oh     4.733    1.946    0.367   -0.735446
C11  Cg    -4.240   -0.550   -0.355    0.549088
C12  Cg    -4.178    0.853    0.229    0.312722
C13  Cg    -2.924    1.550   -0.258    0.275421
O13  Oh    -2.737    2.803    0.371   -0.724714
C14  Cg    -1.706    0.707    0.068    0.270112
O14  Oh    -0.532    1.267   -0.483   -0.713087
C15  Cg    -1.903   -0.692   -0.526    0.178084
O15  Os    -3.069   -1.273    0.022   -0.572713
C16  C     -0.725   -1.551   -0.116    0.829531
O16  O     -0.609   -2.029    0.993   -0.594849
O11  Oh    -5.348   -1.177    0.193   -0.696672
O12  Oh    -5.281    1.631   -0.192   -0.745388
H21  H2     4.726   -0.323   -0.981    0.000000
H22  H1     2.711    1.790   -0.114    0.000000
H23  H1     4.194   -0.341    1.476    0.000000
H43  Ho     2.580    0.408    3.030    0.455401
H24  H1     1.267   -0.056    0.734    0.000000
H44  Ho     1.063   -1.874    1.964    0.447698
H25  H1     3.377   -2.061   -0.187    0.000000
H61  H1     1.656   -2.843   -1.764    0.000000
H62  H1     1.195   -3.145   -0.068    0.000000
```

```
H41   Ho    4.451    0.704   -2.939    0.451663
H42   Ho    4.948    2.409   -0.457    0.451766
H11   H2   -4.298   -0.506   -1.449    0.000000
H12   H1   -4.144    0.759    1.320    0.000000
H13   H1   -2.985    1.671   -1.348    0.000000
H33   Ho   -3.518    3.340    0.173    0.457162
H14   H1   -1.624    0.602    1.156    0.000000
H34   Ho   -0.507    2.192   -0.193    0.446114
H15   H1   -1.951   -0.631   -1.617    0.000000
H31   Ho   -5.559   -1.962   -0.330    0.453804
H32   Ho   -6.080    1.197    0.139    0.458167
```

α-D-Glucopyranosyl 6,6'-α-D-glucopyranose αα-**70**:
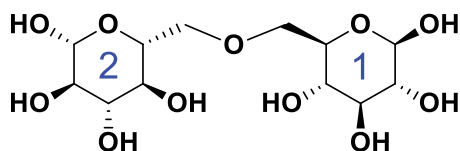
Name	Type	X	Y	Z	Charge
C11	Cg	2.283	-1.436	-0.770	0.526410
C12	Cg	3.655	-1.349	-0.112	0.246599
C13	Cg	3.711	-0.179	0.863	0.361746
O13	Oh	5.019	0.039	1.320	-0.730880
C14	Cg	3.238	1.107	0.206	0.242985
O14	Oh	3.160	2.150	1.134	-0.708142
C15	Cg	1.850	0.871	-0.373	0.250425
O15	Os	1.917	-0.199	-1.293	-0.565472
C16	Cg	1.286	2.058	-1.130	0.256694
O26	Os	-0.007	1.791	-1.615	-0.459010
O11	Oh	1.385	-1.882	0.188	-0.720222
O12	Oh	4.001	-2.545	0.530	-0.696966
C21	Cg	-3.813	0.791	1.121	0.551346
C22	Cg	-4.250	-0.418	0.299	0.232587
C23	Cg	-3.031	-1.134	-0.268	0.369624
O23	Oh	-3.467	-2.121	-1.154	-0.730702
C24	Cg	-2.111	-0.150	-0.981	0.221005
O24	Oh	-0.958	-0.878	-1.331	-0.699096
C25	Cg	-1.781	1.056	-0.099	0.275341
O25	Os	-2.971	1.628	0.400	-0.593337
C26	Cg	-1.116	2.202	-0.861	0.256995
O21	Oh	-3.199	0.305	2.272	-0.723276
O22	Oh	-5.070	-1.248	1.059	-0.696224
H11	H2	2.306	-2.110	-1.617	0.000000
H12	H1	4.395	-1.187	-0.886	0.000000
H13	H1	3.055	-0.389	1.705	0.000000
H33	Ho	5.359	-0.776	1.670	0.440327
H14	H1	3.924	1.362	-0.599	0.000000
H34	Ho	3.988	2.200	1.597	0.433955
H15	H1	1.181	0.616	0.441	0.000000
H61	H1	1.287	2.935	-0.495	0.000000
H62	H1	1.905	2.255	-1.996	0.000000
H31	Ho	0.503	-1.849	-0.176	0.457972
H32	Ho	3.238	-2.863	0.998	0.434352

```
H21   H2   -4.673    1.396    1.376    0.000000
H22   H1   -4.853   -0.066   -0.528    0.000000
H23   H1   -2.473   -1.582    0.553    0.000000
H43   Ho   -2.705   -2.518   -1.556    0.439831
H24   H1   -2.616    0.195   -1.880    0.000000
H44   Ho   -0.348   -0.308   -1.792    0.427646
H25   H1   -1.156    0.724    0.723    0.000000
H63   H1   -0.847    2.988   -0.163    0.000000
H64   H1   -1.843    2.606   -1.554    0.000000
H41   Ho   -3.037    1.018    2.875    0.460762
H42   Ho   -4.607   -1.489    1.852    0.436721
```

Summary of the total conformer space of α-D-Glucopyranosyl 6,6'-α-D-glucopyranose αα-**70** established based on its MD simulation (97% coverage).

Conformer	C4-C5-C6-O6	C5-C6-O6-C6'	C6-O6-C6'-C5'	O6-C6'-C5'-C4'	Count	% abundance
1	58	180	180	58	10150	21%
2	-73	180	180	58	3798	8%
3	-168	180	180	58	3909	8%
4	58	180	180	-73	2926	6%
5	-73	180	180	-73	694	1%
6	-168	180	180	-73	687	1%
7	58	180	180	-168	2727	6%
8	-73	180	180	-168	903	2%
9	-168	180	180	-168	803	2%
10	58	88	180	58	4926	10%
11	-73	88	180	58	151	0%
12	-168	88	180	58	1021	2%
13	58	88	180	-73	412	1%
14	-73	88	180	-73	32	0%
15	-168	88	180	-73	116	0%
16	58	88	180	-168	399	1%
17	-73	88	180	-168	47	0%
18	-168	88	180	-168	327	1%
19	58	-88	180	58	697	1%
20	-73	-88	180	58	501	1%

Conformer	C4-C5-C6-O6	C5-C6-O6-C6'	C6-O6-C6'-C5'	O6-C6'-C5'-C4'	Count	% abundance
21	-168	-88	180	58	651	1%
22	58	-88	180	-73	201	0%
23	-73	-88	180	-73	255	1%
24	-168	-88	180	-73	71	0%
25	58	-88	180	-168	210	0%
26	-73	-88	180	-168	114	0%
27	-168	-88	180	-168	112	0%
28	58	180	88	58	5276	11%
29	-73	180	88	58	475	1%
30	-168	180	88	58	589	1%
31	58	180	88	-73	121	0%
32	-73	180	88	-73	34	0%
33	-168	180	88	-73	50	0%
34	58	180	88	-168	719	1%
35	-73	180	88	-168	153	0%
36	-168	180	88	-168	350	1%
37	58	88	88	58	138	0%
38	-73	88	88	58	16	0%
39	-168	88	88	58	166	0%
40	58	88	88	-73	11	0%
41	-73	88	88	-73	2	0%
42	-168	88	88	-73	8	0%
43	58	88	88	-168	95	0%
44	-73	88	88	-168	8	0%
45	-168	88	88	-168	54	0%
46	58	-88	88	58	27	0%
47	-73	-88	88	58	97	0%
48	-168	-88	88	58	43	0%
49	58	-88	88	-73	0	0%
50	-73	-88	88	-73	0	0%
51	-168	-88	88	-73	0	0%
52	58	-88	88	-168	9	0%
53	-73	-88	88	-168	16	0%
54	-168	-88	88	-168	34	0%
55	58	180	-88	58	616	1%
56	-73	180	-88	58	227	0%
57	-168	180	-88	58	252	1%

Conformer	C4-C5-C6-O6	C5-C6-O6-C6'	C6-O6-C6'-C5'	O6-C6'-C5'-C4'	Count	% abundance
58	58	180	-88	-73	454	1%
59	-73	180	-88	-73	241	0%
60	-168	180	-88	-73	103	0%
61	58	180	-88	-168	538	1%
62	-73	180	-88	-168	67	0%
63	-168	180	-88	-168	190	0%
64	58	88	-88	58	19	0%
65	-73	88	-88	58	0	0%
66	-168	88	-88	58	15	0%
67	58	88	-88	-73	118	0%
68	-73	88	-88	-73	0	0%
69	-168	88	-88	-73	20	0%
70	58	88	-88	-168	48	0%
71	-73	88	-88	-168	0	0%
72	-168	88	-88	-168	45	0%
73	58	-88	-88	58	76	0%
74	-73	-88	-88	58	33	0%
75	-168	-88	-88	58	15	0%
76	58	-88	-88	-73	34	0%
77	-73	-88	-88	-73	30	0%
78	-168	-88	-88	-73	22	0%
79	58	-88	-88	-168	27	0%
80	-73	-88	-88	-168	28	0%
81	-168	-88	-88	-168	15	0%

ß-D-Glucopyranosyl 6,6'-*ß*-D-glucopyranose *ßß*-**70**:
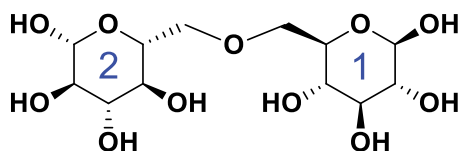
Name	Type	X	Y	Z	Charge
C11	Cg	3.773	1.494	0.610	0.505990
C12	Cg	4.643	0.250	0.733	0.301602
C13	Cg	4.494	−0.598	−0.514	0.253947
O13	Oh	5.181	−1.816	−0.409	−0.723285
C14	Cg	3.028	−0.917	−0.752	0.287313
O14	Oh	2.852	−1.558	−1.984	−0.705483
C15	Cg	2.213	0.374	−0.778	0.185929
O15	Os	2.452	1.122	0.395	−0.509635
C16	Cg	0.719	0.145	−0.891	0.276940
O26	Os	0.295	−0.670	0.166	−0.465434
O11	Oh	3.831	2.258	1.762	−0.693555
O12	Oh	5.996	0.586	0.863	−0.735163
C21	Cg	−3.328	1.377	−0.478	0.495442
C22	Cg	−4.659	0.643	−0.388	0.310281
C23	Cg	−4.593	−0.396	0.714	0.265520
O23	Oh	−5.742	−1.198	0.752	−0.720011
C24	Cg	−3.402	−1.318	0.506	0.271568
O24	Oh	−3.245	−2.178	1.595	−0.699280
C25	Cg	−2.126	−0.489	0.356	0.201409
O25	Os	−2.309	0.452	−0.684	−0.523562
C26	Cg	−0.917	−1.344	0.016	0.275411
O21	Oh	−3.324	2.282	−1.523	−0.695427
O22	Oh	−5.709	1.517	−0.085	−0.733982
H11	H2	4.140	2.121	−0.197	0.000000
H12	H1	4.303	−0.320	1.595	0.000000
H13	H1	4.872	−0.034	−1.364	0.000000
H33	Ho	6.093	−1.634	−0.223	0.457077
H14	H1	2.670	−1.541	0.059	0.000000
H34	Ho	3.419	−2.318	−2.005	0.435546
H15	H1	2.520	0.957	−1.646	0.000000
H61	H1	0.515	−0.330	−1.844	0.000000
H62	H1	0.215	1.103	−0.867	0.000000
H31	Ho	3.208	1.900	2.384	0.443041
H32	Ho	6.100	1.161	1.611	0.450925

```
H21  H2  -3.157   1.951   0.427   0.000000
H22  H1  -4.837   0.143  -1.339   0.000000
H23  H1  -4.468   0.117   1.665   0.000000
H43  Ho  -6.500  -0.639   0.871   0.452503
H24  H1  -3.564  -1.886  -0.409   0.000000
H44  Ho  -4.076  -2.609   1.757   0.435049
H25  H1  -1.928   0.032   1.289   0.000000
H63  H1  -1.024  -1.729  -0.995   0.000000
H64  H1  -0.890  -2.179   0.701   0.000000
H41  Ho  -3.163   1.809  -2.330   0.448870
H42  Ho  -5.732   2.212  -0.731   0.450448
```

Summary of the total conformer space of *ß*-D-Glucopyranosyl 6,6'-*ß*-D-glucopyranose *ßß*-**70** established based on its MD simulation (97% coverage).

Conformer	C4-C5-C6-O6	C5-C6-O6-C6'	C6-O6-C6'-C5'	O6-C6'-C5'-C4'	Count	% abundance
1	58	180	180	58	7810	16%
2	-73	180	180	58	3246	7%
3	-168	180	180	58	3250	7%
4	58	180	180	-73	2873	6%
5	-73	180	180	-73	865	2%
6	-168	180	180	-73	624	1%
7	58	180	180	-168	3253	7%
8	-73	180	180	-168	785	2%
9	-168	180	180	-168	1001	2%
10	58	88	180	58	5761	12%
11	-73	88	180	58	140	0%
12	-168	88	180	58	770	2%
13	58	88	180	-73	553	1%
14	-73	88	180	-73	31	0%
15	-168	88	180	-73	142	0%
16	58	88	180	-168	768	2%
17	-73	88	180	-168	40	0%
18	-168	88	180	-168	211	0%
19	58	-88	180	58	775	2%
20	-73	-88	180	58	570	1%

Conformer	C4-C5-C6-O6	C5-C6-O6-C6′	C6-O6-C6′-C5′	O6-C6′-C5′-C4′	Count	% abundance
21	-168	-88	180	58	613	1%
22	58	-88	180	-73	188	0%
23	-73	-88	180	-73	235	0%
24	-168	-88	180	-73	183	0%
25	58	-88	180	-168	273	1%
26	-73	-88	180	-168	226	0%
27	-168	-88	180	-168	242	0%
28	58	180	88	58	5253	11%
29	-73	180	88	58	618	1%
30	-168	180	88	58	834	2%
31	58	180	88	-73	123	0%
32	-73	180	88	-73	27	0%
33	-168	180	88	-73	24	0%
34	58	180	88	-168	871	2%
35	-73	180	88	-168	155	0%
36	-168	180	88	-168	179	0%
37	58	88	88	58	277	1%
38	-73	88	88	58	26	0%
39	-168	88	88	58	132	0%
40	58	88	88	-73	20	0%
41	-73	88	88	-73	0	0%
42	-168	88	88	-73	4	0%
43	58	88	88	-168	138	0%
44	-73	88	88	-168	11	0%
45	-168	88	88	-168	20	0%
46	58	-88	88	58	19	0%
47	-73	-88	88	58	116	0%
48	-168	-88	88	58	45	0%
49	58	-88	88	-73	0	0%
50	-73	-88	88	-73	0	0%
51	-168	-88	88	-73	1	0%
52	58	-88	88	-168	15	0%
53	-73	-88	88	-168	19	0%
54	-168	-88	88	-168	115	0%
55	58	180	-88	58	808	2%
56	-73	180	-88	58	209	0%
57	-168	180	-88	58	281	1%

Conformer	C4-C5-C6-O6	C5-C6-O6-C6'	C6-O6-C6'-C5'	O6-C6'-C5'-C4'	Count	% abundance
58	58	180	-88	-73	509	1%
59	-73	180	-88	-73	261	1%
60	-168	180	-88	-73	164	0%
61	58	180	-88	-168	649	1%
62	-73	180	-88	-168	229	0%
63	-168	180	-88	-168	232	0%
64	58	88	-88	58	24	0%
65	-73	88	-88	58	0	0%
66	-168	88	-88	58	19	0%
67	58	88	-88	-73	117	0%
68	-73	88	-88	-73	0	0%
69	-168	88	-88	-73	24	0%
70	58	88	-88	-168	54	0%
71	-73	88	-88	-168	2	0%
72	-168	88	-88	-168	44	0%
73	58	-88	-88	58	50	0%
74	-73	-88	-88	58	56	0%
75	-168	-88	-88	58	42	0%
76	58	-88	-88	-73	30	0%
77	-73	-88	-88	-73	29	0%
78	-168	-88	-88	-73	25	0%
79	58	-88	-88	-168	42	0%
80	-73	-88	-88	-168	63	0%
81	-168	-88	-88	-168	60	0%

Summary of the total conformer space of acetyl 2,3,4,6-tetra-*O*-acetyl-α-D-glucopyranoside α-**58** established based on its MD simulation (92% coverage).

Conformer #	C4-C5-C6-O6	C5-C6-O6-C11′	O5-C1-O1-C1′	C1-C2-O2-C3′	C3-C4-O4-C7′	Count	% abundance
1	53	180	89	83	100	2243	4.9%
2	53	118	89	83	100	371	0.8%
3	53	-116	89	83	100	1826	4.0%
4	53	180	142	83	100	5561	12.1%
5	53	118	142	83	100	1167	2.5%
6	53	-116	142	83	100	4368	9.5%
7	53	180	89	139	100	2813	6.1%
8	53	118	89	139	100	517	1.1%
9	53	-116	89	139	100	2215	4.8%
10	53	180	142	139	100	2917	6.3%
11	53	118	142	139	100	611	1.3%
12	53	-116	142	139	100	2330	5.1%
13	53	-180	89	83	-73	101	0.2%
14	53	118	89	83	-73	20	0.0%
15	53	-116	89	83	-73	22	0.0%
16	53	-180	142	83	-73	196	0.4%
17	53	118	142	83	-73	54	0.1%
18	53	-116	142	83	-73	54	0.1%
19	53	-180	89	139	-73	141	0.3%
20	53	118	89	139	-73	18	0.0%
21	53	-116	89	139	-73	28	0.1%
22	53	-180	142	139	-73	104	0.2%
23	53	118	142	139	-73	26	0.1%
24	53	-116	142	139	-73	27	0.1%
25	-68	180	89	83	100	1571	3.4%
26	-68	118	89	83	100	474	1.0%
27	-68	-116	89	83	100	533	1.2%
28	-68	180	142	83	100	3735	8.1%
29	-68	118	142	83	100	934	2.0%
30	-68	-116	142	83	100	1501	3.3%
31	-68	180	89	139	100	2037	4.4%
32	-68	118	89	139	100	455	1.0%
33	-68	-116	89	139	100	642	1.4%
34	-68	180	142	139	100	1938	4.2%
35	-68	118	142	139	100	424	0.9%

Conformer #	C4-C5-C6-O6	C5-C6-O6-C11'	O5-C1-O1-C1'	C1-C2-O2-C3'	C3-C4-O4-C7'	Count	% abundance
36	-68	-116	142	139	100	726	1.6%
37	-68	180	89	83	-73	76	0.2%
38	-68	118	89	83	-73	41	0.1%
39	-68	-116	89	83	-73	20	0.0%
40	-68	180	142	83	-73	154	0.3%
41	-68	118	142	83	-73	59	0.1%
42	-68	-116	142	83	-73	39	0.1%
43	-68	180	89	139	-73	108	0.2%
44	-68	118	89	139	-73	60	0.1%
45	-68	-116	89	139	-73	22	0.0%
46	-68	180	142	139	-73	84	0.2%
47	-68	118	142	139	-73	38	0.1%
48	-68	-116	142	139	-73	17	0.0%
49	-163	180	89	83	100	199	0.4%
50	-163	118	89	83	100	106	0.2%
51	-163	-116	89	83	100	45	0.1%
52	-163	180	142	83	100	696	1.5%
53	-163	118	142	83	100	312	0.7%
54	-163	-116	142	83	100	161	0.3%
55	-163	180	89	139	100	247	0.5%
56	-163	118	89	139	100	119	0.3%
57	-163	-116	89	139	100	65	0.1%
58	-163	180	142	139	100	337	0.7%
59	-163	118	142	139	100	162	0.4%
60	-163	-116	142	139	100	89	0.2%
61	-163	180	89	83	-73	6	0.0%
62	-163	118	89	83	-73	3	0.0%
63	-163	-116	89	83	-73	0	0.0%
64	-163	180	142	83	-73	25	0.1%
65	-163	118	142	83	-73	24	0.1%
66	-163	-116	142	83	-73	8	0.0%
67	-163	180	89	139	-73	9	0.0%
68	-163	118	89	139	-73	5	0.0%
69	-163	-116	89	139	-73	4	0.0%
70	-163	180	142	139	-73	12	0.0%
71	-163	118	142	139	-73	11	0.0%
72	-163	-116	142	139	-73	2	0.0%

Summary of the total conformational space of acetyl 2,3,4,6-tetra-*O*-acetyl-*α*-D-galactopyranoside *α*-**59** established based on its MD simulation (88% coverage).

Conformer #	C4-C5-C6-O6 ω / °	C5-C6-O6-C11' θ / °	O5-C1-O1-C1' φ_1 / °	C1-C2-O2-C3' φ_2 / °	C2-C3-O3-C5' φ_3 / °	Count	% abundance
1	-56	130	145	85	-148	10102	22.9%
2	-56	130	145	85	-99	1850	4.2%
3	-56	130	145	143	-148	1795	4.1%
4	-56	130	145	143	-99	970	2.2%
5	-56	130	90	85	-148	4676	10.6%
6	-56	130	90	85	-99	1059	2.4%
7	-56	130	90	143	-148	1868	4.2%
8	-56	130	90	143	-99	1228	2.8%
9	-56	180	145	85	-148	7379	16.7%
10	-56	180	145	85	-99	1562	3.5%
11	-56	180	145	143	-148	1389	3.2%
12	-56	180	145	143	-99	898	2.0%
13	-56	180	90	85	-148	3174	7.2%
14	-56	180	90	85	-99	791	1.8%
15	-56	180	90	143	-148	1281	2.9%
16	-56	180	90	143	-99	955	2.2%
17	-56	-87	145	85	-148	1346	3.1%
18	-56	-87	145	85	-99	283	0.6%
19	-56	-87	145	143	-148	246	0.6%
20	-56	-87	145	143	-99	143	0.3%
21	-56	-87	90	85	-148	557	1.3%
22	-56	-87	90	85	-99	140	0.3%
23	-56	-87	90	143	-148	220	0.5%
24	-56	-87	90	143	-99	145	0.3%